

UNCLASSIFIED

AD NUMBER

AD368357

CLASSIFICATION CHANGES

TO: unclassified

FROM: confidential

LIMITATION CHANGES

TO:
Approved for public release, distribution
unlimited

FROM:
Distribution: DoD only: others to
Director, Naval Research Lab., Washington,
D. C. 20390.

AUTHORITY

1970, Group-4, DoDD 5200.10, 26 Jul 1962.;
NRL ltr, 26 Feb 2001.

THIS PAGE IS UNCLASSIFIED

CONFIDENTIAL

958357

**SUMMARY OF NAVY STUDY PROGRAM
FOR**

F4H-1 and FBU-3 WEAPON SYSTEMS

(Parameter Plots for Co-Altitude Attacks)

VOLUME VII

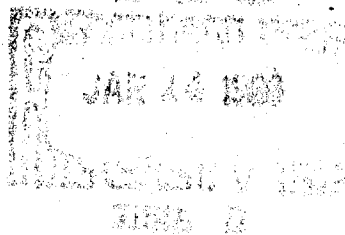
I. N. Bellavin

R. L. Lister

C. N. Loughmiller

J. C. Ryan

RADAR DIVISION



**U. S. NAVAL RESEARCH LABORATORY
Washington, D.C.**

CONFIDENTIAL

In addition to security requirements which apply to this document and must be met, each transmittal outside the Department of Defense must have prior approval of the Director, U.S. Naval Research Laboratory, Washington, D.C.

Declassified at 1 year intervals
Declassified after 1 year

CONFIDENTIAL

MEMORANDUM REPORT

(6) SUMMARY OF NAVY STUDY PROGRAM
FOR
F4H-1 AND F8U-3 WEAPON SYSTEMS
(Parameter Plots for Co-Altitude Attacks), VOLUME VII

(10) I. N. Bellavin, C. M. Loughmiller 2nd
R. L. Lister, J. C. Ryon

(11)

(12)

248p.

(14) AIRL 145-754-Vol-7

NAVY DEPARTMENT
NAVAL RESEARCH LABORATORY
EQUIPMENT RESEARCH BRANCH
RADAR DIVISION

CONFIDENTIAL

DE

CONFIDENTIAL

TABLE OF CONTENTS

| | PAGE |
|--|------|
| INTRODUCTION | 1 |
| DEFINITION OF PARAMETERS | 1 |
| PHASE I-SYSTEM PERFORMANCE UNDER IDEAL CONDITIONS-HORIZONTAL ATTACKS | 3 |
| Interceptor at V_{max} at AI Radar Detection | 3 |
| Interceptor Under V_{cruise} Conditions at AI Radar Detection - Increased Thrust at Detection | 7 |
| PHASE II-SYSTEM CAPABILITIES FOR SNAP-UP ATTACK UNDER IDEAL CONDITIONS | 7 |
| PHASE III-F4H-1/F8U-3 WEAPON CONTROL SYSTEMS PERFORMANCE UNDER EXPECTED TACTICAL CONDITIONS | 7 |
| ACKNOWLEDGEMENTS | 8 |

CONFIDENTIAL

~~CONFIDENTIAL~~

INTRODUCTION

An investigation is reported of

The Bureau of Aeronautics has contracted with Westinghouse, Air Arm Division, for analytical services to be used in a study to establish the tactical use capability of the F4H-1 and F8U-3 Weapon Systems. This study is conducted under the technical direction of the Naval Research Laboratory with all inputs derived from Navy sources. Westinghouse, using these inputs, will submit analytical results to the Navy. Recommendations and conclusions to be drawn from analytical results are assumed to be a Navy responsibility and in particular the responsibility of the technical directors (NRL). This report is the seventh in a series directed toward carrying out this responsibility.

In Volumes I and III of this series, the effective attack zones for perfectly vectored, co-altitude attacks were presented. Selected samples of plots of parameter variations during the various fire control runs were presented. This volume is a continuation of the parameter plots for these co-altitude attacks. All of the runs presented are for the system employing the current A1 radar (AN/APQ-50 or XN-2, AN/APQ-72). These runs originate at the 85% probability of detection point for this radar (12-13 naut mi head-on against B-47 size target). A later volume will present the results for runs made with a system utilizing the improved radar (AN/APQ-72).

The study results, as presented to date, have been separated into study phases (see Volumes I and III). Table I is a summation of these study phases. This same format will be followed in presenting the material of this volume. Table II gives an index of figures contained in this volume. Starting with Fig. III it is seen that the remaining figures are grouped consistent with the format given on Table I. Each of the major categories are indicated by tabs along the edge of the report.

DEFINITION OF PARAMETERS

Since this volume is restricted to those phases of the study which are related to perfectly vectored co-altitude attacks, the parameters which are investigated are those associated with target and interceptor motion during this type of engagement. The parameters, for which graphs showing the variation during the co-altitude attacks are given in this volume, are defined as follows:

CONFIDENTIAL

- R = Range between interceptor and target position
- T = Time elapsed from AI radar detection (t_0)
- λ_a = Azimuth gimbal angle. This is the angle between the radar gimbal mechanical axis (RGMA) and the line of sight (LOS) in the plane of the azimuth gimbal
- λ_e = Elevation gimbal angle. This is the angle between the radar gimbal mechanical axis (RGMA) and the line of sight (LOS) in the plane of the elevation gimbal
- $\dot{\lambda}_a$ = Rate of change of azimuth gimbal angle
- $\dot{\lambda}_e$ = Rate of change of elevation gimbal angle
- λ = Total lead angle (angle between line of sight to target and line of flight of the interceptor)
- τ = Target aspect angle (angle between the line of sight to the target and line of flight of the target)
- ψ = Angle between the space reference vector and the interceptor velocity vector
- ω_j = Angular rate of the line of sight in the elevation plane of the antenna
- L/W = Load factor
- ϕ = Roll angle
- V_F = Fighter velocity
- α = Fighter angle of attack. This is the angle between the path frame reference line (FRL) and the fighter flight path

CONFIDENTIAL

PHASE I-SYSTEM PERFORMANCE UNDER IDEAL CONDITIONS-HORIZONTAL ATTACKS

Following the format used in presenting study results to date, the first case for which parameter plots will be given is that of horizontal attacks under "ideal" conditions.

Figure I gives a pictorial representation of the perfectly vectored co-altitude attack. The target in the illustration is assumed to be non-maneuvering (cases for maneuvering targets will also be included later in this volume). The interceptor is assumed to start on a perfectly vectored lead pursuit course. On this sketch, λ (total gimbal angle), is the angle between the line of sight (LOS) fighter to target and the line of flight of the fighter. τ_0 is the angle between the target heading and the LOS target to fighter. τ_0 will be referred to in the remainder of this document as initial target aspect angle (aspect angle at AI radar detection). Figure II shows the courses flown, relative to the target, by the interceptor during a particular situation. Along these courses the interceptor heading is shown by vectors.

The conditions listed on Table I describe the speed and altitude cases of interest. Partial results for these cases are given in Volumes I and II of this series. This phase of this volume is intended as a continuation of these results.

Interceptor at V_{\max} at AI Radar Detection

In Volume I the effective attack zones and associated parameter plots for horizontal attacks against a nonmaneuvering target at 30,000 ft and 50,000 ft where $V_T/V_F = 1.0, 0.8$, and 0.45 (V_T = target velocity, V_F = fighter velocity = V_{\max}) were given and will not be repeated here. In Volume III the effective attack zones and associated parameter plots for horizontal attacks against a nonmaneuvering target at 1000 ft where $V_T/V_F = 0.8$ ($V_F = V_{\max}$) were given and also will not be repeated.

Figures III and IV are copies from Volume III of effective attack zones for the ideal horizontal attack conditions for engagements occurring at 1000 ft altitude for speed ratios of $V_T/V_F = 1.0$ and 0.45 . These are repeated here so that the reader can quickly correlate the parameter plots with the corresponding interceptor courses on the polar plots depicting the effective attack zones.

CONFIDENTIAL

The polar plot of Fig. III shows the effective attack zone for horizontal attacks occurring at 1000 ft altitude under ideal conditions. Detailed description of the polar plots for each condition studied has been given previously in Volumes I and III. However, a general description of this first polar plot (Fig. III) is repeated at this point to assist the reader in utilizing subsequent polar plots and associated parameter variation graphs.

For the situation which resulted in the effective attack zone shown on Fig. III the attack occurred at 1000 ft. The interceptor velocity is 1189 ft/sec and $V_T/V_F = 1.0$. The interceptor was assumed to be on a perfectly vectored lead pursuit course. The target is nonmaneuvering. Curve A gives the 85% probability of detection range for the current radar (AN/APQ-50 or XN-2, AN/APQ-72). Curve B gives the range at AI radar lock on time (estimated as 10 sec after detection throughout the study). The curve labeled C represents the Sparrow III maximum aerodynamic range (interlock equation) and the curve labeled D represents the Sparrow III minimum aerodynamic range (interlock equation). Curve E describes the constant load factor boundary for $N_z = 3$. The 90% cumulative probability of Sparrow III seeker lock-on range is given by Curve F. Sparrow III is currently further limited by a 6.5 naut mi interlock which is shown by Curve G. The effective attack zone is that bounded by the heavy curve. The trajectories for each interceptor course investigated are shown. These courses originated from $\tau = 0^\circ, 30^\circ, 60^\circ, 70.8^\circ, 90^\circ, 120^\circ$, and 150° . The interceptor is restricted to a 3g turn. Referring to the figure, it is seen that the usable approach courses are those between 30° and approximately 70° off the target's nose. The numbers on each of the trajectories represent the time elapsed from t_0 (AI radar detection).

Referring to Table II (index of figures) it is seen that the parameter plots have been grouped under the basic polar plot for the target and interceptor conditions of interest. For example, Figs. III-1 thru III-14b give the parameter variations for each of the interceptor trajectories given on the polar plot of Fig. III. (Trajectory for $\tau_0 = 0^\circ$ not given.)

With the preceding background information, it is now of interest to investigate the actual parameter plots. A complete description of the first family is in order as an assist to the reader in using the remaining graphs. Throughout this report the first parameter plot of each

CONFIDENTIAL

family will show the resulting variation in range versus time. This is presented not only to show variation in range, but in order that a ready transformation of the data on the subsequent graphs can be made (some of the parameters are plotted versus time, others versus range). In addition, on the range versus time plot, the following points are labeled:

O = R_{max}

■ = R_{min}

X = Impact for missile launch at R_{min}

□ = $L/W = 3$

These labeled points can then be transferred readily to the other parameter plots in the associated family.

As far as possible two graphs have been included on one sheet and thus under one figure number. For example, Fig. III-1 consists of two graphs which give the resulting range variation as a function of time for the interceptor trajectories of Fig. III. The top graph gives the range variation for trajectories starting at $\tau_0 = 30^\circ, 60^\circ, 70.8^\circ, 120^\circ$, and 150° . The lower graph gives the range variation for the case of $\tau_0 = 90^\circ$. Referring to the parameter plots, it is seen that for $\tau_0 = 30^\circ$, R_{max} is reached at 5.0 seconds after detection (range = 23,500 ft). R_{min} is reached at 12.2 seconds after detection (range = 8800 ft). The point of impact (arbitrarily chosen for a missile launched at R_{min}) is seen to occur at 15.0 seconds after detection. In following the required lead pursuit course the interceptor encountered $L/W = 3$ conditions at 13.5 seconds after detection (range = 6000 ft). For the case of $\tau_0 = 60^\circ$, R_{max} occurred at 18 seconds after detection. However, R_{min} was never reached, thus this point and the corresponding impact point is not plotted. In following the required lead pursuit course the interceptor never encountered $L/W = 3$. Referring to the curves for $\tau_0 = 70.8^\circ, 90^\circ, 120^\circ$, and 150° , it is seen that none of the points described previously are labeled. For these conditions, R_{max} was never reached. Reference to Fig. III will indicate graphically the same factors brought out above.

CONFIDENTIAL

Figure III-2 gives curves showing the variation in azimuth gimbal angle (λ_a) as a function of range. Referring to the curve for $\tau_0 = 30^\circ$, it is seen that the azimuth gimbal angle varies from -5° at the range for missile impact to approximately -15° . For the case of $\tau_0 = 60^\circ$ the variation is from -9° to -25° during the run.

The curves of Fig. III-3 give the resulting variation in elevation gimbal angle (λ_e) as a function of range. For the case of $\tau_0 = 30^\circ$, the elevation gimbal angle varies from -4° at the start of the run to -26° at the range for missile impact. It is interesting to note that in flying a lead pursuit trajectory much of the gimbal angle requirement is translated into the elevation axis because of the roll of the interceptor.

Figures III-4a thru III-4c give the rate of change of azimuth gimbal angle ($\dot{\lambda}_a$) as a function of range. For $\tau_0 = 30^\circ$, $\dot{\lambda}_a$ varies from 0 deg/sec to approximately 1.9 deg/sec. Figures III-5a and III-5b give the rate of change of elevation gimbal angle ($\dot{\lambda}_e$) as a function of range. For $\tau_0 = 30^\circ$, $\dot{\lambda}_e$ varies from -0.5 deg/sec to -5 deg/sec.

The curves of Fig. III-6 give the total lead angle (λ) as a function of range. These curves show the combined effects of Figs. III-3 and III-4. Figure III-7 gives the target aspect angle (τ) as a function of range for the corresponding trajectories of Fig. III. The heading angle (ψ) as a function of range is shown on Fig. III-8.

Figure III-9 gives the azimuth antenna rate (ω_k) versus range. For the case of $\tau_0 = 30^\circ$, ω_k varies from 0.4 deg/sec to 1.2 deg/sec. The elevation antenna rate (ω_j) versus range is shown on Fig. III-10a and Fig. III-10b. Again referring to the curve for $\tau_0 = 30^\circ$, it is seen that ω_j varies from 0 deg/sec at the start of the run to 6 deg/sec at the range for missile impact.

Load factor (L/W) versus range is given by Fig. III-11. The curves of this figure illustrate the "g" build-up as the attack progresses. As was stated previously, one of the barriers in the overlays depicting the effective attack zones is the locus of points described by $L/W = 3$.

Figure III-12 gives the variation in roll angle (ϕ) versus range. As can be seen from these plots, for the perfect situation (1000 ft altitude attacks), roll angles of 70° and higher can be expected. Figure III-13 gives plots of interceptor velocity (V_F) as a function of time.

CONFIDENTIAL

These curves illustrate the slowdown of the interceptor while on the approach course. The curves of Fig. III-14a and Fig. III-14b show the angle of attack (α) as a function of time. For the case of $\tau_0 = 30$, α at the beginning of the run is approximately 1° and at 10 seconds after detection starts building up rapidly.

Figure IV gives the co-altitude lead pursuit attack zone overlay for attacks occurring at 1000 ft altitude where the speed ratio (V_T/V_F) is 0.45 and the interceptor starts the engagement at V_{max} . The corresponding parameter plots are given on Figures IV-1 thru IV-14.

Interceptor Under V_{cruise} Conditions at AI Radar Detection-Increased Thrust at Detection

In Volume III, the co-altitude lead pursuit attack zone overlays for conditions where the interceptor starts the attack (AI radar detection) under V_{cruise} conditions and increased thrust is then applied were given. These overlays are repeated here by Figs. V, VI, VII, VIII, and IX. The corresponding parameter plots for the interceptor trajectories are grouped following each of the related attack zone overlays. For example, Fig. V gives the attack zone overlay for attacks occurring at 50,000 ft altitude. The target velocity is 1940 ft/sec. The interceptor starts the attack at V_{cruise} (873 ft/sec). Maximum thrust is applied. The corresponding parameter plots are given by Figs. V-1 thru V-14.

PHASE II-SYSTEM CAPABILITIES FOR SNAP-UP ATTACK UNDER IDEAL CONDITIONS

The results of this phase of study are detailed in Volumes I and III. The related parameter plots are given in Volume VIII.

PHASE III-F4H-1/F8U-3 WEAPON CONTROL SYSTEMS PERFORMANCE UNDER EXPECTED TACTICAL CONDITIONS

In Volume III of this series, the results of the investigation of the effects of target maneuver on the tactical use capability of Sparrow III were detailed. For this phase of the study, the target maneuver was assumed to start at AI radar detection and consisted of a lg lateral turn which crisscrossed the desired flight. The maximum deviation of target heading from this path is 30° . The polar plots showing the effective attack zone for the co-altitude, perfectly vectored situation are repeated here as Figs. X and XI. The attack altitude was 30,000 ft and $V_T/V_F = 0.8$ where $V_F = 1897$ ft/sec. Figure X gives the results for a target maneuver initially to the right. Figure XI gives the results for a target maneuver initially to the left. The corresponding parameter variations are given by Figs. X-1a thru X-14c and Figs. XI-1 thru XI-14c.

CONFIDENTIAL

ACKNOWLEDGEMENTS

The data presented in this report represents a continuation of the results of the Navy's Air-to-Air Missile Study Program. The analytical results, including those from which the figures were derived, are the results of the computation work underway at Westinghouse Air Arm Division. The authors would like to thank the Analytical Section of this division for their major contribution to this report. In addition, the authors would like to thank Laurence F. Gilchrist of the Equipment Research Branch, Naval Research Laboratory for his assistance in the preparation of this report.

TABLE I

OUTLINE OF NAVY AIR-TO-AIR MISSILE SYSTEM STUDY PROGRAM

PHASE I System Performance Under Ideal Conditions

A. Aircraft Characteristics

1. F4H-1
2. F8U-3

B. Altitudes (co-altitude case)

1. 1000 feet or less
2. 30,000 feet
3. 50,000 feet

C. Interceptor Velocity

1. F4H-1 at altitude (V_{max} & V_{cruise})
2. F8U-3 at altitude (V_{max} & V_{cruise})

D. Target to interceptor speed ratio for interceptor at V_{max}

1. 0.45
 2. 0.8
 3. 1.0
- } Some cases may be trivial and will not be used

Target speed resulting from above will be used for interceptor at V_{cruise}

E. Conditions

1. Perfect vectoring
2. Straight line flight path
3. Current AI detection capability
4. B-47 size target
5. Preparation time - two cases determined by study
6. Sparrow III - capability of current seeker is to be used
7. Sparrow III - aerodynamic capability of current missile is to be used
8. Gimbal angle limits in F4H-1 and F8U-3 aircraft
 - a. APQ-72
 - b. Seeker

9. Illumination consideration - Geometry of keeping both target and missile illuminated. Illumination requirements to be determined by study.

PHASE II System Snap-up Performance Under Ideal Conditions

- A. A, C, D, and E - same as Phase I
- B. Altitudes (snap-up case)
 1. Target
 - a. 30,000 feet
 - b. 50,000 feet
 - c. 65,000 feet
 2. Interceptor Altitude - To be determined by study of system capability.

PHASE III System Performance Under Expected Tactical Conditions

- A. Target maneuver
- B. Vectoring accuracy
- C. Weather
- D. Limits imposed by interceptor tactics
 1. Climb capability
 2. Endurance
 3. Dead time
- E. Countermeasures
 1. Airborne weapons system

PHASE IV System Performance Under Expected Tactical Conditions With Addition of Currently Proposed Improvements

- A. Improvements proposed:
 1. Search volume optimization

CONFIDENTIAL

TABLE II
INDEX OF FIGURES

FIGURE I LEAD PURSUIT PROFILE

FIGURE II LEAD PURSUIT TRAJECTORIES

FIGURE III CO-ALTITUDE LEAD PURSUIT ATTACK ZONE OVERLAY

$V_T = 1189$ ft/sec $V_P = 1189$ ft/sec Altitude, 1000 ft
(Initial Target Aspect Angle $\tau_0 = 30^\circ, 60^\circ, 70.8^\circ, 90^\circ, 120^\circ, 150^\circ$)

| | |
|--------------|--|
| Fig. III-1 | Range vs Time |
| Fig. III-2 | Azimuth Gimbal Angle vs Range |
| Fig. III-3 | Elevation Gimbal Angle vs Range |
| Fig. III-4a | Rate of Change of the Azimuth Gimbal Angle vs Range ($\tau_0 = 30^\circ, 60^\circ$) |
| Fig. III-4b | Rate of Change of the Azimuth Gimbal Angle vs Range ($\tau_0 = 70.8^\circ, 90^\circ$) |
| Fig. III-4c | Rate of Change of the Azimuth Gimbal Angle vs Range ($\tau_0 = 120^\circ$) |
| Fig. III-5a | Rate of Change of the Elevation Gimbal Angle vs Range ($\tau_0 = 30^\circ, 60^\circ, 70.8^\circ$) |
| Fig. III-5b | Rate of Change of the Elevation Gimbal Angle vs Range ($\tau_0 = 90^\circ, 120^\circ$) |
| Fig. III-6 | Total Lead Angle vs Range |
| Fig. III-7 | Target Aspect Angle vs Range |
| Fig. III-8 | Heading Angle vs Range |
| Fig. III-9 | Azimuth Antenna Rate vs Range |
| Fig. III-10a | Elevation Antenna Rate vs Range ($\tau_0 = 30^\circ, 60^\circ$) |

CONFIDENTIAL

- Fig. III-10b Elevation Antenna Rate vs Range ($\tau_0 = 70.8^\circ, 90^\circ, 120^\circ, 150^\circ$)
- Fig. III-11 Load Factor vs Range
- Fig. III-12 Roll Angle vs Range
- Fig. III-13 Fighter Speed vs Time
- Fig. III-14a Angle of Attack vs Time ($\tau_0 = 30^\circ, 60^\circ, 70.8^\circ, 120^\circ, 150^\circ$)
- Fig. III-14b Angle of Attack vs Time ($\tau_0 = 90^\circ$)

FIGURE IV CO-ALTITUDE LEAD PURSUIT ATTACK ZONE OVERLAY

$V_T = 533$ ft/sec $V_F = 1189$ ft/sec Altitude = 1000 ft
(Initial Target Aspect Angle $\tau_0 = 30^\circ, 60^\circ, 90^\circ, 120^\circ, 150^\circ$)

- Fig. IV-1 Range vs Time
- Fig. IV-2 Azimuth Gimbal Angle vs Range
- Fig. IV-3 Elevation Gimbal Angle vs Range
- Fig. IV-4a Rate of Change of the Azimuth Gimbal Angle vs Range
($\tau_0 = 30^\circ, 60^\circ$)
- Fig. IV-4b Rate of Change of the Azimuth Gimbal Angle vs Range
($\tau_0 = 90^\circ, 120^\circ$)
- Fig. IV-4c Rate of Change of the Azimuth Gimbal Angle vs Range
($\tau_0 = 150^\circ$)
- Fig. IV-5a Rate of Change of the Elevation Gimbal Angle vs Range
($\tau_0 = 30^\circ, 60^\circ, 90^\circ$)
- Fig. IV-5b Rate of Change of the Elevation Gimbal Angle vs Range
($\tau_0 = 120^\circ, 150^\circ$)
- Fig. IV-6 Total Load Angle vs Range
- Fig. IV-7 Target Aspect Angle vs Range

CONFIDENTIAL

| | |
|-------------|---|
| Fig. IV-8 | Heading Angle vs Range |
| Fig. IV-9a | Azimuth Antenna Rate vs Range ($\tau_0 = 30^\circ, 60^\circ, 90^\circ$) |
| Fig. IV-9b | Azimuth Antenna Rate vs Range ($\tau_0 = 120^\circ, 150^\circ$) |
| Fig. IV-10a | Elevation Antenna Rate vs Range ($\tau_0 = 30^\circ, 60^\circ$) |
| Fig. IV-10b | Elevation Antenna Rate vs Range ($\tau_0 = 90^\circ, 120^\circ$) |
| Fig. IV-10c | Elevation Antenna Rate vs Range ($\tau_0 = 150^\circ$) |
| Fig. IV-11a | Load Factor vs Range ($\tau_0 = 30^\circ, 60^\circ$) |
| Fig. IV-11b | Load Factor vs Range ($\tau_0 = 90^\circ, 120^\circ$) |
| Fig. IV-11c | Load Factor vs Range ($\tau_0 = 150^\circ$) |
| Fig. IV-12 | Roll Angle vs Range |
| Fig. IV-13 | Fighter Speed vs Time |
| Fig. IV-14 | Angle of Attack vs Time |

FIGURE V CO-ALTITUDE LEAD PURSUIT ATTACK ZONE OVERLAY
 $V_T = 1940$ ft/sec $V_p = 873$ (Veruise-Increased Thrust at
Detection) Altitude = 50,000 ft
(Initial Target Aspect Angle $\tau_0 = 30^\circ, 60^\circ$)

| | |
|----------|---|
| Fig. V-1 | Range vs Time |
| Fig. V-2 | Azimuth Gimbal Angle vs Range |
| Fig. V-3 | Elevation Gimbal Angle vs Range |
| Fig. V-4 | Rate of Change of the Azimuth Gimbal Angle vs Range |
| Fig. V-5 | Rate of Change of the Elevation Gimbal Angle vs Range |
| Fig. V-6 | Total Lead Angle vs Range |

CONFIDENTIAL

- Fig. V-7 Target Aspect Angle vs Range
- Fig. V-8 Heading Angle vs Range
- Fig. V-9 Azimuth Antenna Rate vs Range
- Fig. V-10 Elevation Antenna Rate vs Range
- Fig. V-11 Load Factor vs Range
- Fig. V-12 Roll Angle vs Range
- Fig. V-13 Fighter Speed vs Time
- Fig. V-14 Angle of Attack vs Time

FIGURE VI CO-ALTITUDE LEAD PURSUIT ATTACK ZONE OVERLAY
 $V_T = 1552$ ft/sec $V_F = 873$ ft/sec (V_{cruise} -Increased Thrust at Detection) Altitude = 50,000 ft)
(Initial Target Aspect Angle $\tau_0 = 30^\circ, 60^\circ, 90^\circ$)

- Fig. VI-1a Range vs Time ($\tau_0 = 30^\circ, 60^\circ$)
- Fig. VI-1b Range vs Time ($\tau_0 = 90^\circ$)
- Fig. VI-2 Azimuth Gimbal Angle vs Range
- Fig. VI-3 Elevation Gimbal Angle vs Range
- Fig. VI-4a Rate of Change of the Azimuth Gimbal Angle vs Range
 ($\tau_0 = 30^\circ, 60^\circ$)
- Fig. VI-4b Rate of Change of the Azimuth Gimbal Angle vs Range
 ($\tau_0 = 90^\circ$)
- Fig. VI-5a Rate of Change of the Elevation Gimbal Angle vs Range
 ($\tau_0 = 30^\circ, 60^\circ$)
- Fig. VI-5b Rate of Change of the Elevation Gimbal Angle vs Range
 ($\tau_0 = 90^\circ$)

CONFIDENTIAL

- Fig. VI-6 Total Lead Angle vs Range
Fig. VI-7 Target Aspect Angle vs Range
Fig. VI-8 Heading Angle vs Range
Fig. VI-9 Azimuth Antenna Rate vs Range
Fig. VI-10 Elevation Antenna Rate vs Range
Fig. VI-11 Load Factor vs Range
Fig. VI-12 Roll Angle vs Range
Fig. VI-13a Fighter Speed vs Time ($\tau_0 = 30^\circ, 60^\circ$)
Fig. VI-13b Fighter Speed vs Time ($\tau_0 = 90^\circ$)
Fig. VI-14 Angle of Attack vs Time

FIGURE VII CO-ALTITUDE LEAD PURSUIT ATTACK ZONE OVERLAY
 $V_T = 873$ ft/sec $V_F = 873$ ft/sec ($V_{\text{cruise-Increased}}$
Thrust at Detection) Altitude = 50,000 ft
(Initial Target Aspect Angle $\tau_0 = 30^\circ, 60^\circ, 90^\circ, 120^\circ, 150^\circ$)

- Fig. VII-1 Range vs Time
Fig. VII-2a Azimuth Gimbal Angle vs Range ($\tau_0 = 30^\circ, 60^\circ, 90^\circ$)
Fig. VII-2b Azimuth Gimbal Angle vs Range ($\tau_0 = 120^\circ, 150^\circ$)
Fig. VII-3 Elevation Gimbal Angle vs Range
Fig. VII-4a Rate of Change of the Azimuth Gimbal Angle vs Range
($\tau_0 = 30^\circ, 60^\circ$)
Fig. VII-4b Rate of Change of the Azimuth Gimbal Angle vs Range
($\tau_0 = 90^\circ, 120^\circ$)
Fig. VII-4c Rate of Change of the Azimuth Gimbal Angle vs Range
($\tau_0 = 150^\circ$)

CONFIDENTIAL

Fig. VII-5a Rate of Change of the Elevation Gimbal Angle vs Range
 ($\tau_0 = 30^\circ, 60^\circ$)

Fig. VII-5b Rate of Change of the Elevation Gimbal Angle vs Range
 ($\tau_0 = 90^\circ, 120^\circ, 150^\circ$)

Fig. VII-6 Total Lead Angle vs Range

Fig. VII-7 Target Aspect Angle vs Range

Fig. VII-8 Heading Angle vs Range

Fig. VII-9a Azimuth Antenna Rate vs Range ($\tau_0 = 30^\circ, 60^\circ$)

Fig. VII-9b Azimuth Antenna Rate vs Range ($\tau_0 = 90^\circ, 120^\circ, 150^\circ$)

Fig. VII-10a Elevation Antenna Rate vs Range ($\tau_0 = 30^\circ, 60^\circ$)

Fig. VII-10b Elevation Antenna Rate vs Range ($\tau_0 = 90^\circ, 120^\circ$)

Fig. VII-10c Elevation Antenna Rate vs Range ($\tau_0 = 150^\circ$)

Fig. VII-11a Load Factor vs Range ($\tau_0 = 30^\circ, 60^\circ, 90^\circ, 120^\circ$)

Fig. VII-11b Load Factor vs Range ($\tau_0 = 150^\circ$)

Fig. VII-12 Roll Angle vs Range

Fig. VII-13a Fighter Speed vs Time ($\tau_0 = 30^\circ, 60^\circ, 90^\circ$)

Fig. VII-13b Fighter Speed vs Time ($\tau_0 = 120^\circ, 150^\circ$)

Fig. VII-14a Angle of Attack vs Time ($\tau_0 = 30^\circ, 60^\circ, 90^\circ$)

Fig. VII-14b Angle of Attack vs Time ($\tau_0 = 120^\circ, 150^\circ$)

CONFIDENTIAL

FIGURE VIII CO-ALTITUDE LEAD PURSUIT ATTACK ZONE OVERLAY

$V_T = 1897$ ft/sec $V_F = 894$ ft/sec ($V_{\text{cruise-Increased}}$
Thrust at Detection) Altitude = 30,000 ft
(Initial Target Aspect Angle $\tau_0 = 30^\circ$)

- Fig. VIII-1 Range vs Time
- Fig. VIII-2 Azimuth Gimbal Angle vs Range
- Fig. VIII-3 Elevation Gimbal Angle vs Range
- Fig. VIII-4 Rate of Change of the Azimuth Gimbal Angle vs Range
- Fig. VIII-5 Rate of Change of the Elevation Gimbal Angle vs Range
- Fig. VIII-6 Total Lead Angle vs Range
- Fig. VIII-7 Target Aspect Angle vs Range
- Fig. VIII-8 Heading Angle vs Range
- Fig. VIII-9 Azimuth Antenna Rate vs Range
- Fig. VIII-10 Elevation Antenna Rate vs Range
- Fig. VIII-11 Load Factor vs Range
- Fig. VIII-12 Roll Angle vs Range
- Fig. VIII-13 Fighter Speed vs Time
- Fig. VIII-14 Angle of Attack vs Time

FIGURE IX CO-ALTITUDE LEAD PURSUIT ATTACK ZONE OVERLAY

$V_T = 1518$ ft/sec $V_F = 894$ ft/sec ($V_{\text{cruise-Increased}}$
Thrust at Detection) Altitude = 30,000 ft
(Initial Target Aspect Angle $\tau_0 = 30^\circ, 60^\circ, 90^\circ$)

- Fig. IX-1a Range vs Time ($\tau_0 = 30^\circ, 60^\circ$)
- Fig. IX-1b Range vs Time ($\tau_0 = 90^\circ$)

CONFIDENTIAL

Fig. IX-2 Azimuth Gimbal Angle vs Range

Fig. IX-3 Elevation Gimbal Angle vs Range

Fig. IX-4a Rate of Change of the Azimuth Gimbal Angle vs Range
($\tau_0 = 30^\circ, 60^\circ$)

Fig. IX-4b Rate of Change of the Azimuth Gimbal Angle vs Range
($\tau_0 = 90^\circ$)

Fig. IX-5a Rate of Change of the Elevation Gimbal Angle vs Range
($\tau_0 = 30^\circ, 60^\circ$)

Fig. IX-5b Rate of Change of the Elevation Gimbal Angle vs Range
($\tau_0 = 90^\circ$)

Fig. IX-6 Total Lead Angle vs Range

Fig. IX-7 Target Aspect Angle vs Range

Fig. IX-8 Heading Angle vs Range

Fig. IX-9 Azimuth Antenna Rate vs Range

Fig. IX-10a Elevation Antenna Rate vs Range ($\tau_0 = 30^\circ, 60^\circ$)

Fig. IX-10b Elevation Antenna Rate vs Range ($\tau_0 = 90^\circ$)

Fig. IX-11a Load Factor vs Range ($\tau_0 = 30^\circ, 60^\circ$)

Fig. IX-11b Load Factor vs Range ($\tau_0 = 90^\circ$)

Fig. IX-12 Roll Angle vs Range

Fig. IX-13 Fighter Speed vs Time

Fig. IX-14a Angle of Attack vs Time ($\tau_0 = 30^\circ, 60^\circ$)

Fig. IX-14b Angle of Attack vs Time ($\tau_0 = 90^\circ$)

CONFIDENTIAL

FIGURE X CO-ALTITUDE LEAD PURSUIT ATTACK ZONE OVERLAYS

$V_T = 1518$ ft/sec $V_P = 1897$ ft/sec Altitude = 30,000 ft
Maneuvering Target - Initial Right Turn
(Initial Target Aspect Angle $\tau_0 = 30^\circ, 60^\circ, 90^\circ, 120^\circ, 150^\circ$)

- Fig. X-1a Range vs Time ($\tau_0 = 30^\circ, 60^\circ$)
- Fig. X-1b Range vs Time ($\tau_0 = 90^\circ, 120^\circ$)
- Fig. X-1c Range vs Time ($\tau_0 = 150^\circ$)
- Fig. X-2a Azimuth Gimbal Angle vs Range ($\tau_0 = 30^\circ, 60^\circ$)
- Fig. X-2b Azimuth Gimbal Angle vs Range ($\tau_0 = 90^\circ, 120^\circ$)
- Fig. X-2c Azimuth Gimbal Angle vs Range ($\tau_0 = 150^\circ$)
- Fig. X-3a Elevation Gimbal Angle vs Range ($\tau_0 = 30^\circ, 60^\circ$)
- Fig. X-3b Elevation Gimbal Angle vs Range ($\tau_0 = 90^\circ, 120^\circ$)
- Fig. X-3c Elevation Gimbal Angle vs Range ($\tau_0 = 150^\circ$)
- Fig. X-4a Rate of Change of the Azimuth Gimbal Angle vs Range ($\tau_0 = 30^\circ, 60^\circ$)
- Fig. X-4b Rate of Change of the Azimuth Gimbal Angle vs Range ($\tau_0 = 90^\circ, 120^\circ$)
- Fig. X-4c Rate of Change of the Azimuth Gimbal Angle vs Range ($\tau_0 = 150^\circ$)
- Fig. X-5a Rate of Change of the Elevation Gimbal Angle vs Range ($\tau_0 = 30^\circ, 60^\circ$)
- Fig. X-5b Rate of Change of the Elevation Gimbal Angle vs Range ($\tau_0 = 90^\circ, 120^\circ$)
- Fig. X-5c Rate of Change of the Elevation Gimbal Angle vs Range ($\tau_0 = 150^\circ$)

CONFIDENTIAL

Fig. X-6a Total Lead Angle vs Range ($\tau_0 = 30^\circ, 60^\circ$)
Fig. X-6b Total Lead Angle vs Range ($\tau_0 = 90^\circ, 120^\circ$)
Fig. X-6c Total Lead Angle vs Range ($\tau_0 = 150^\circ$)
Fig. X-7a Target Aspect Angle vs Range ($\tau_0 = 30^\circ, 60^\circ$)
Fig. X-7b Target Aspect Angle vs Range ($\tau_0 = 90^\circ, 120^\circ$)
Fig. X-7c Target Aspect Angle vs Range ($\tau_0 = 150^\circ$)
Fig. X-8a Heading Angle vs Range ($\tau_0 = 30^\circ, 60^\circ$)
Fig. X-8b Heading Angle vs Range ($\tau_0 = 90^\circ, 120^\circ$)
Fig. X-8c Heading Angle vs Range ($\tau_0 = 150^\circ$)
Fig. X-9a Azimuth Antenna Rate vs Range ($\tau_0 = 30^\circ, 60^\circ$)
Fig. X-9b Azimuth Antenna Rate vs Range ($\tau_0 = 90^\circ, 120^\circ$)
Fig. X-9c Azimuth Antenna Rate vs Range ($\tau_0 = 150^\circ$)
Fig. X-10a Elevation Antenna Rate vs Range ($\tau_0 = 30^\circ, 60^\circ$)
Fig. X-10b Elevation Antenna Rate vs Range ($\tau_0 = 90^\circ, 120^\circ$)
Fig. X-10c Elevation Antenna Rate vs Range ($\tau_0 = 150^\circ$)
Fig. X-11a Load Factor vs Range ($\tau_0 = 30^\circ, 60^\circ$)
Fig. X-11b Load Factor vs Range ($\tau_0 = 90^\circ, 120^\circ$)
Fig. X-11c Load Factor vs Range ($\tau_0 = 150^\circ$)
Fig. X-12a Roll Angle vs Range ($\tau_0 = 30^\circ, 60^\circ$)
Fig. X-12b Roll Angle vs Range ($\tau_0 = 90^\circ, 120^\circ$)
Fig. X-12c Roll Angle vs Range ($\tau_0 = 150^\circ$)

CONFIDENTIAL

- Fig. X-13a Fighter Speed vs Time ($\tau_0 = 30^\circ, 60^\circ, 90^\circ$)
Fig. X-13b Fighter Speed vs Time ($\tau_0 = 120^\circ, 150^\circ$)
Fig. X-14a Angle of Attack vs Time ($\tau_0 = 30^\circ, 60^\circ$)
Fig. X-14b Angle of Attack vs Time ($\tau_0 = 90^\circ, 120^\circ$)
Fig. X-14c Angle of Attack vs Time ($\tau_0 = 150^\circ$)

FIGURE XI CO-ALTITUDE LEAD PURSUIT ATTACK ZONE OVERLAYS
 $V_T = 1518$ ft/sec $V_F = 1897$ ft/sec Altitude = 30,000 ft
Maneuvering Target - Initial Left Turn
(Initial Target Aspect Angle $\tau_0 = 0^\circ, 30^\circ, 60^\circ, 90^\circ, 120^\circ, 150^\circ$)

- Fig. XI-1 Range vs Time
Fig. XI-2a Azimuth Gimbal Angle vs Range ($\tau_0 = 0^\circ, 30^\circ$)
Fig. XI-2b Azimuth Gimbal Angle vs Range ($\tau_0 = 60^\circ, 90^\circ$)
Fig. XI-2c Azimuth Gimbal Angle vs Range ($\tau_0 = 120^\circ, 150^\circ$)
Fig. XI-3a Elevation Gimbal Angle vs Range ($\tau_0 = 0^\circ, 30^\circ, 60^\circ$)
Fig. XI-3b Elevation Gimbal Angle vs Range ($\tau_0 = 90^\circ, 120^\circ$)
Fig. XI-3c Elevation Gimbal Angle vs Range ($\tau_0 = 150^\circ$)
Fig. XI-4a Rate of Change of the Azimuth Gimbal Angle vs Range
($\tau_0 = 0^\circ, 30^\circ$)
Fig. XI-4b Rate of Change of the Azimuth Gimbal Angle vs Range
($\tau_0 = 60^\circ, 90^\circ$)
Fig. XI-4c Rate of Change of the Azimuth Gimbal Angle vs Range
($\tau_0 = 120^\circ, 150^\circ$)
Fig. XI-5a Rate of Change of the Elevation Gimbal Angle vs Range
($\tau_0 = 0^\circ, 30^\circ, 60^\circ$)

CONFIDENTIAL

Fig. XI-5b Rate of Change of the Elevation Gimbal Angle vs Range
 ($\tau_0 = 90^\circ, 120^\circ$)

Fig. XI-5c Rate of Change of the Elevation Gimbal Angle vs Range
 ($\tau_0 = 150^\circ$)

Fig. XI-6a Total Lead Angle vs Range ($\tau_0 = 0^\circ, 30^\circ$)

Fig. XI-6b Total Lead Angle vs Range ($\tau_0 = 60^\circ, 90^\circ$)

Fig. XI-6c Total Lead Angle vs Range ($\tau_0 = 120^\circ, 150^\circ$)

Fig. XI-7a Target Aspect Angle vs Range ($\tau_0 = 0^\circ, 30^\circ$)

Fig. XI-7b Target Aspect Angle vs Range ($\tau_0 = 60^\circ, 90^\circ$)

Fig. XI-7c Target Aspect Angle vs Range ($\tau_0 = 120^\circ, 150^\circ$)

Fig. XI-8a Heading Angle vs Range ($\tau_0 = 0^\circ, 30^\circ$)

Fig. XI-8b Heading Angle vs Range ($\tau_0 = 60^\circ, 90^\circ$)

Fig. XI-8c Heading Angle vs Range ($\tau_0 = 120^\circ, 150^\circ$)

Fig. XI-9a Azimuth Antenna Rate vs Range ($\tau_0 = 0^\circ, 30^\circ$)

Fig. XI-9b Azimuth Antenna Rate vs Range ($\tau_0 = 60^\circ, 90^\circ$)

Fig. XI-9c Azimuth Antenna Rate vs Range ($\tau_0 = 120^\circ, 150^\circ$)

Fig. XI-10a Elevation Antenna Rate vs Range ($\tau_0 = 0^\circ, 30^\circ$)

Fig. XI-10b Elevation Antenna Rate vs Range ($\tau_0 = 60^\circ, 90^\circ$)

Fig. XI-10c Elevation Antenna Rate vs Range ($\tau_0 = 120^\circ, 150^\circ$)

Fig. XI-11a Load Factor vs Range ($\tau_0 = 0^\circ, 30^\circ$)

Fig. XI-11b Load Factor vs Range ($\tau_0 = 60^\circ, 90^\circ$)

CONFIDENTIAL

Fig. XI-11c Load Factor vs Range ($\tau_0 = 120^\circ, 150^\circ$)
Fig. XI-12a Roll Angle vs Range ($\tau_0 = 0^\circ, 30^\circ$)
Fig. XI-12b Roll Angle vs Range ($\tau_0 = 60^\circ, 90^\circ$)
Fig. XI-12c Roll Angle vs Range ($\tau_0 = 120^\circ, 150^\circ$)
Fig. XI-13a Fighter Speed vs Time ($\tau_0 = 0^\circ, 30^\circ, 60^\circ$)
Fig. XI-13b Fighter Speed vs Time ($\tau_0 = 90^\circ, 120^\circ$)
Fig. XI-13c Fighter Speed vs Time ($\tau_0 = 150^\circ$)
Fig. XI-14a Angle of Attack vs Time ($\tau_0 = 0^\circ, 30^\circ, 60^\circ$)
Fig. XI-14b Angle of Attack vs Time ($\tau_0 = 90^\circ, 120^\circ$)
Fig. XI-14c Angle of Attack vs Time ($\tau_0 = 150^\circ$)

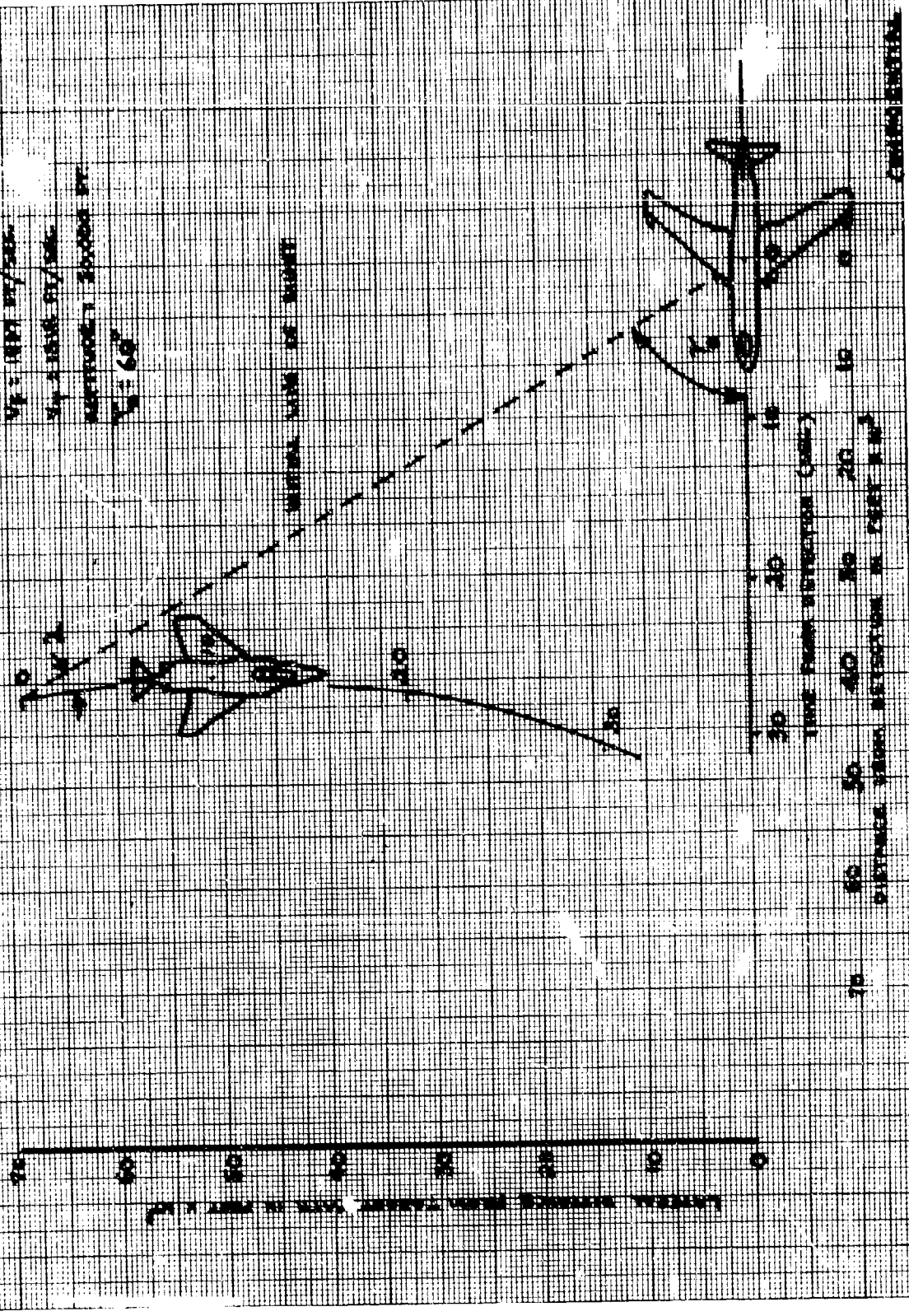
FIG. 1 - LEAD CORRECTION GRAPH

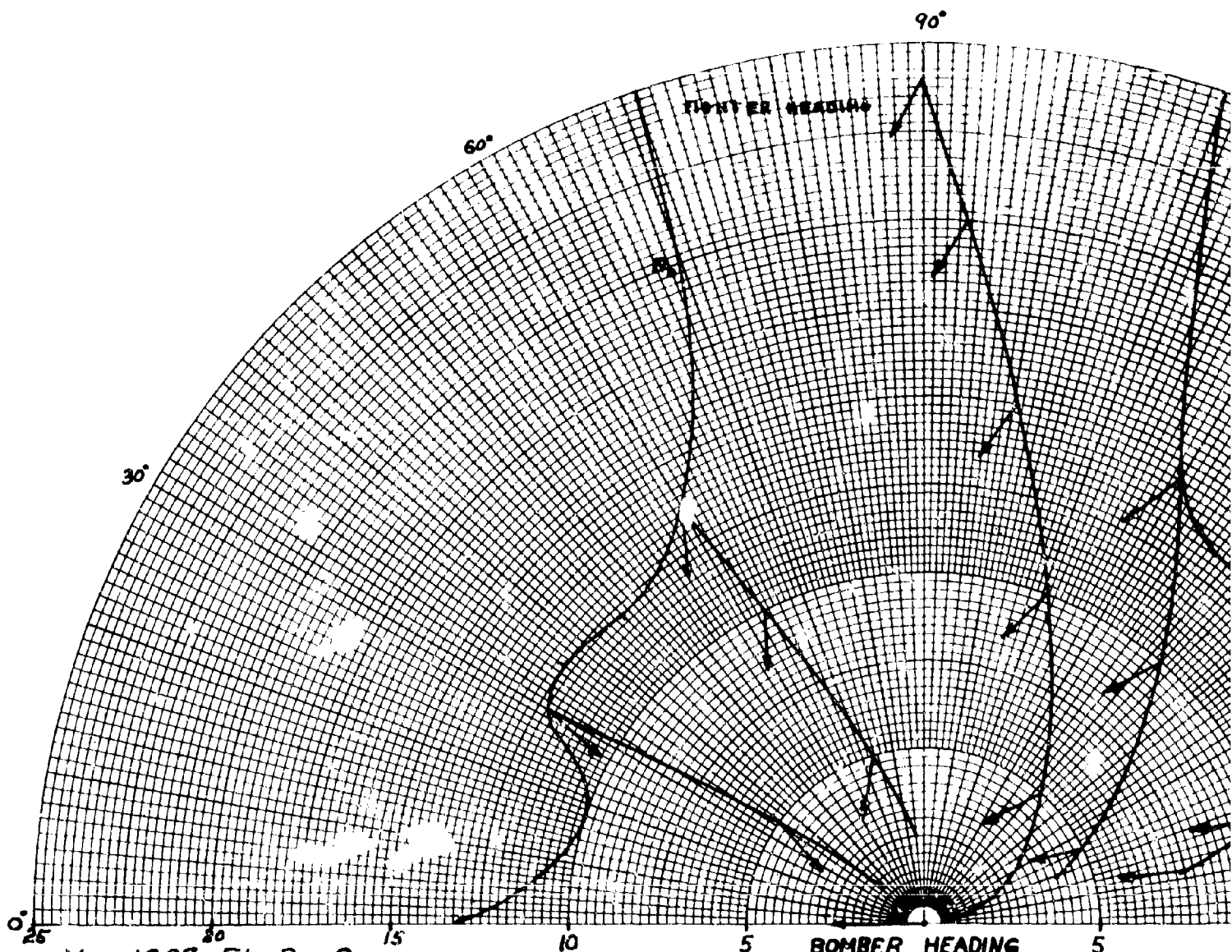
$V_p = 1800$ FT/SEC.

$V_t = 1500$ FT/SEC.

HEIGHT = 25,000 FT.

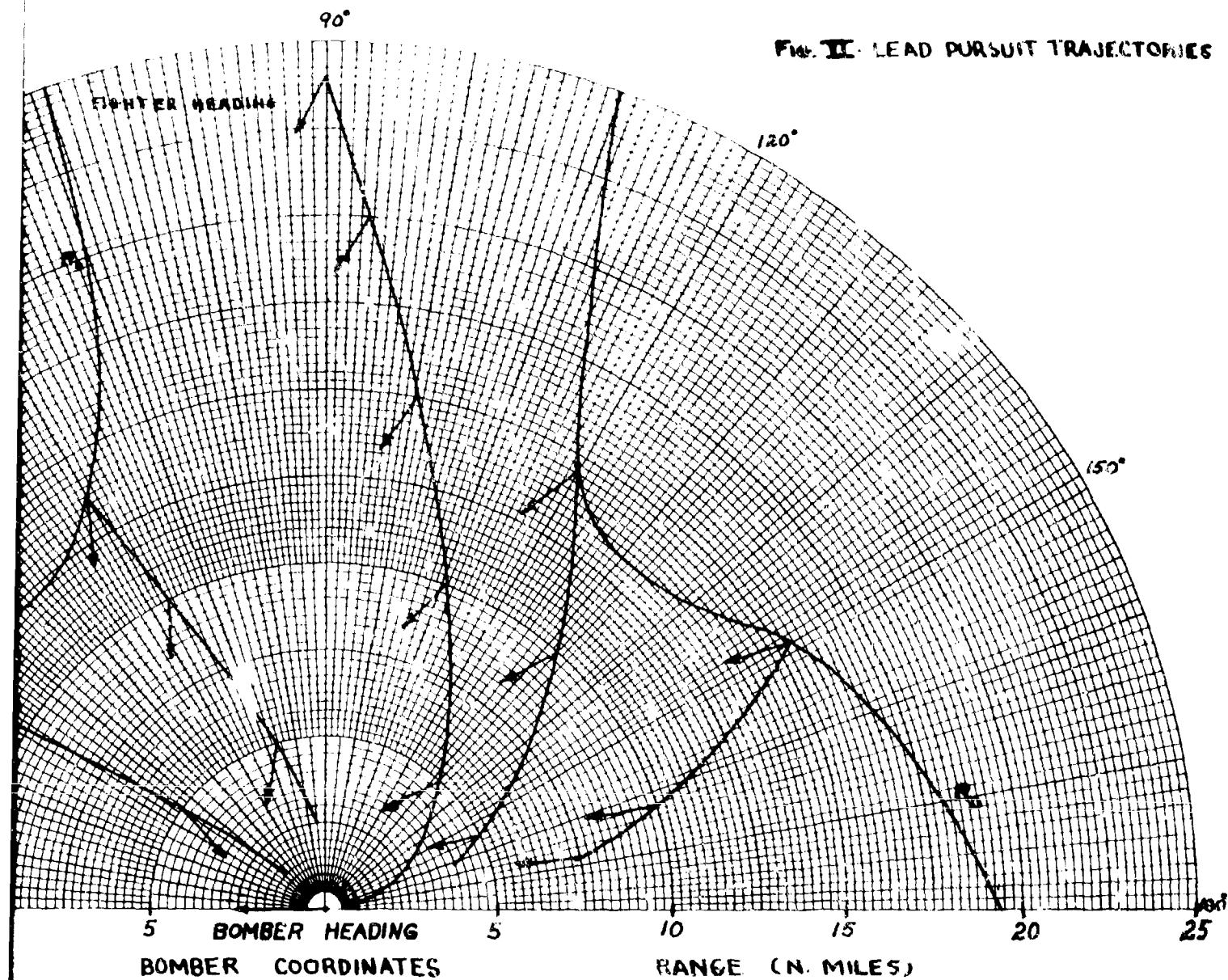
$\theta = 60^\circ$



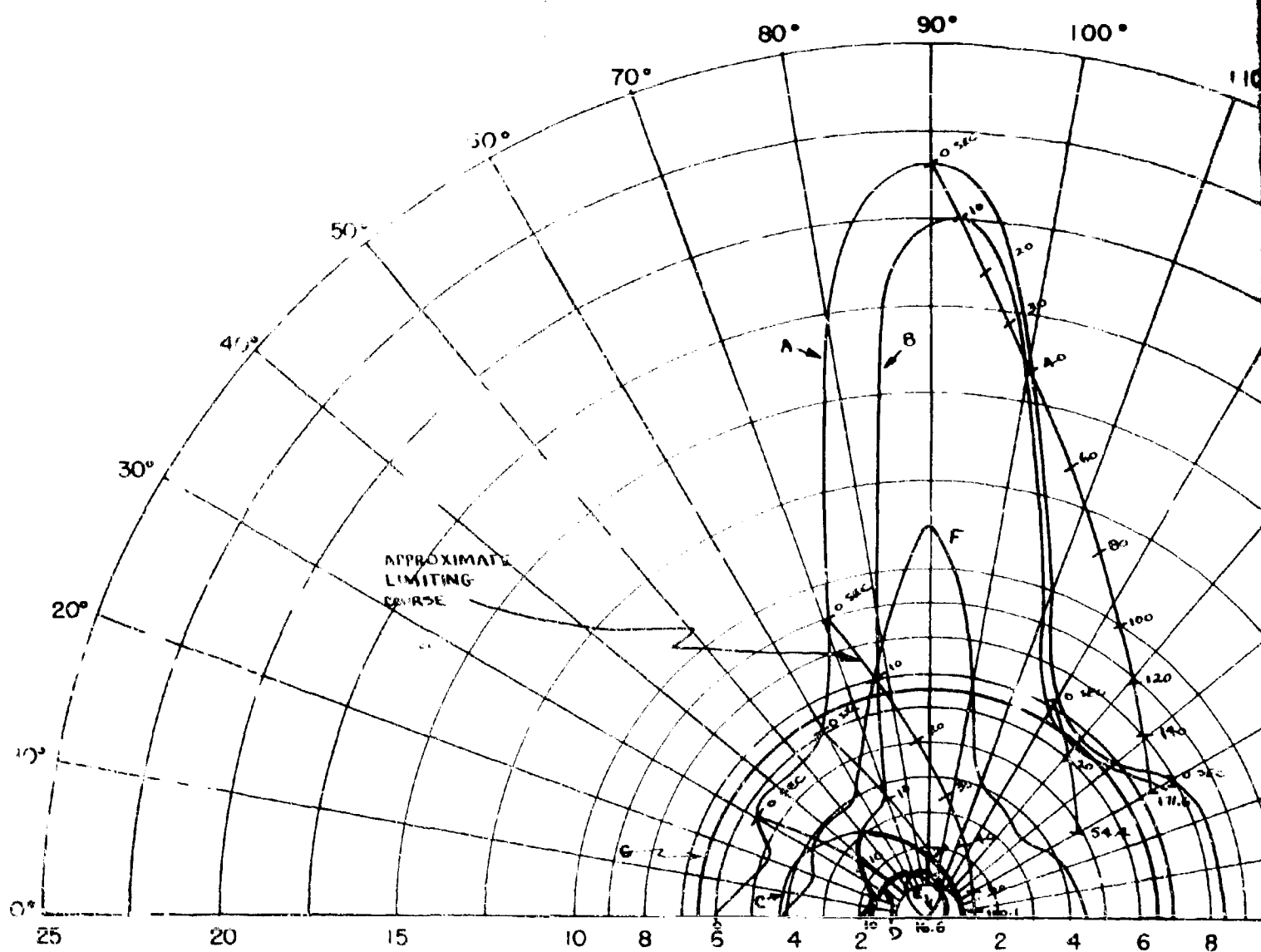


$V_r = 1897$ Ft. Per Sec.
 $V_r = 1518$ Ft. Per Sec.
 ALTITUDE = 30,000 Ft.
 → = FIGHTER HEADING

FIG. II. LEAD PURSUIT TRAJECTORIES



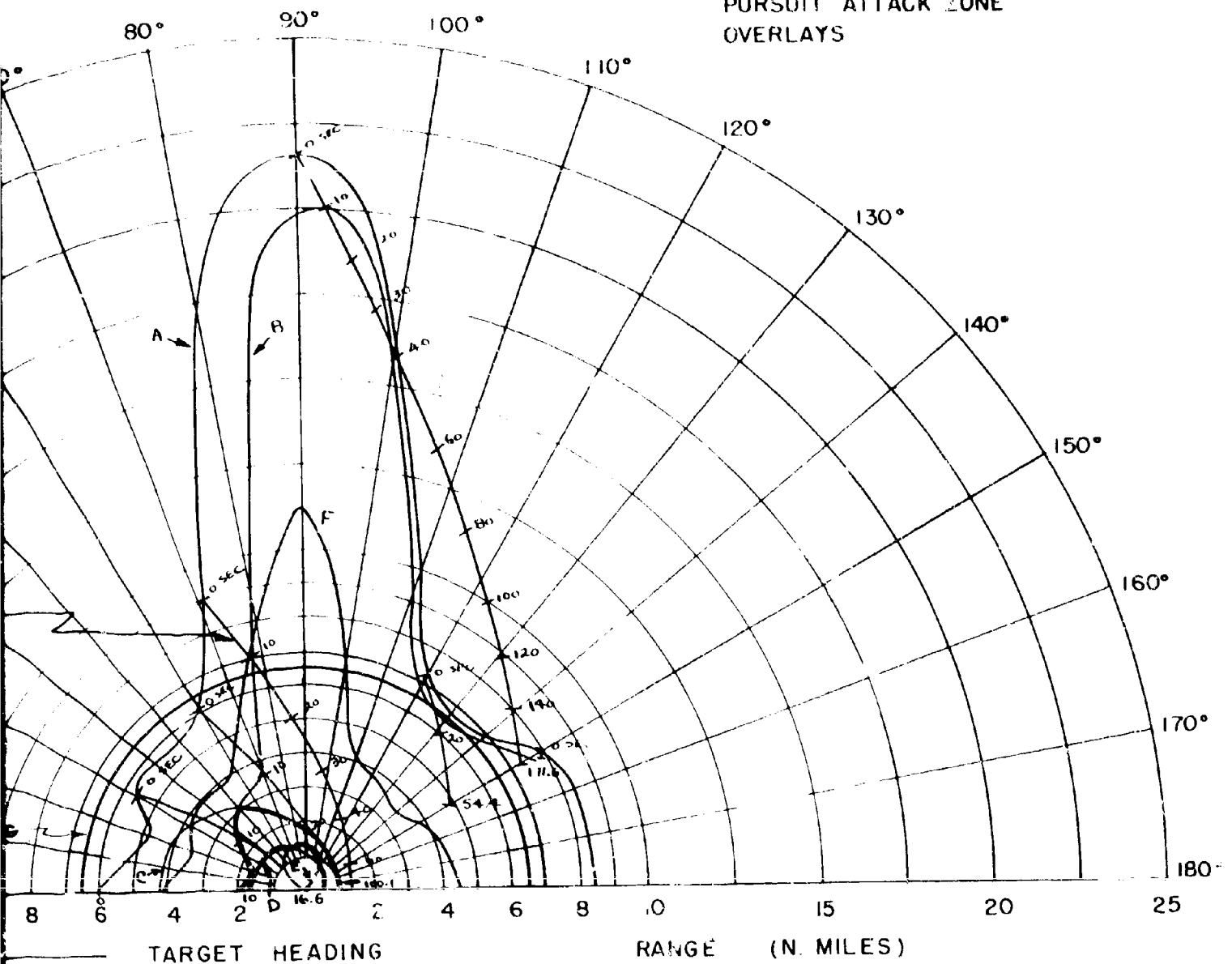
CONFIDENTIAL



$V_F = 1189$ FT/SEC (F4H-1)(F8U-3)
 $V_T = 1189$ FT/SEC
 ALTITUDE = 1000 FT.

- A - 85% DETECTION RANGE
- B - LOCK-ON RANGE (10 SEC. LOCK-ON TIME)
- C - SPARROW III MAX. AERODYNAMIC RANGE
- D - SPARROW III MIN. AERODYNAMIC RANGE
- E - CONSTANT LOAD FACTOR LOCUS ($N_Z = 3$)
- F - 90% SPARROW III SEEKER LOCK-ON RANGE
- G - 6.5 N.M. INTERLOCK

FIG. III - CO-ALTITUDE LEAD
PURSUIT ATTACK ZONE
OVERLAYS



85% DETECTION RANGE
LOCK-ON RANGE (10 SEC. LOCK-ON TIME)
SPARROW III MAX. AERODYNAMIC RANGE
SPARROW III MIN. AERODYNAMIC RANGE
CONSTANT LOAD FACTOR LOCUS ($N_z = 3$)
90% SPARROW III SEEKER LOCK-ON RANGE
6.5 N.M. INTERLOCK

CONFIDENTIAL

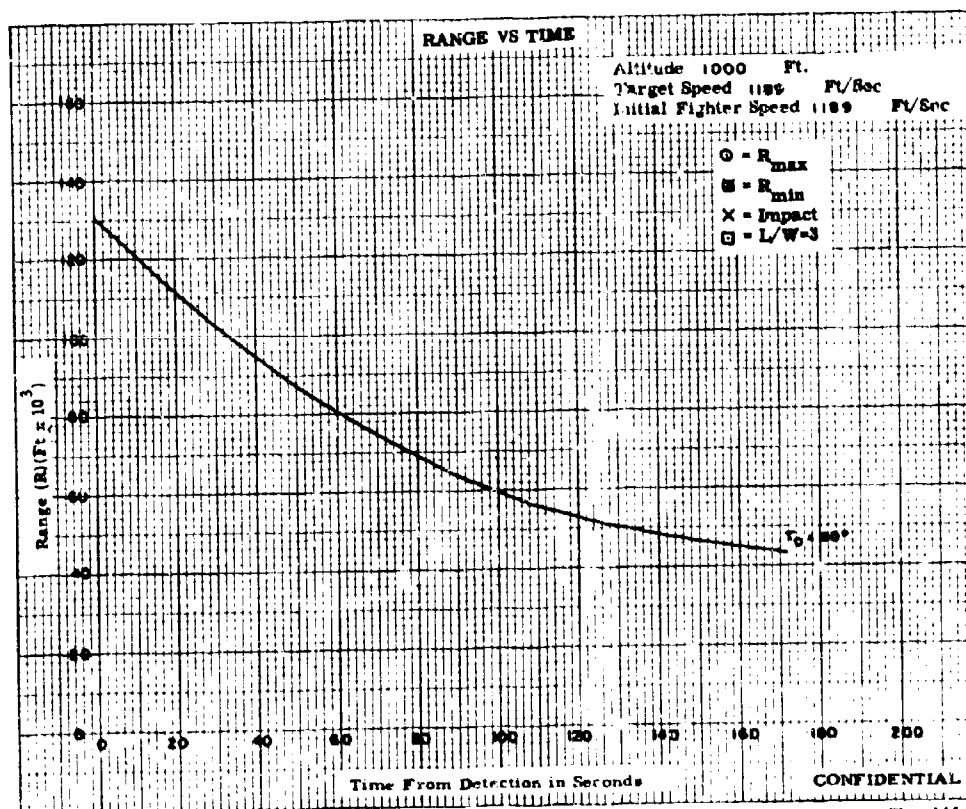
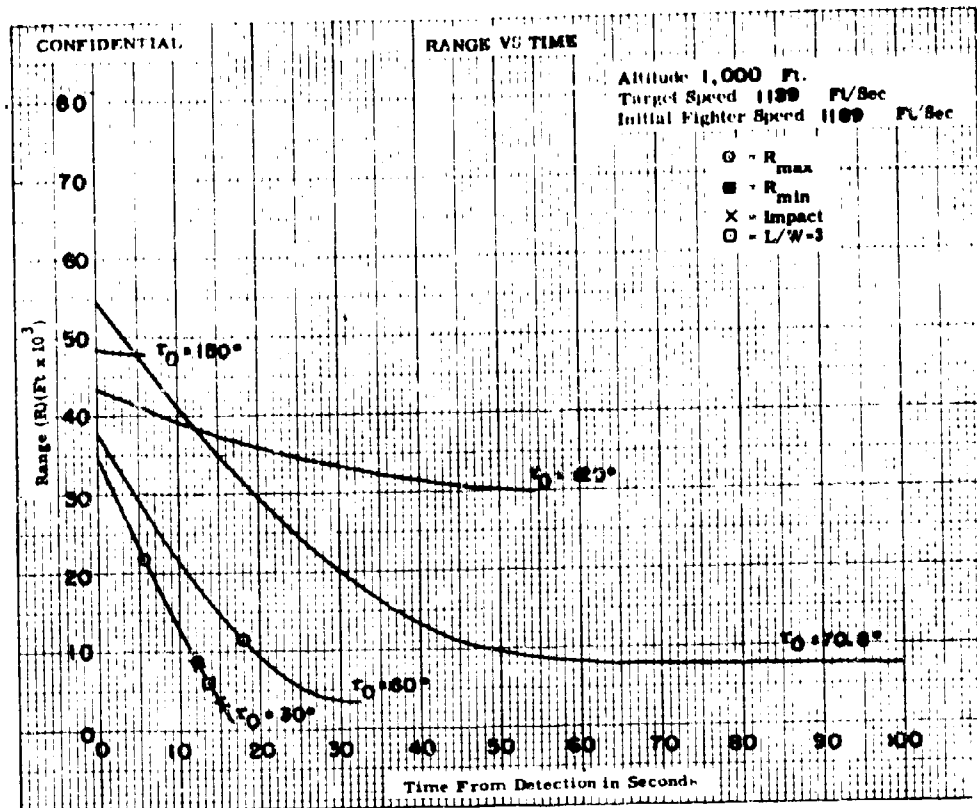


Fig. III-1

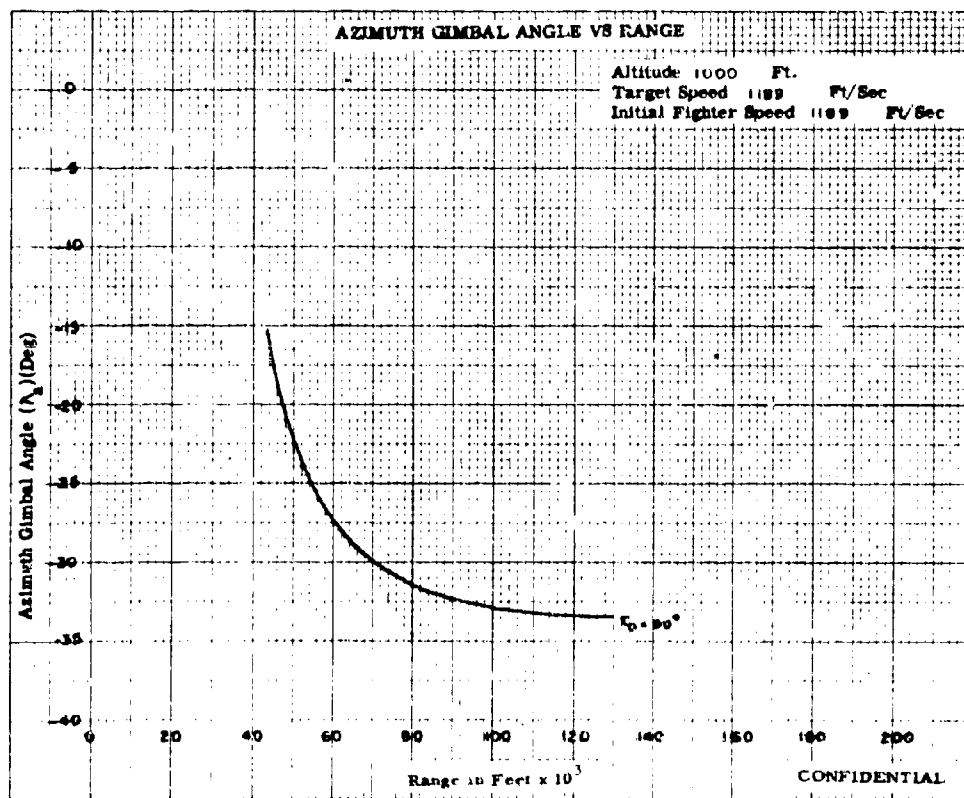
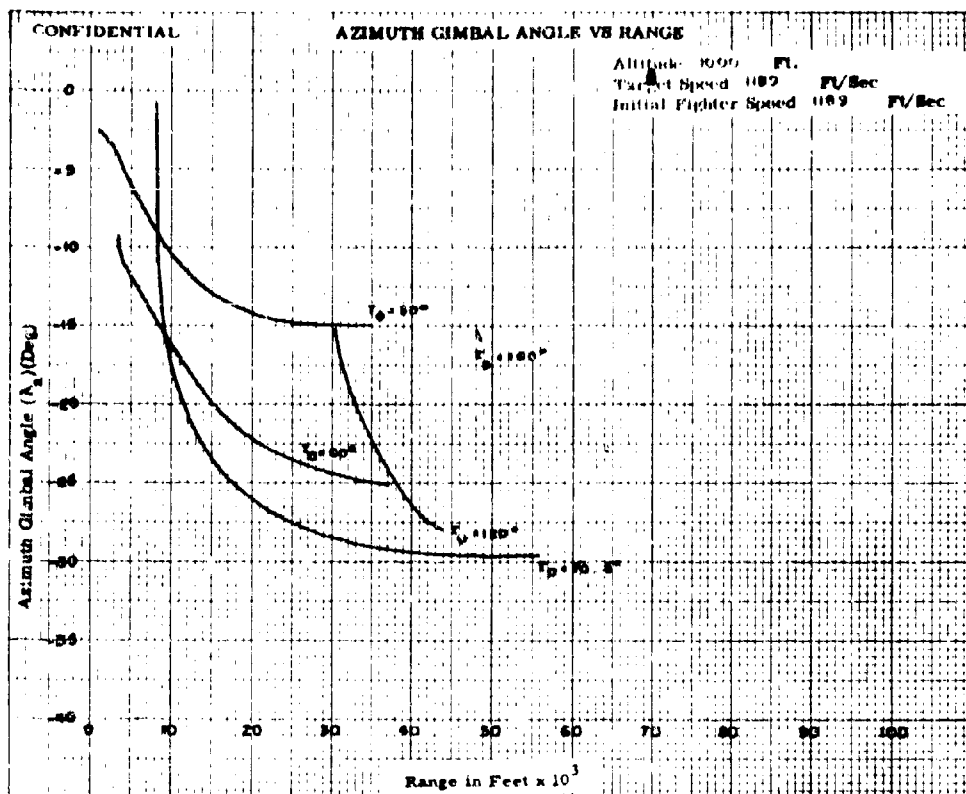


Fig. 111-2

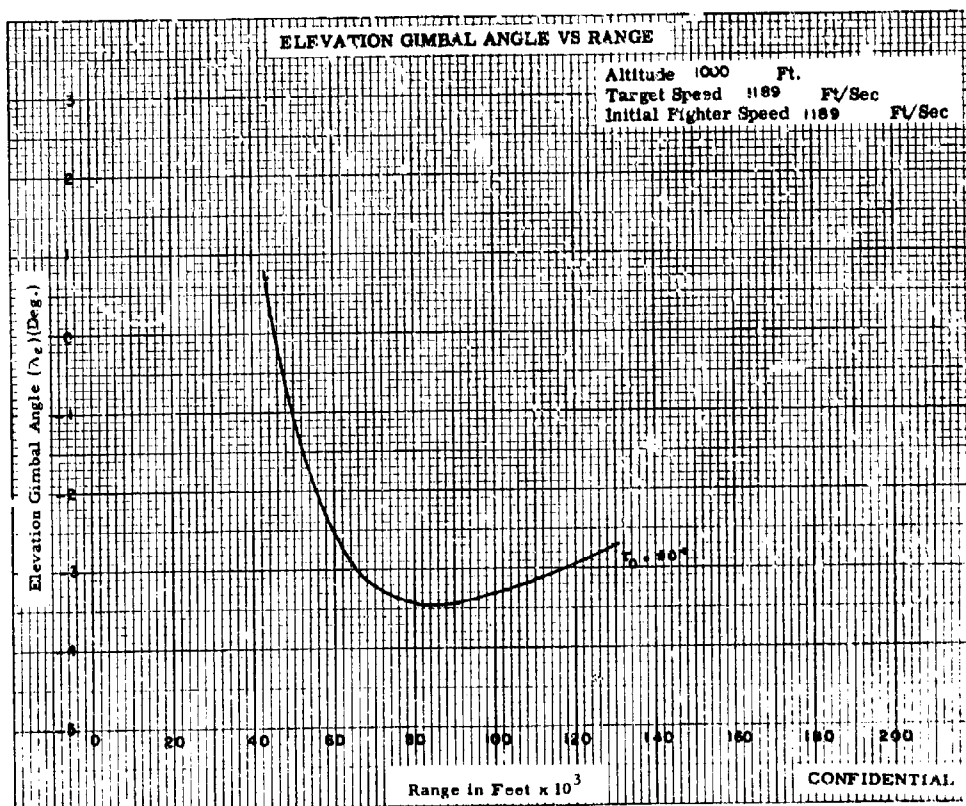
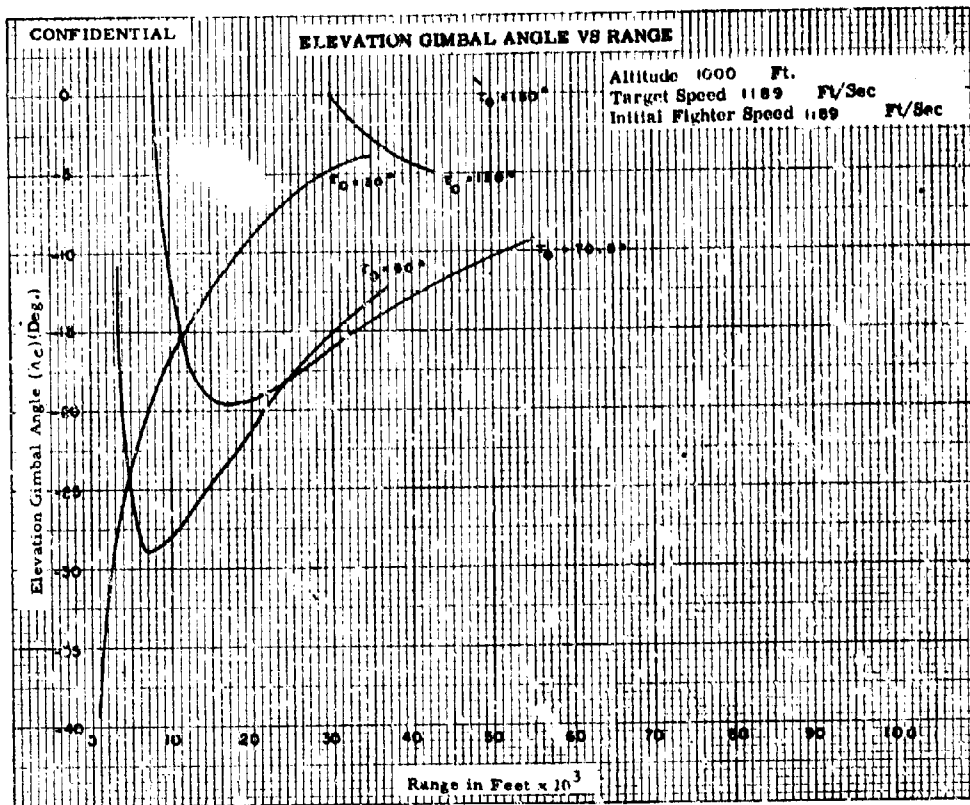


Fig. III-3

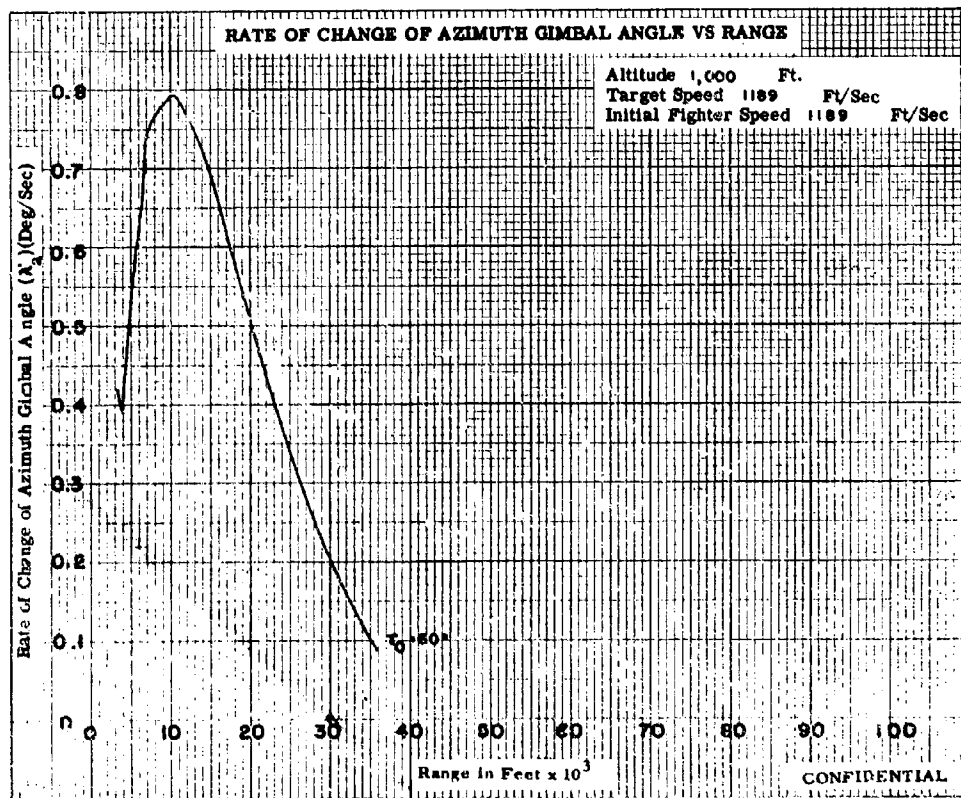
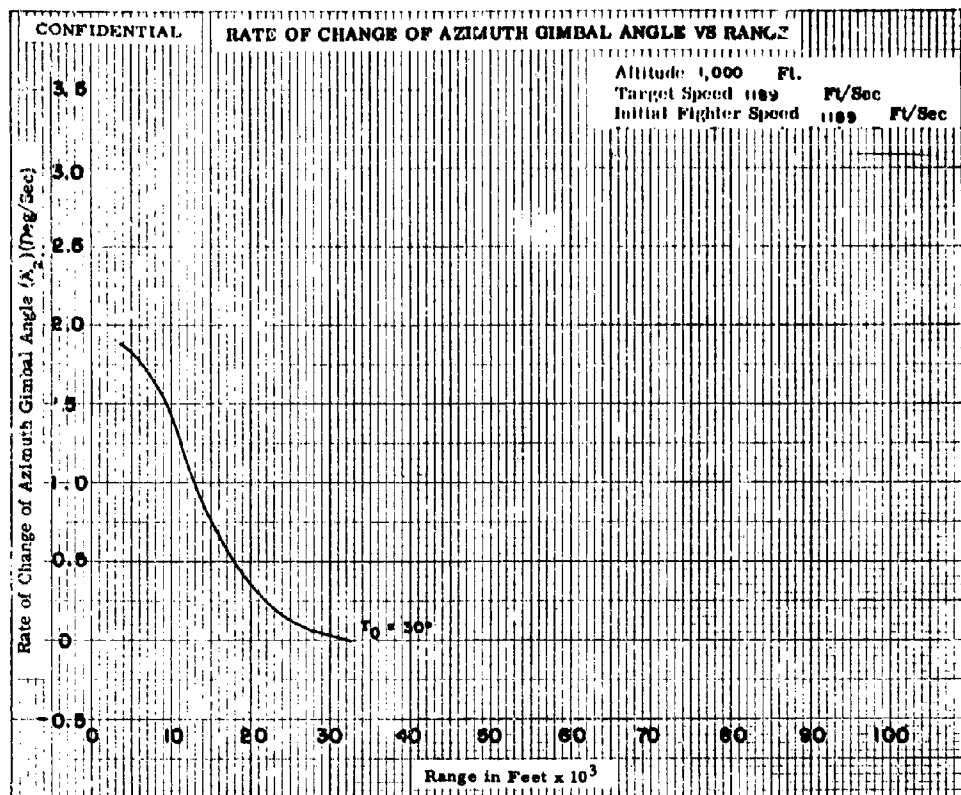


Fig. 111-4a

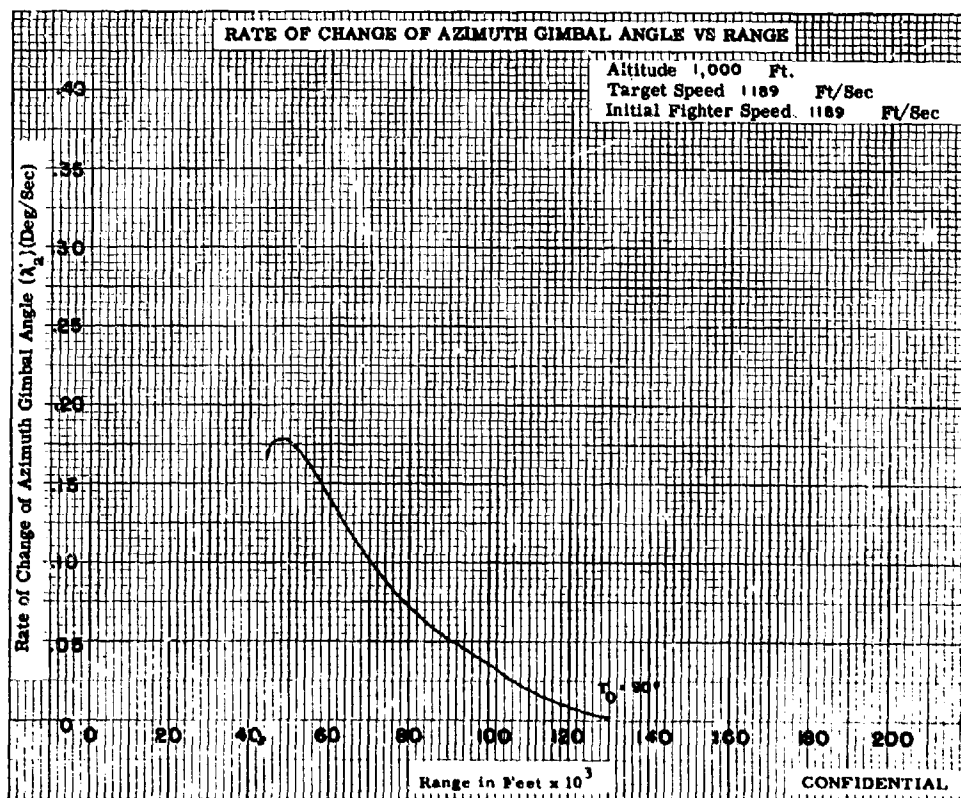
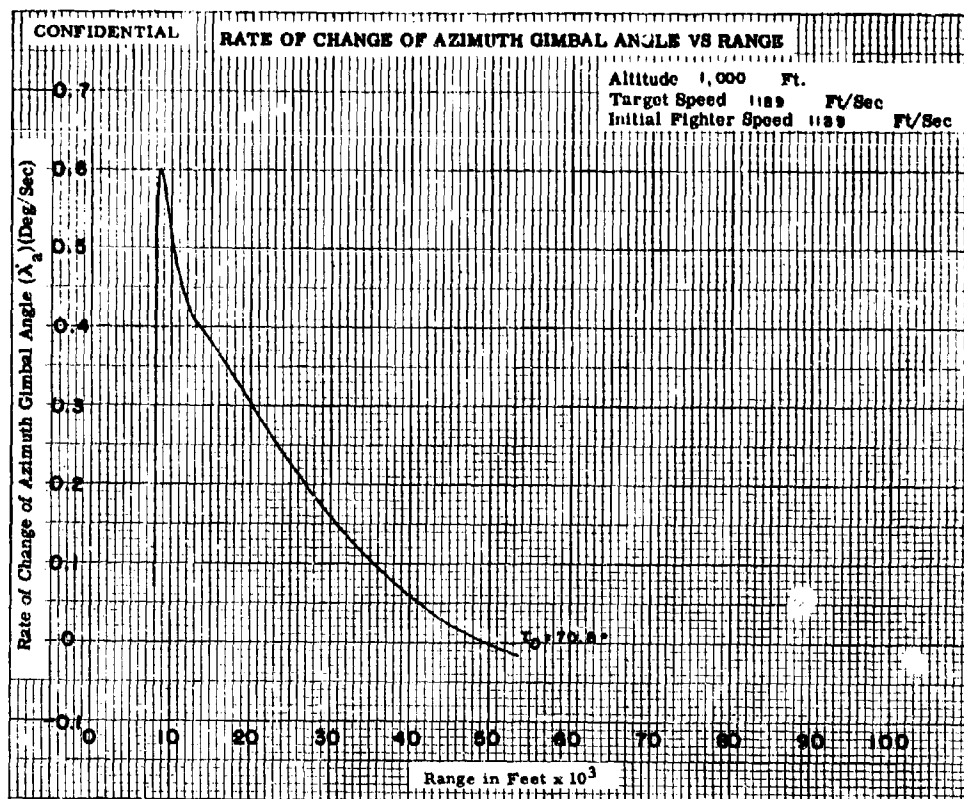


Fig. 111-40

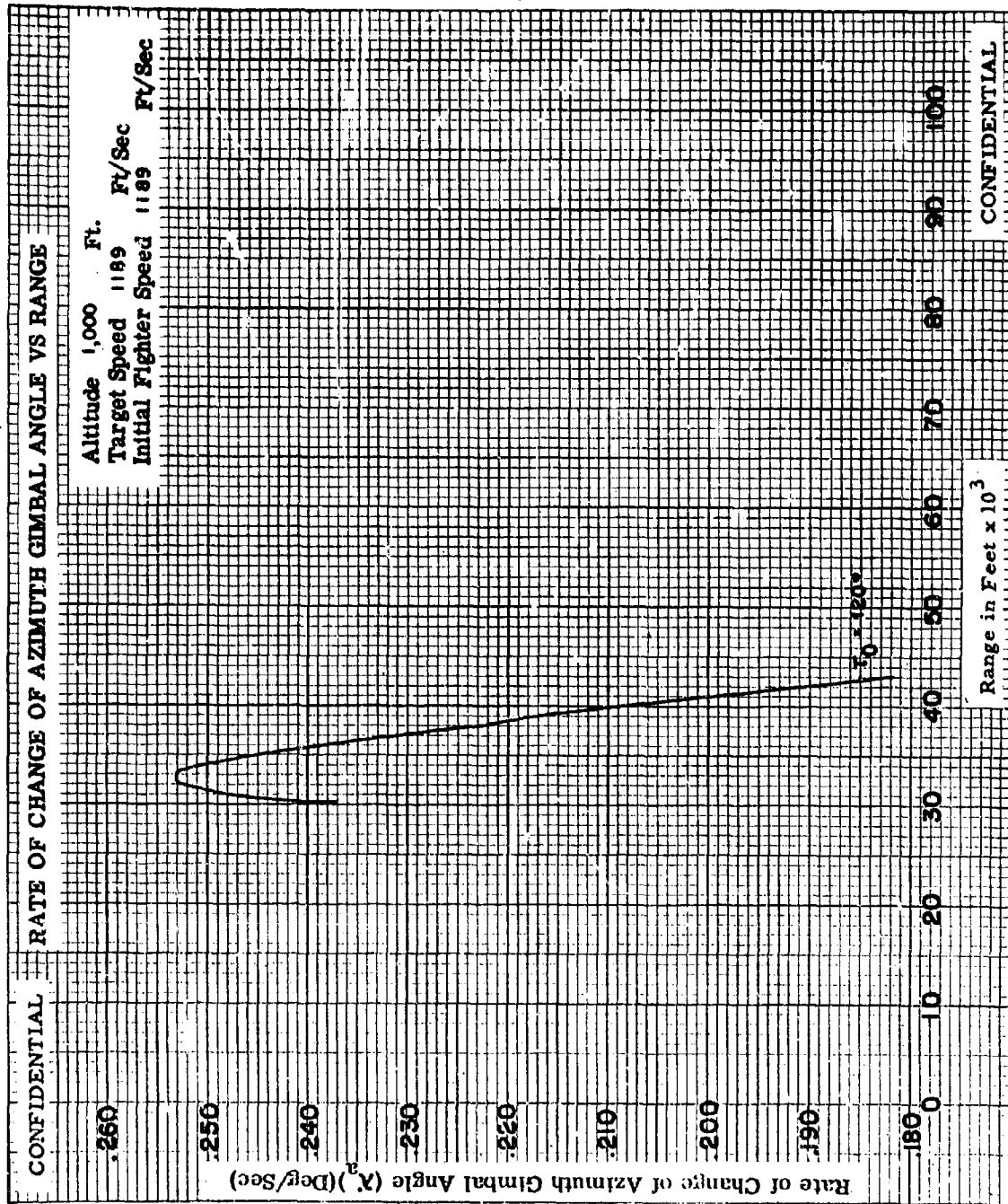


Fig. III-4c

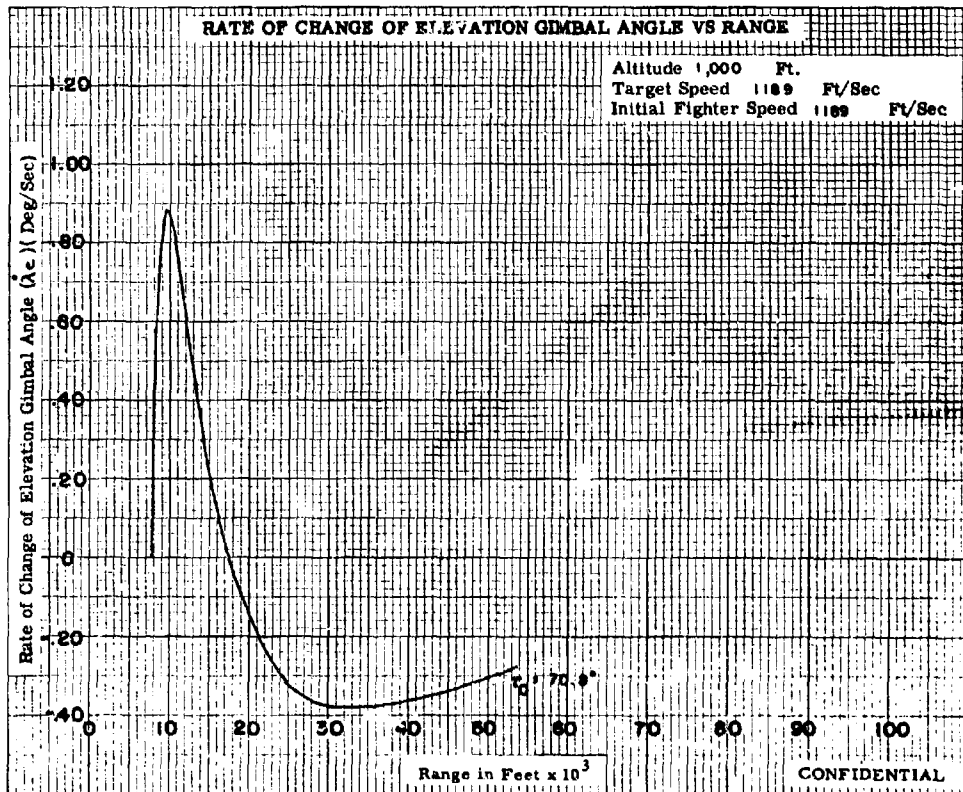
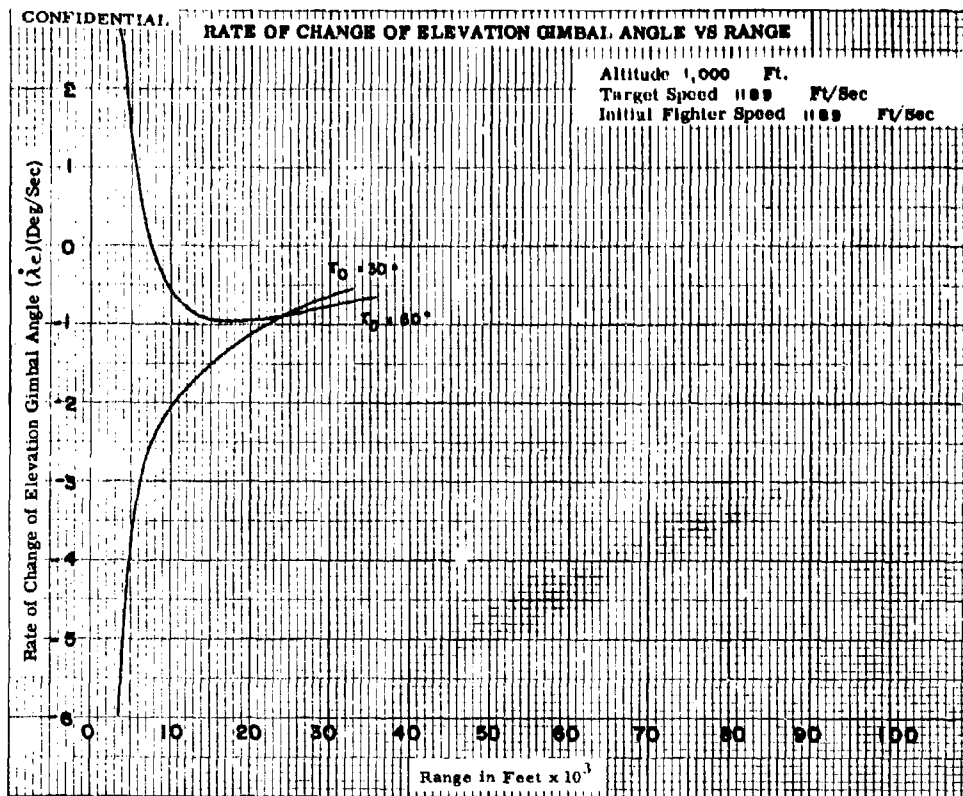


Fig. 111-5a

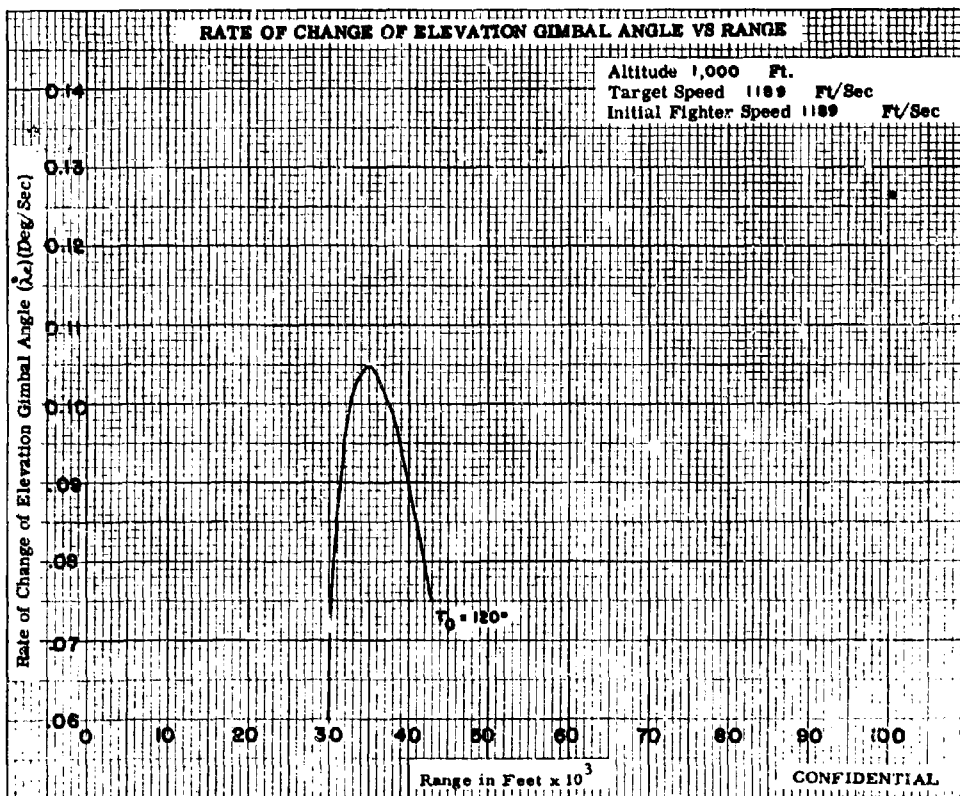
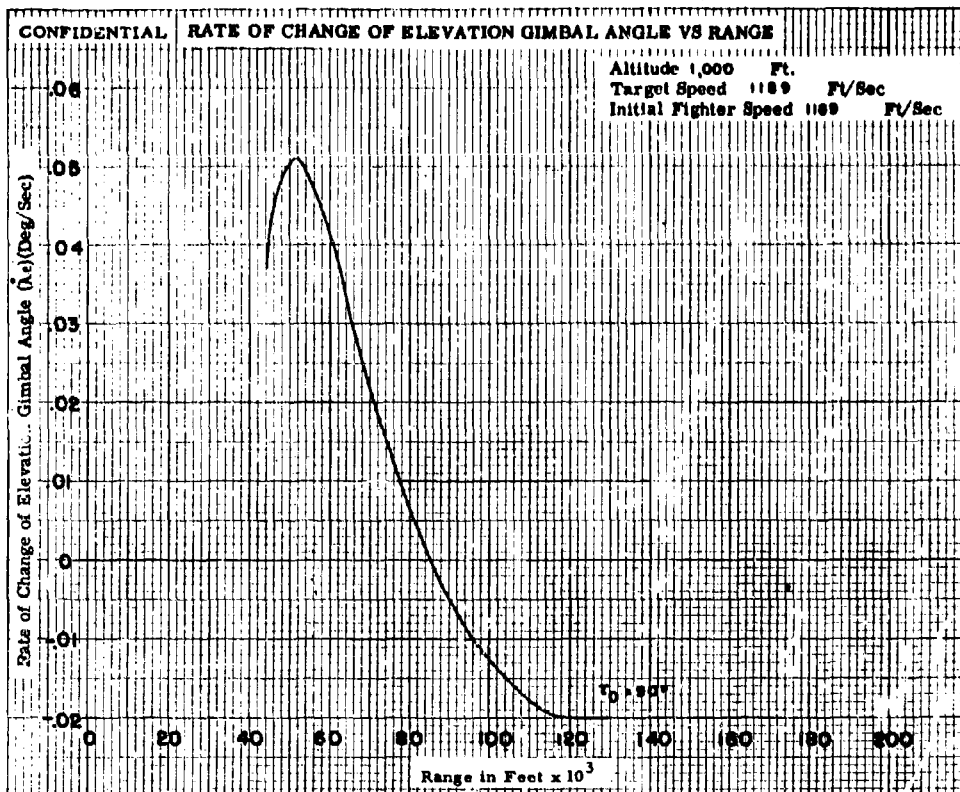


Fig. 111-5b

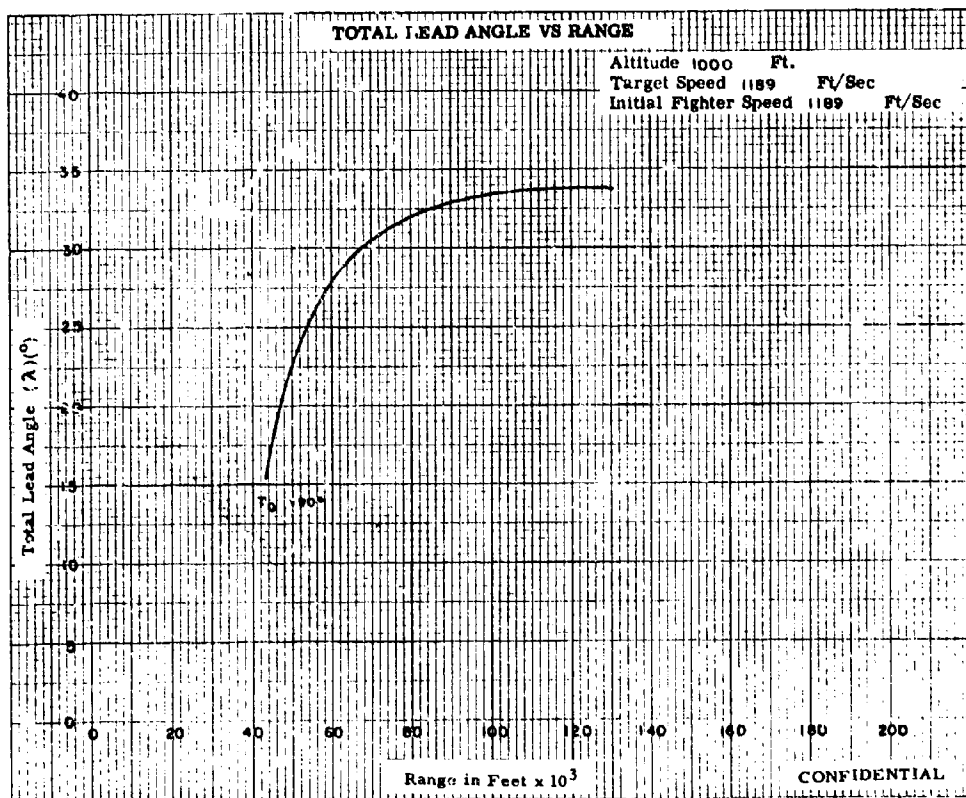
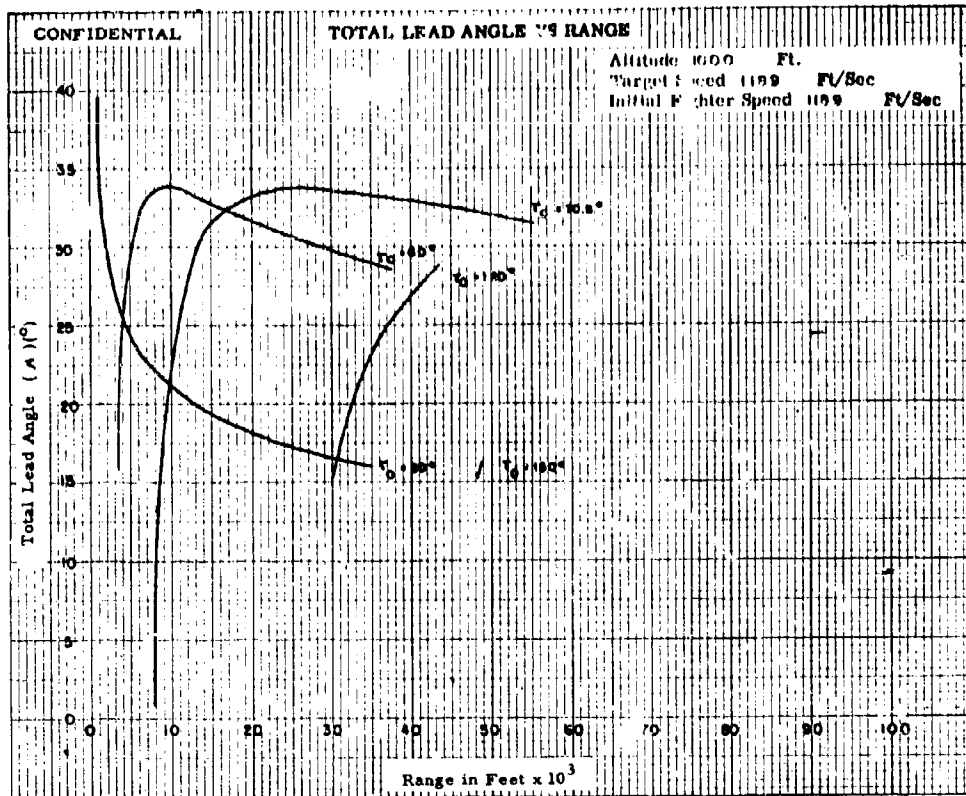


Fig. 111-6

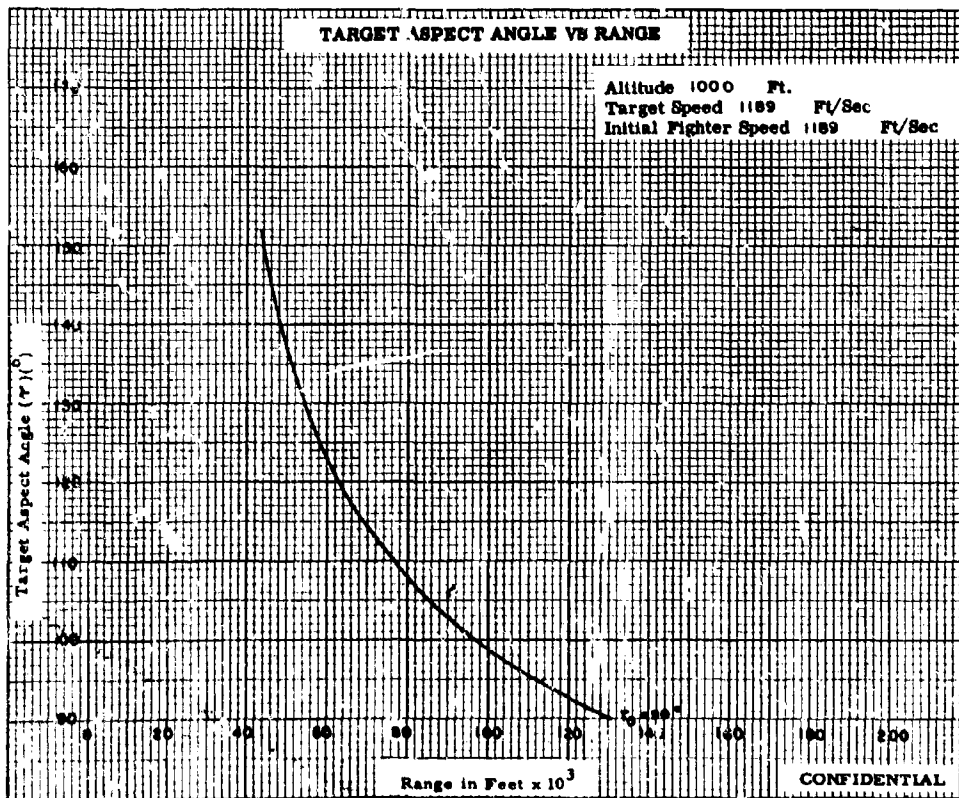
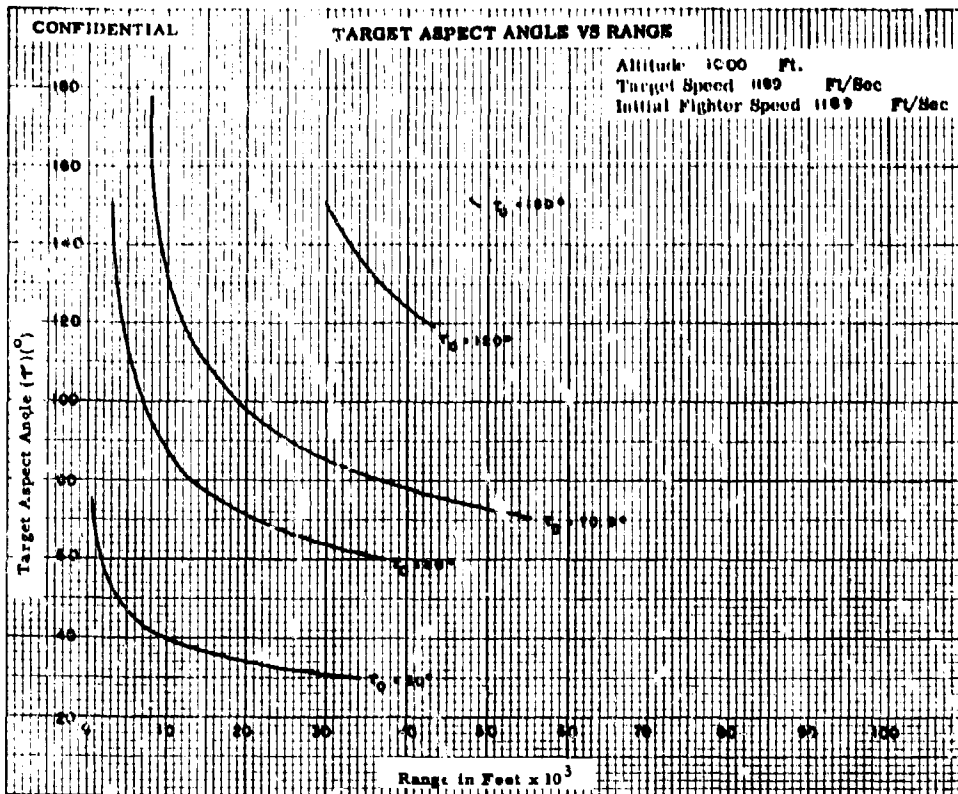


Fig. 111-7

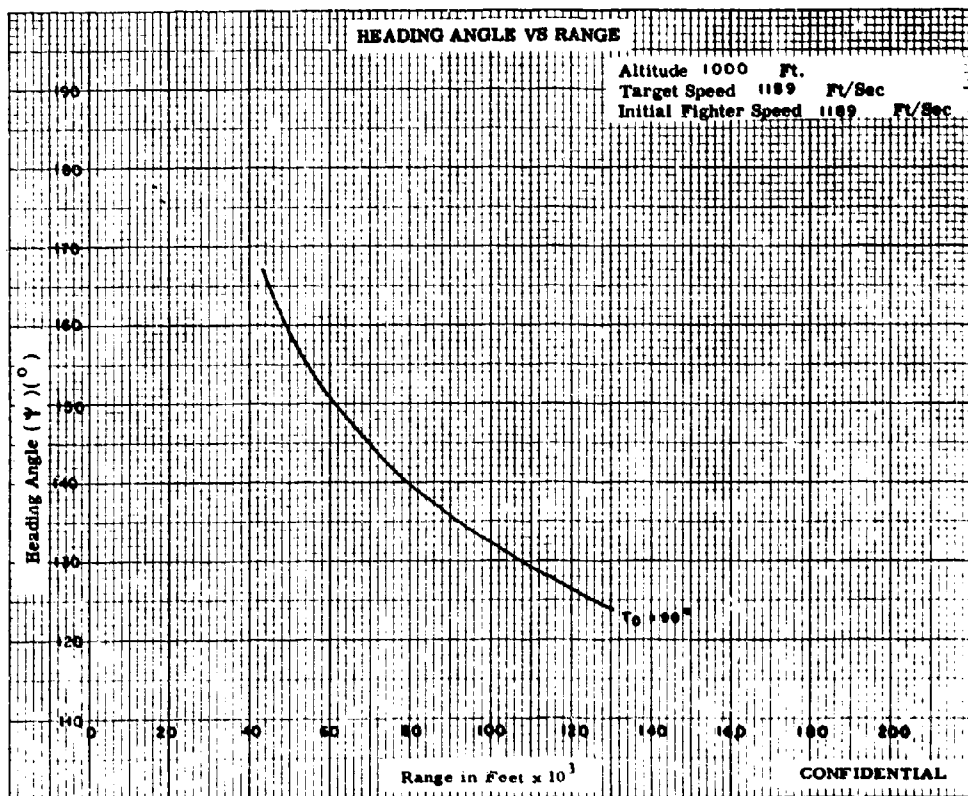
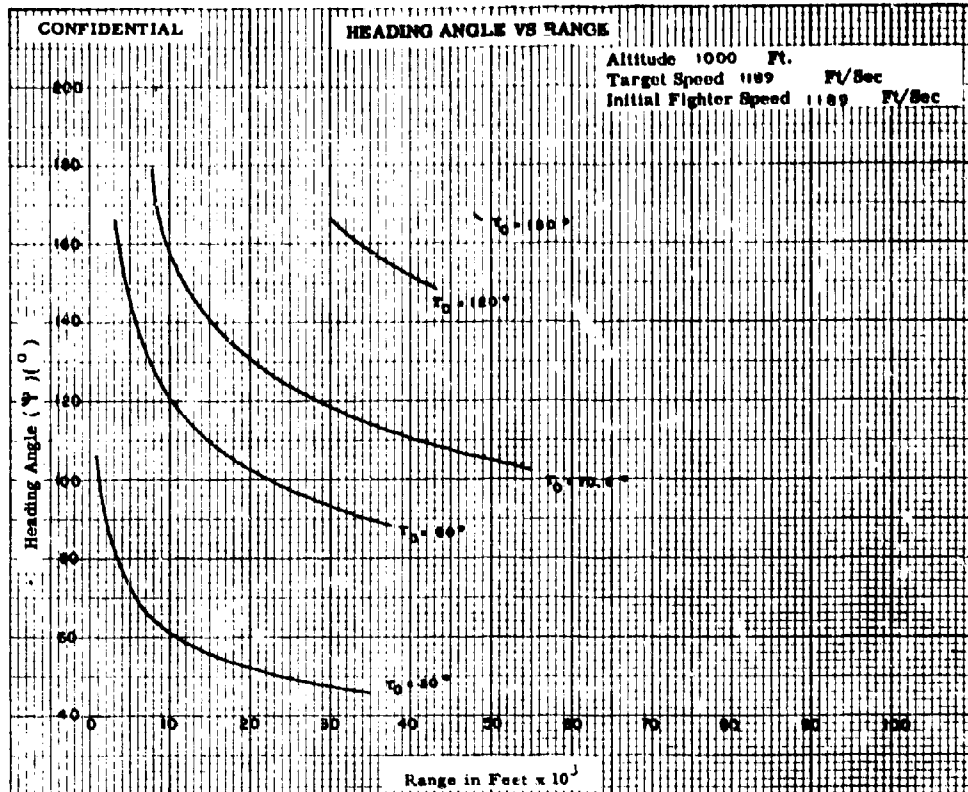


Fig. 111-8

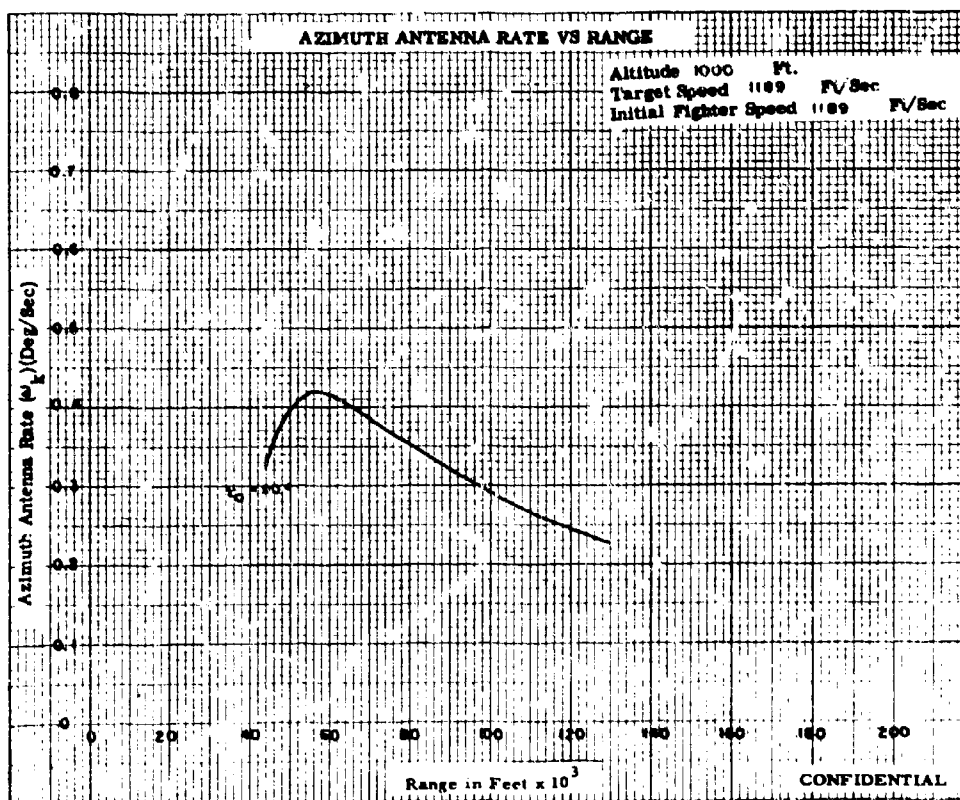
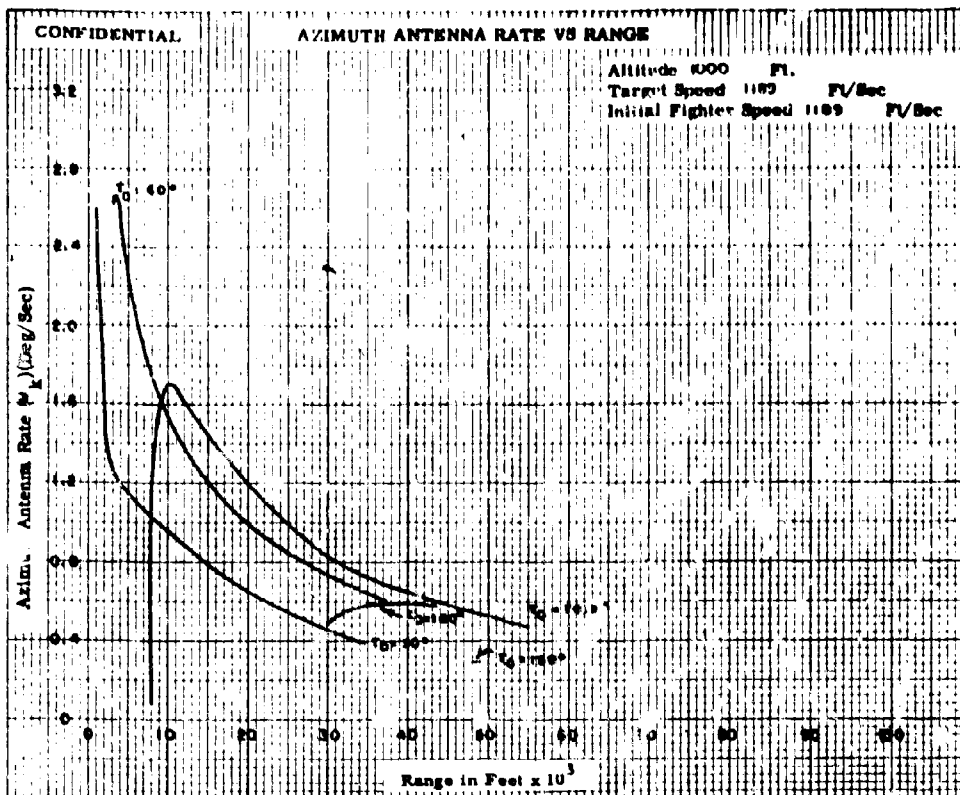


Fig. 111-9

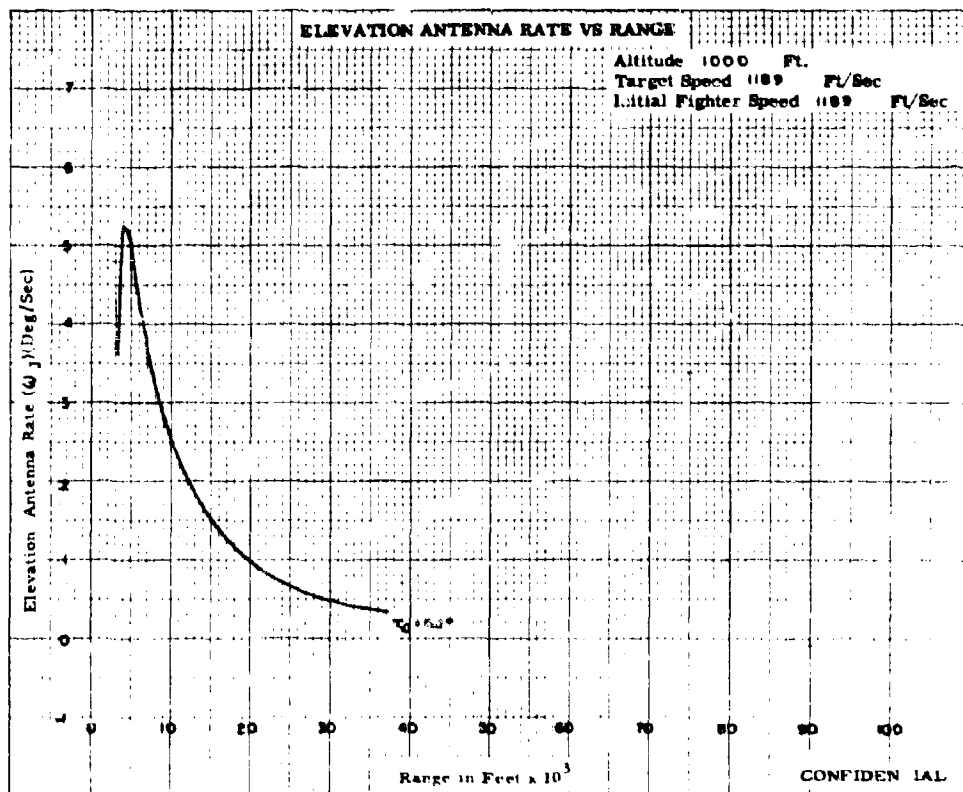
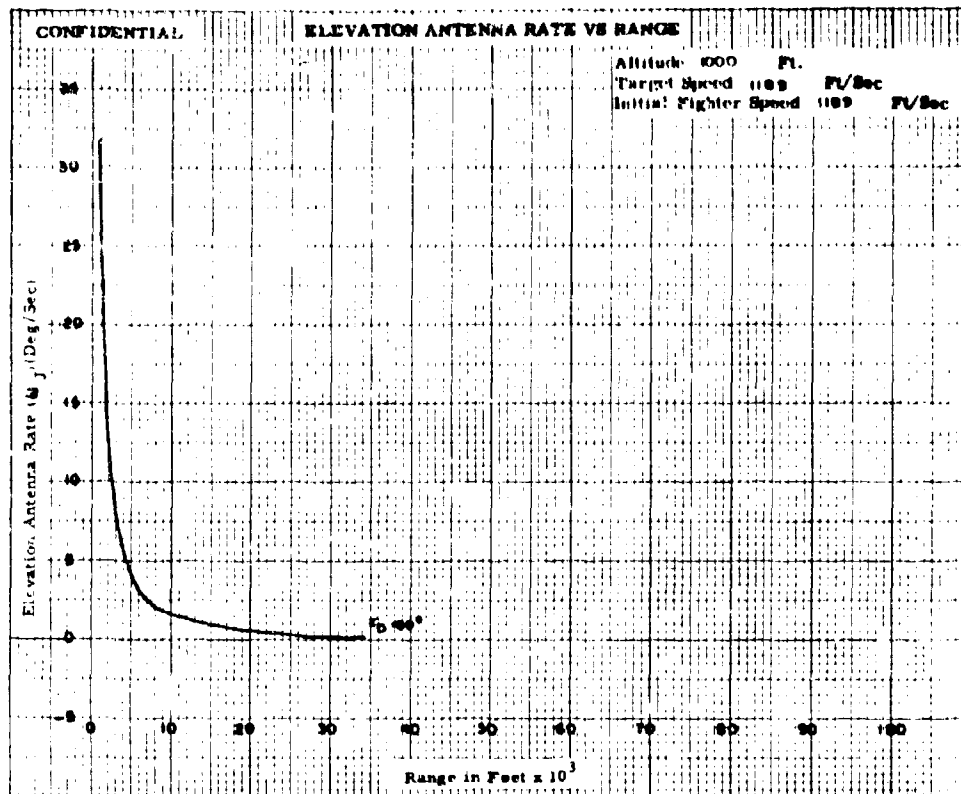


Fig. 111-20a

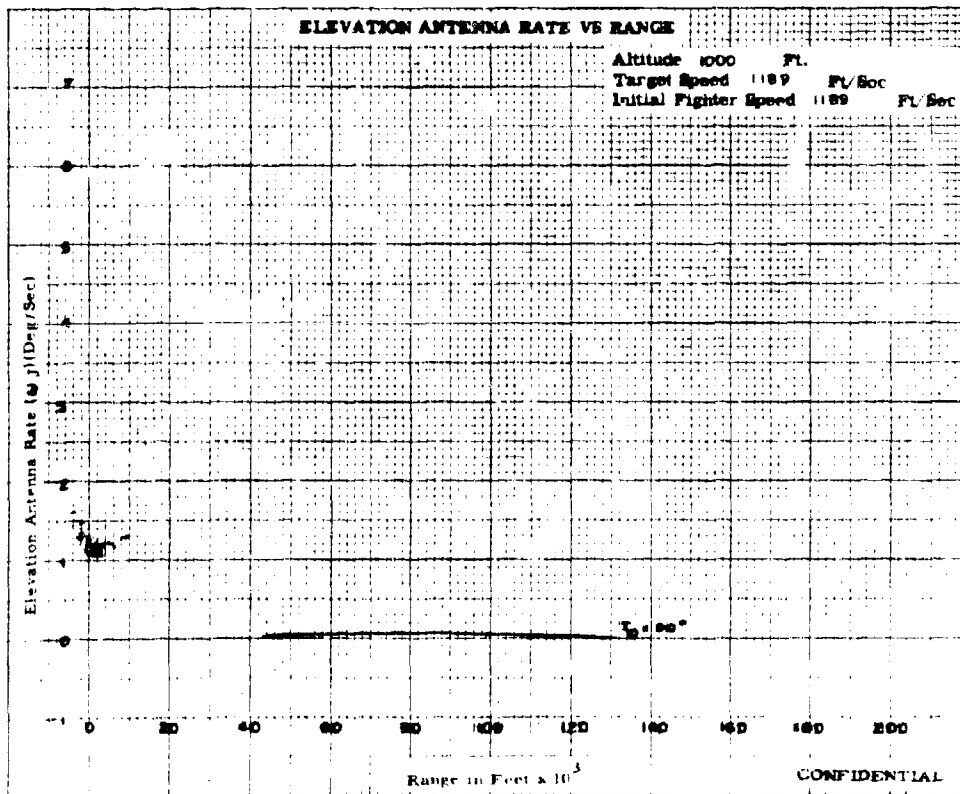
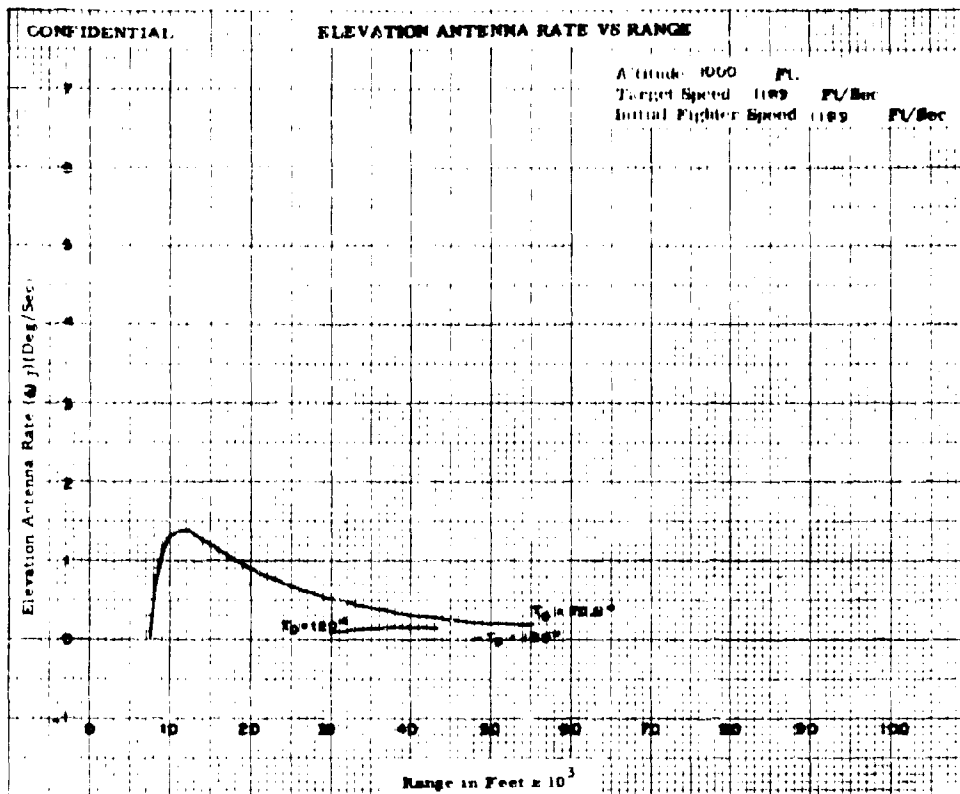


Fig. 111-10b

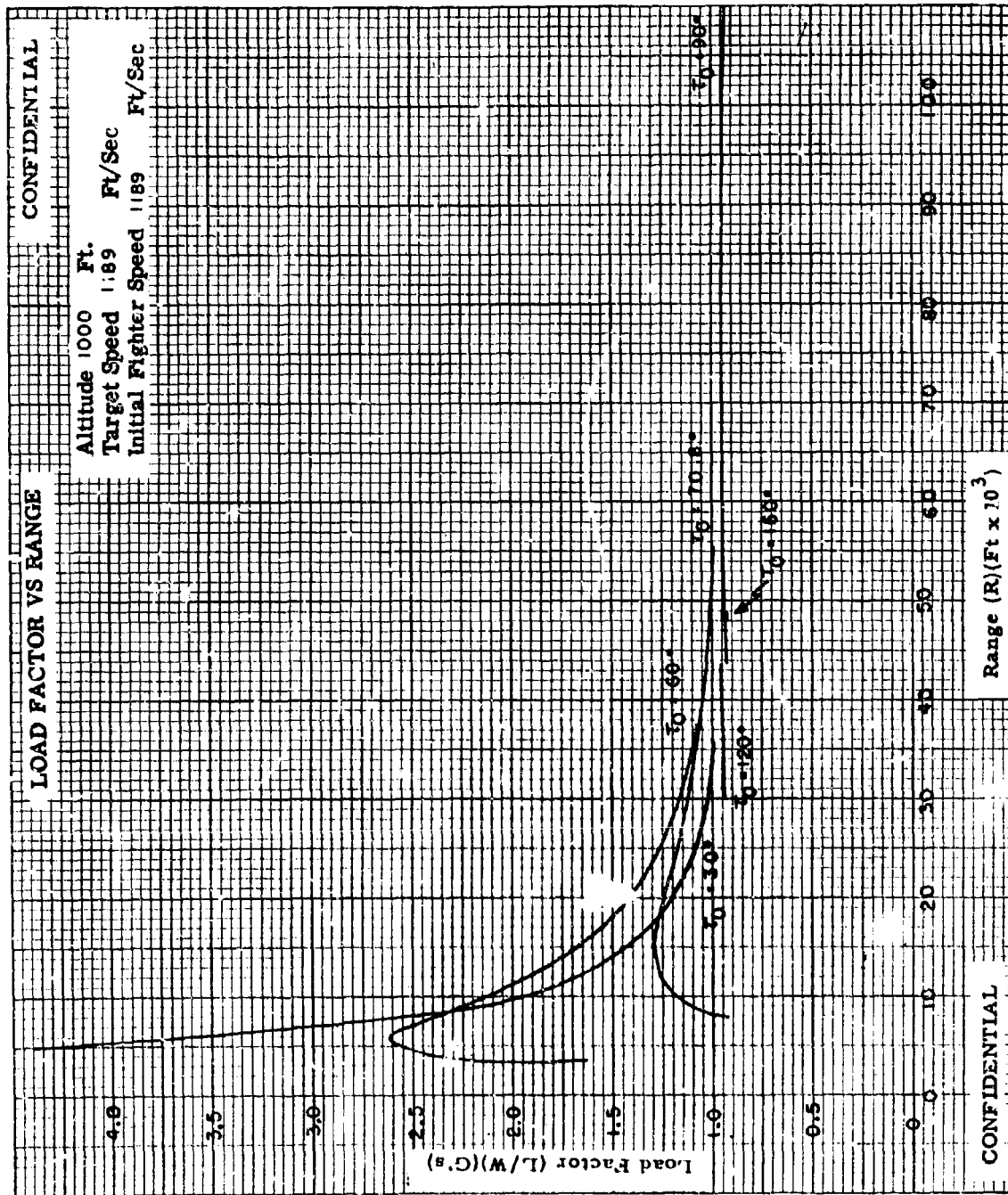


Fig. III-11

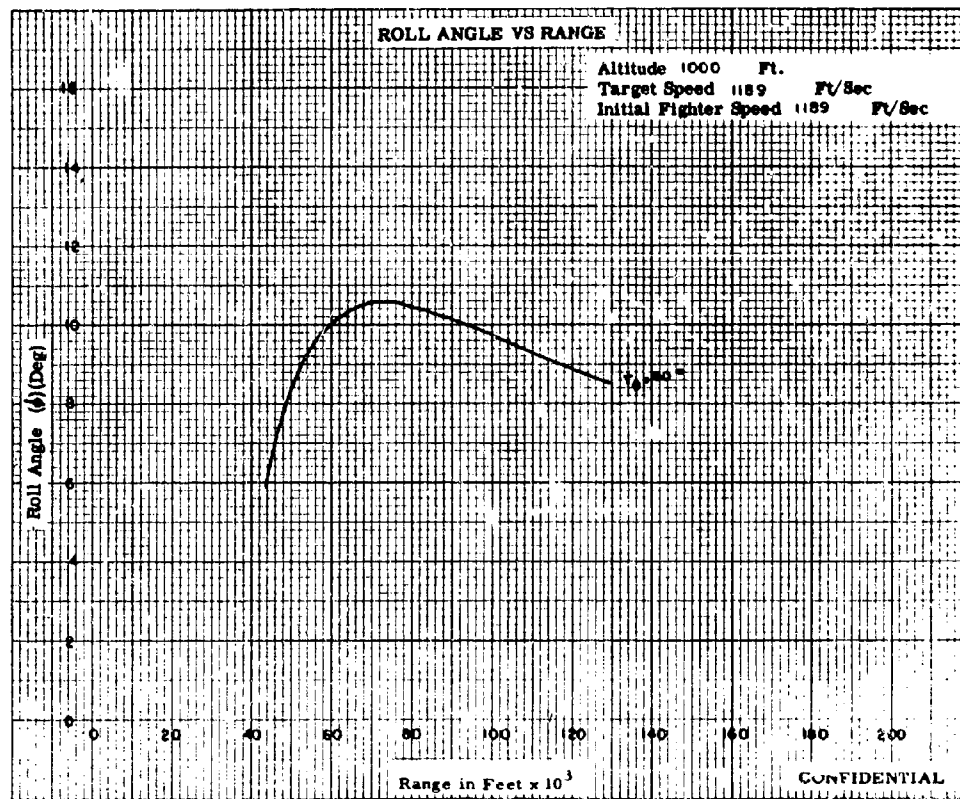
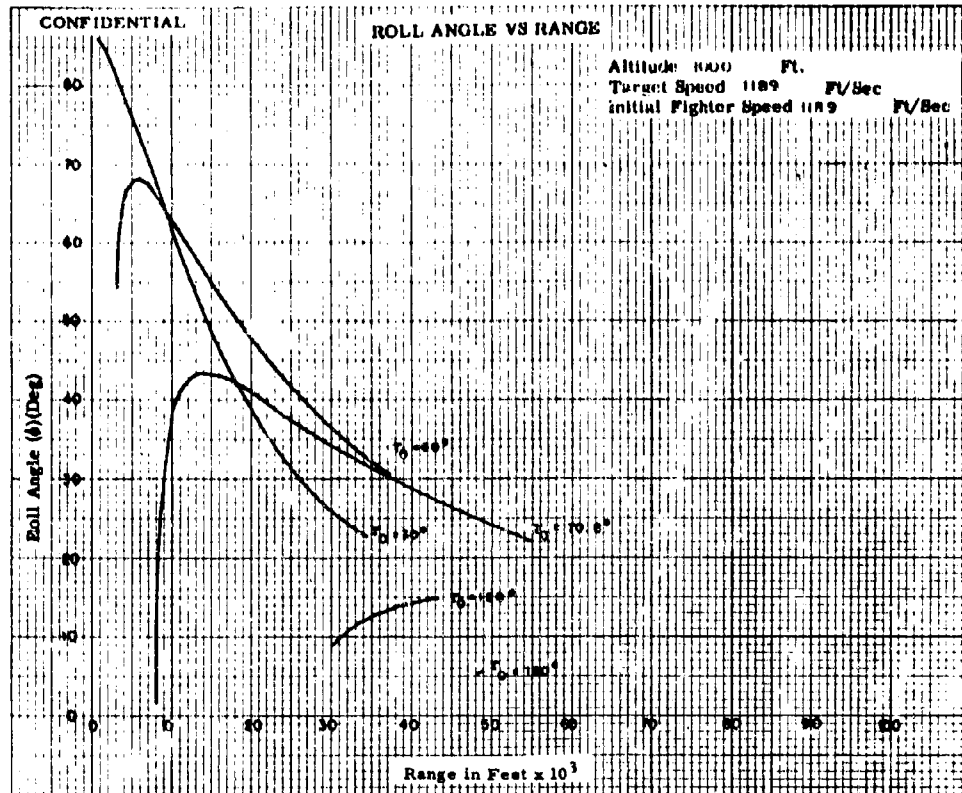


Fig. 111-12

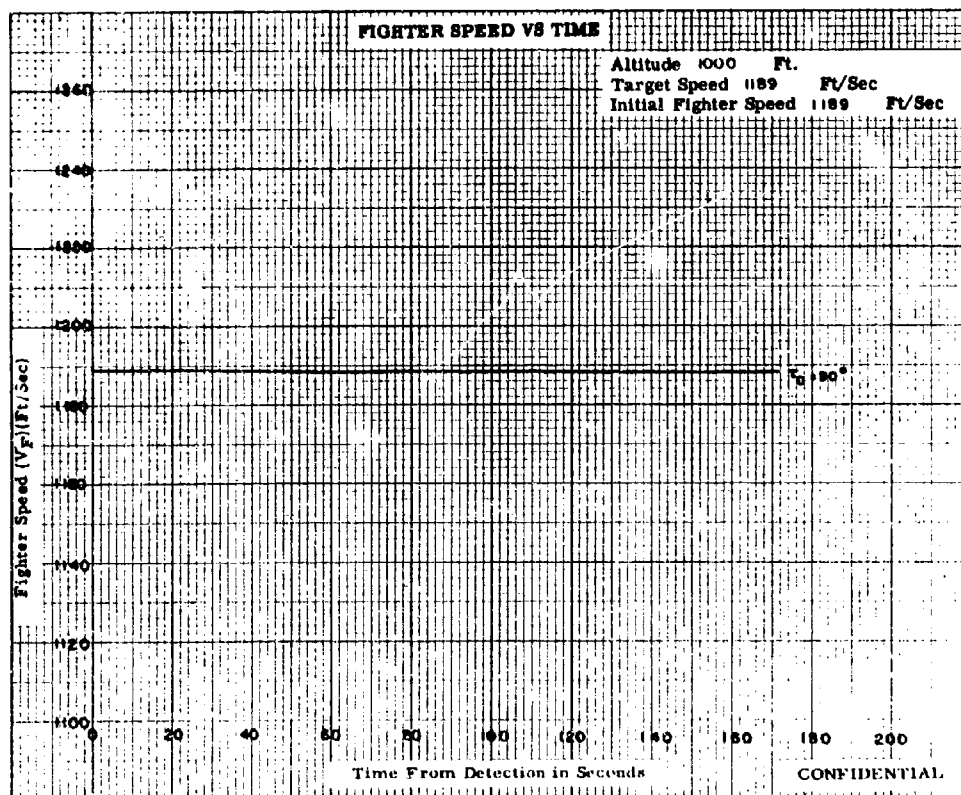
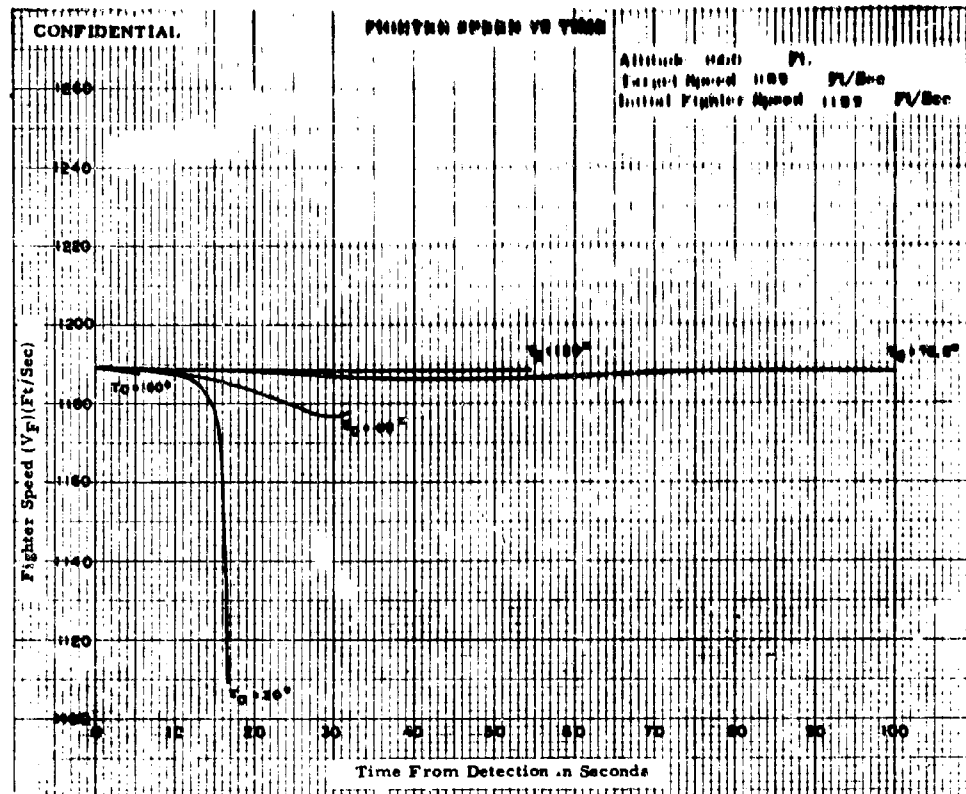


Fig. III-13

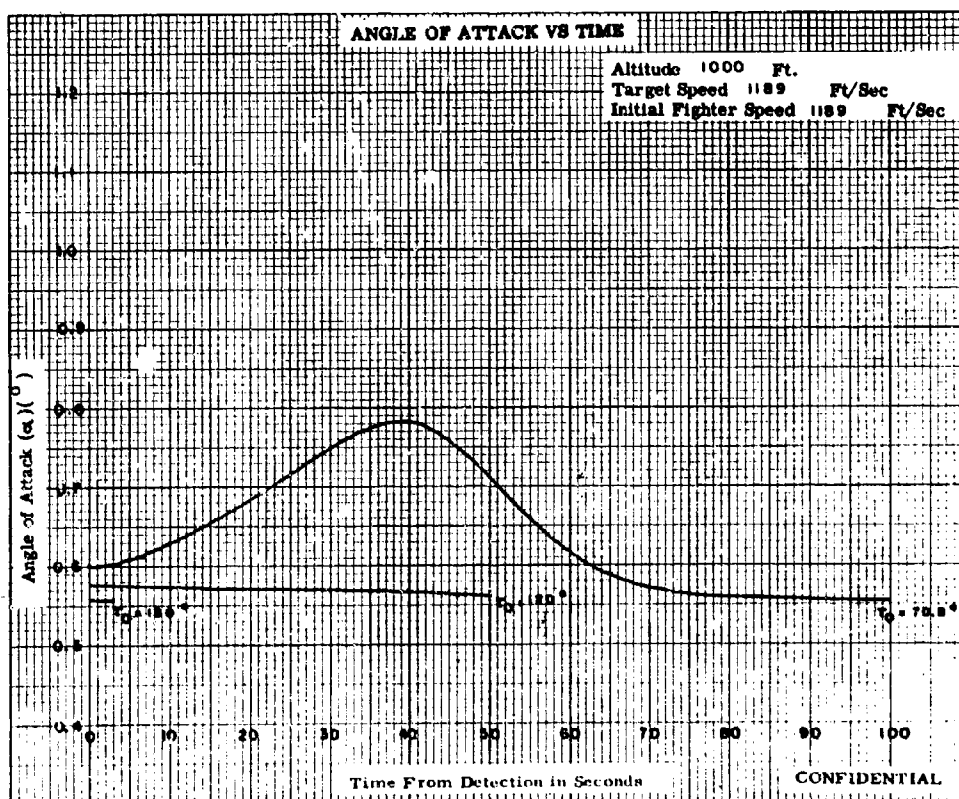
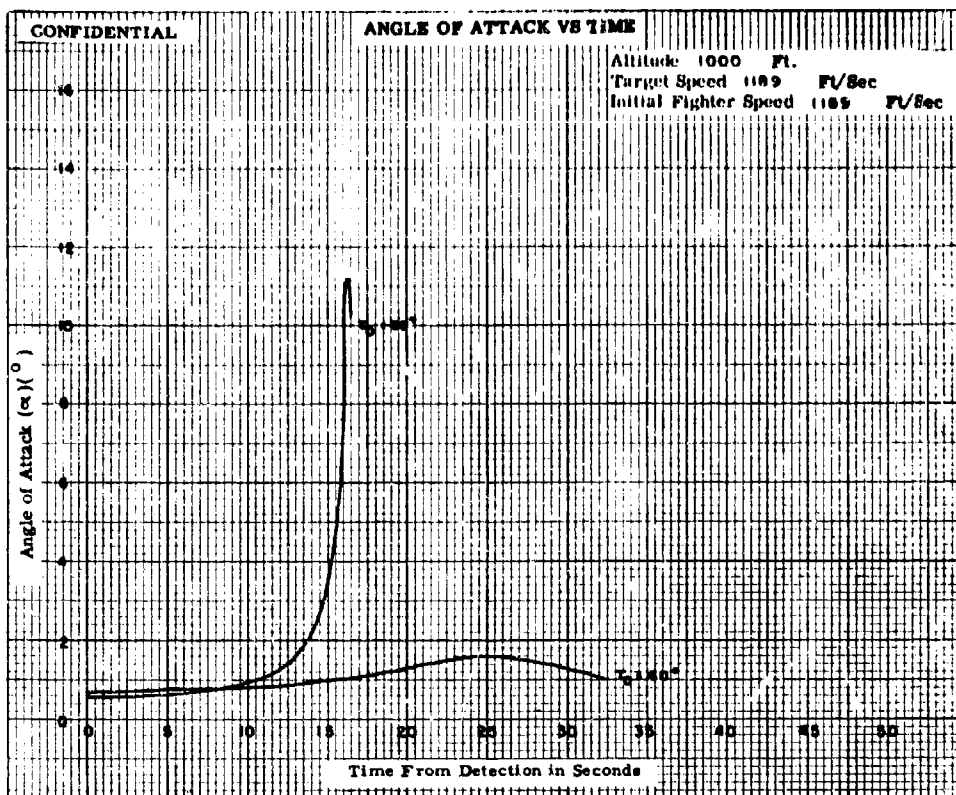


Fig. 111-14a

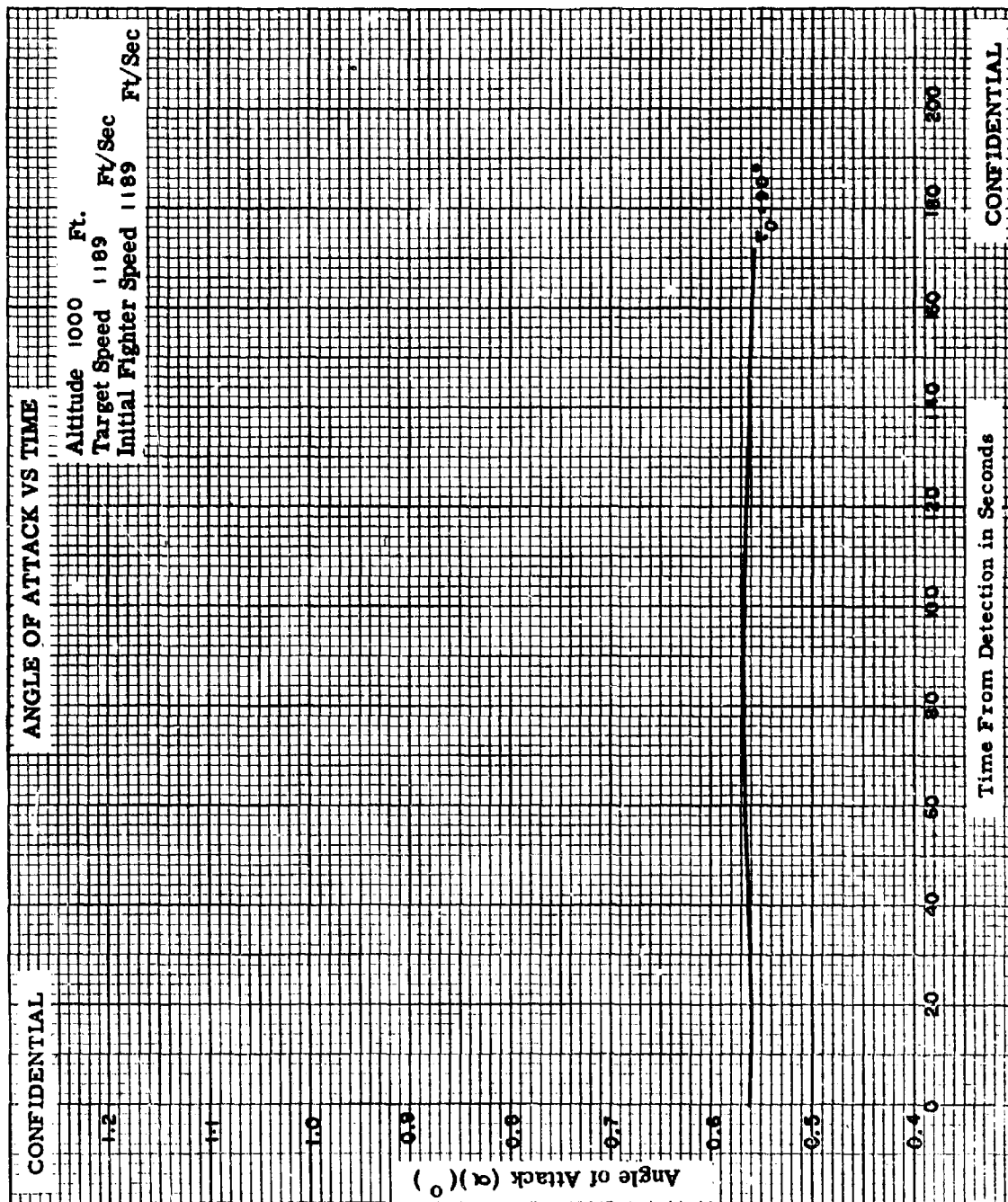
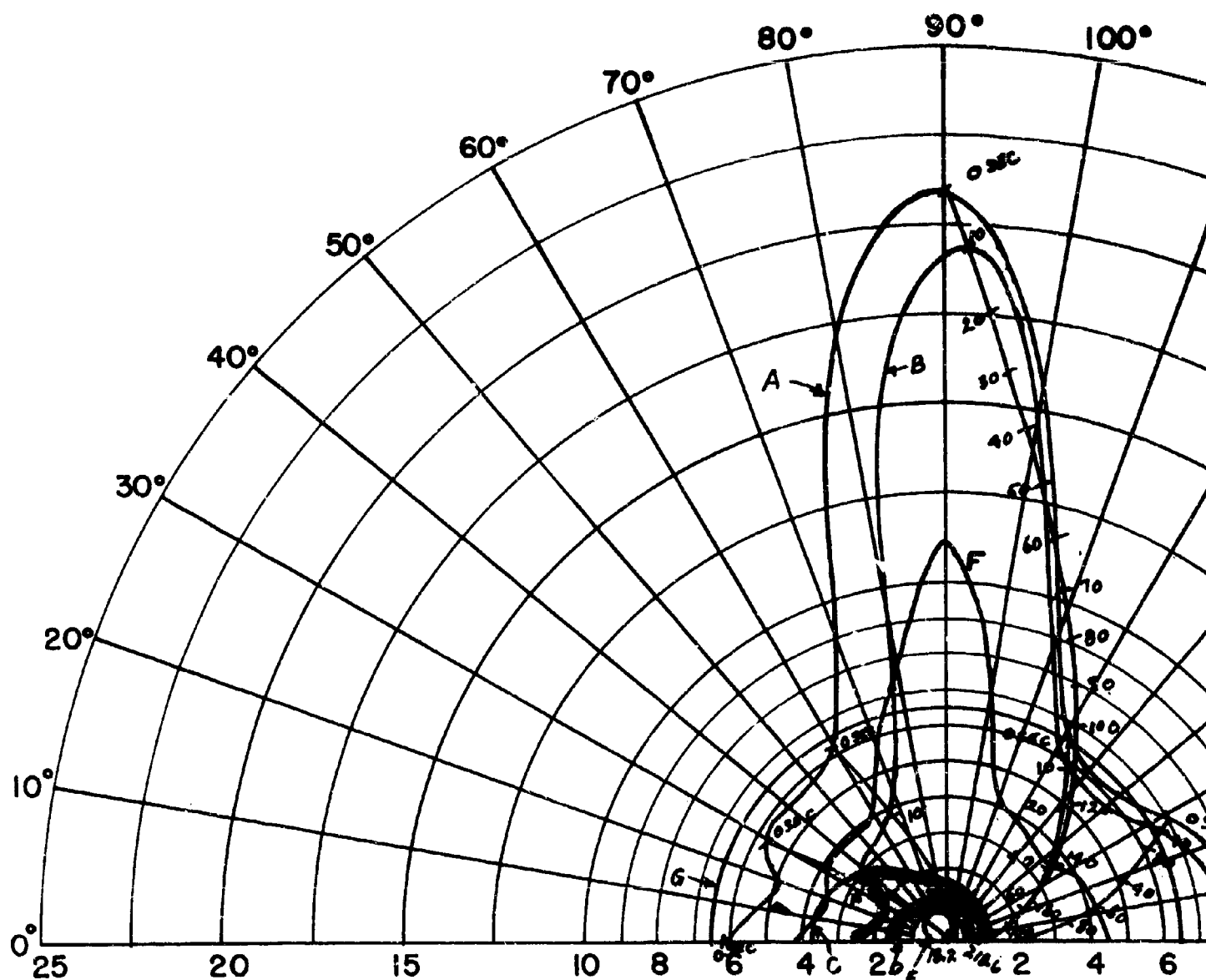


Fig. 111-14b



$V_F = 1189$ FT/SEC (F4H-1)(F8U-3)
 $V_T = 951$ FT/SEC
 ALTITUDE = 1000 FT.

← TARGET HEADING

- A - 85% DETECTION RANGE
- B - LOCK-ON RANGE (10 SEC. LOCK-ON)
- C - SPARROW III MAX. AERODYNAMIC
- D - SPARROW III MIN. AERODYNAMIC
- E - CONSTANT LOAD FACTOR LOCUS
- F - 90% SPARROW III SEEKER LOCK-
- G - 6.5 N.M. INTERLOCK

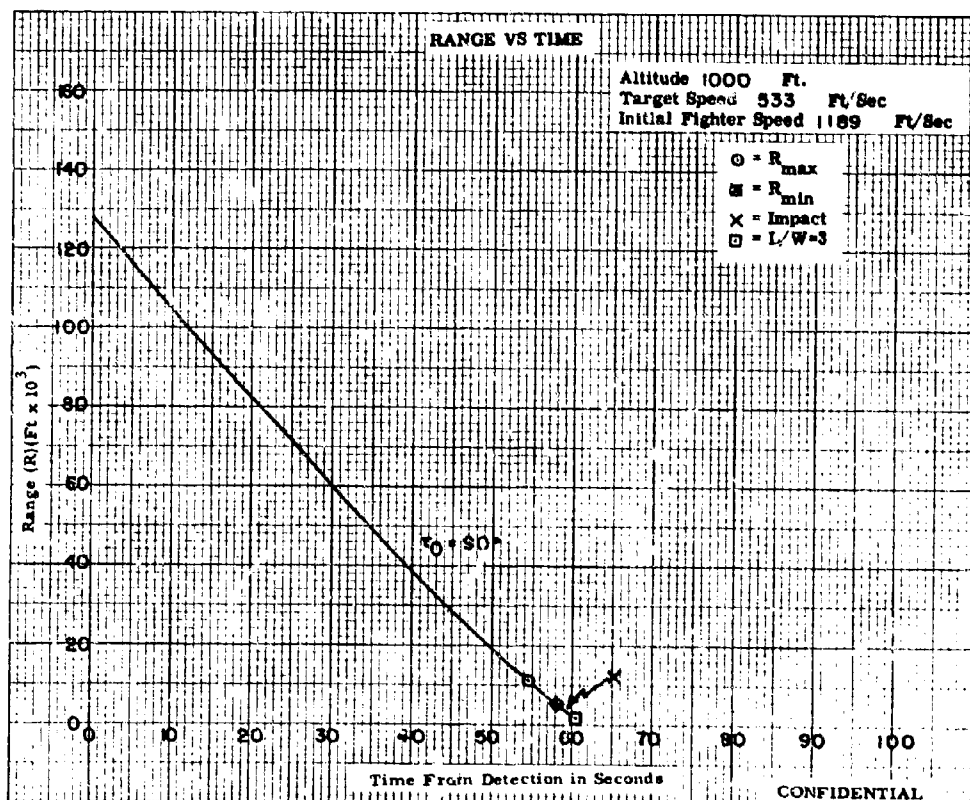
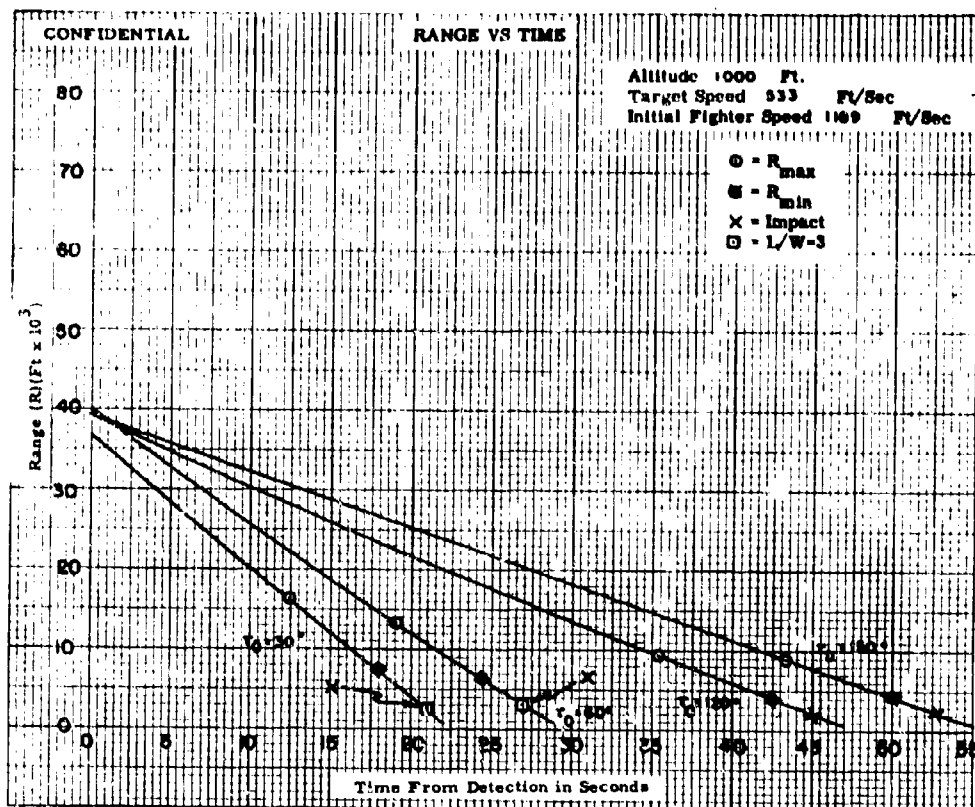


Fig. IV-1

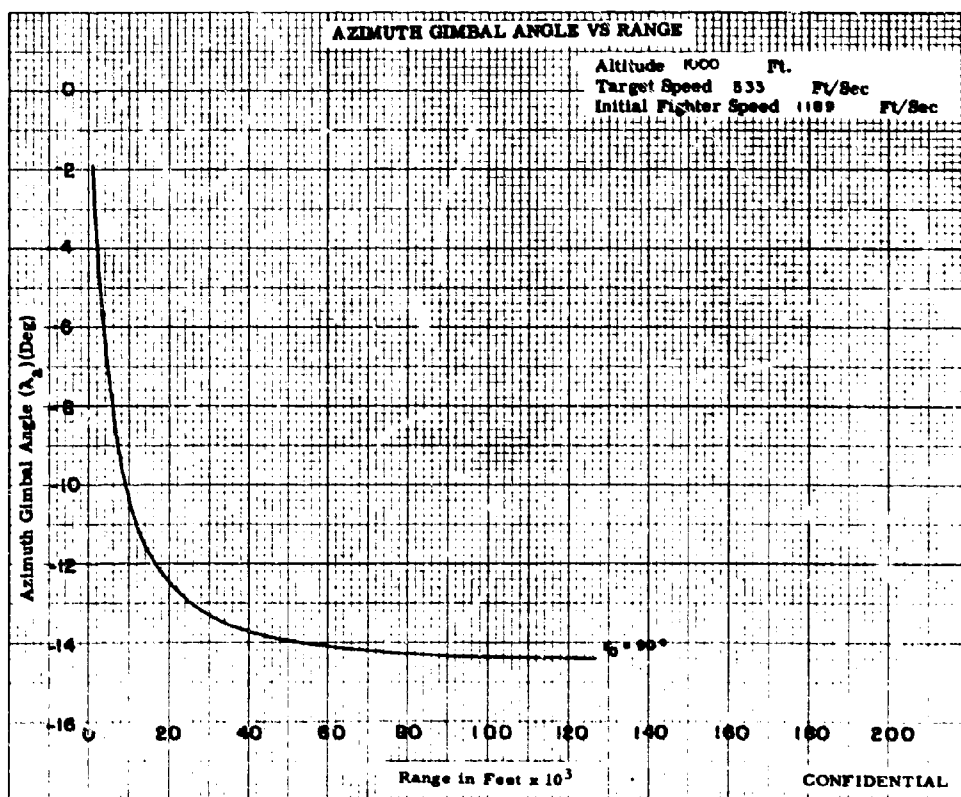
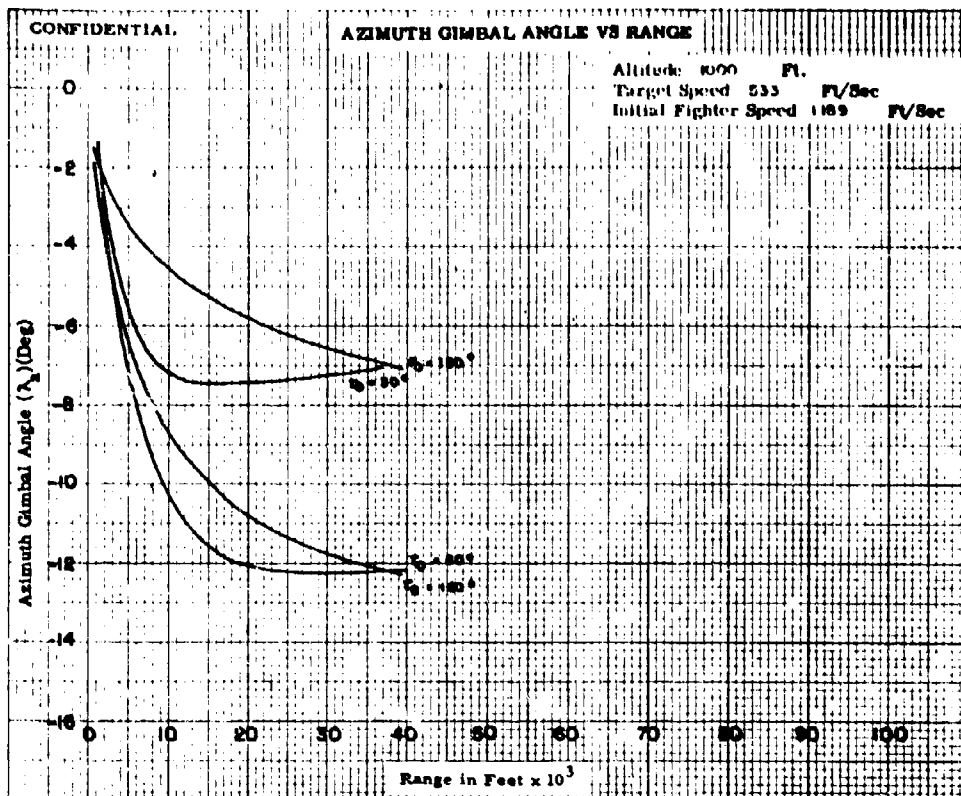


Fig. IV-2

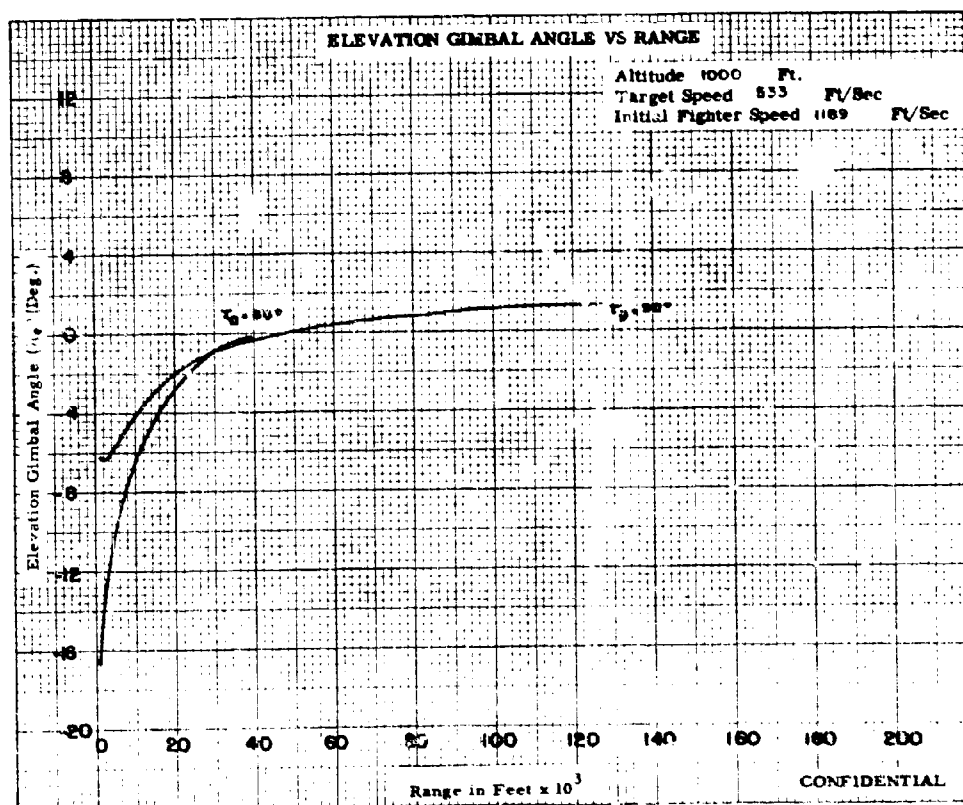
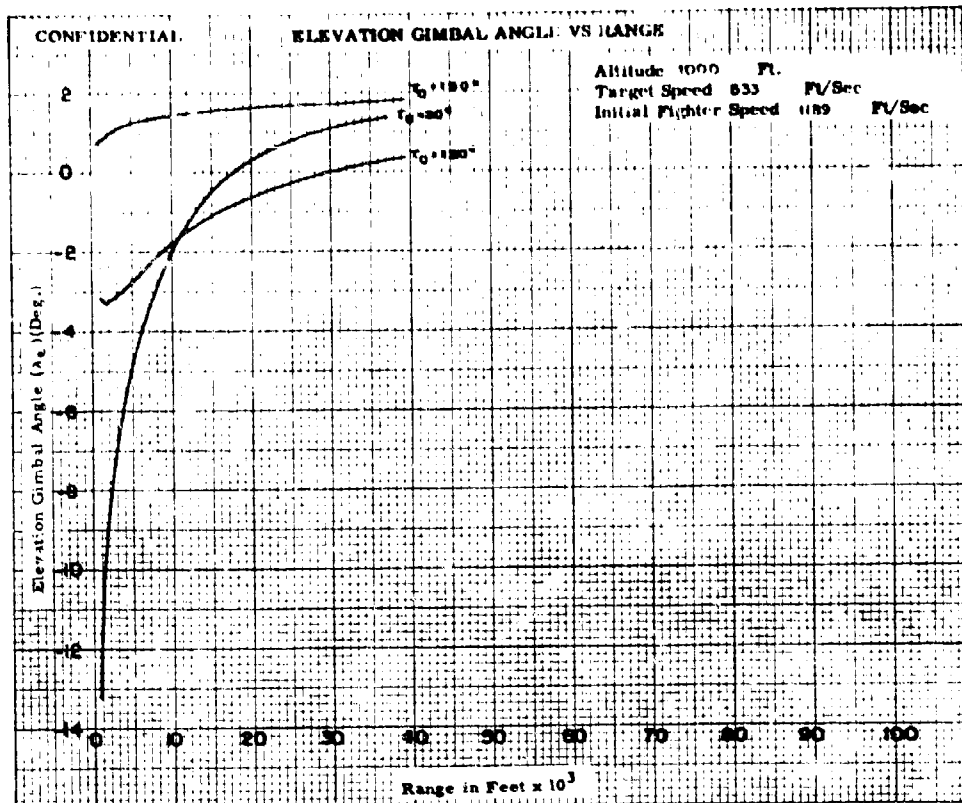


Fig. IV-3

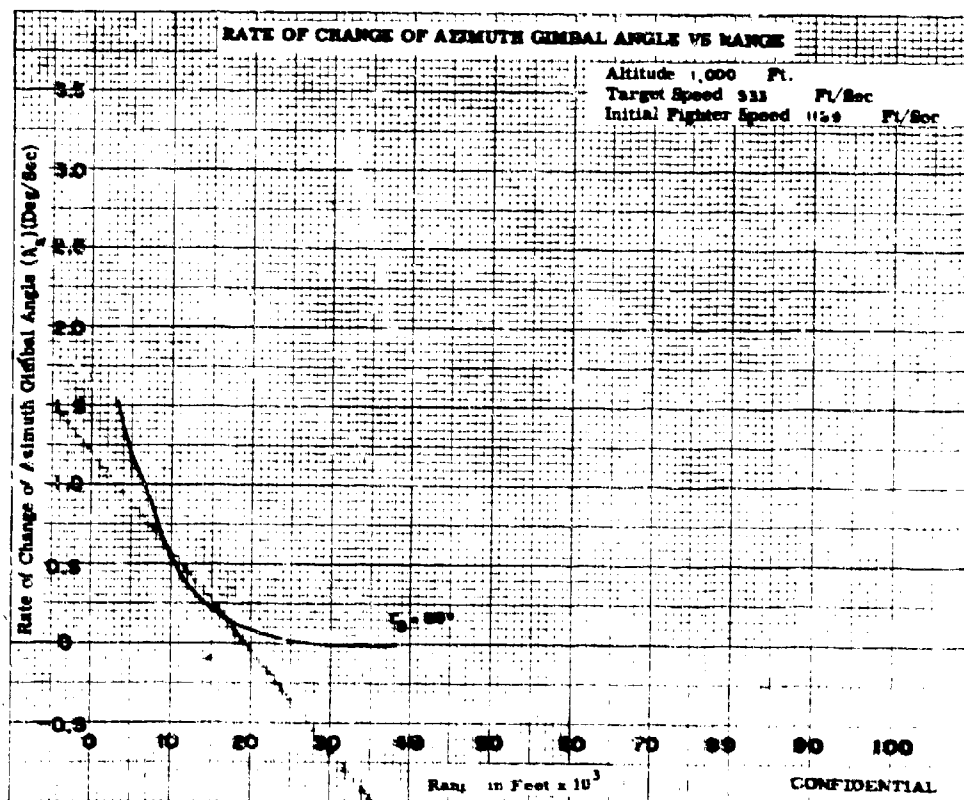
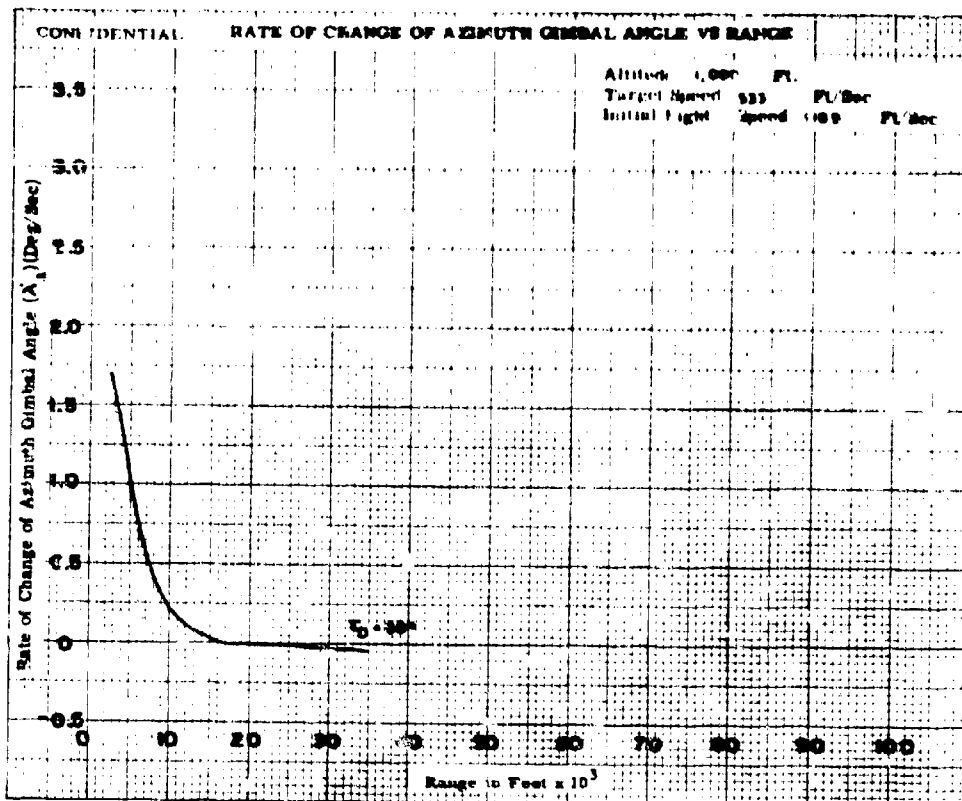
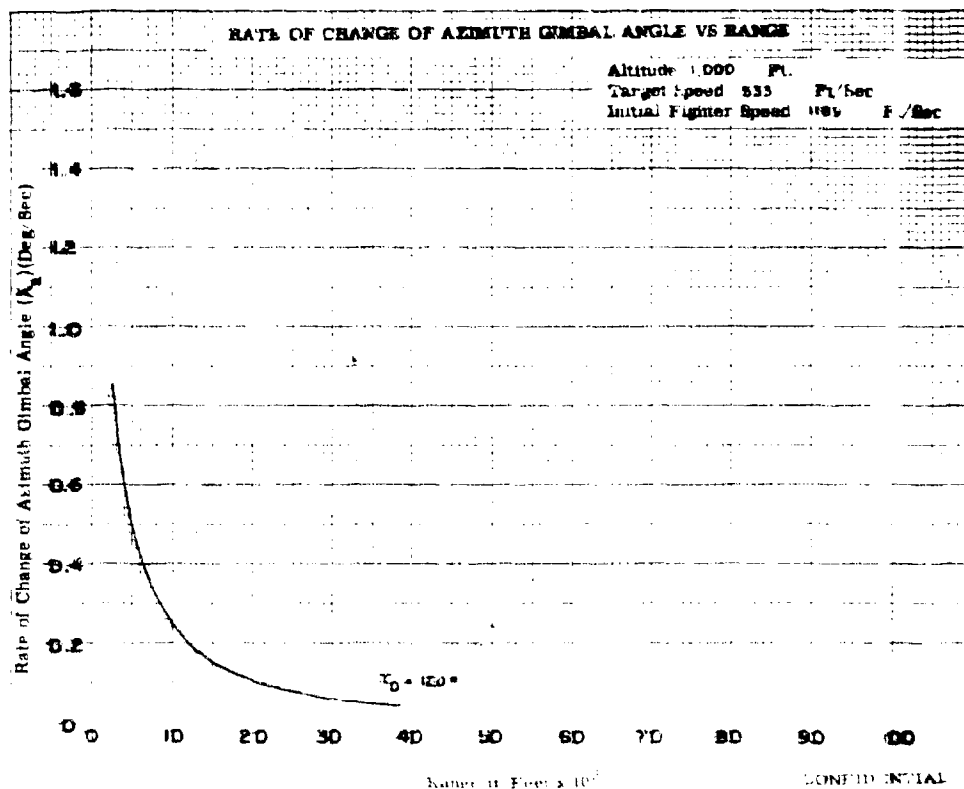
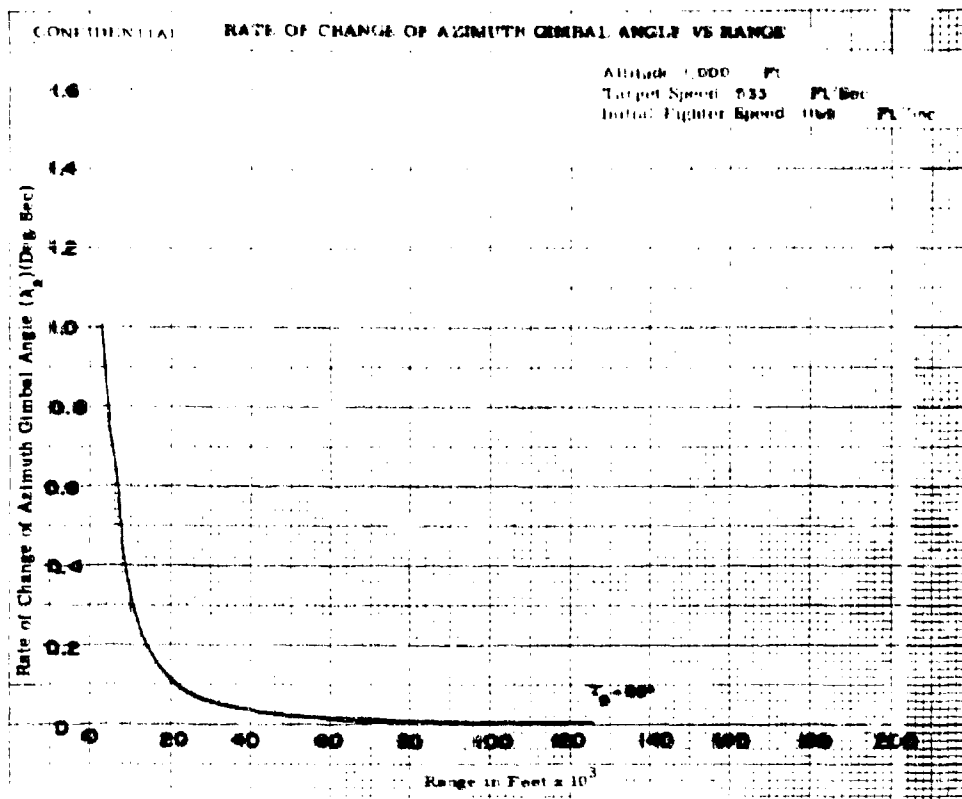


Fig. IV-4b



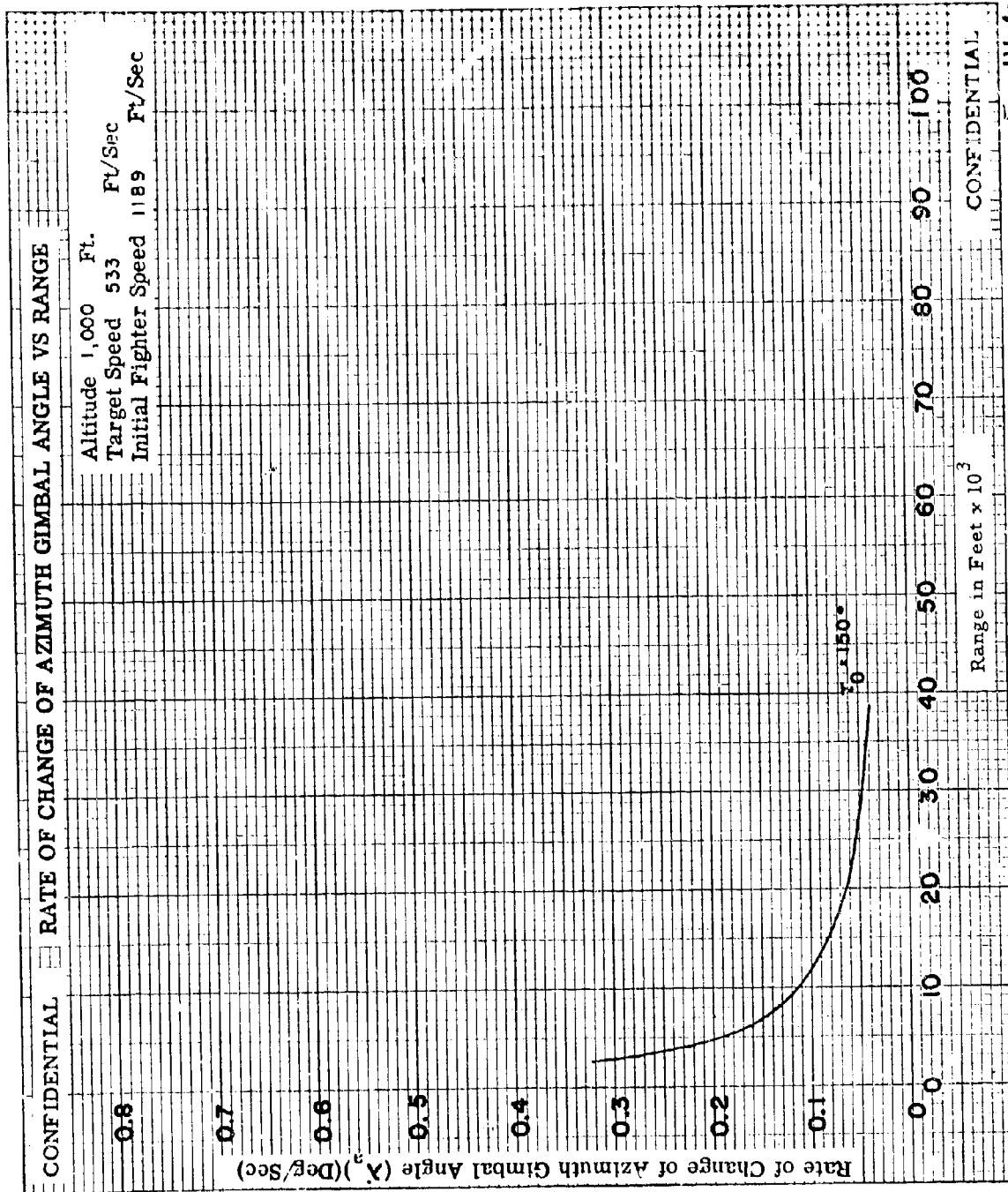


Fig. IV-4c

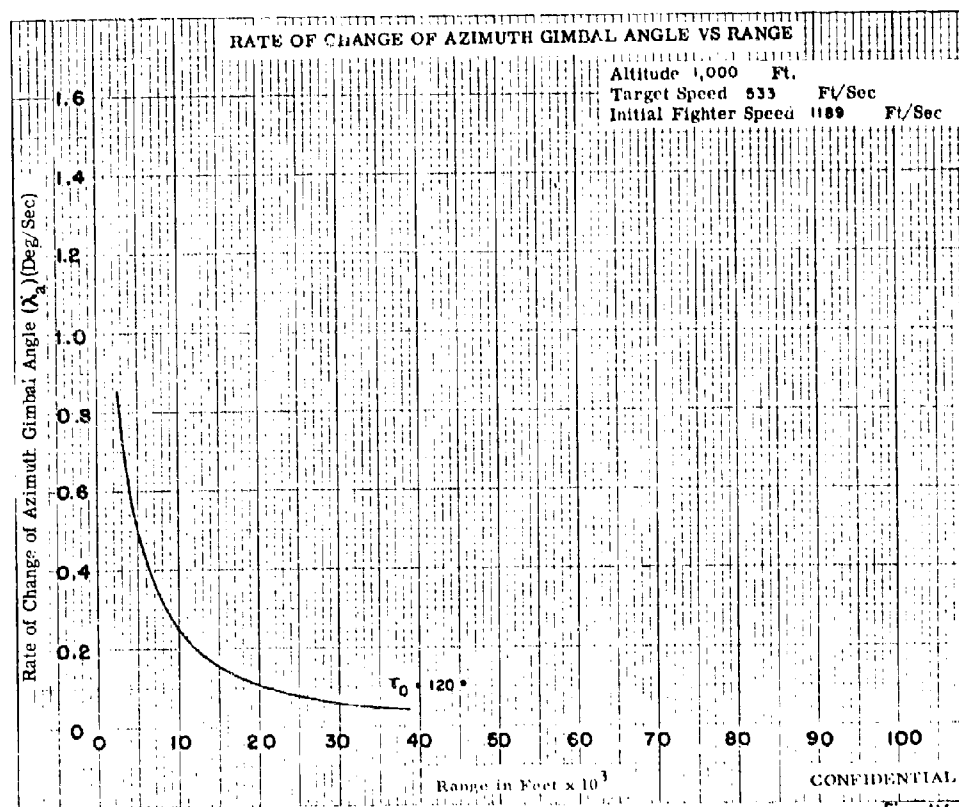
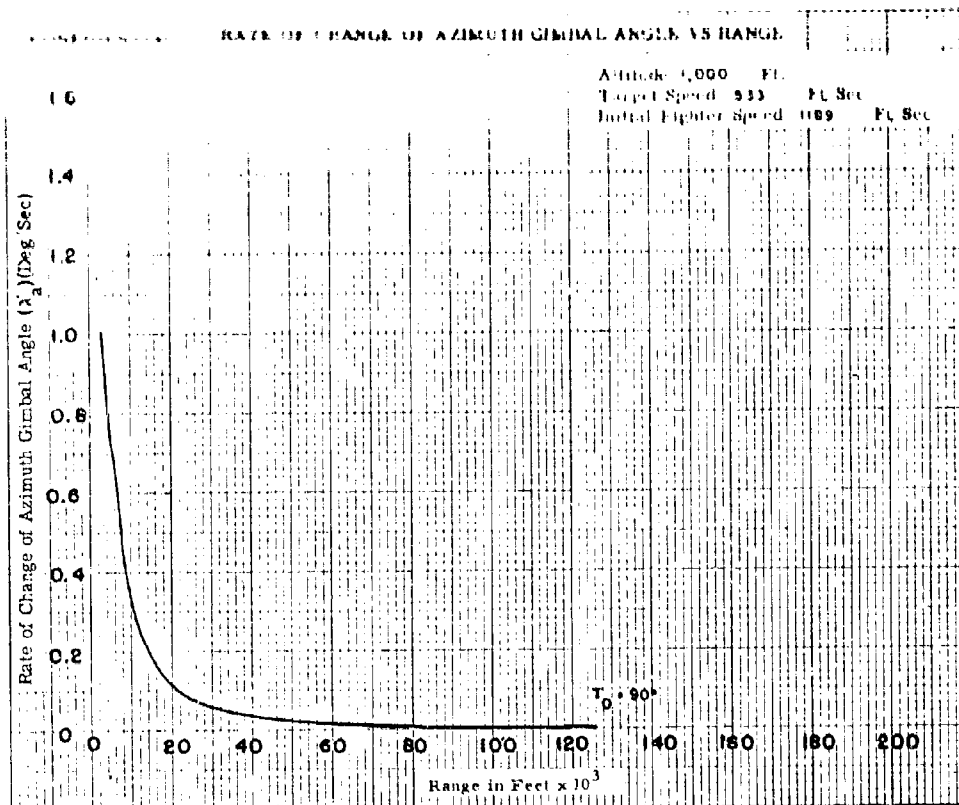


Fig. IV-4b

CONFIDENTIAL

RATE OF CHANGE OF AZIMUTH GIMBAL ANGLE VS RANGE

Altitude 1,000 Ft.
 Target Speed 533 Ft./Sec
 Initial Fighter Speed 1189 Ft./Sec

Rate of Change of Azimuth Gimbal Angle ($\dot{\lambda}_g$) (Deg/Sec)

0.8

0.7

0.6

0.5

0.4

0.3

0.2

0.1

0.0

0 10 20 30 40 50 60 70 80 90 100

$\theta_0 = 150^\circ$

Range in Feet $\times 10^3$

CONFIDENTIAL

Fig. IV-4c

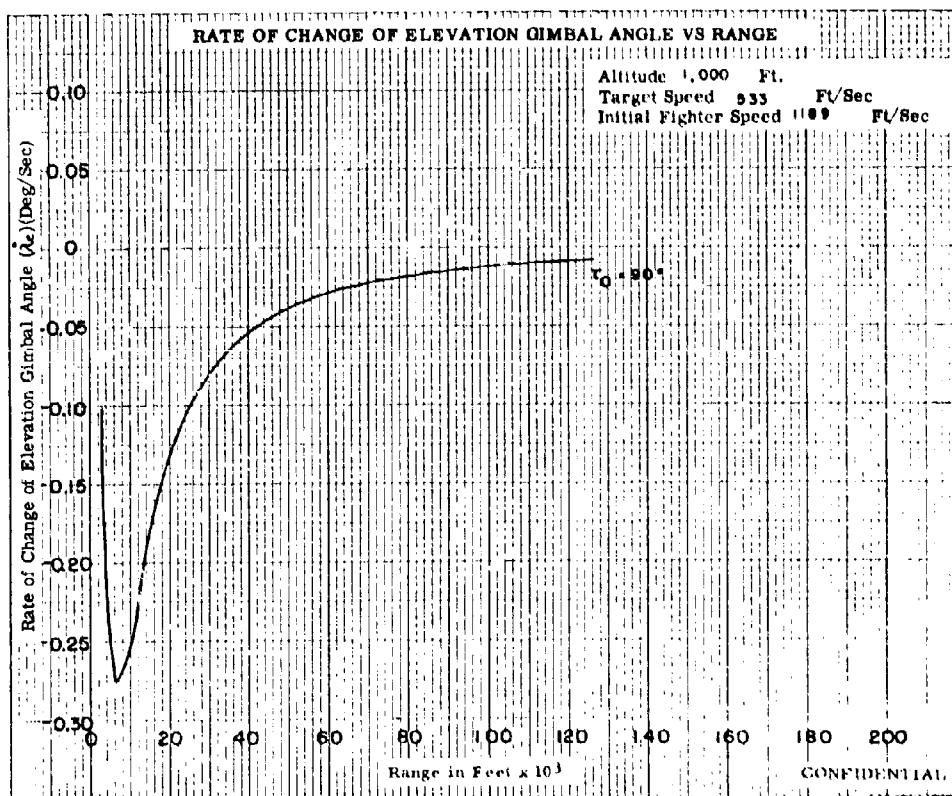
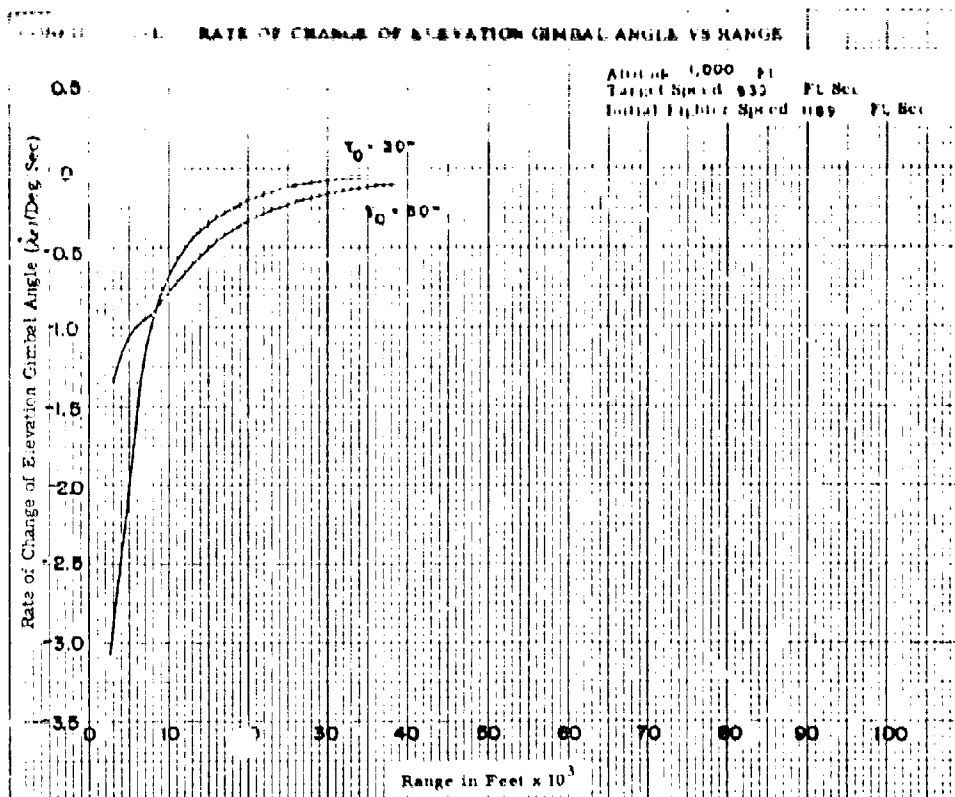


Fig. IV-5a

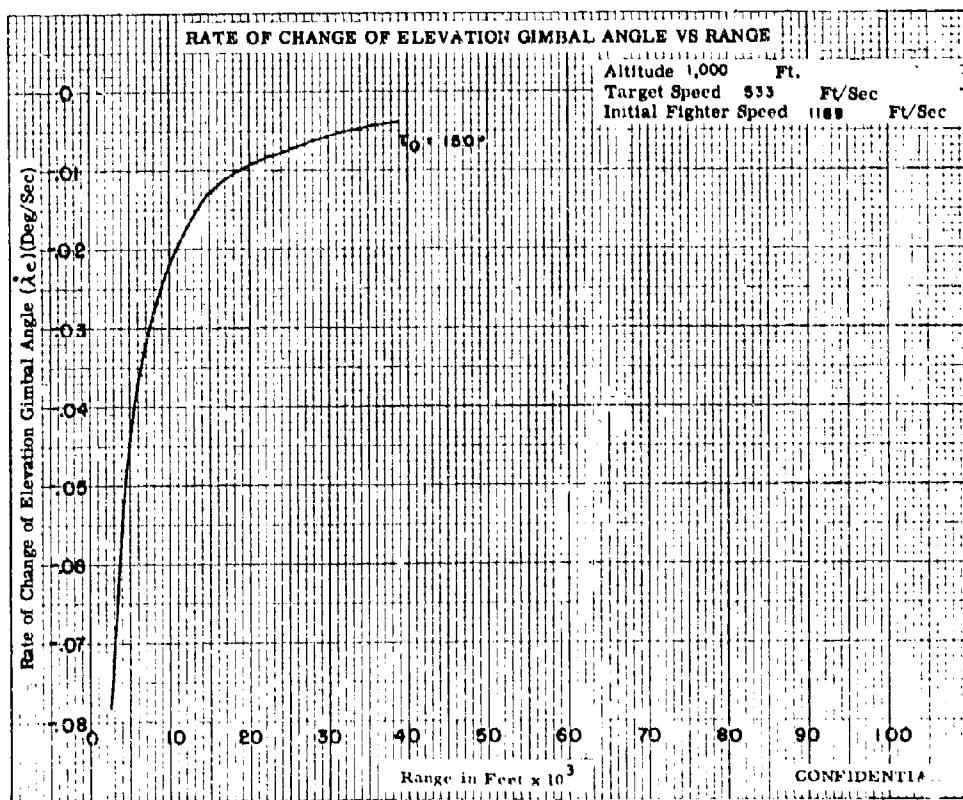
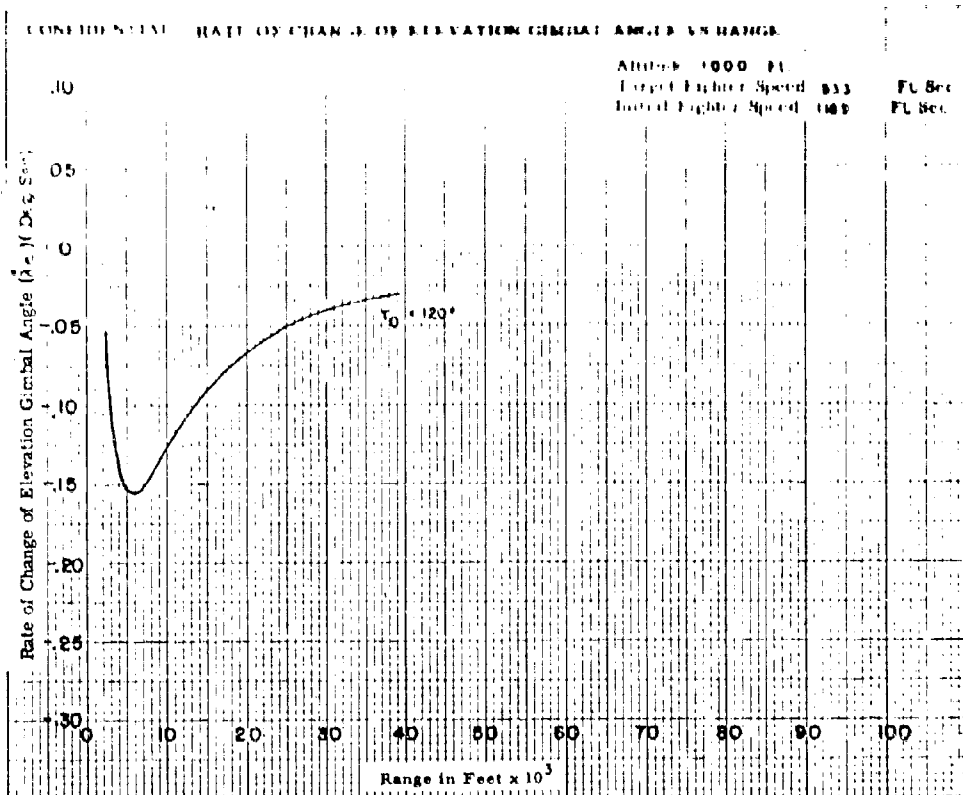


Fig. IV-5b

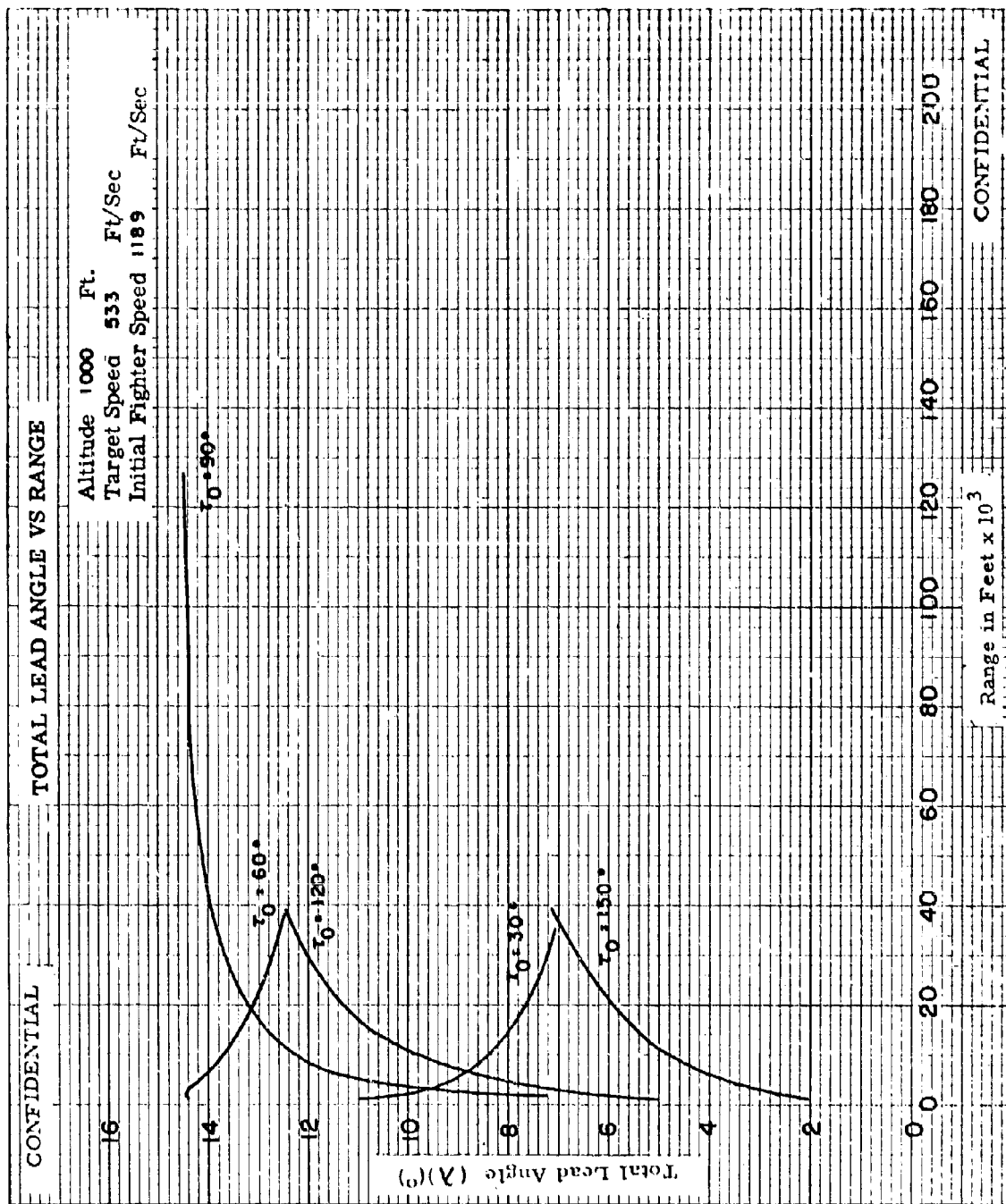


Fig. IV-6

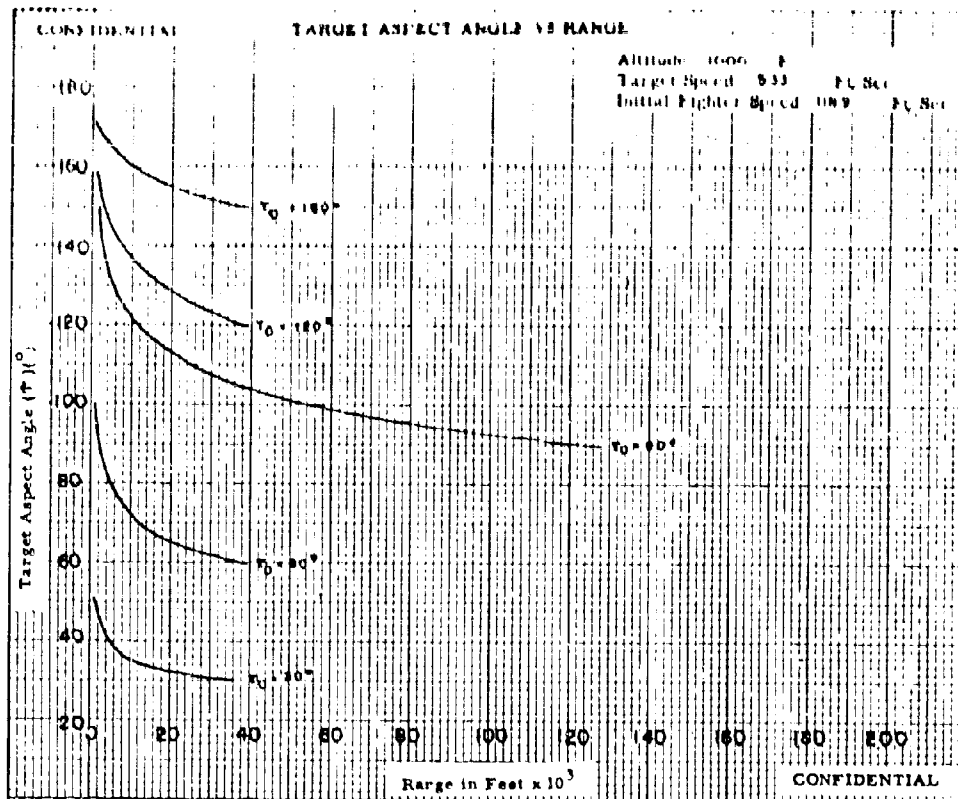


Fig. IV-7

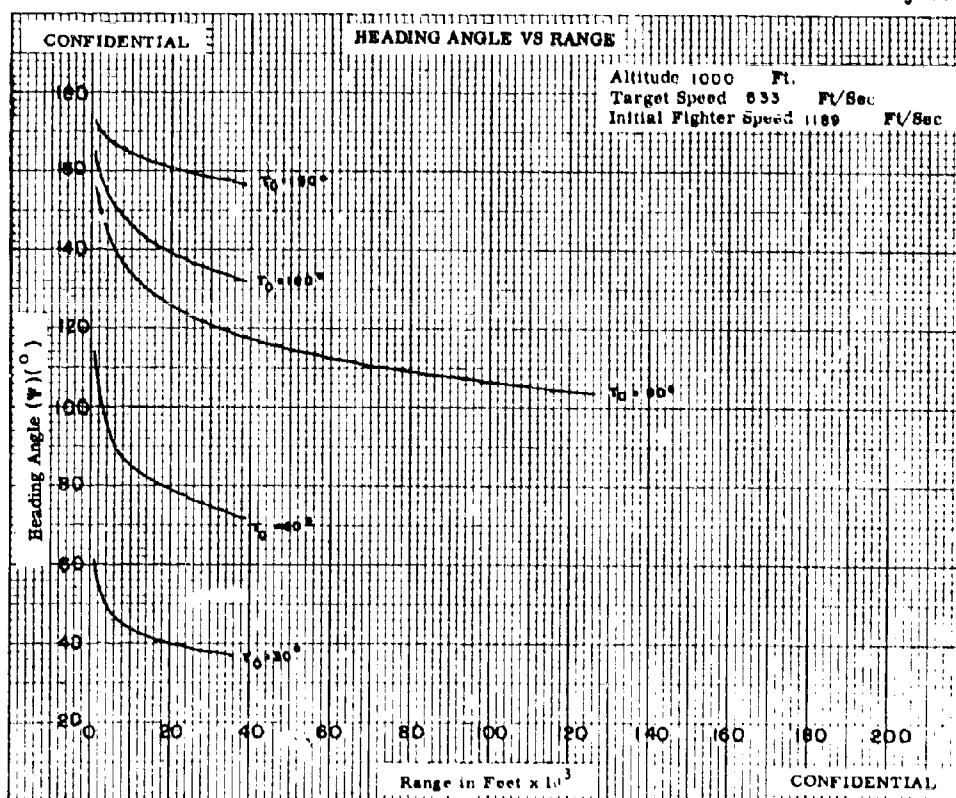


Fig. IV-8

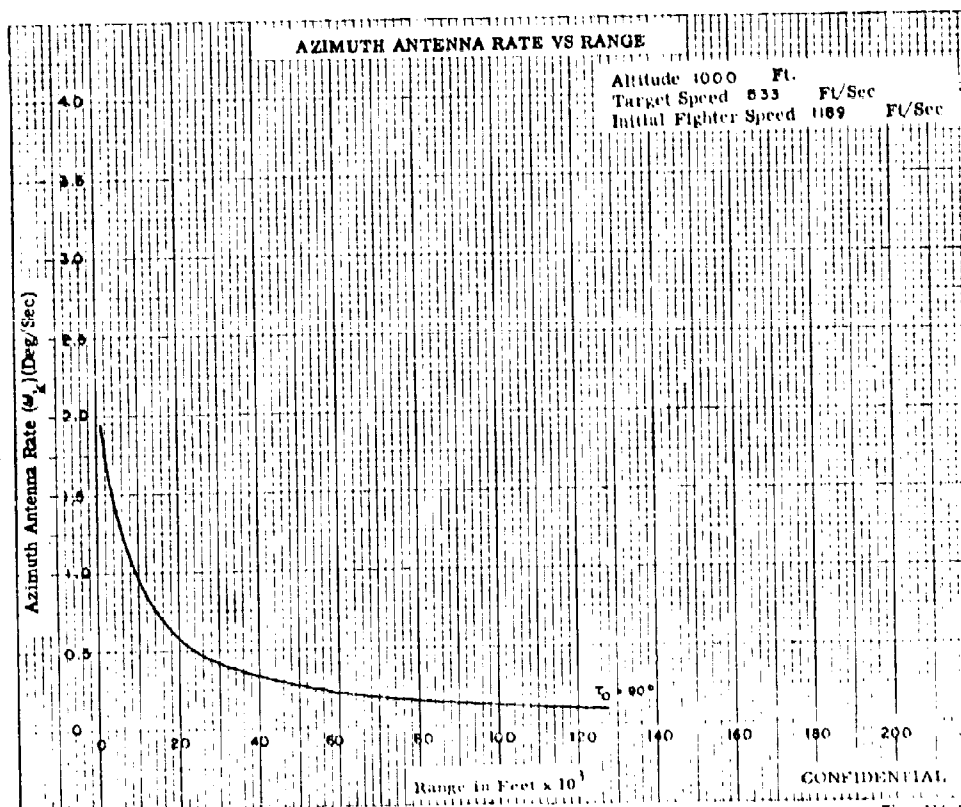
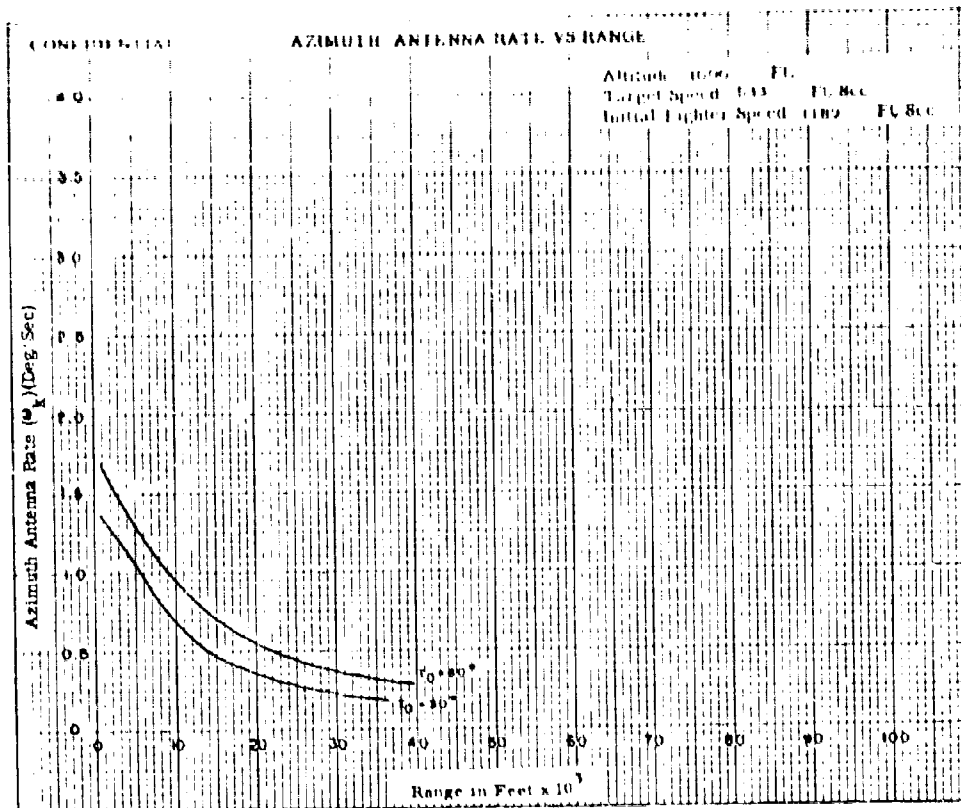


Fig. IV-9a

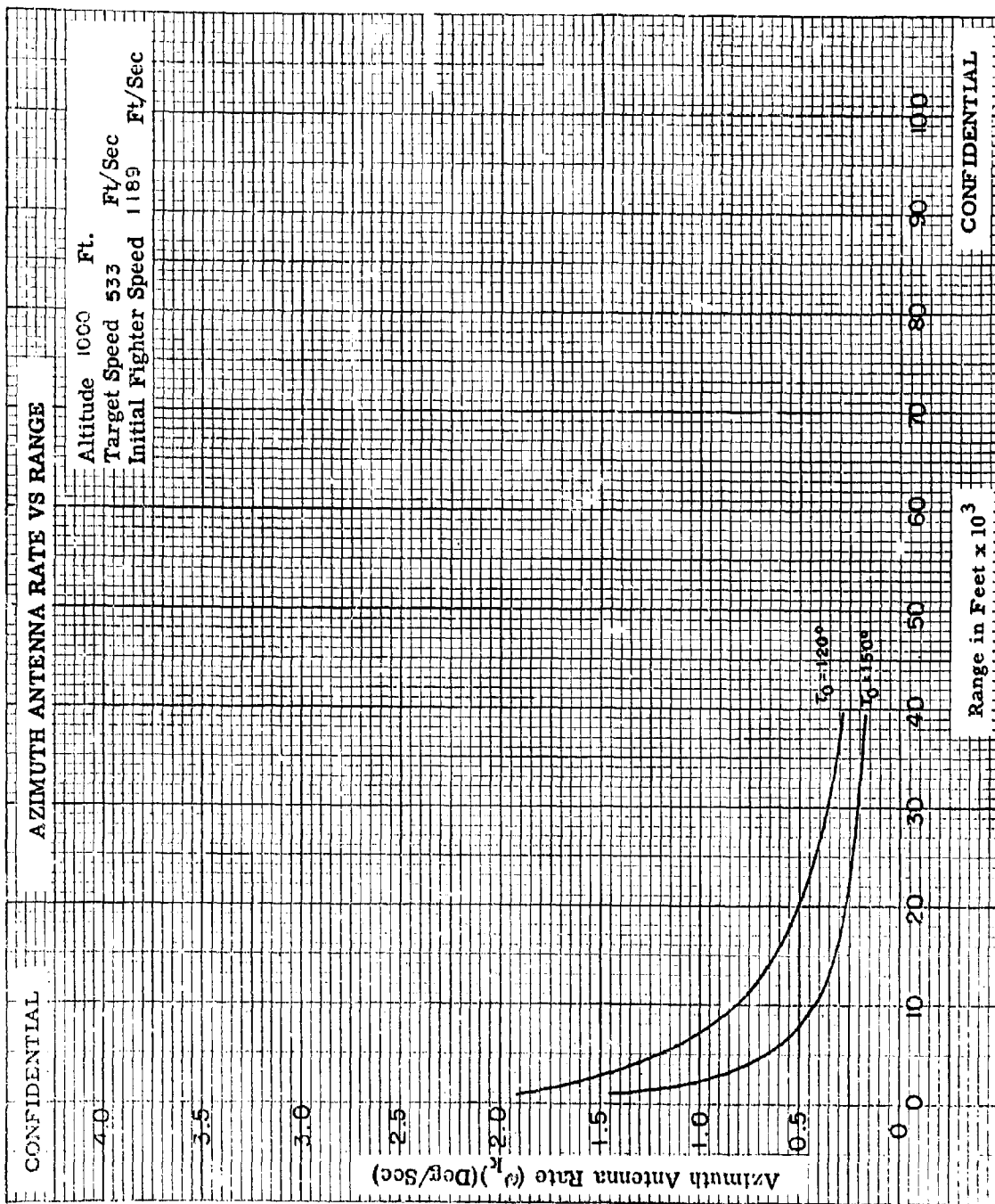


Fig. IV-9b

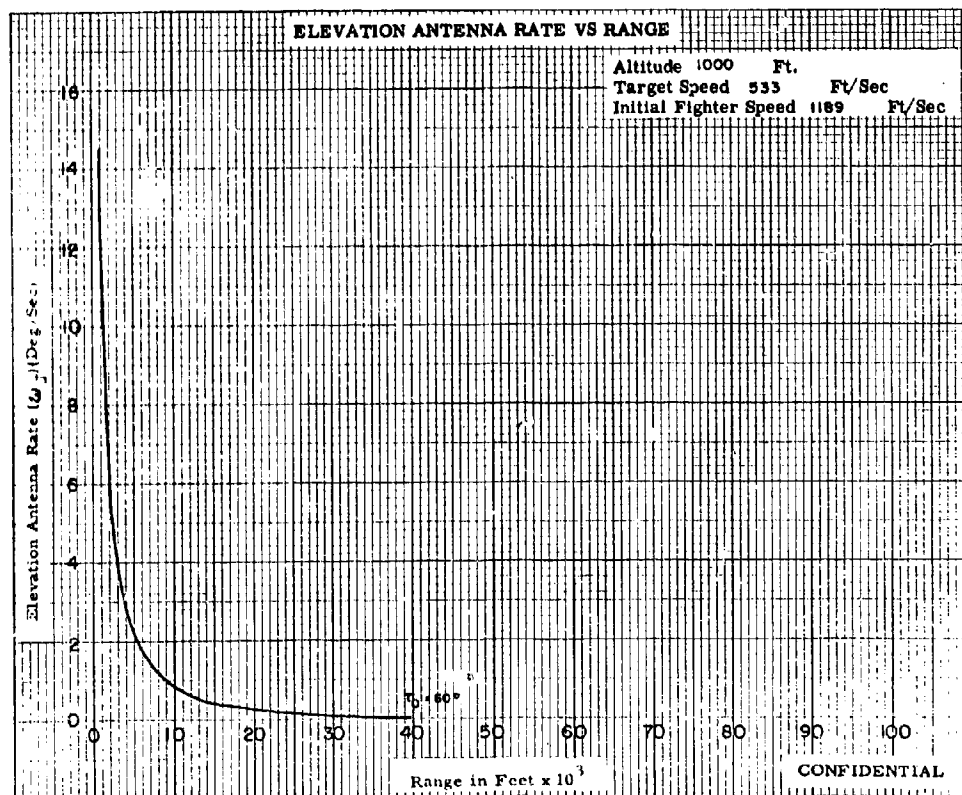
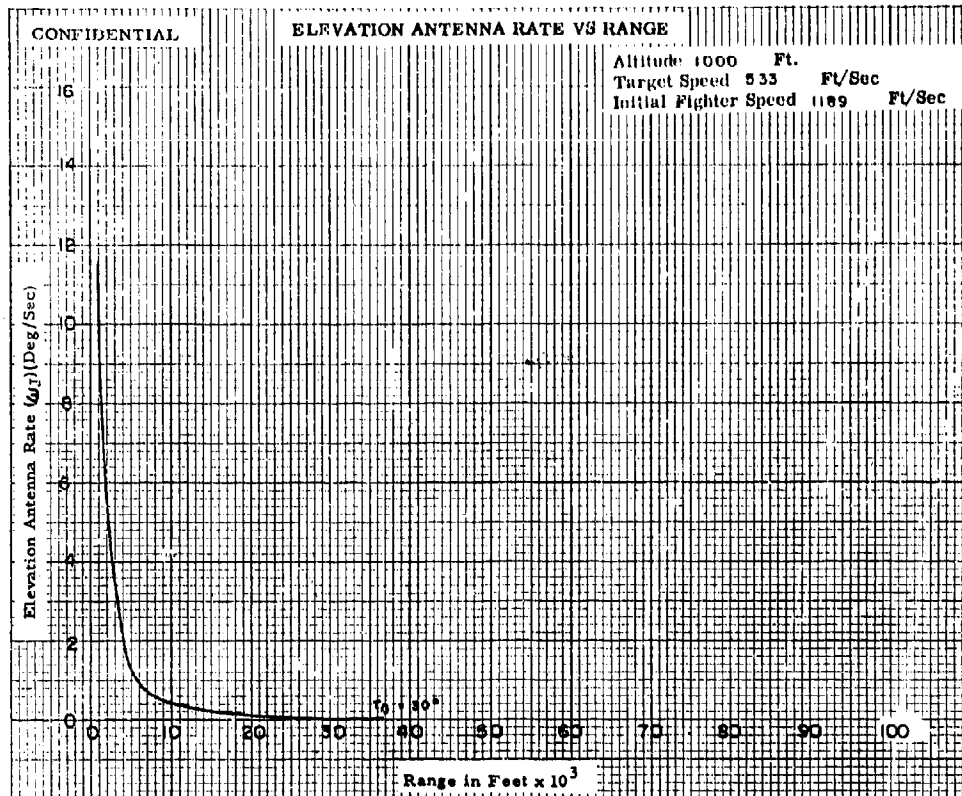


Fig. IV-10a

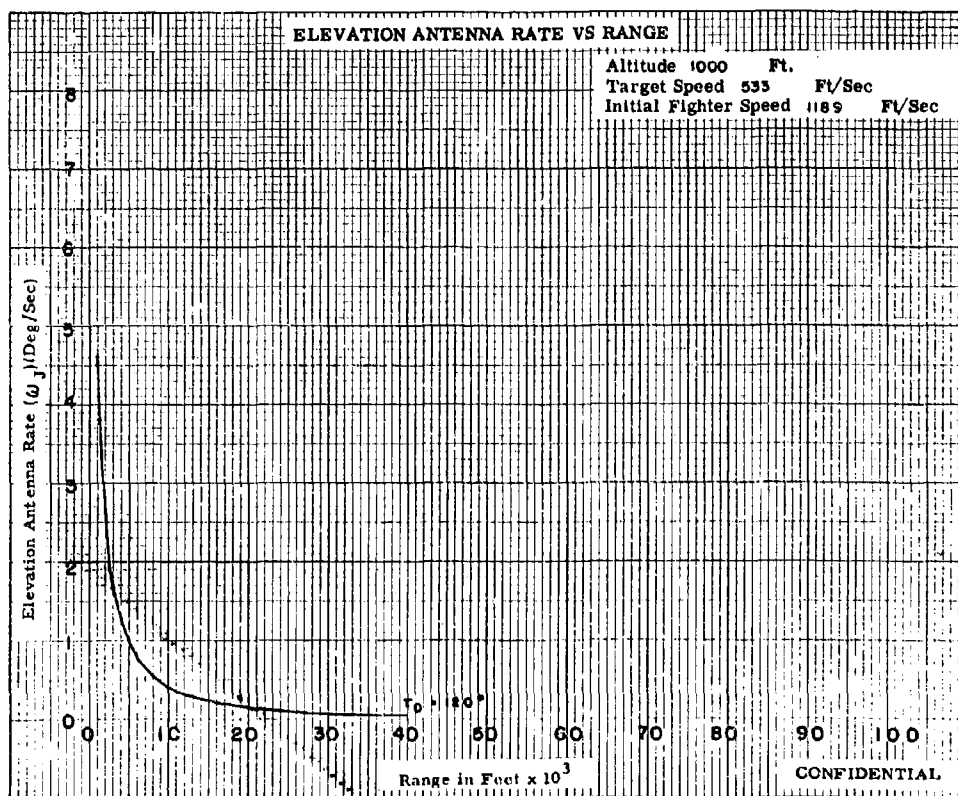
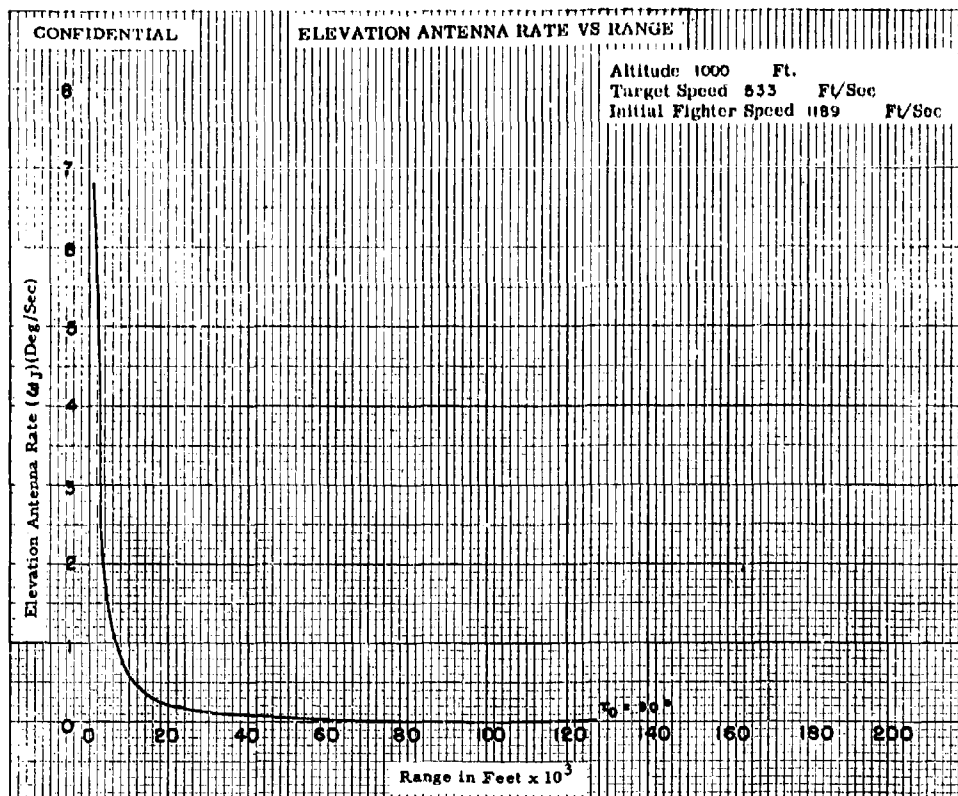


Fig. IV-10b

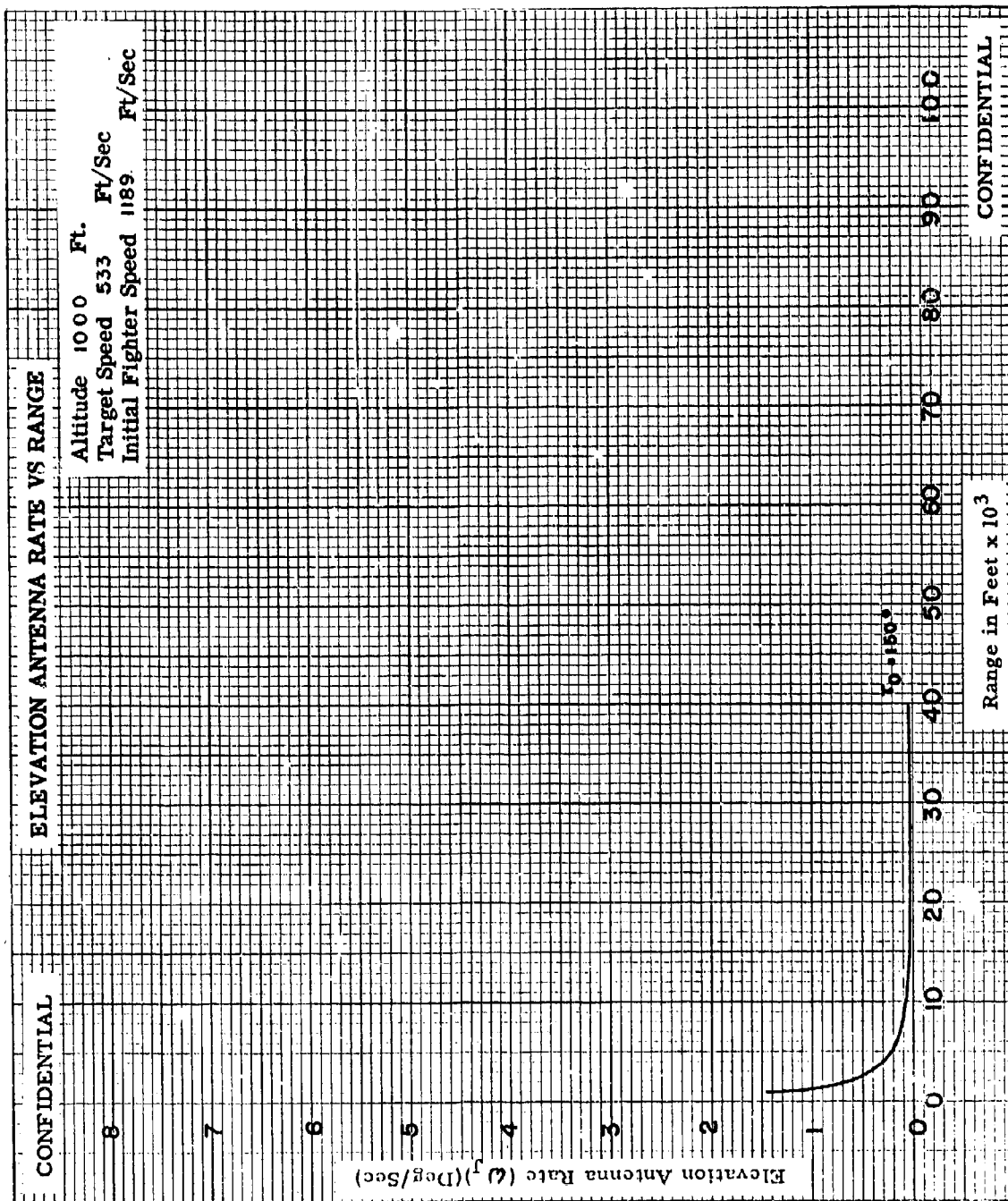


Fig. IV-10c

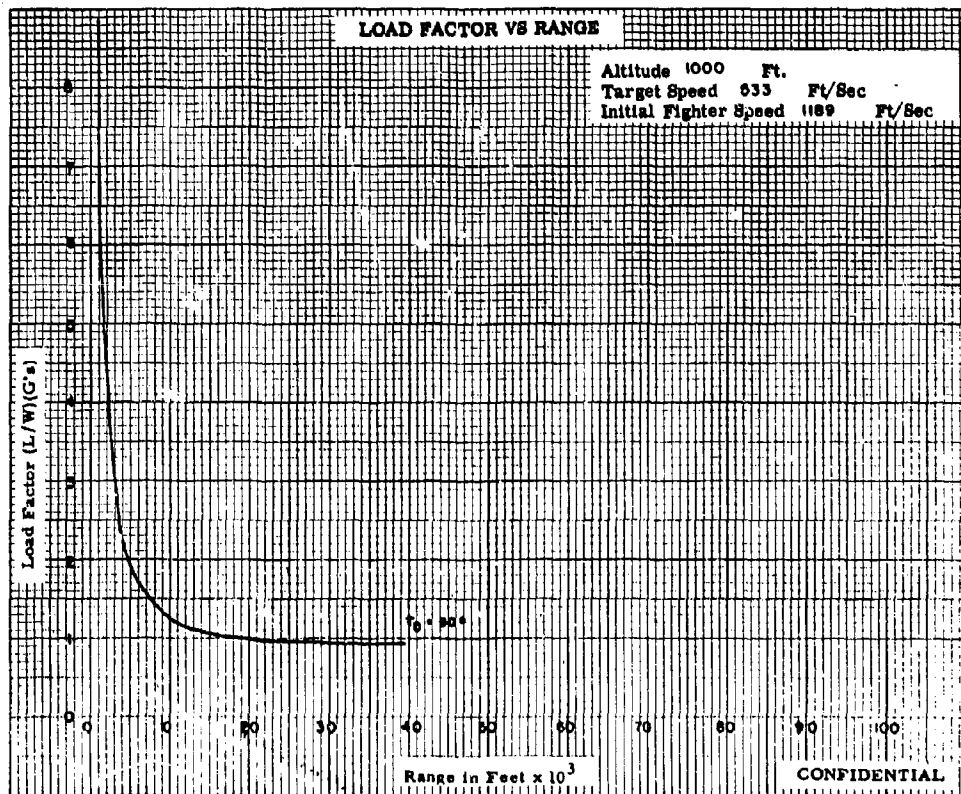
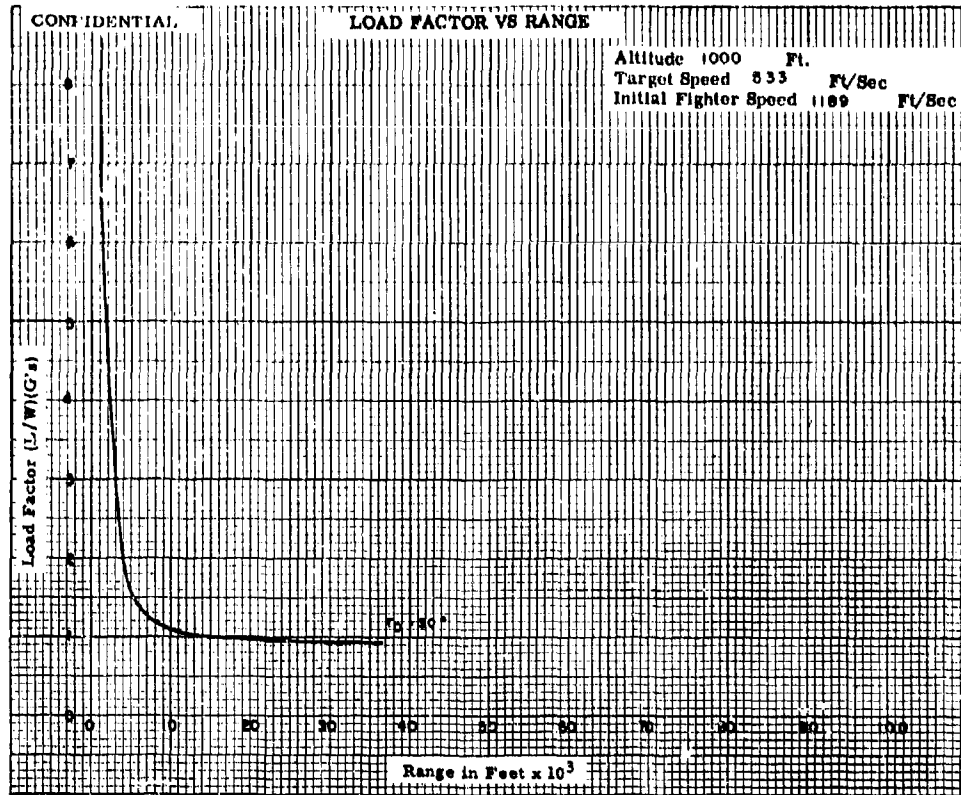


Fig. IV-11a

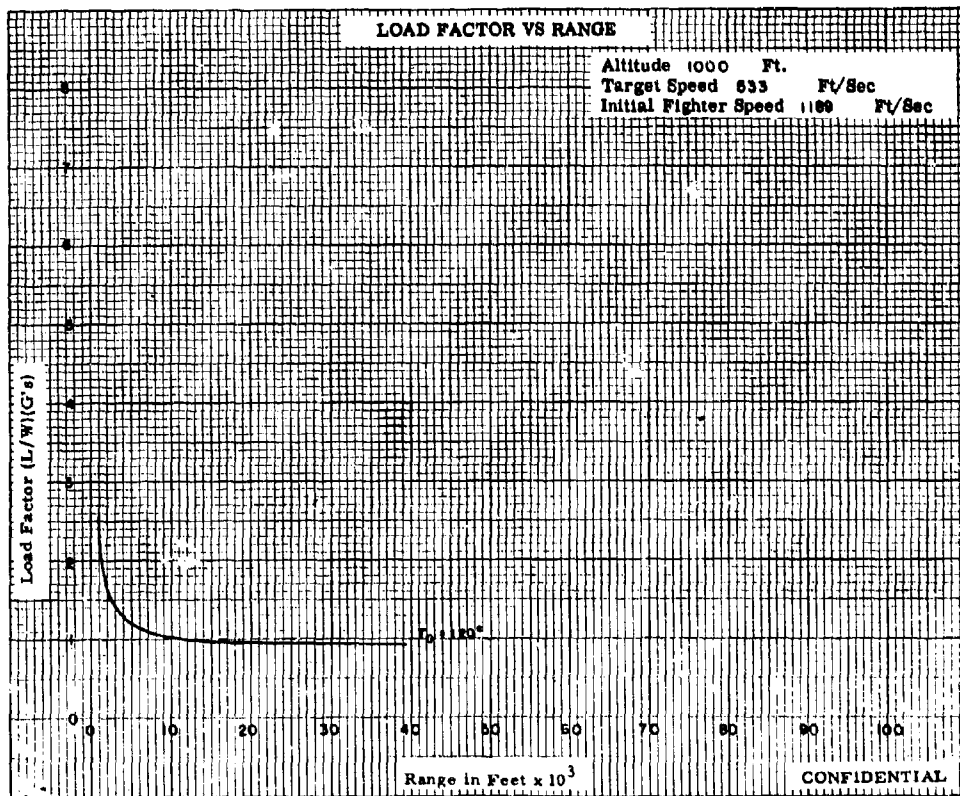
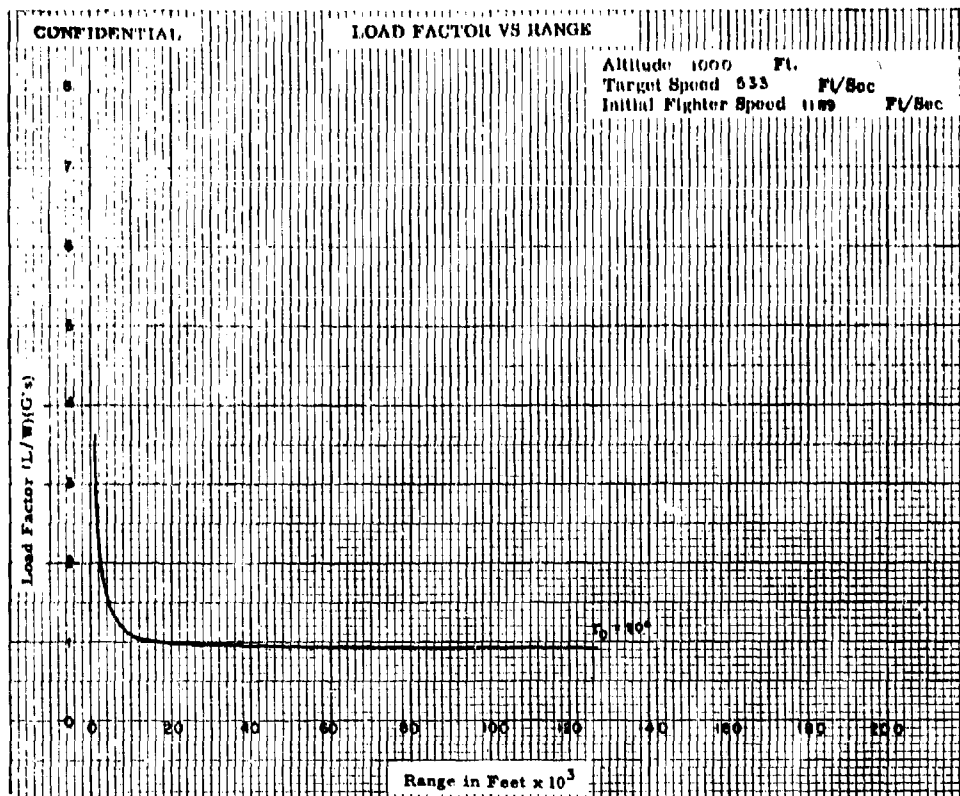


Fig. IV-11b

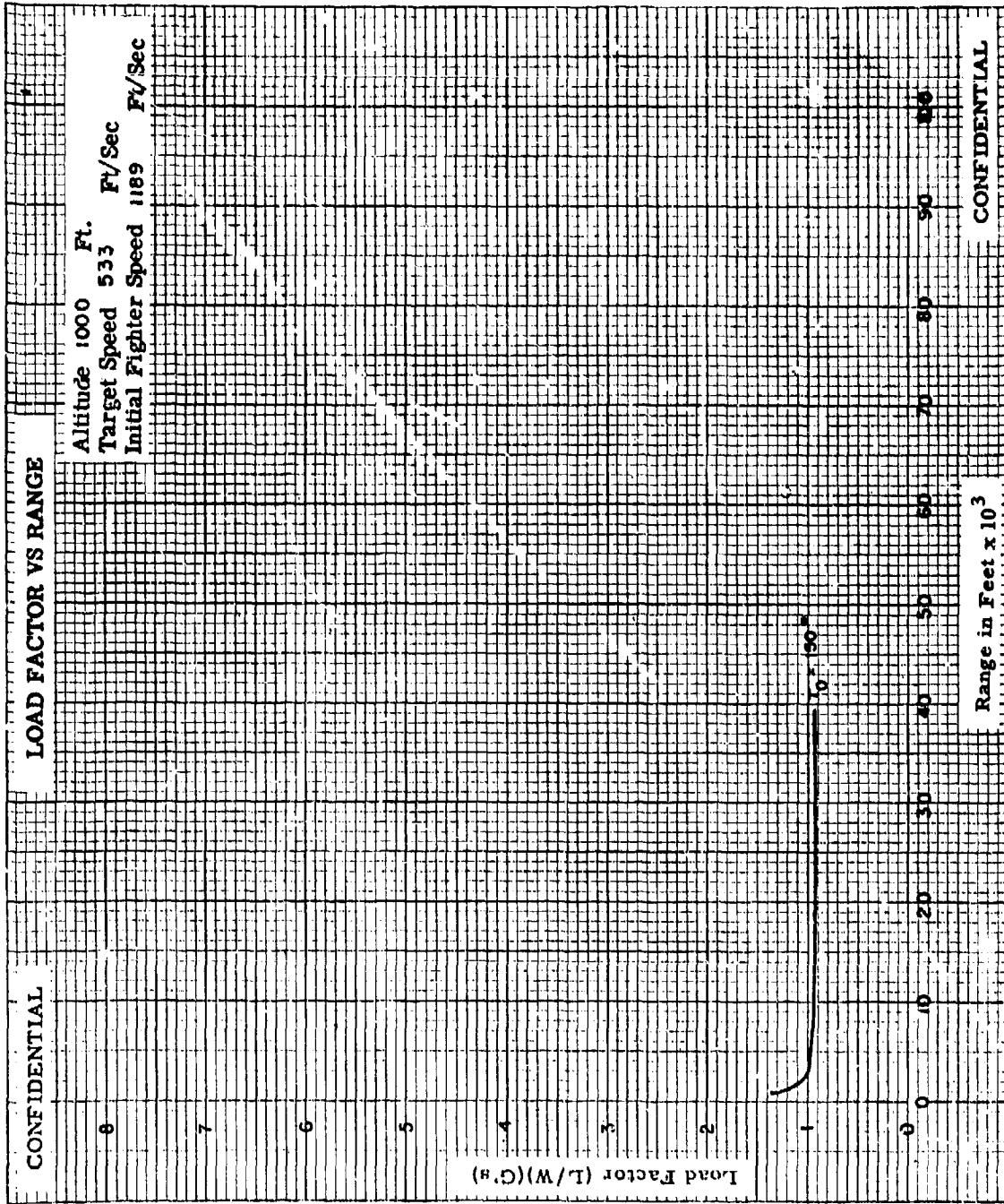


Fig. IV-11c

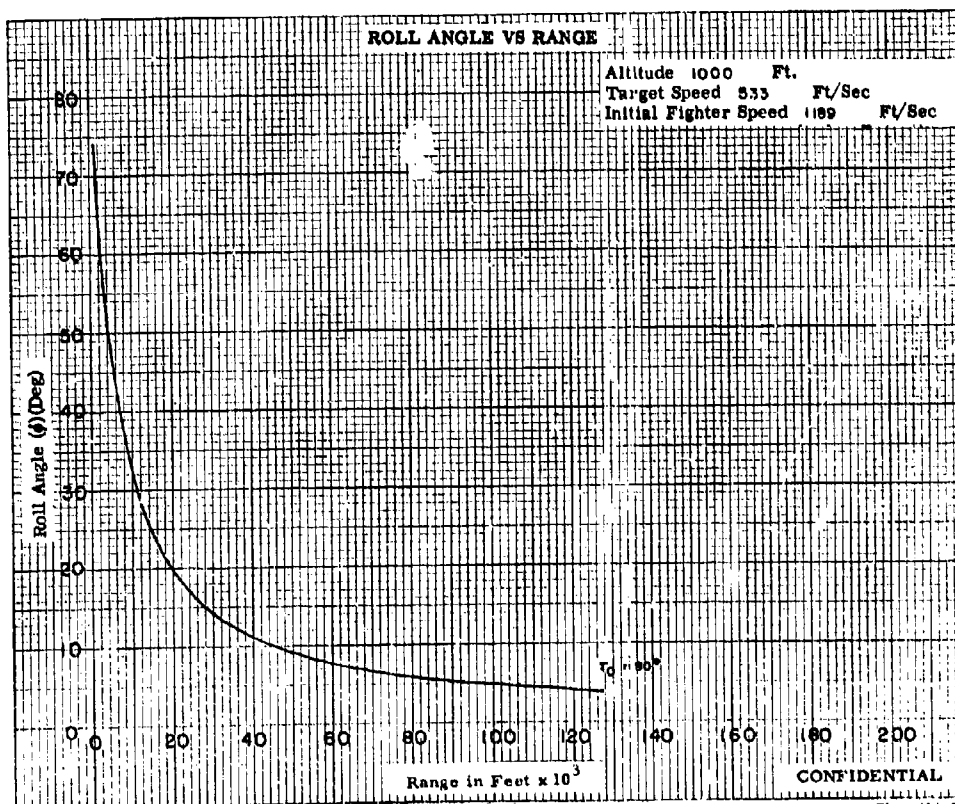
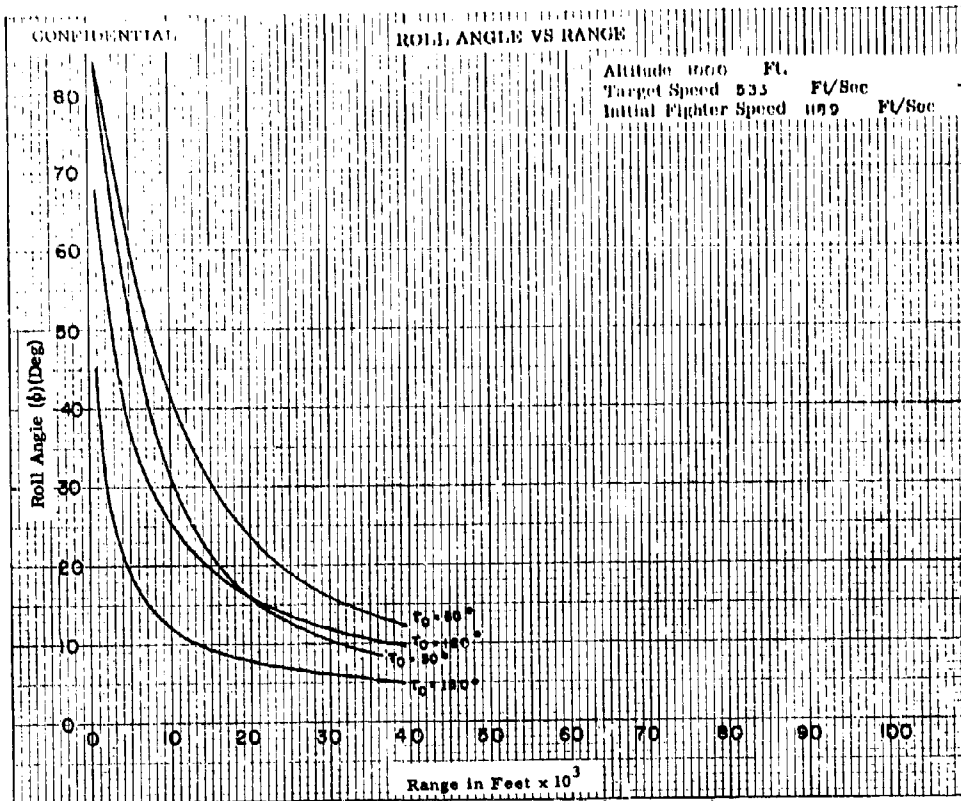


Fig. IV-12

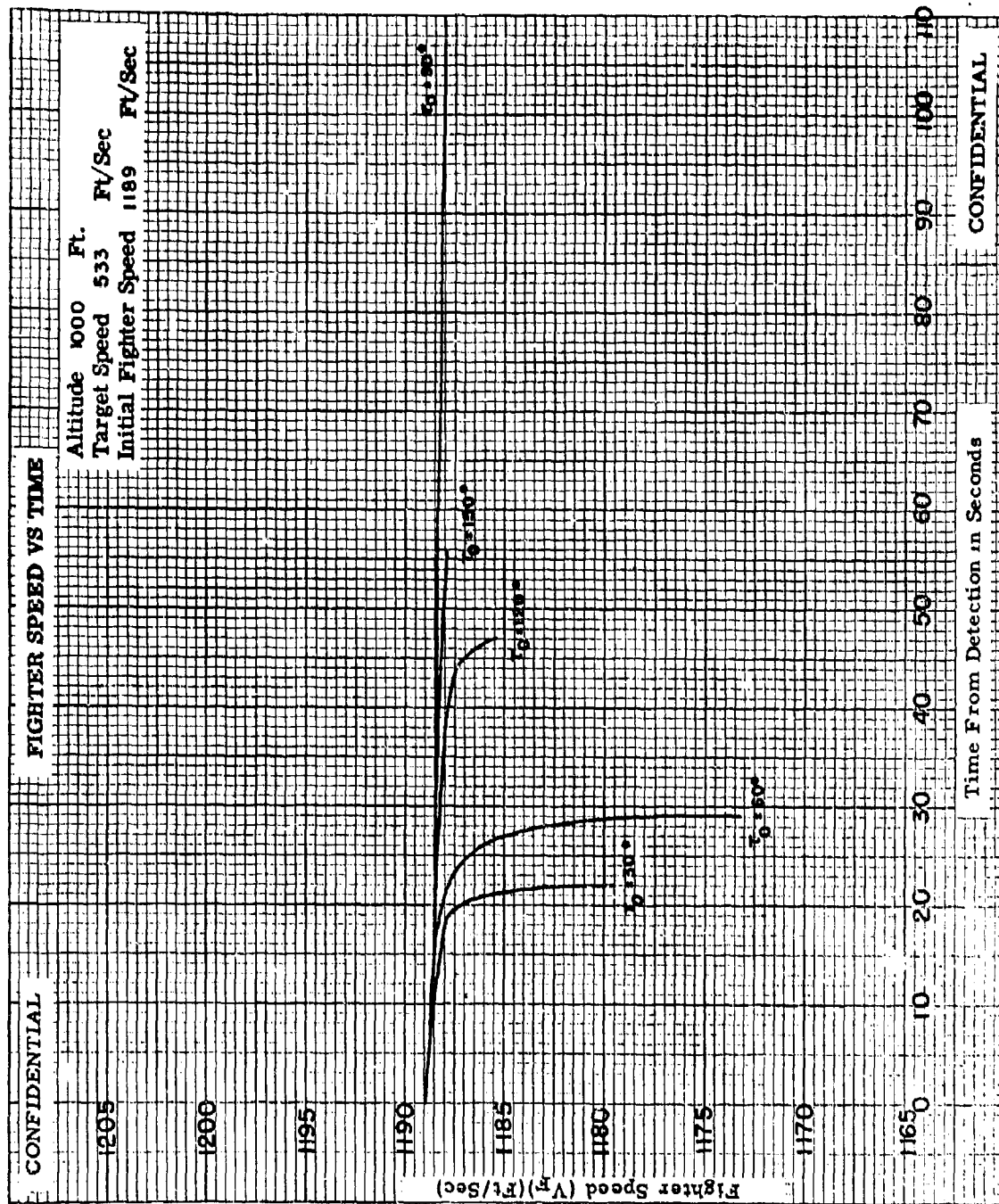


Fig. IV-13

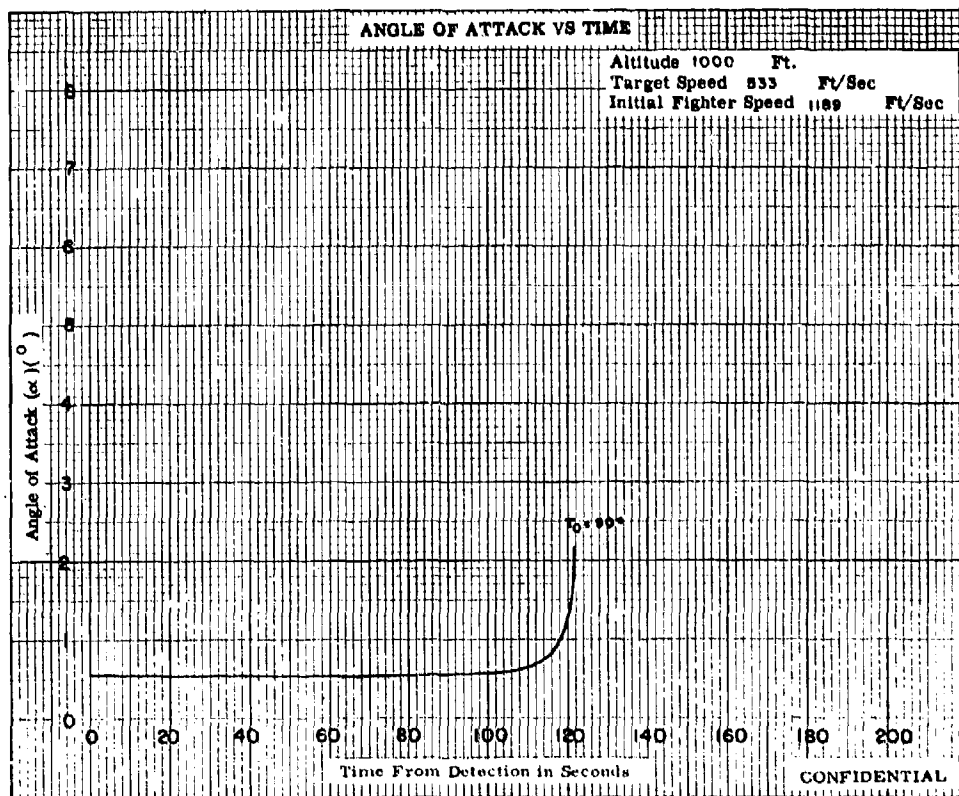
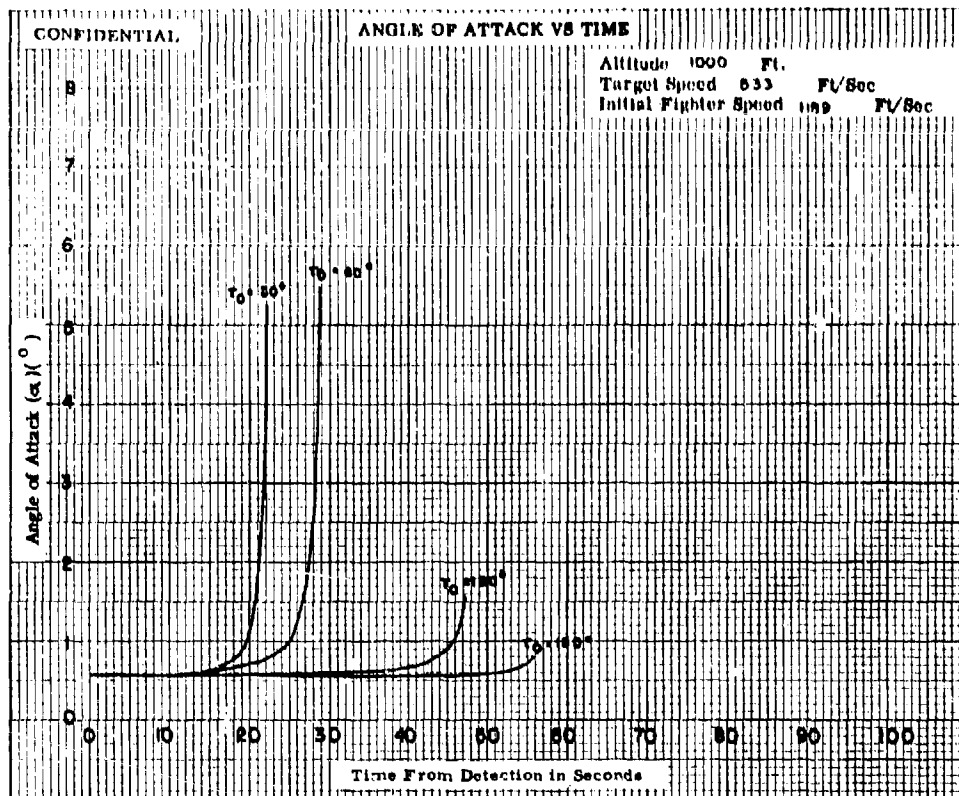
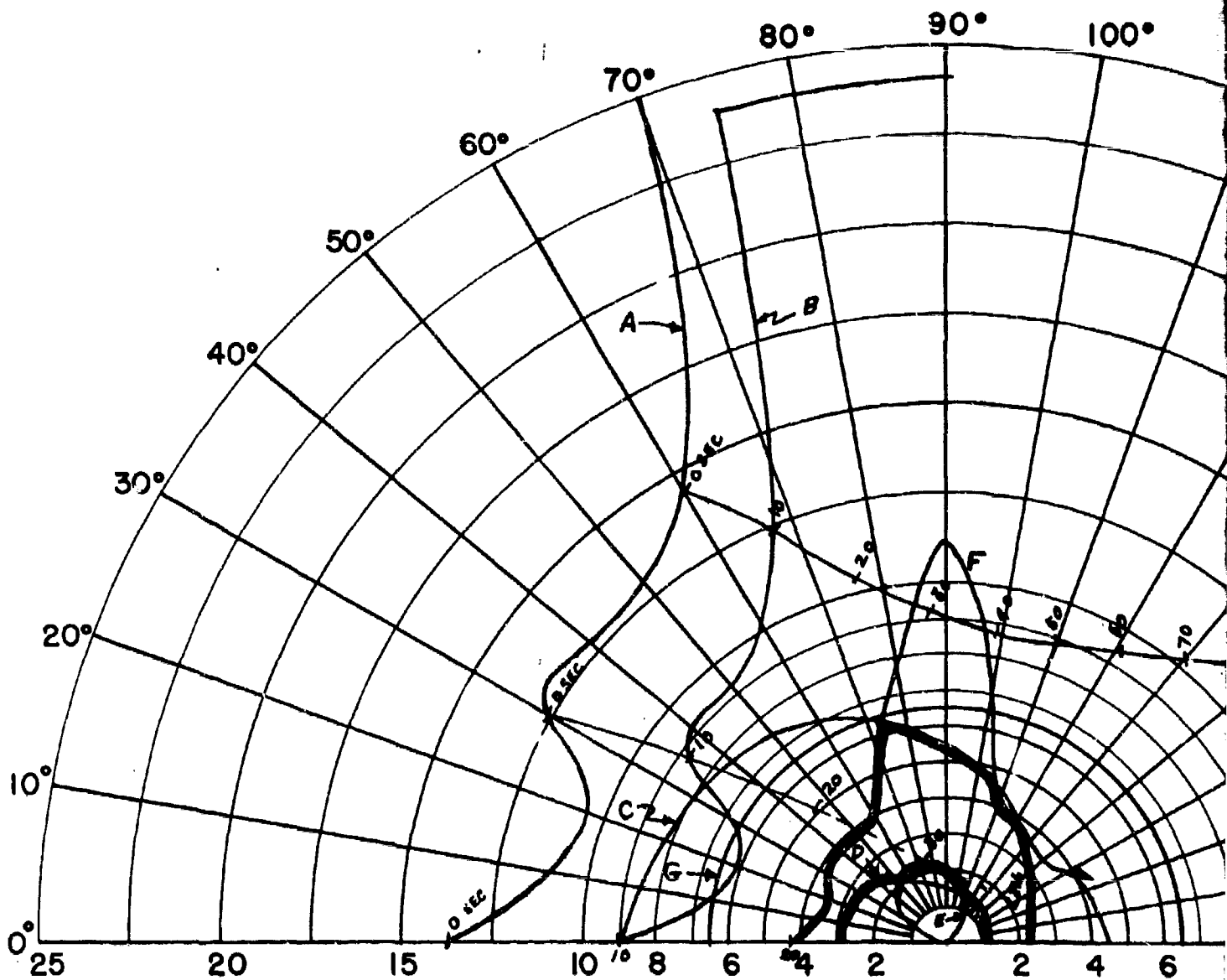


Fig. IV-14



$V_F = 873$ FT/SEC (F4H-1)(F8U-3)

$V_T = 1940$ FT/SEC

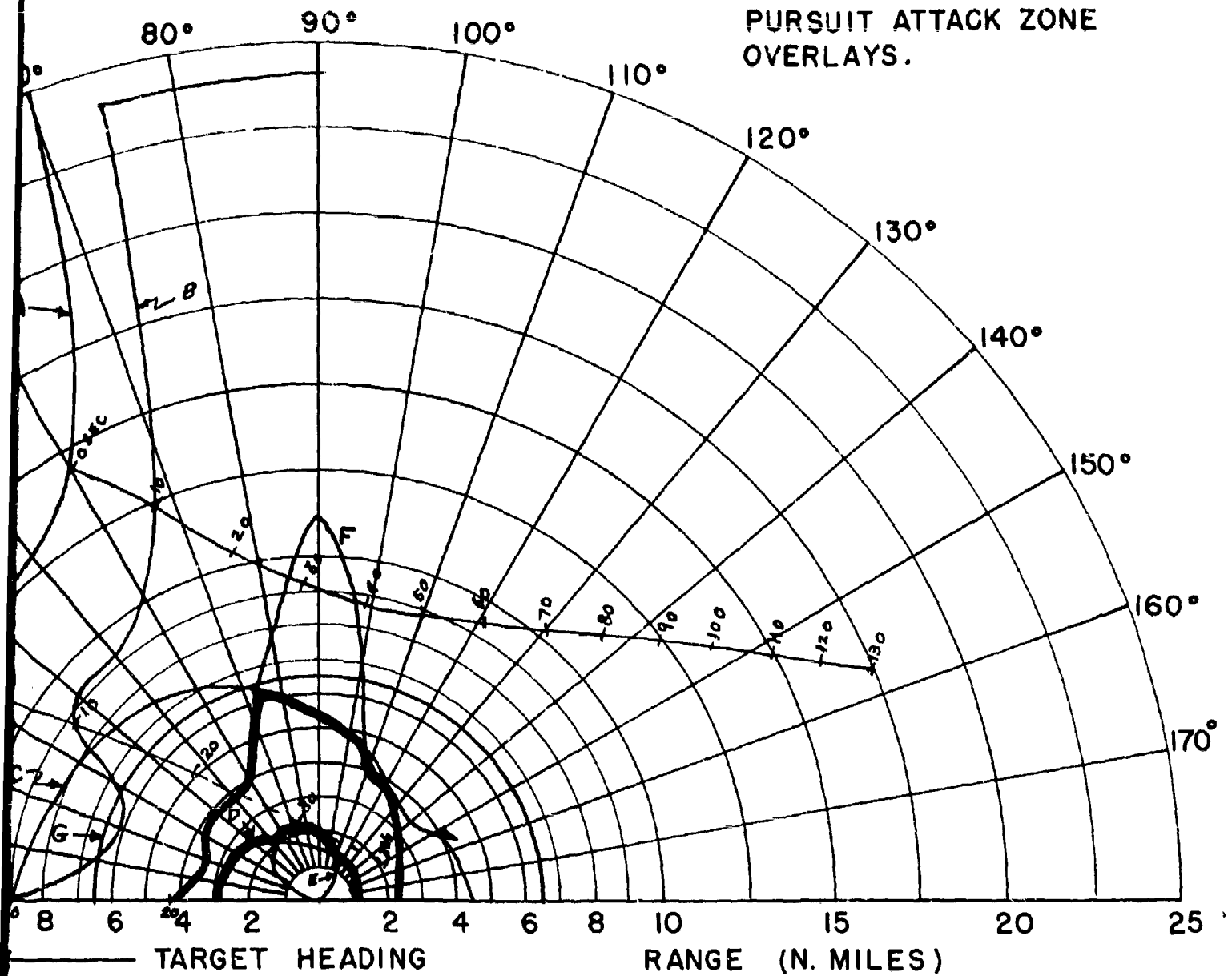
ALTITUDE = 50,000 FT.

INCREASED THRUST AT DETECTION

← TARGET HEADING

- A - 85% DETECTION RANGE
- B - LOCK-ON RANGE (10 SEC. LOCK-ON)
- C - SPARROW III MAX. AERODYNAMIC R
- D - SPARROW III MIN. AERODYNAMIC R
- E - CONSTANT LOAD FACTOR LOCUS (
- F - 90% SPARROW III SEEKER LOCK-C
- G - 6.5 N.M. INTERLOCK

FIG. V - CO-ALTITUDE LEAD
PURSUIT ATTACK ZONE
OVERLAYS.



- 85% DETECTION RANGE
- LOCK-ON RANGE (10 SEC. LOCK-ON TIME)
- SPARROW III MAX. AERODYNAMIC RANGE
- SPARROW III MIN. AERODYNAMIC RANGE
- CONSTANT LOAD FACTOR LOCUS ($N_z = 3$)
- 90% SPARROW III SEEKER LOCK-ON RANGE
- 6.5 N.M. INTERLOCK

CONFIDENTIAL

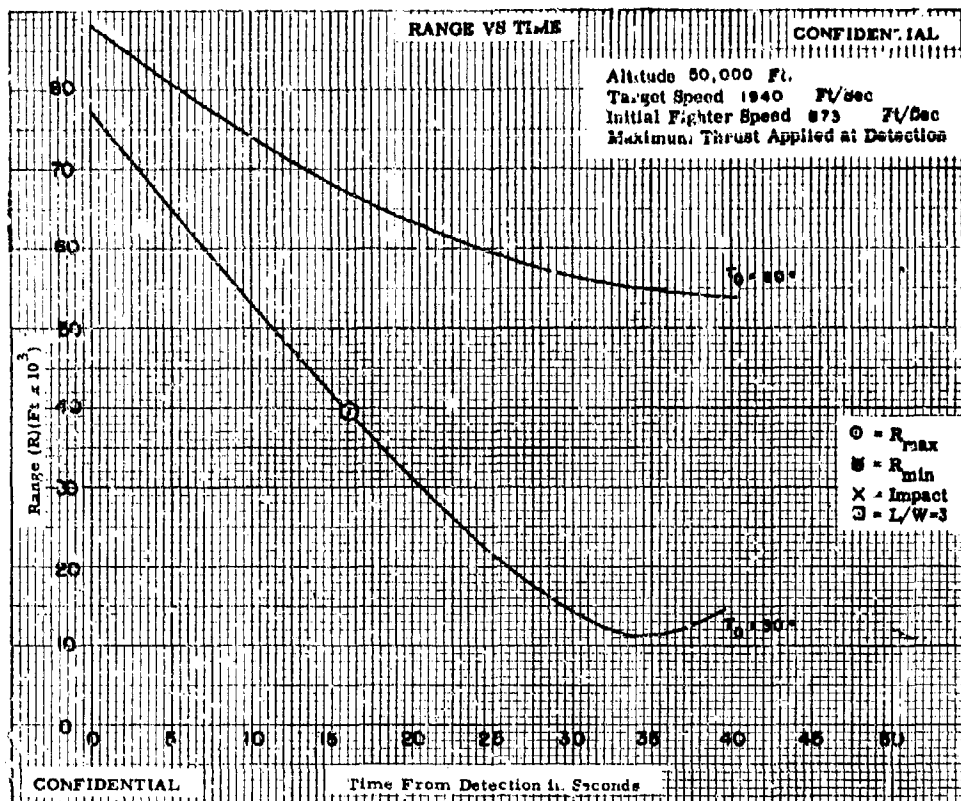


Fig. V-1

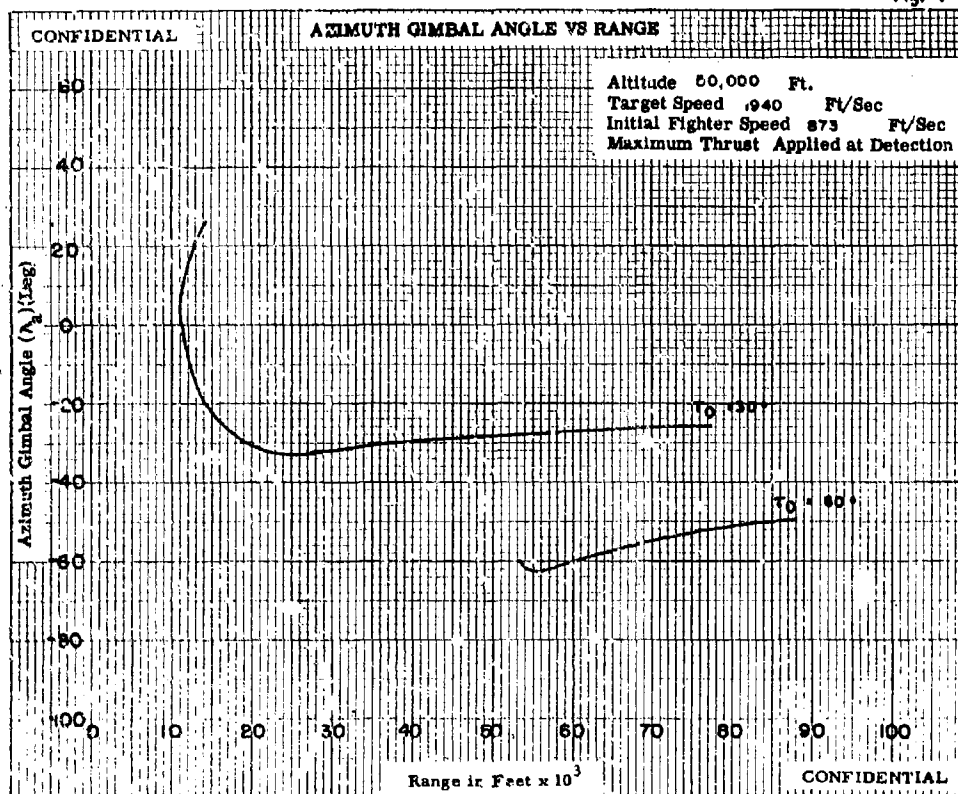


Fig. V-2

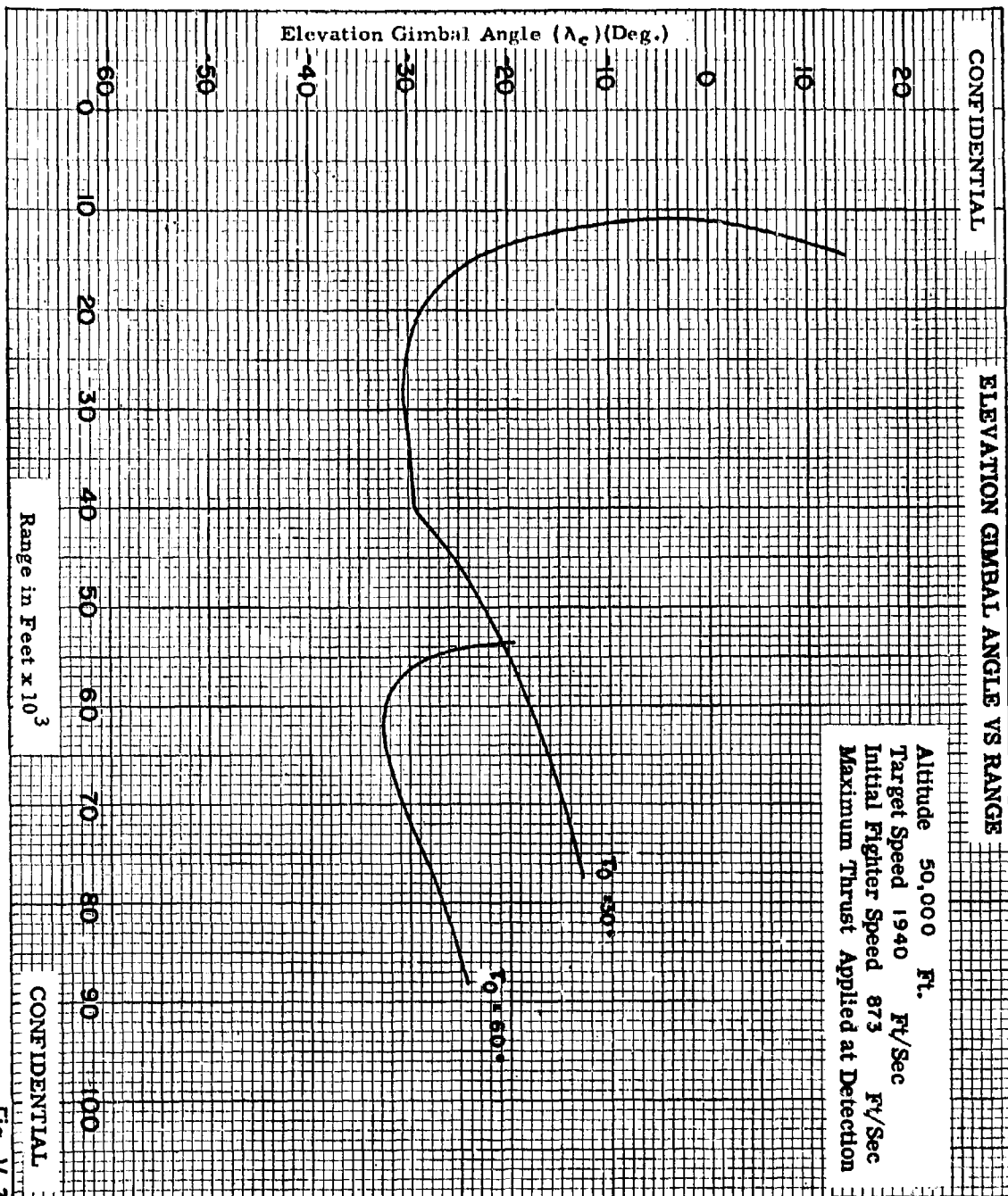


Fig. V-3

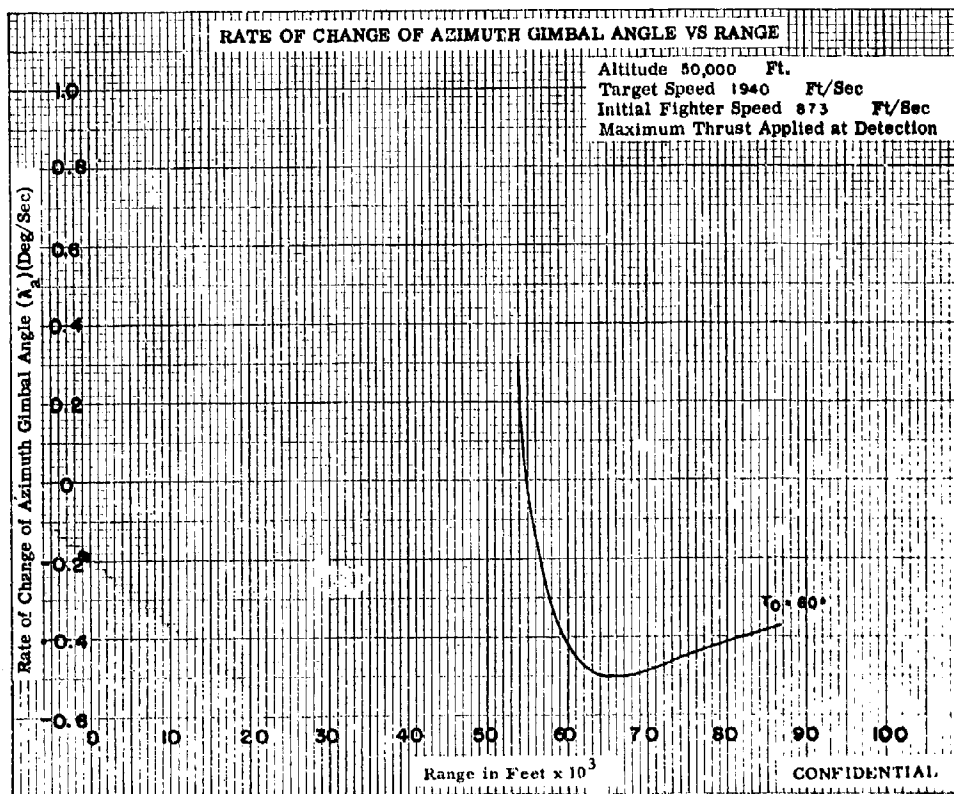
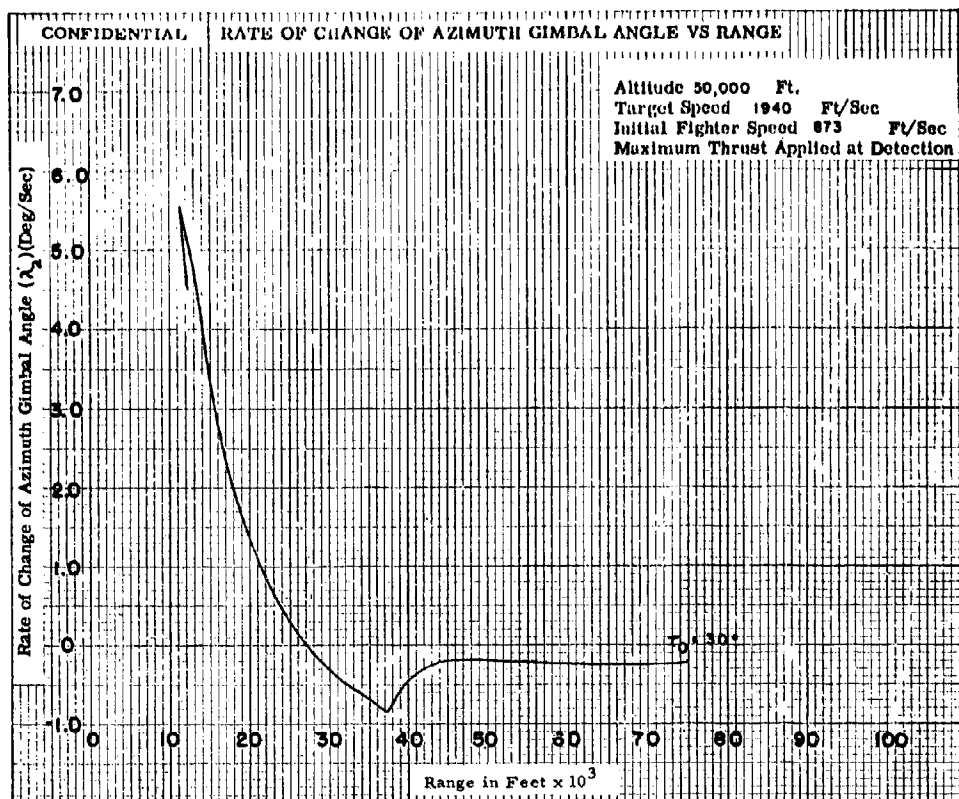
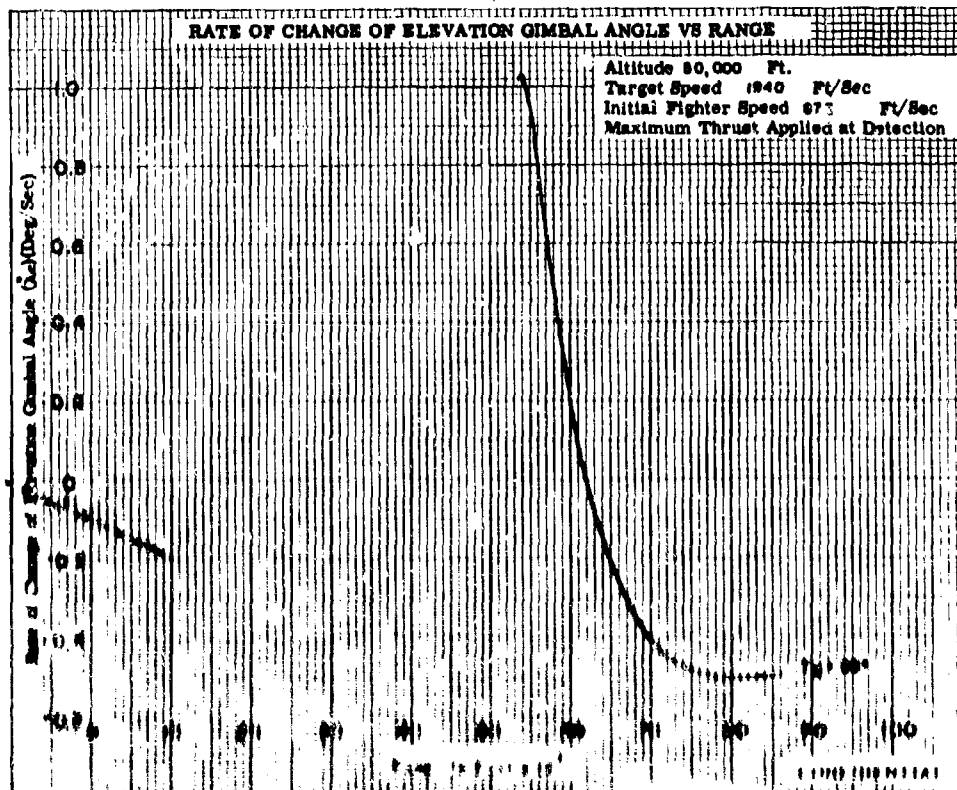
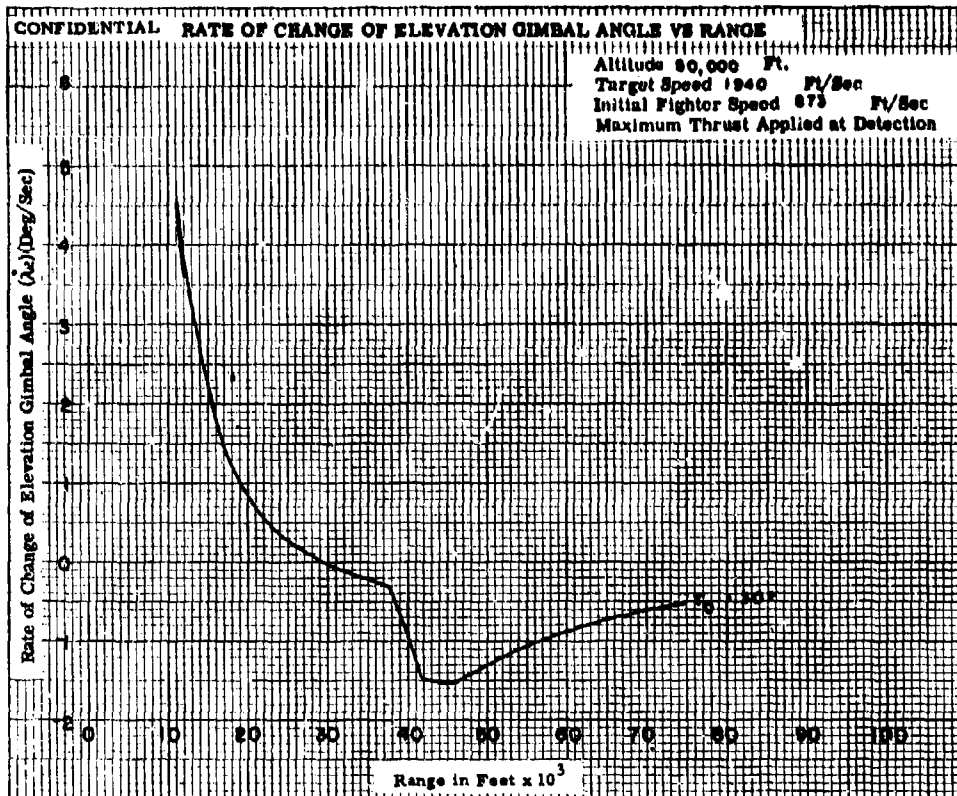


Fig. V-4



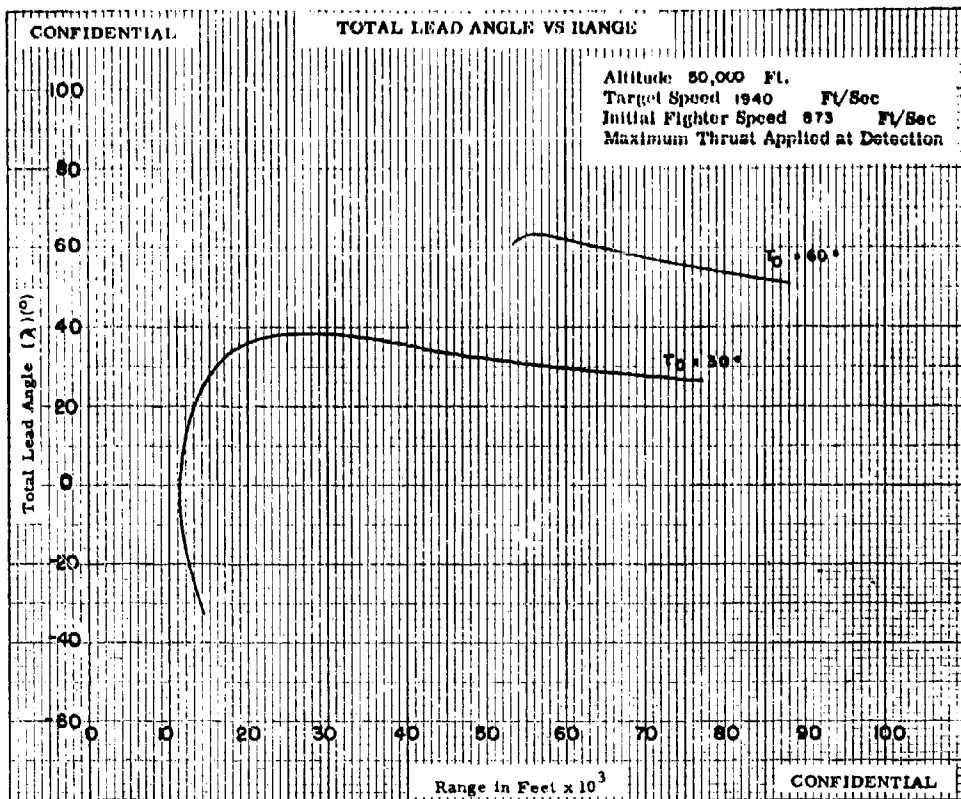


Fig. V-6

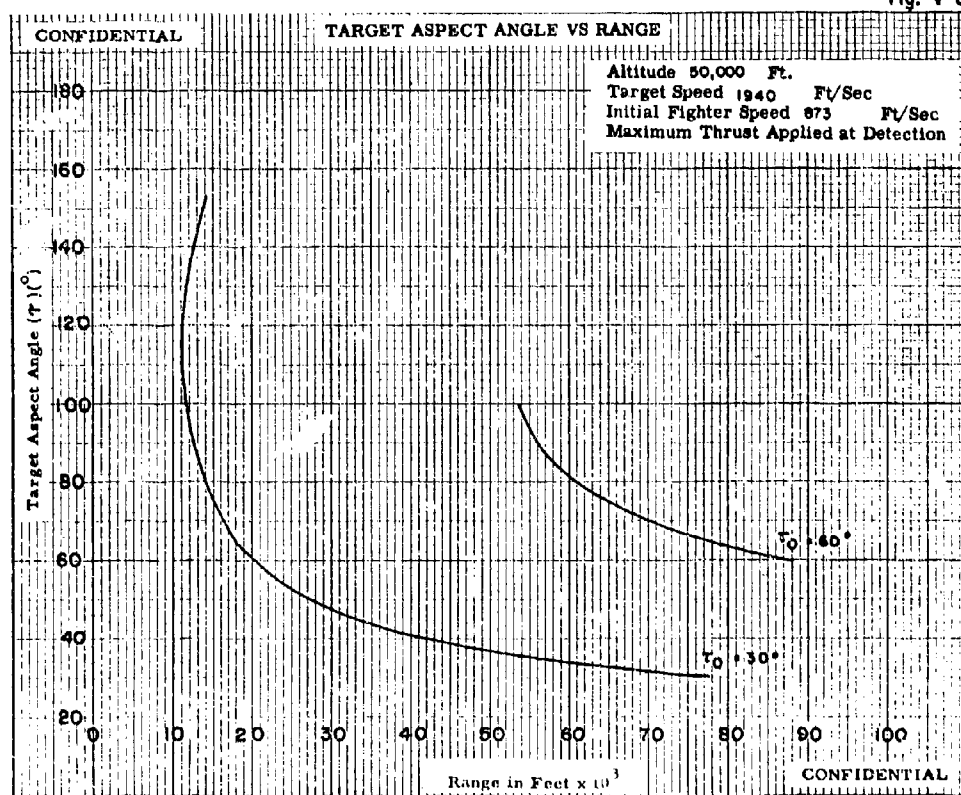


Fig. V-7

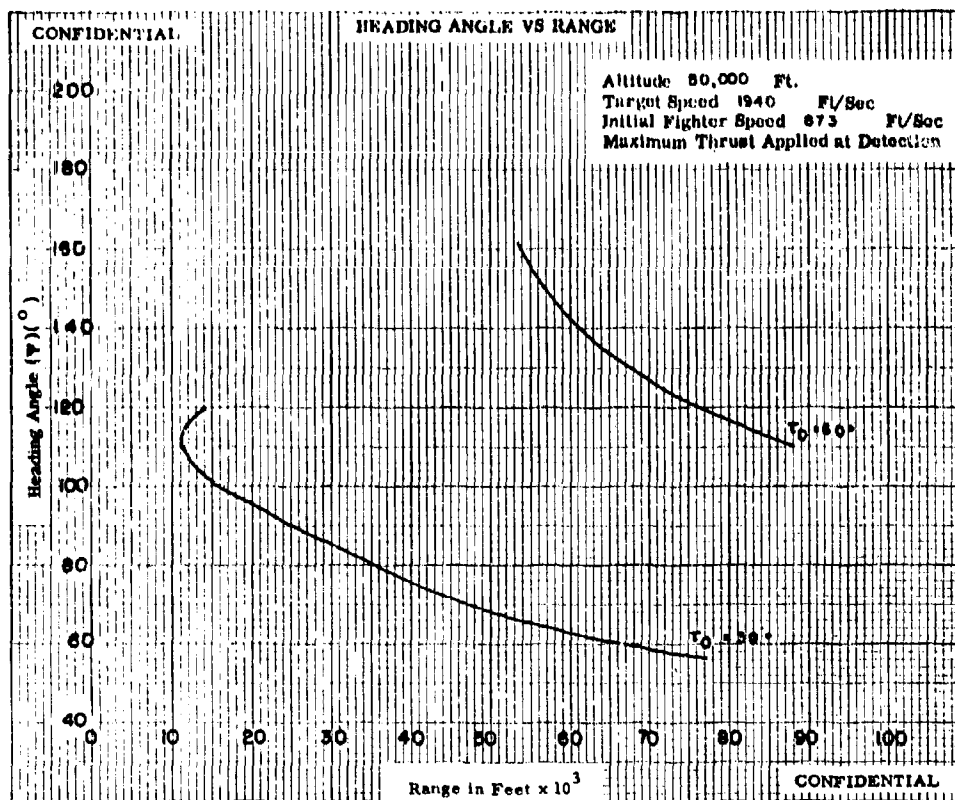


Fig. V-8

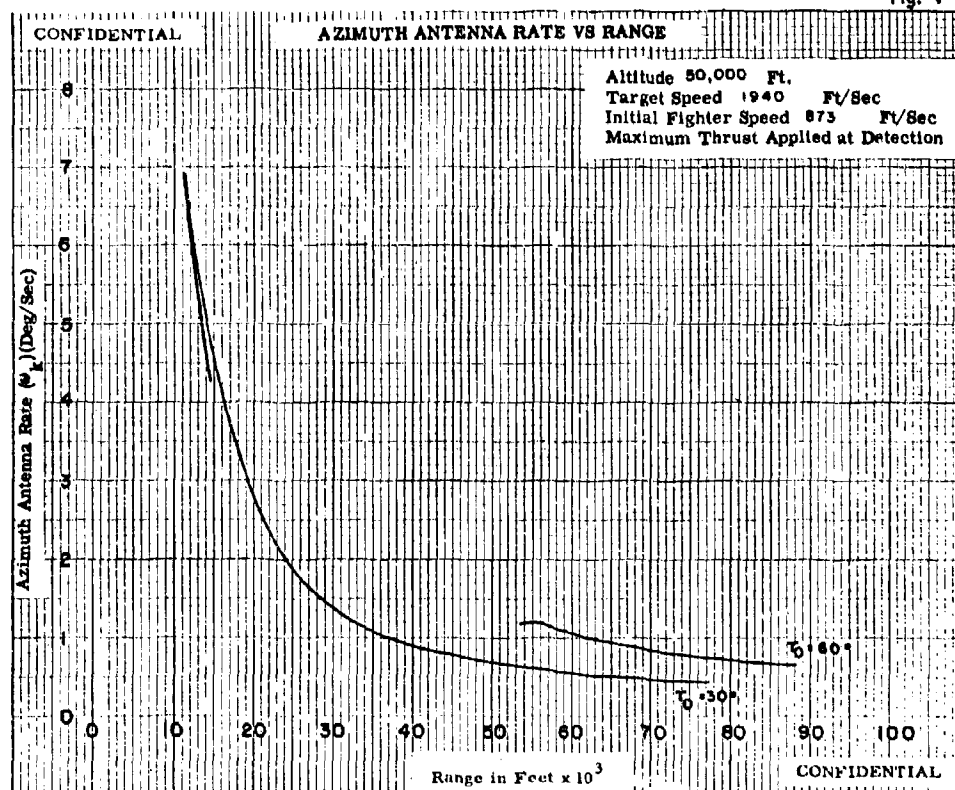


Fig. V-9

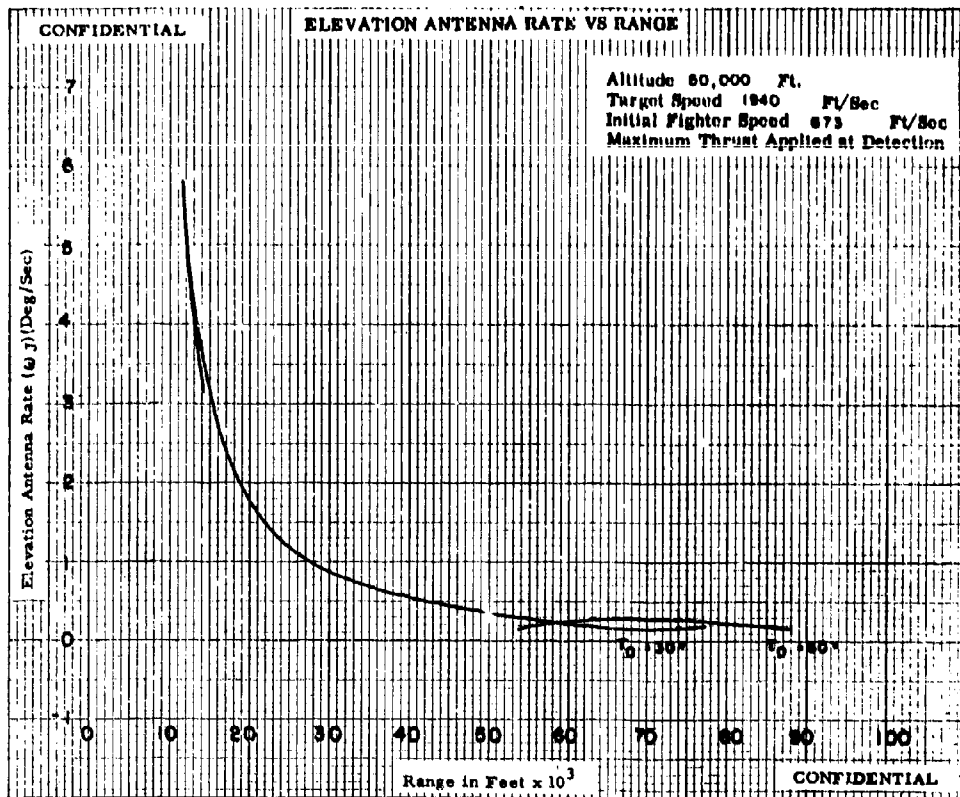


Fig. V-10

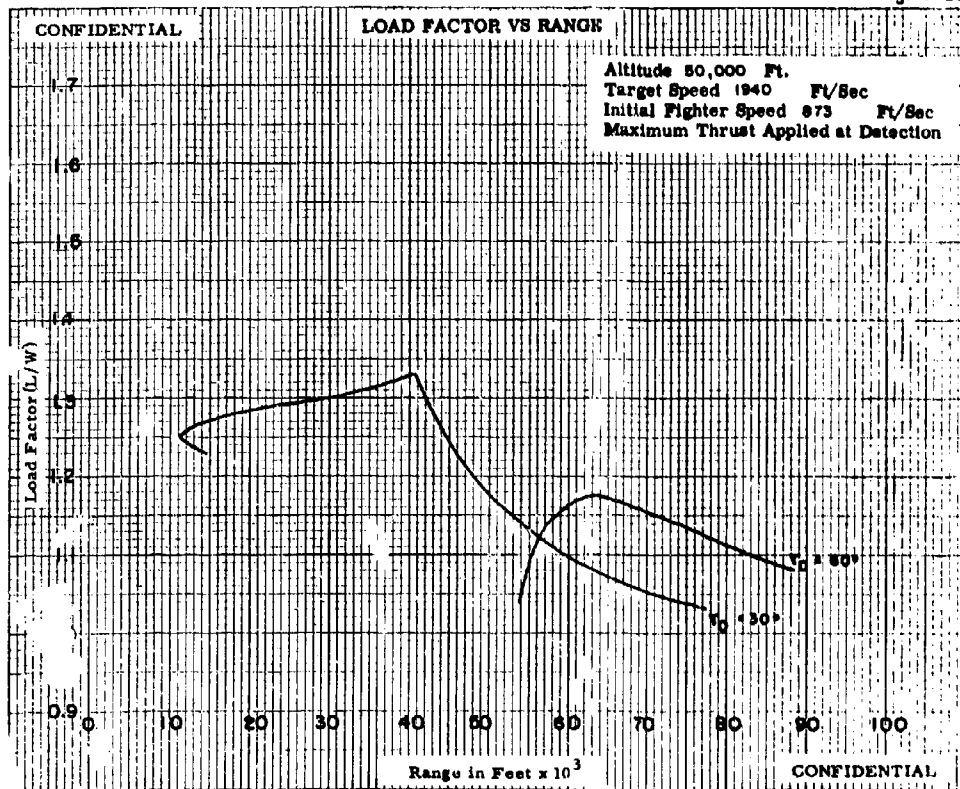


Fig. V-11

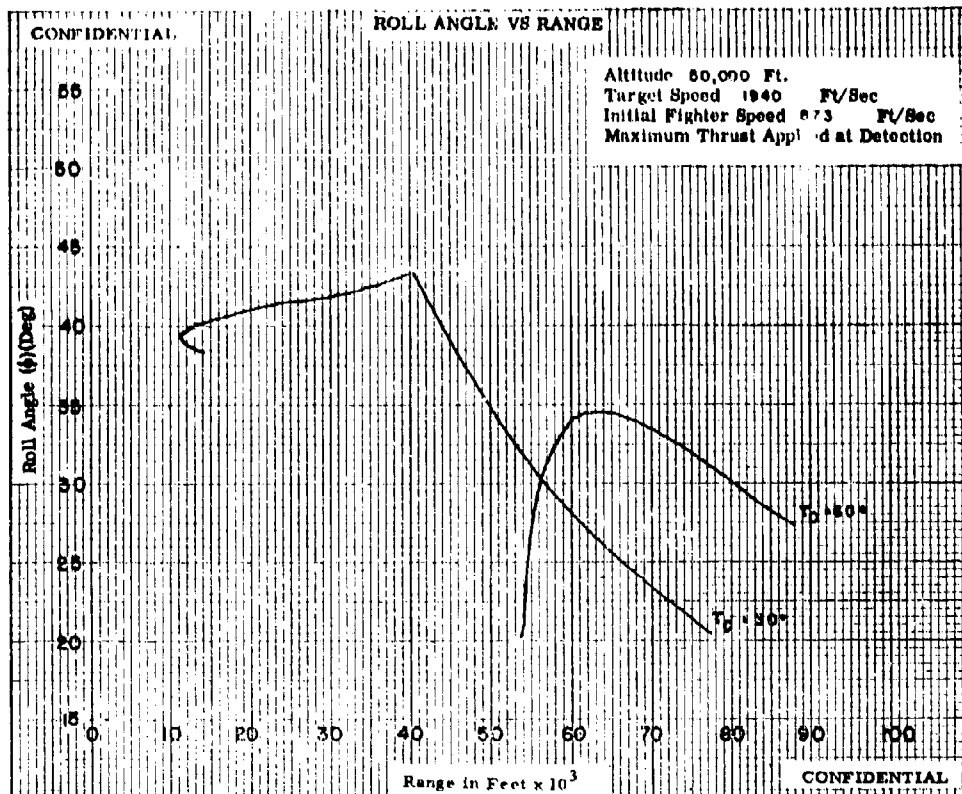


Fig. V-12

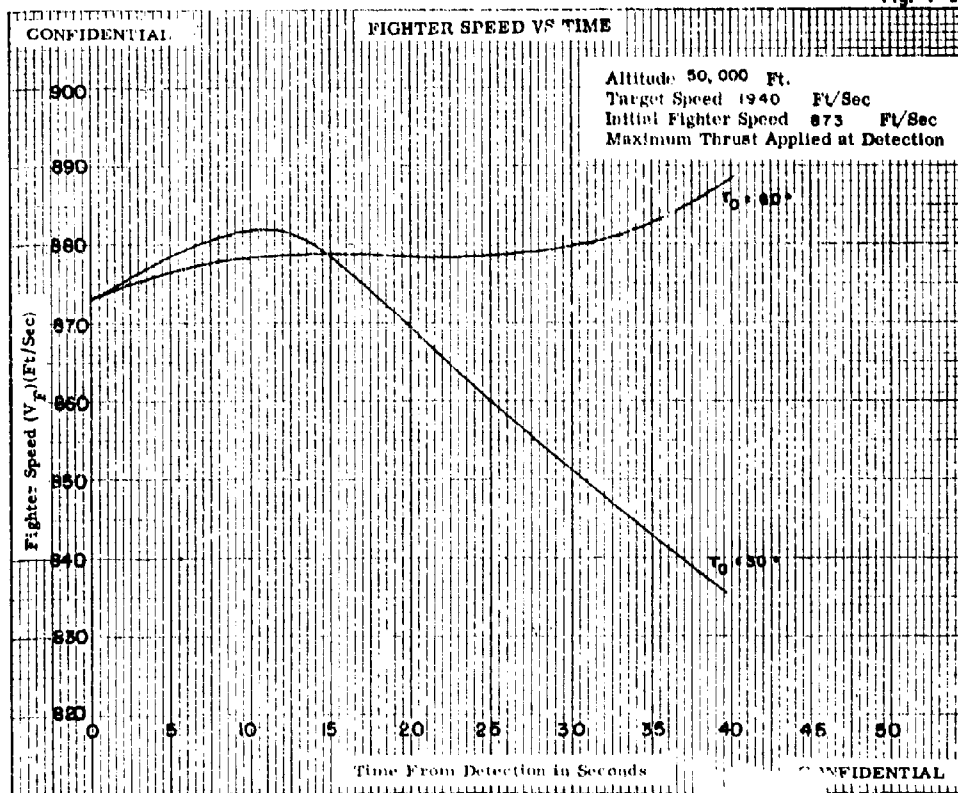


Fig. V-13

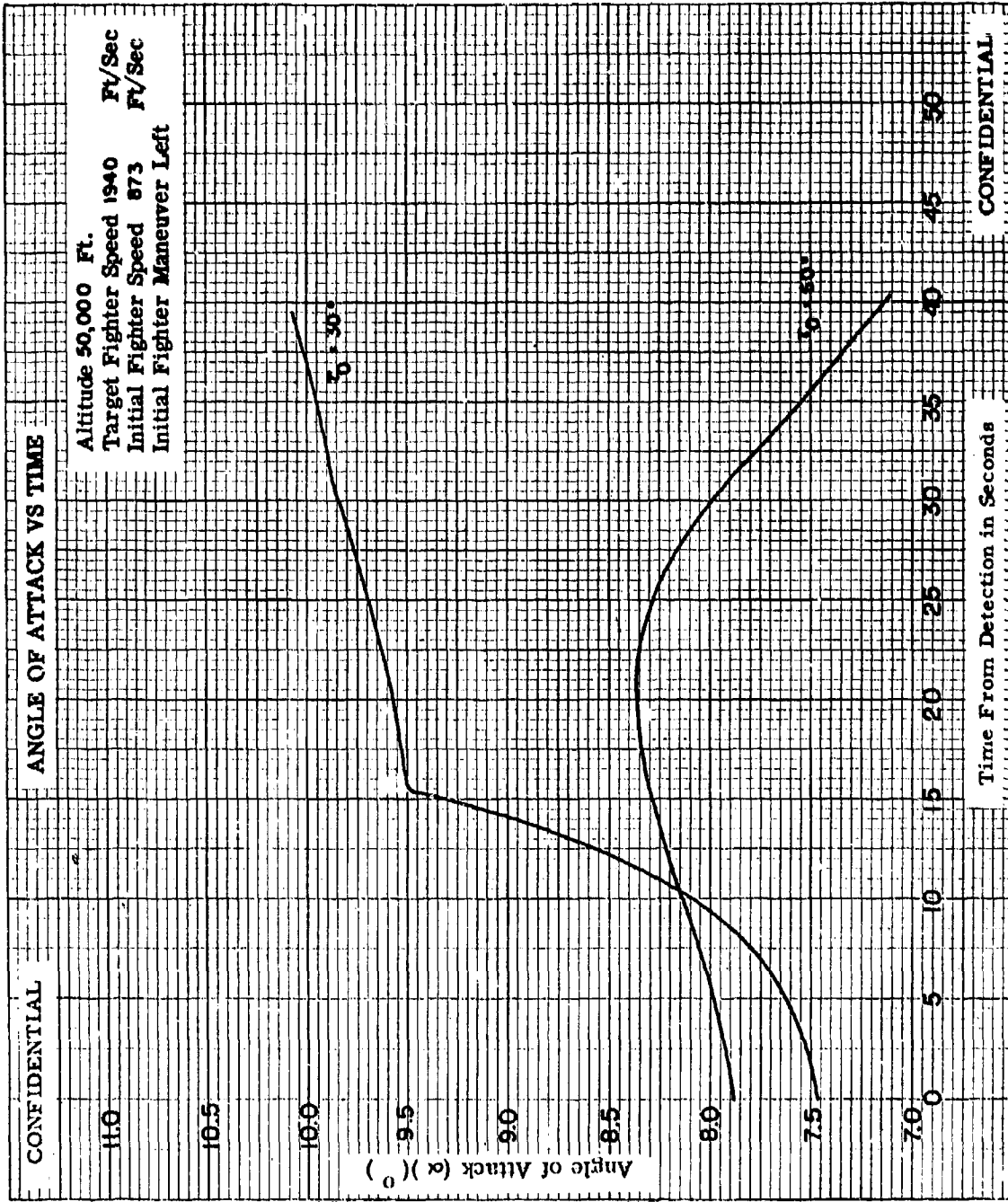
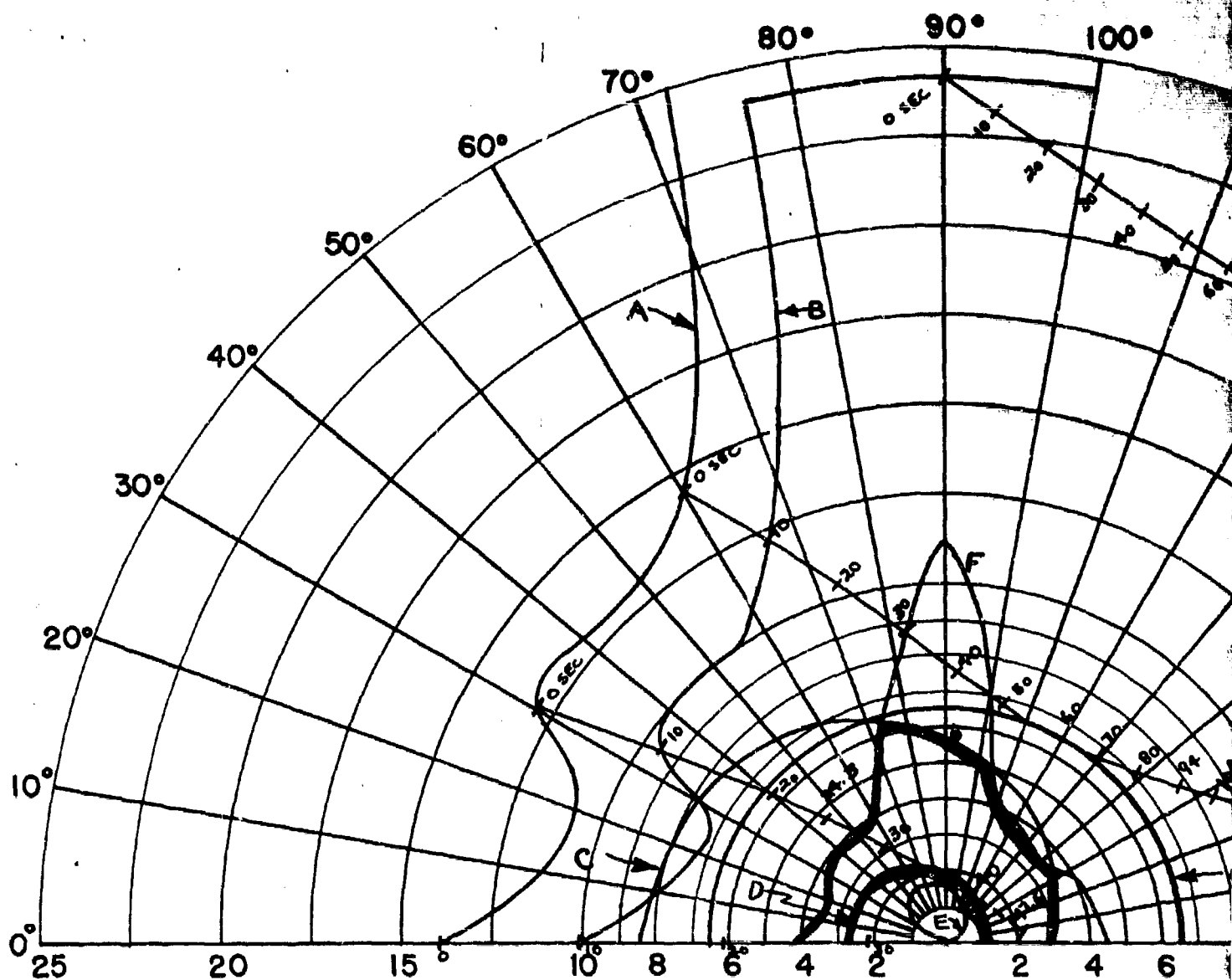


Fig. V-14



$V_F = 873$ FT/SEC (F4H-1)(F8U-3)

$V_T = 1552$ FT/SEC

ALTITUDE = 50,000 FT.
INCREASED THRUST AT DETECTION

← TARGET HEADING

- A - 85% DETECTION RANGE
- B - LOCK-ON RANGE (10 SEC. LOCK-ON T
- C - SPARROW III MAX. AERODYNAMIC R
- D - SPARROW III MIN. AERODYNAMIC R
- E - CONSTANT LOAD FACTOR LOCUS (I
- F - 90% SPARROW III SEEKER LOCK-O
- G - 6.5 N.M. INTERLOCK

[illegible]

CONFIDENTIAL

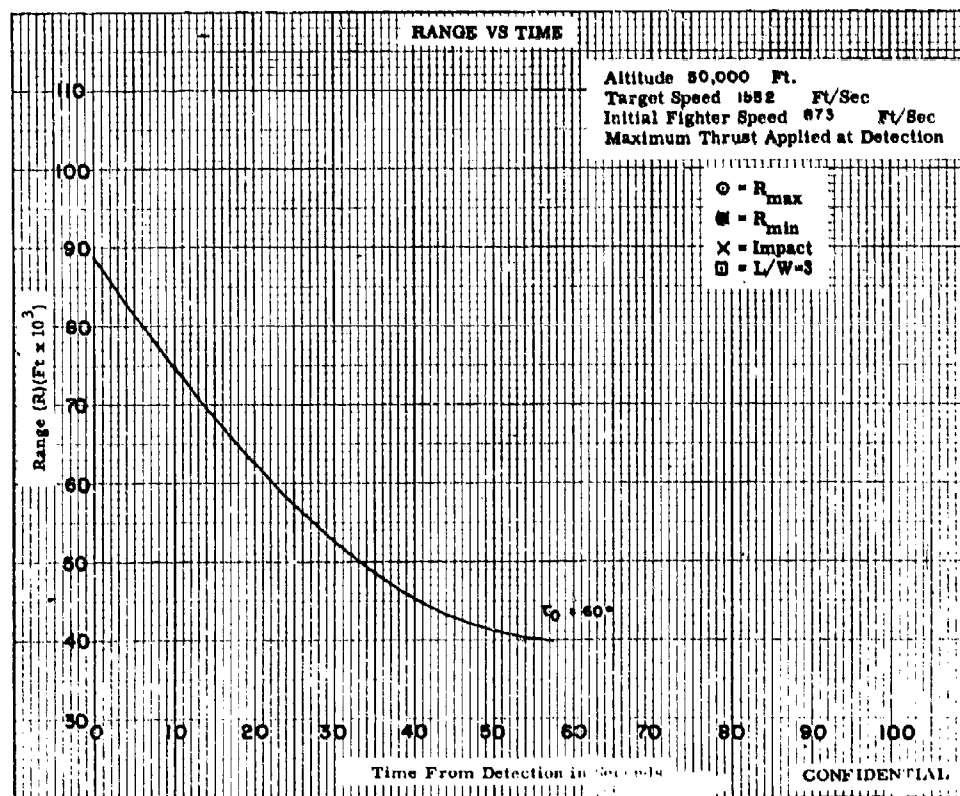
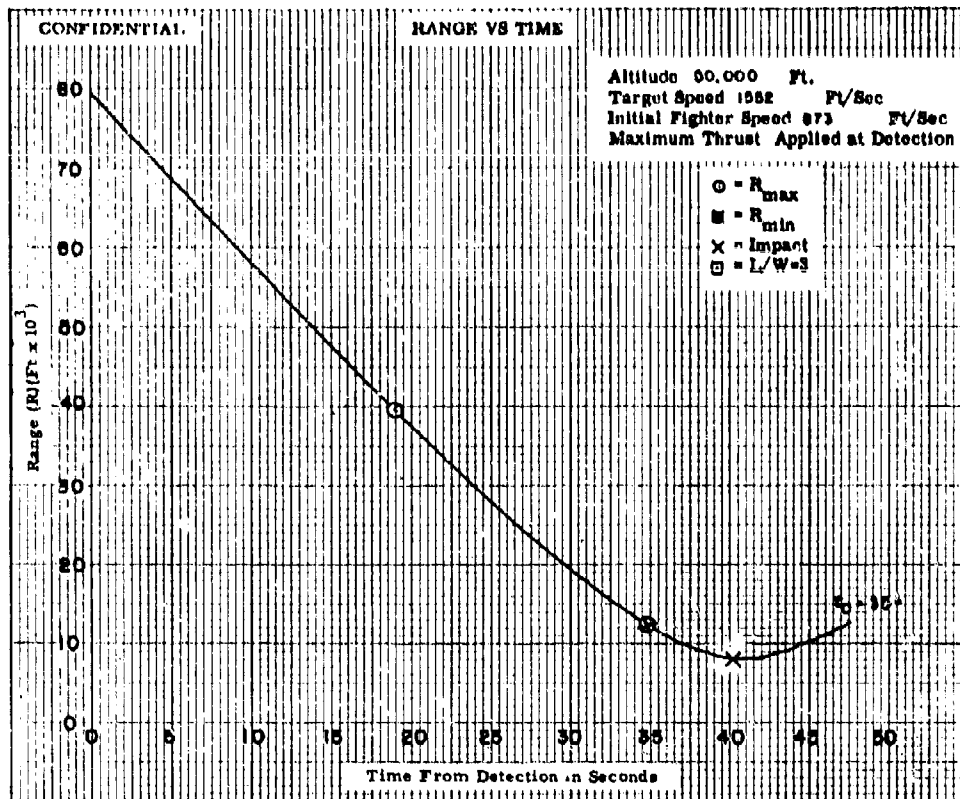


Fig. VI-1a

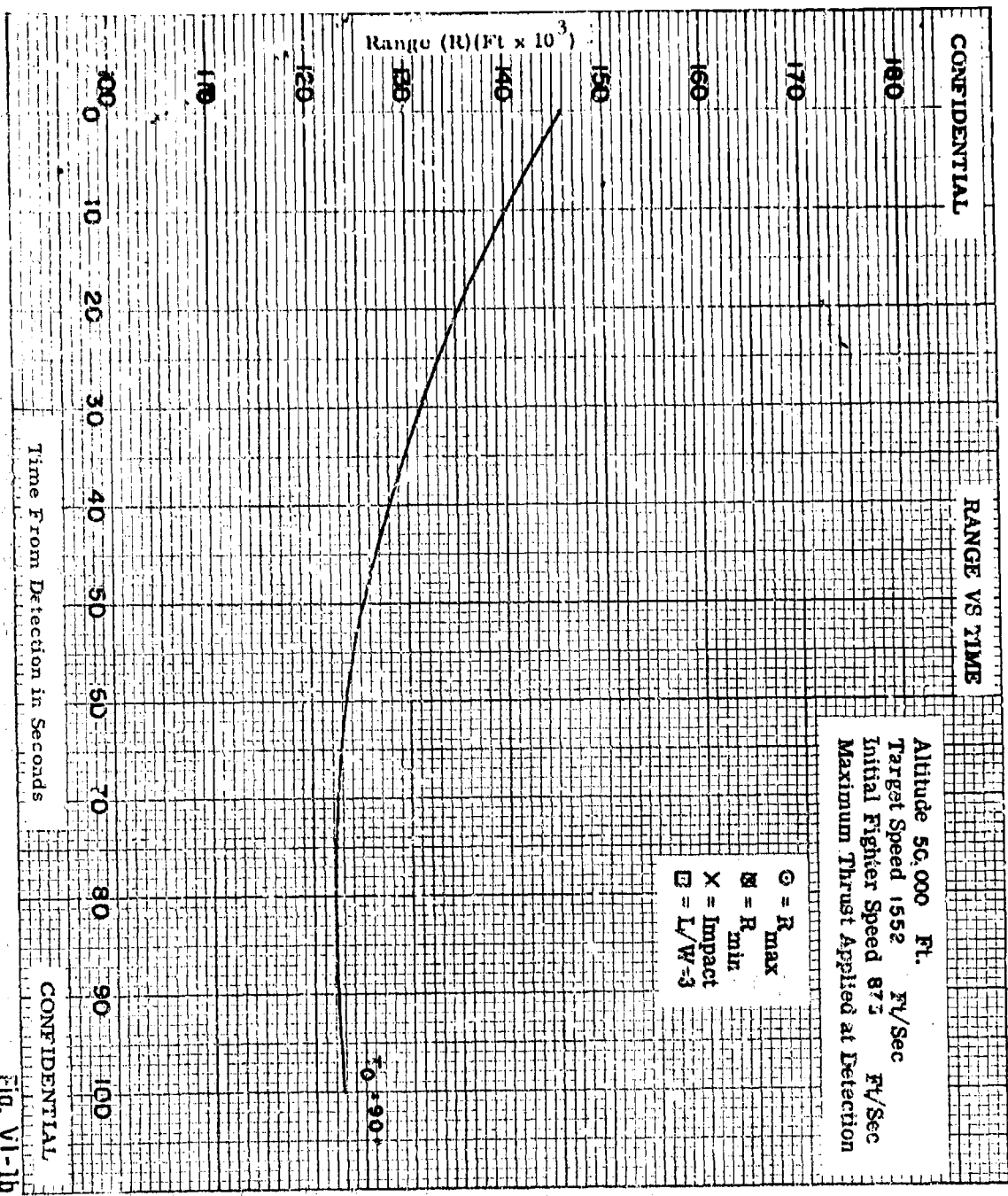


Fig. VI-1b

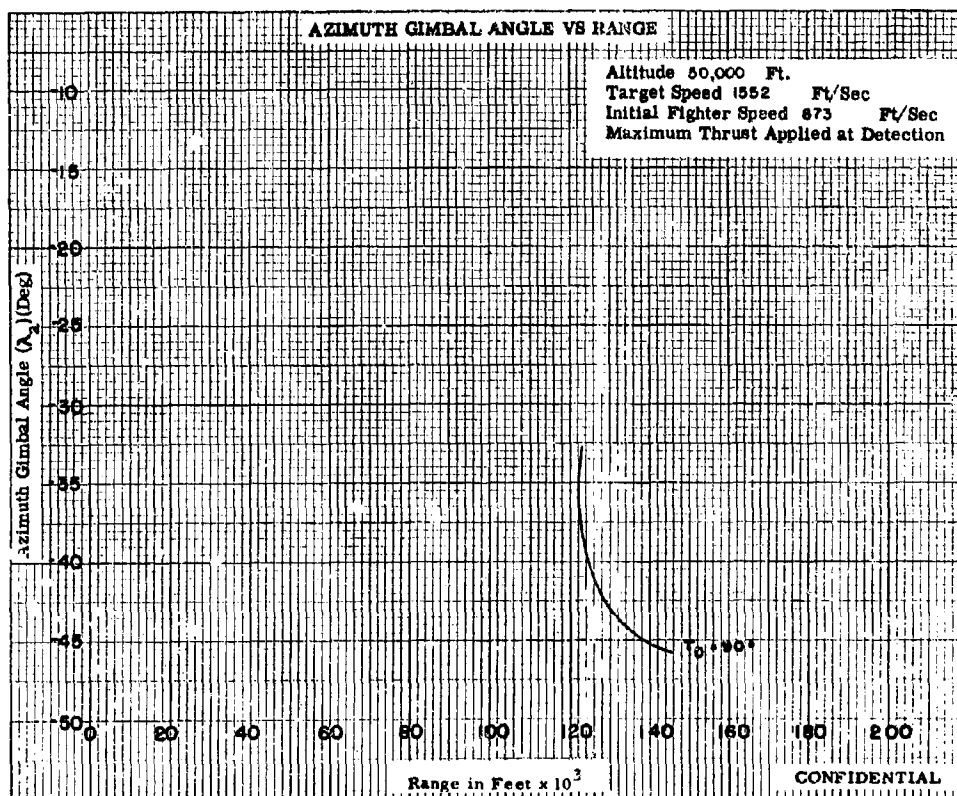
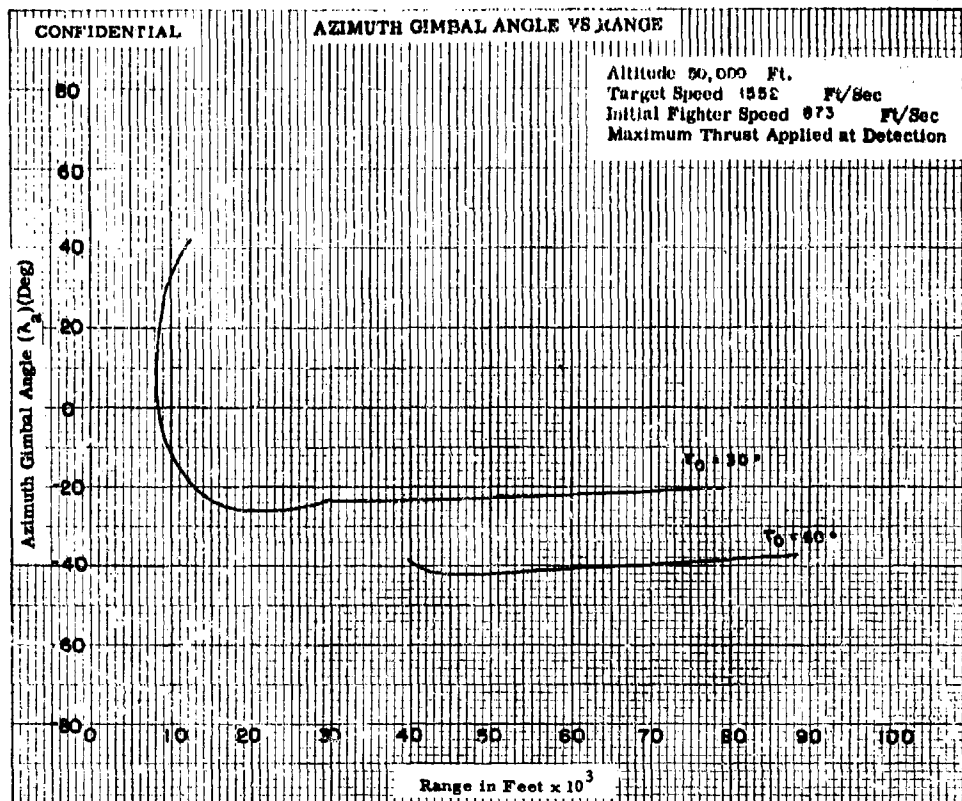


Fig. VI-2

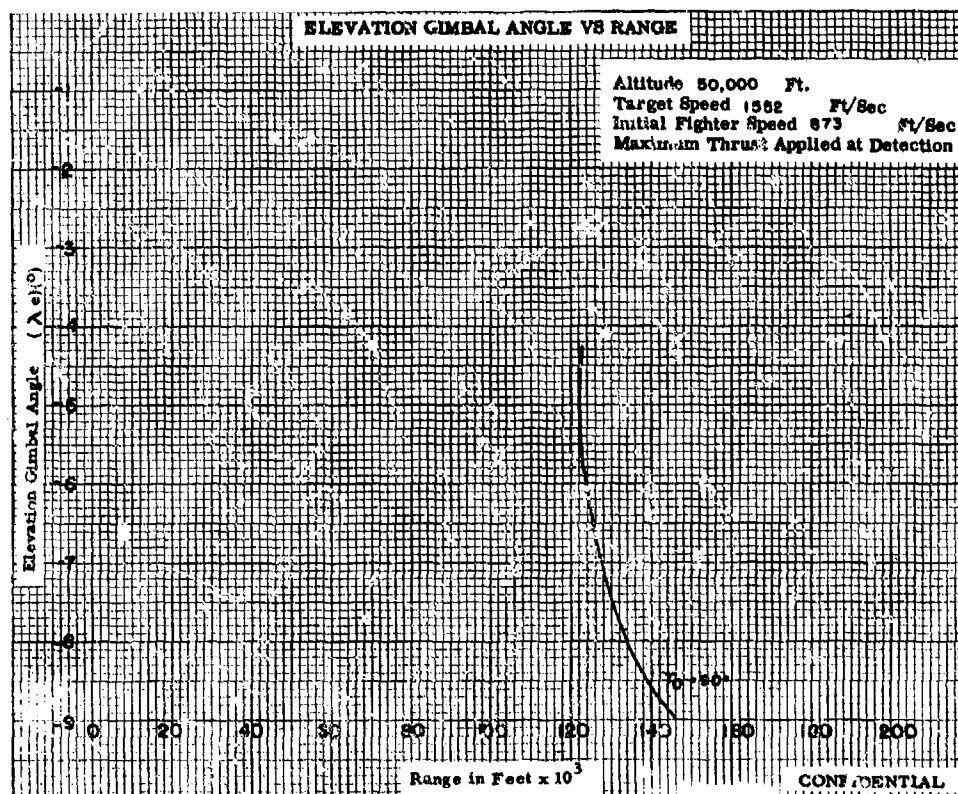
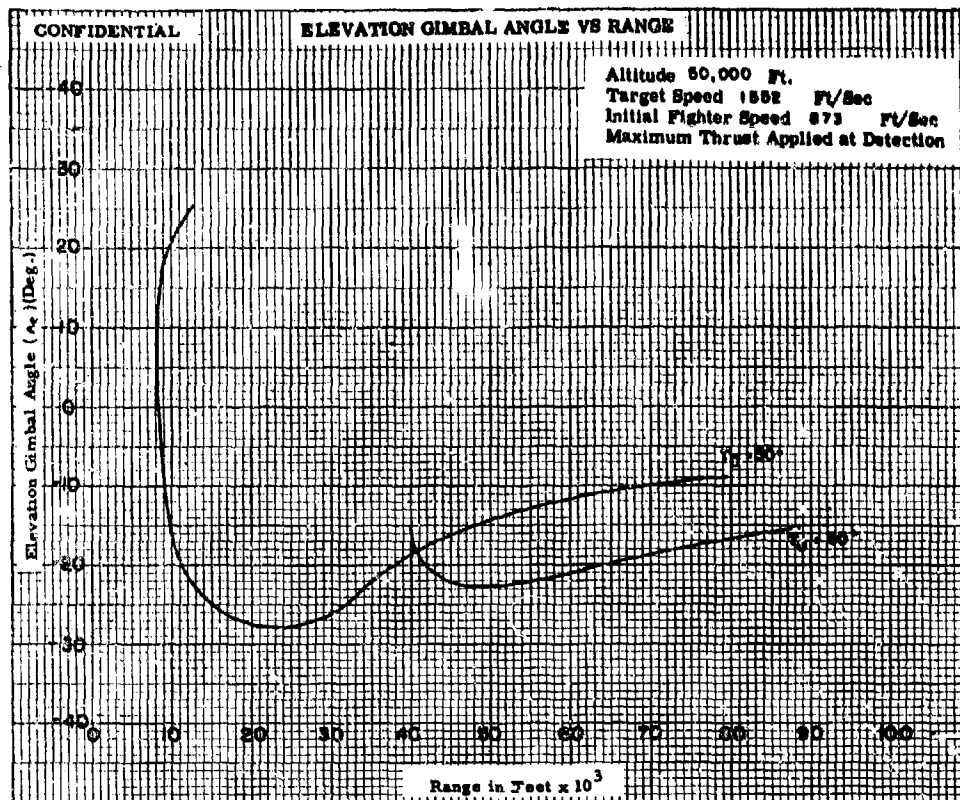


Fig. VI-3

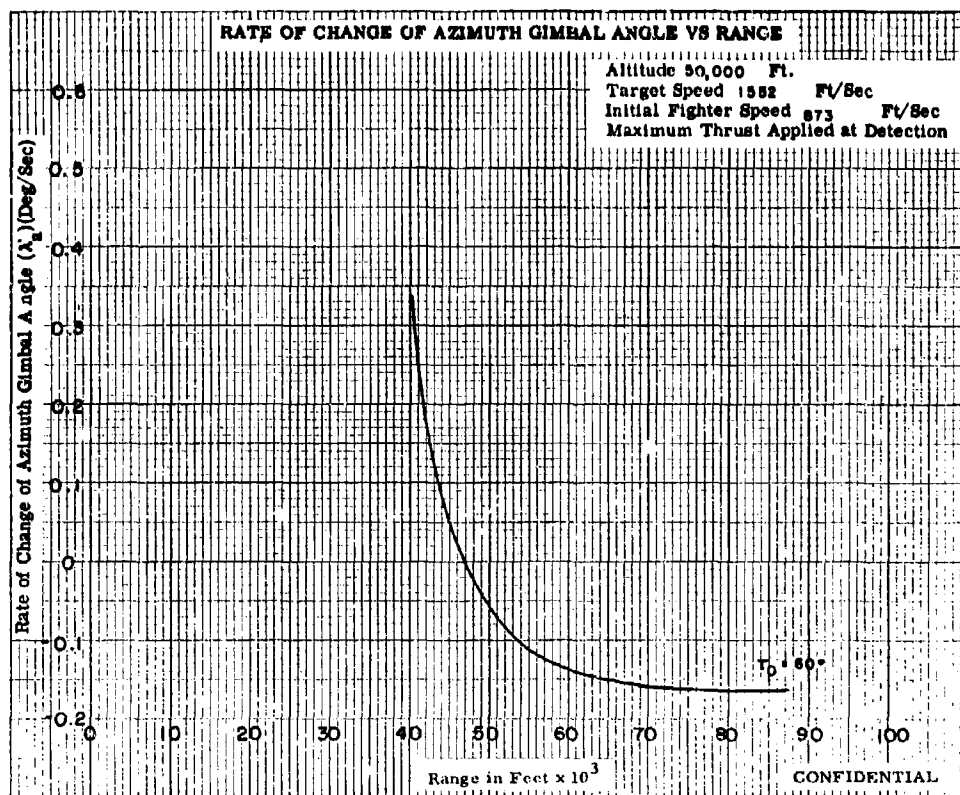
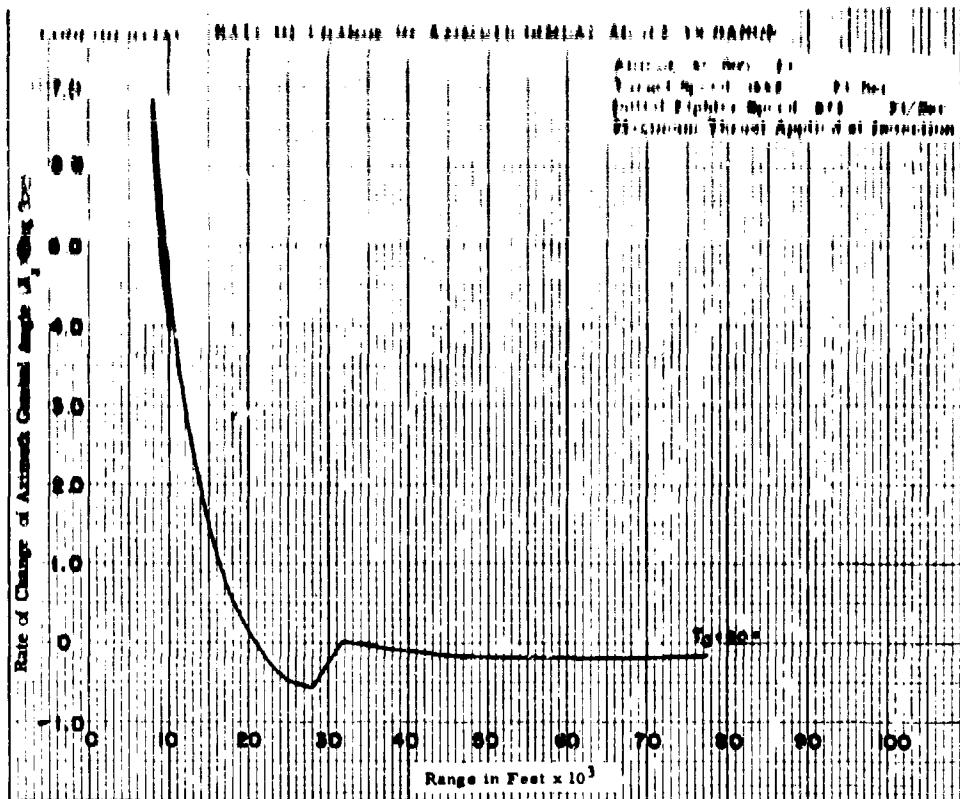


Fig. VI-4a

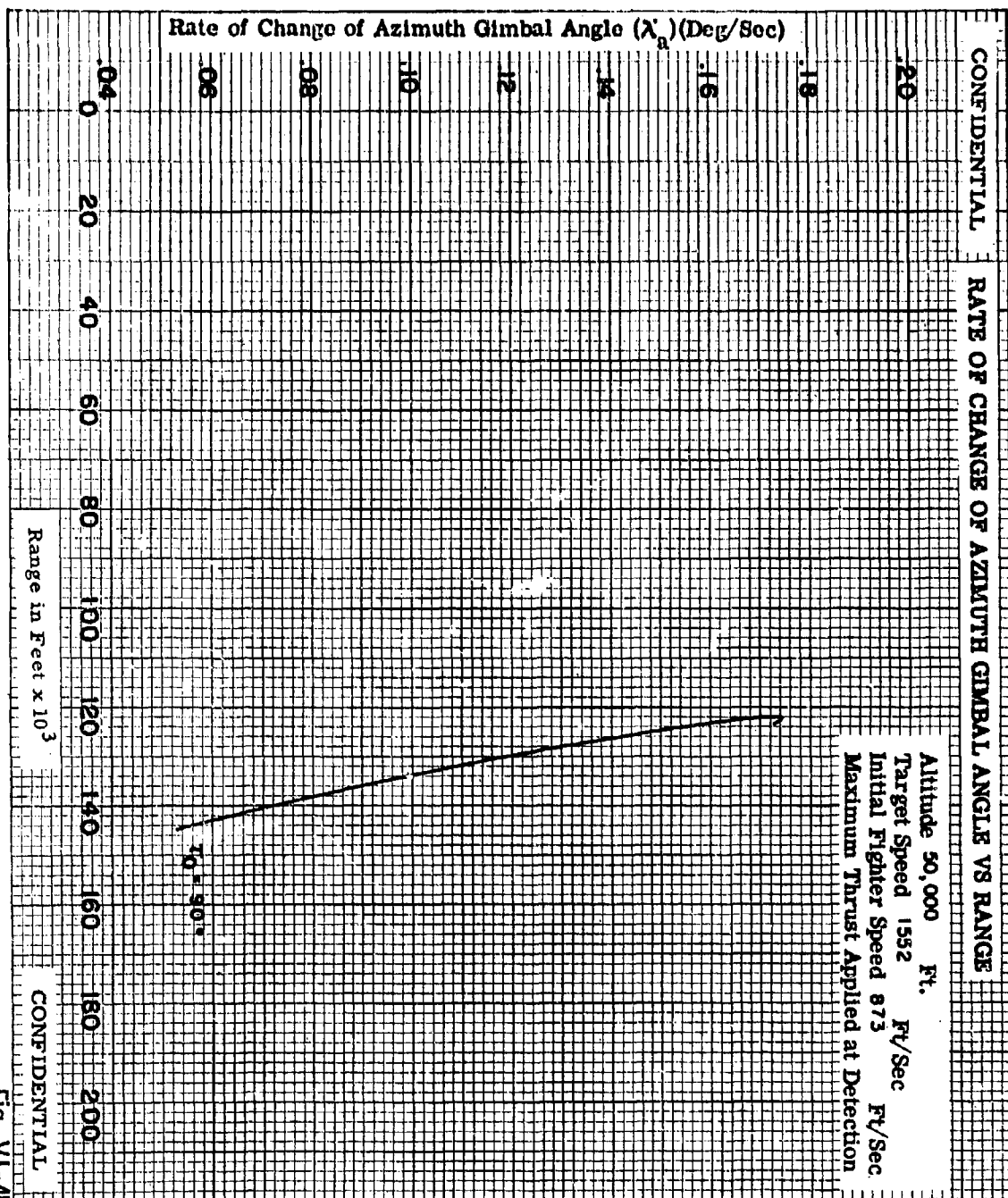


Fig. VI-4b

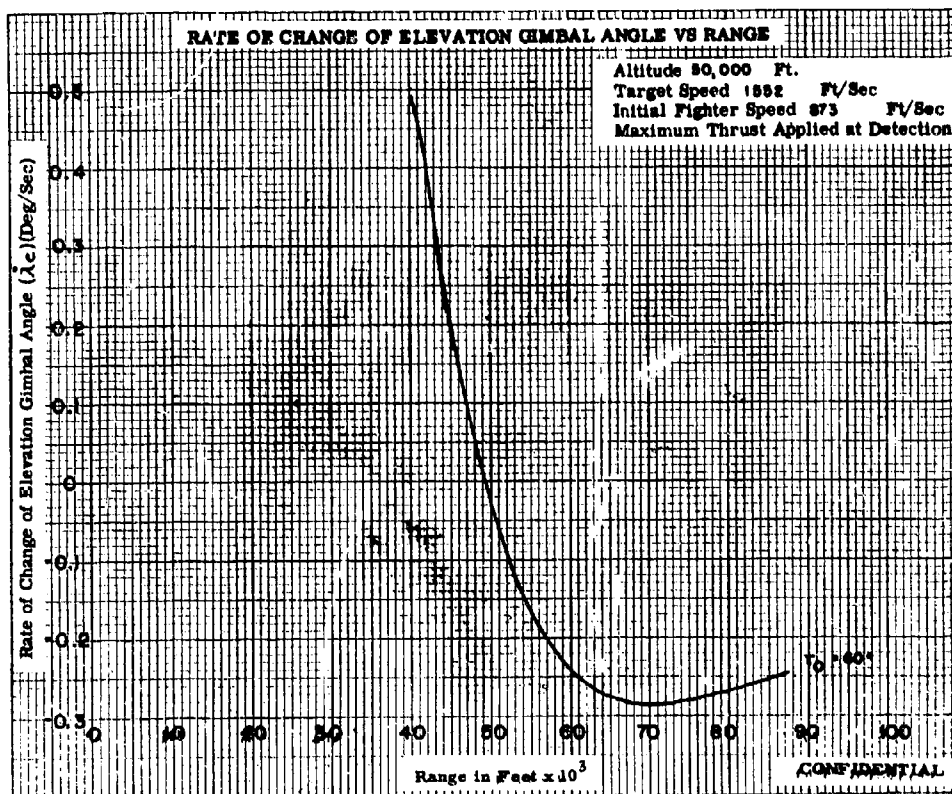
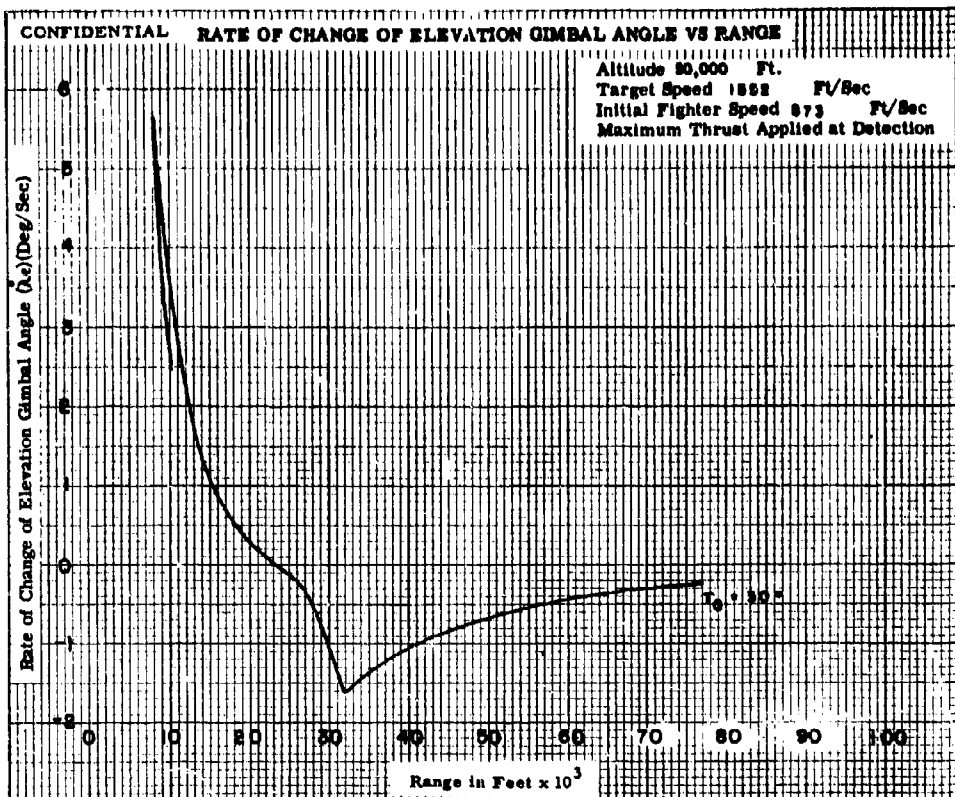


Fig. VI-5a

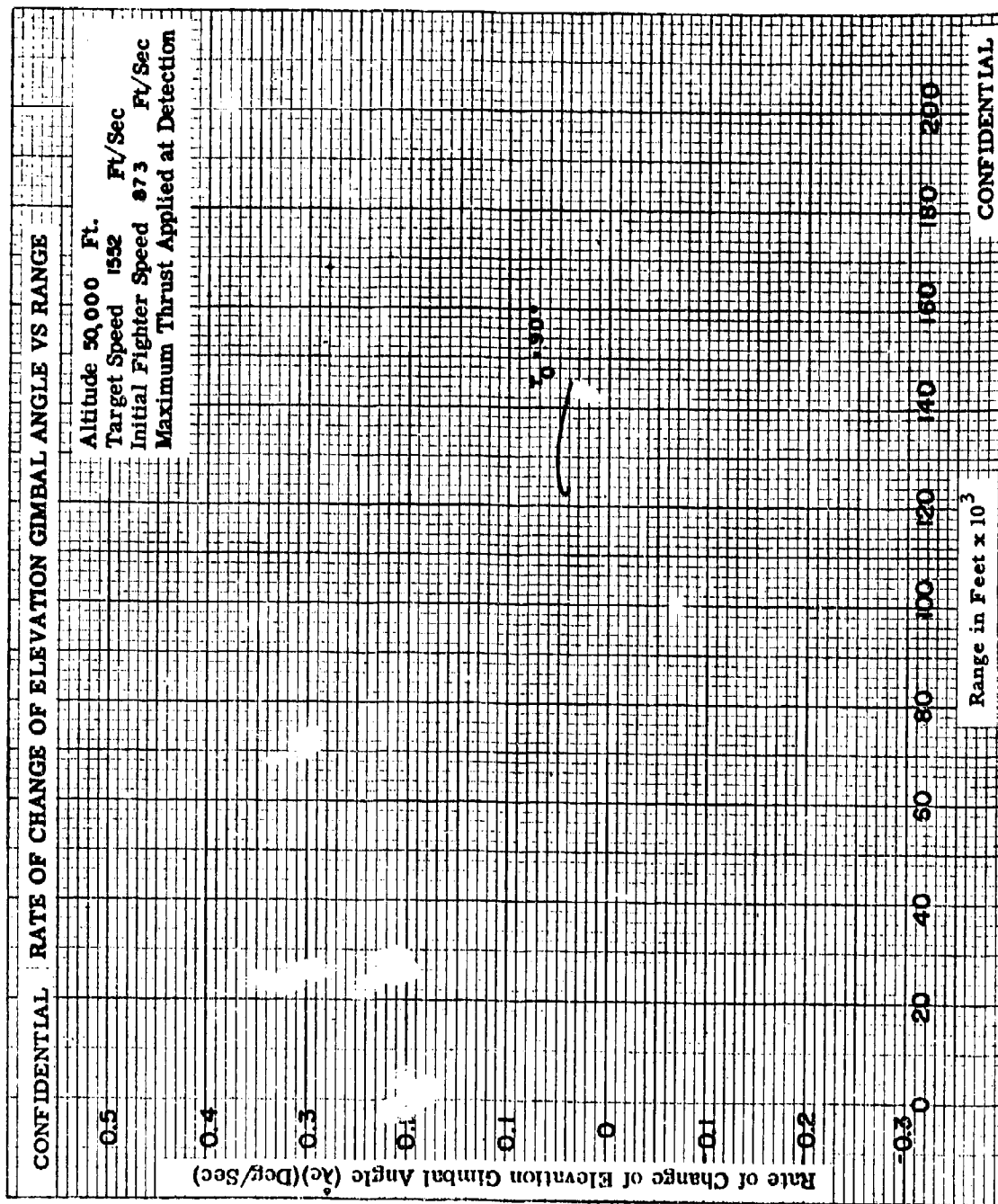


Fig. VI-50

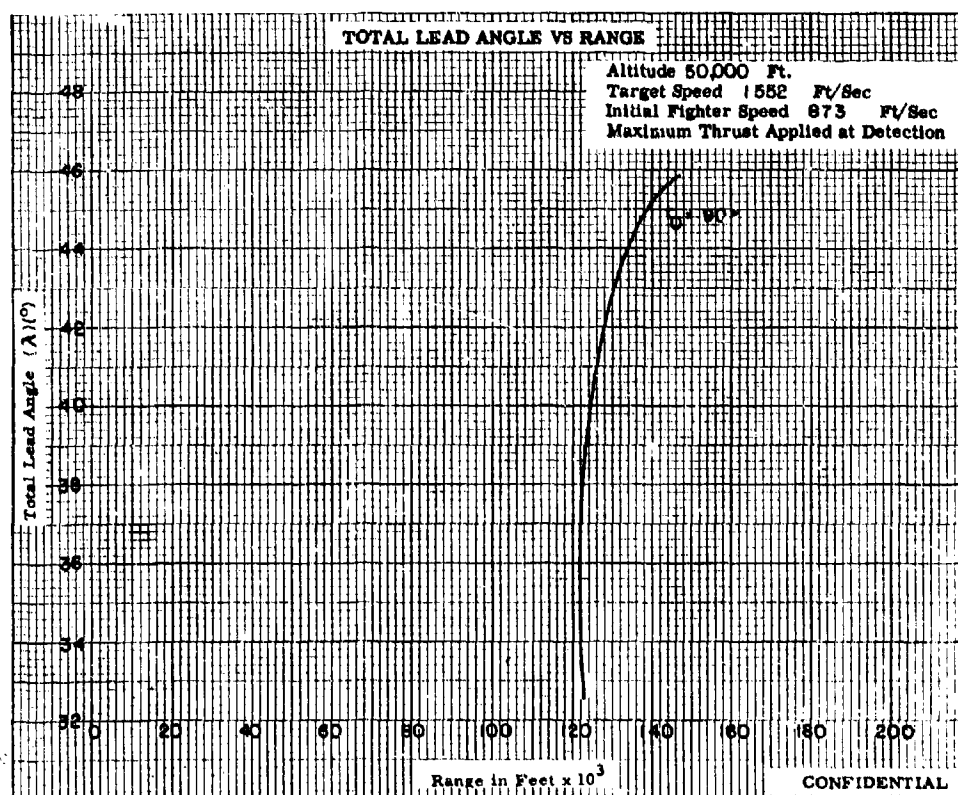
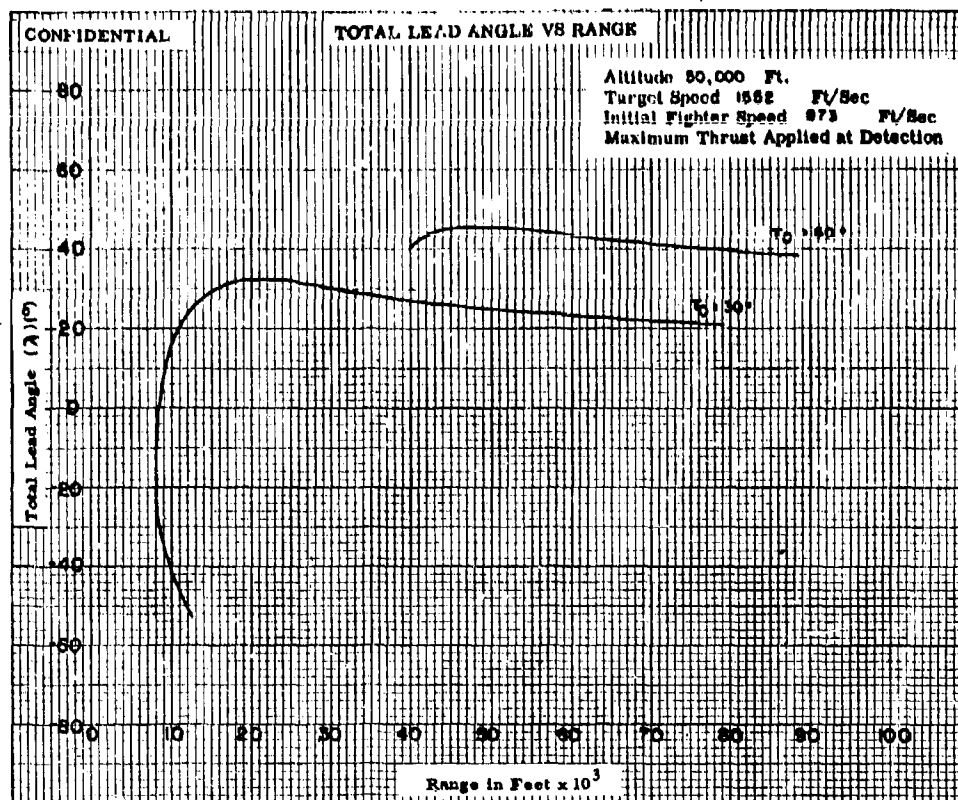


Fig. VI-6

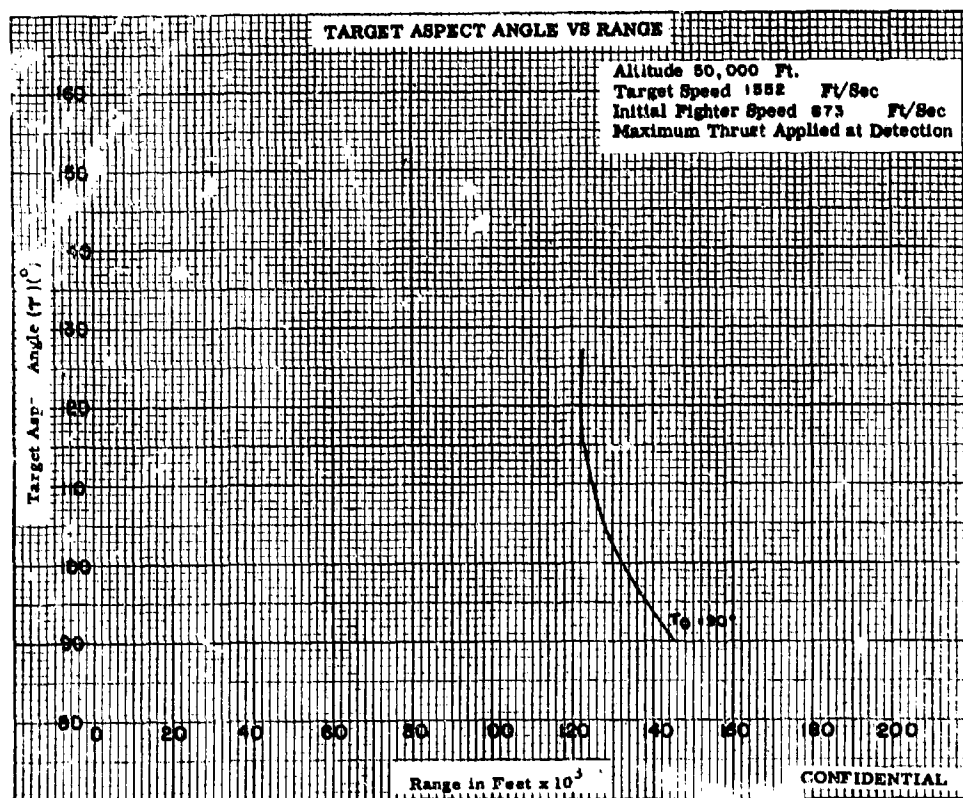
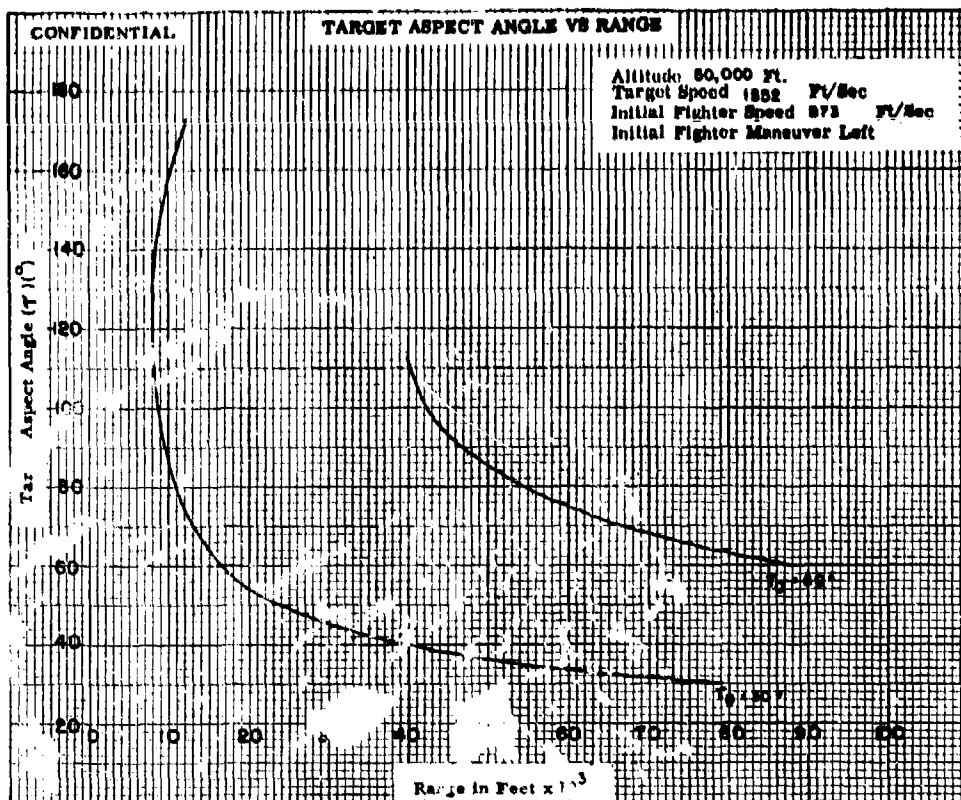


Fig. VI-7

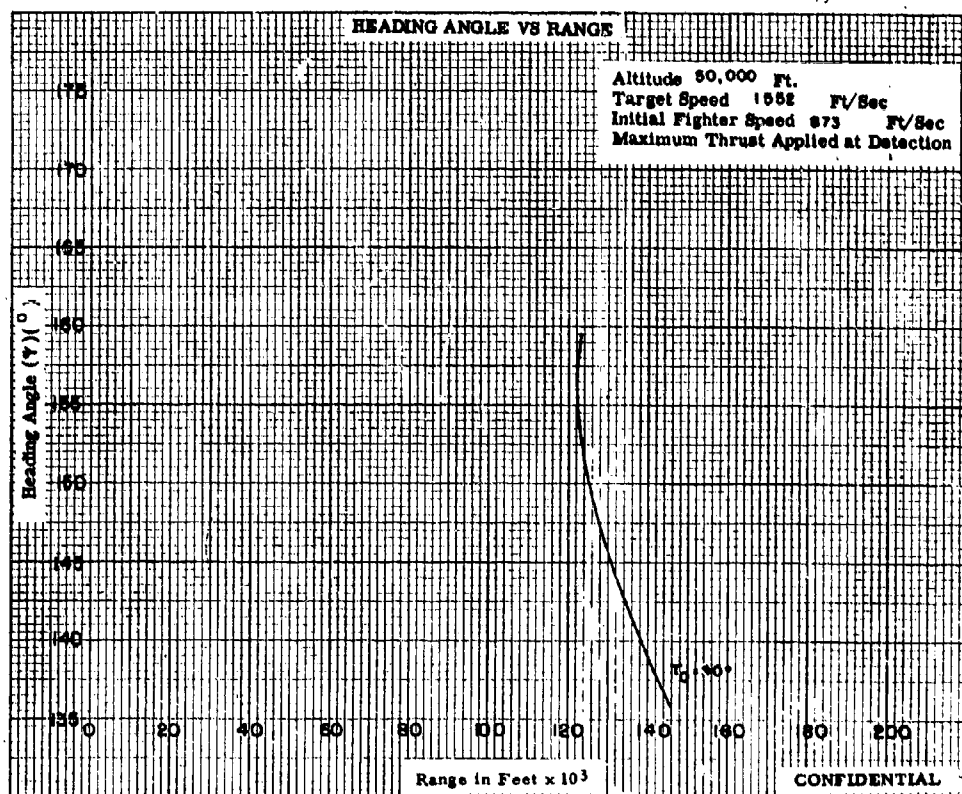
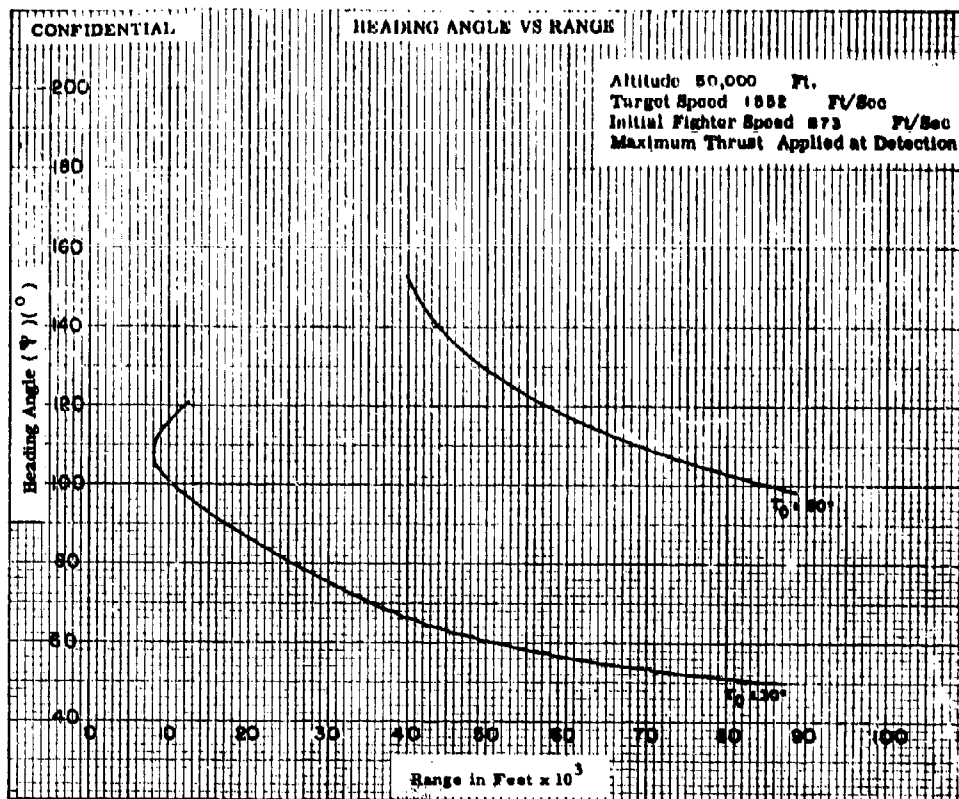


Fig. VI-8

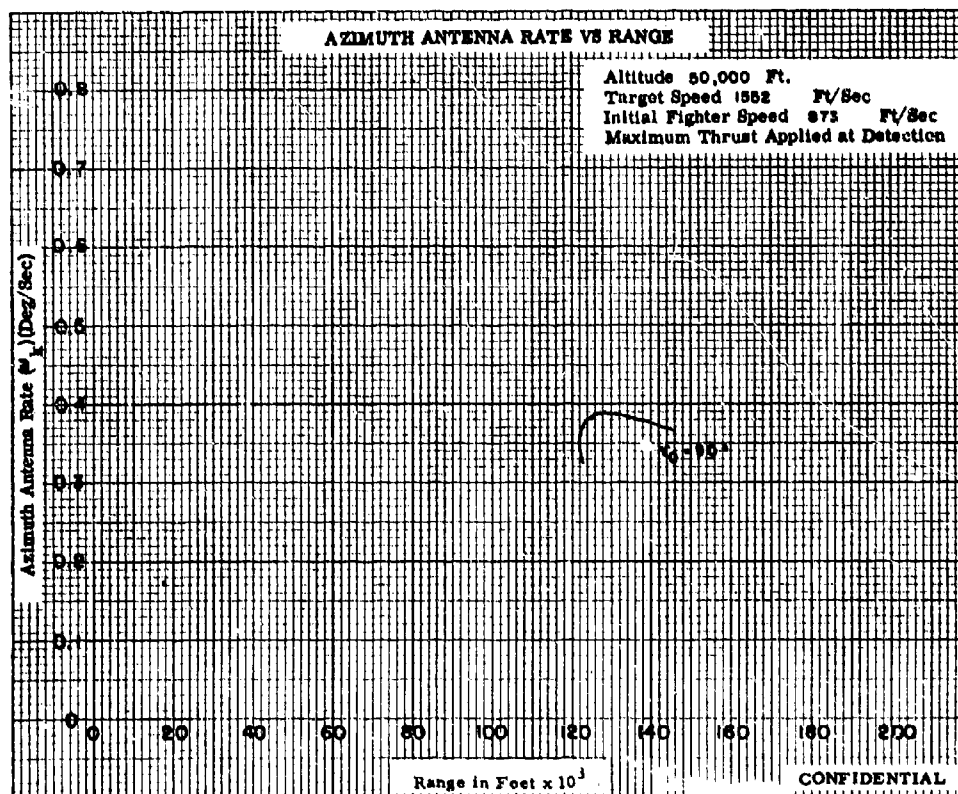
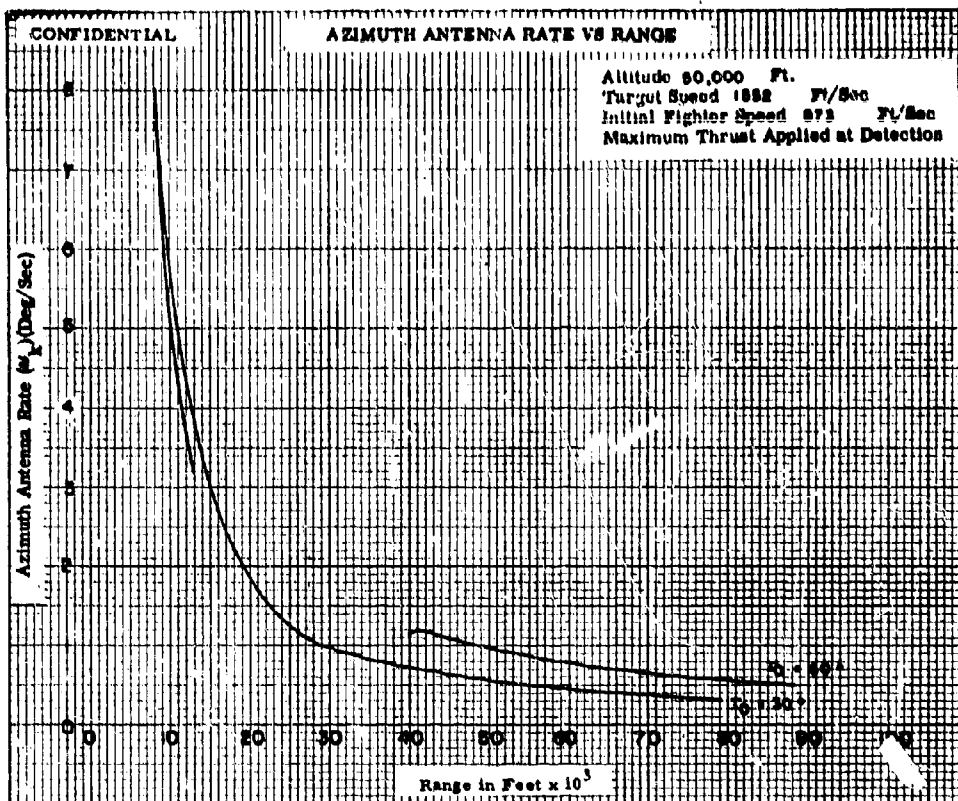


Fig. VI-9

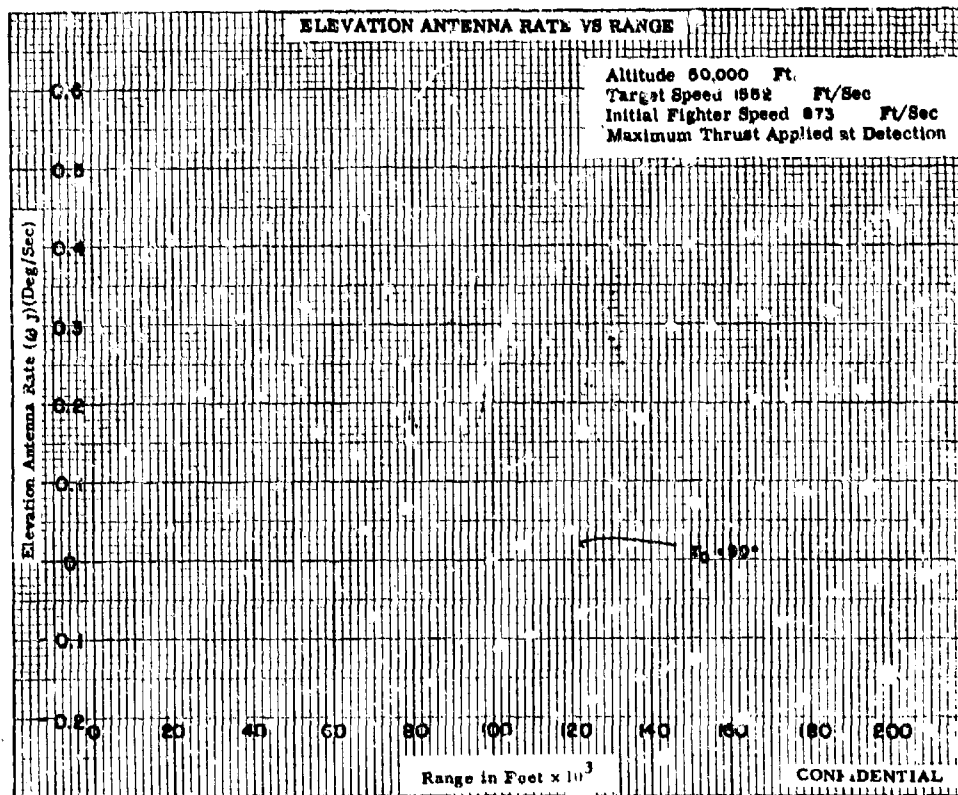
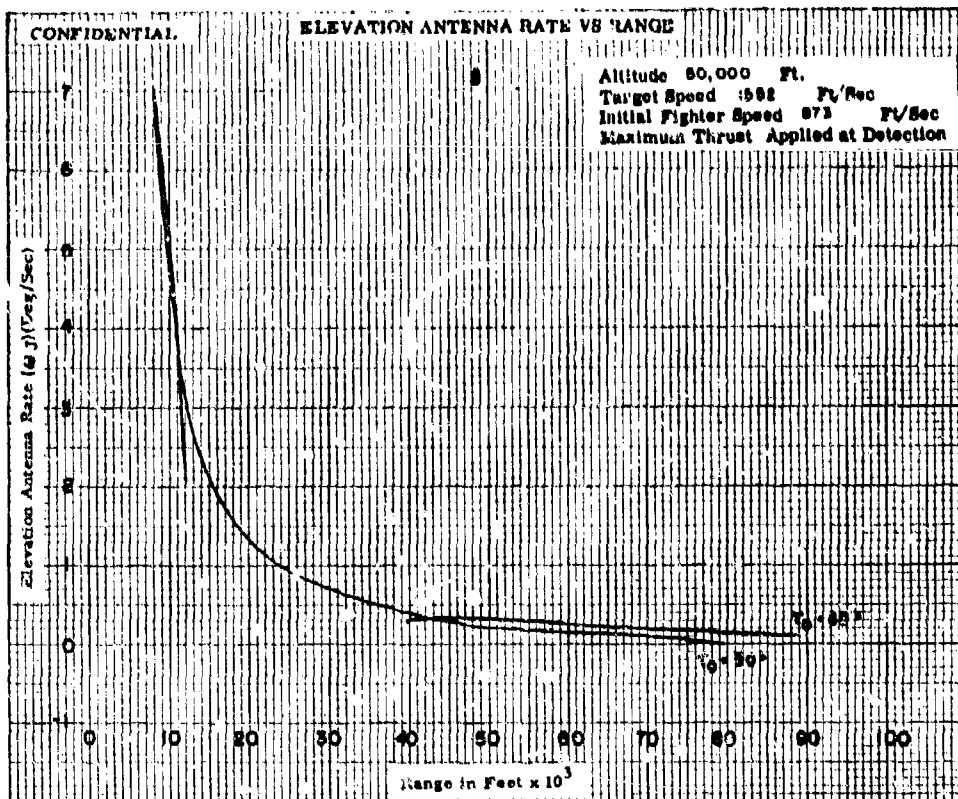


Fig. VI-10

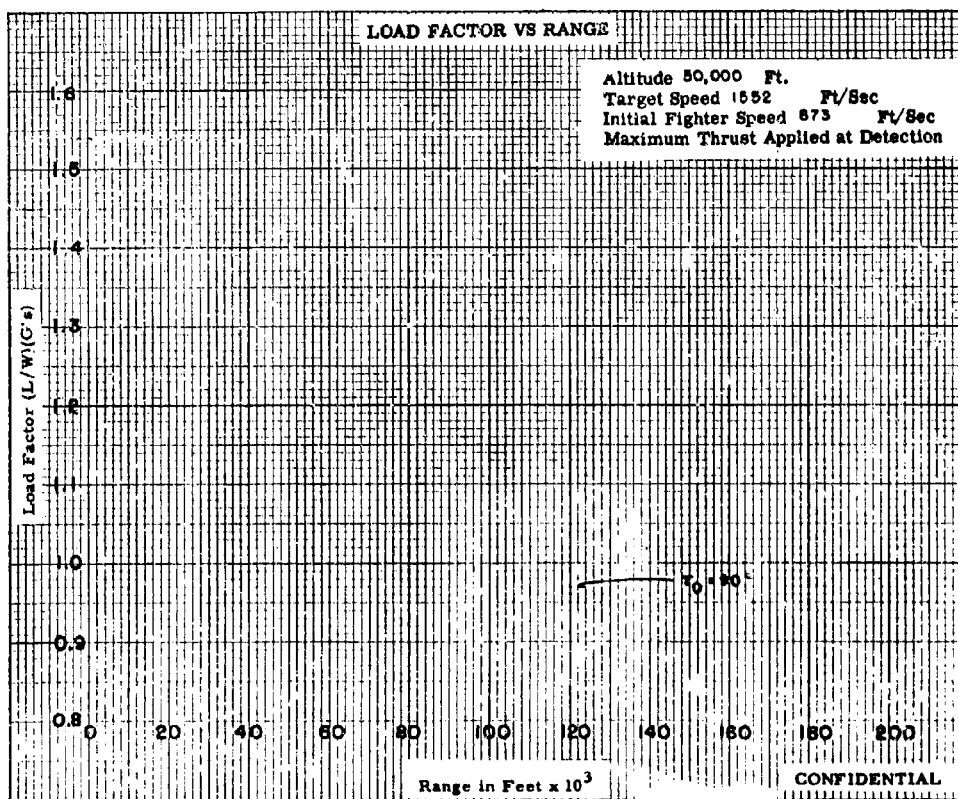
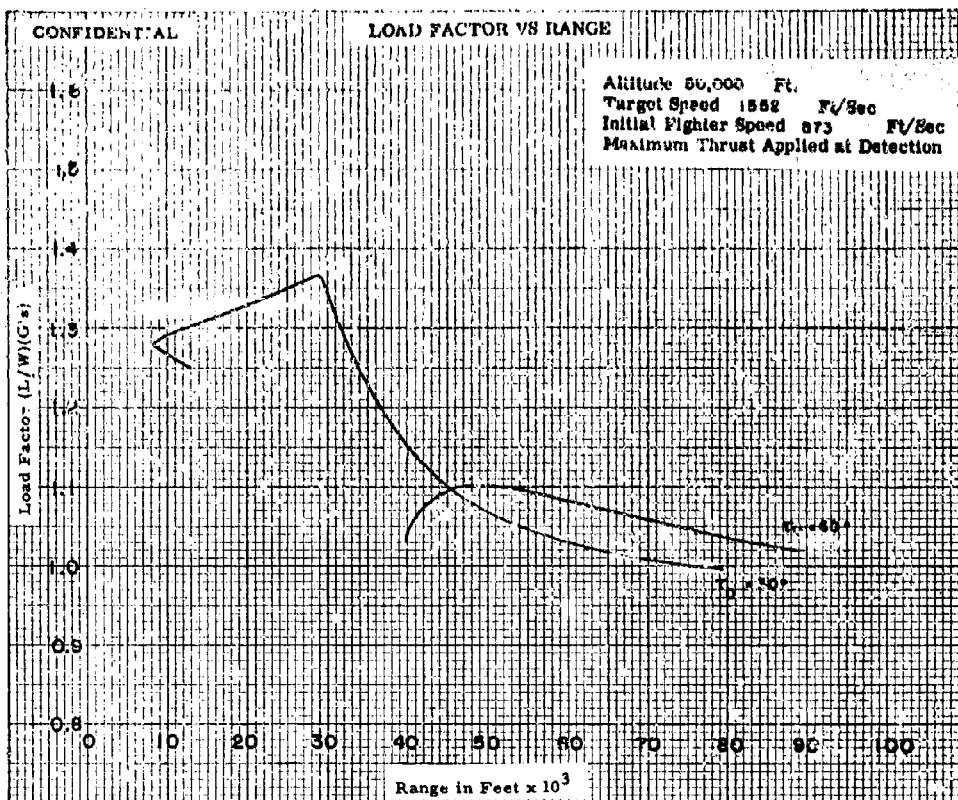


Fig. VI-11

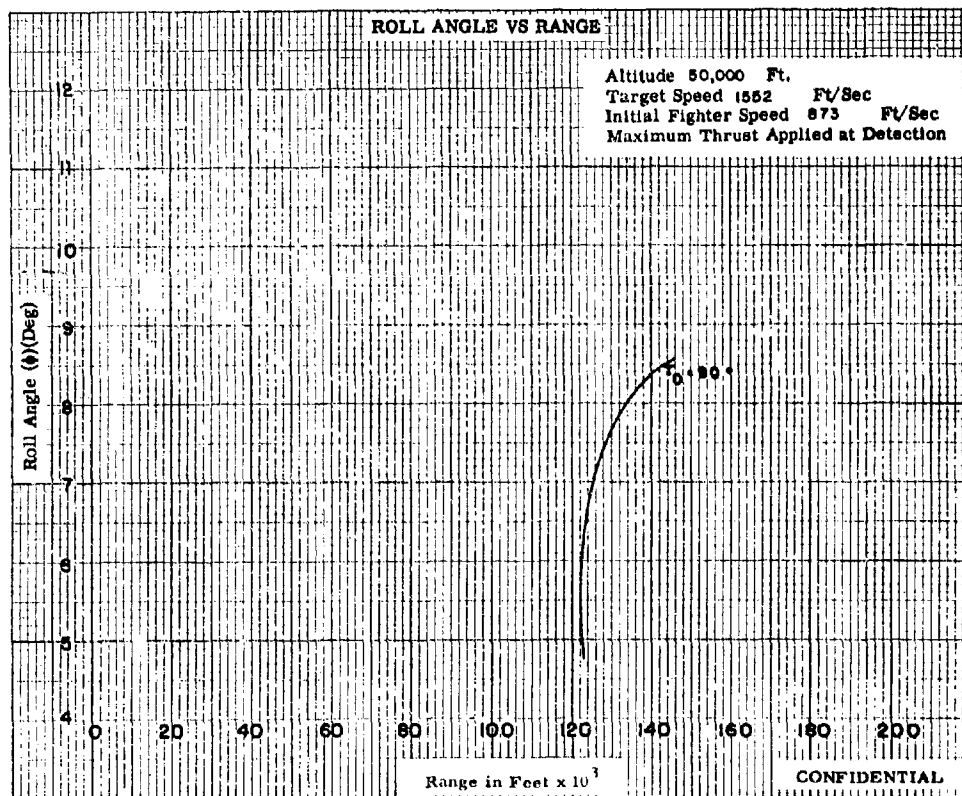
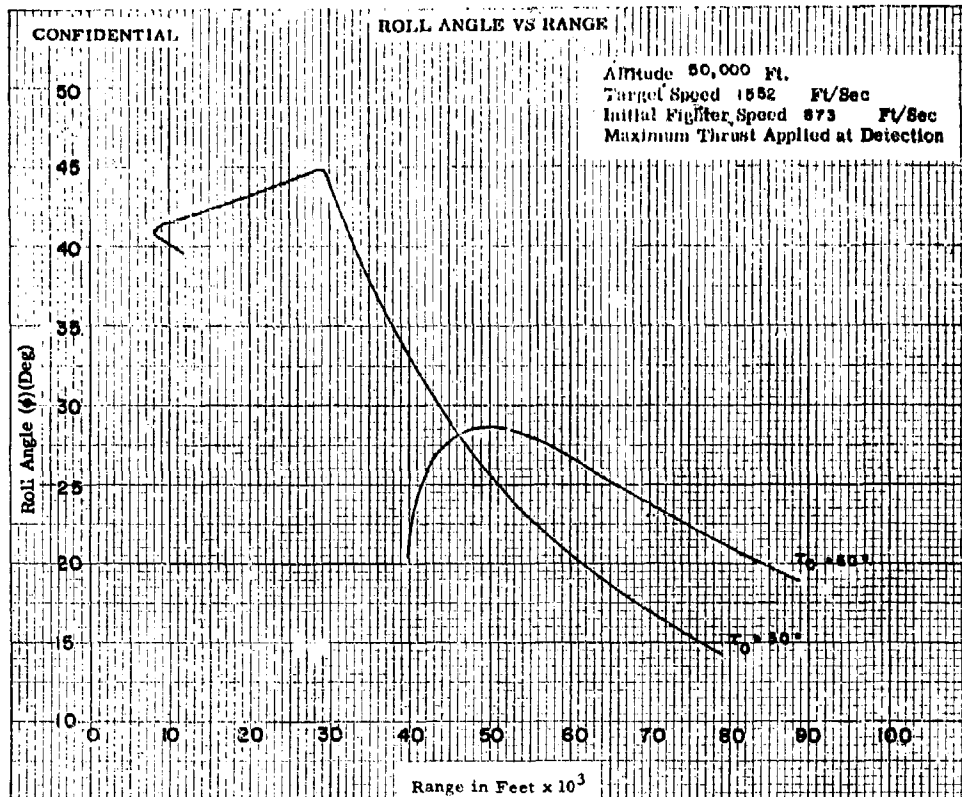


Fig. VI-12

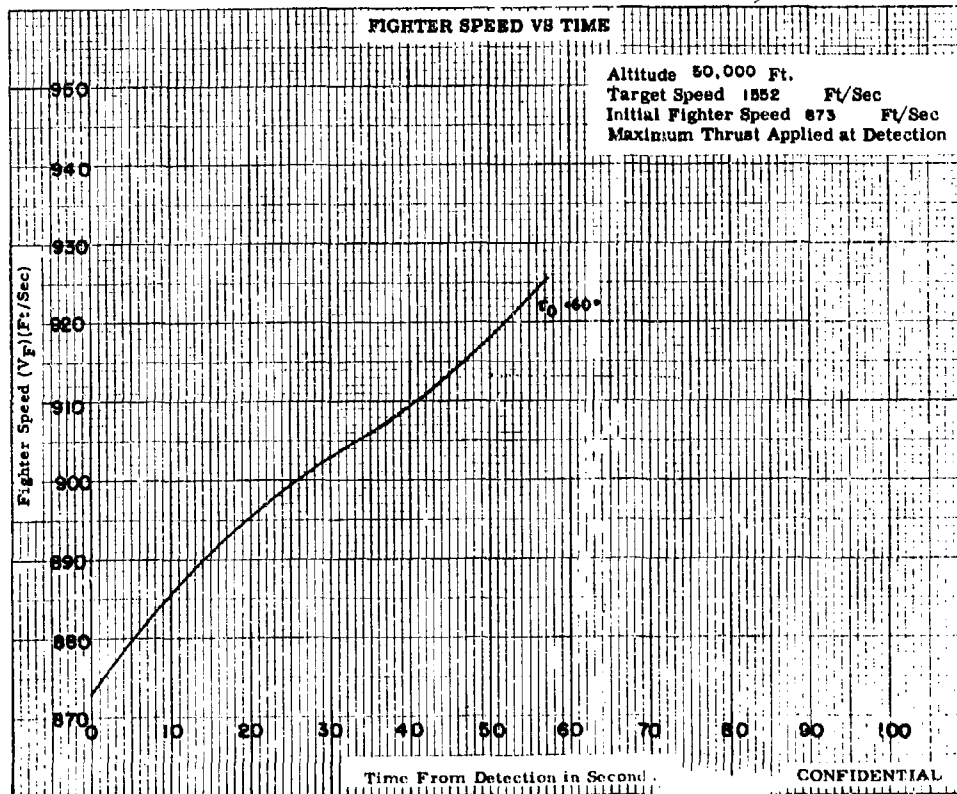
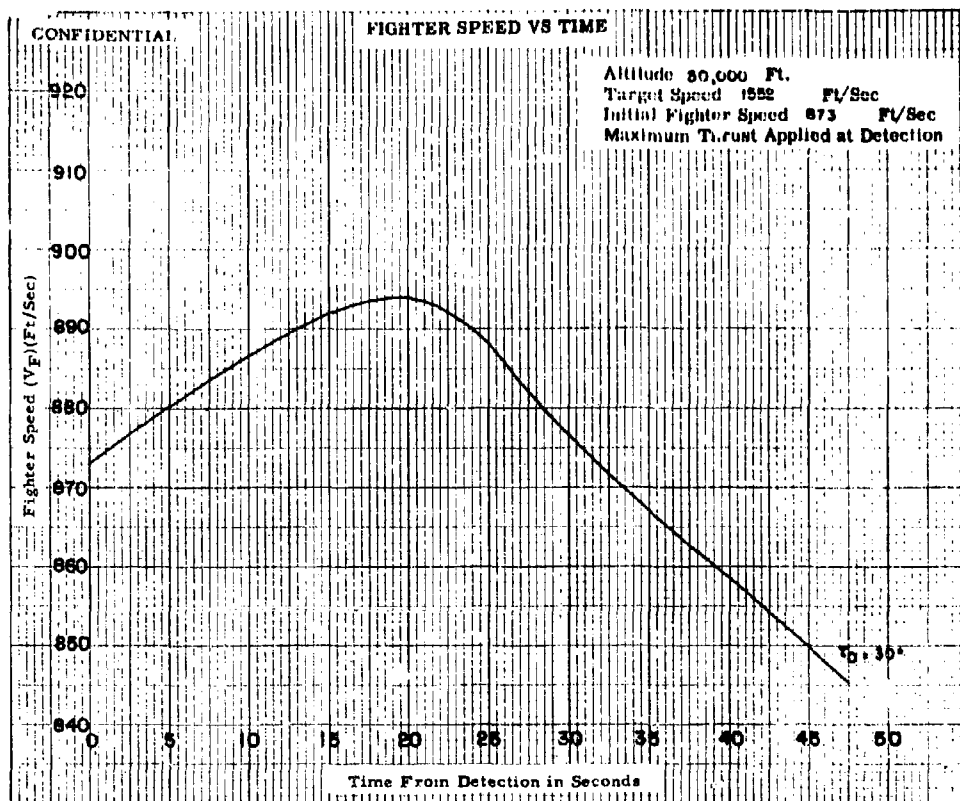


Fig. VI-13a

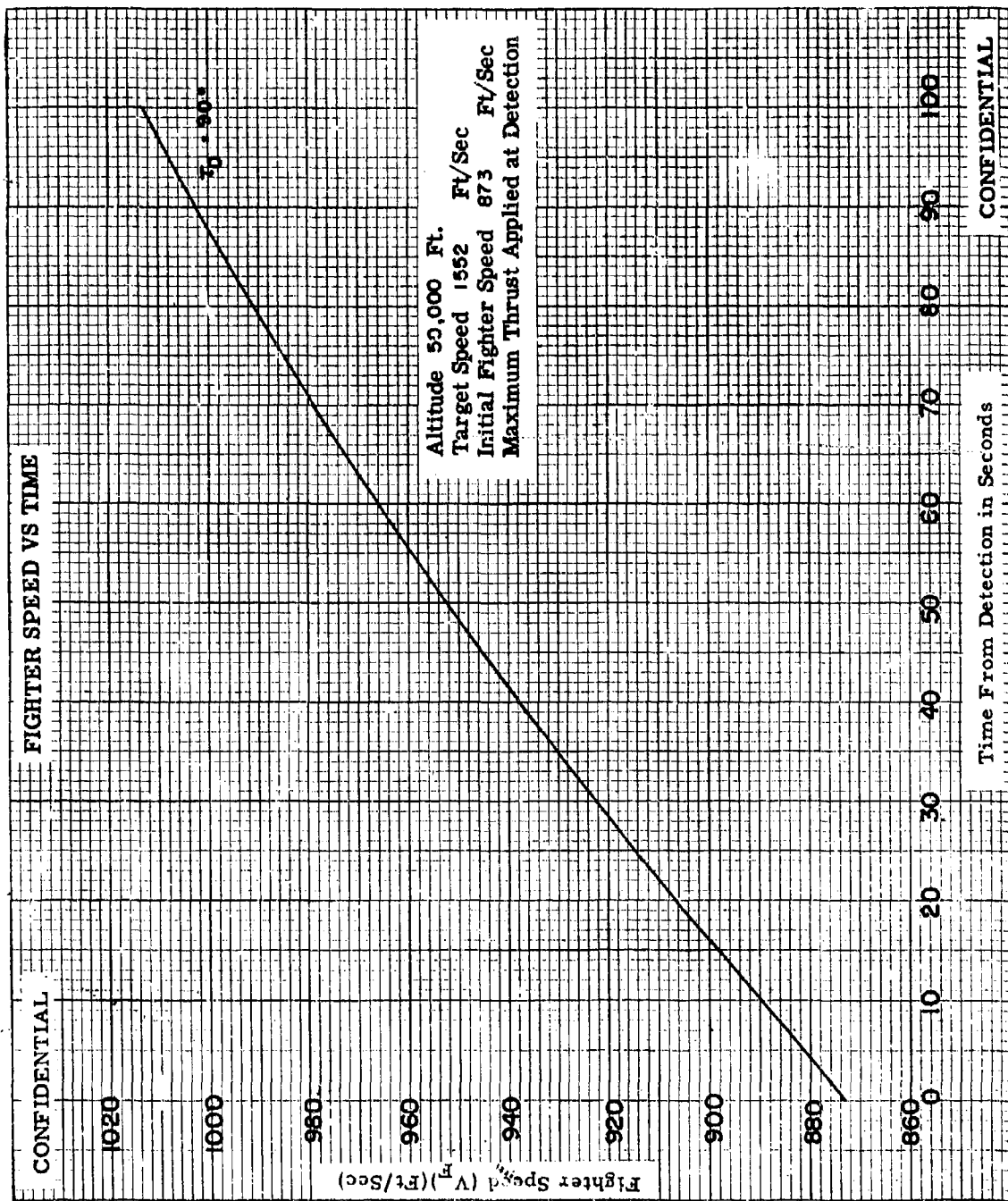


Fig. VI-13b

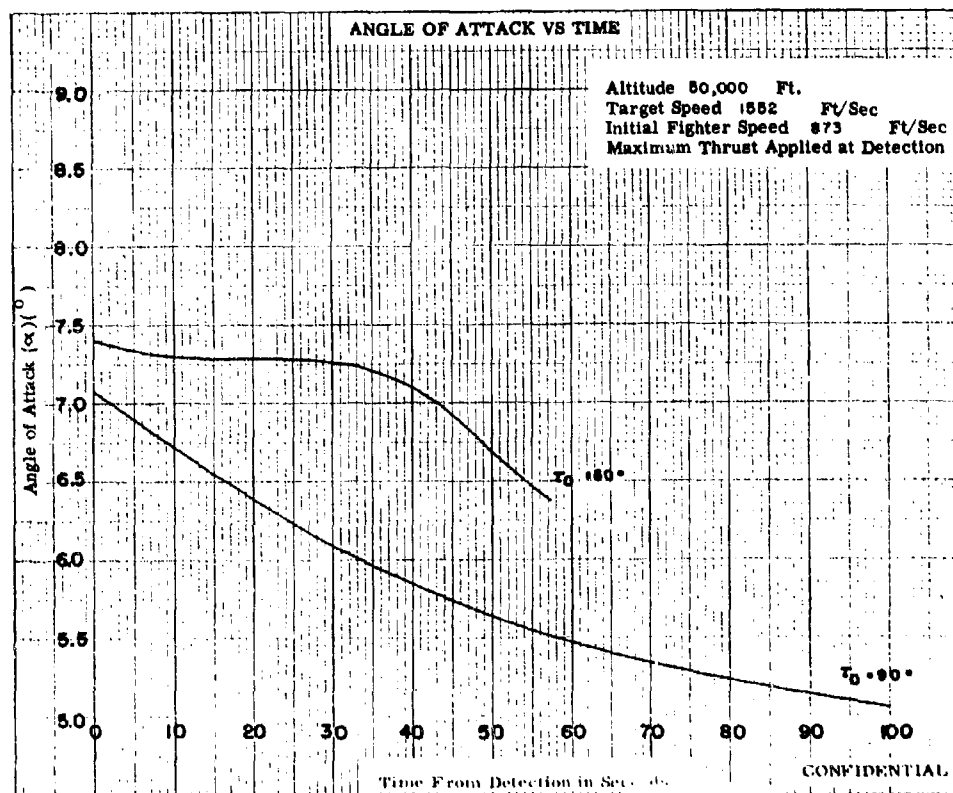
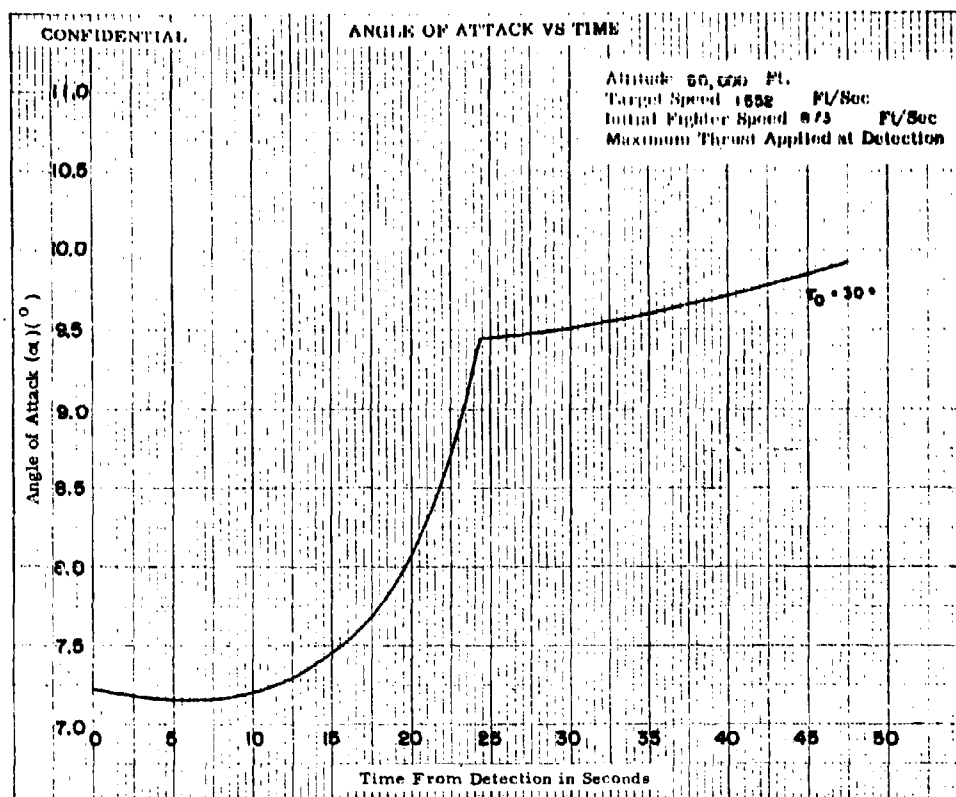
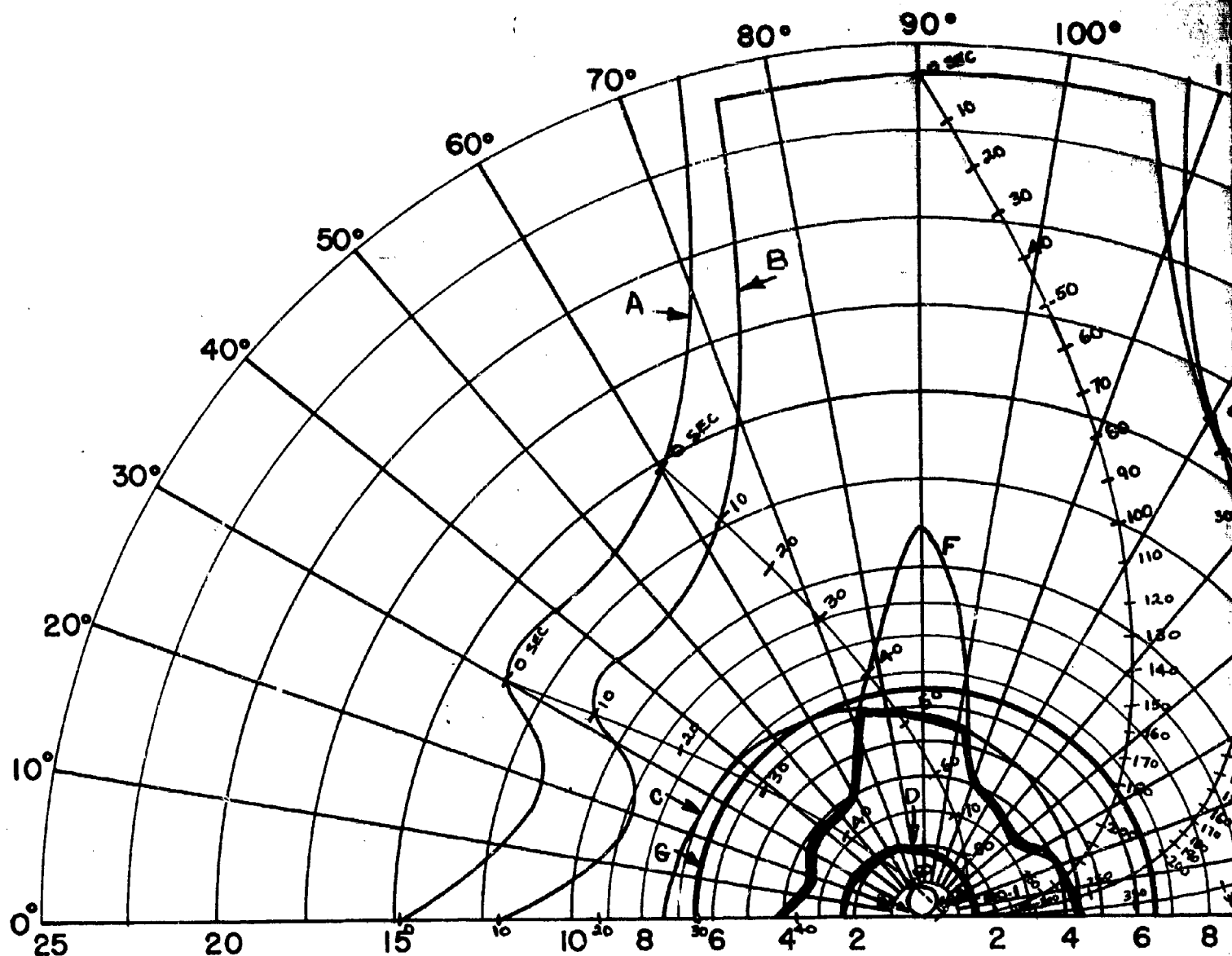


Fig. VI-14



$V_F = 873$ FT/SEC (F4H-1)(F8U-3)

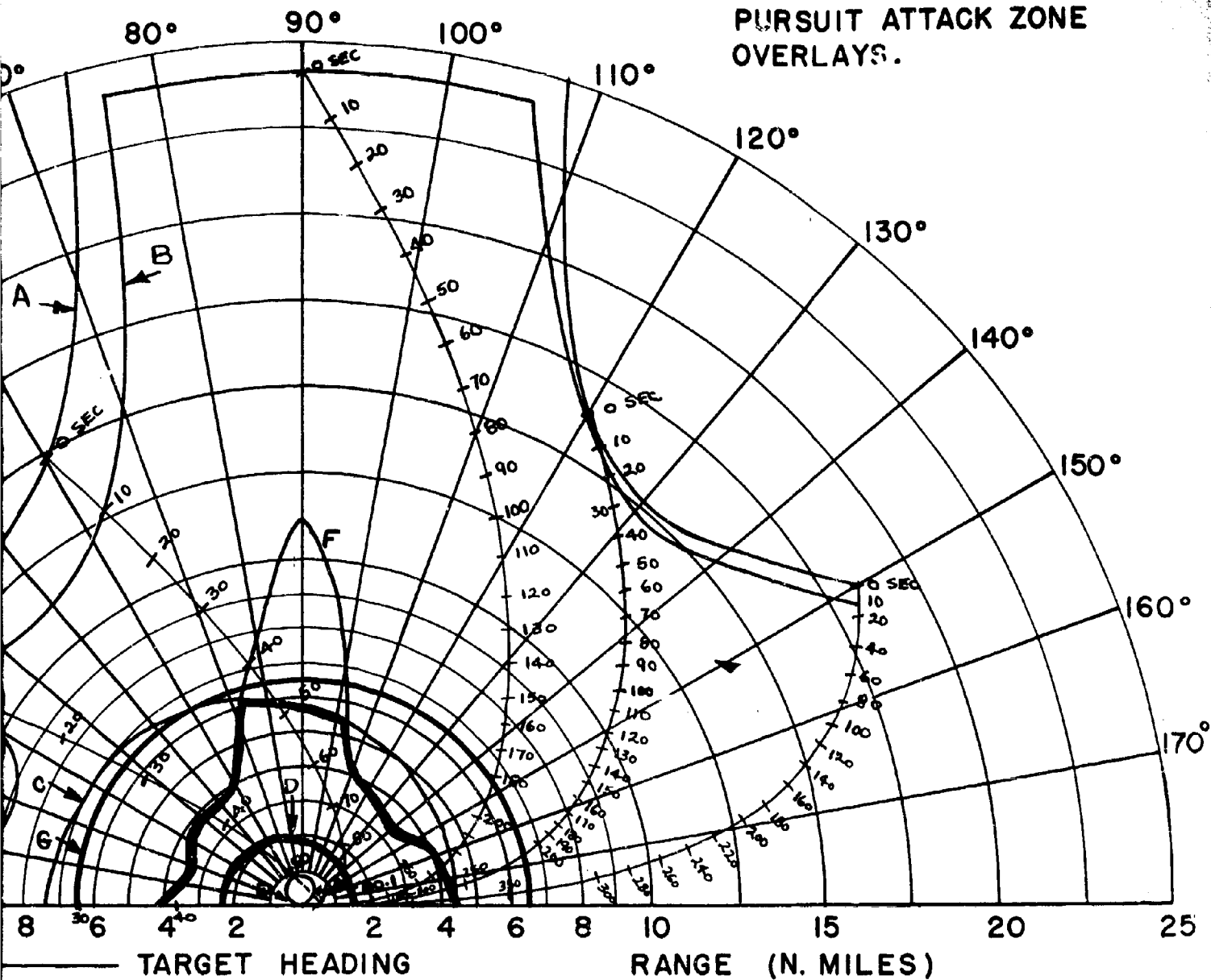
$V_T = 873$ FT/SEC

ALTITUDE = 50,000 FT.
INCREASED THRUST AT DETECTION

← TARGET HEADING

- A - 85% DETECTION RANGE
- B - LOCK-ON RANGE (10 SEC. LOCK-ON TIME)
- C - SPARROW III MAX. AERODYNAMIC RANGE
- D - SPARROW III MIN. AERODYNAMIC RANGE
- E - CONSTANT LOAD FACTOR LOCUS (N_z)
- F - 90% SPARROW III SEEKER LOCK-ON RANGE
- G - 6.5 N.M. INTERLOCK

FIG. VII - CO-ALTITUDE LEAD
PURSUIT ATTACK ZONE
OVERLAYS.



85% DETECTION RANGE
LOCK-ON RANGE (10 SEC. LOCK-ON TIME)
SPARROW III MAX. AERODYNAMIC RANGE
SPARROW III MIN. AERODYNAMIC RANGE
CONSTANT LOAD FACTOR LOCUS ($N_z = 3$)
90% SPARROW III SEEKER LOCK-ON RANGE
6.5 N.M. INTERLOCK

CONFIDENTIAL

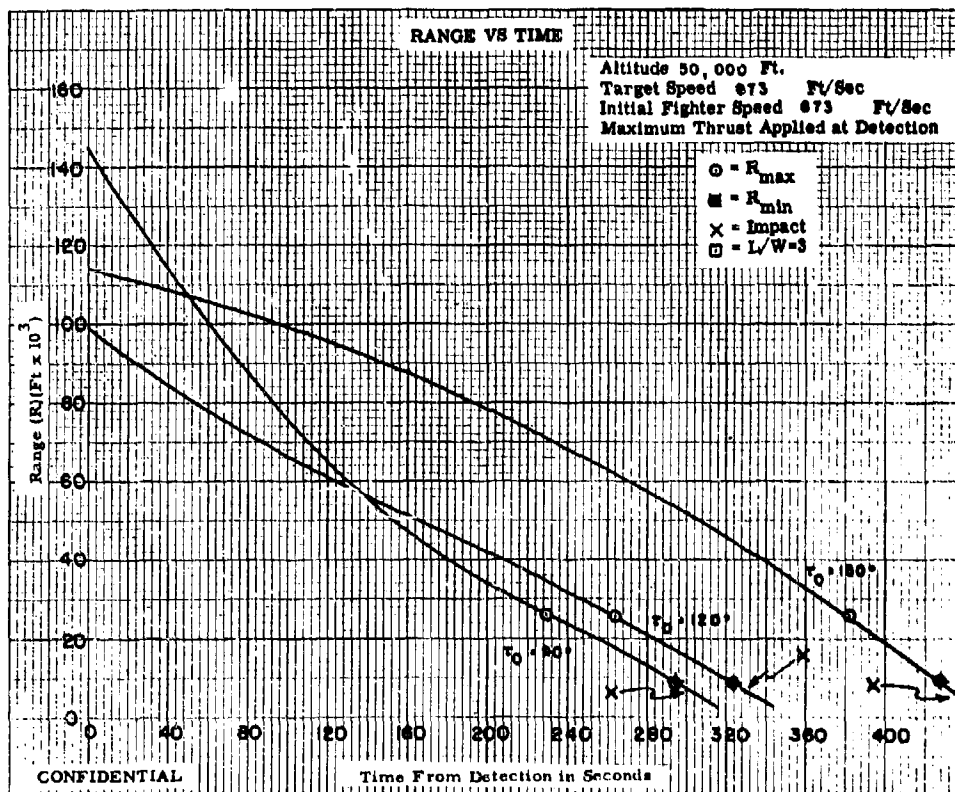
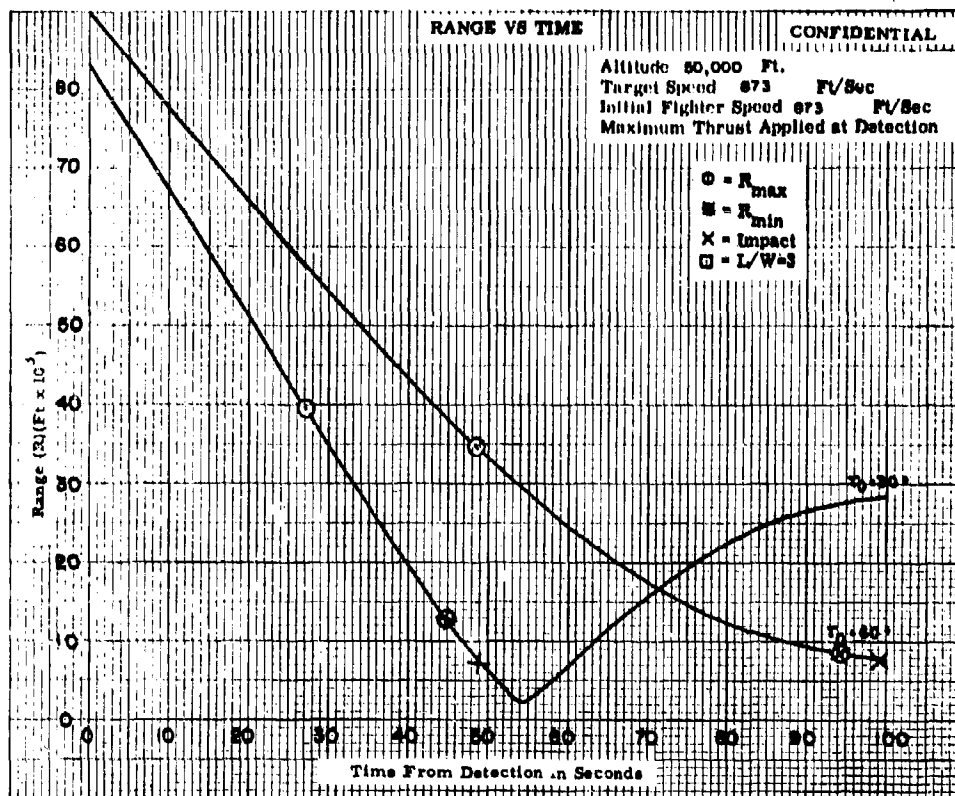


Fig. VII-1

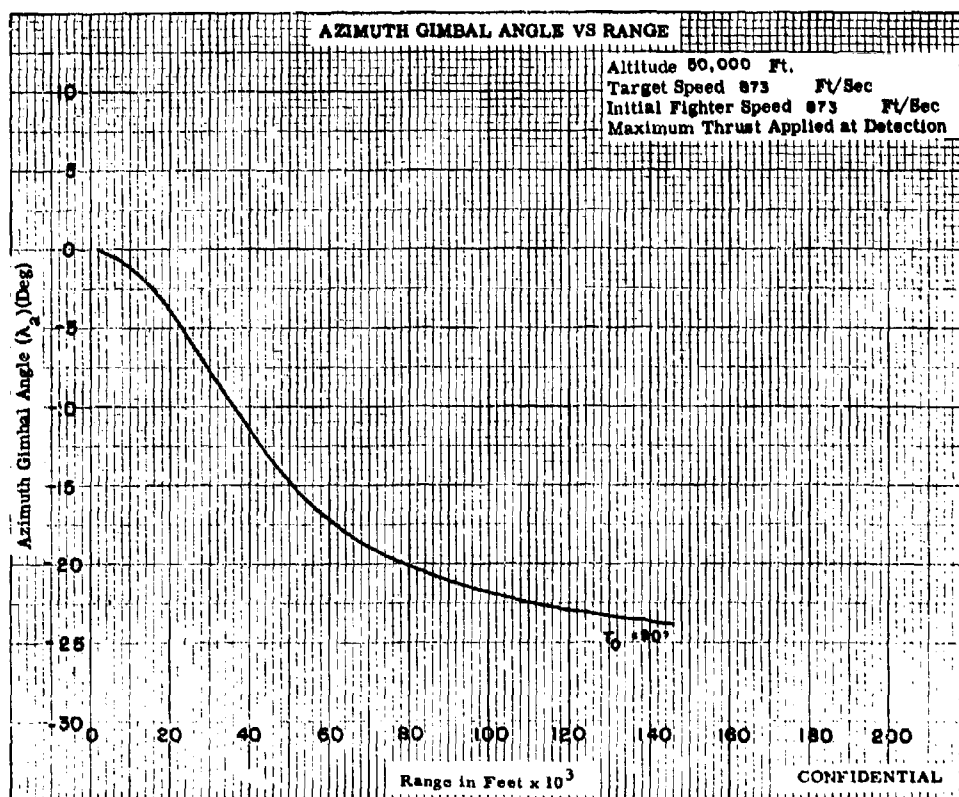
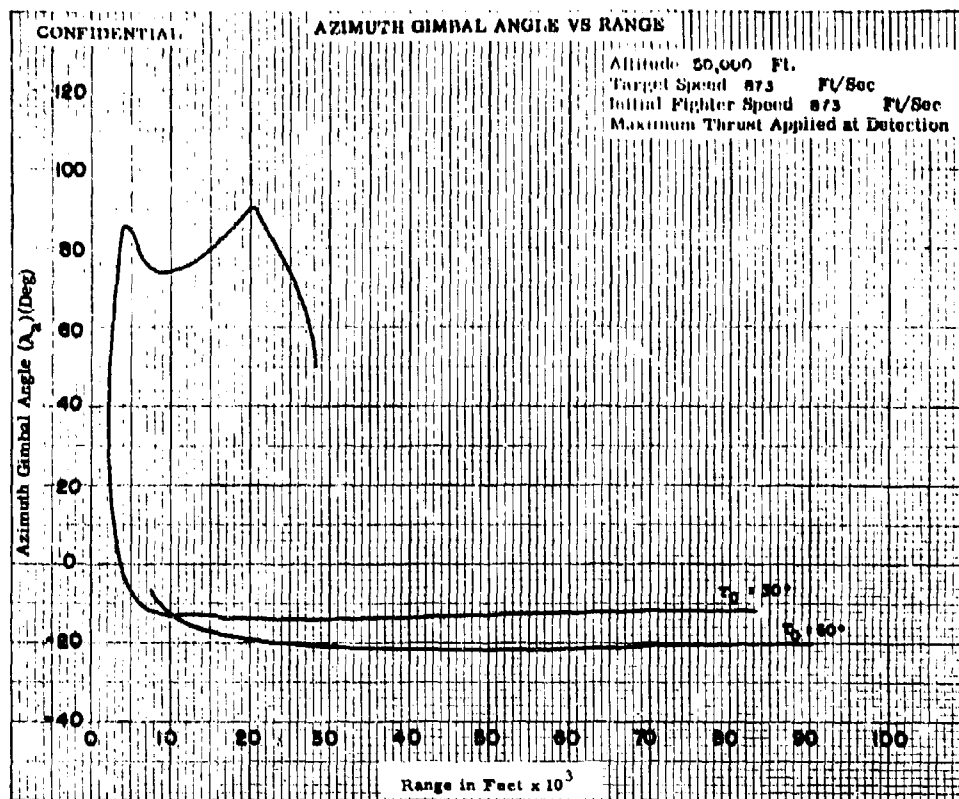


Fig. VII-2a

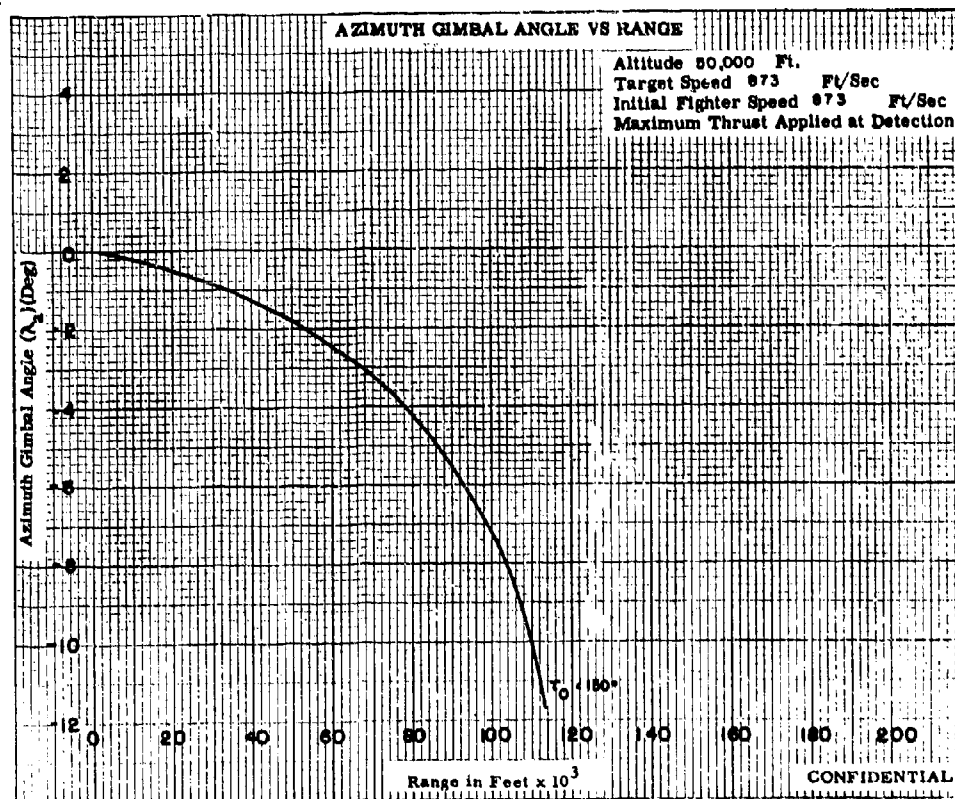
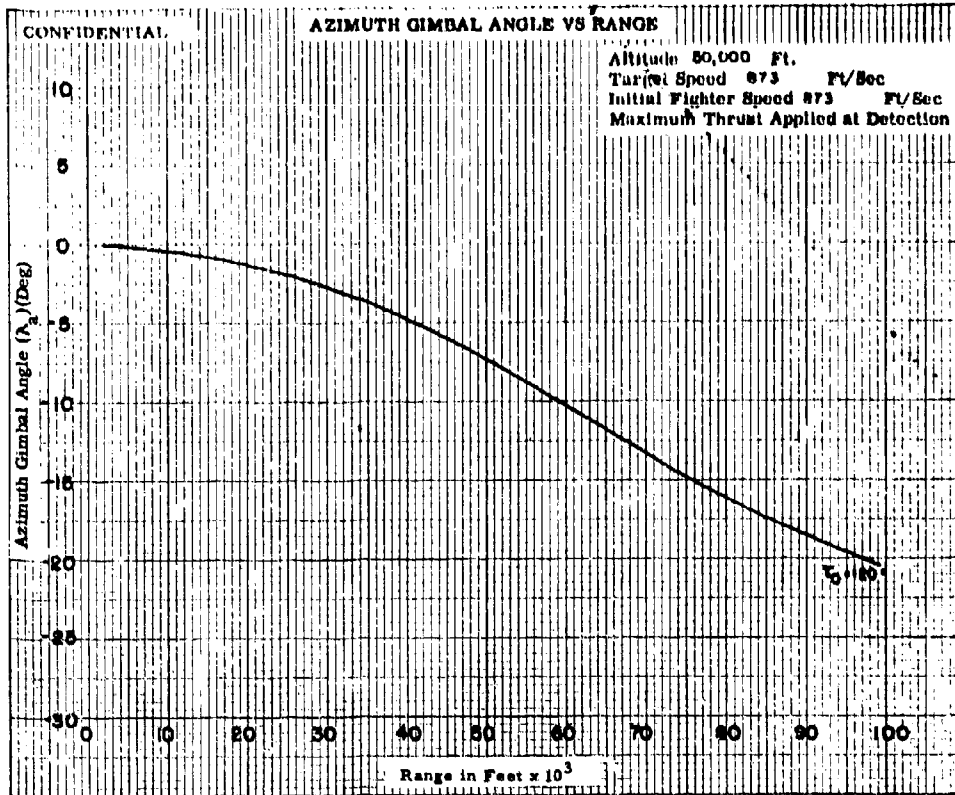


Fig. VII-2b

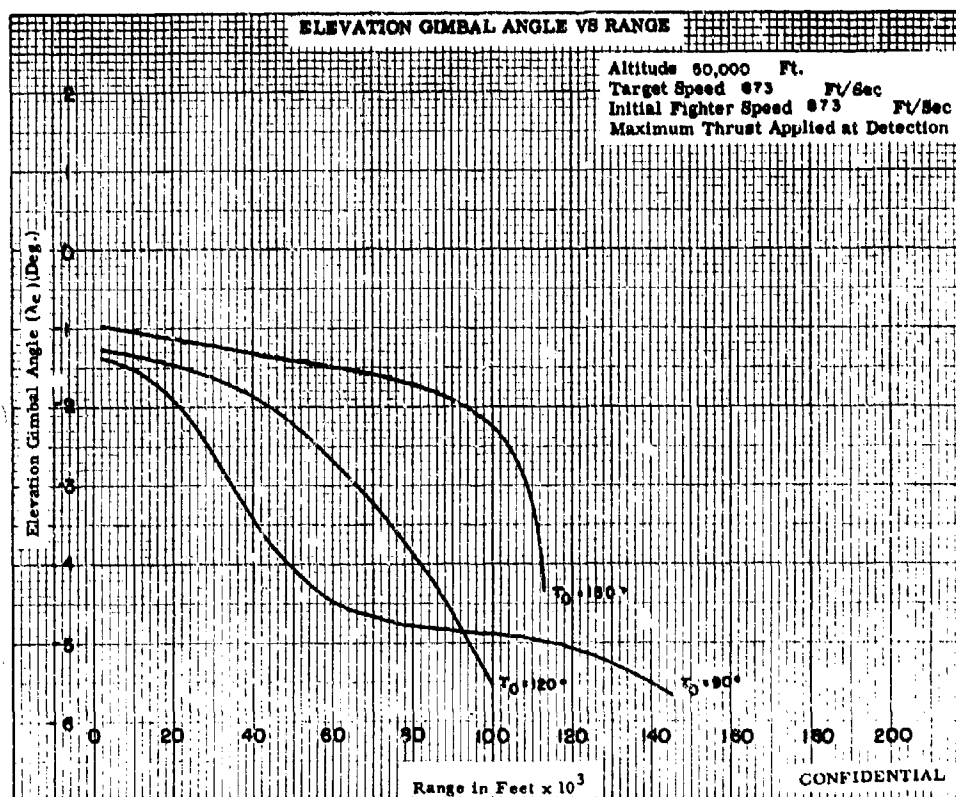
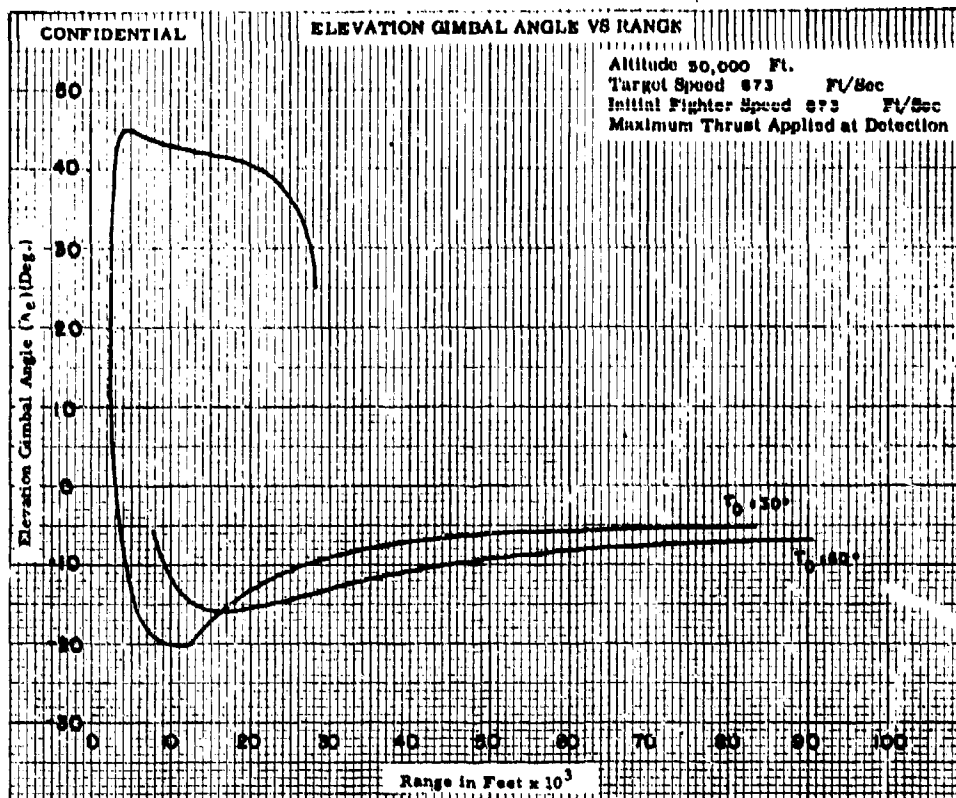


Fig. VII-3

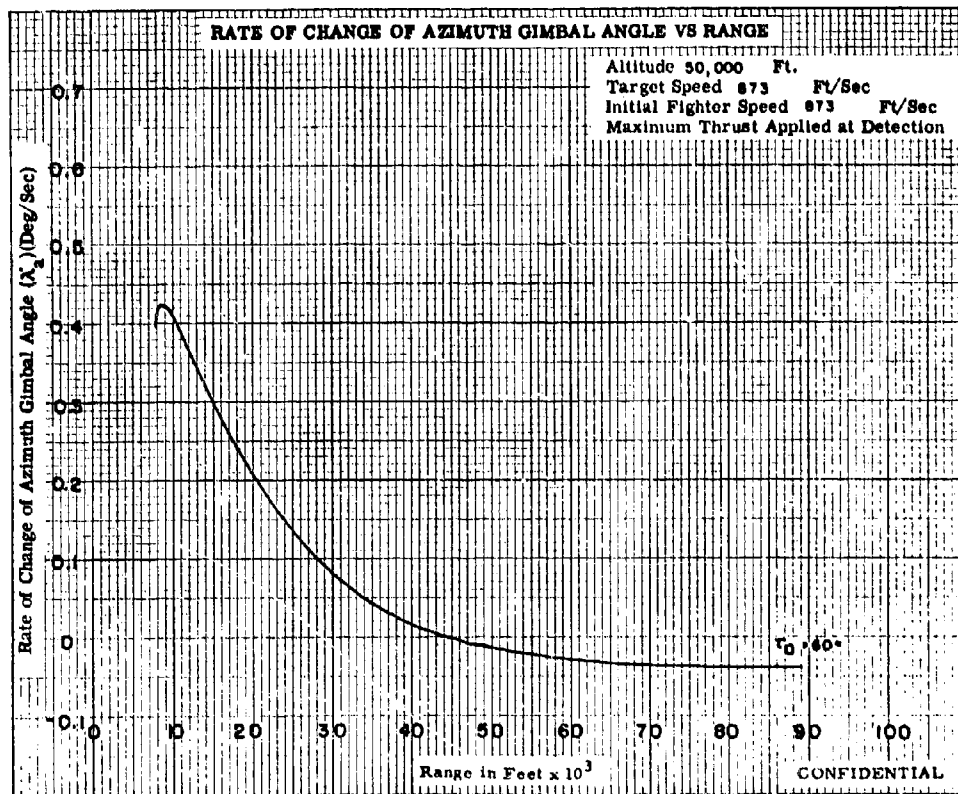
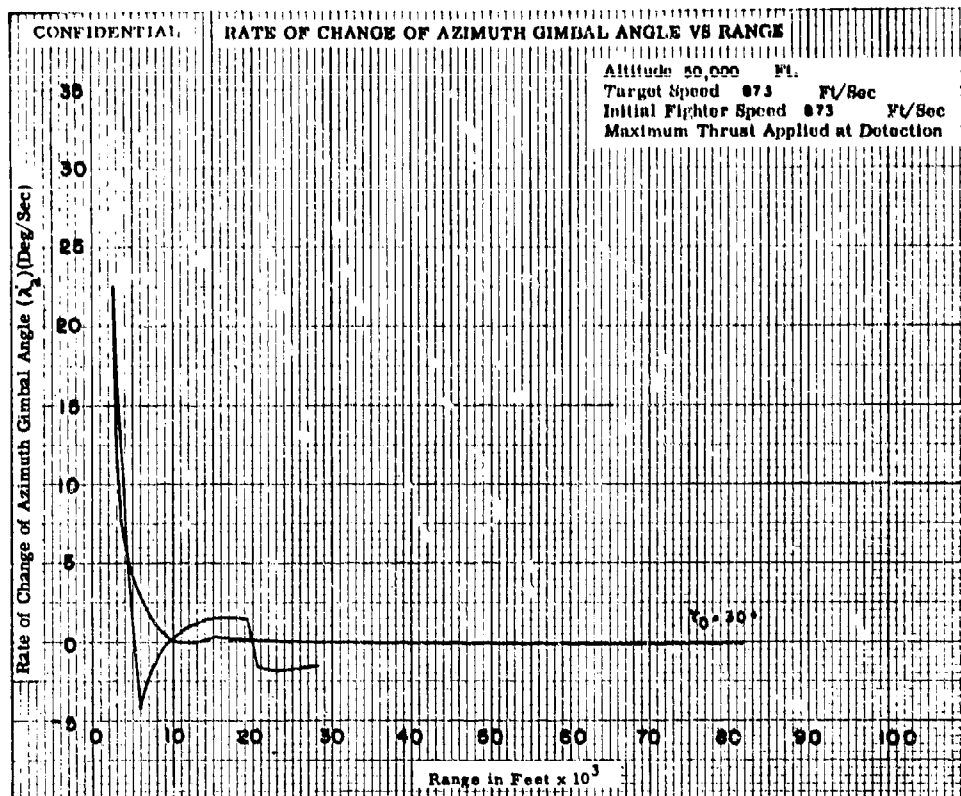


Fig. VII-4a

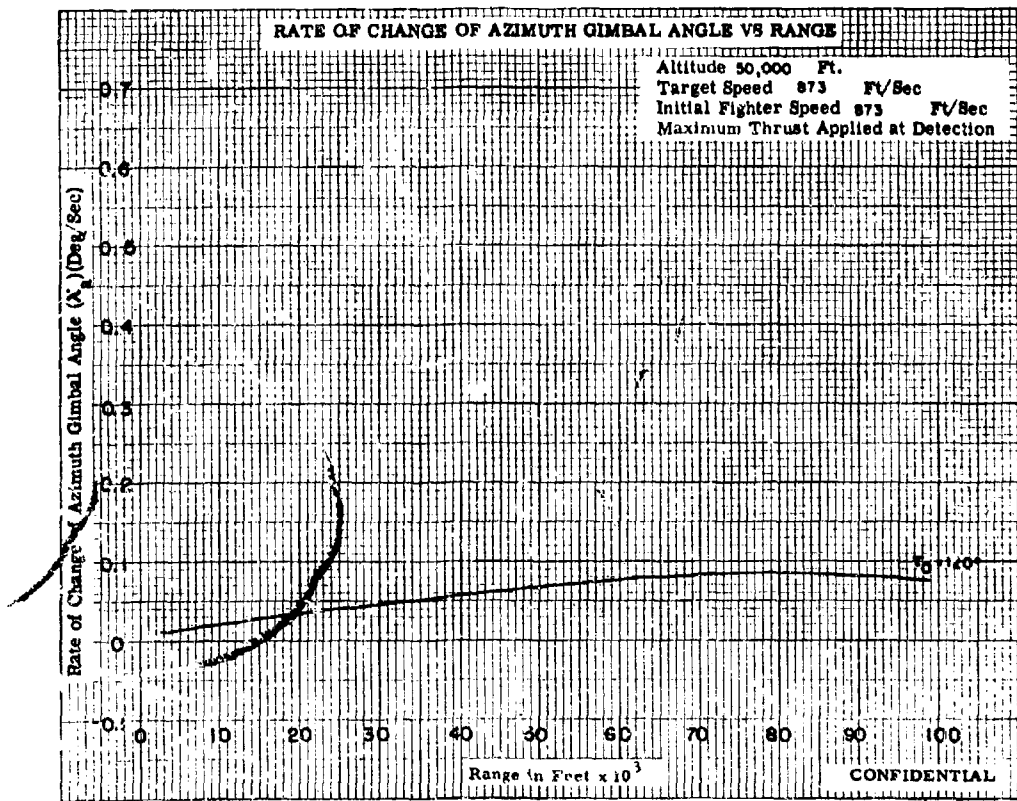
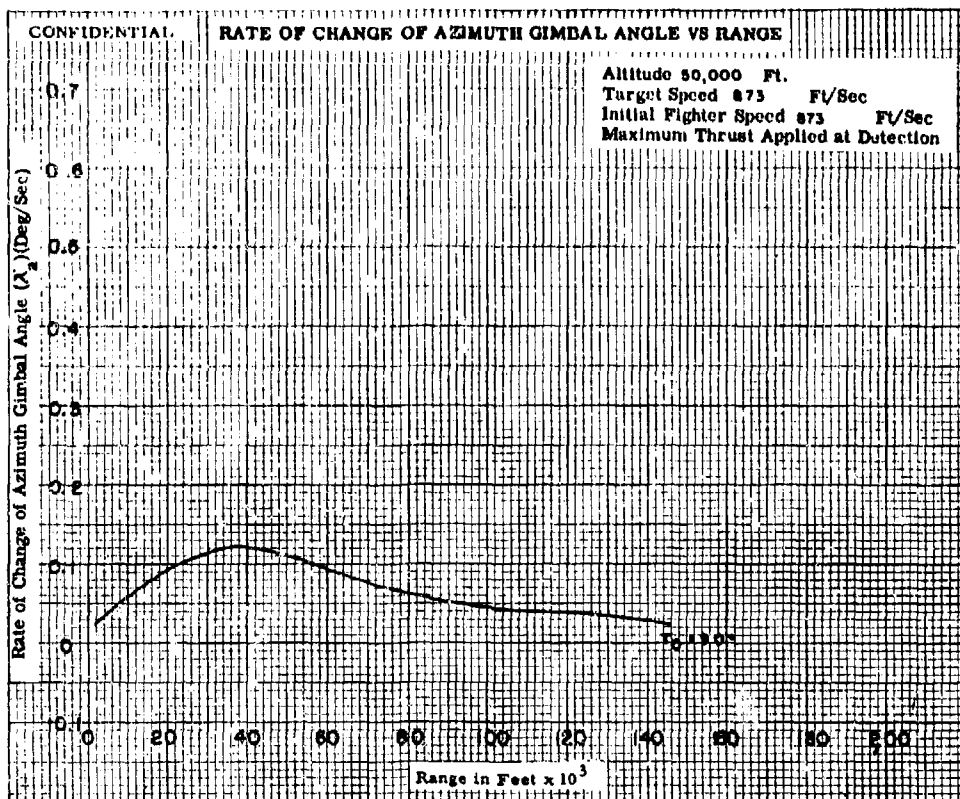


Fig. VII-4b

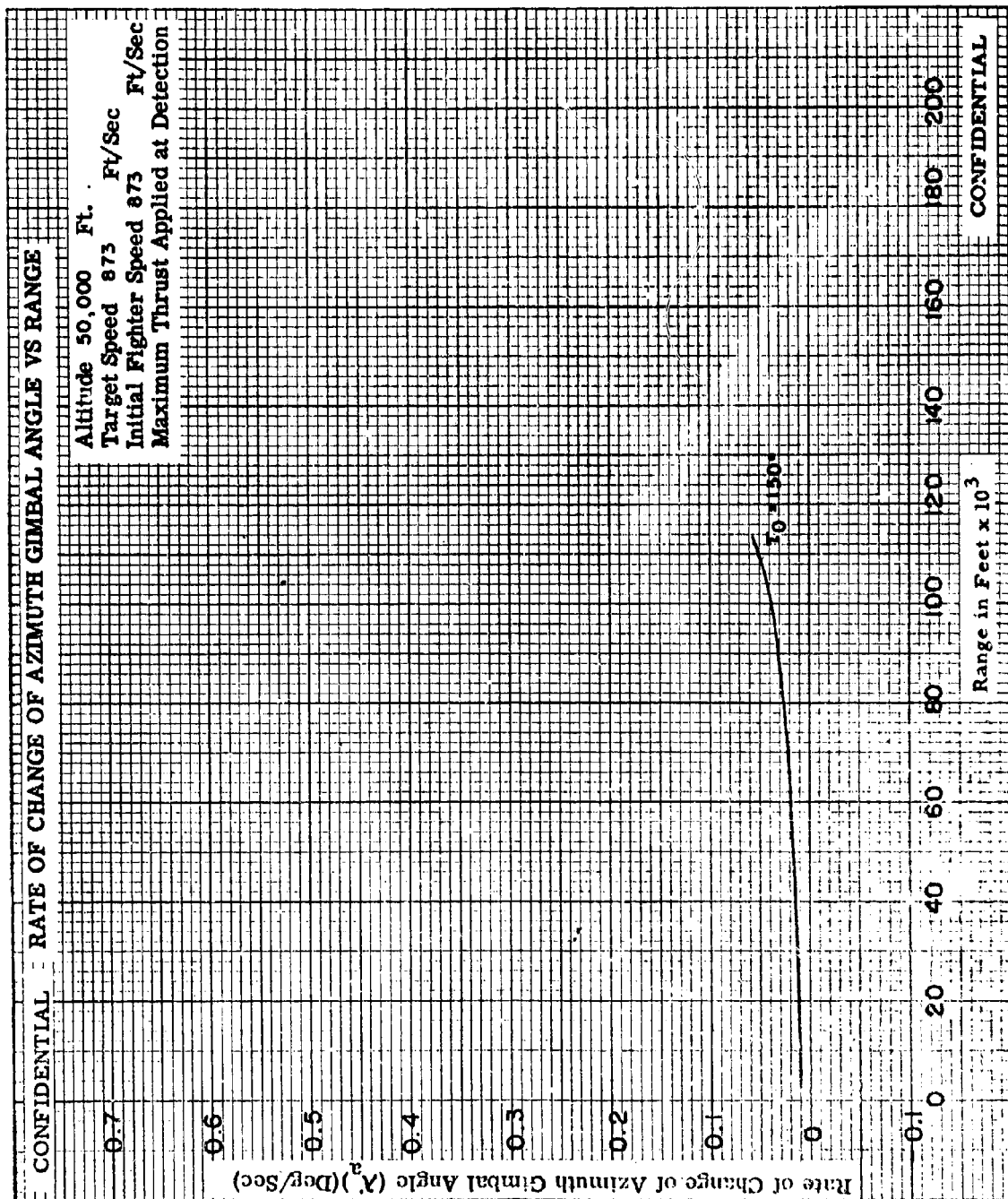


Fig. VII-4c

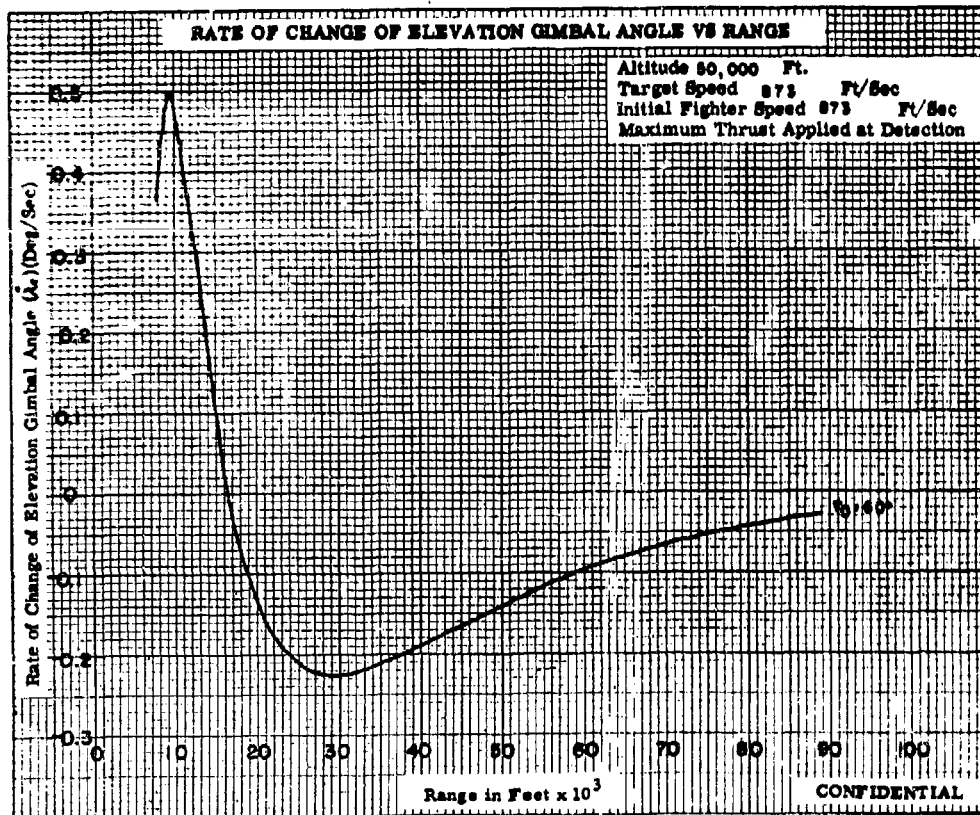
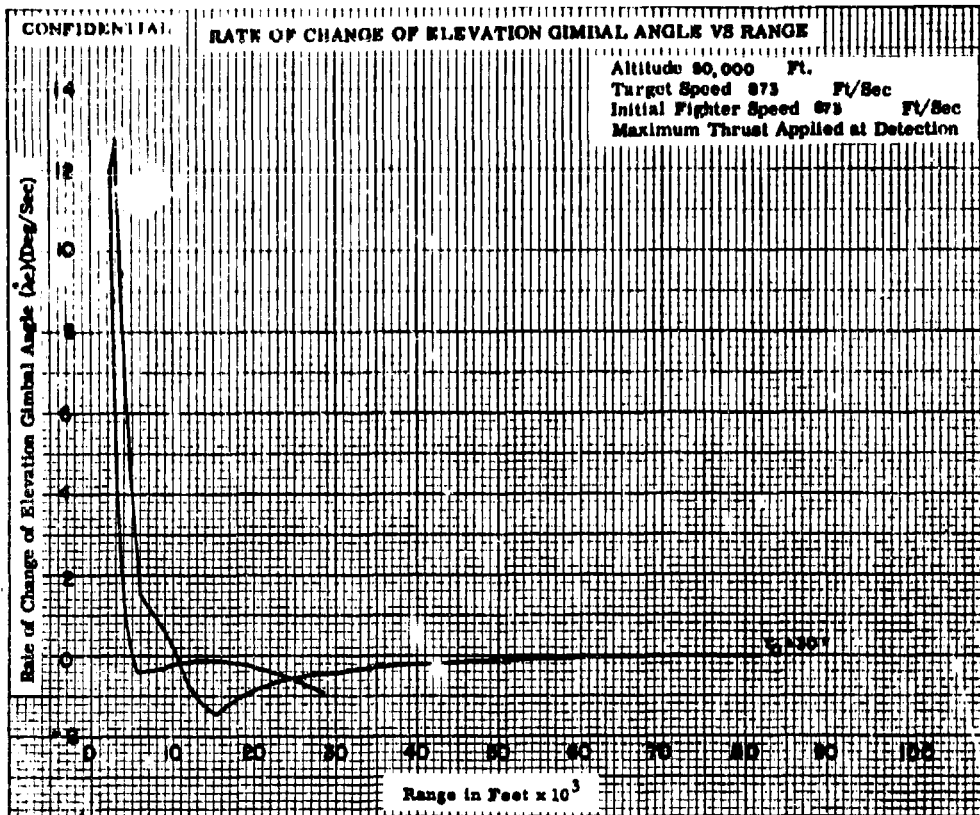


Fig. VII-3a

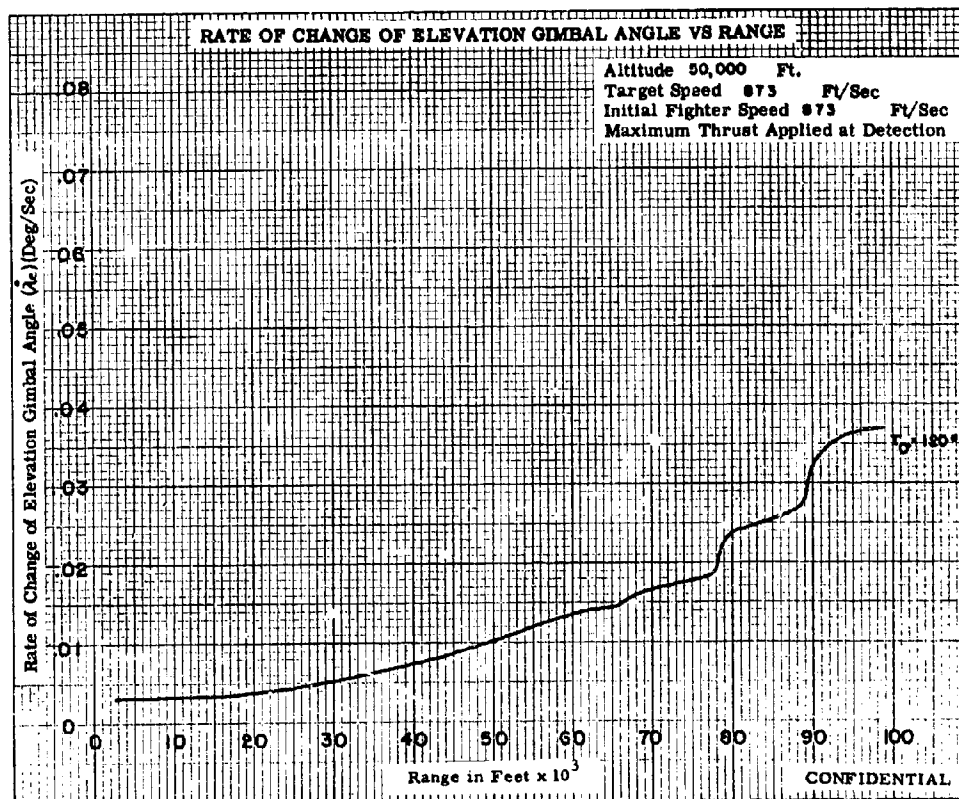
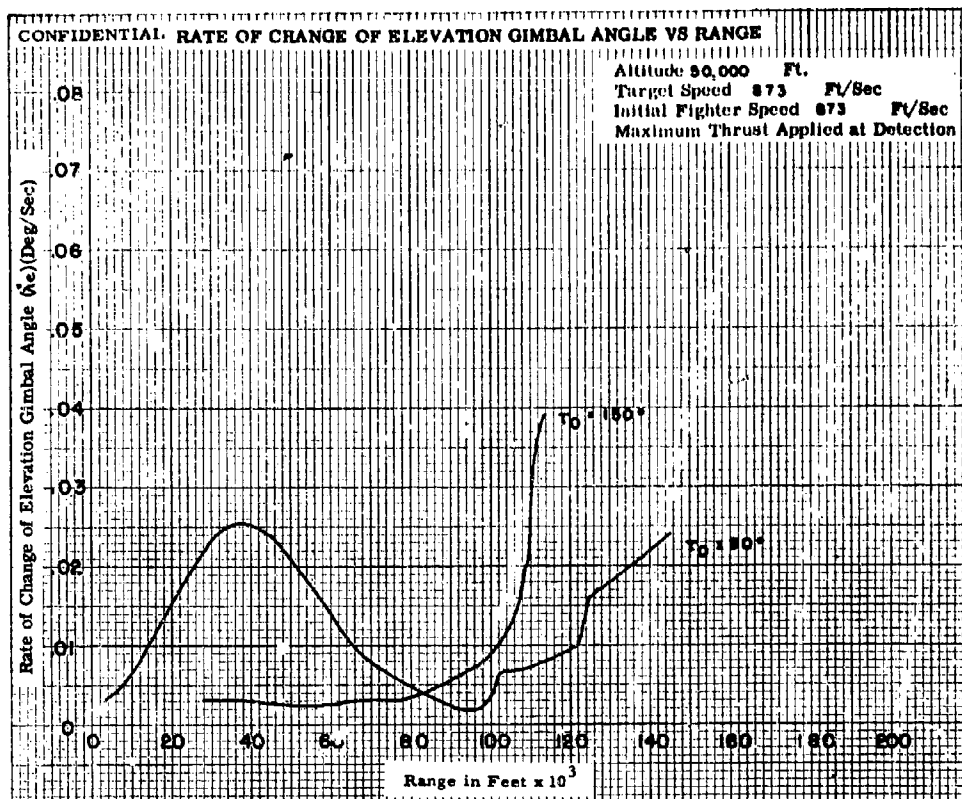


Fig. VII-5b

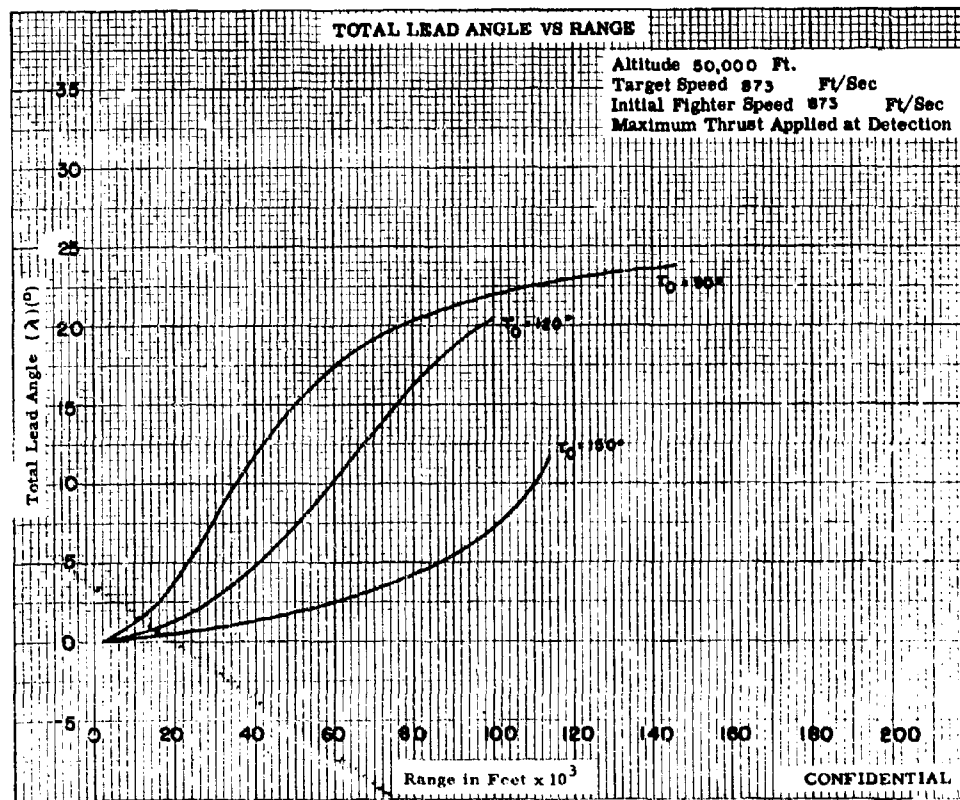
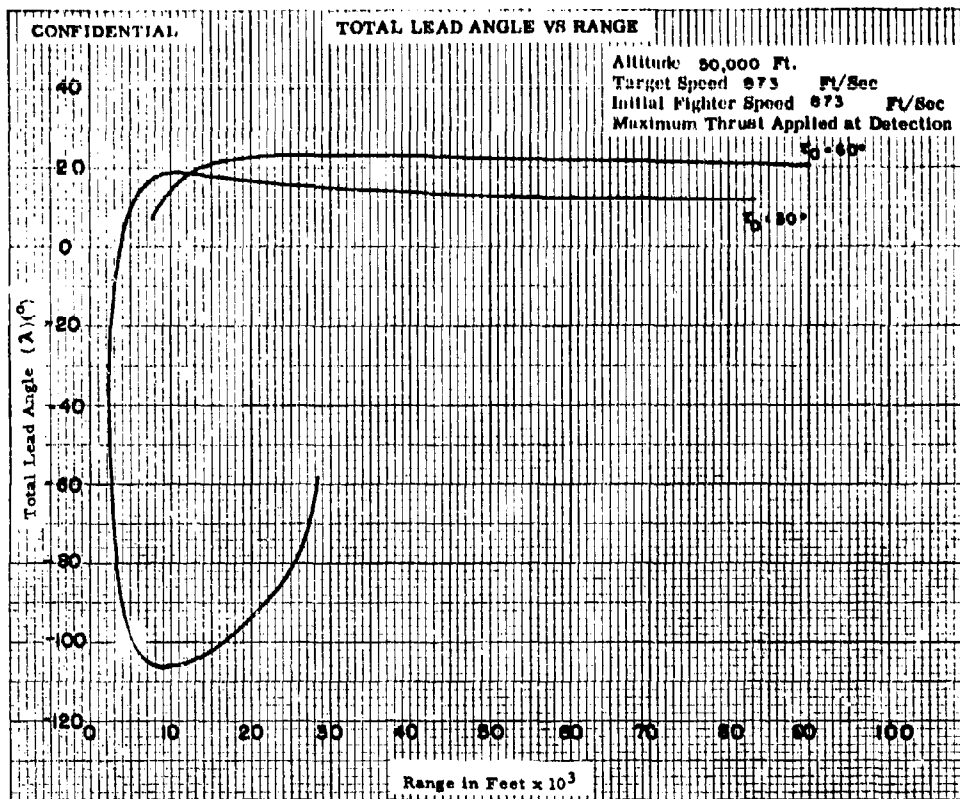


Fig. VII-6

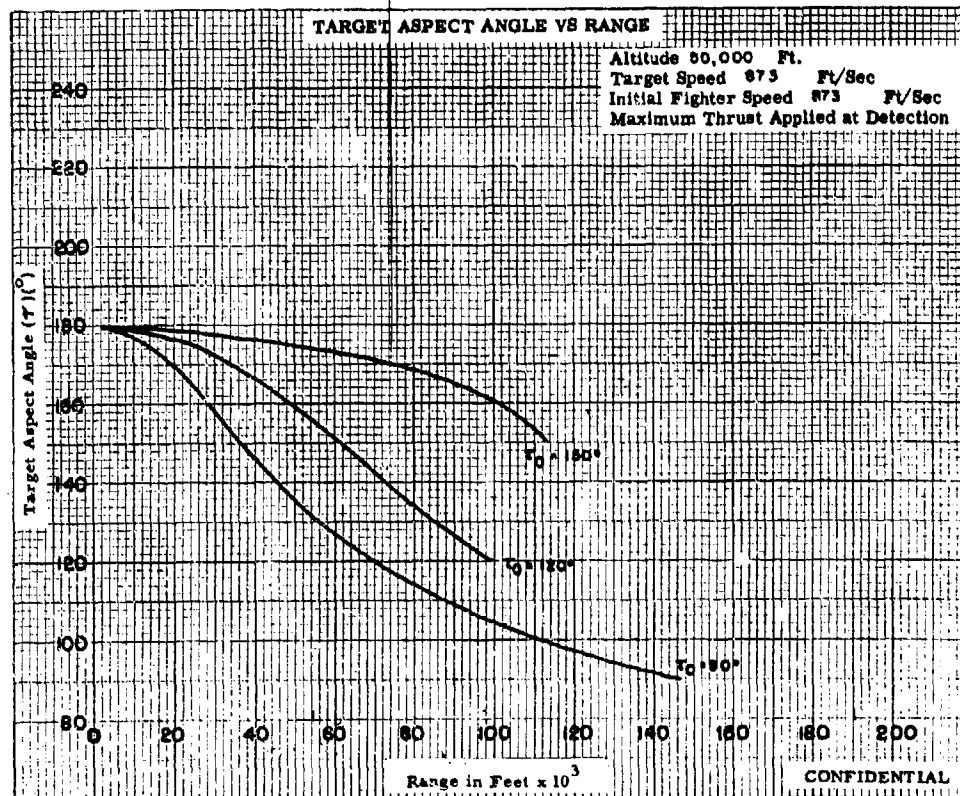
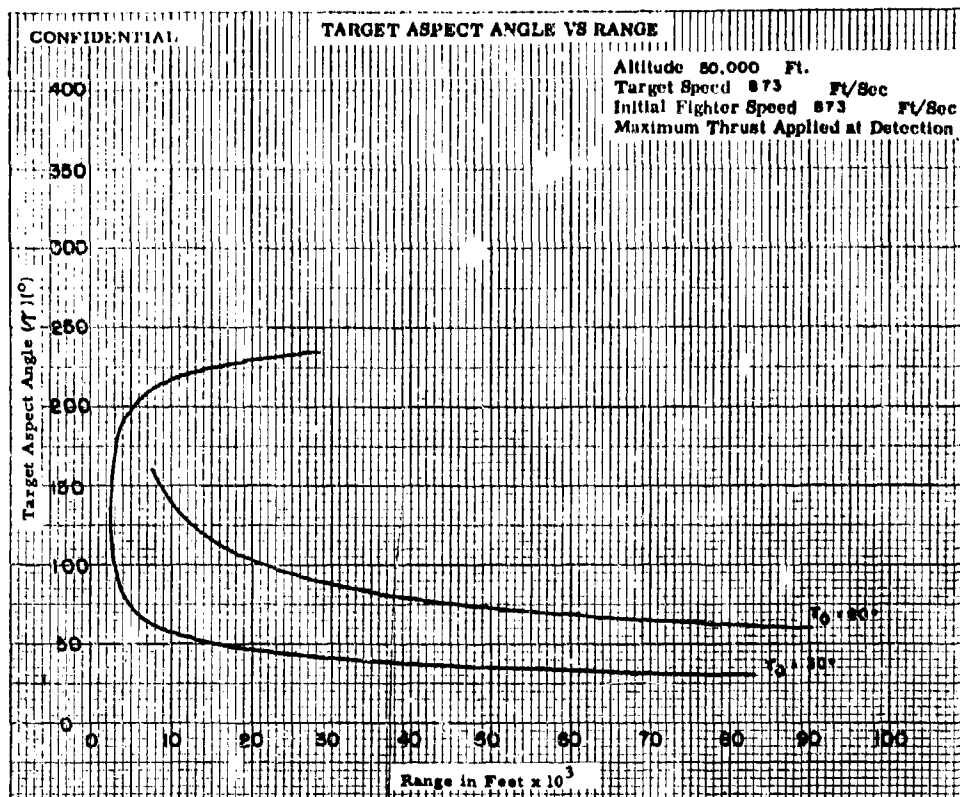


Fig. VII-7

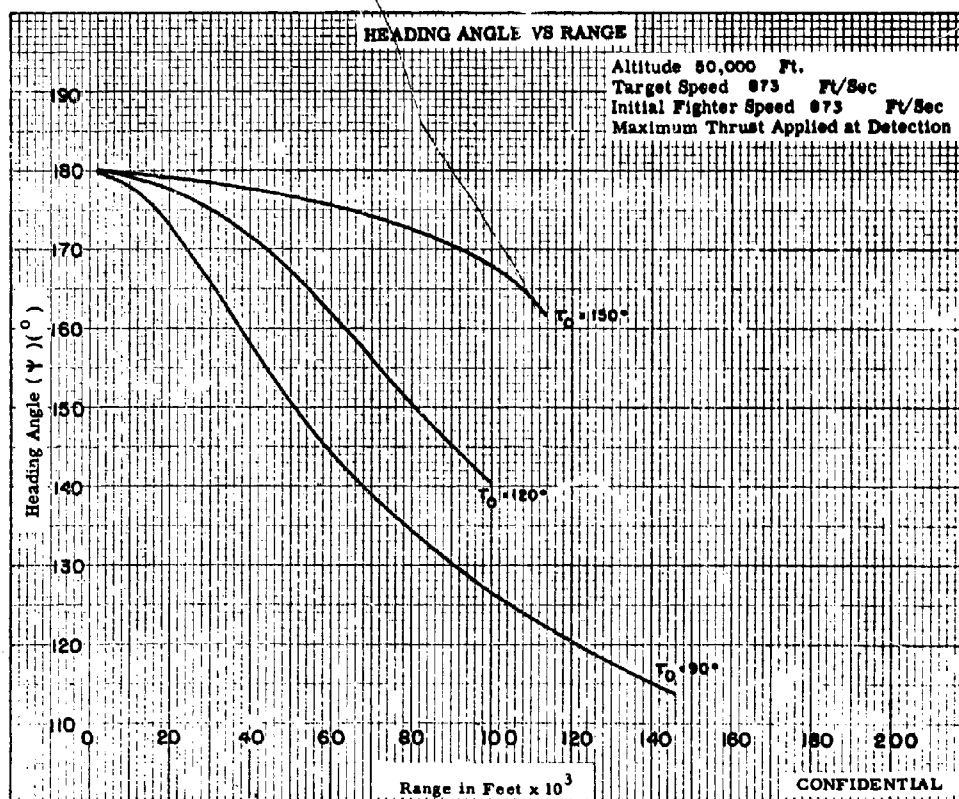
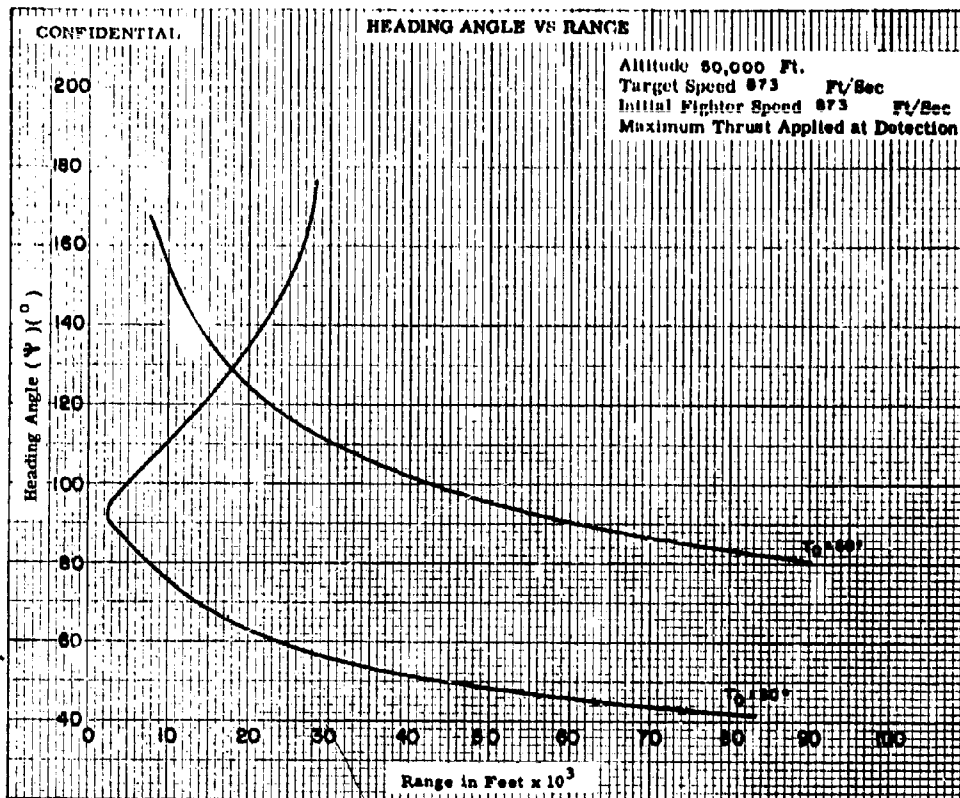


Fig. VII-8

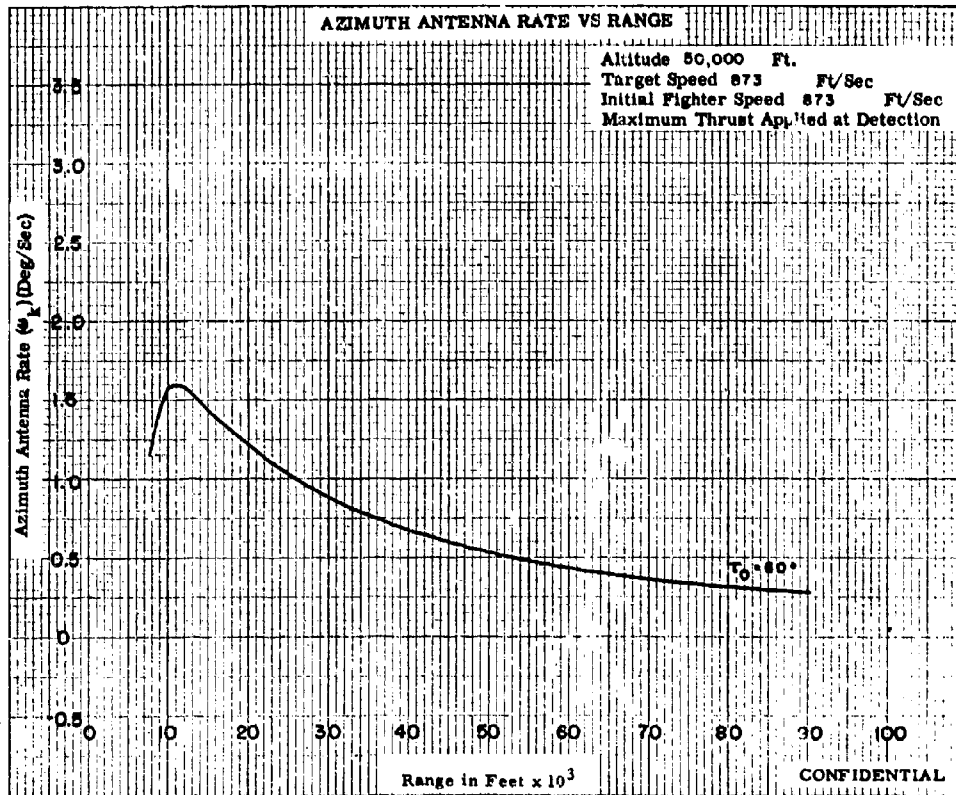
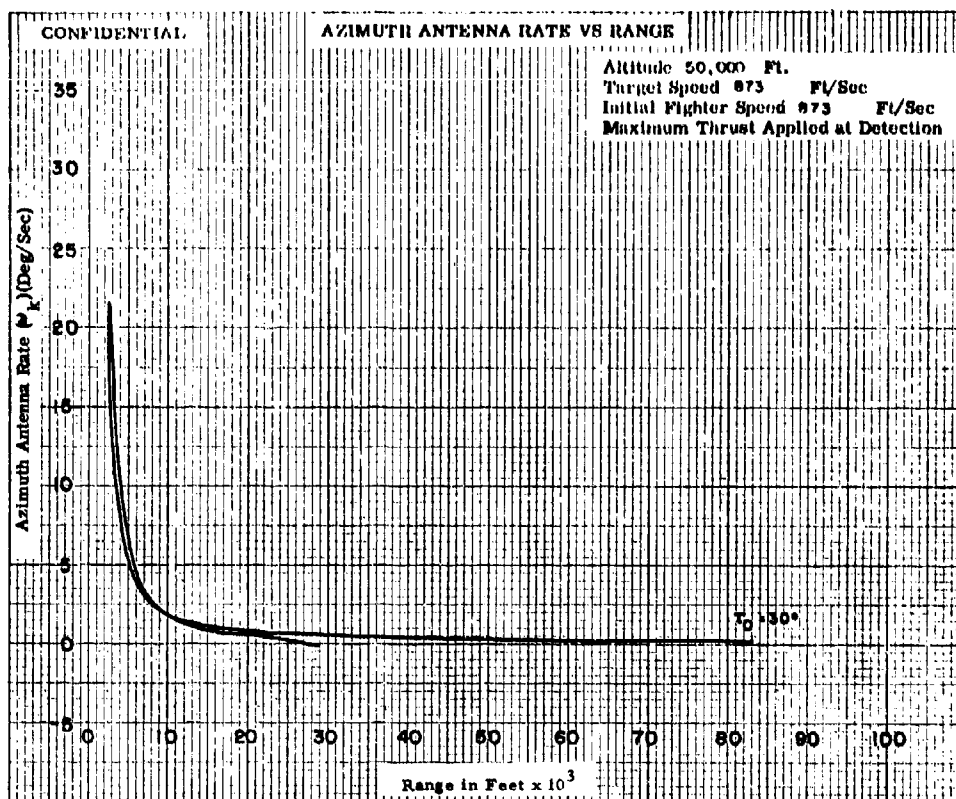


Fig. VII-9a

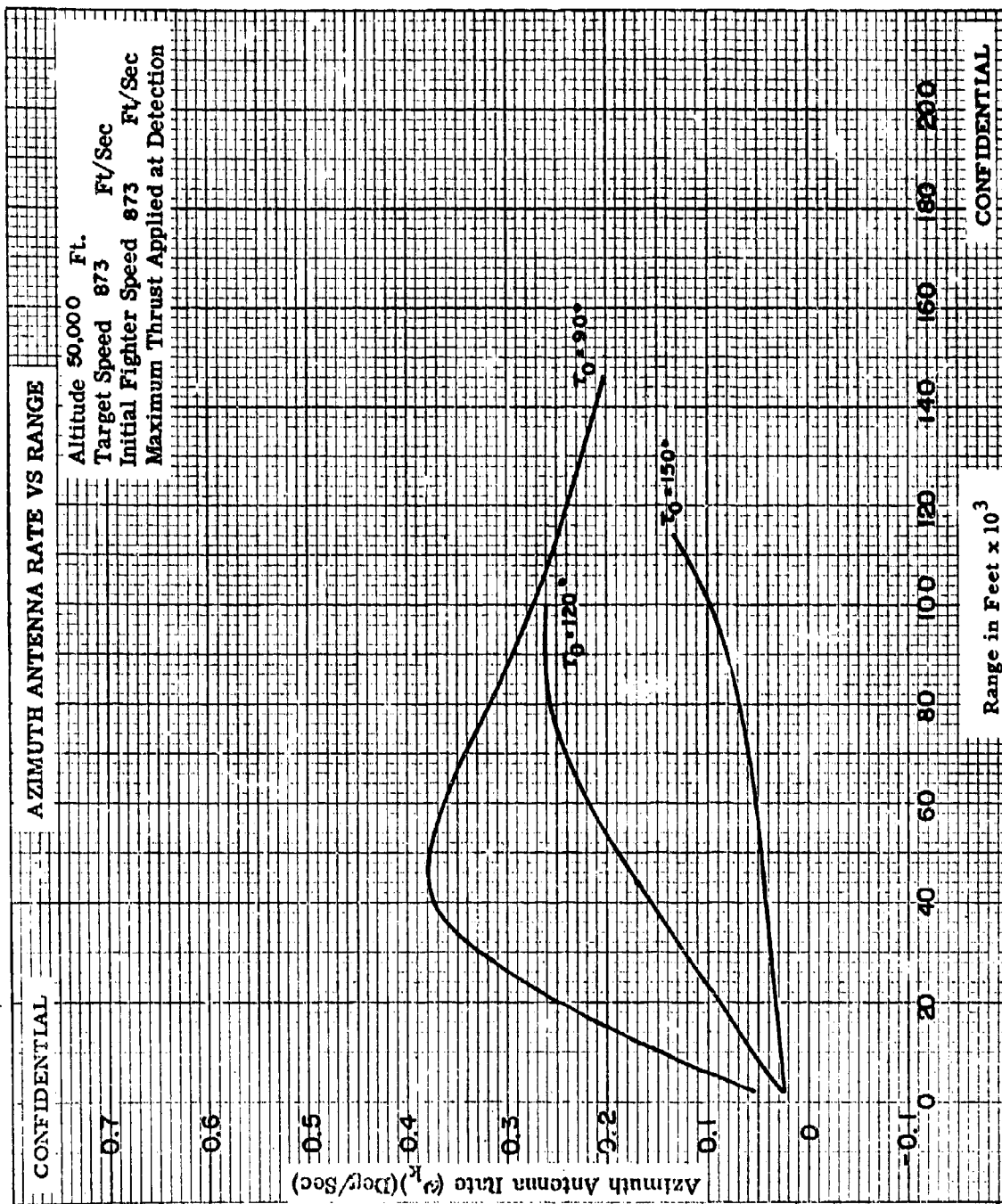


Fig. VII-9b

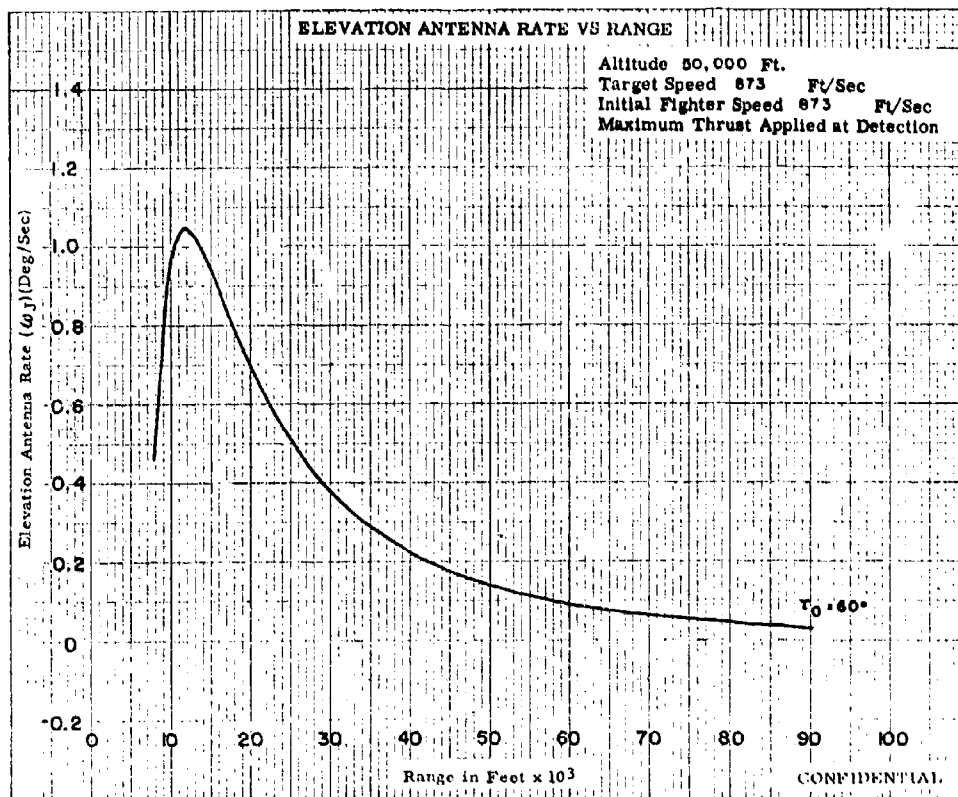
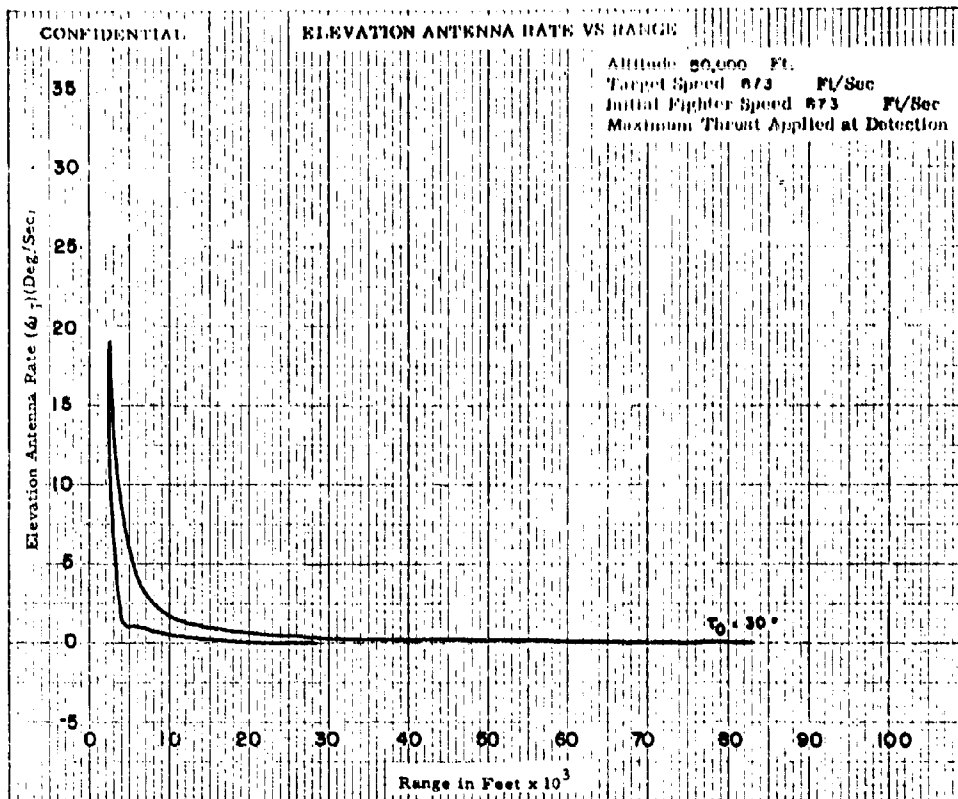


Fig. VII-10a

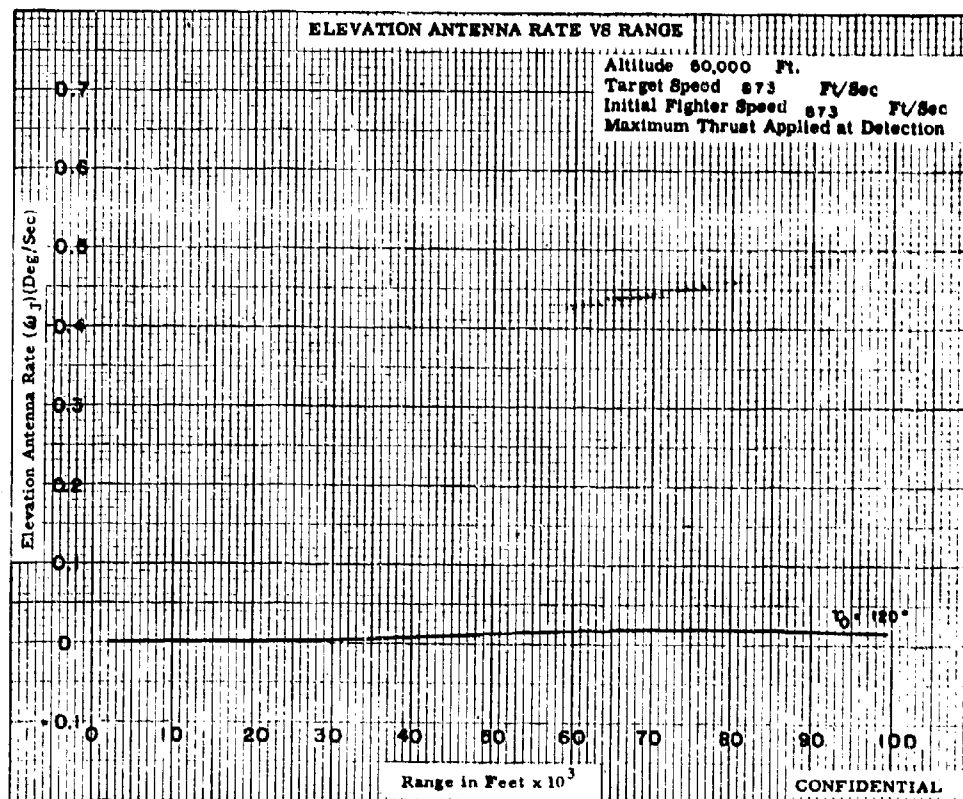
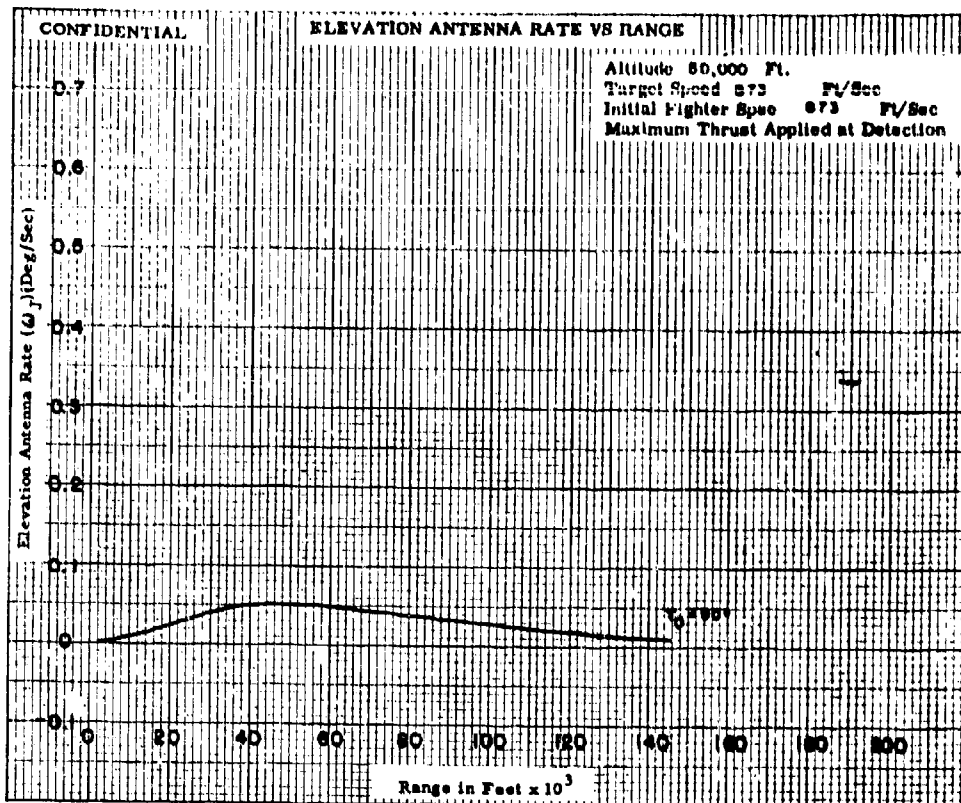


Fig. VII-10b

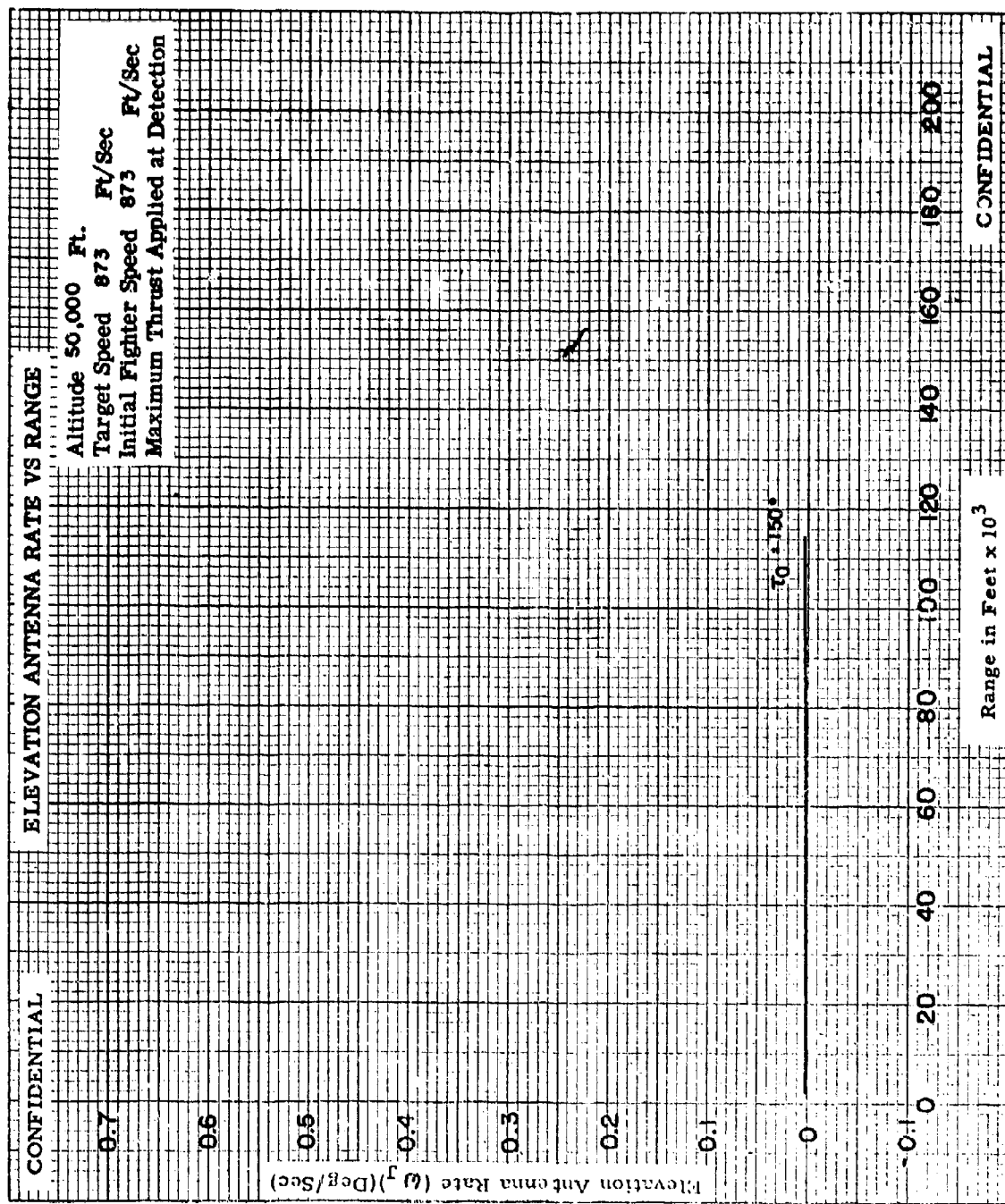


Fig. VII-10c

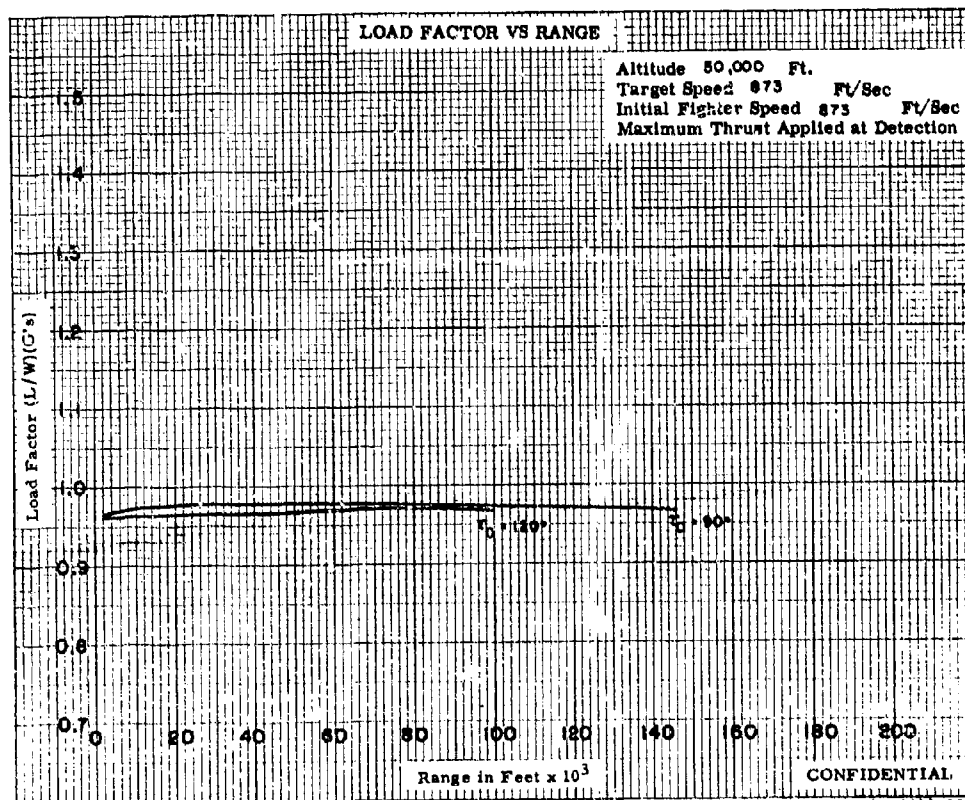
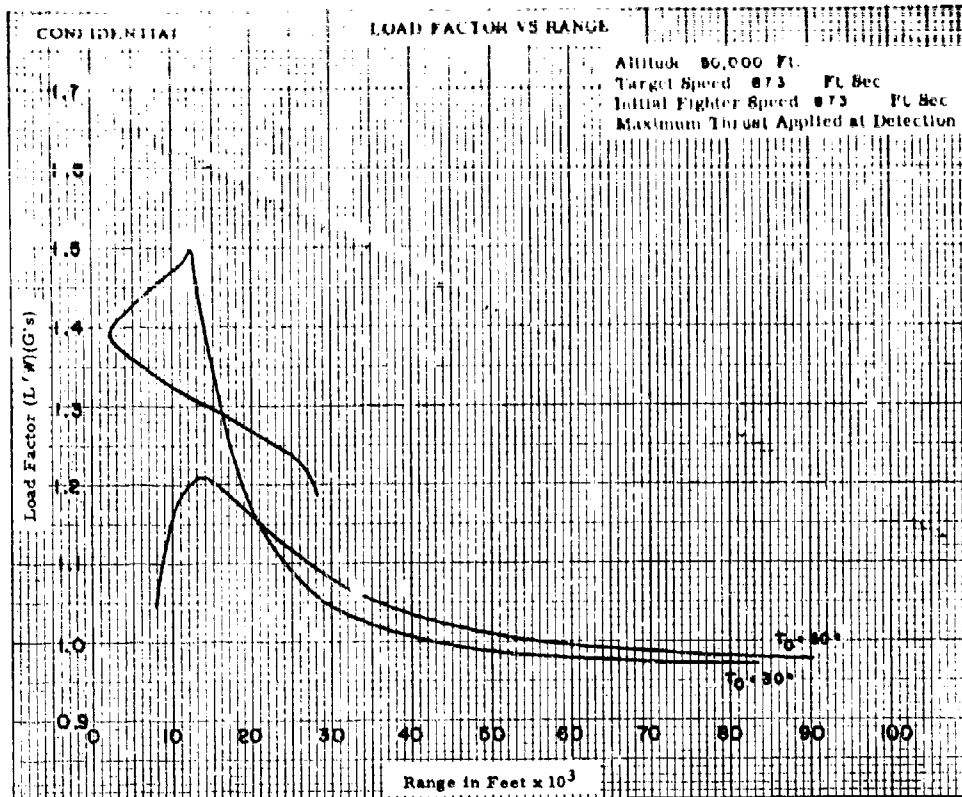


Fig. VII-11a

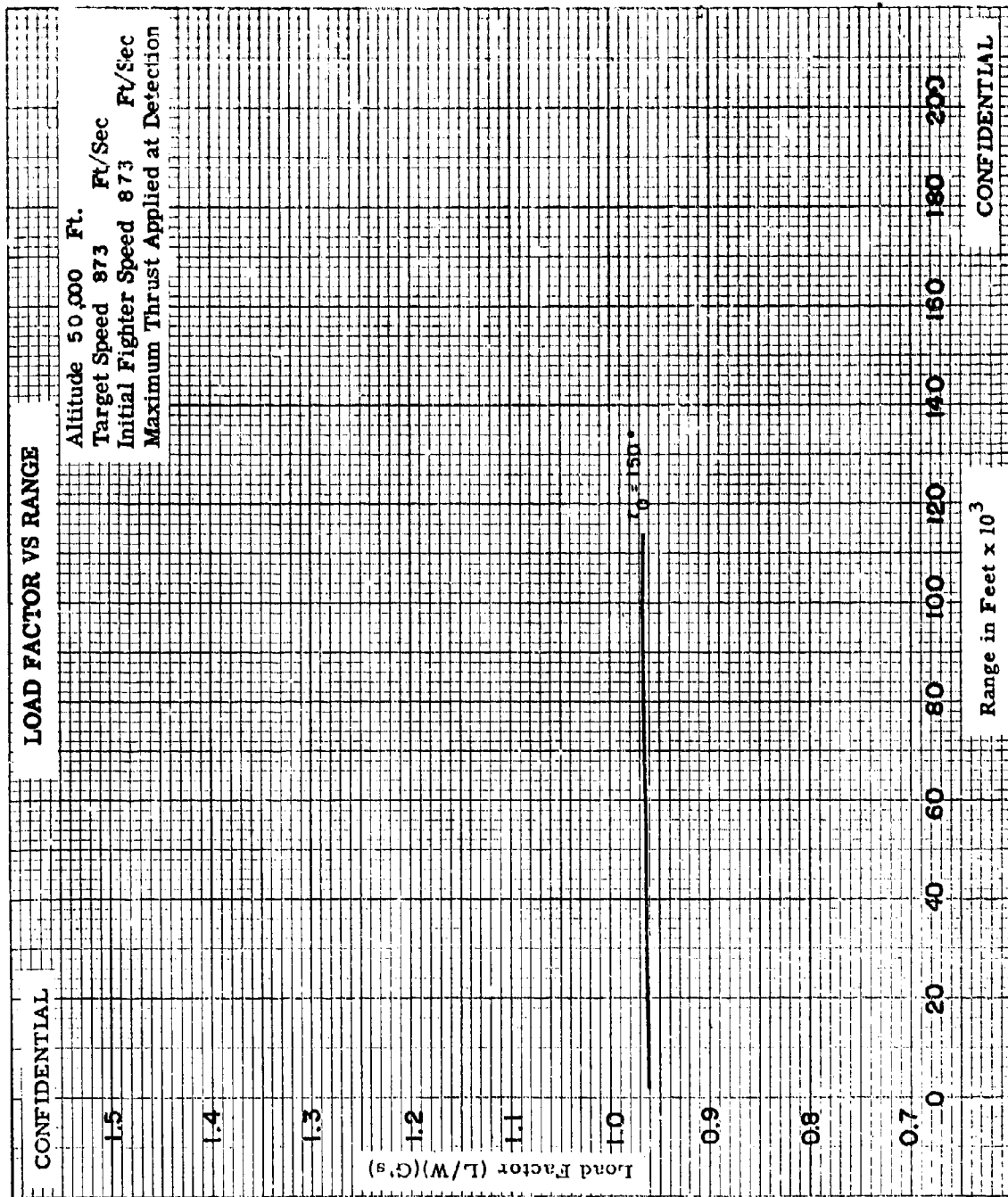


Fig. VI-11b

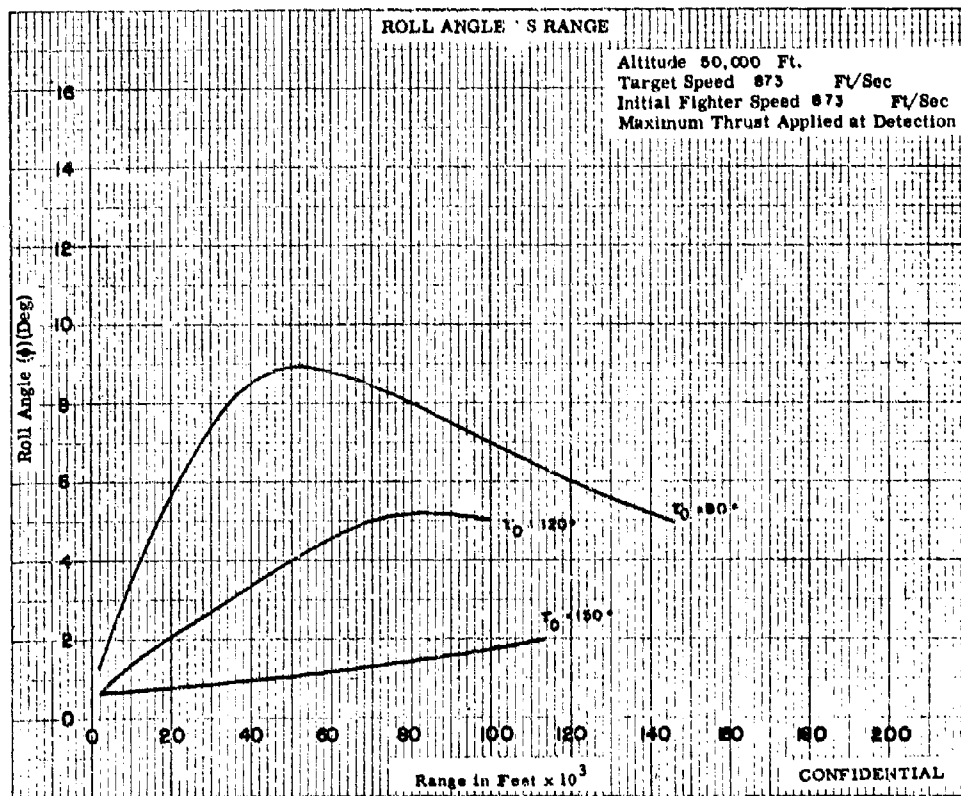
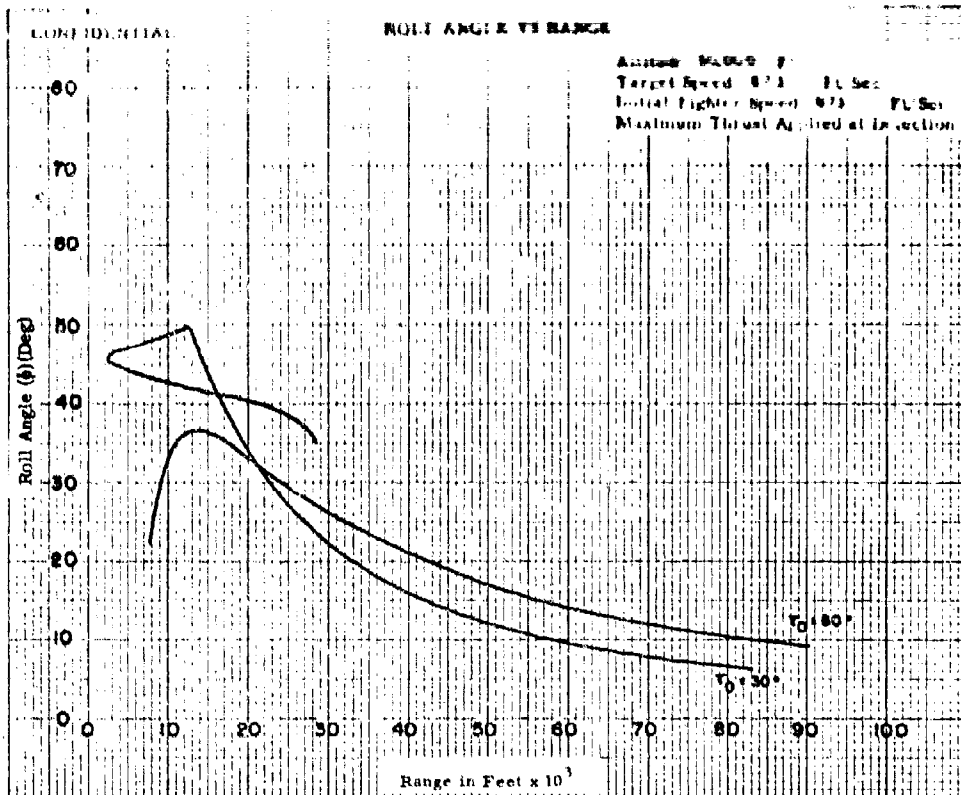


Fig. VII-12

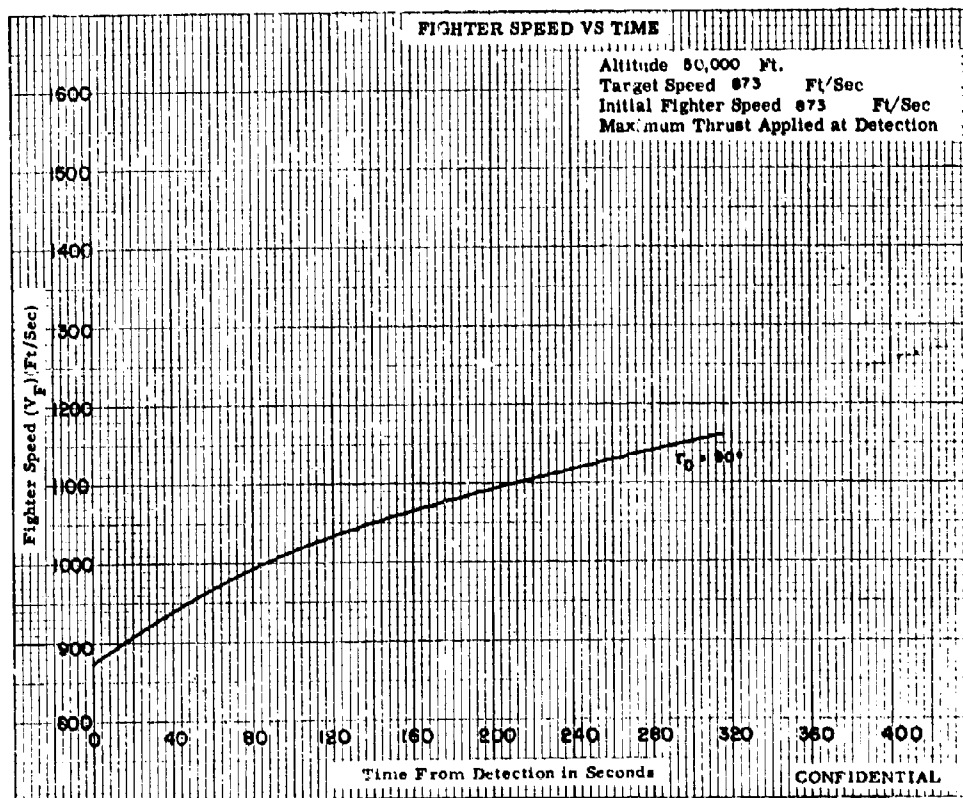
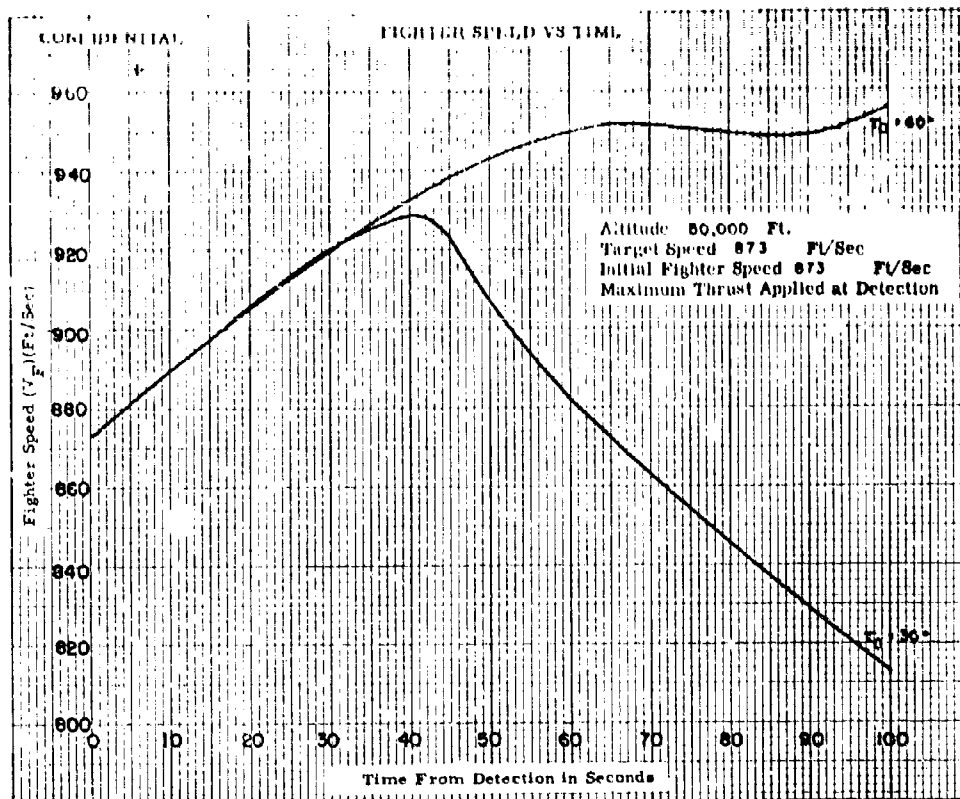


Fig. VII-13a

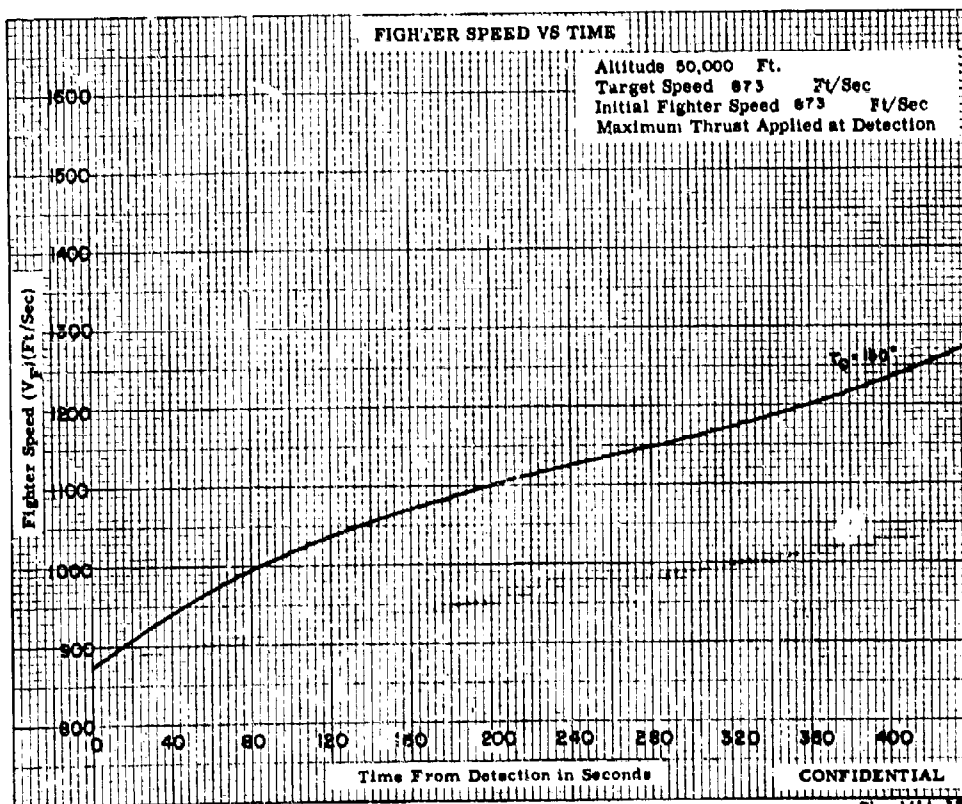
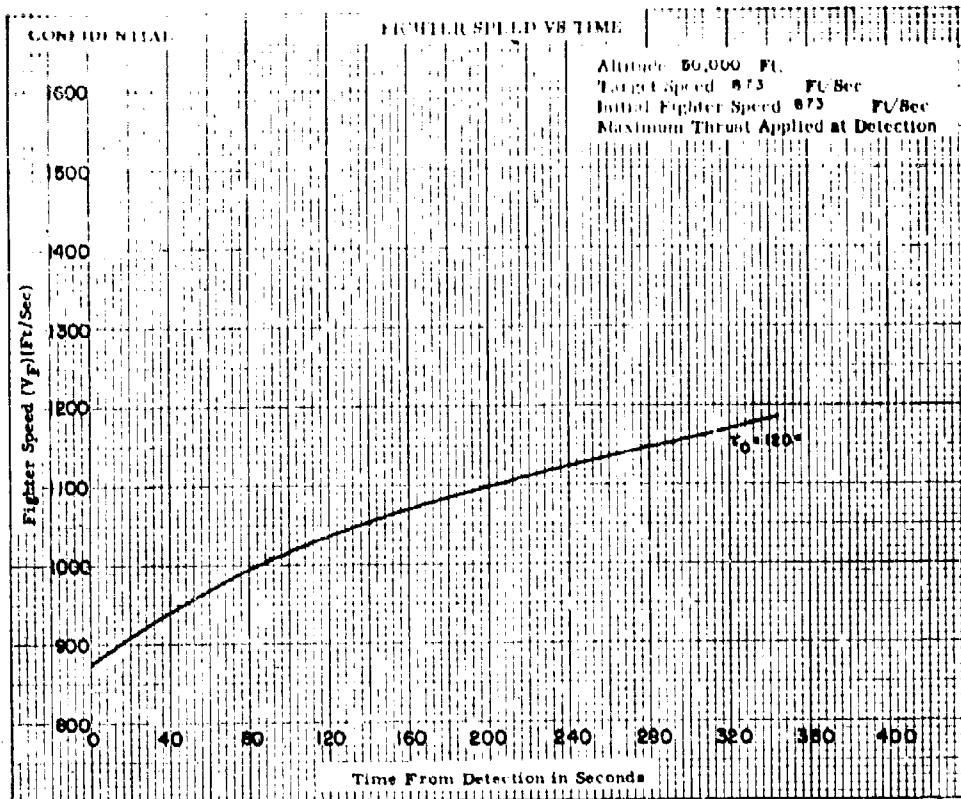


Fig. VII-13b

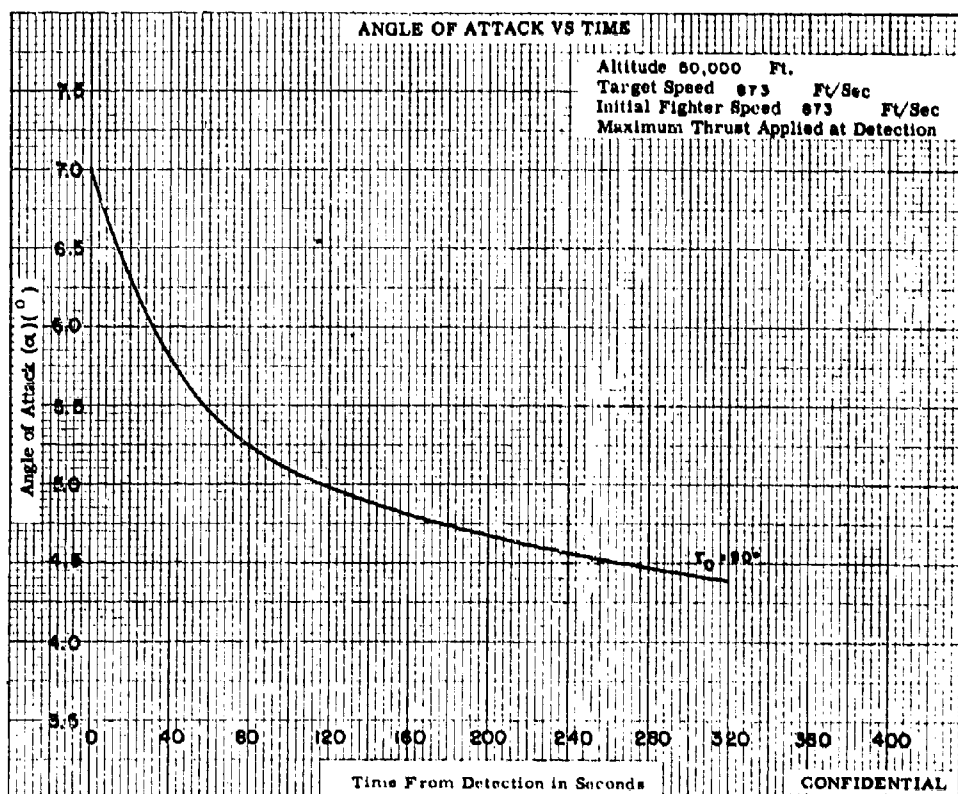
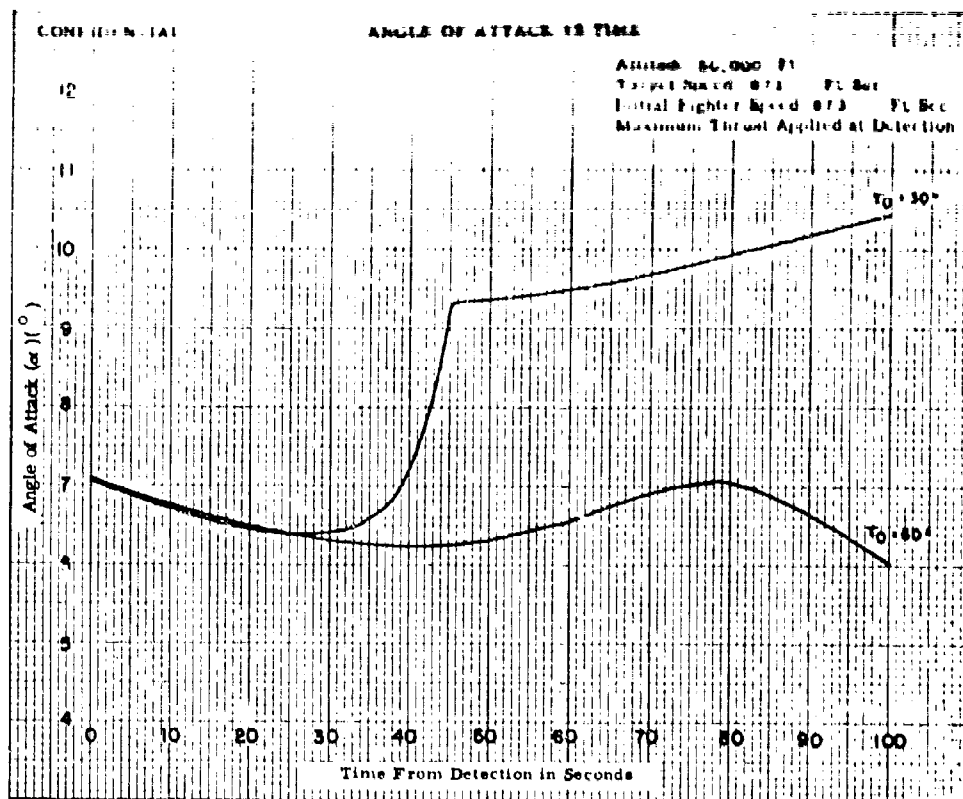


Fig. VII-14a

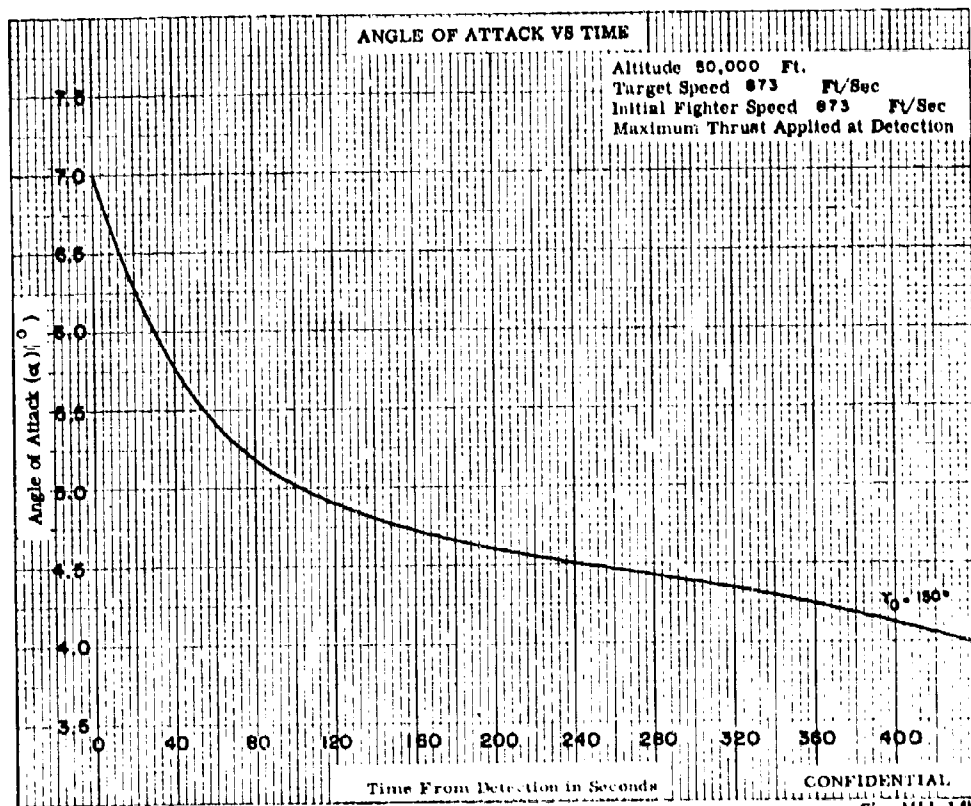
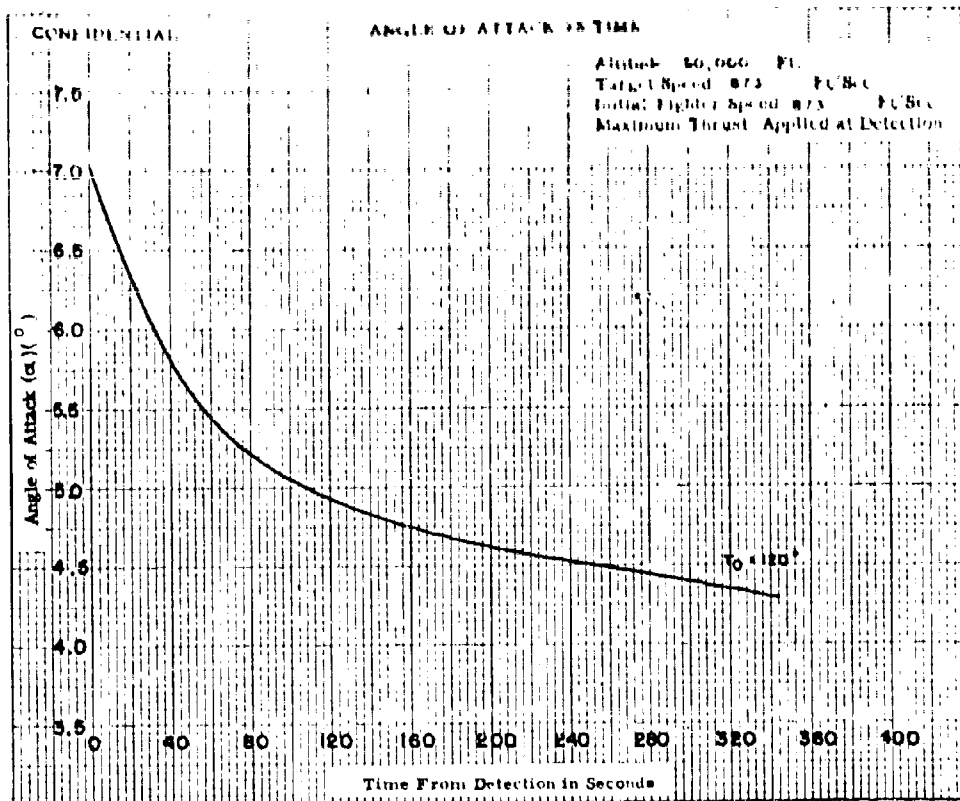
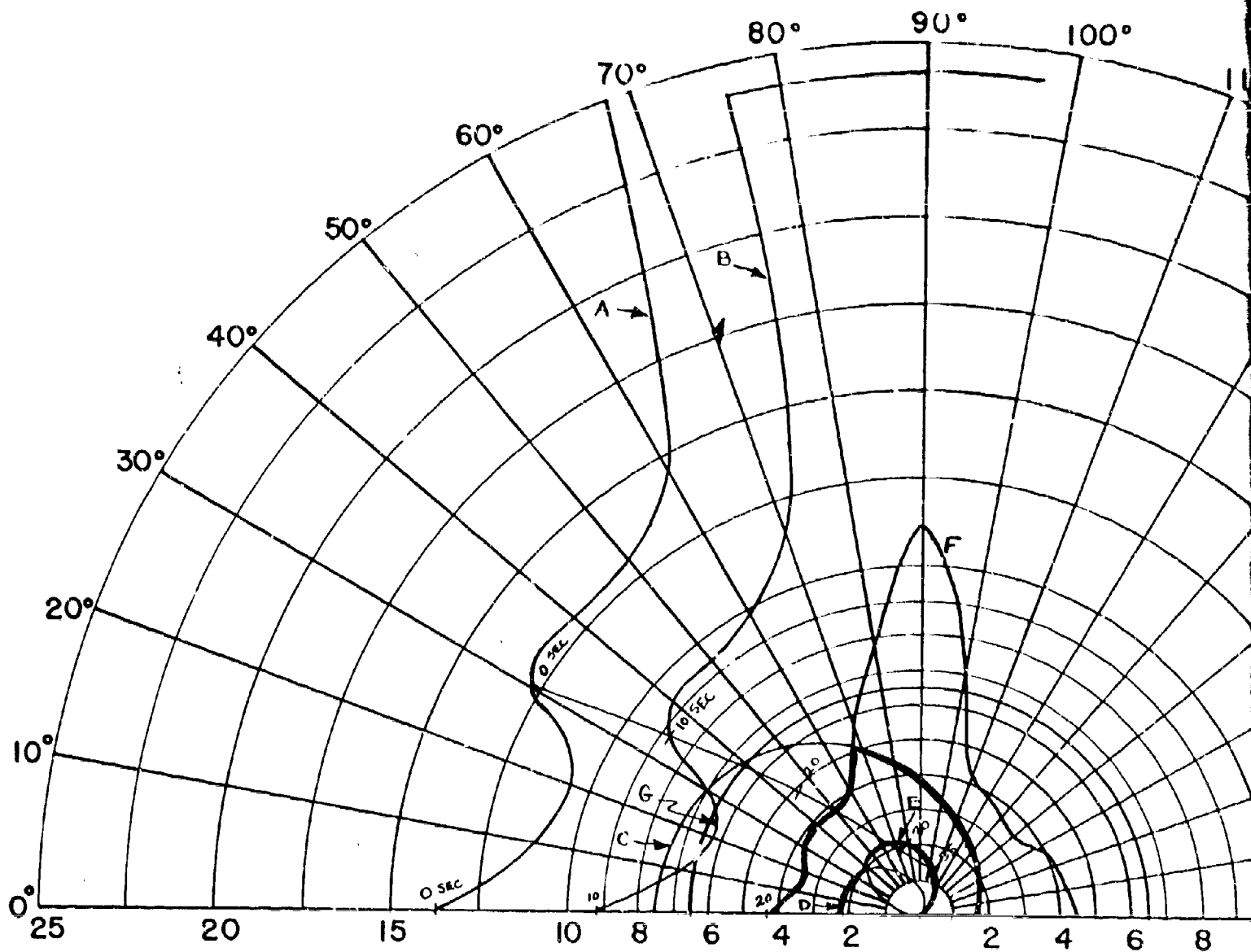


Fig. VII-14b



$V_F = 894$ FT/SEC (F4H-1)(F8U-3)

$V_T = 1897$ FT/SEC

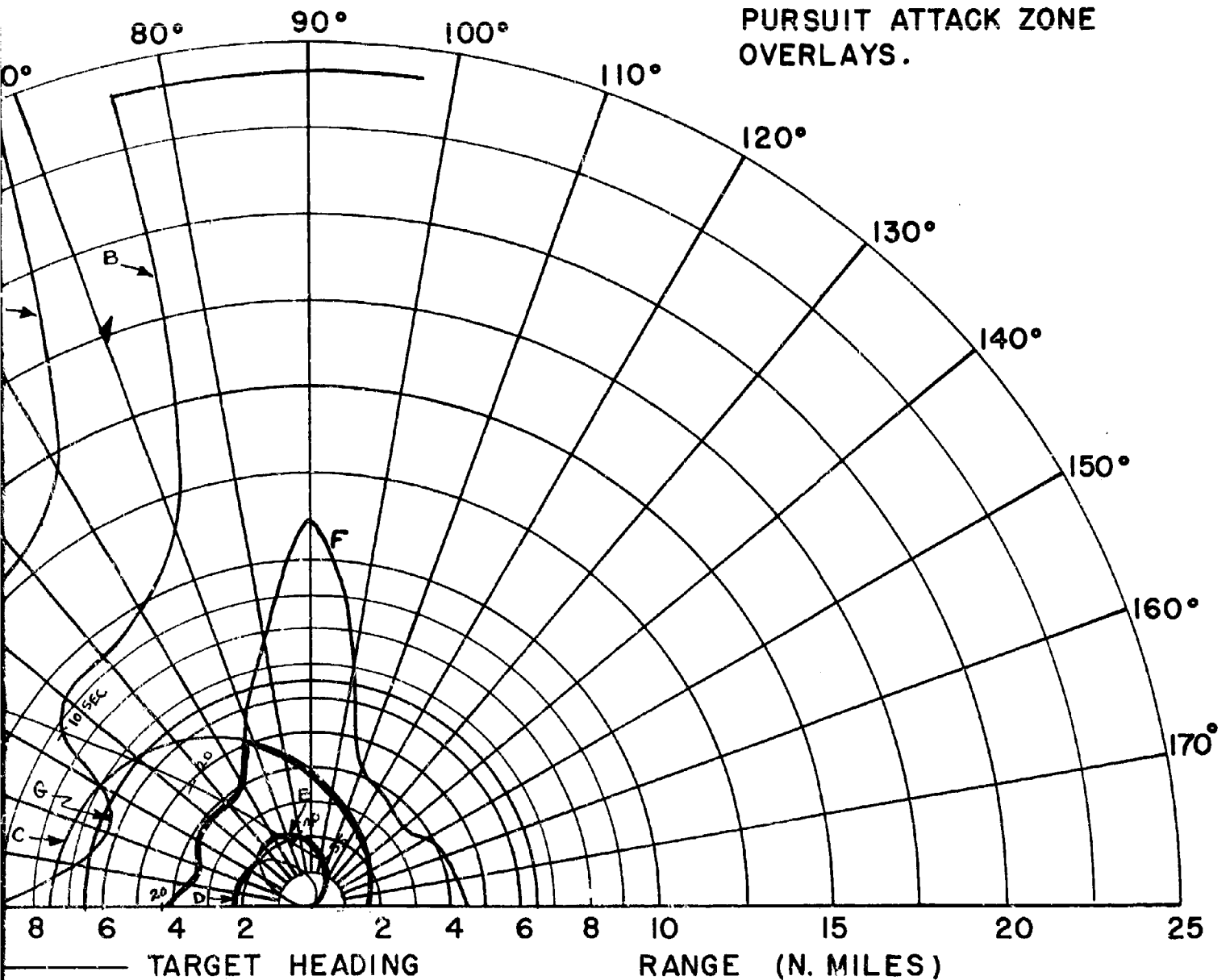
ALTITUDE = 30,000 FT.

INCREASED THRUST AT DETECTION

TARGET HEADING

- A - 85% DETECTION RANGE
- B - LOCK-ON RANGE (10 SEC. LOCK-ON TIME)
- C - SPARROW III MAX. AERODYNAMIC RANGE
- D - SPARROW III MIN. AERODYNAMIC RANGE
- E - CONSTANT LOAD FACTOR LOCUS ($N_z = 1$)
- F - 90% SPARROW III SEEKER LOCK-ON RANGE
- G - 6.5 N.M. INTERLOCK

FIG. VIII - CO-ALTITUDE LEAD
PURSUIT ATTACK ZONE
OVERLAYS.



85% DETECTION RANGE
 LOCK-ON RANGE (10 SEC. LOCK-ON TIME)
 SPARROW III MAX. AERODYNAMIC RANGE
 SPARROW III MIN. AERODYNAMIC RANGE
 CONSTANT LOAD FACTOR LOCUS ($N_z = 3$)
 90% SPARROW III SEEKER LOCK-ON RANGE
 6.5 N.M. INTERLOCK

CONFIDENTIAL

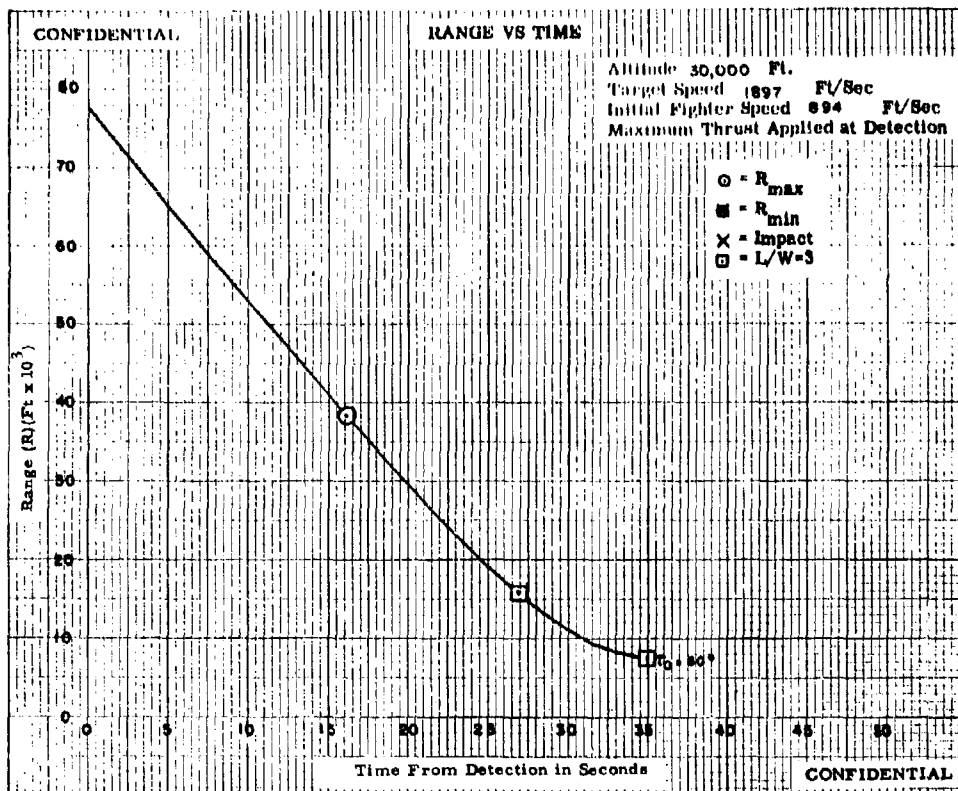


Fig. VIII-1

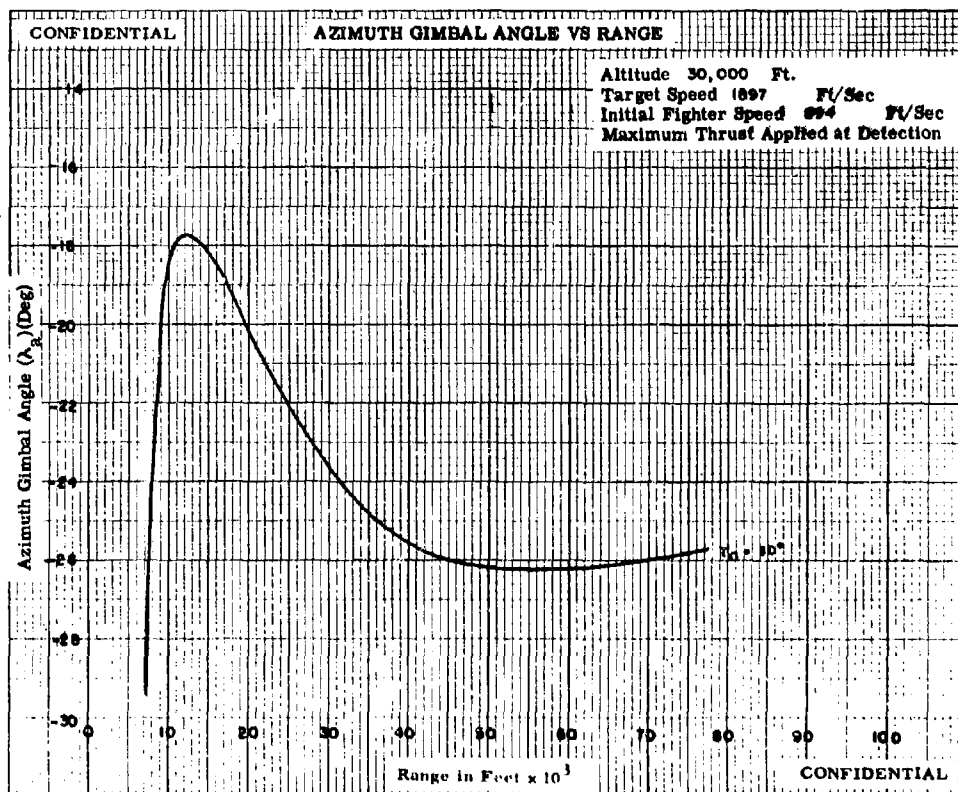


Fig. VIII-2

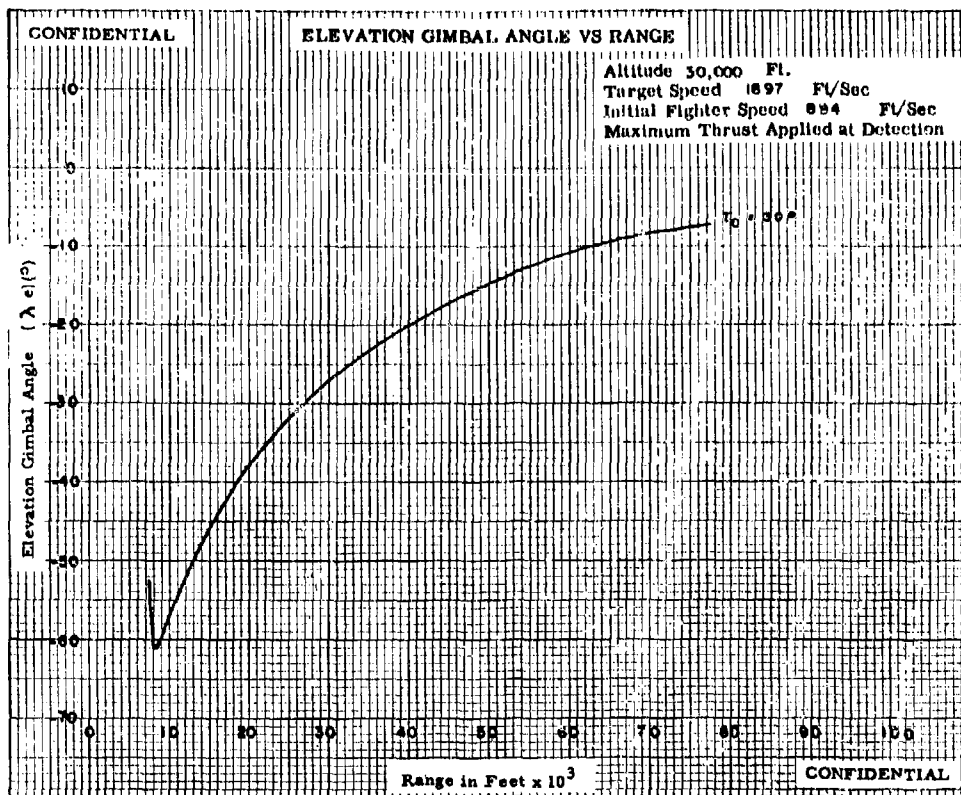


Fig. VIII-3

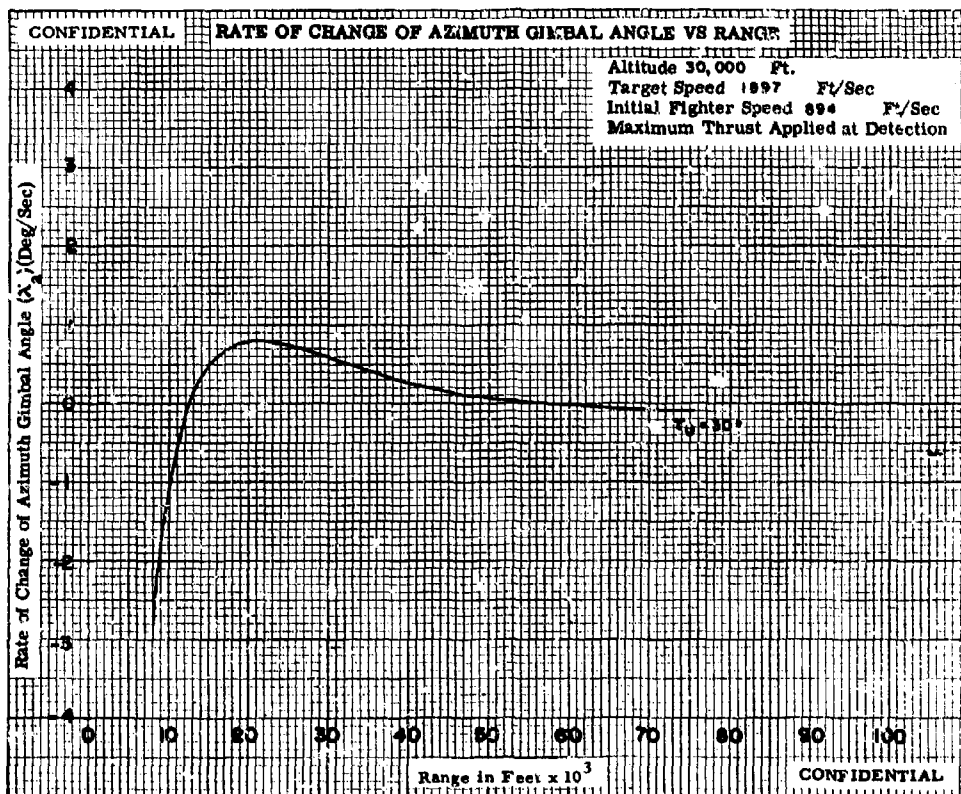


Fig. VIII-4

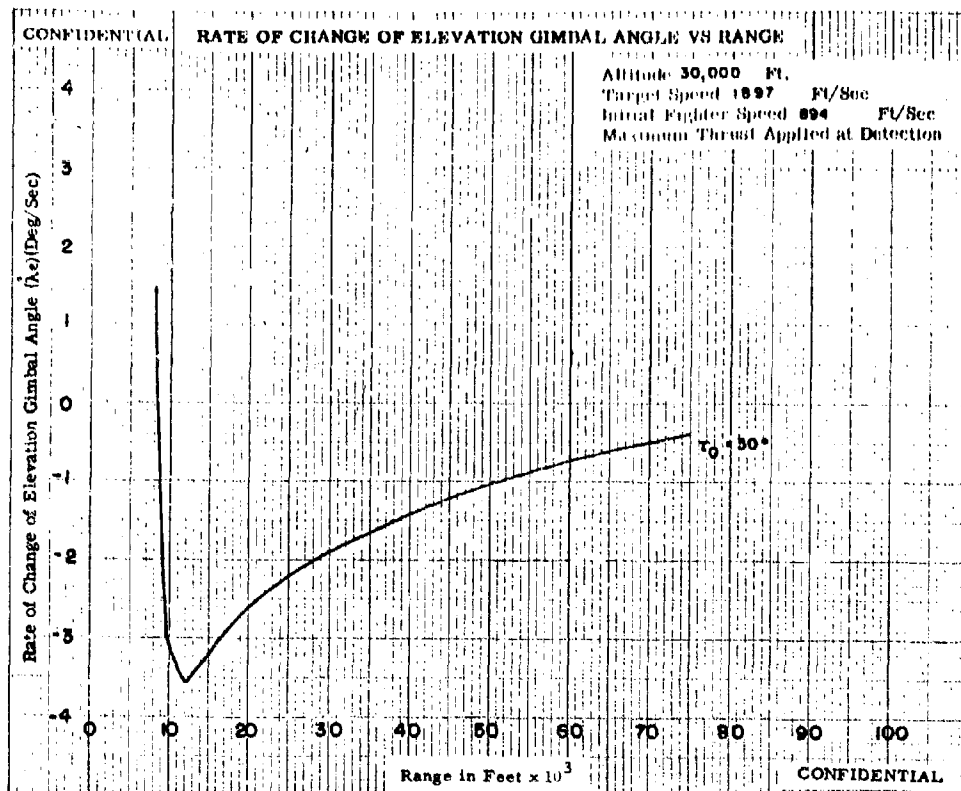


Fig. VIII-5

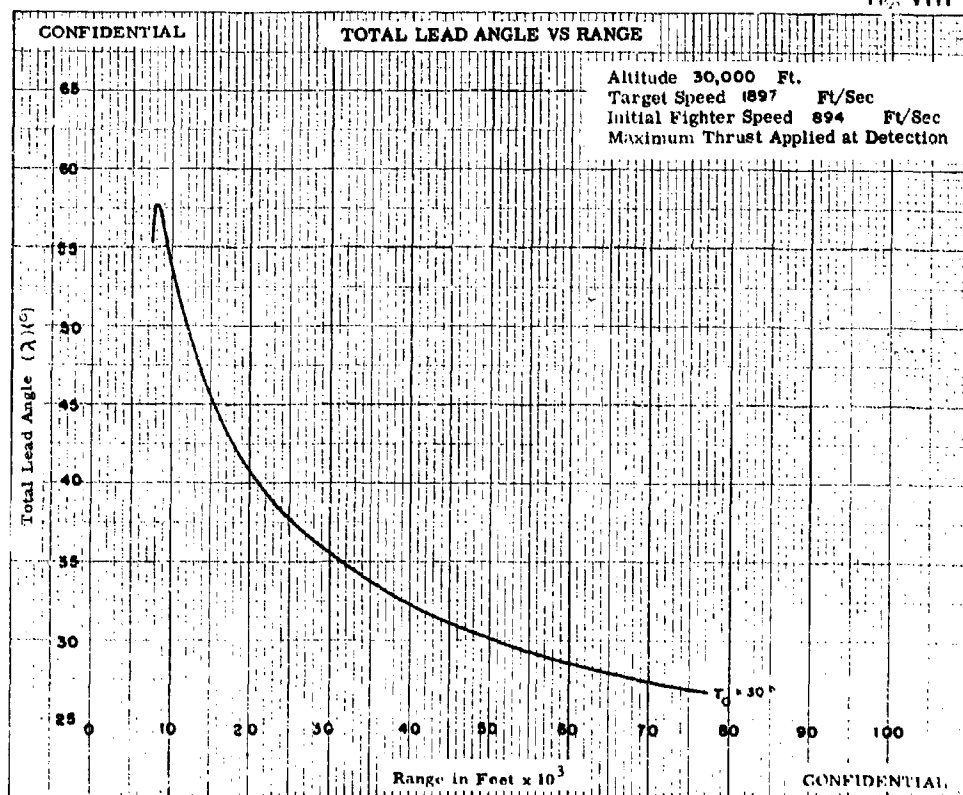


Fig. VIII-6

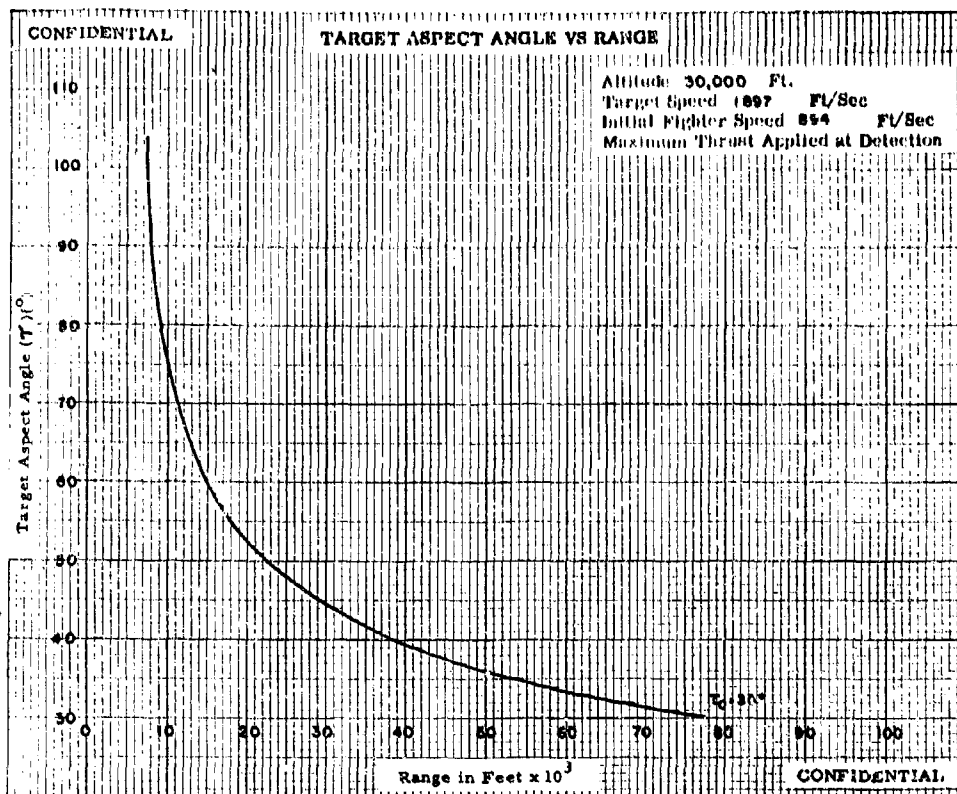


Fig. VIII-7

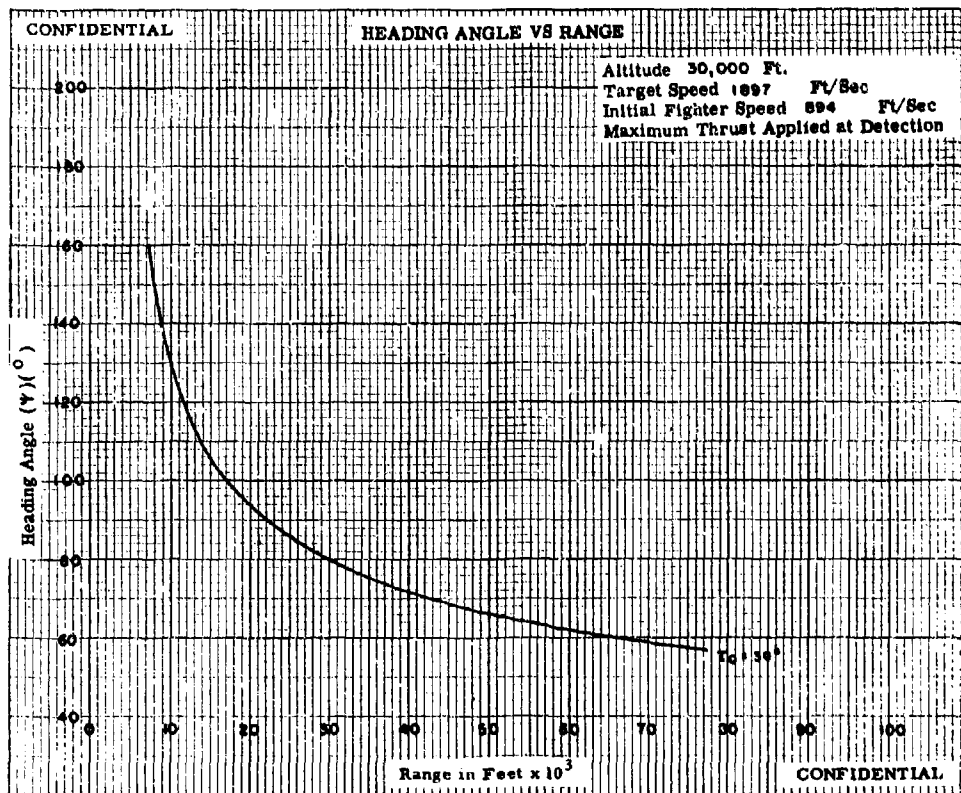


Fig. VIII-8

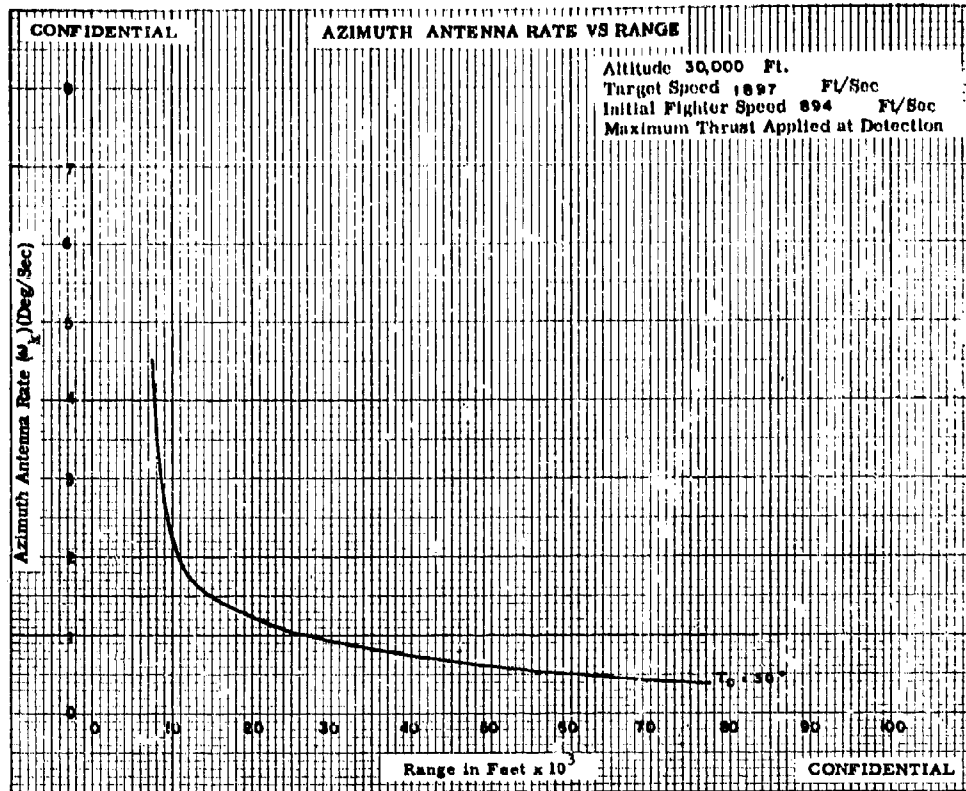


Fig. VIII-9

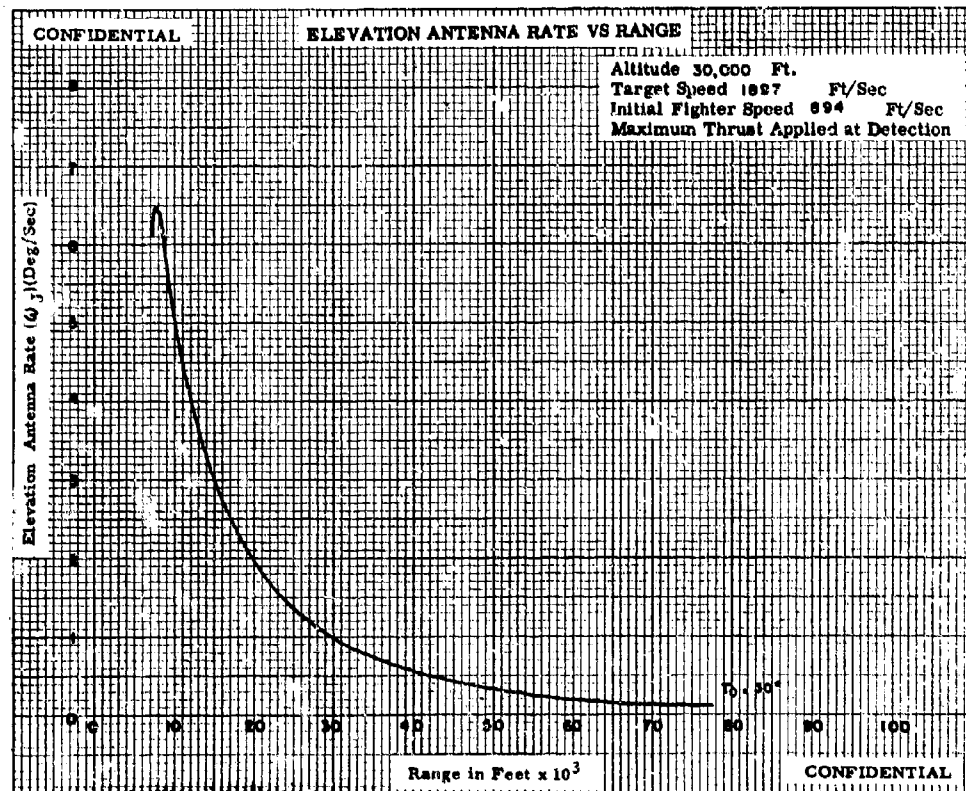


Fig. VIII-10

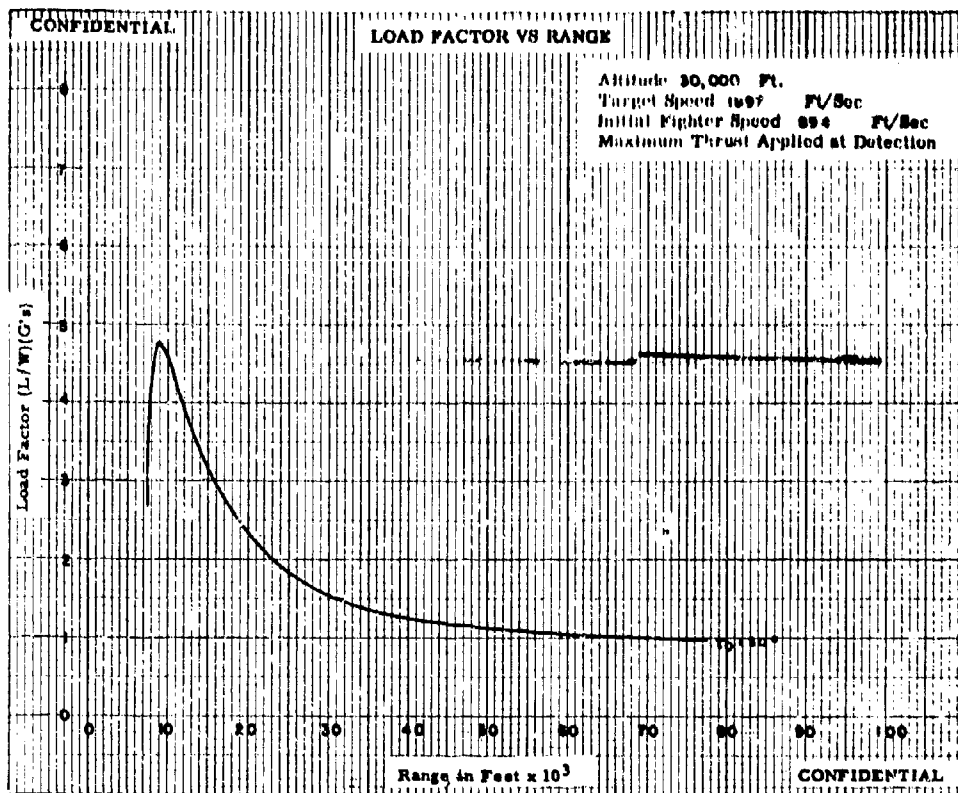


Fig. VIII-11

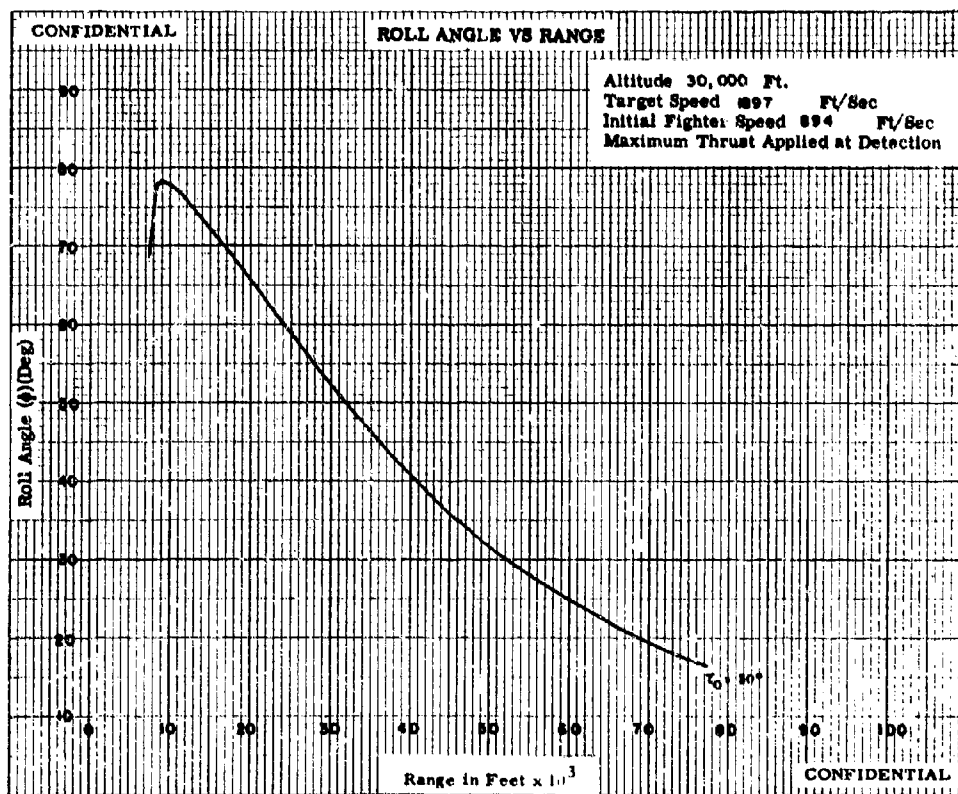


Fig. VIII-12

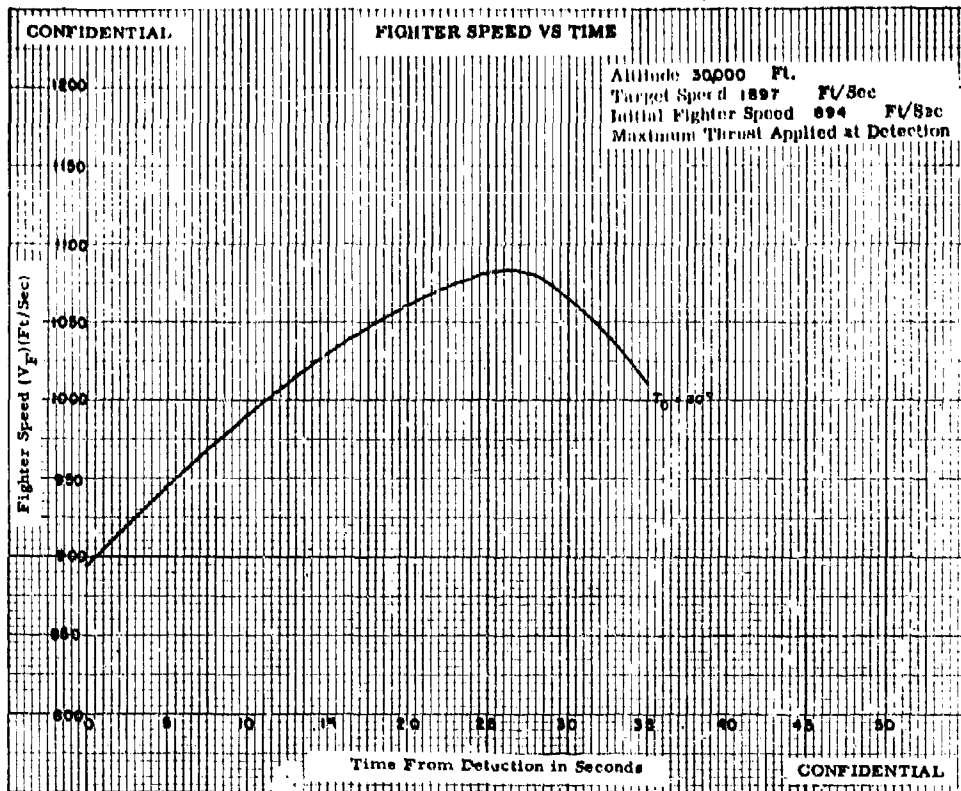


Fig. VIII-13

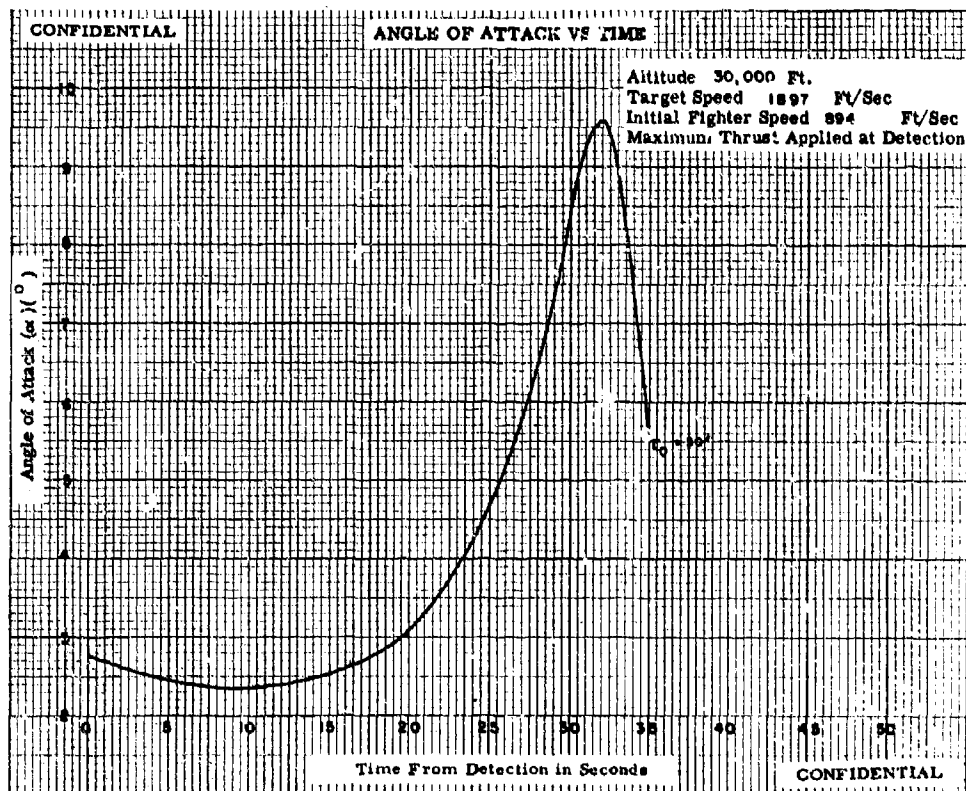
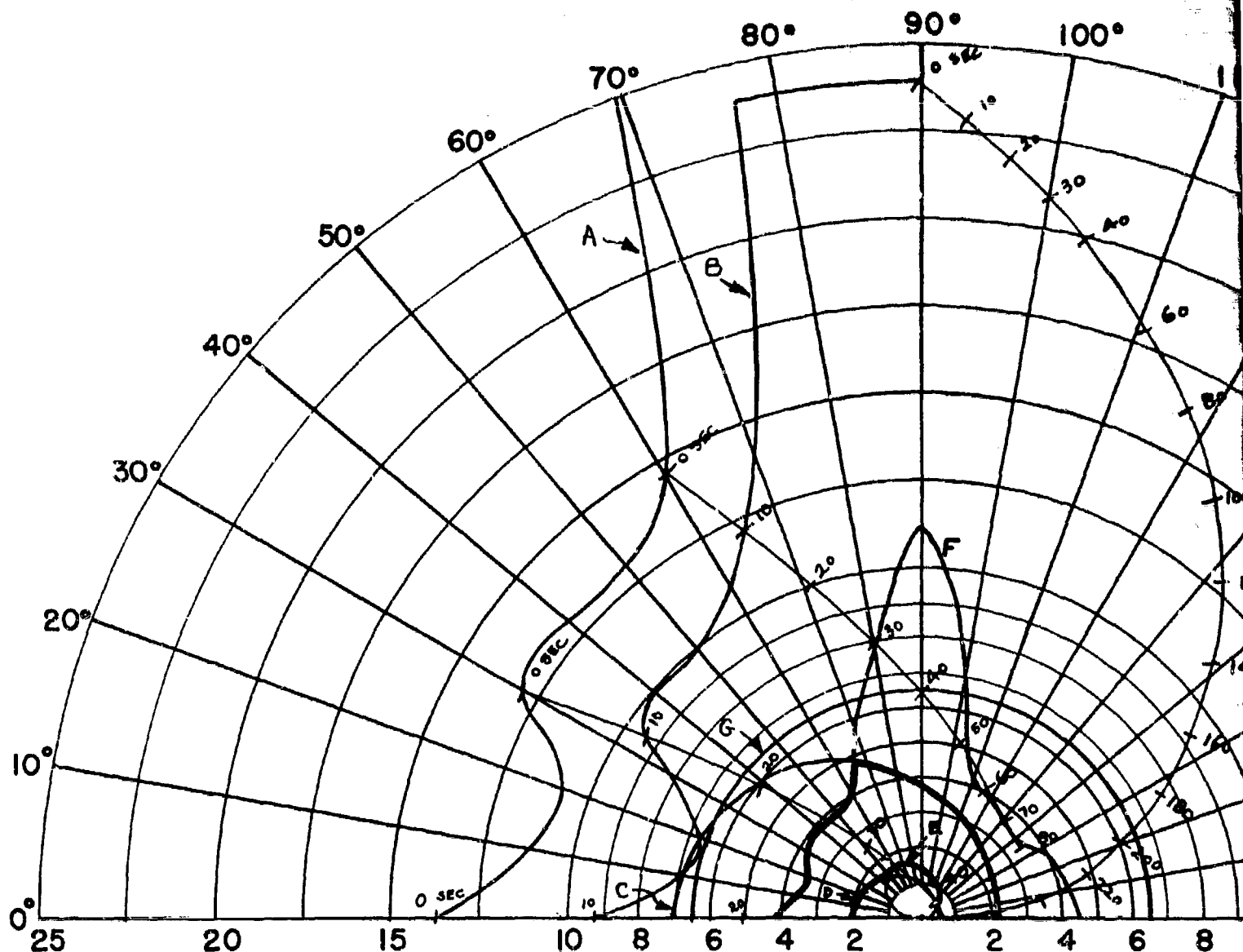


Fig. VIII-14



$V_F = 894$ FT/SEC (F4H-1)(F8U-3)

$V_T = 1518$ FT/SEC

ALTITUDE = 30,000 FT.

INCREASED THRUST AT DETECTION

TARGET HEADING

A - 85% DETECTION RANGE

B - LOCK-ON RANGE (10 SEC. LOCK-ON TIME)

C - SPARROW III MAX. AERODYNAMIC RANGE

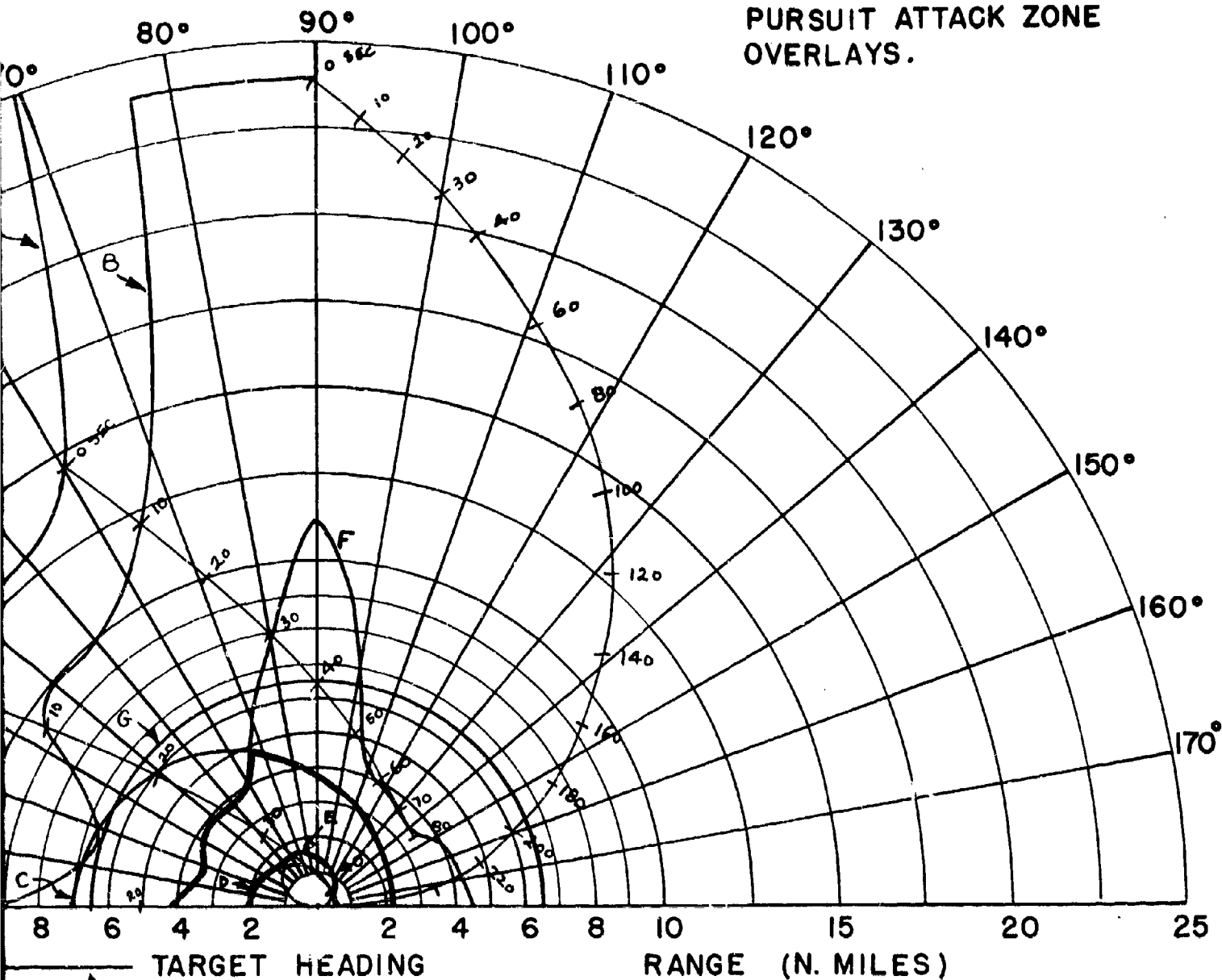
D - SPARROW III MIN. AERODYNAMIC RANGE

E - CONSTANT LOAD FACTOR LOCUS ($N_z =$

F - 90% SPARROW III SEEKER LOCK-ON R

G - 6.5 N.M. INTERLOCK

FIG. IX - CO-ALTITUDE LEAD
PURSUIT ATTACK ZONE
OVERLAYS.



85% DETECTION RANGE
LOCK-ON RANGE (10 SEC. LOCK-ON TIME)
SPARROW III MAX. AERODYNAMIC RANGE
SPARROW III MIN. AERODYNAMIC RANGE
CONSTANT LOAD FACTOR LOCUS ($N_z = 3$)
90% SPARROW III SEEKER LOCK-ON RANGE
6.5 N.M. INTERLOCK

CONFIDENTIAL

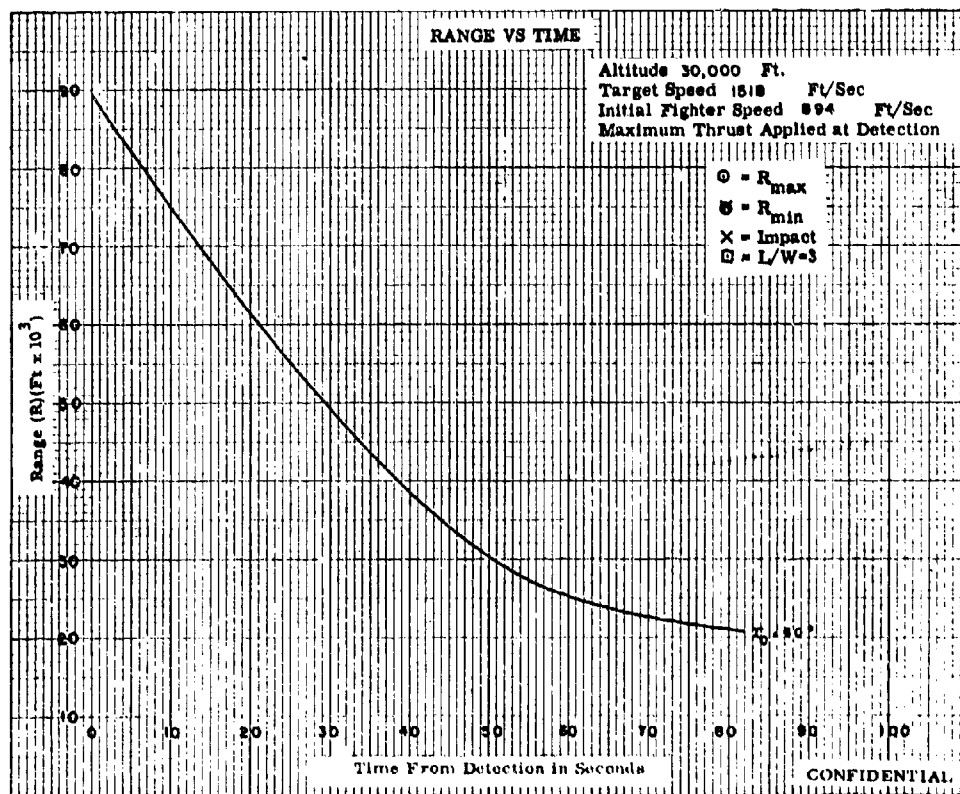
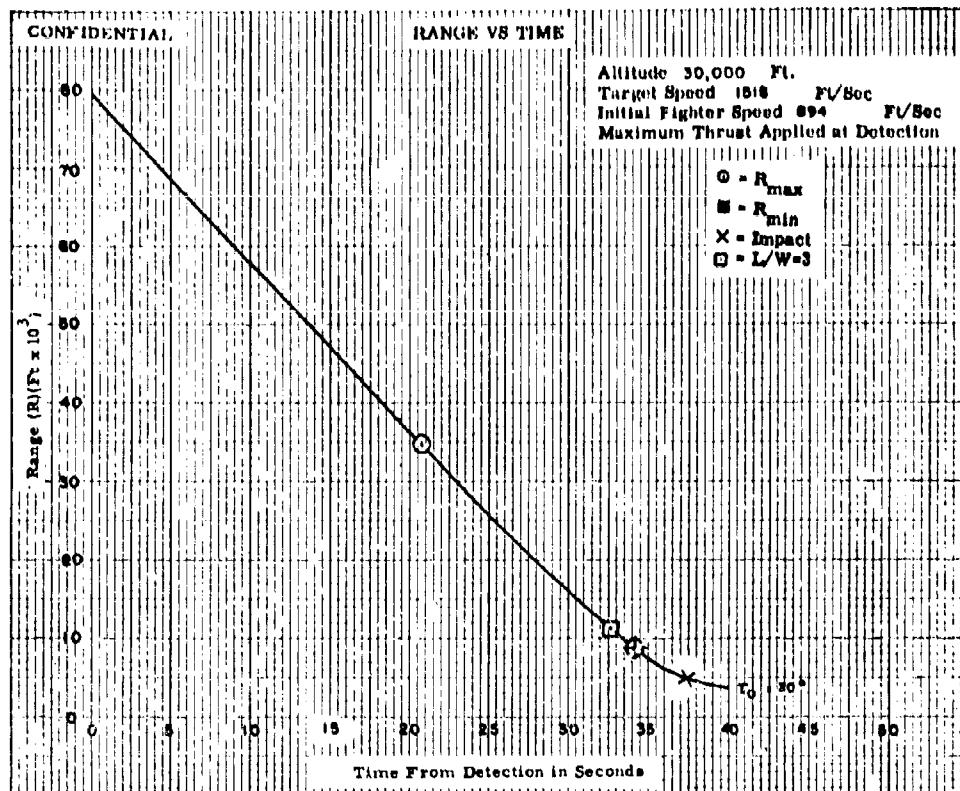


Fig. 1X-1a

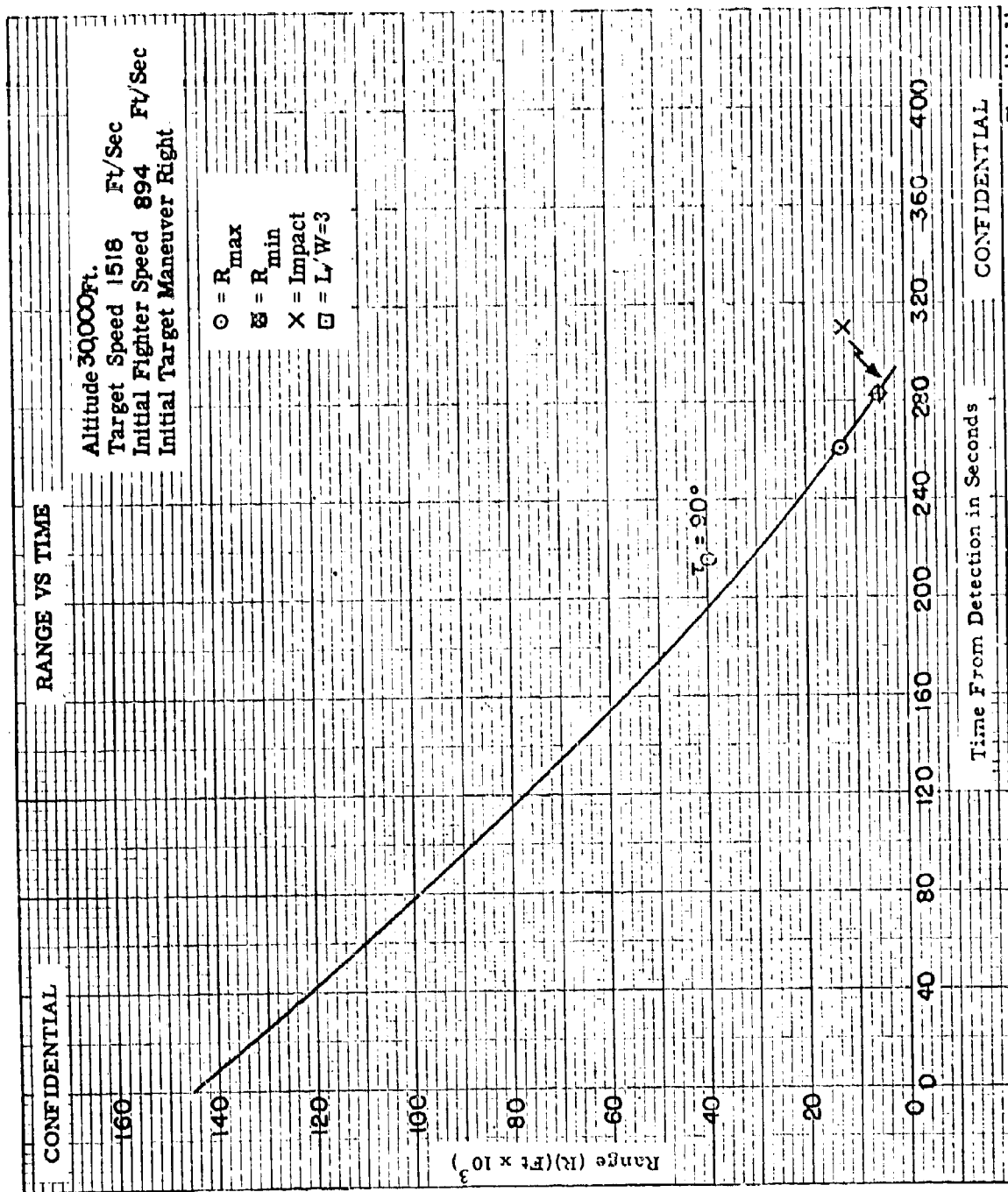


Fig. IX-1b

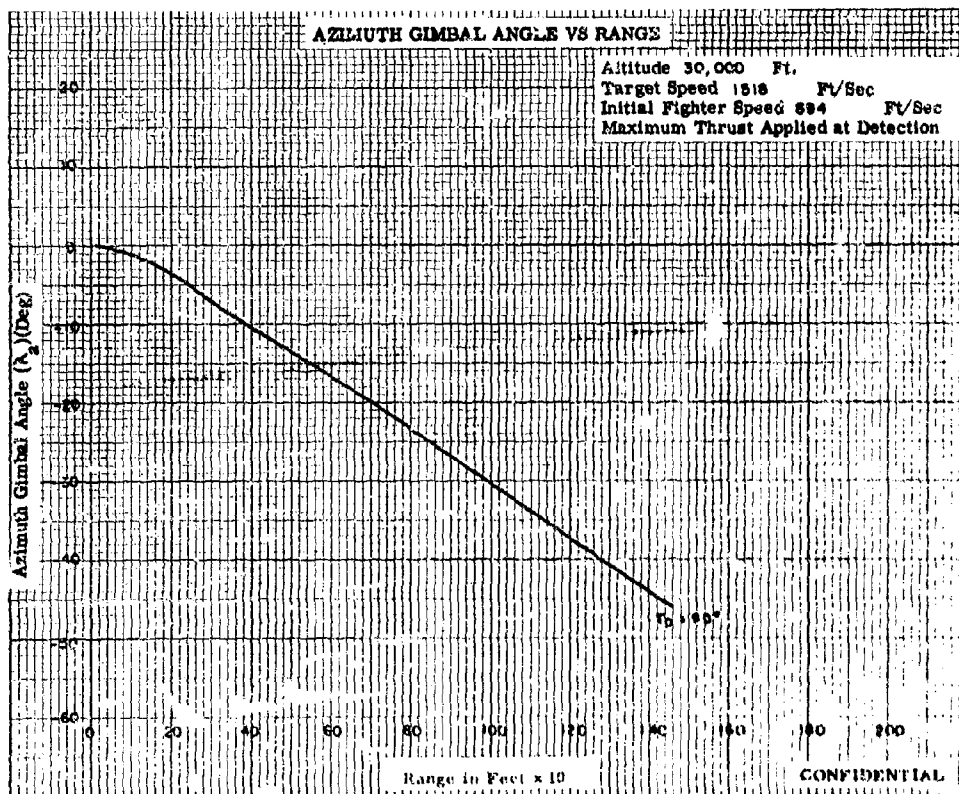
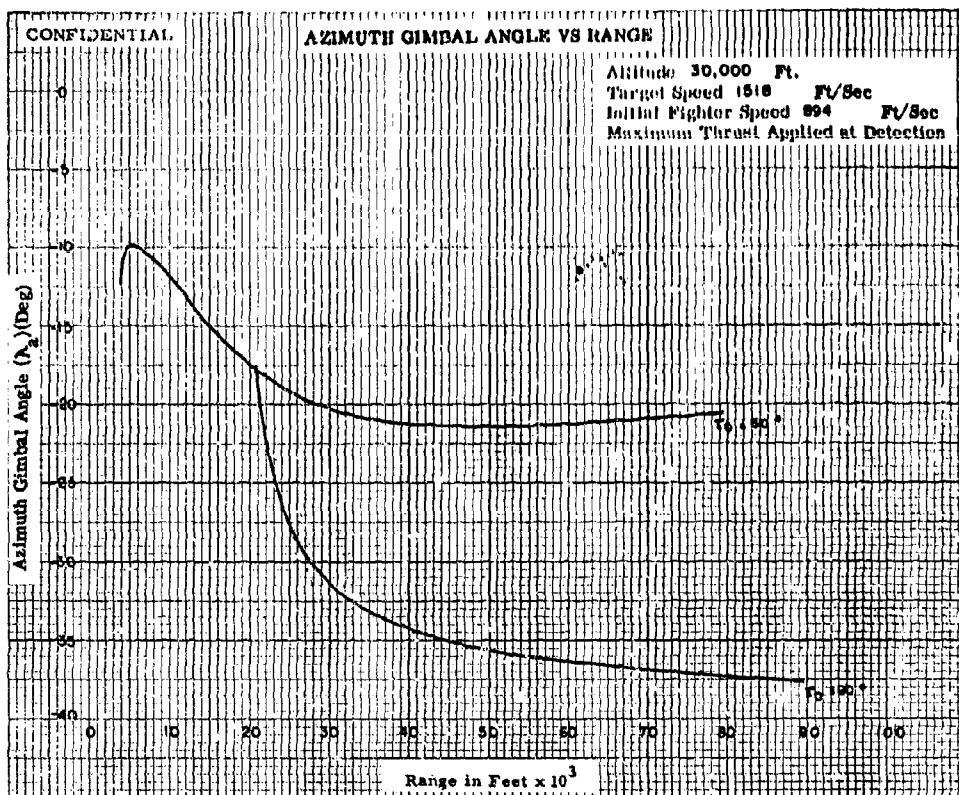


Fig. 1X-2

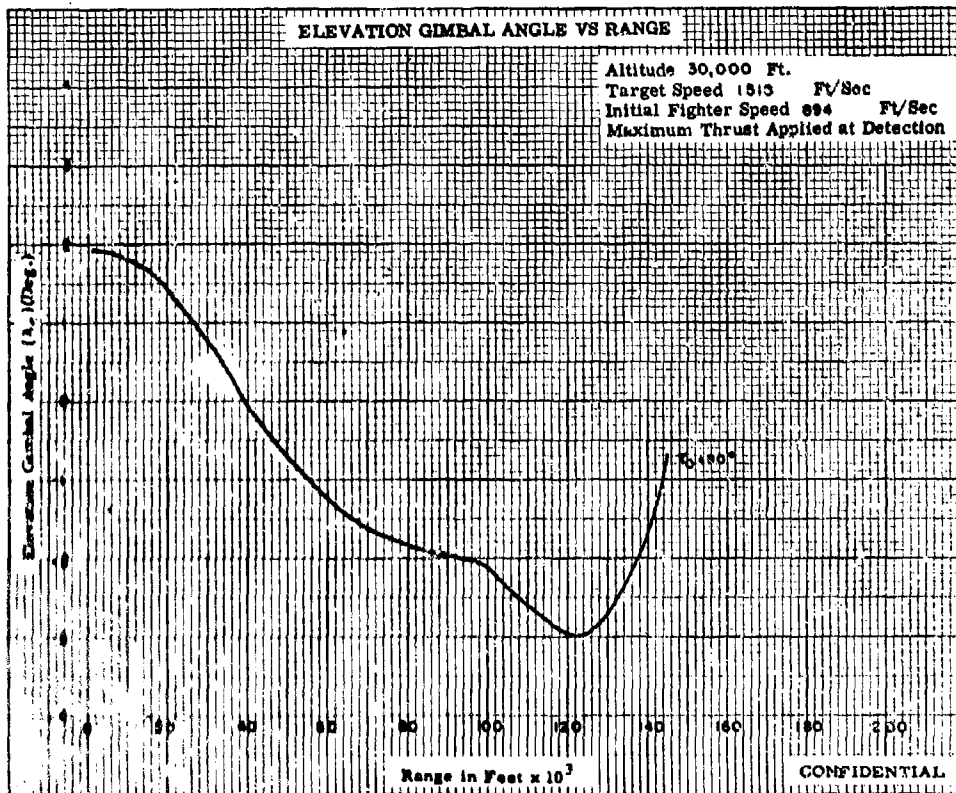
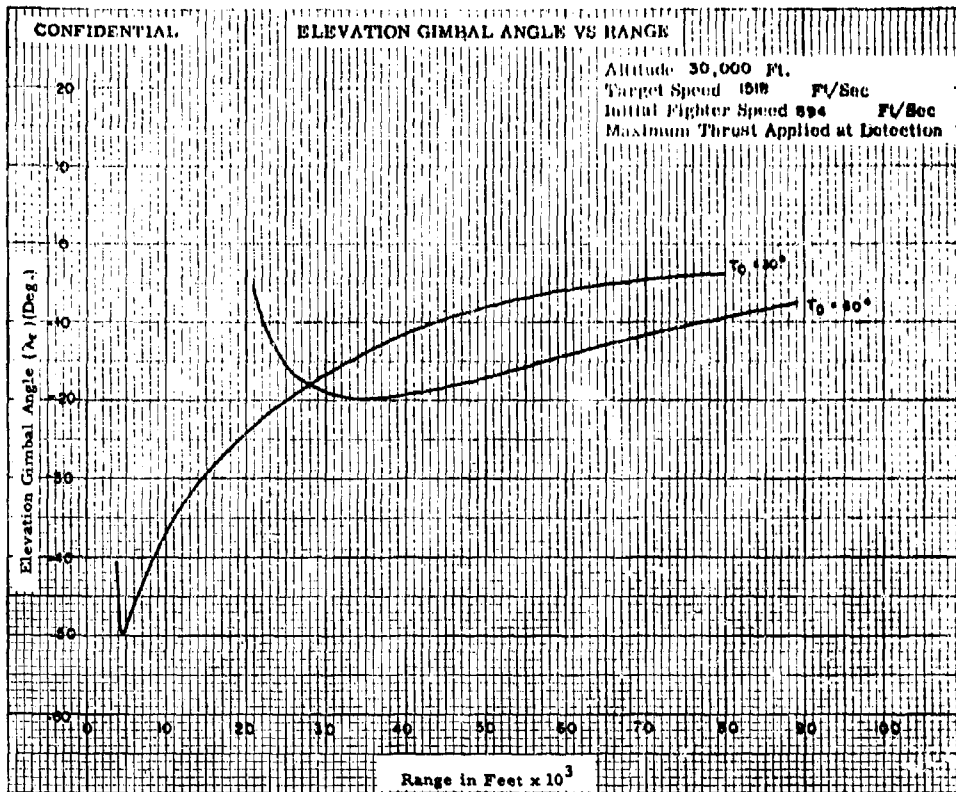


Fig. IX-3

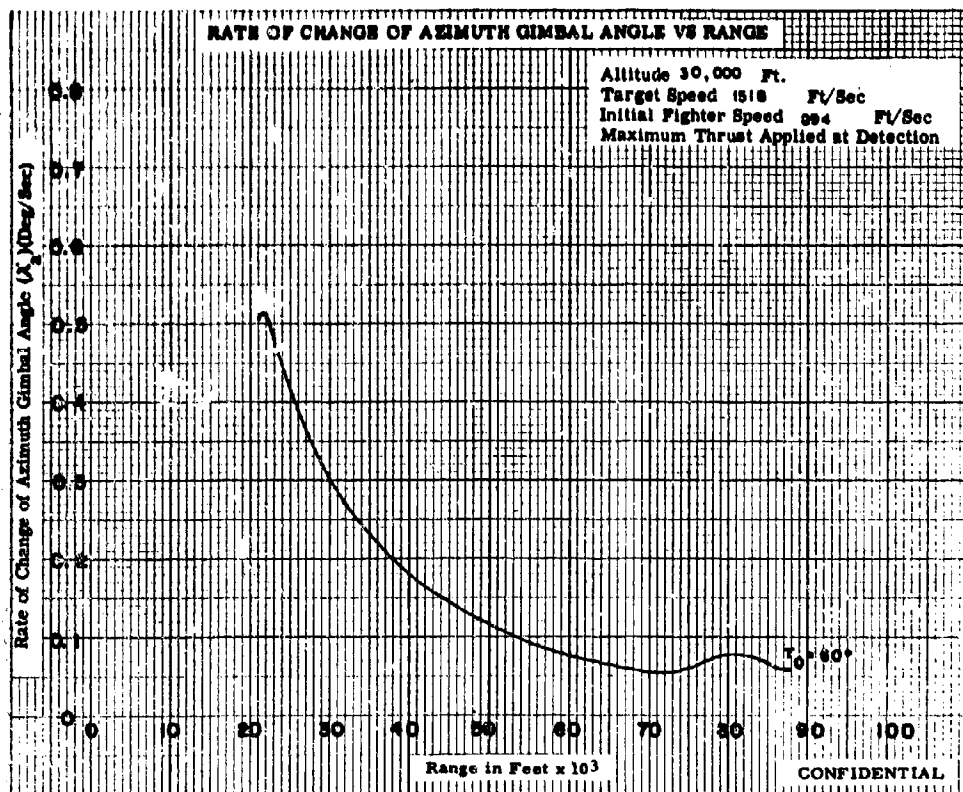
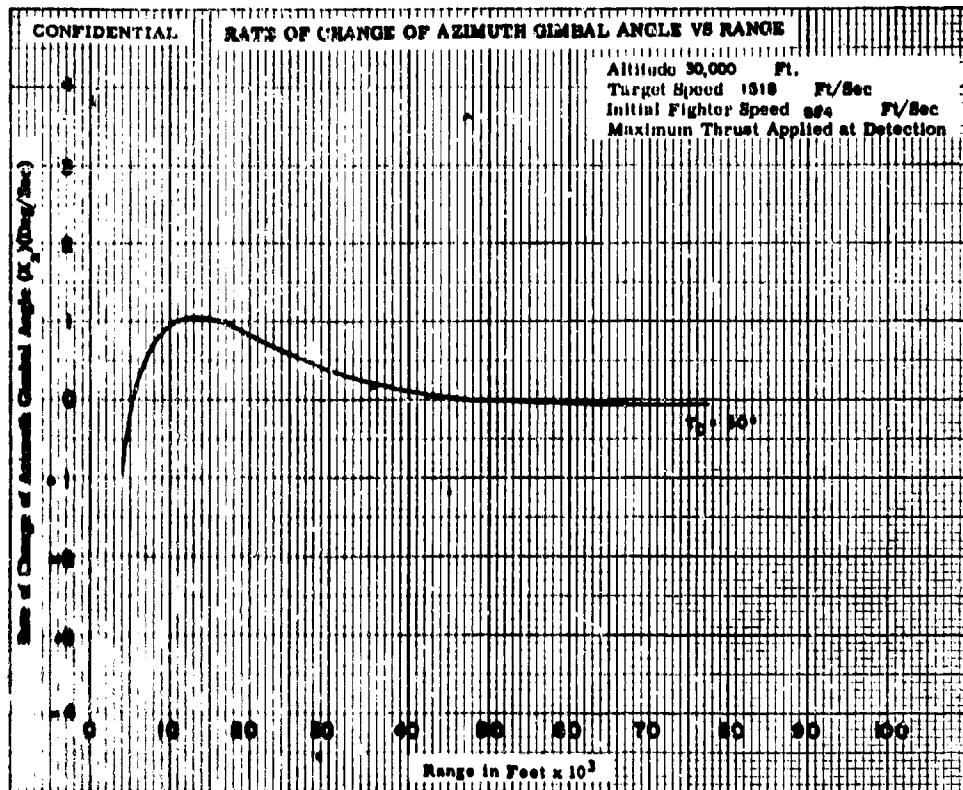


Fig. IX-4a

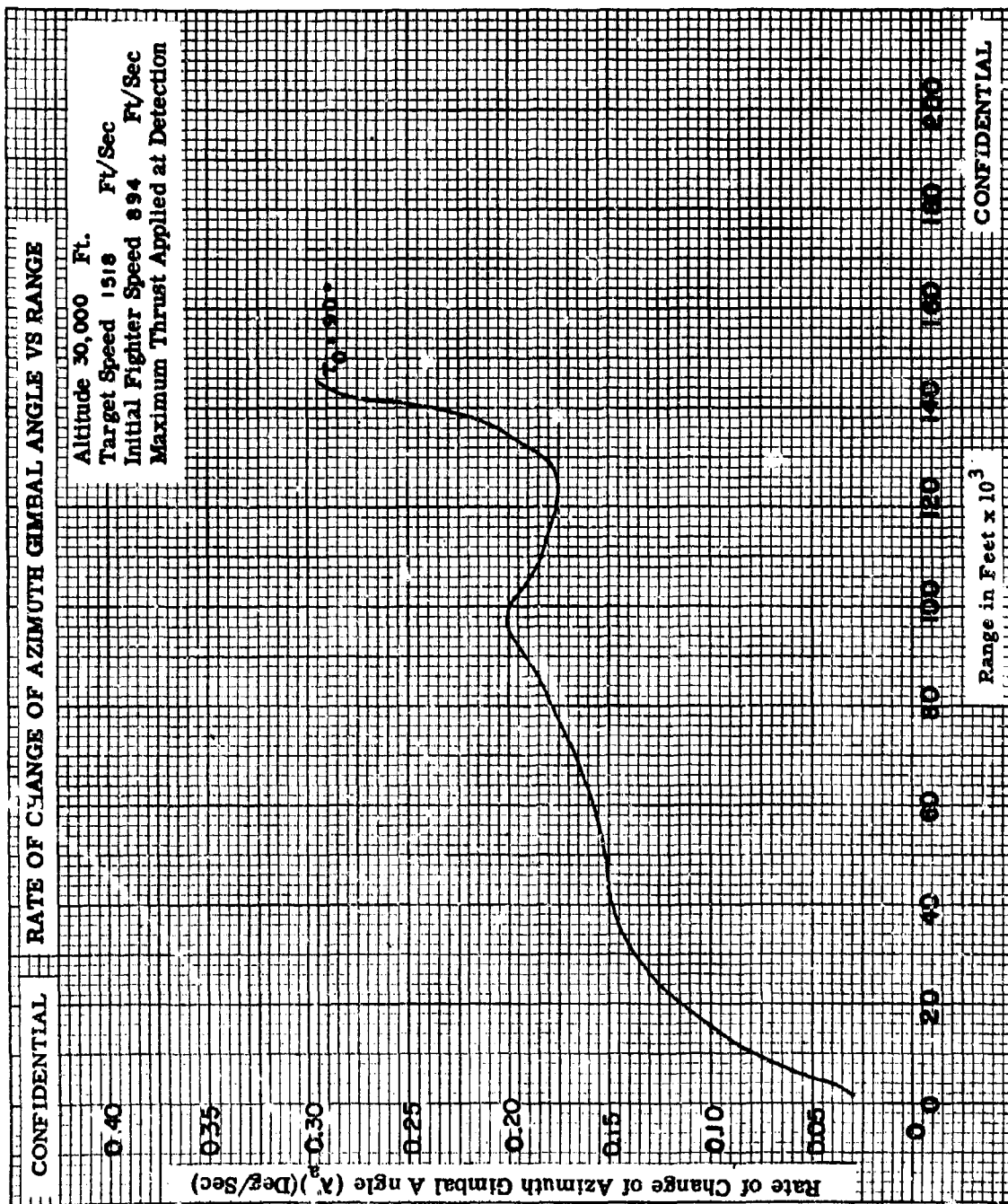


Fig. IX-4b

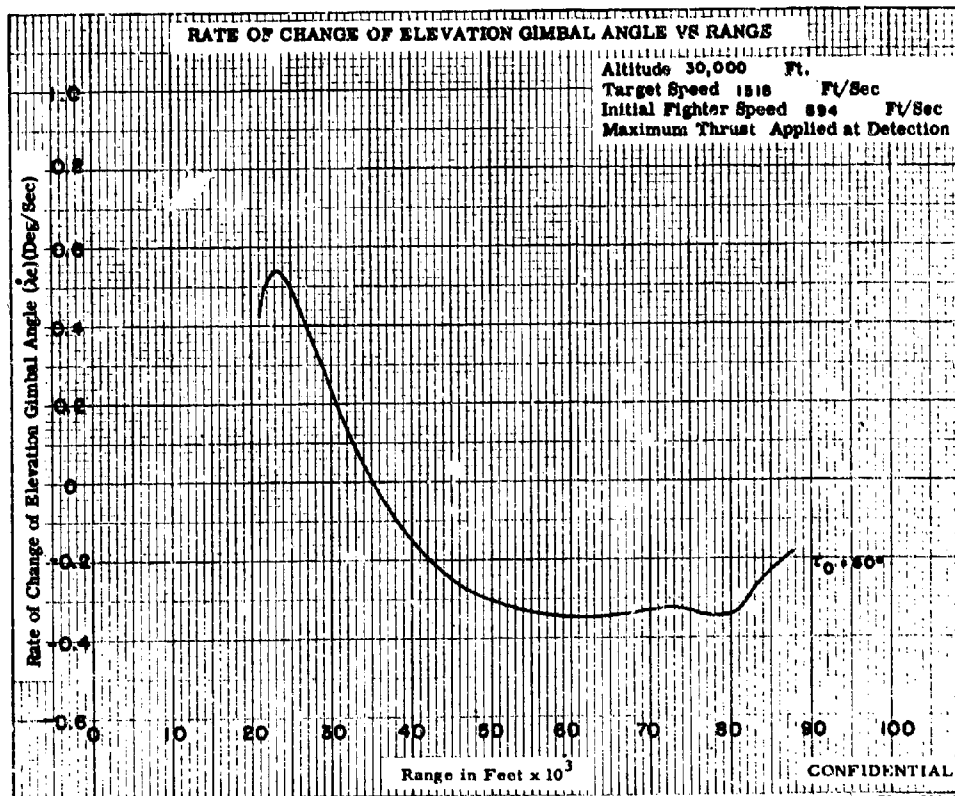
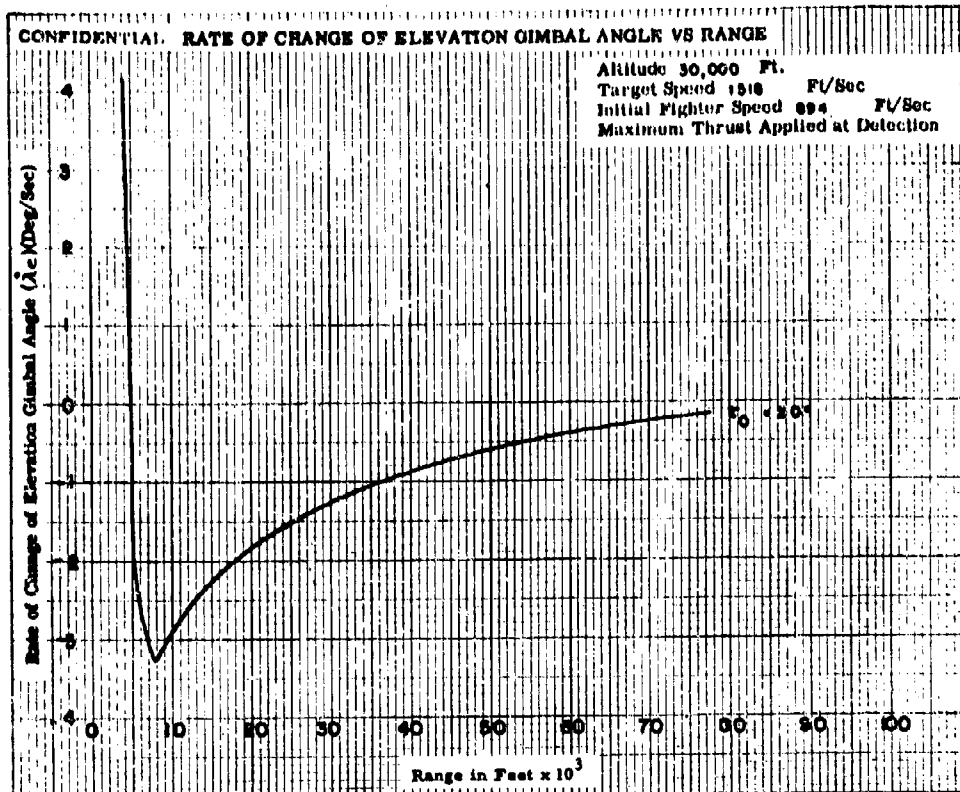


Fig. IX-5a

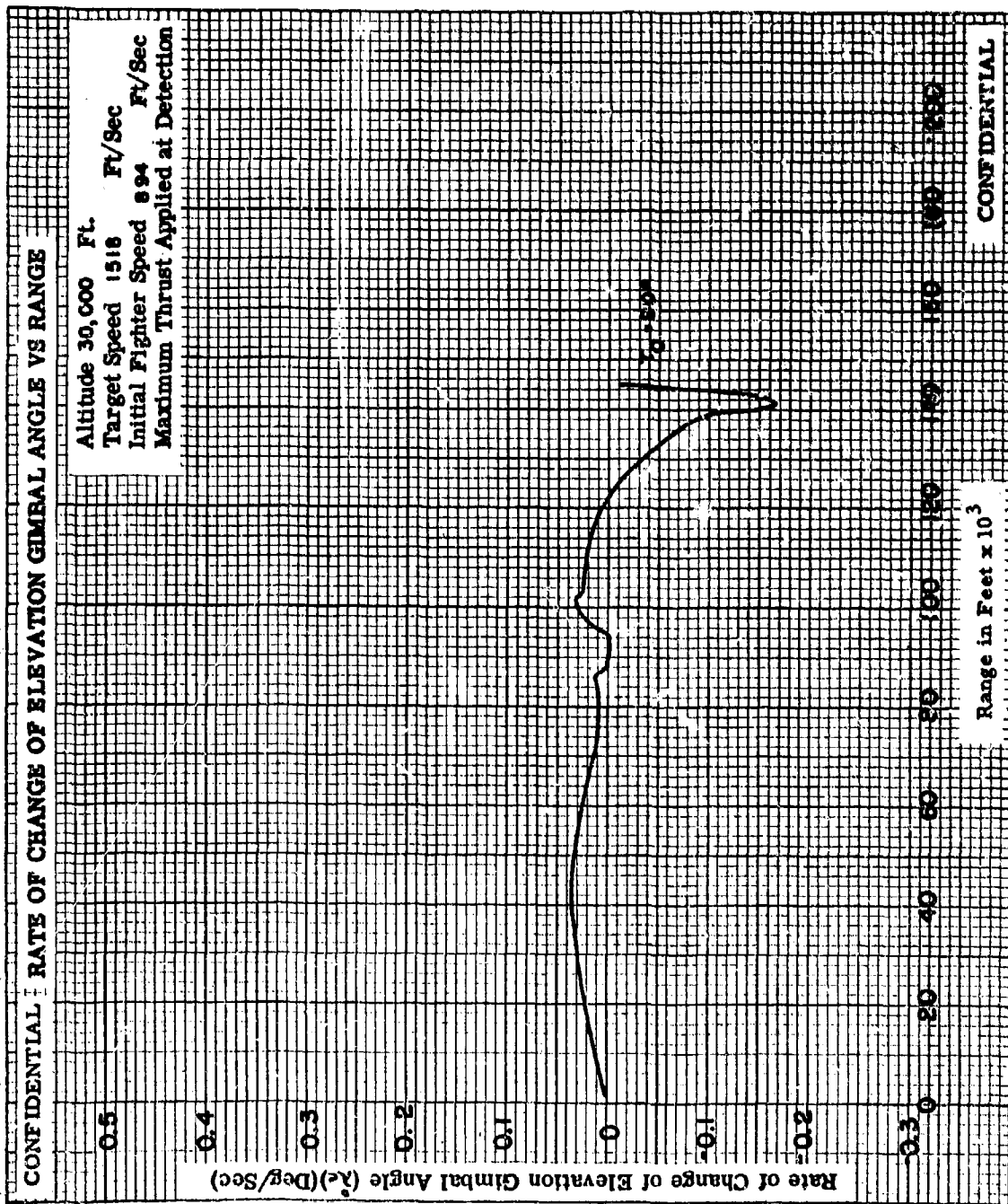


Fig. IX-5b

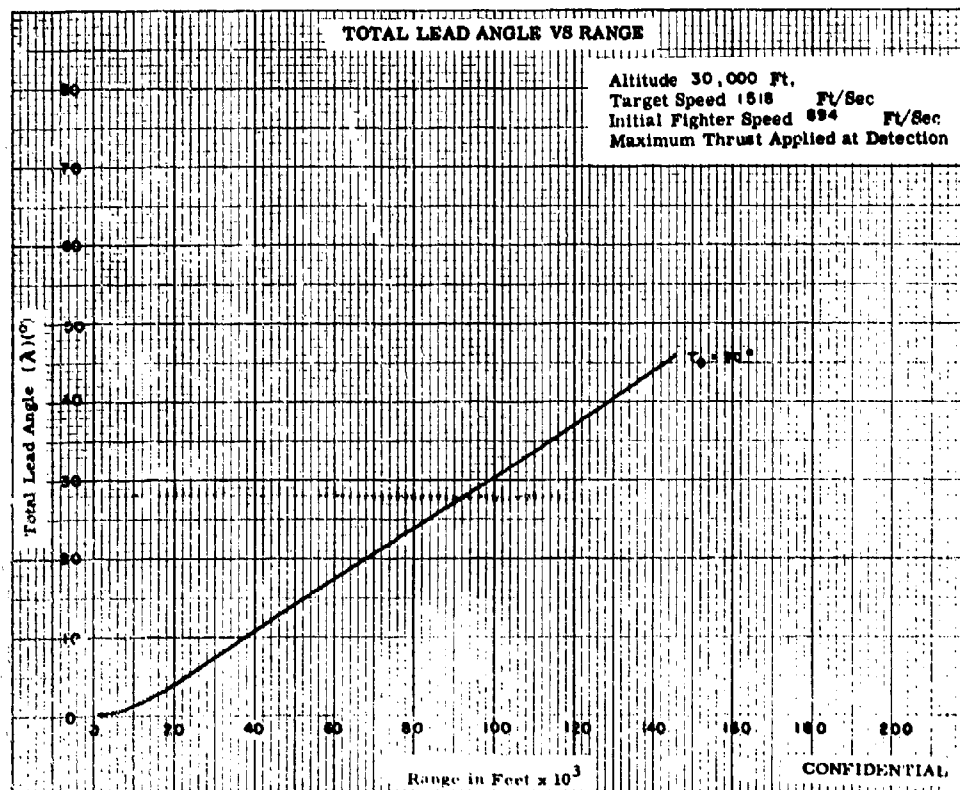
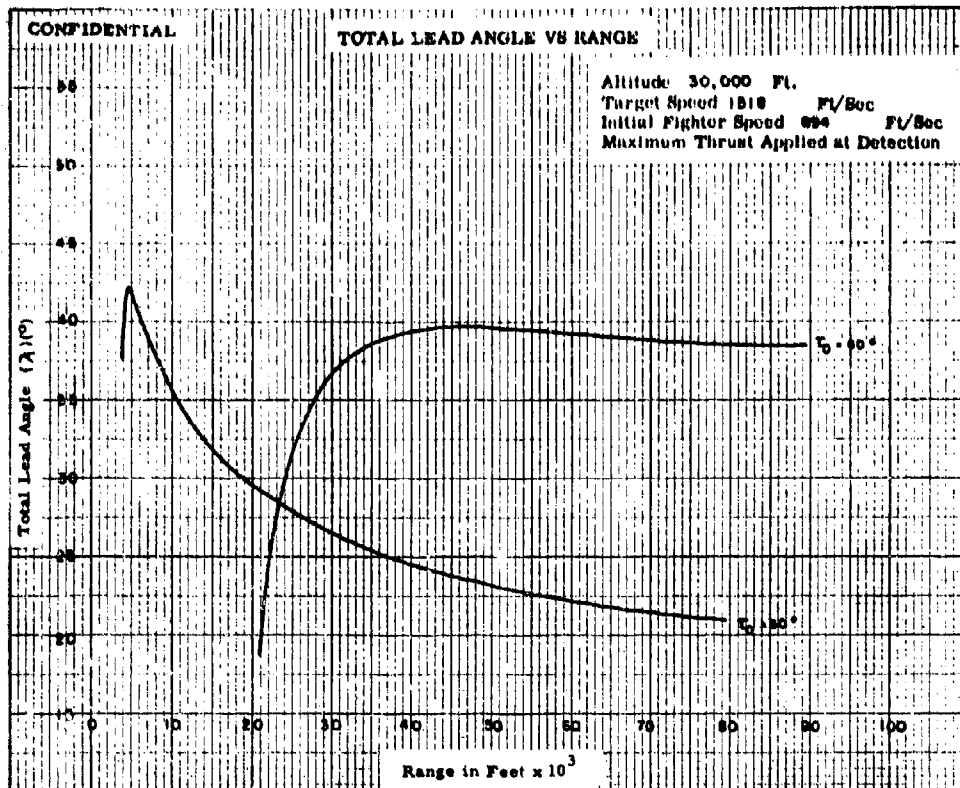


Fig. IX-6

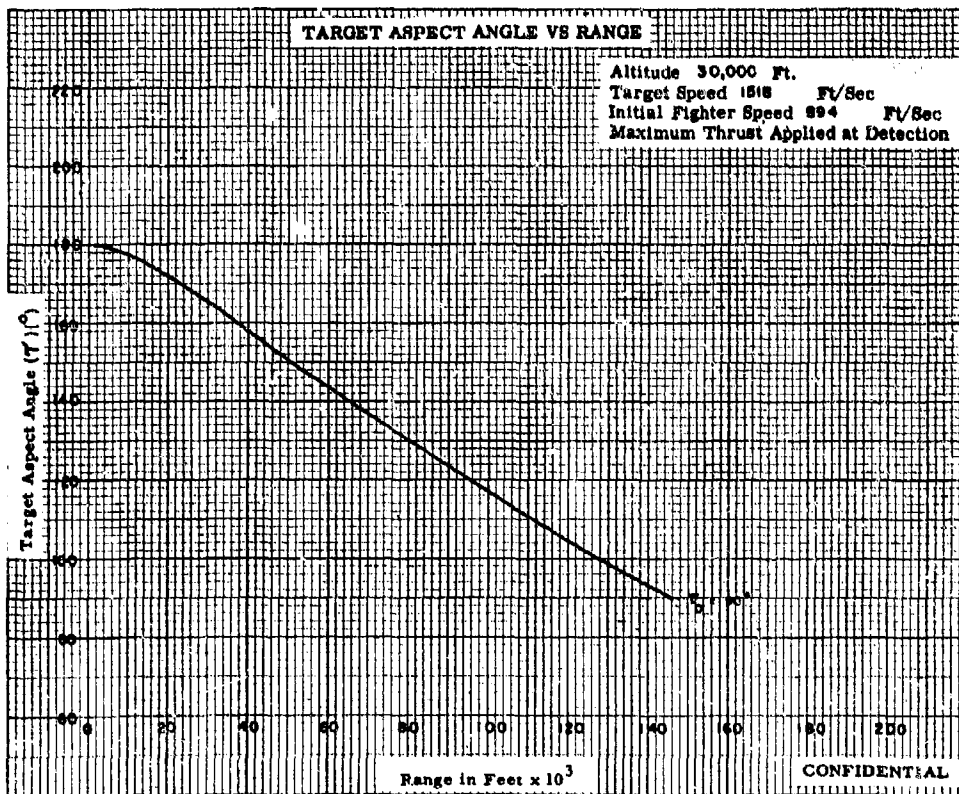
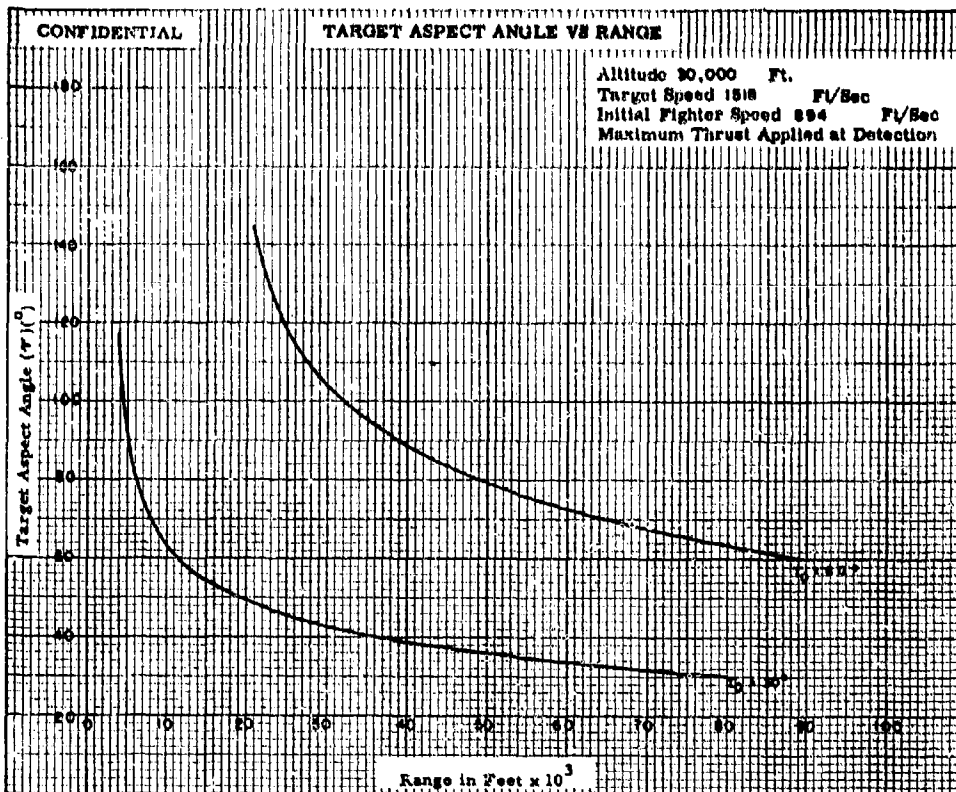


Fig. IX-7

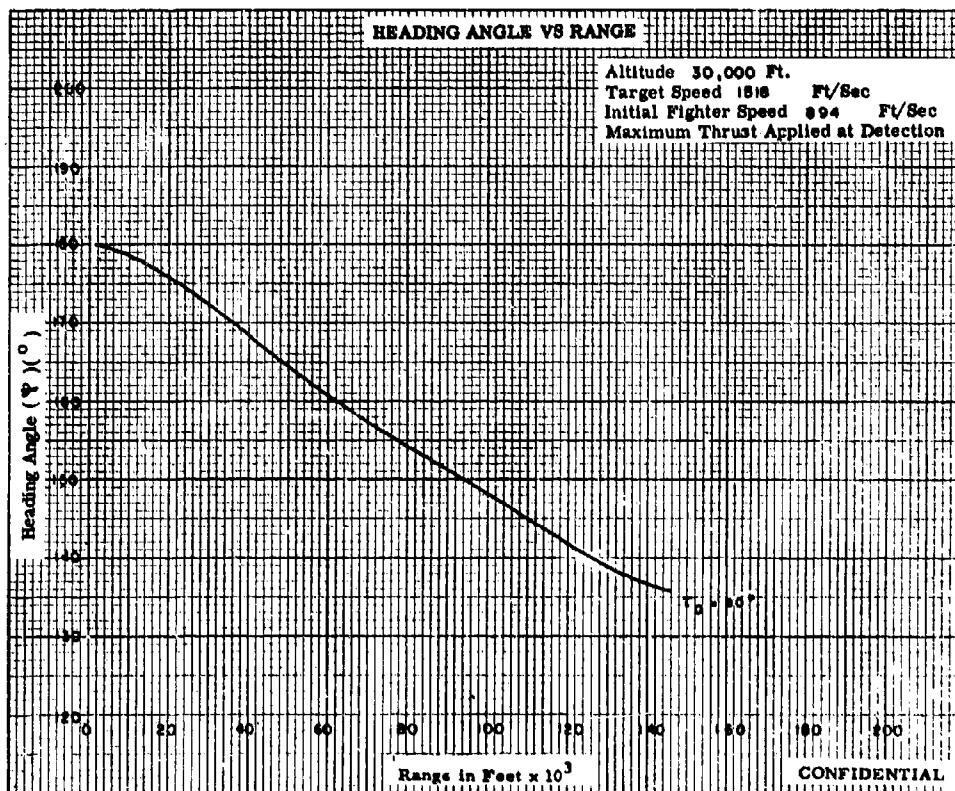
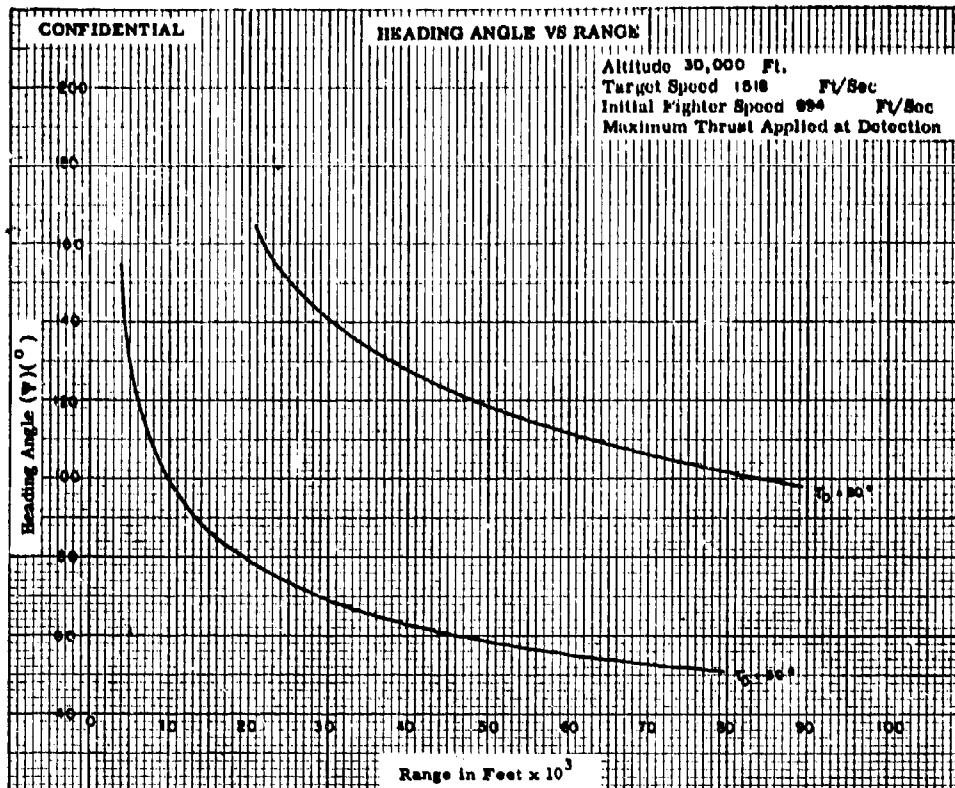


Fig. IX-8

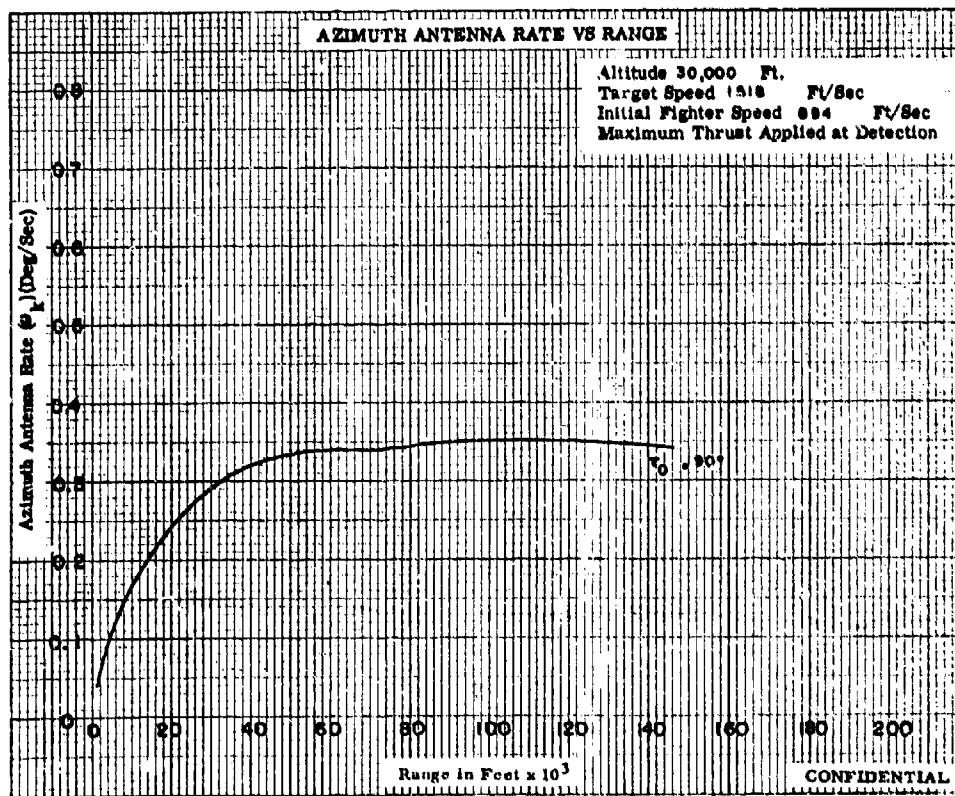
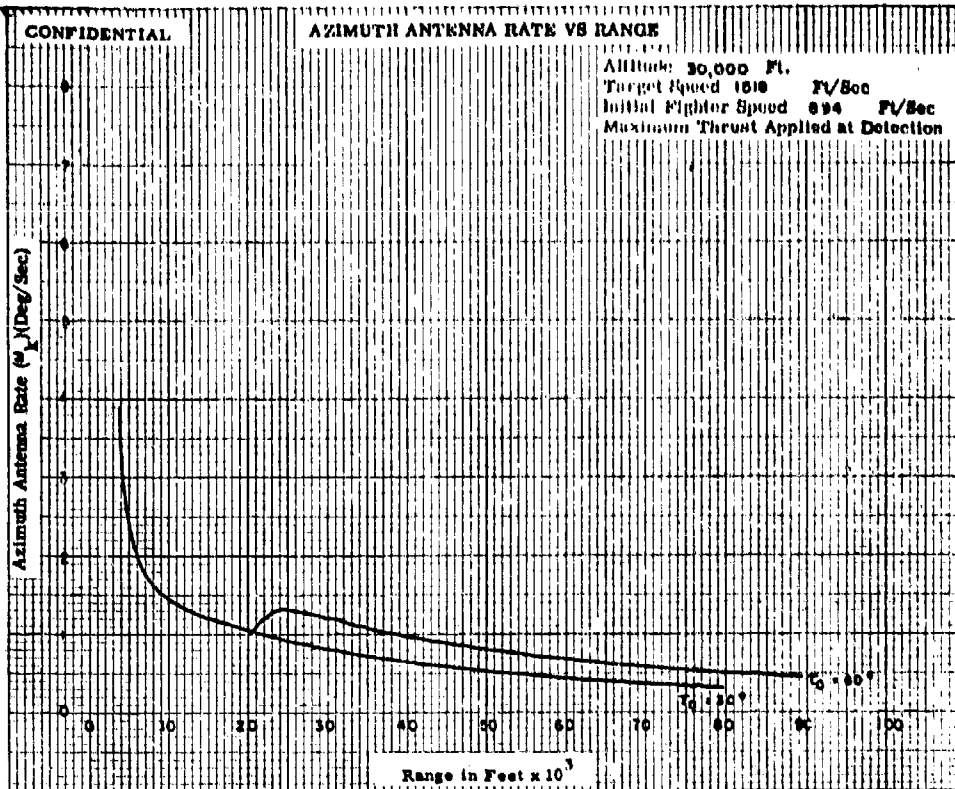


Fig. 1X-9

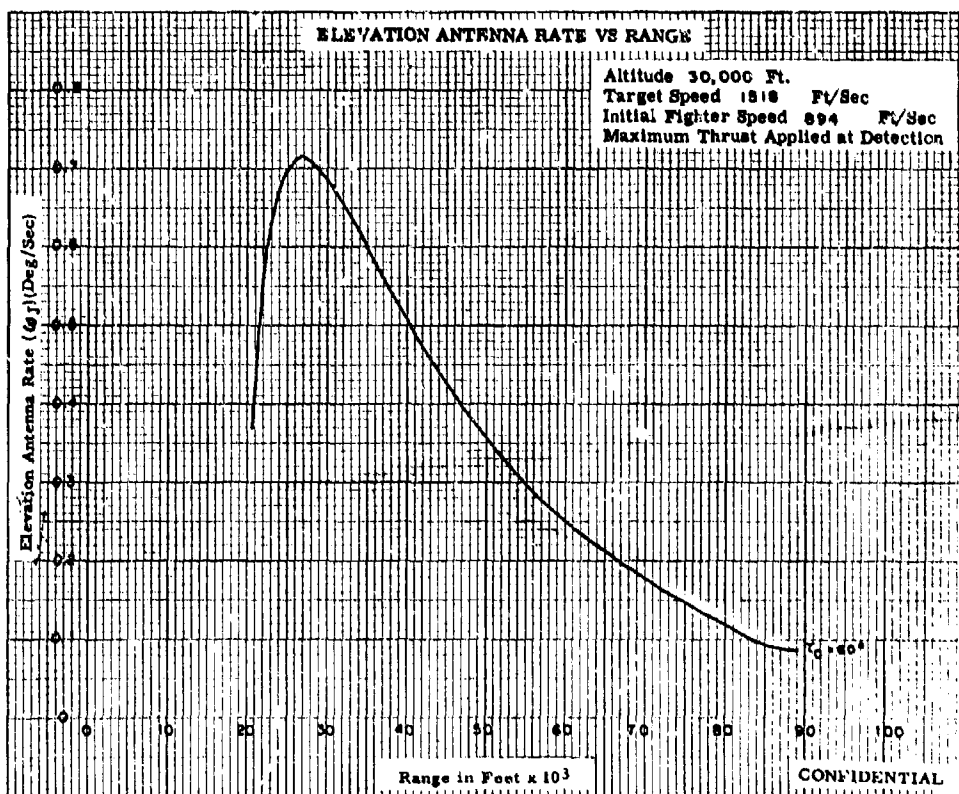
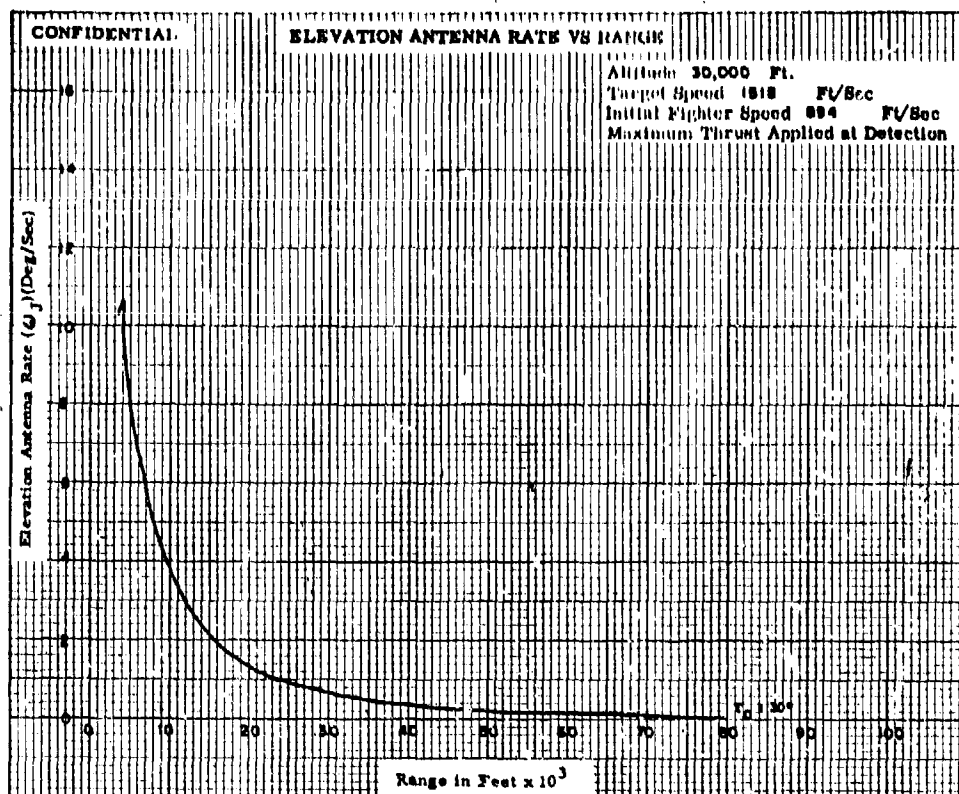


Fig. 1X-10a

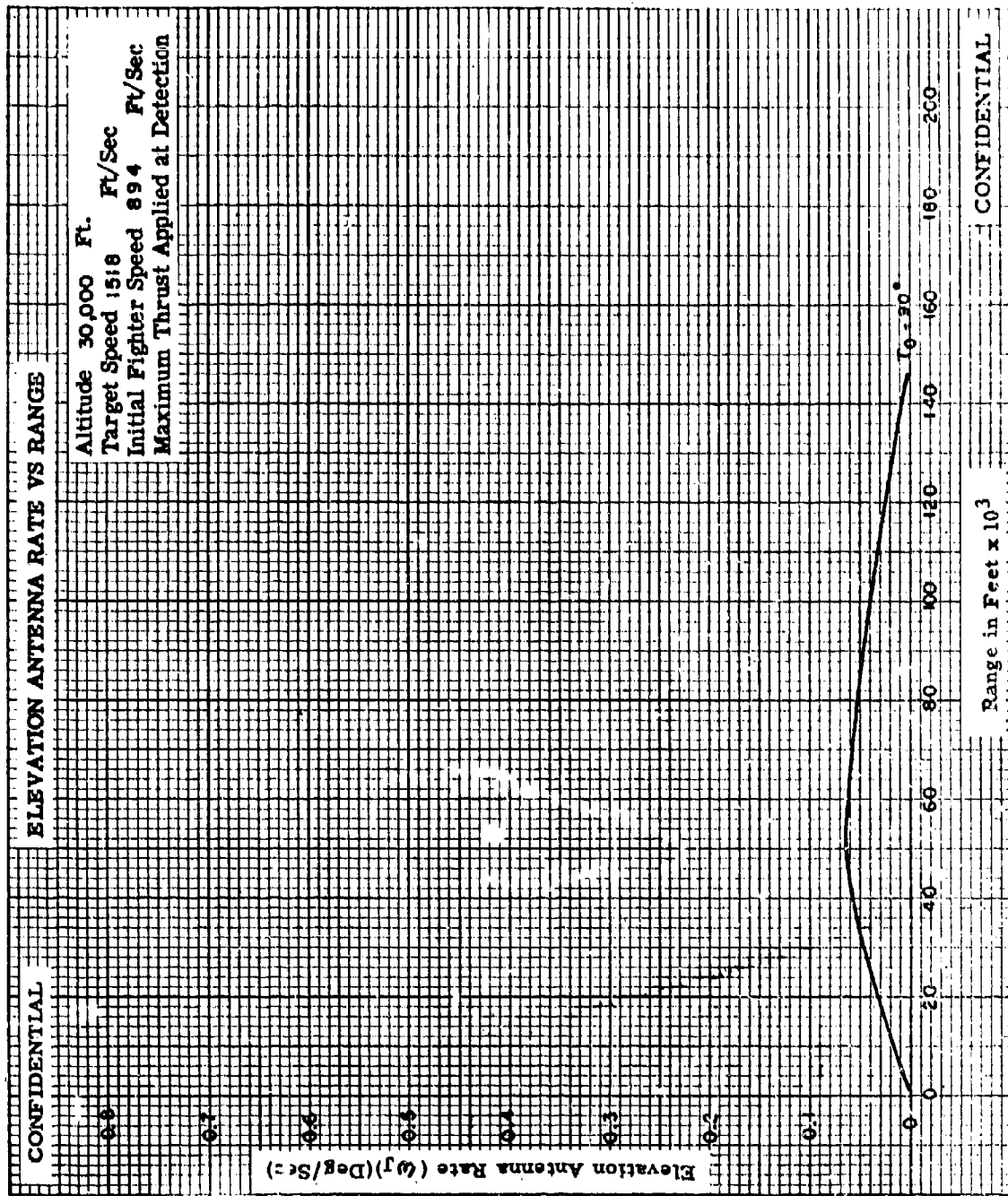


Fig. IX-10b

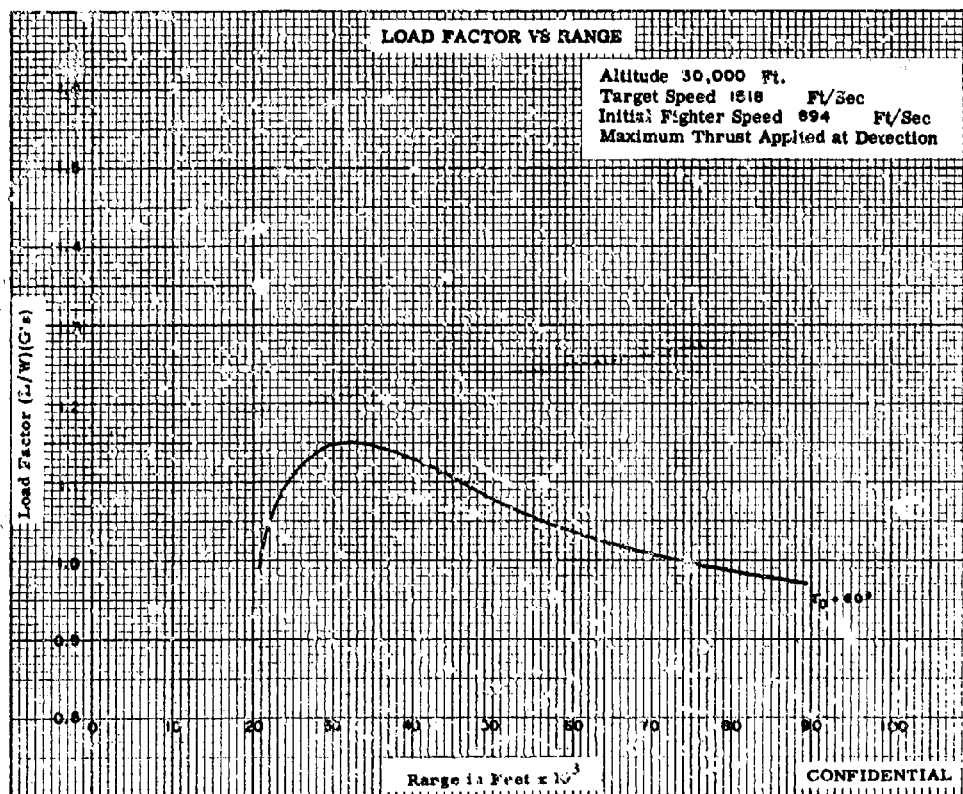
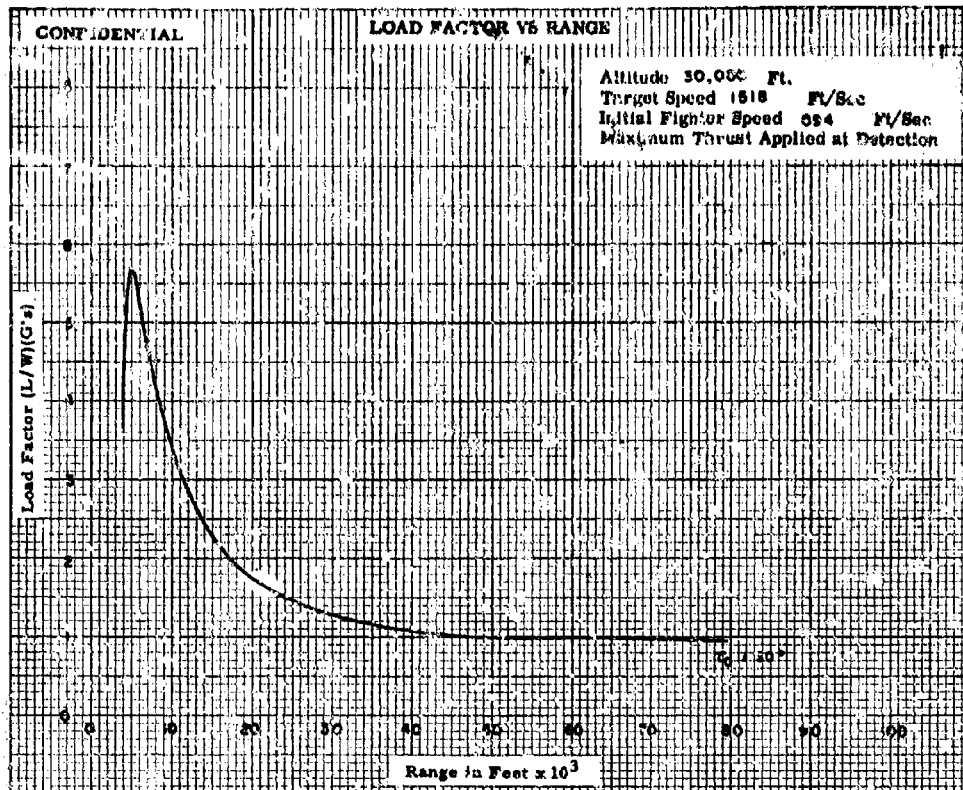


Fig. IX-11a

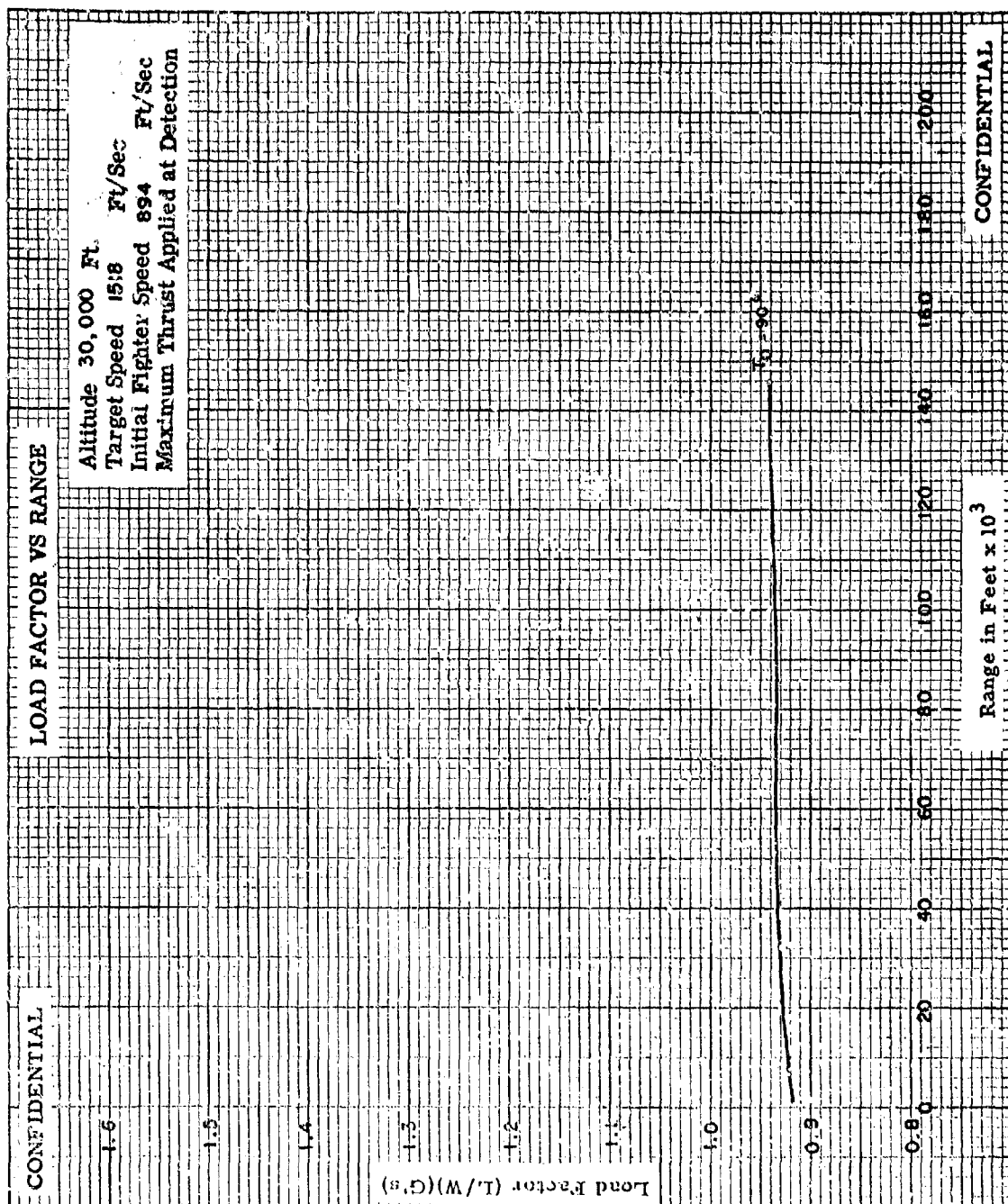


Fig. IX-11b

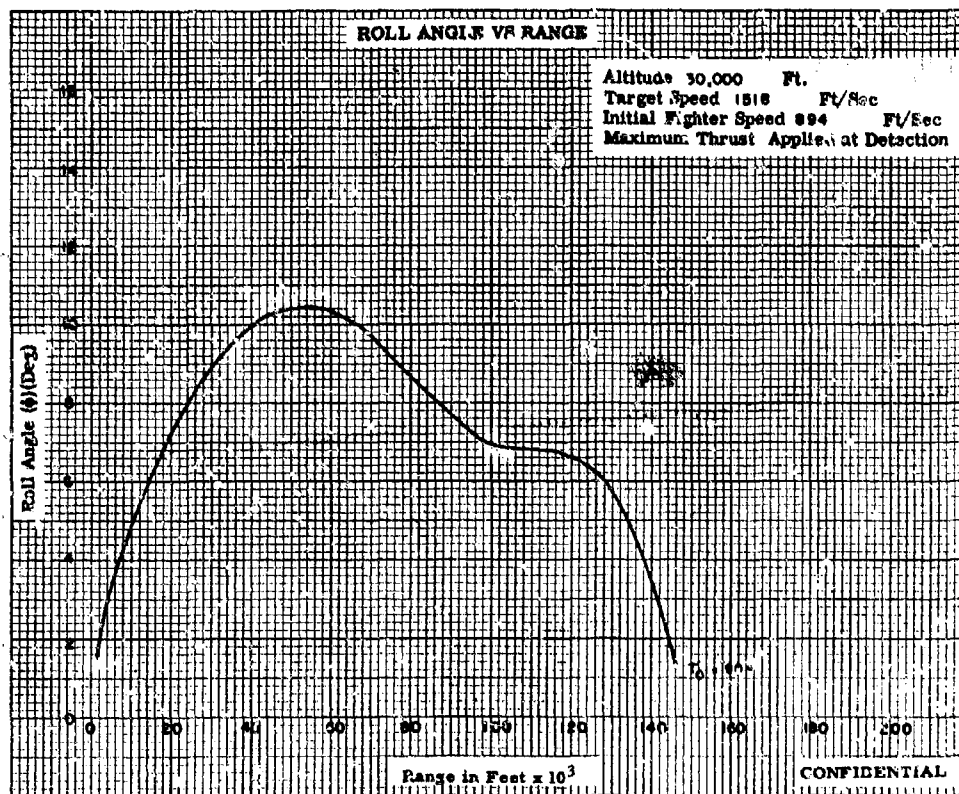
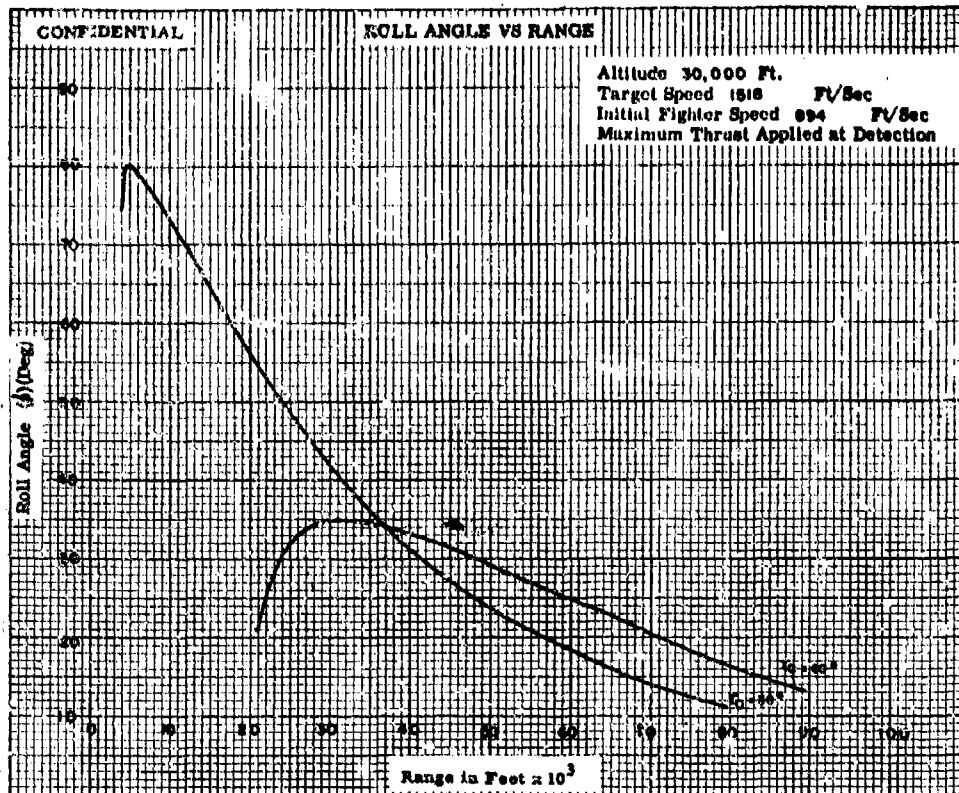


Fig. IX-12

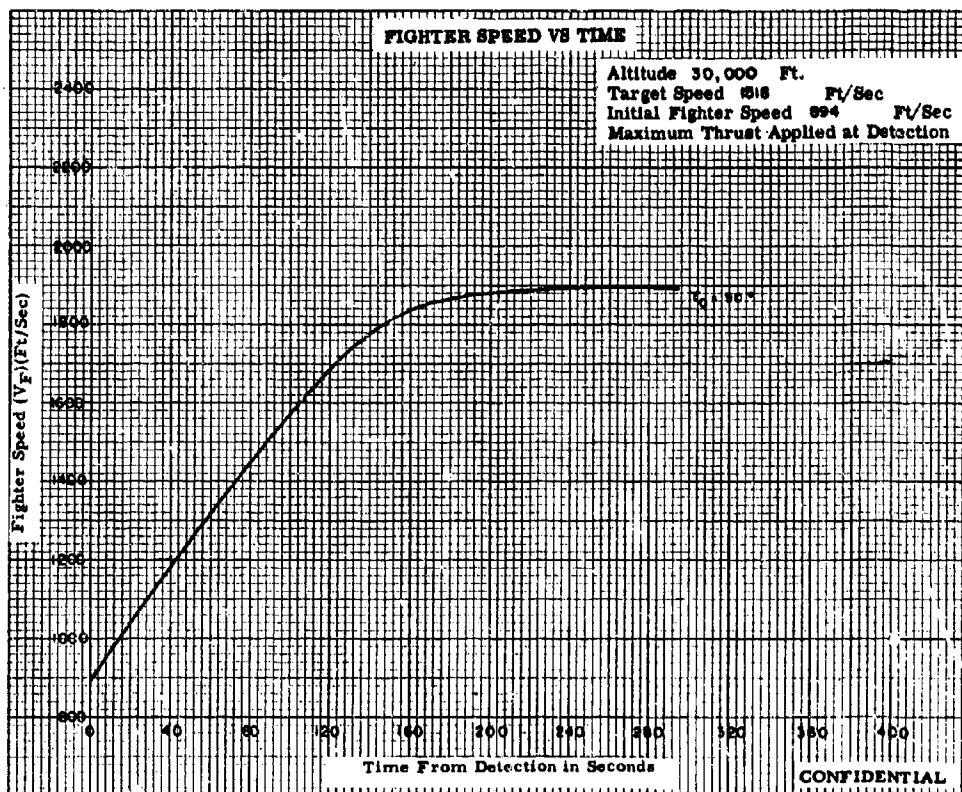
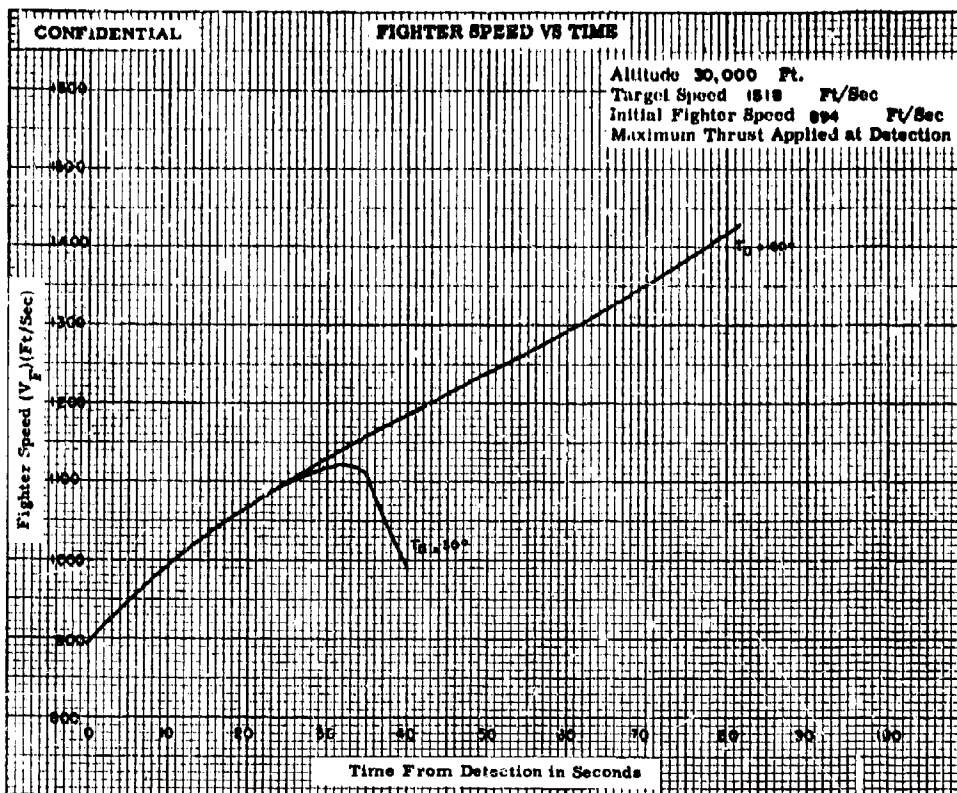


Fig. IX-13

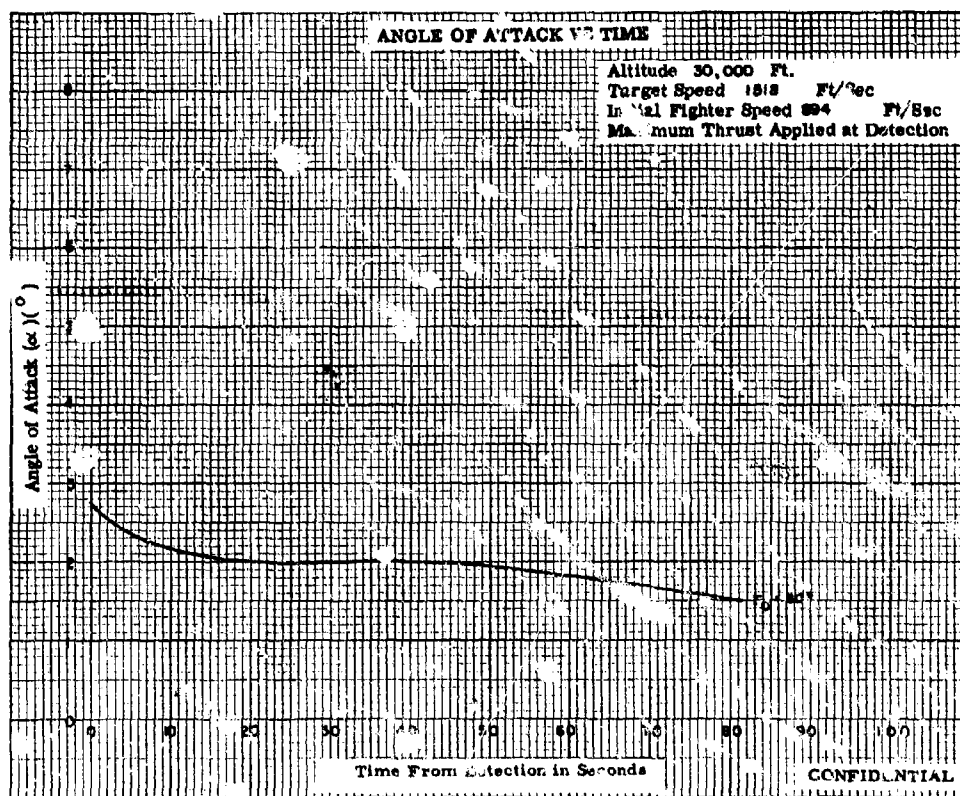
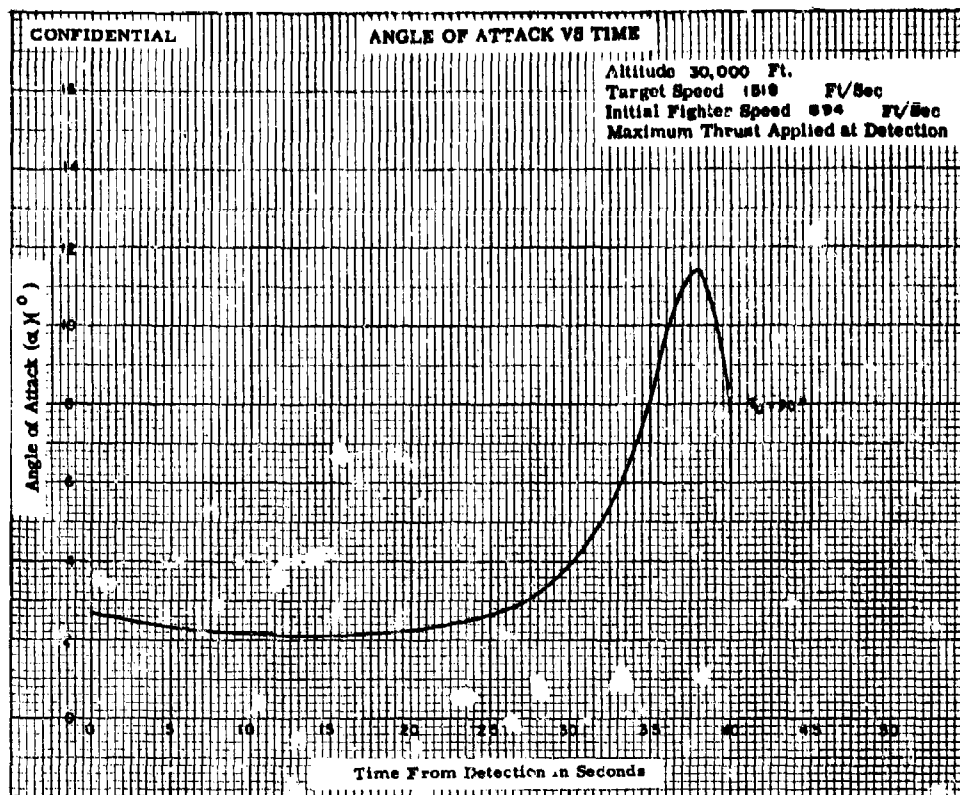


Fig. IX-14a

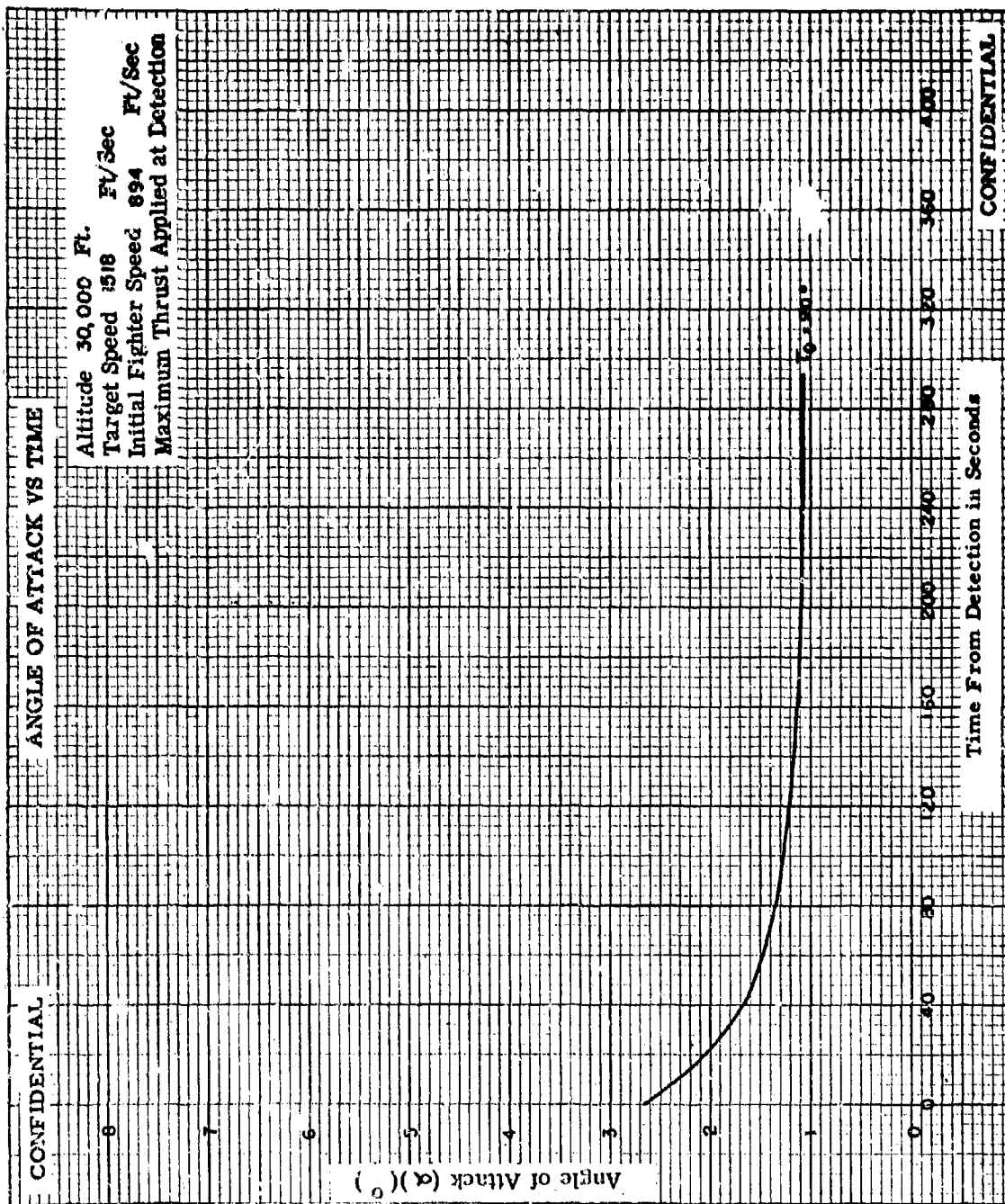
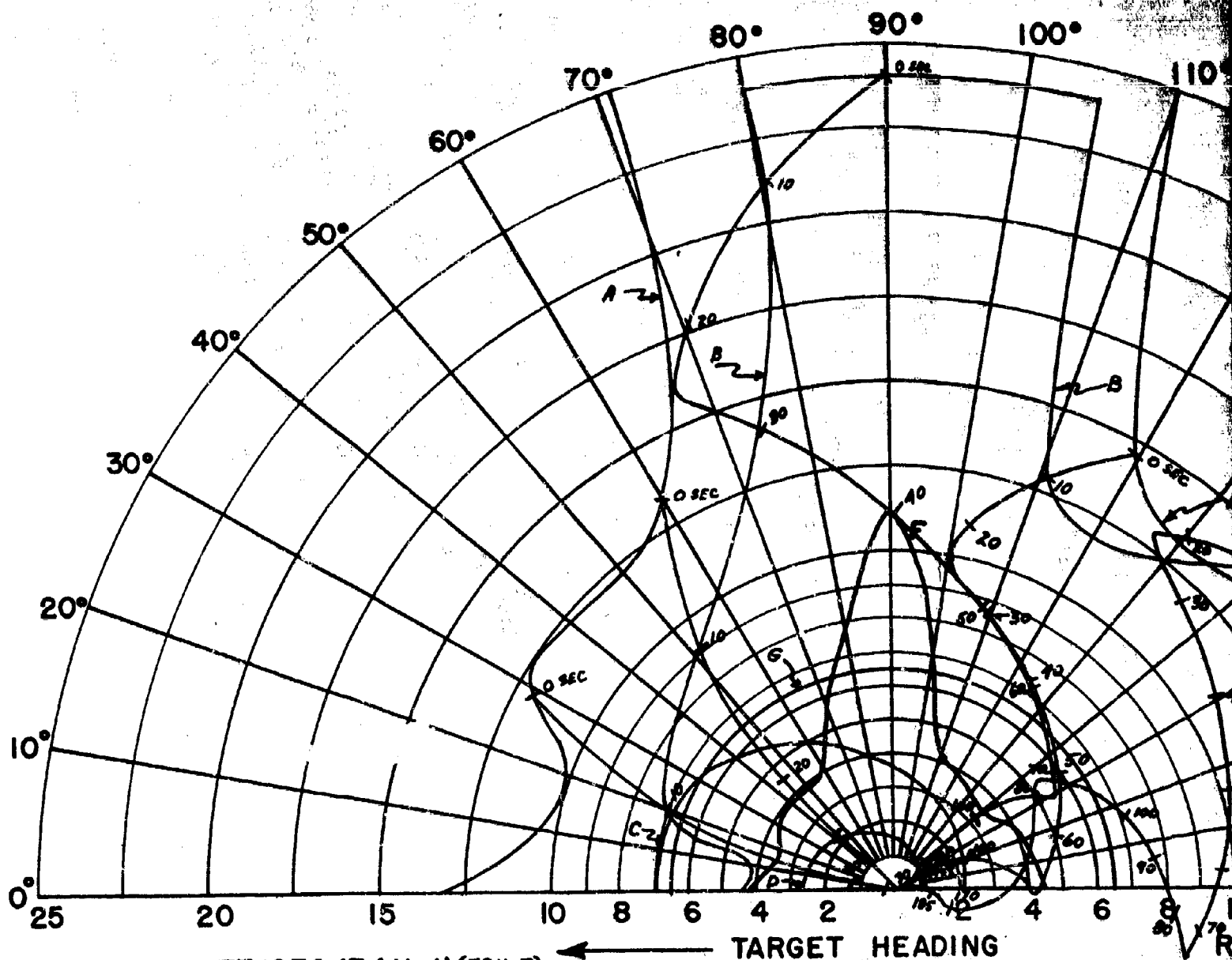


Fig. IX-14b

F18



$V_F = 1897$ FT/SEC (F4H-1)(F8U-3)

$V_T = 1518$ FT/SEC

ALTITUDE = 30,000 FT.

MANEUVERING TARGET-IN TARGET

COORDINATES

INITIAL RIGHT TURN

A - 85% DETECTION RANGE

B - LOCK-ON RANGE (10 SEC. LOCK-ON TIME)

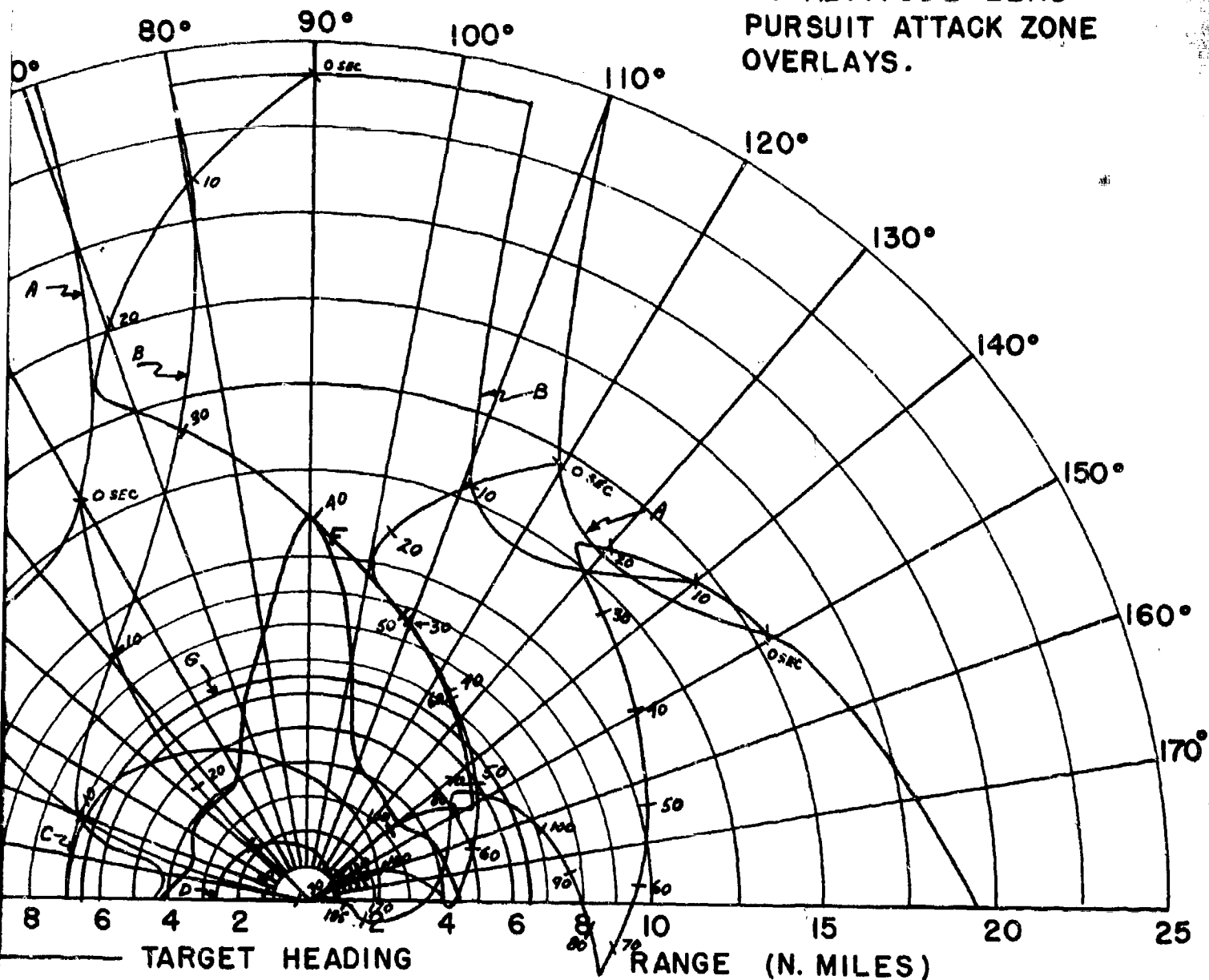
C - SPARROW III MAX. AERODYNAMIC RANGE

D - SPARROW III MIN. AERODYNAMIC RANGE

E - 90% SPARROW III SEEKER LOCK-ON R

G - 6.5 N.M. INTERLOCK

FIG. X - CO-ALTITUDE LEAD
PURSUIT ATTACK ZONE
OVERLAYS.



85% DETECTION RANGE
 LOCK-ON RANGE (10 SEC. LOCK-ON TIME)
 SPARROW III MAX. AERODYNAMIC RANGE
 SPARROW III MIN. AERODYNAMIC RANGE
 90% SPARROW III SEEKER LOCK-ON RANGE
 6.5 N.M. INTERLOCK

CONFIDENTIAL

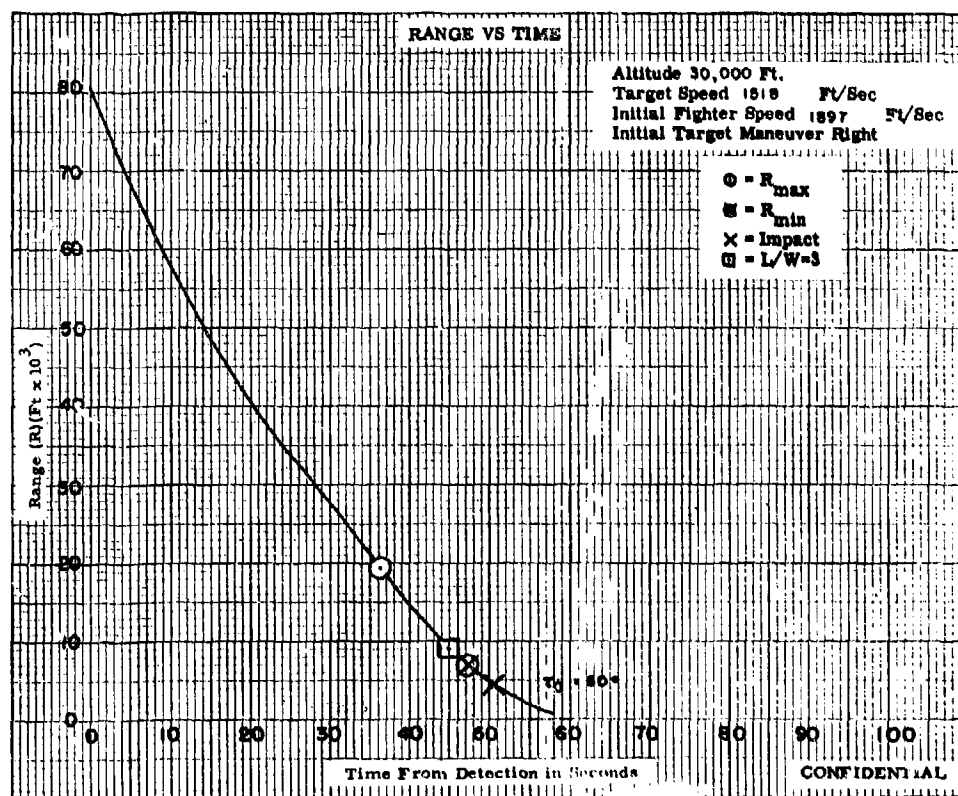
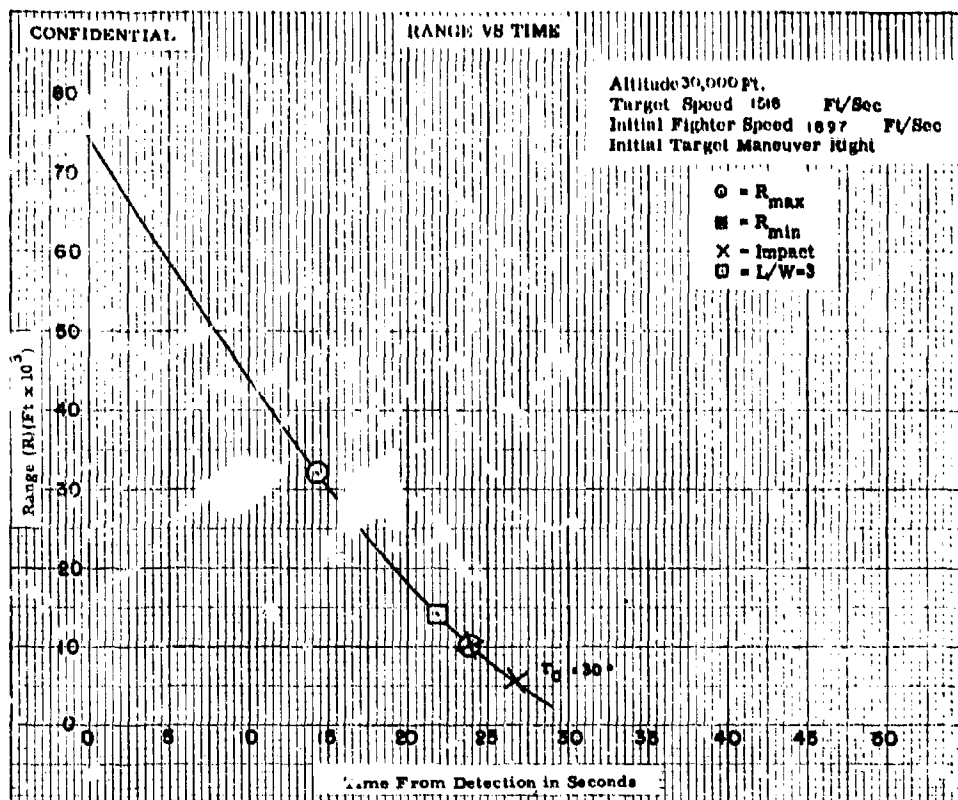


Fig. X-1a

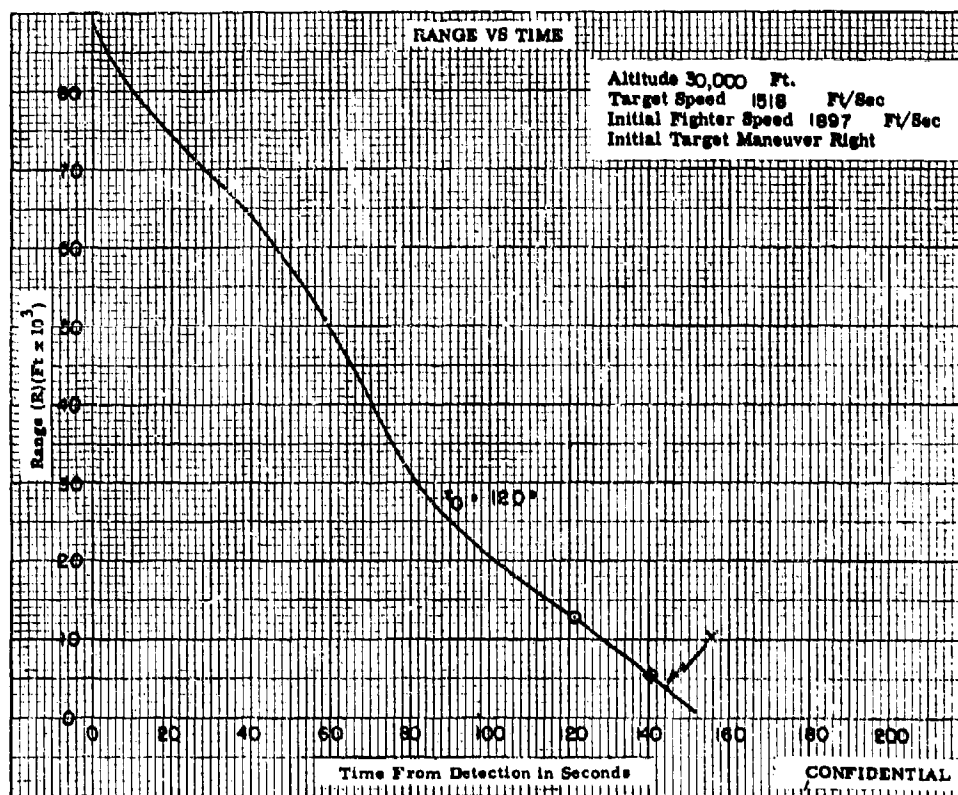
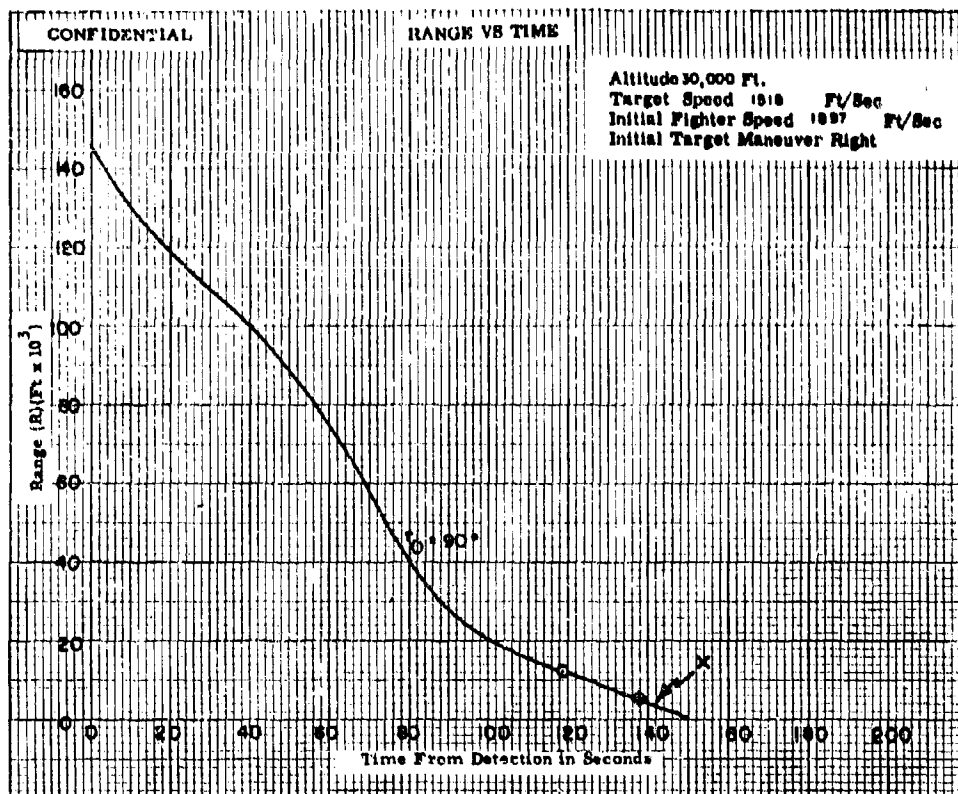


Fig. X-1b

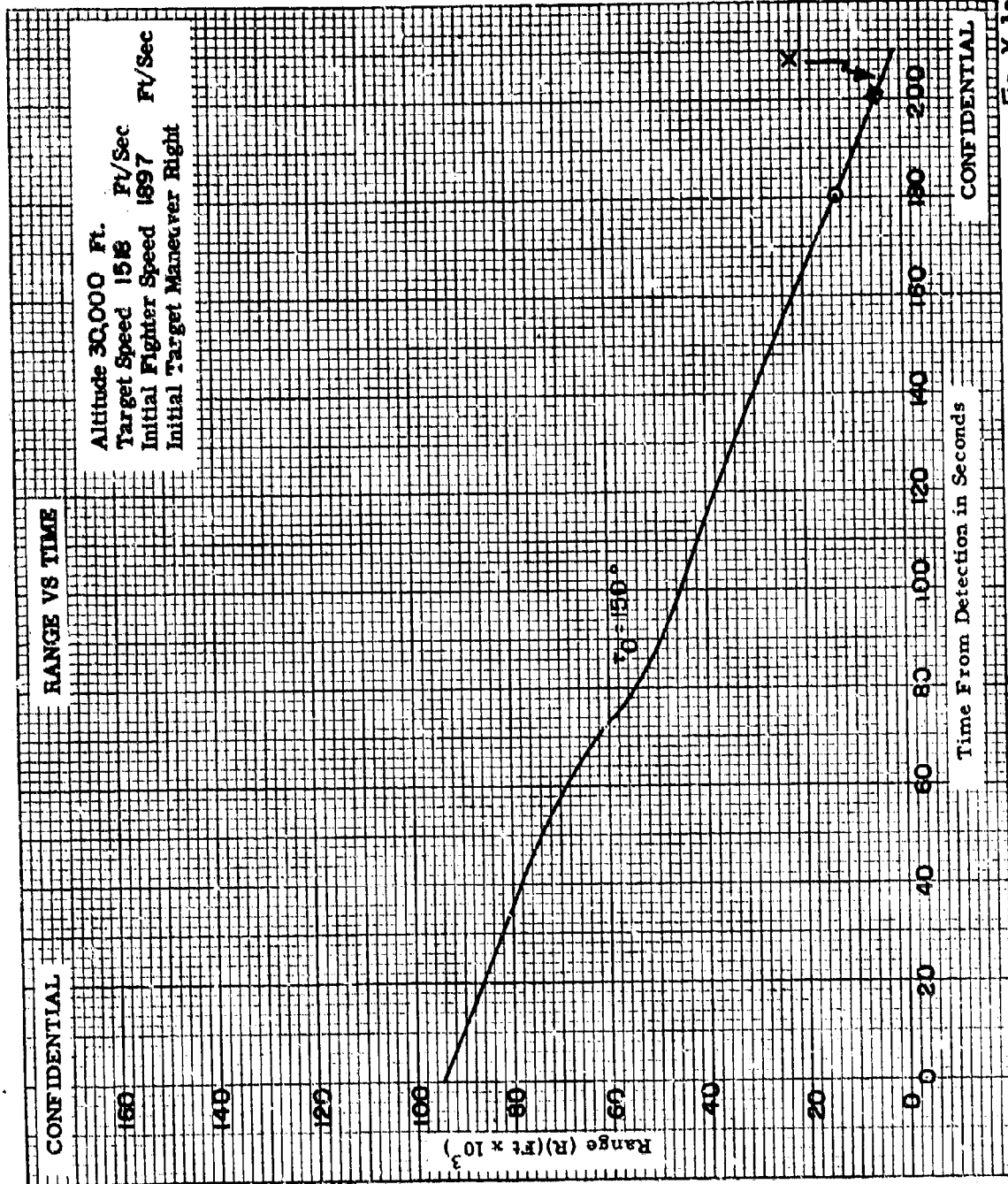


Fig X-1c

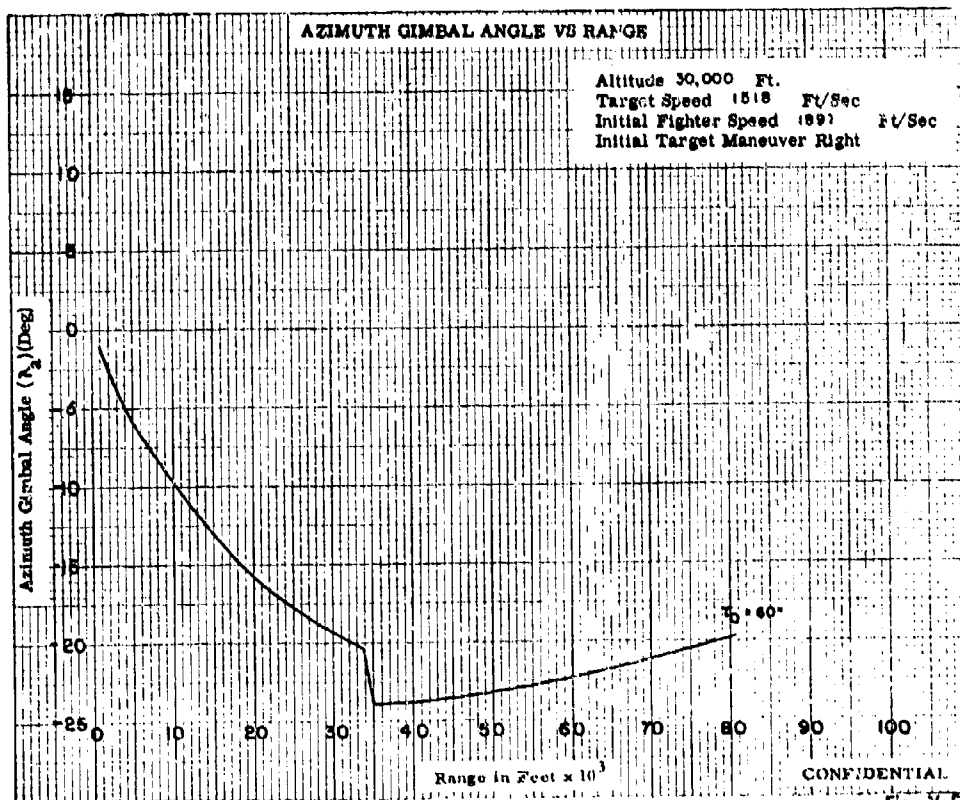
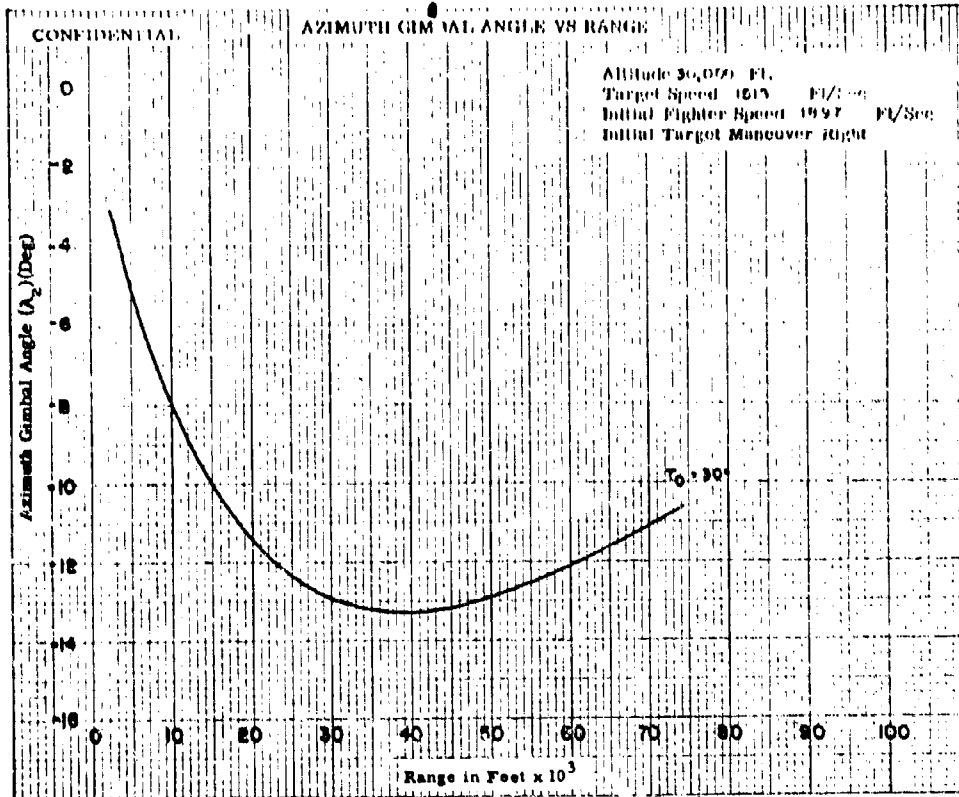


Fig. X-2a

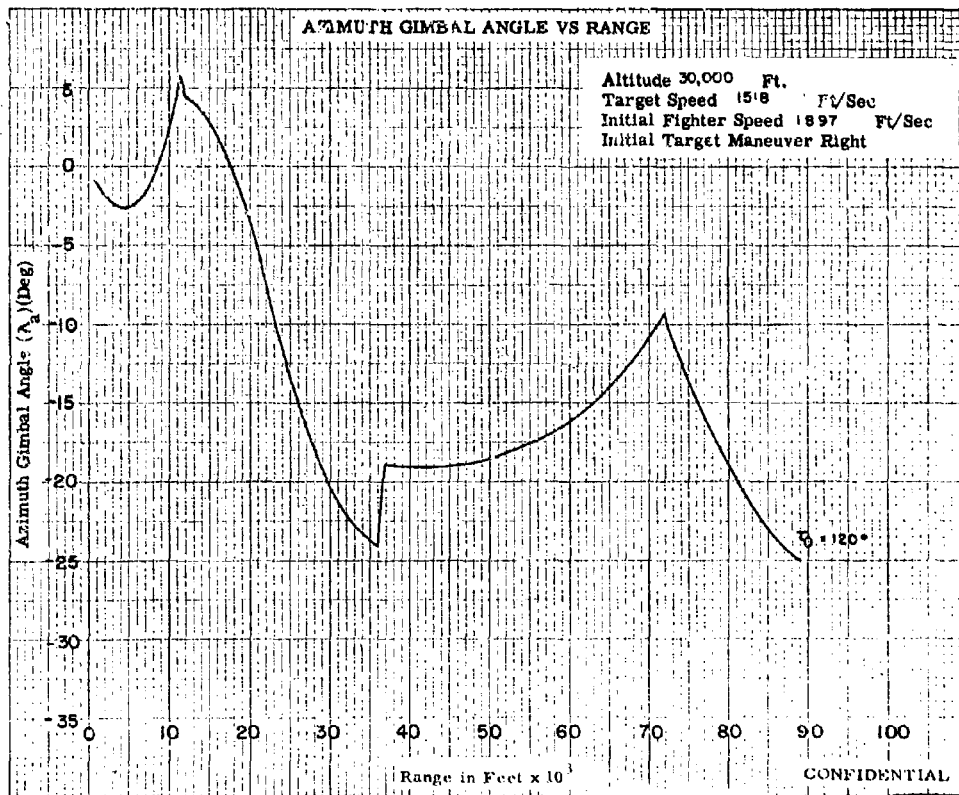
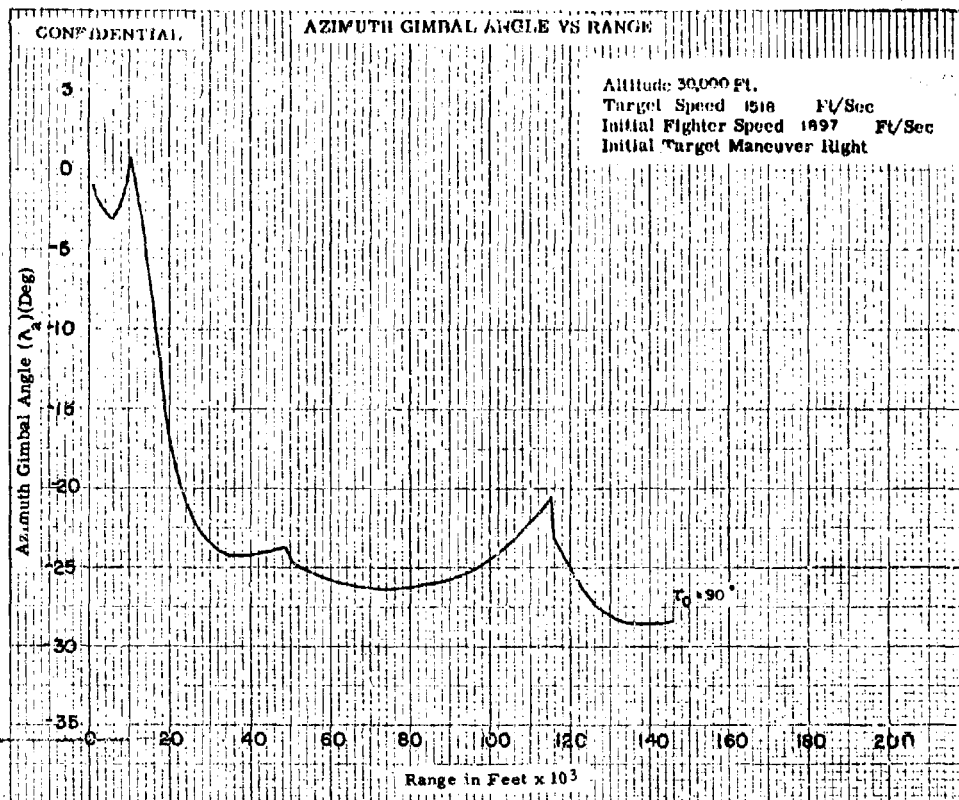


Fig. X-2b

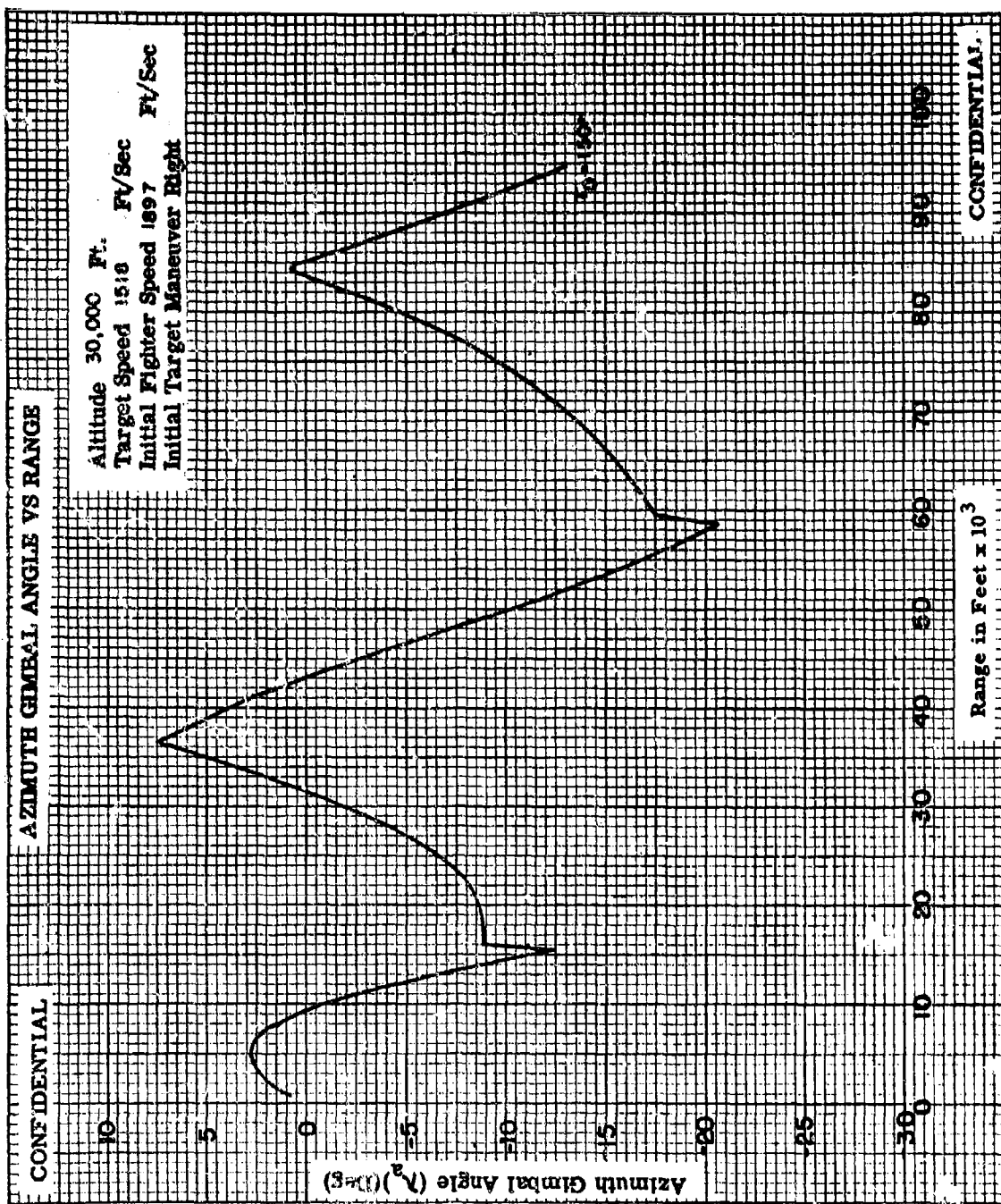


Fig. X-2c

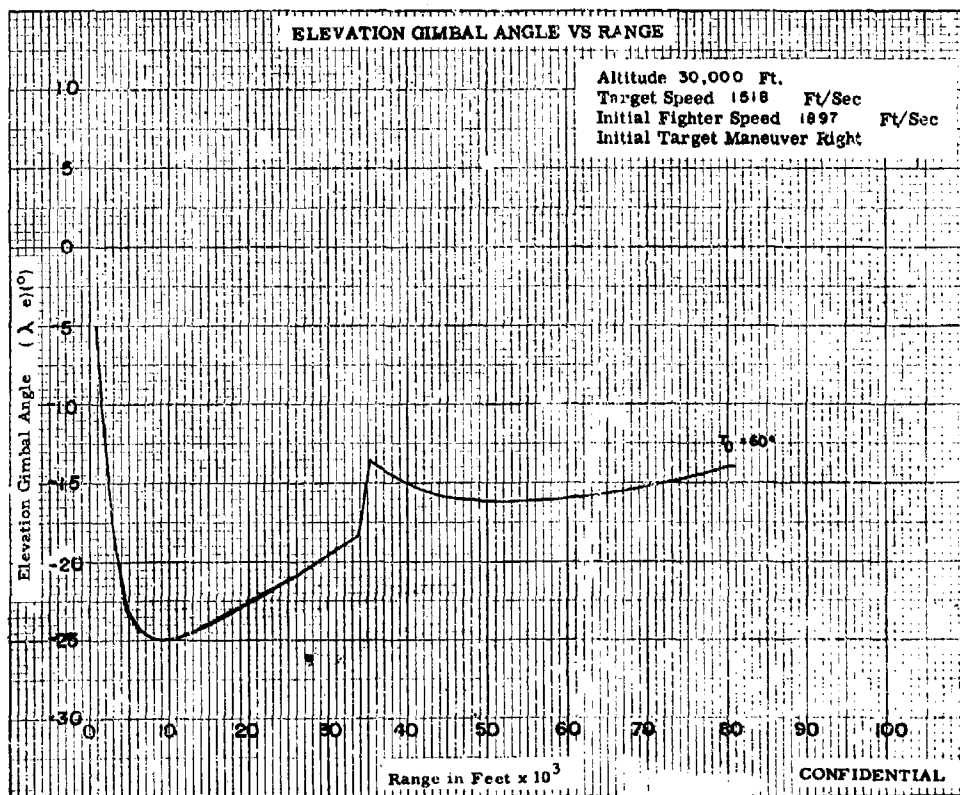
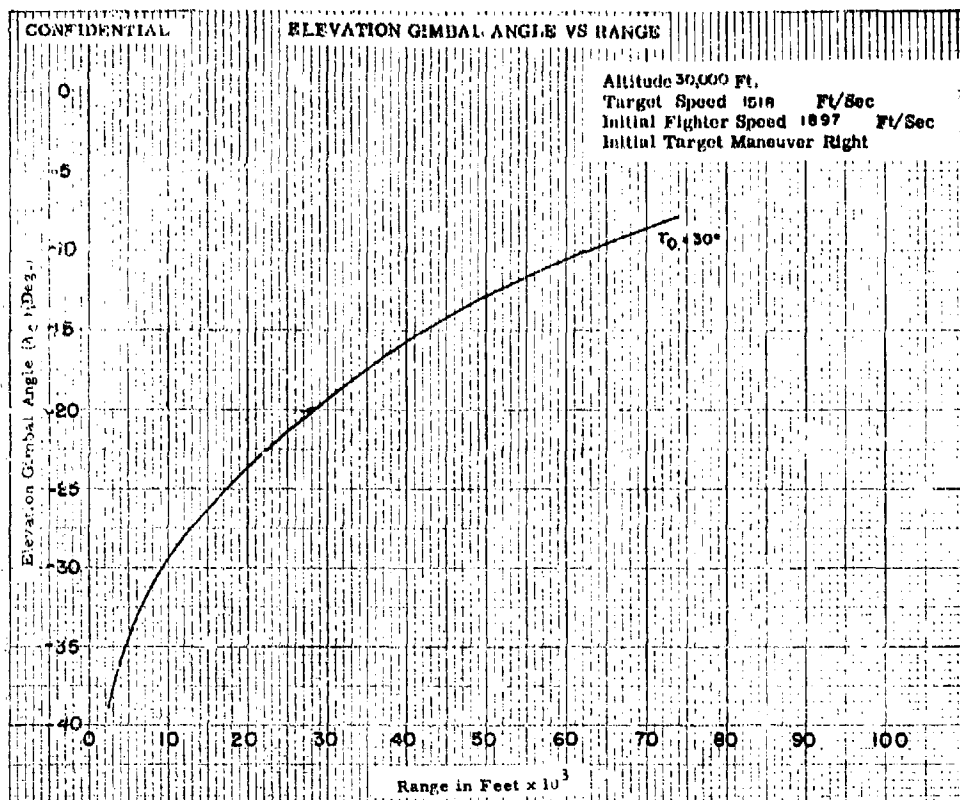


Fig. X-3a

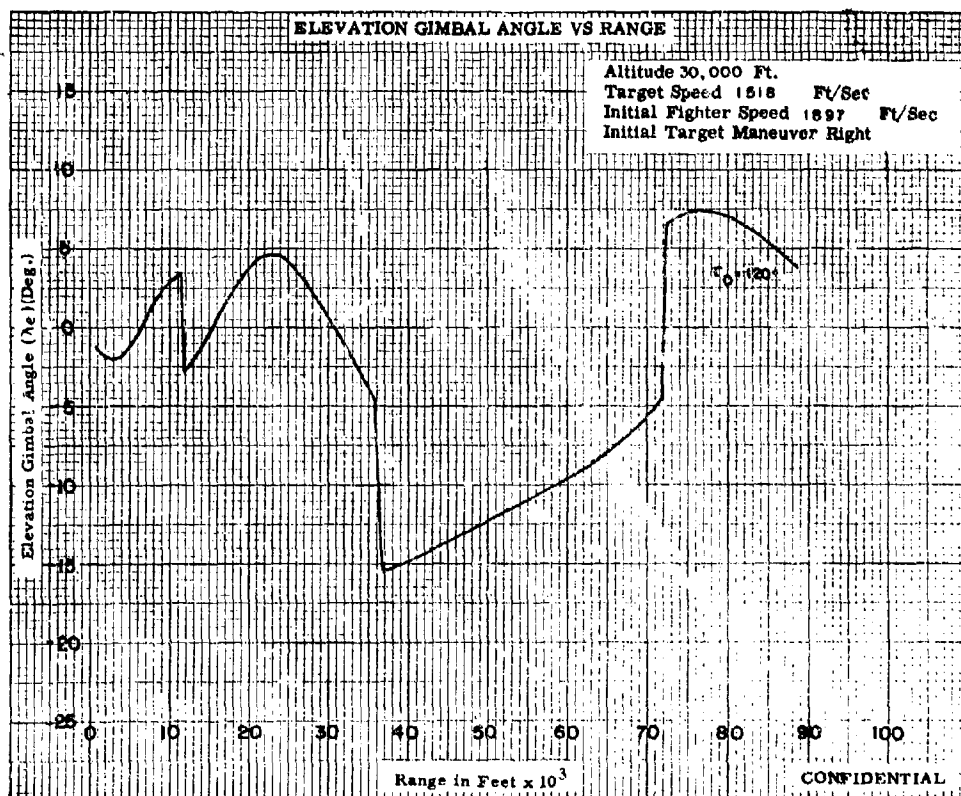
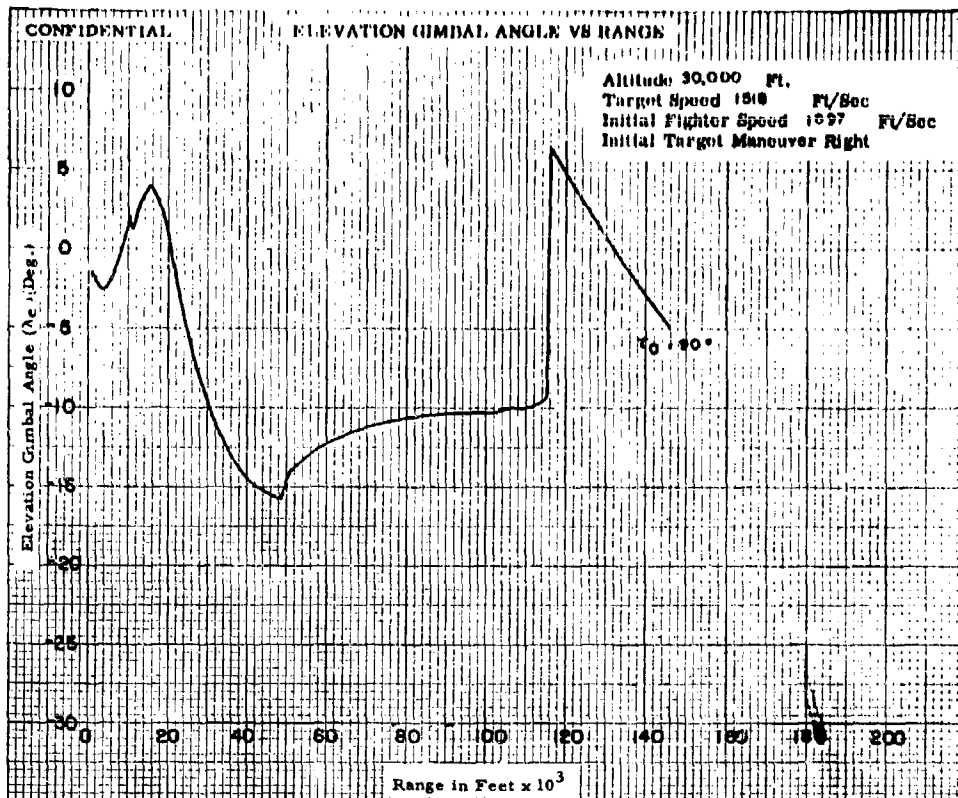


Fig. X-3b

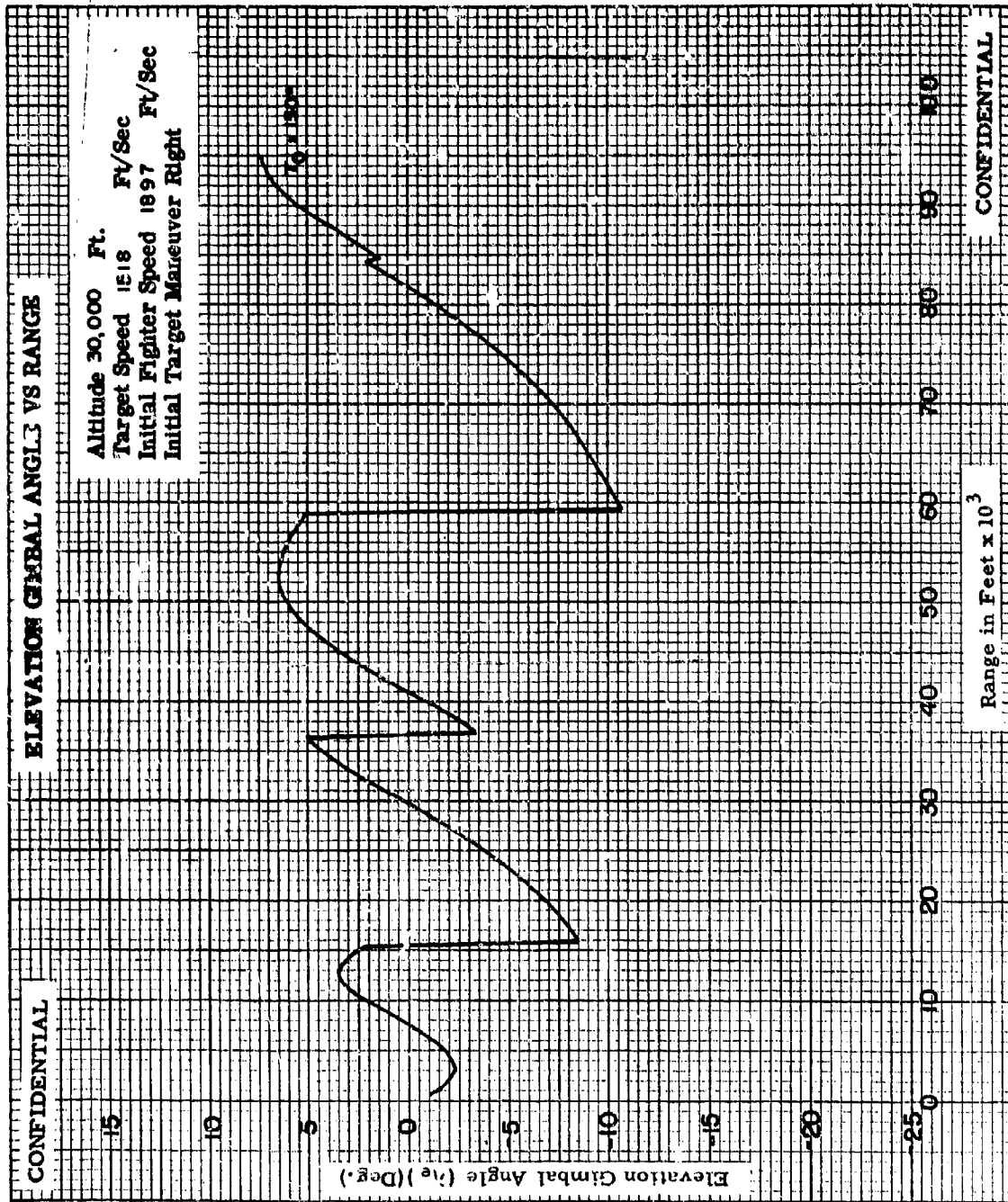


Fig. X-3c

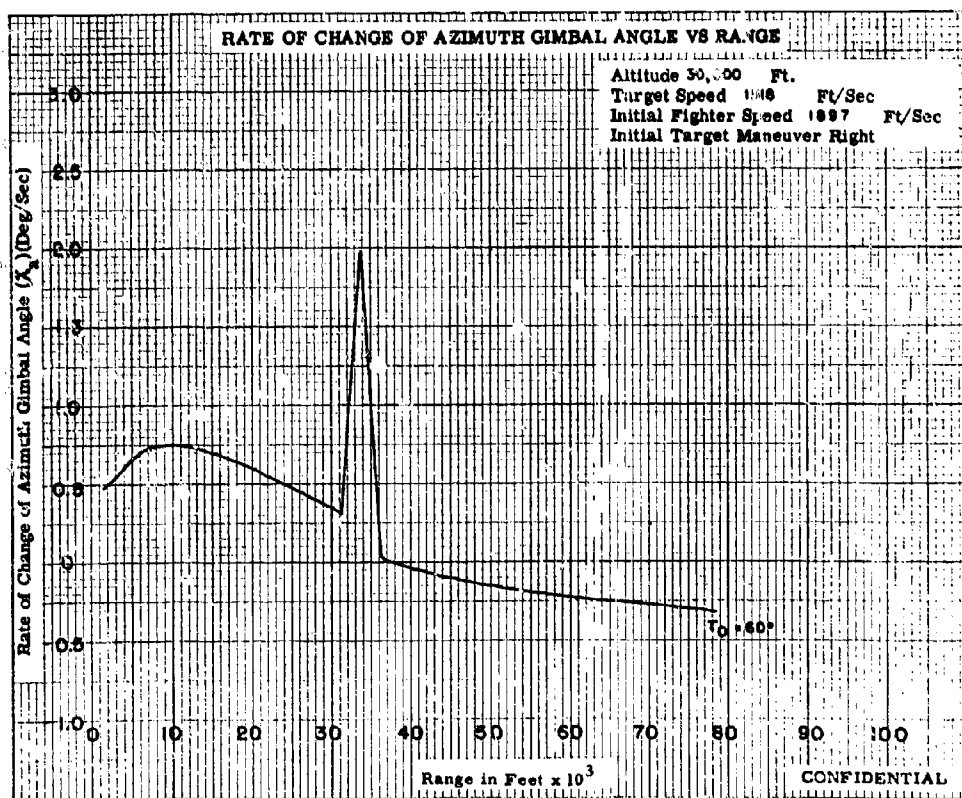
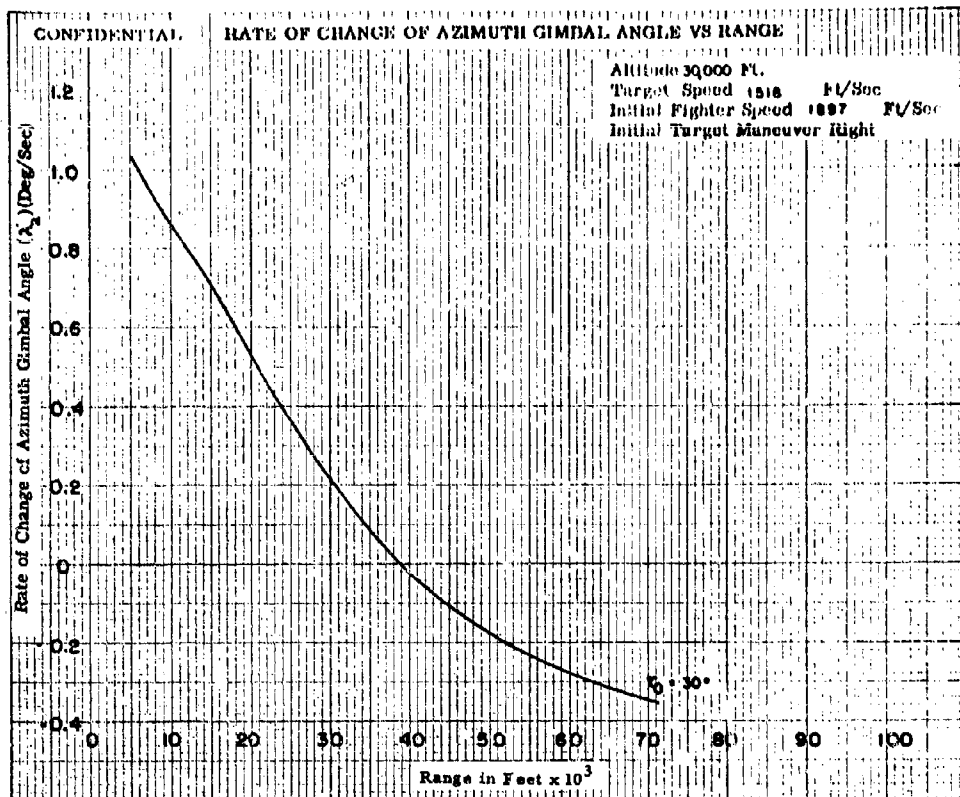


Fig. X-4a

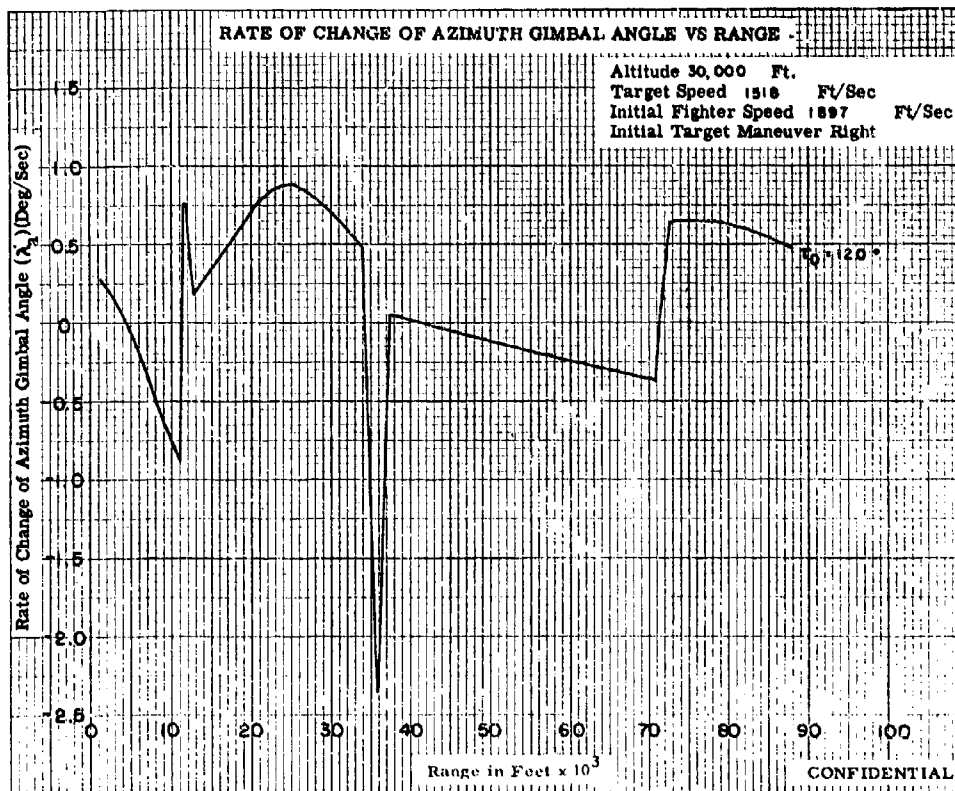
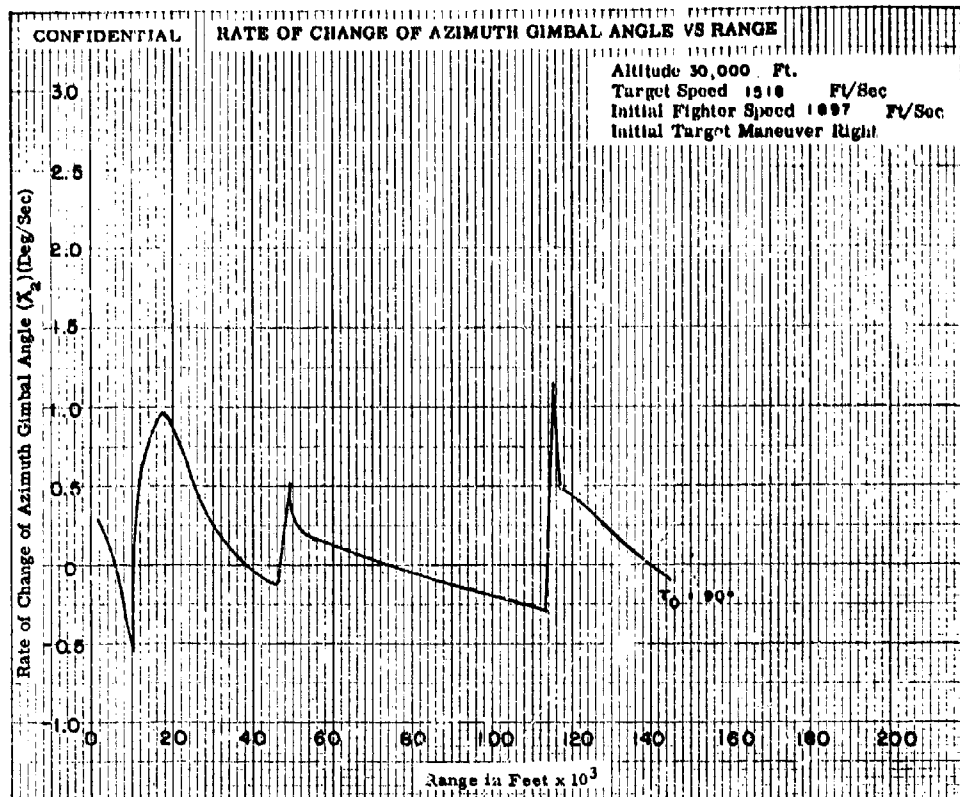


Fig. X-4b

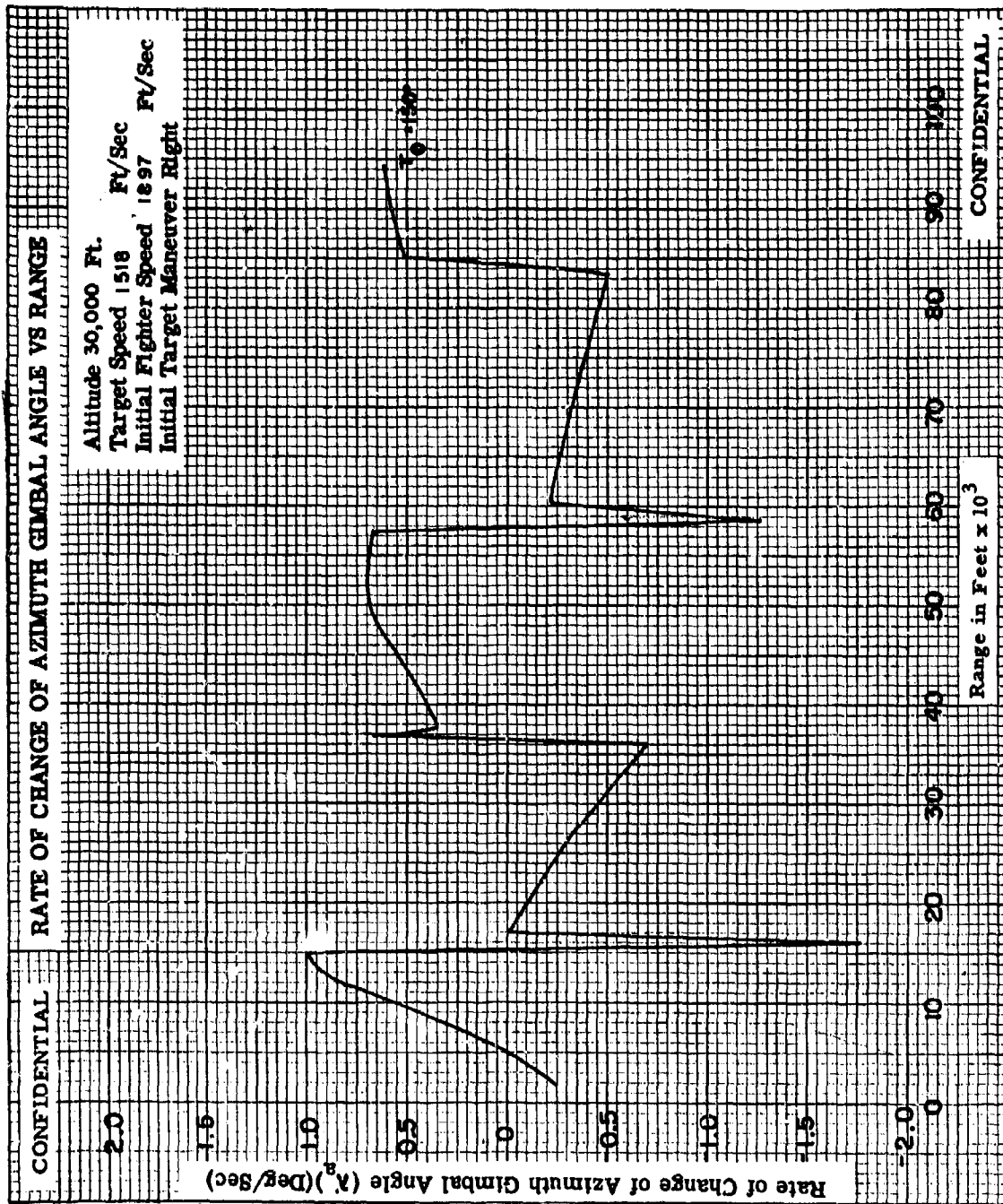


Fig X-4c

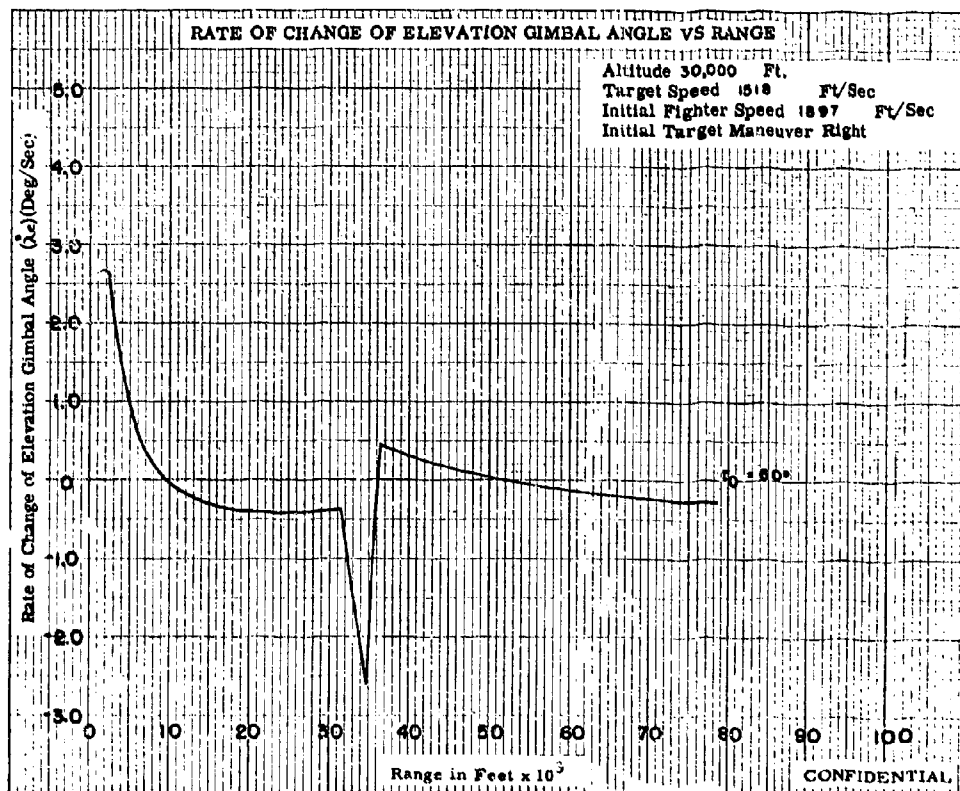
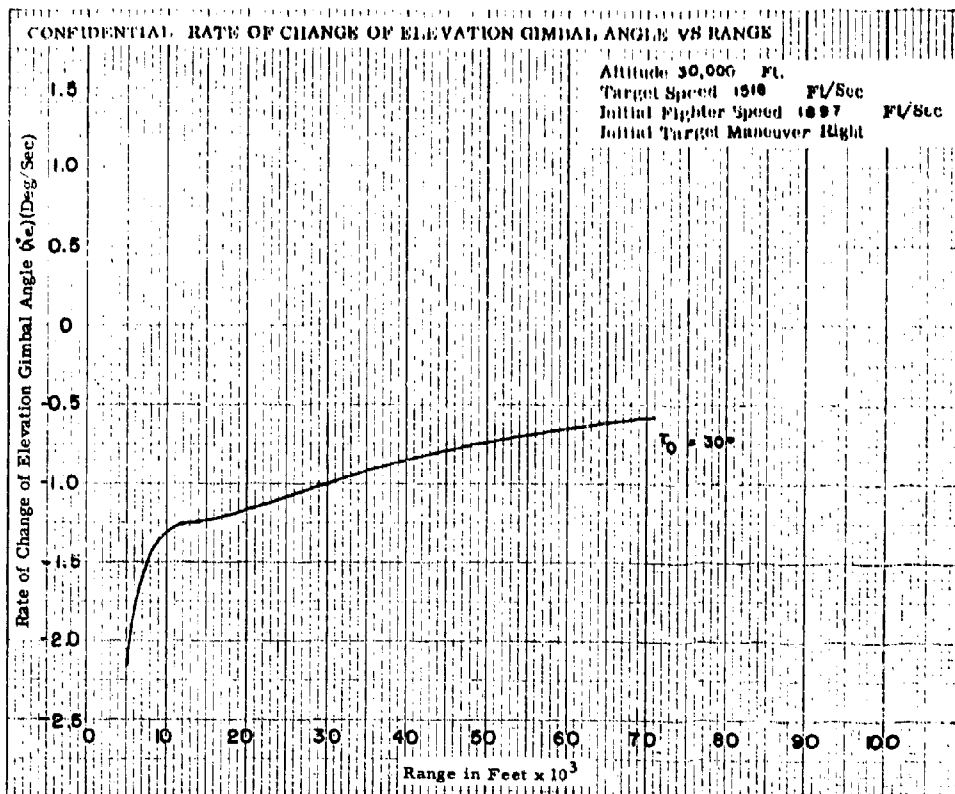


Fig. X-5a

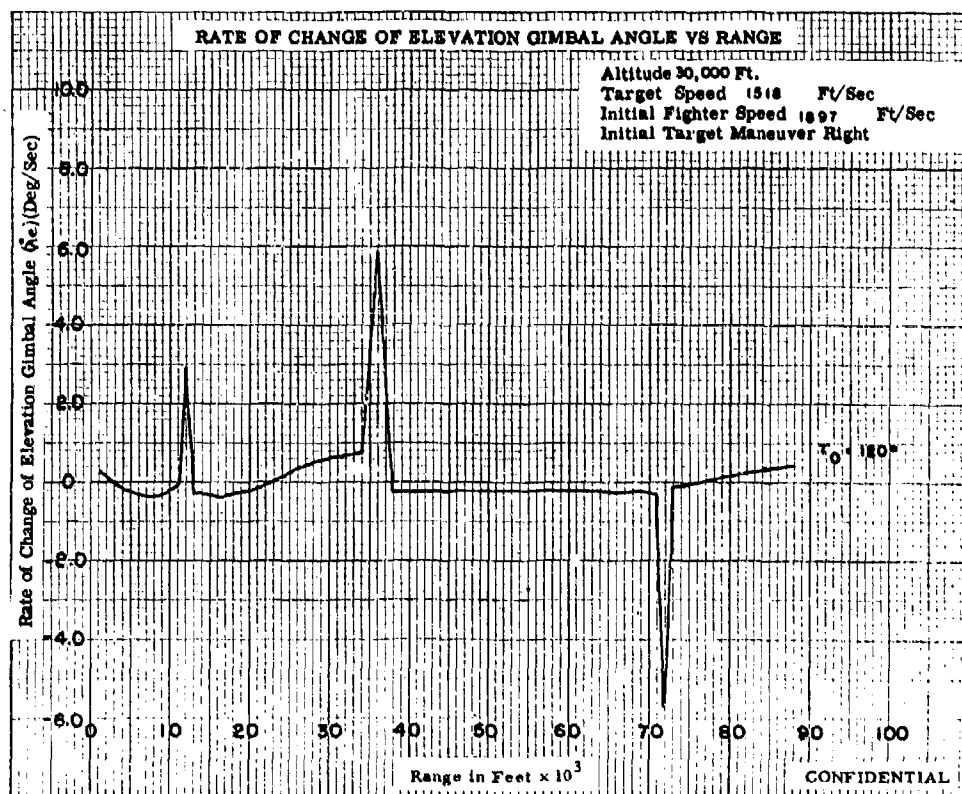
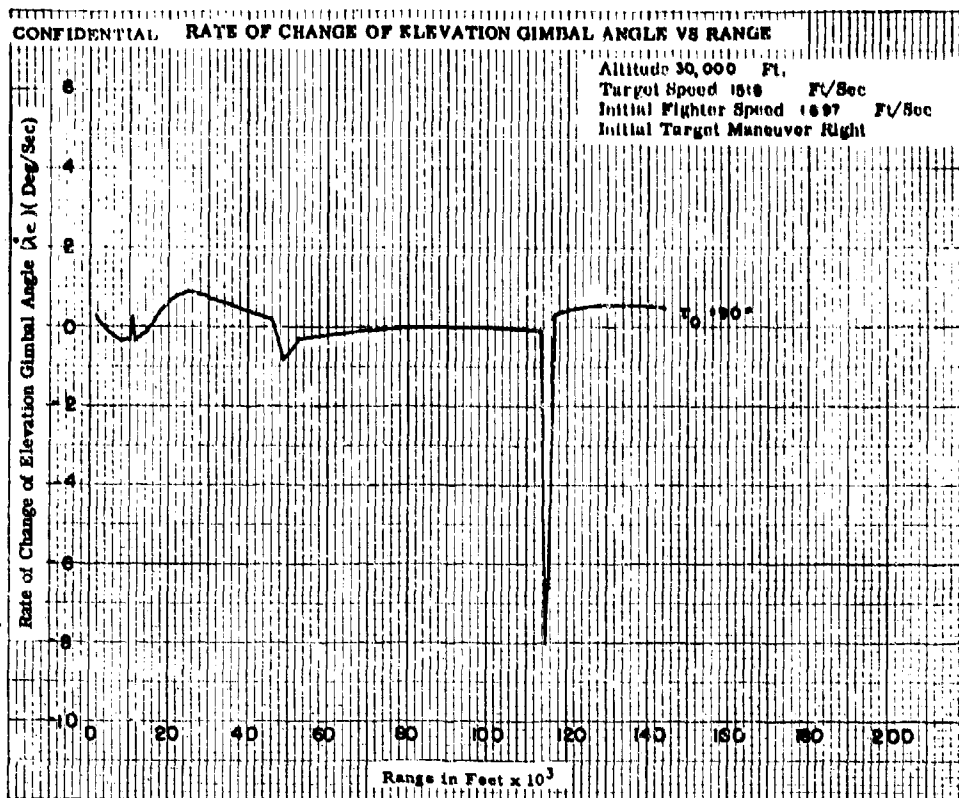


Fig. X-5b

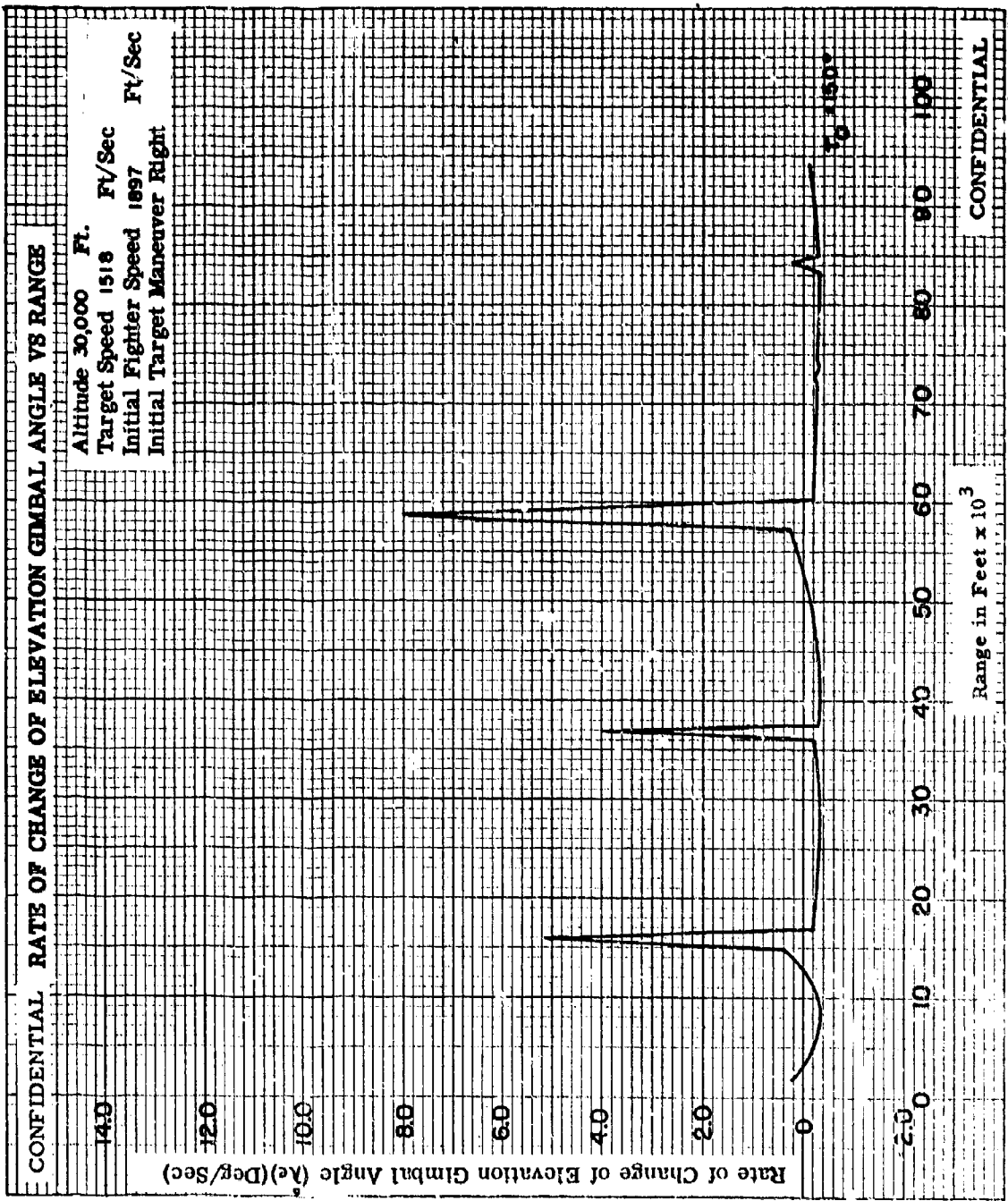


Fig. X-5

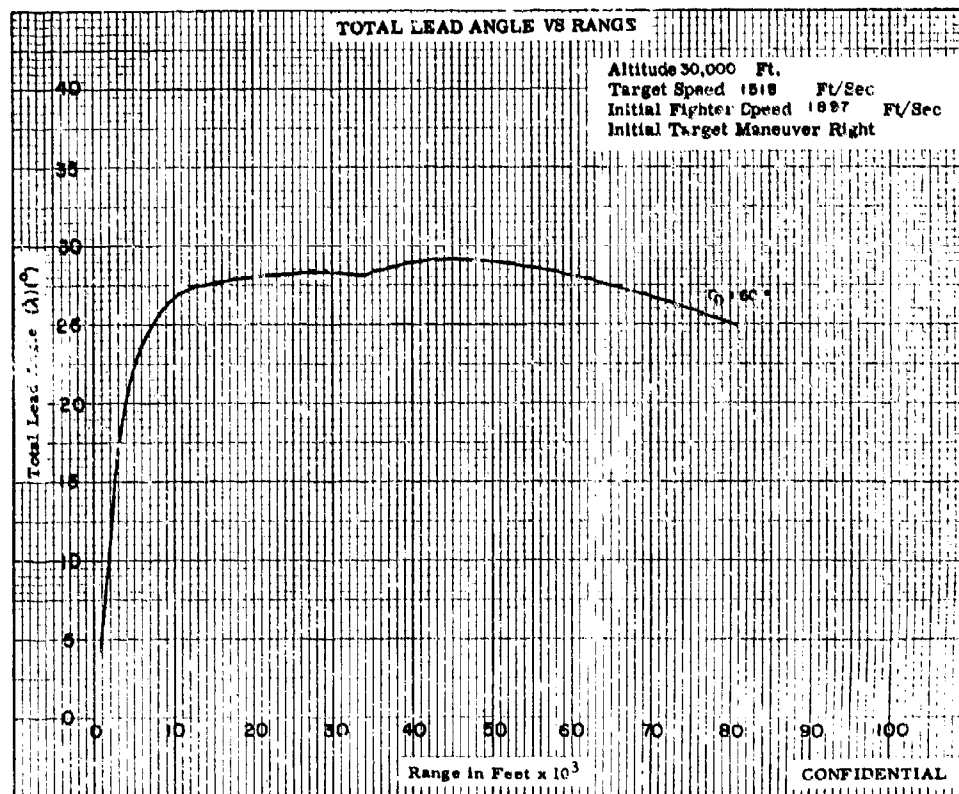
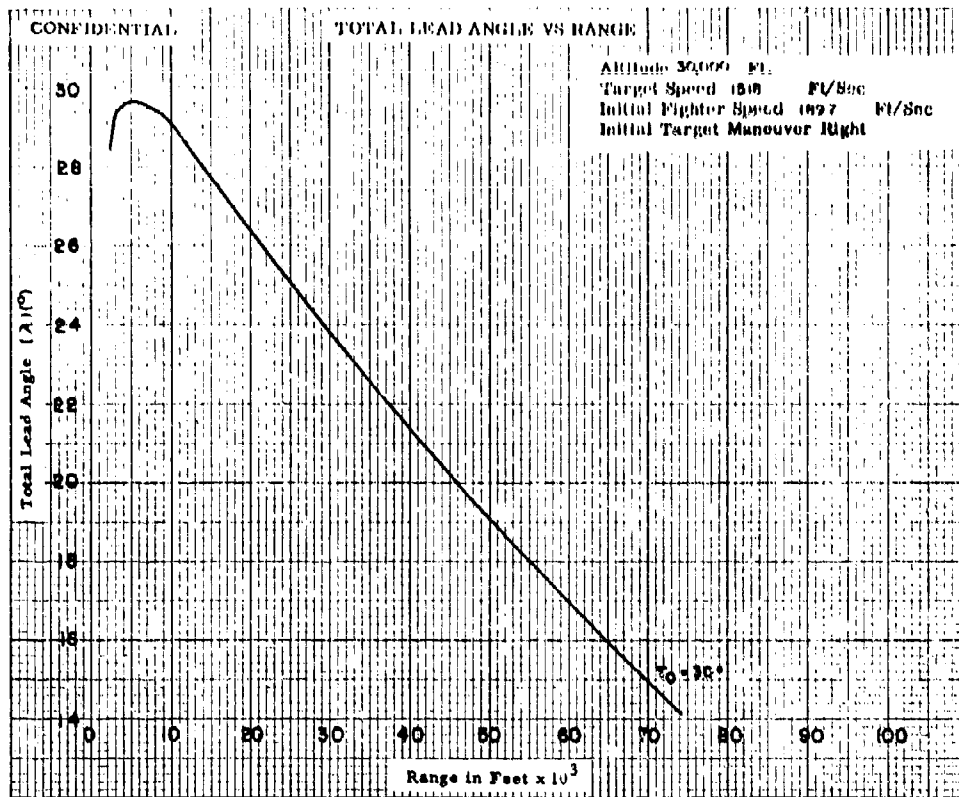


Fig. X-6a

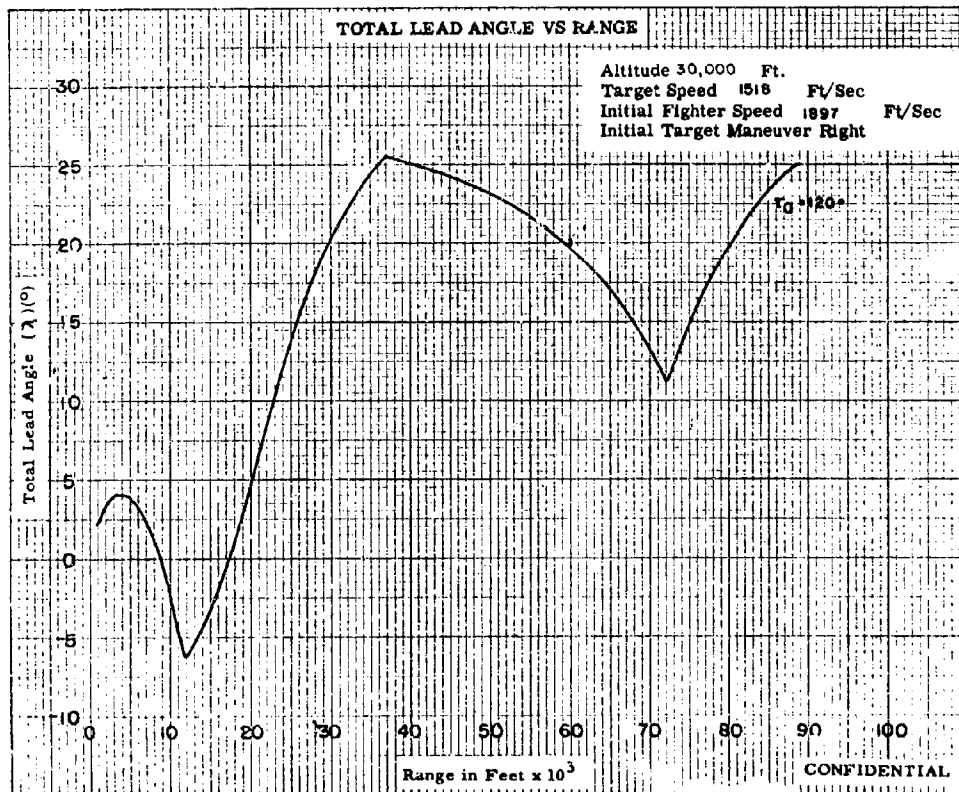
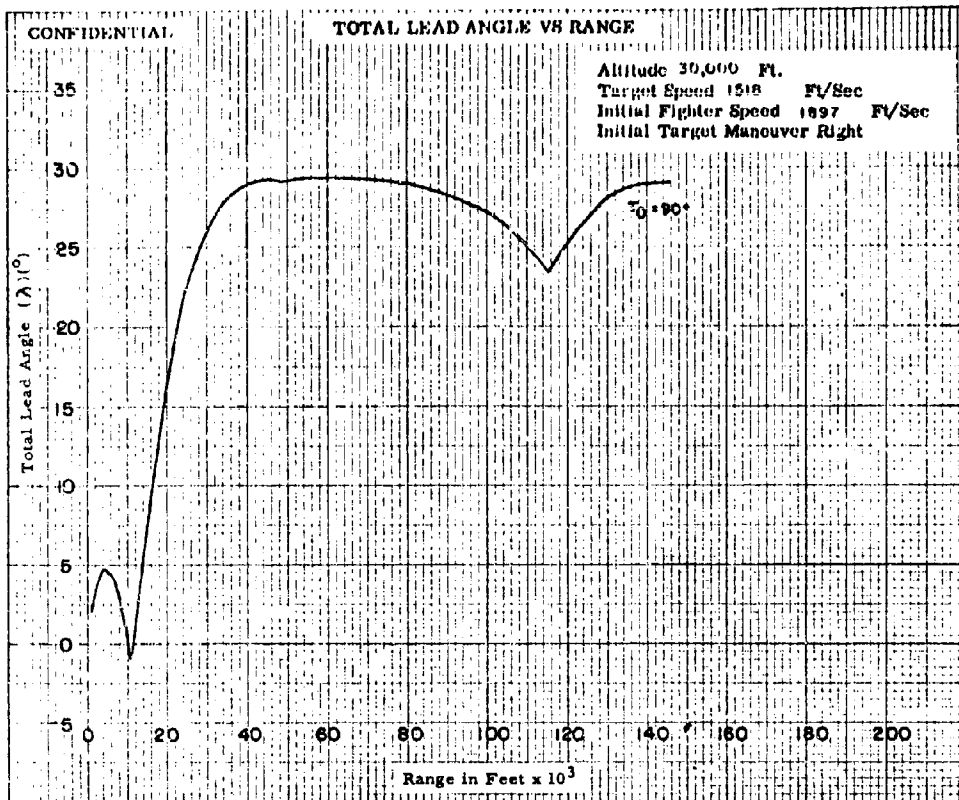


Fig. X-6b

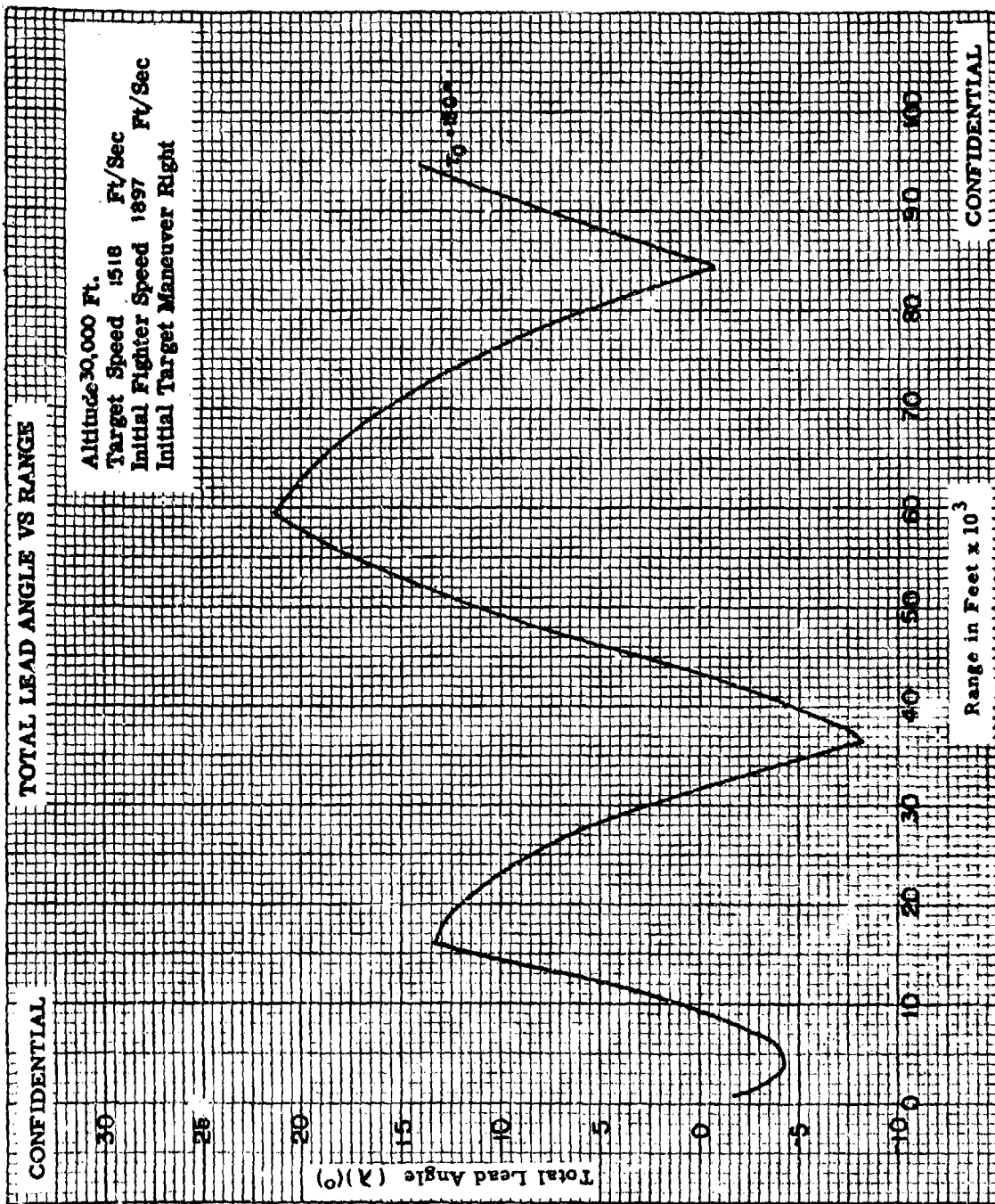


Fig. X-6c

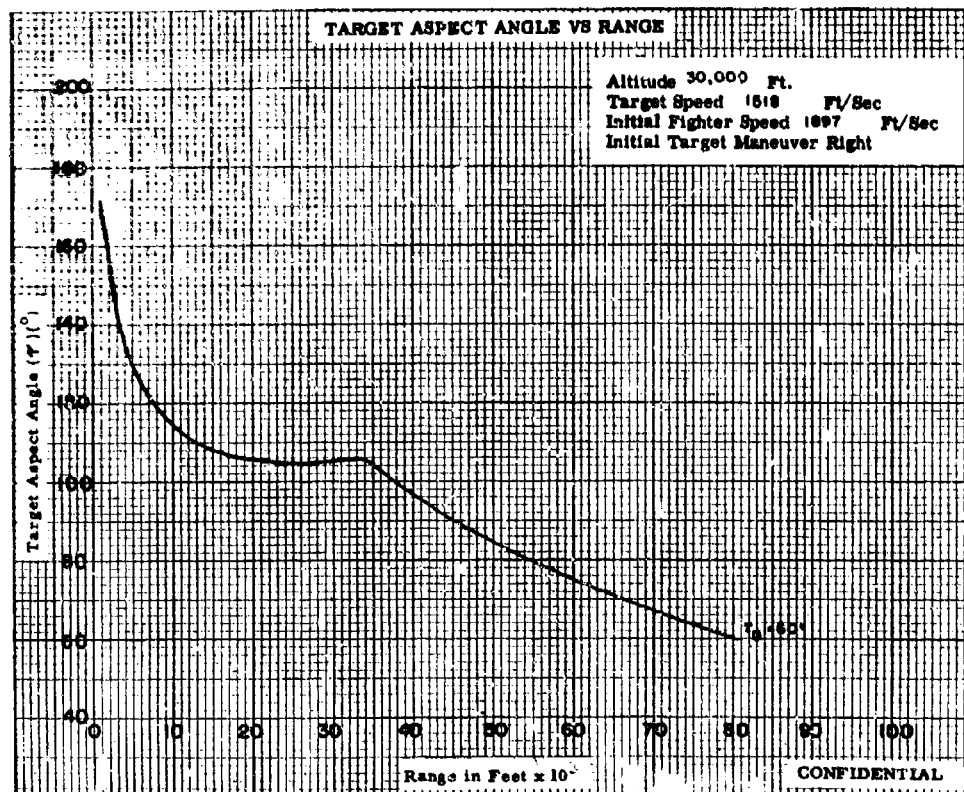
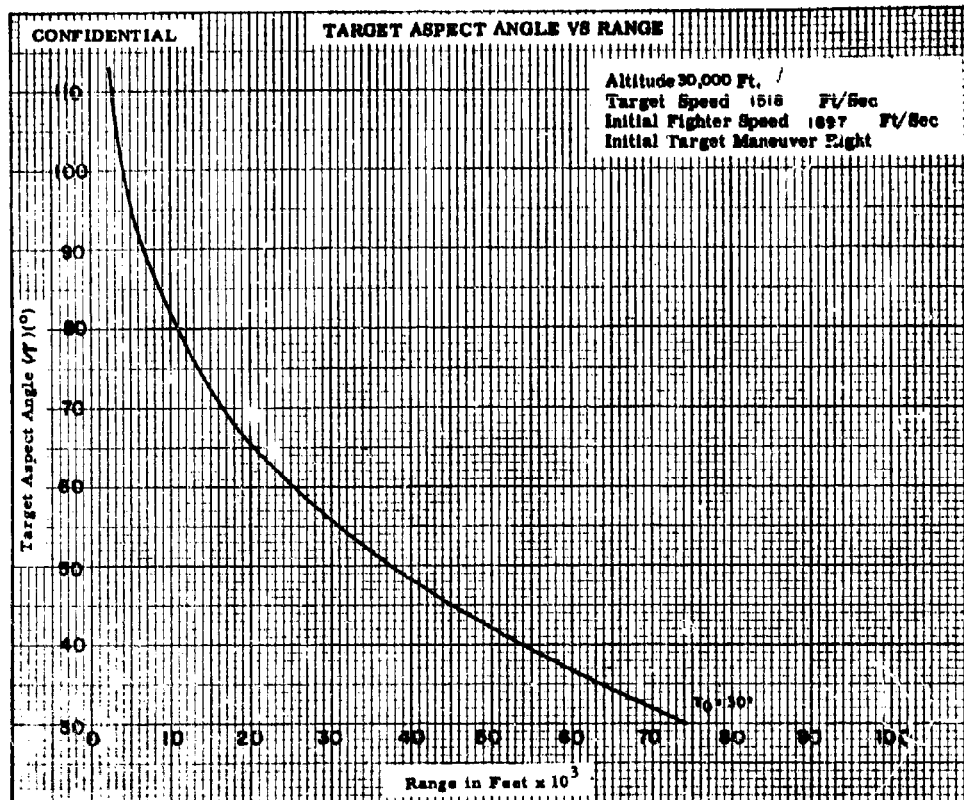


Fig. X-7a

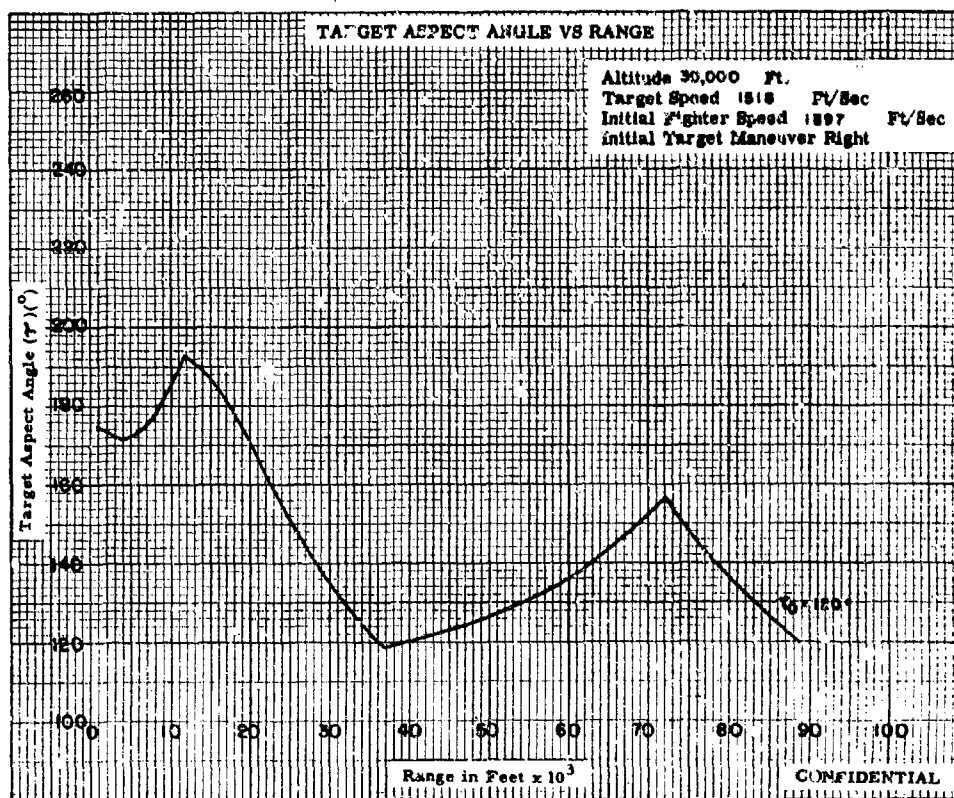
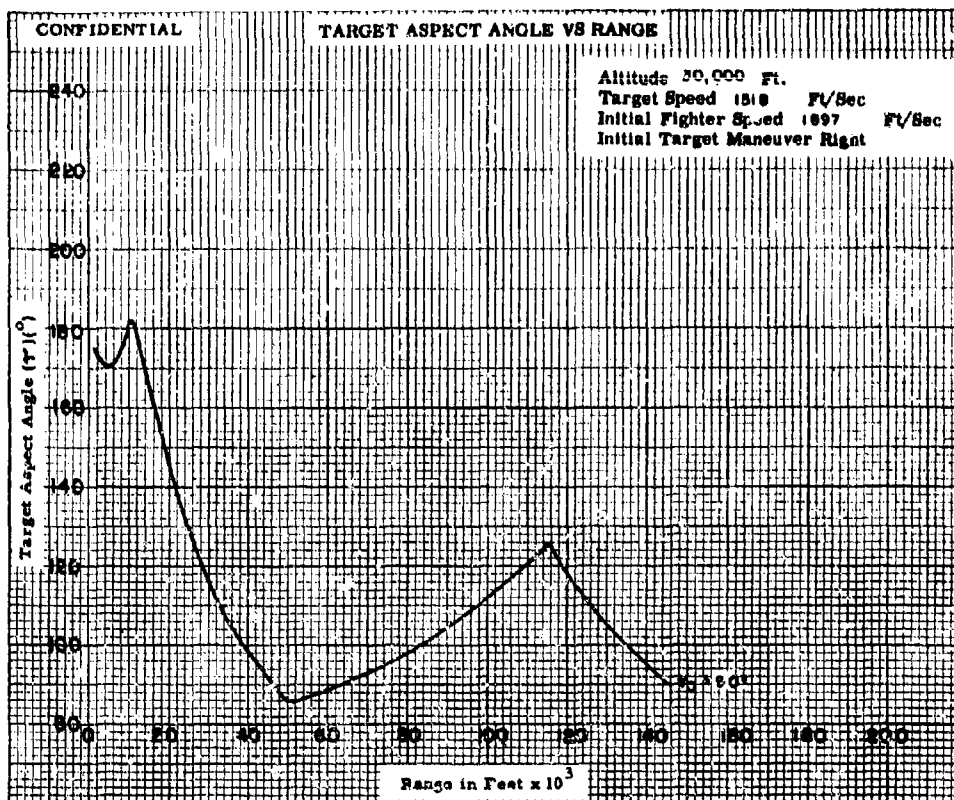


Fig. X-7b

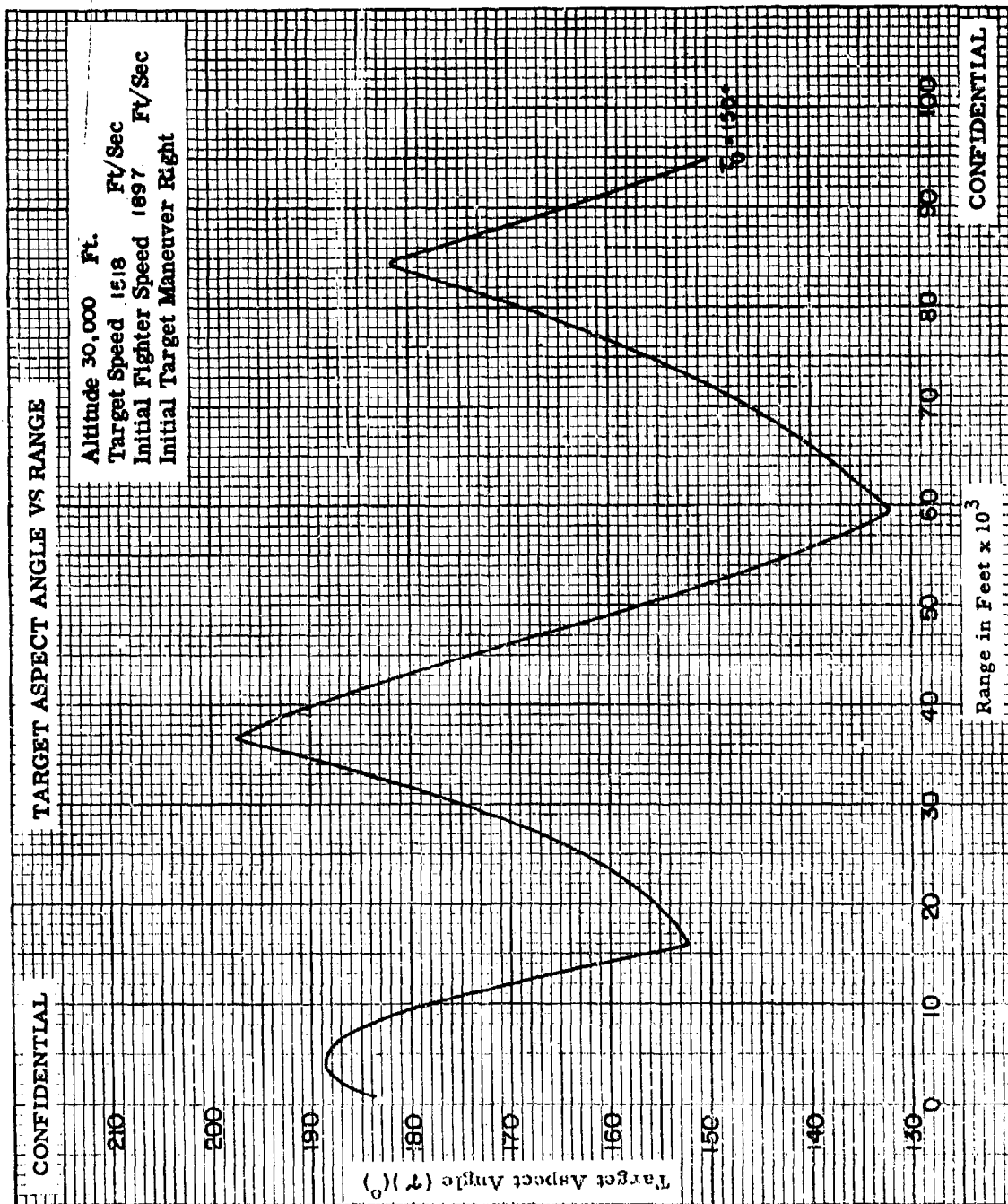


Fig. X-7c

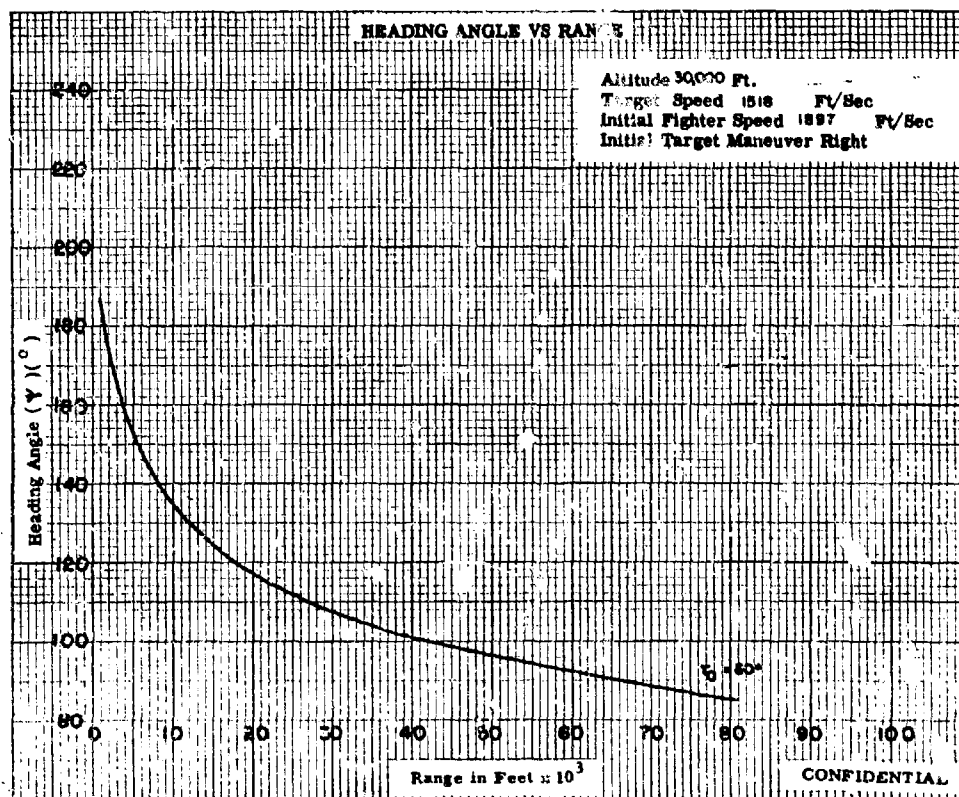
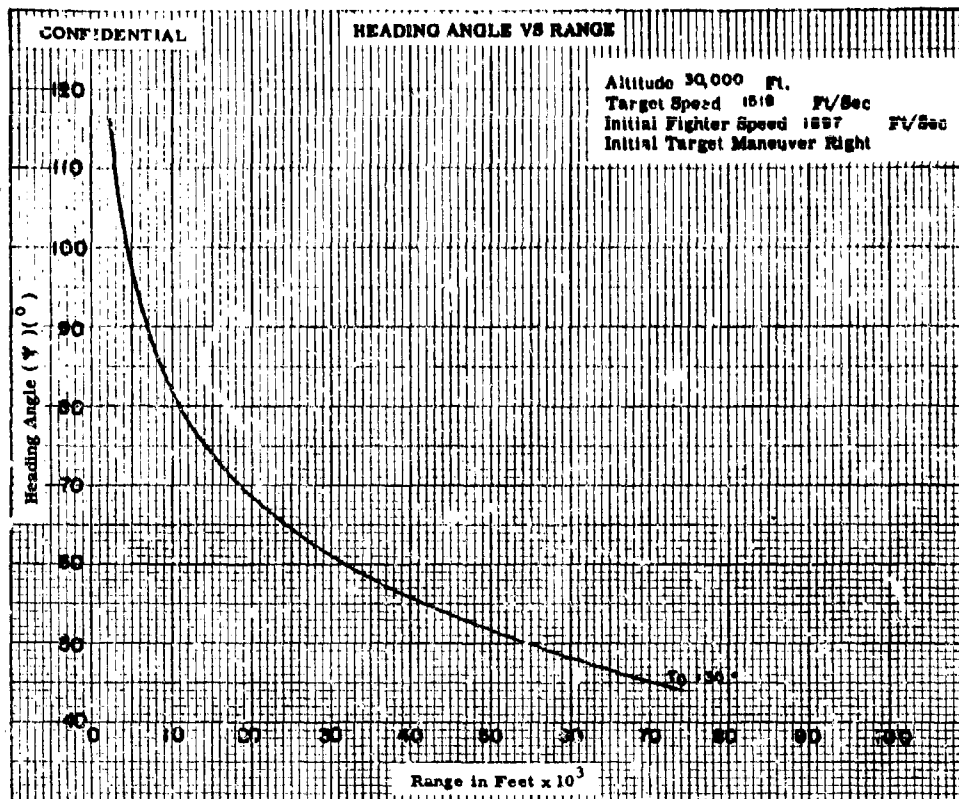


Fig. X-8a

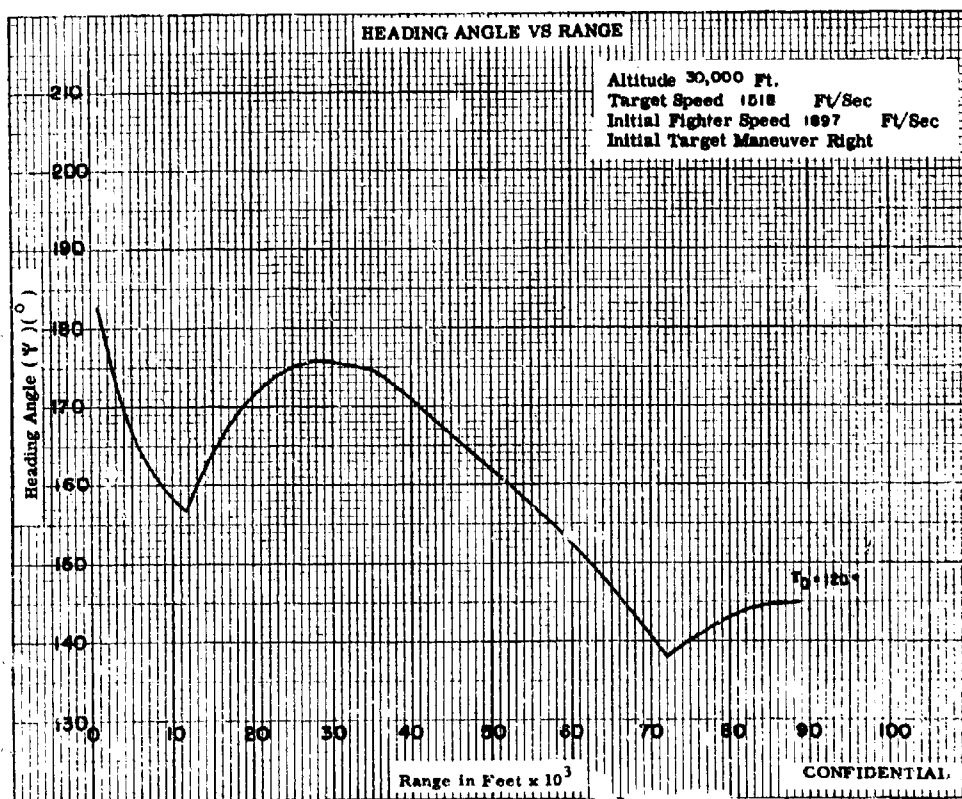
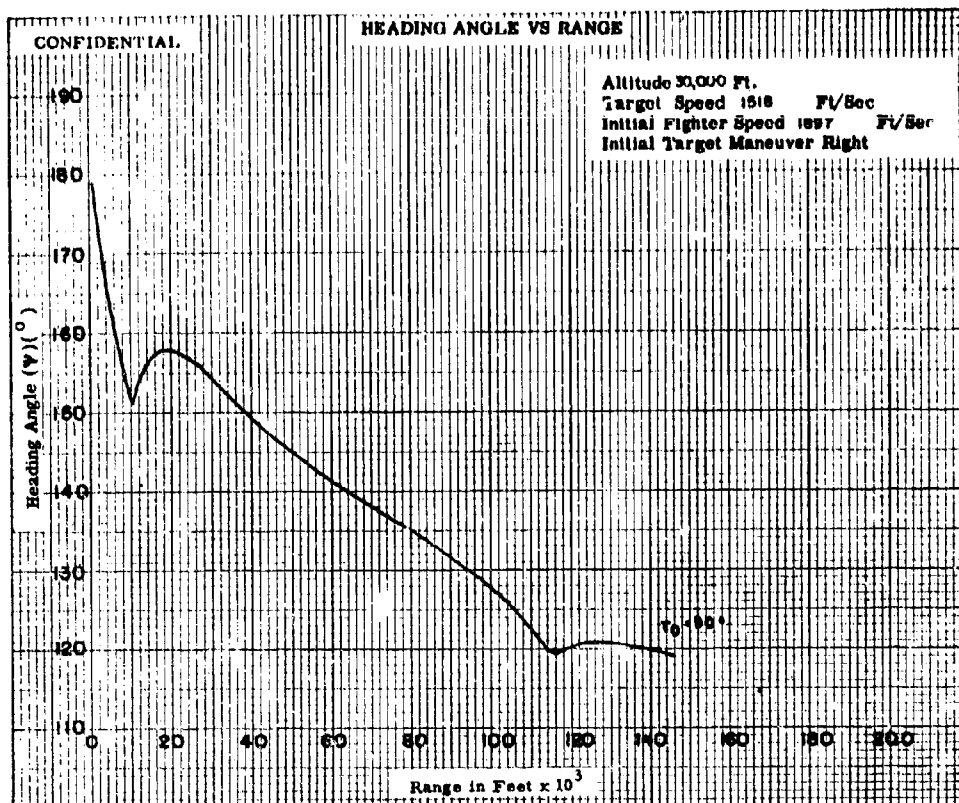


Fig. X-80

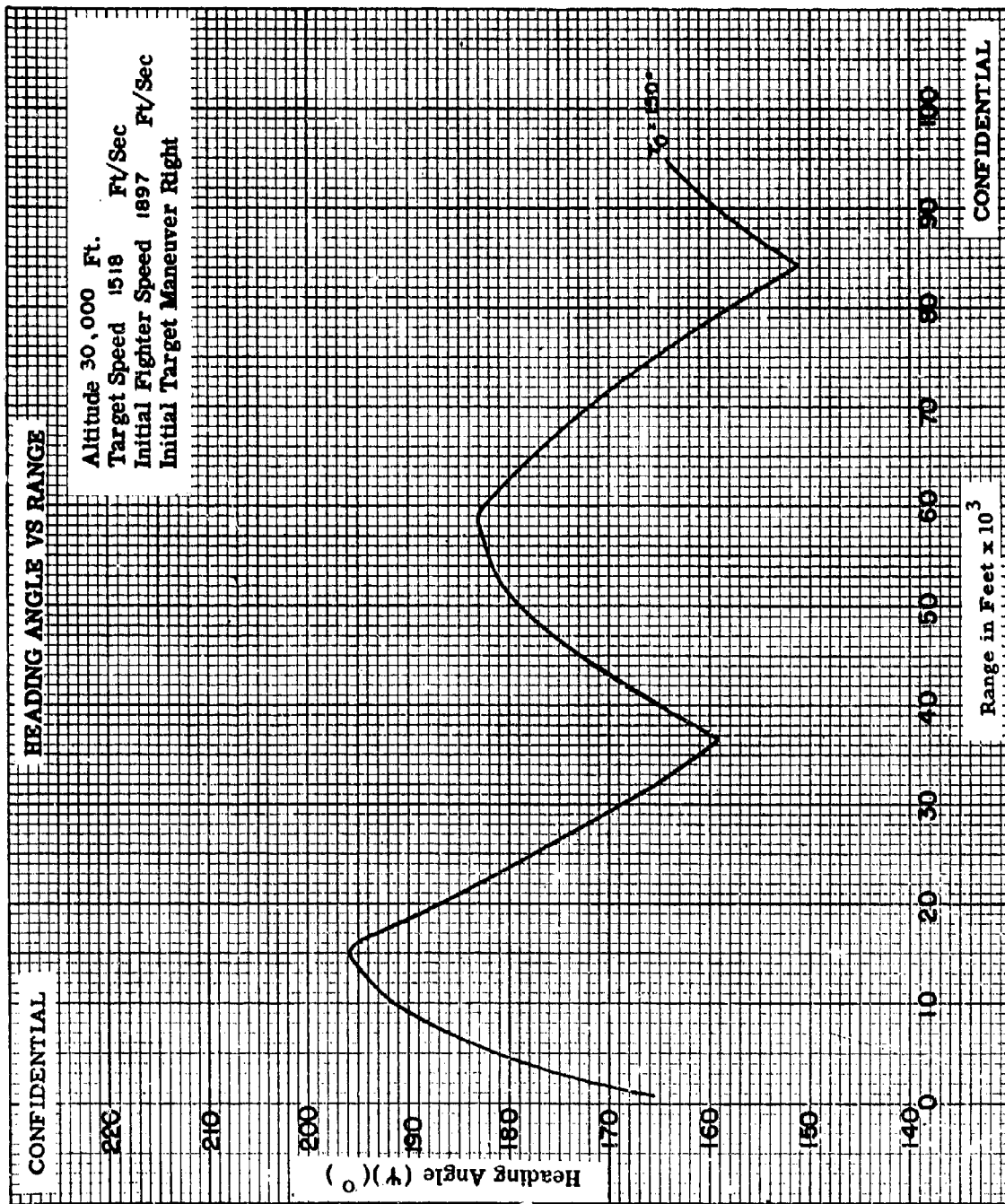


Fig. X-8c

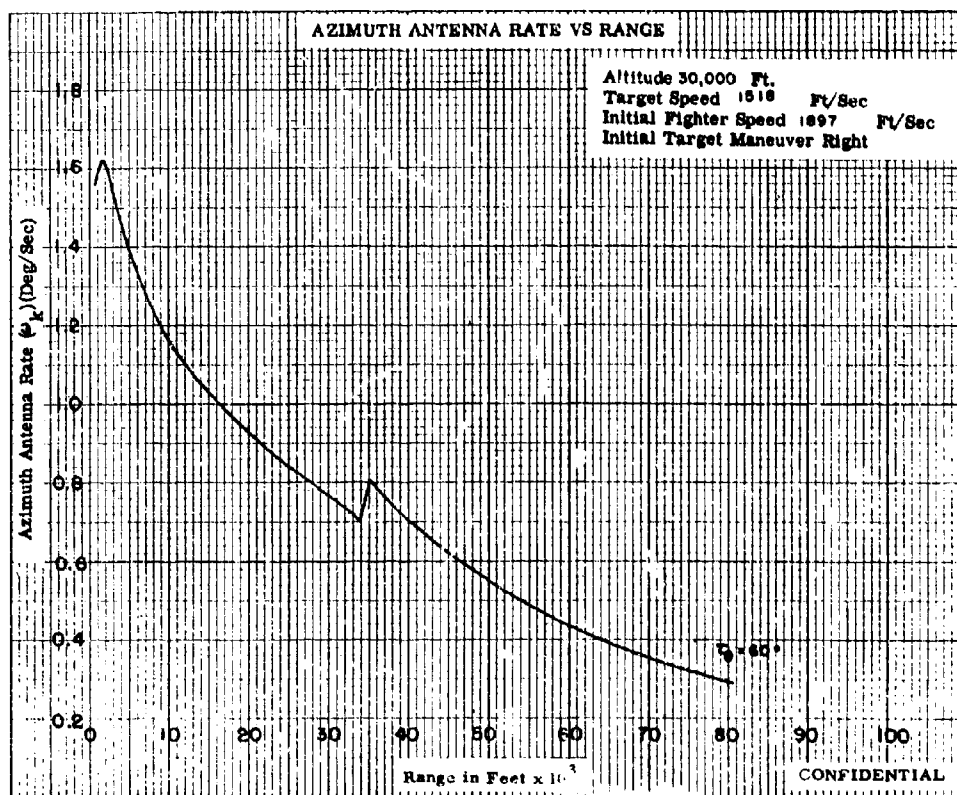
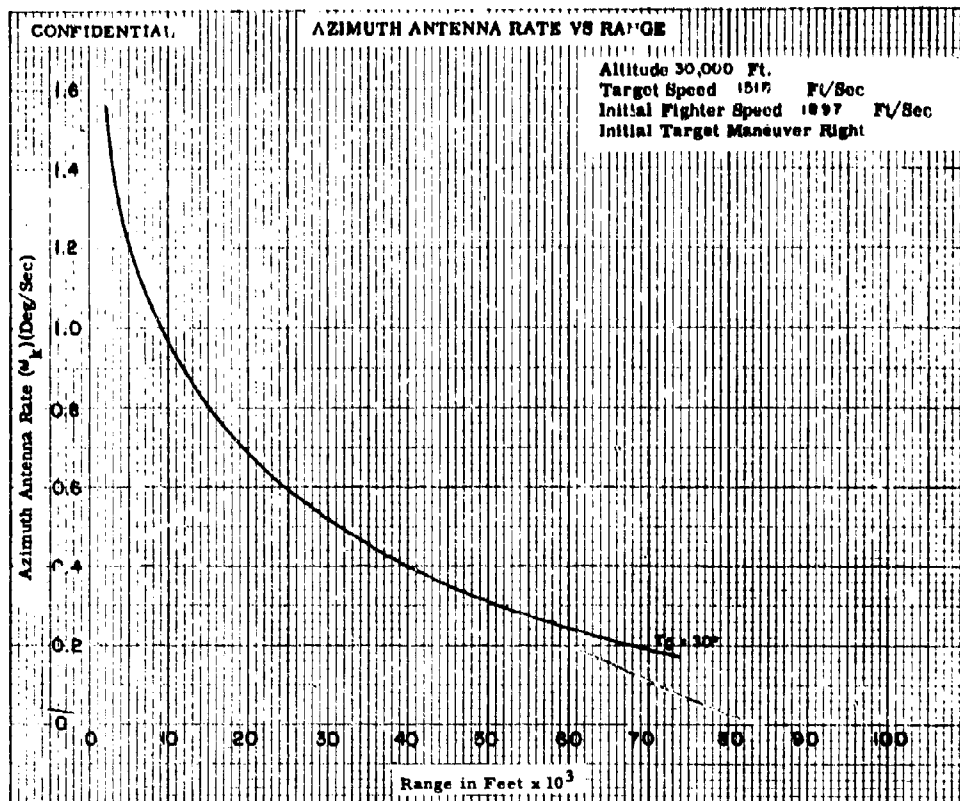


Fig. X-9a

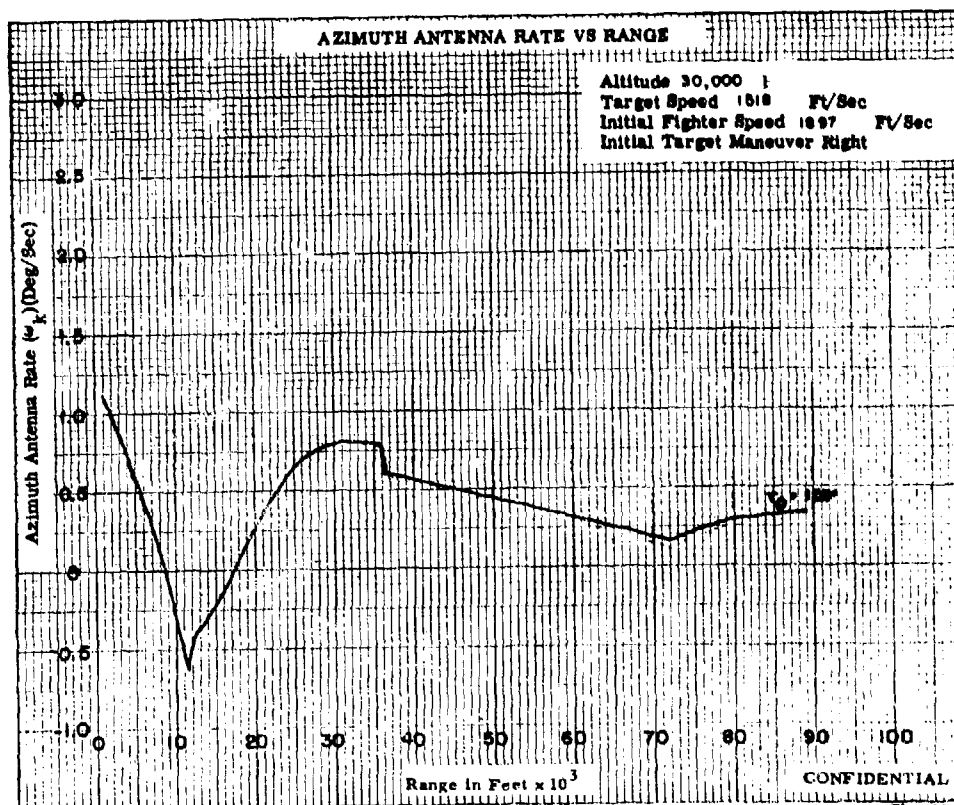
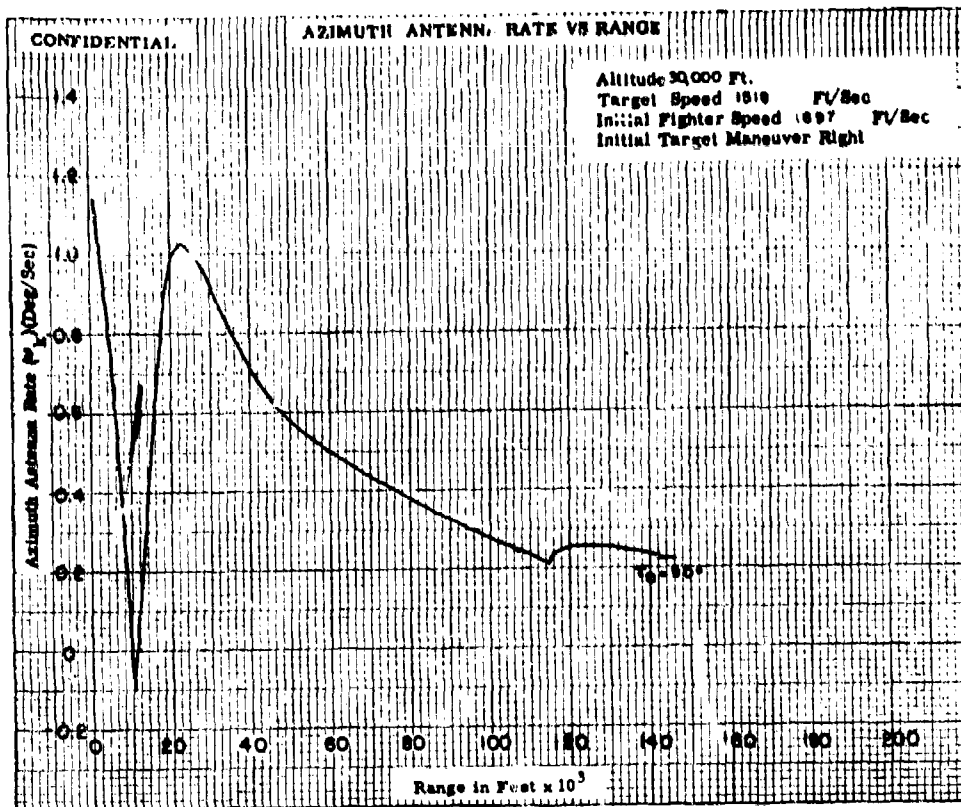


Fig. X-9b

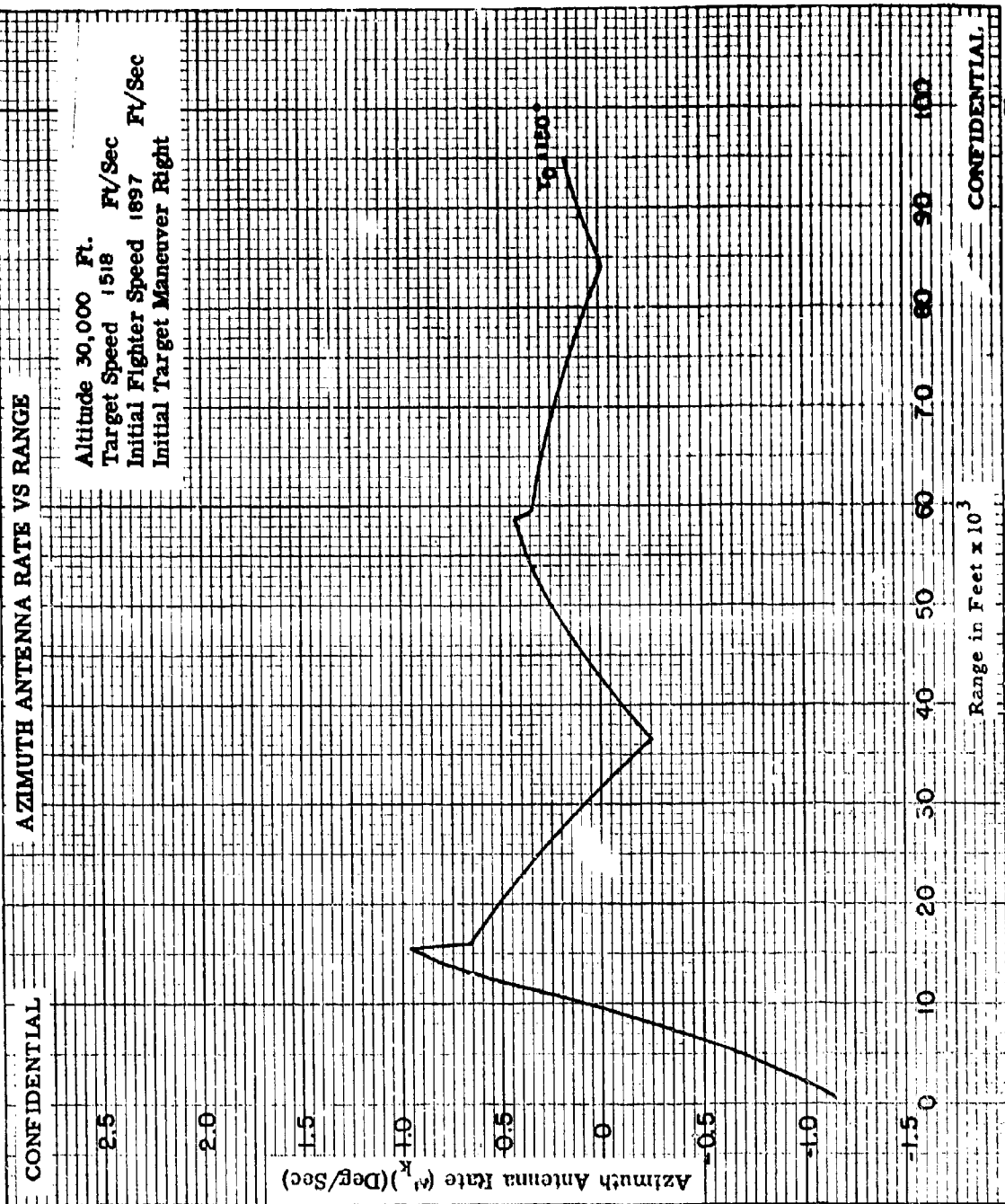


Fig. X-9c

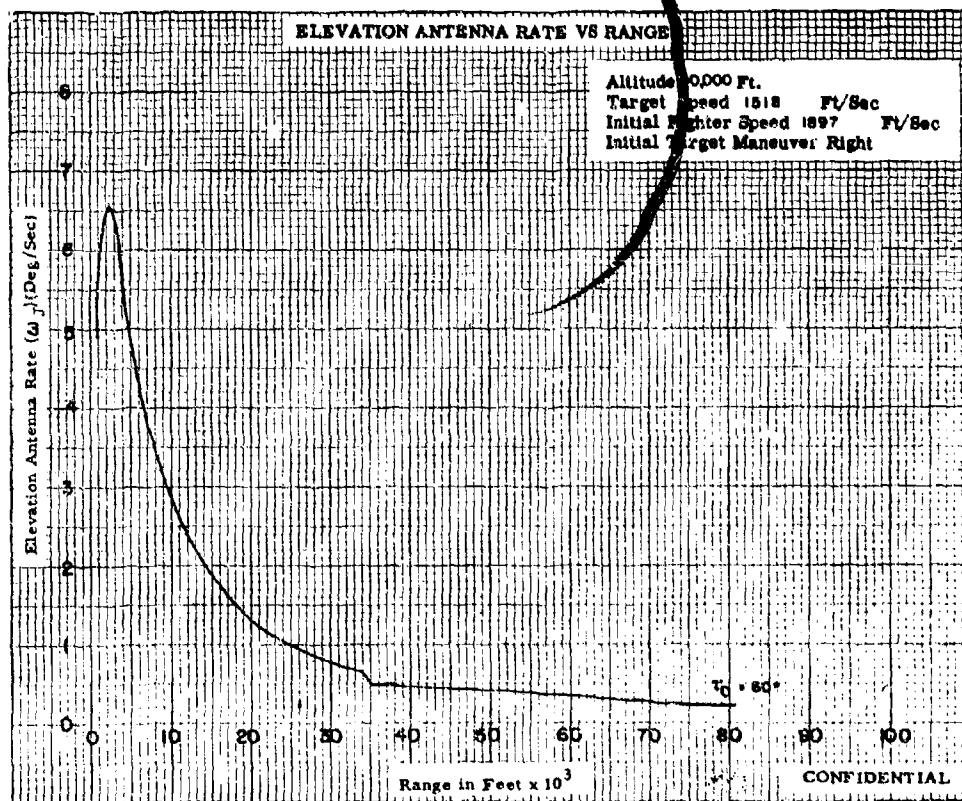
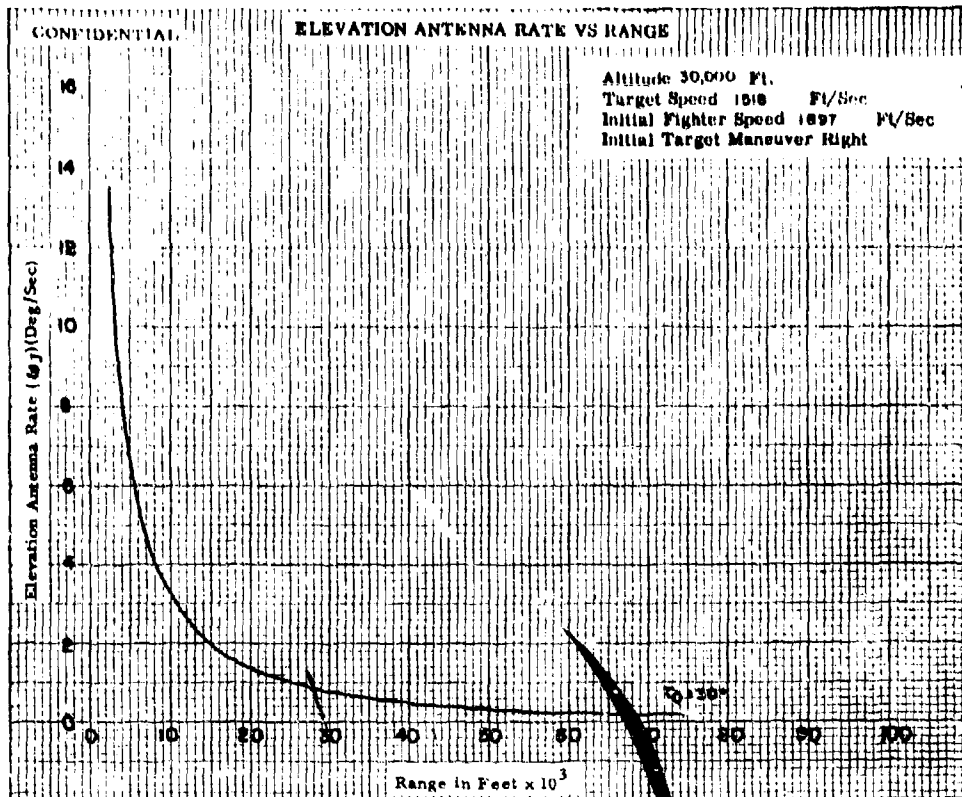


Fig. X-10a

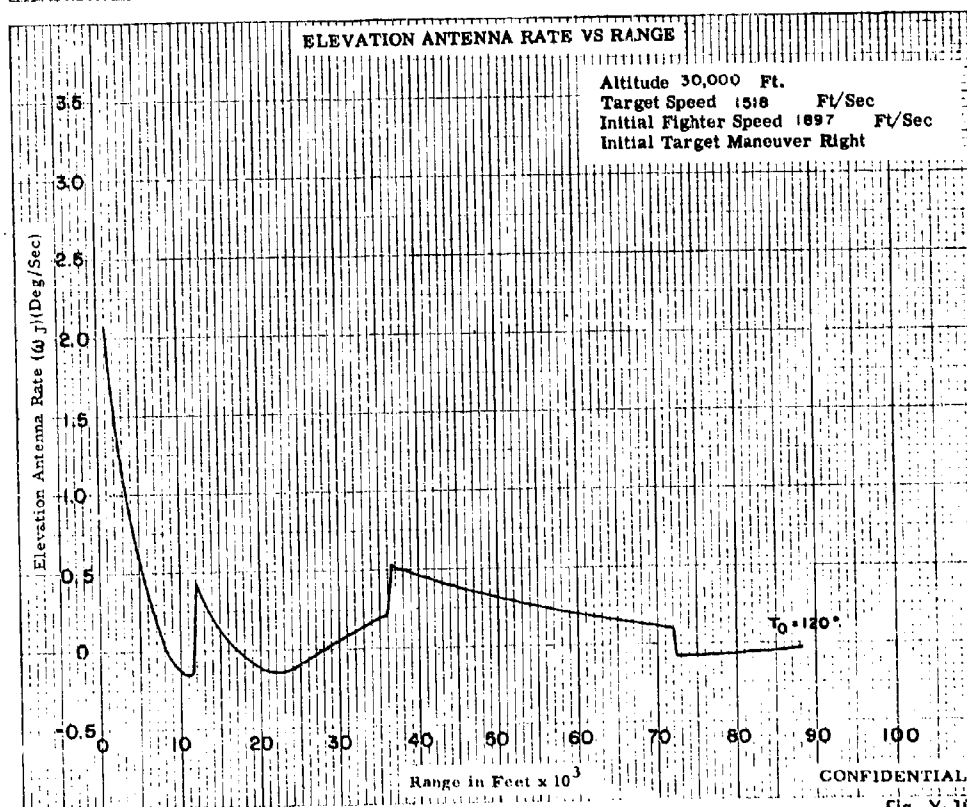
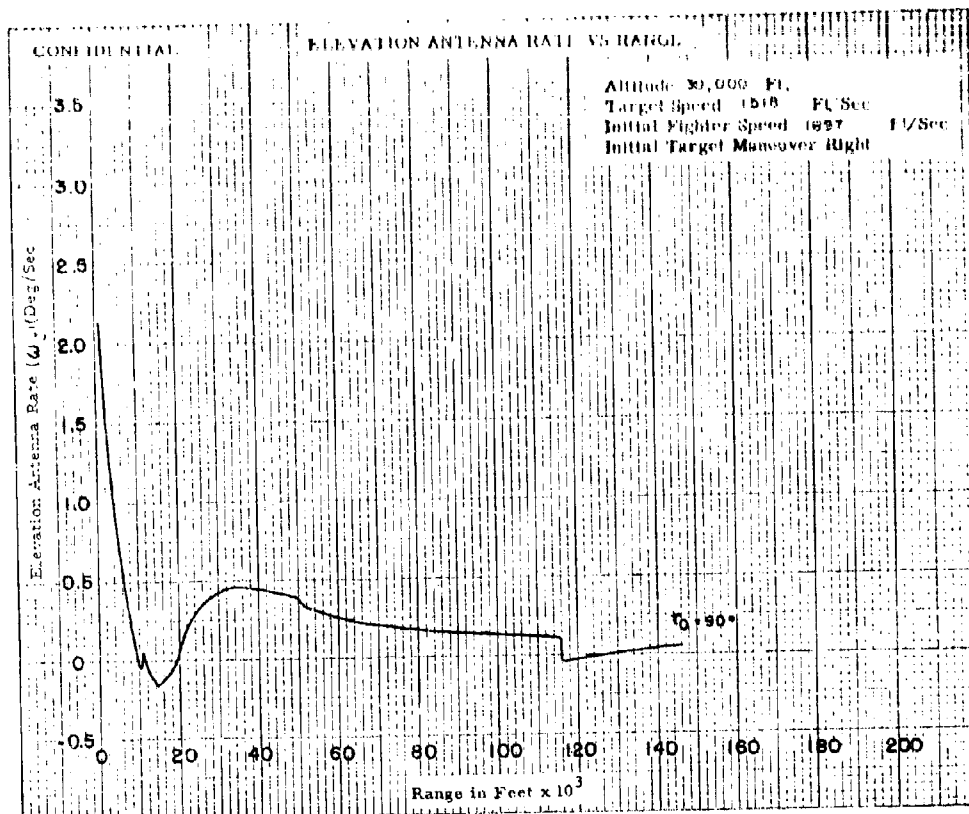


Fig. X-10b

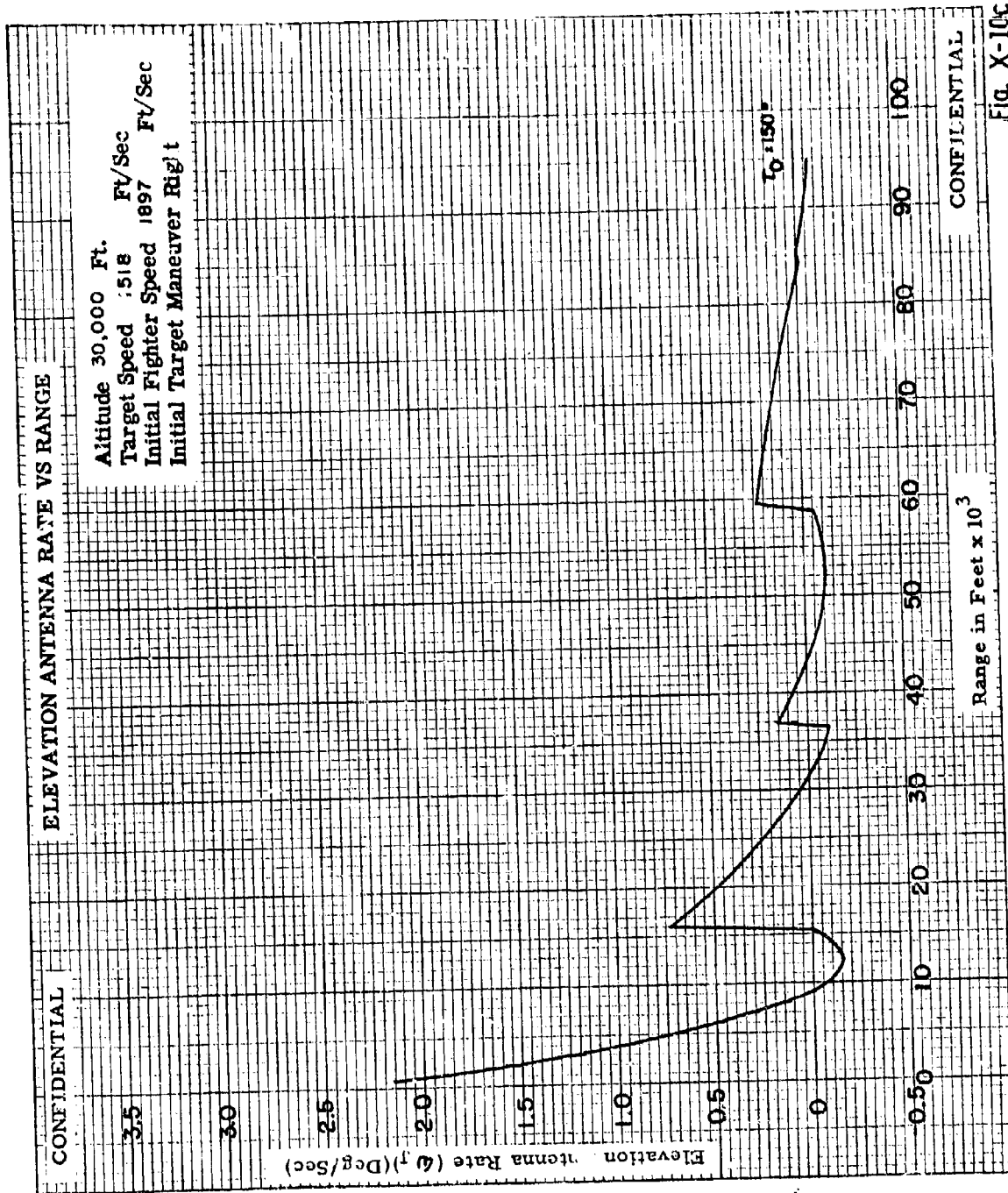


Fig. X-10c

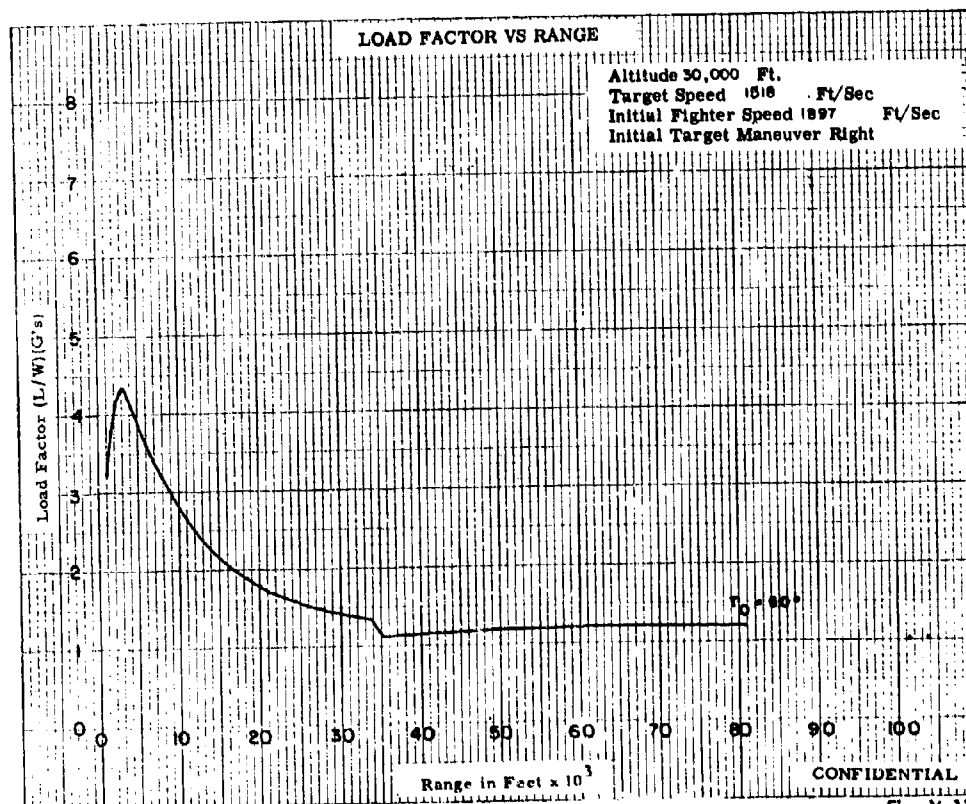
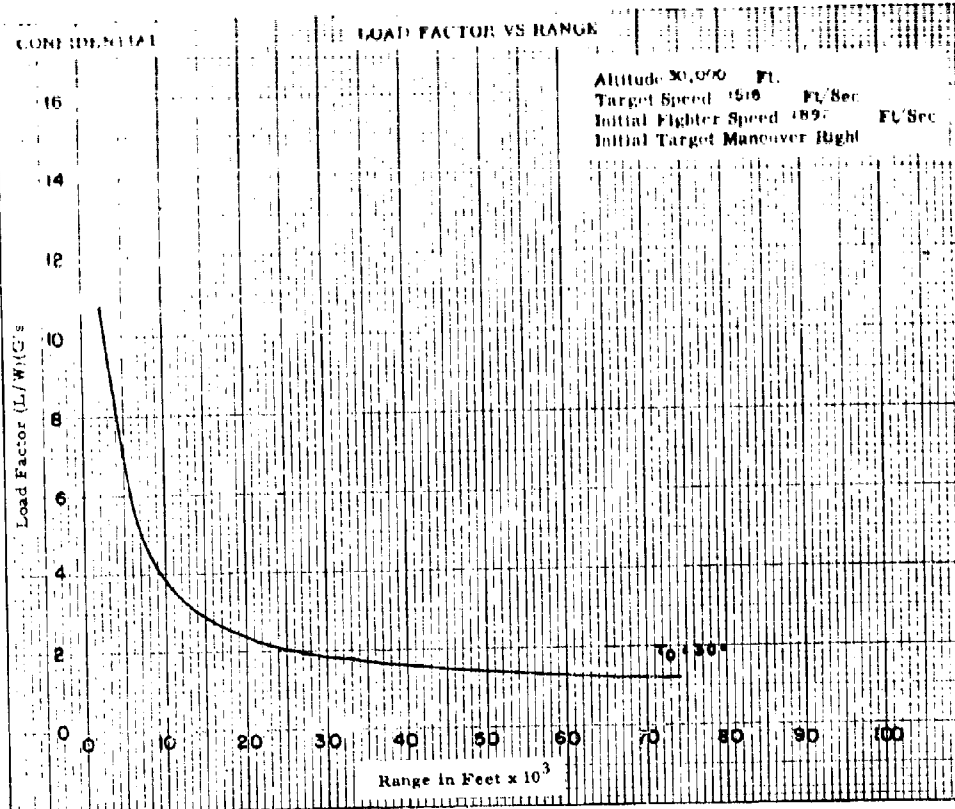


Fig. X-11a

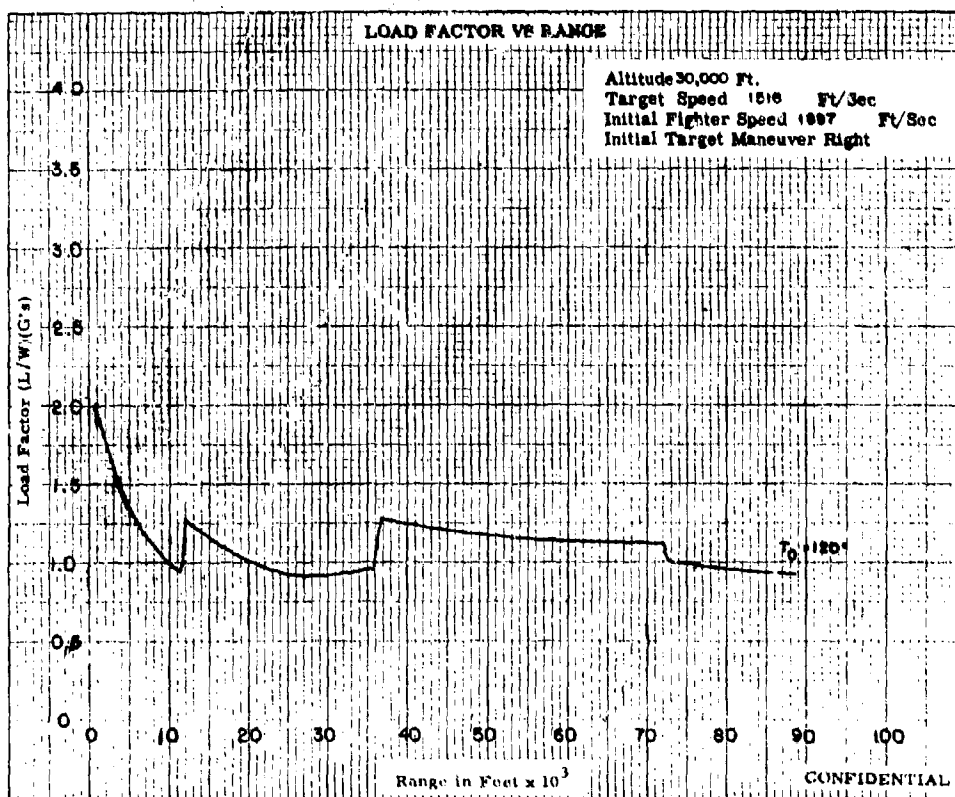
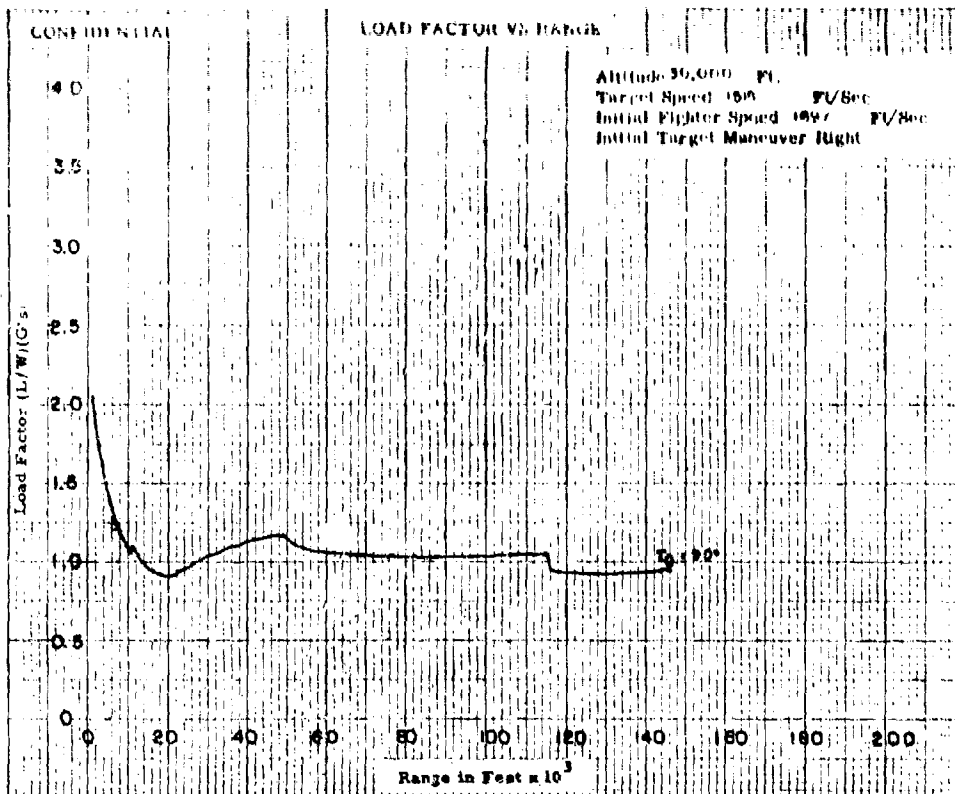


Fig. X-11b

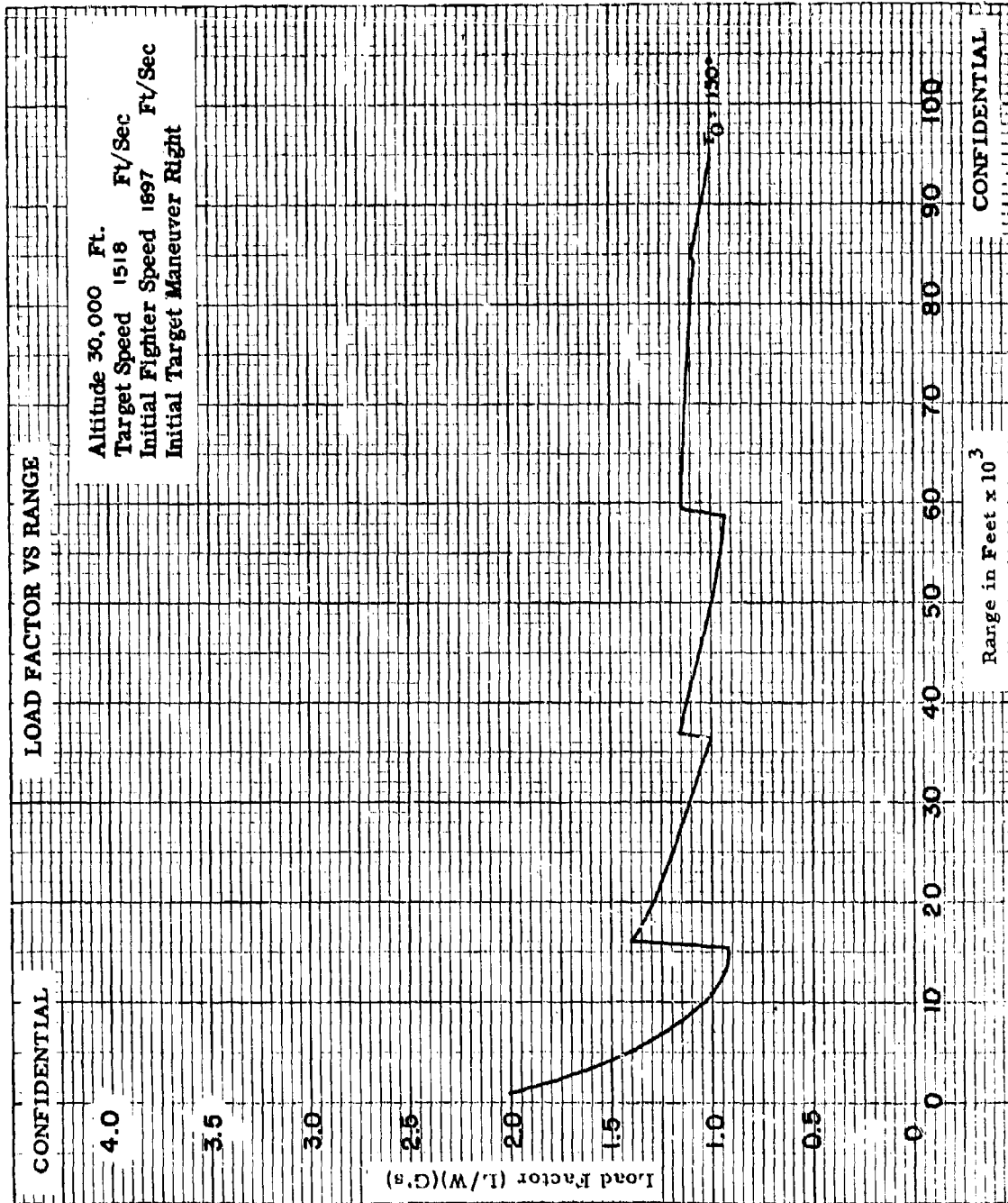


Fig X-11c

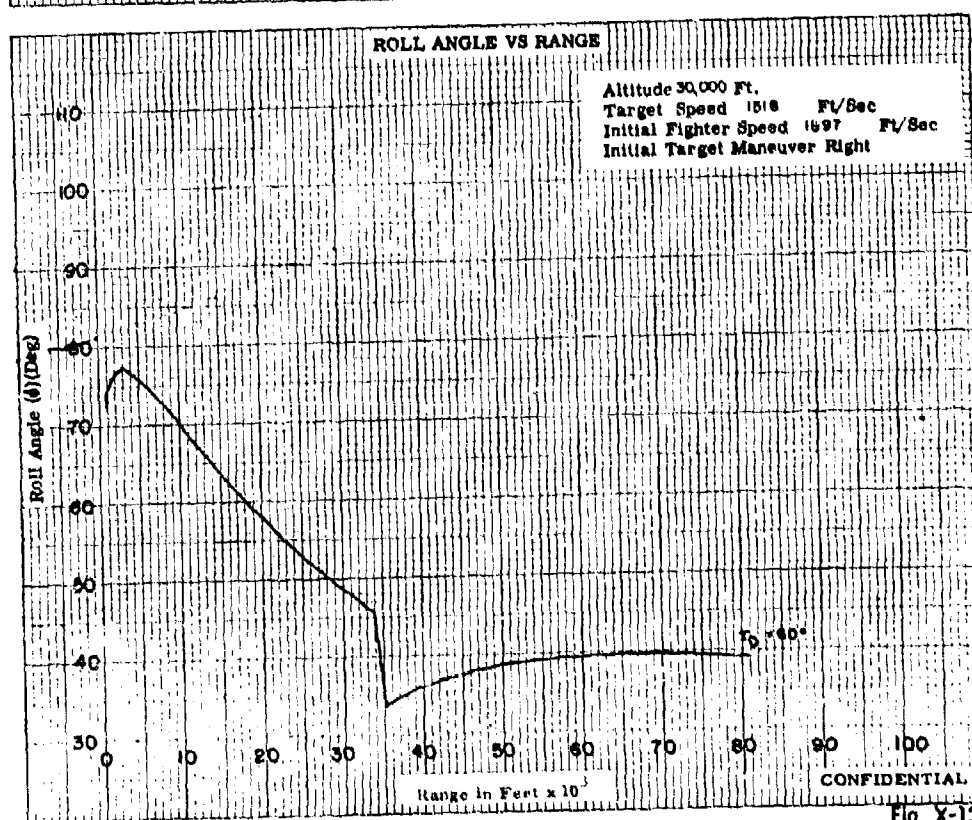
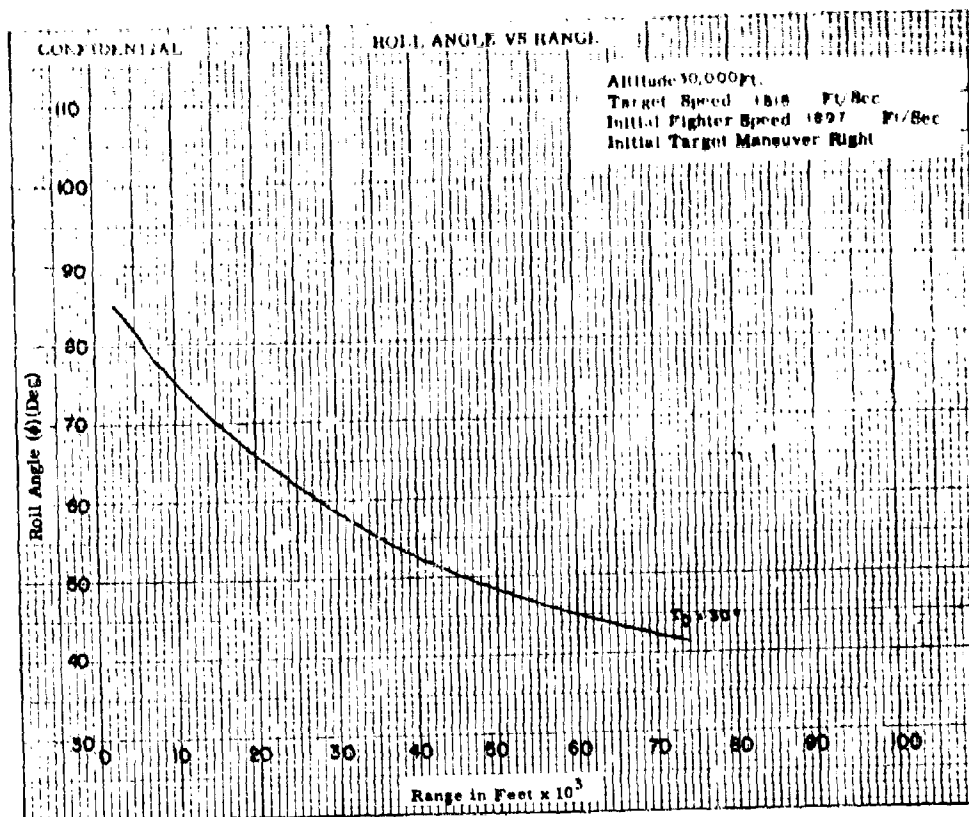


Fig. X-12a

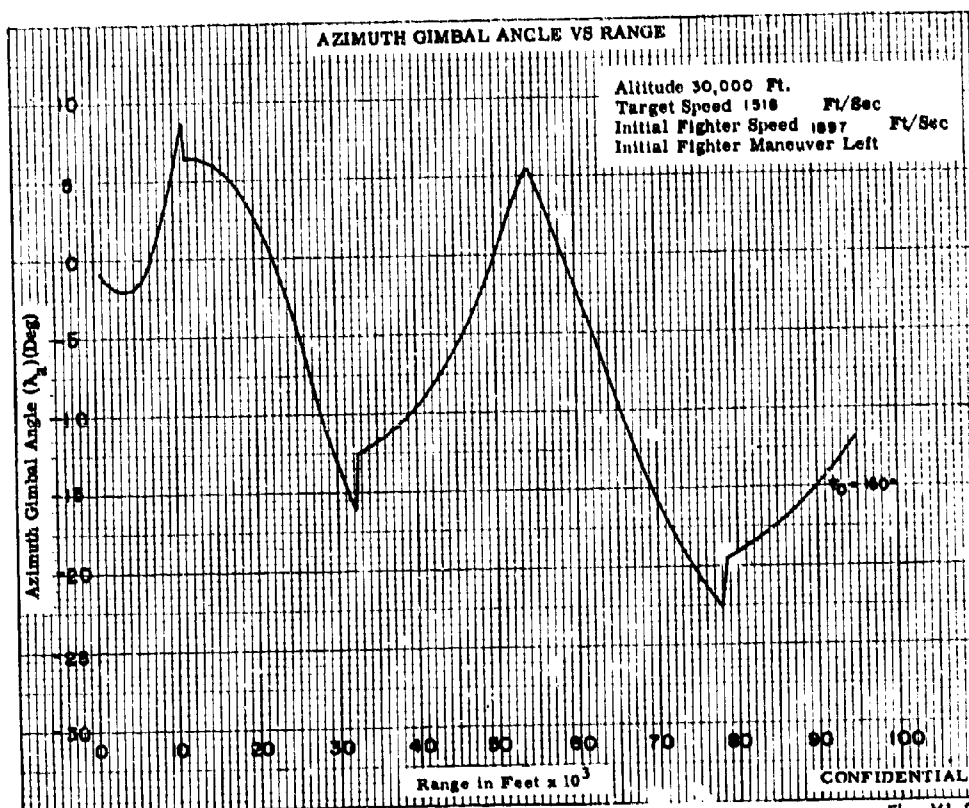
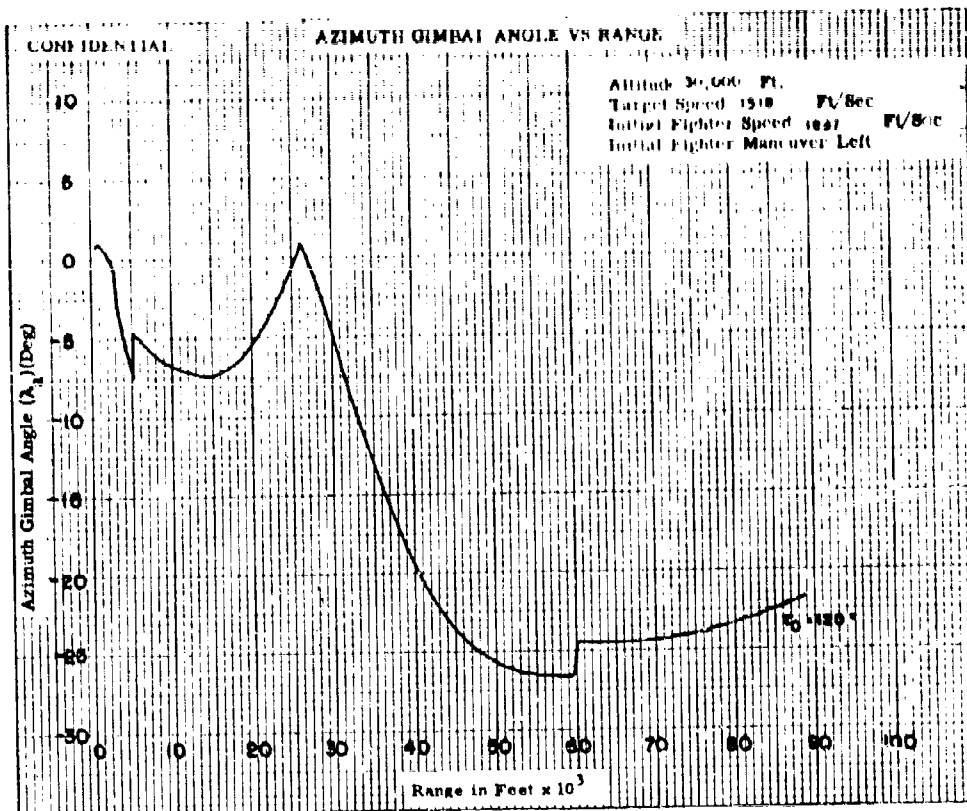


Fig. XI-2c

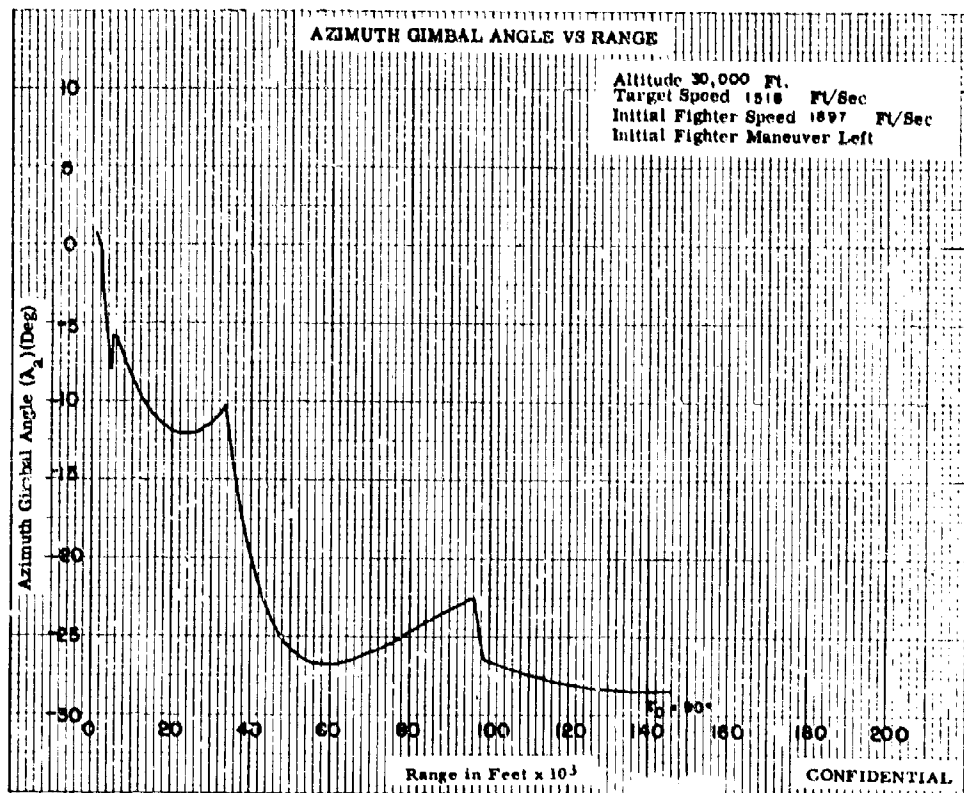
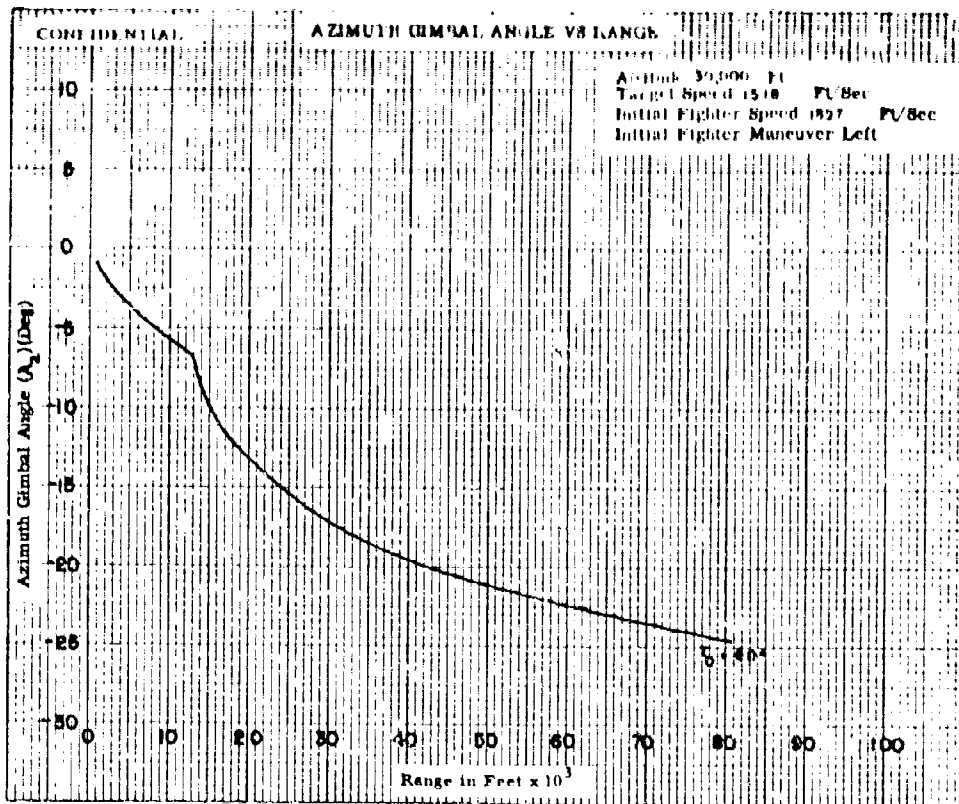


Fig. XI-2b

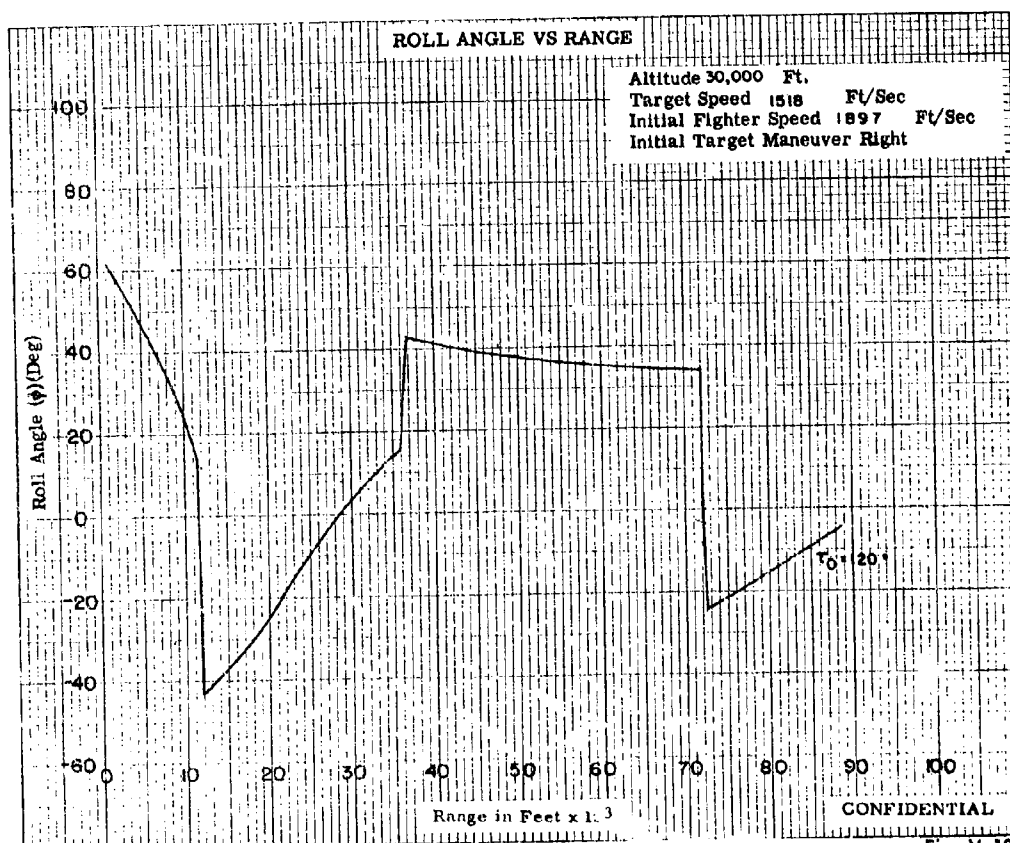
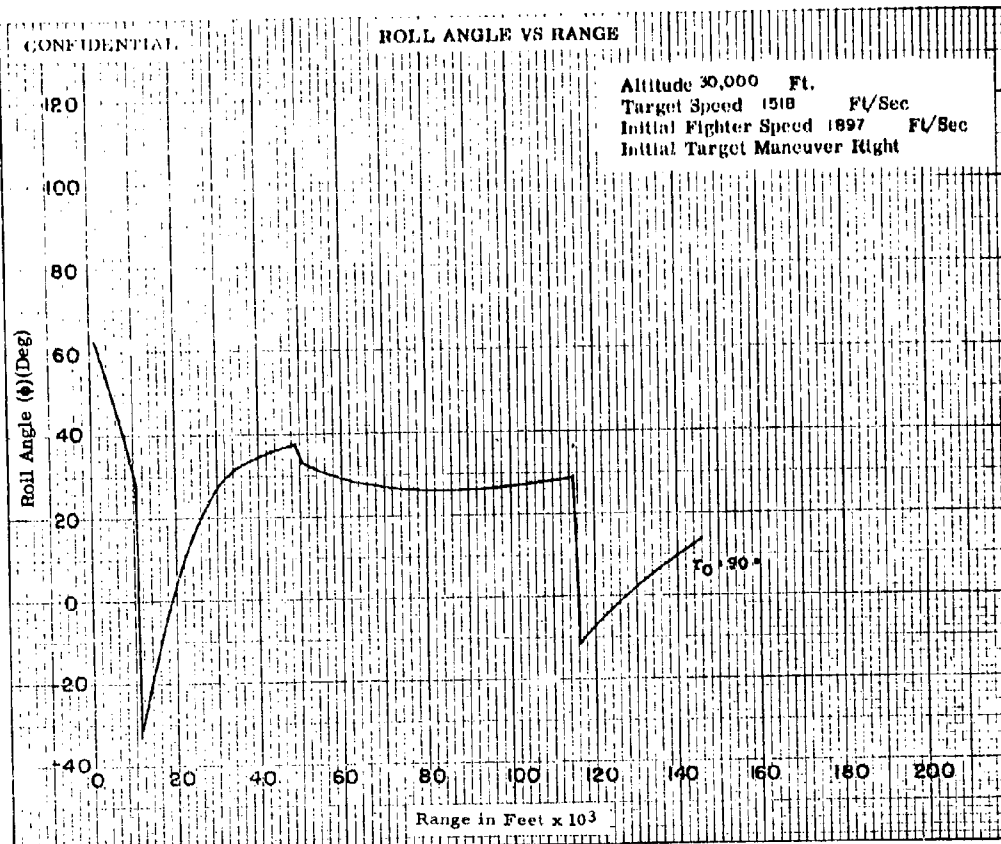


Fig. X-12b

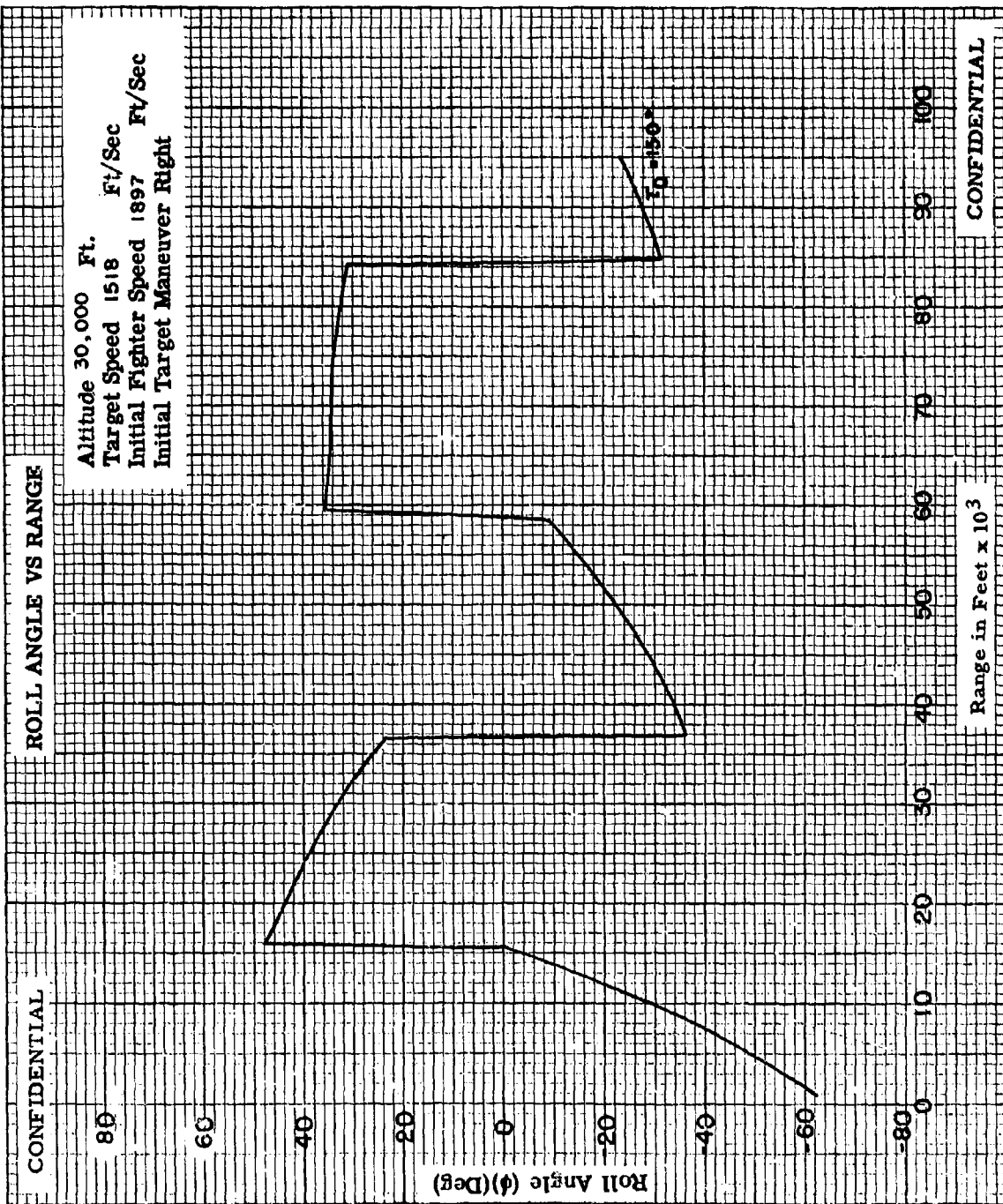


Fig. X-12c

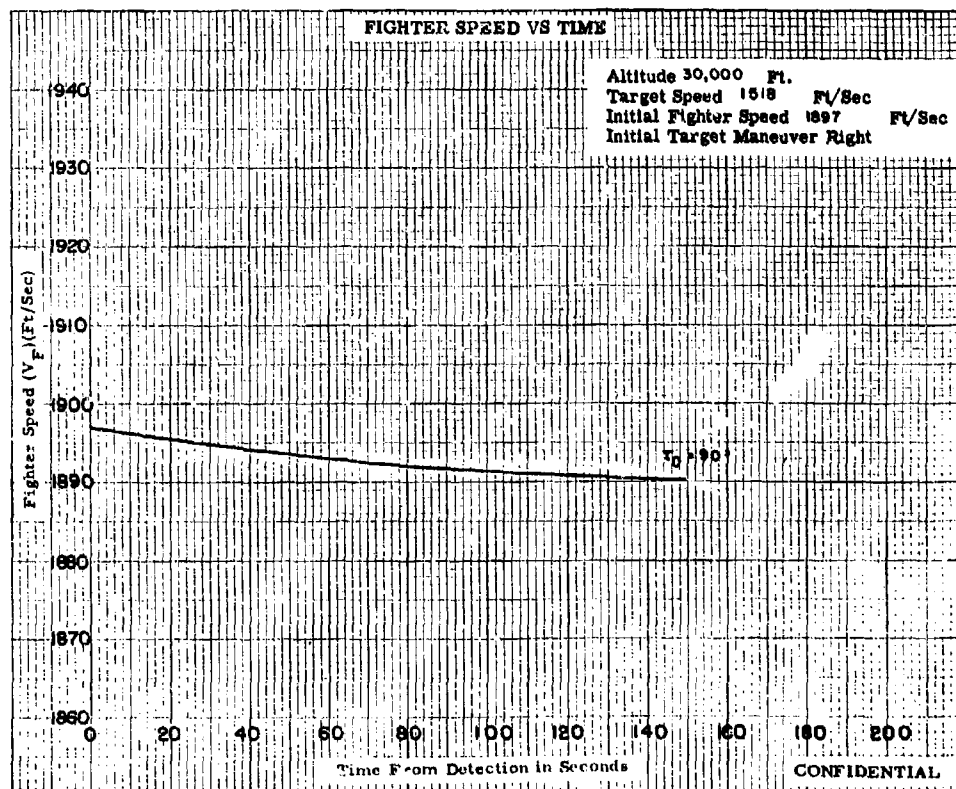
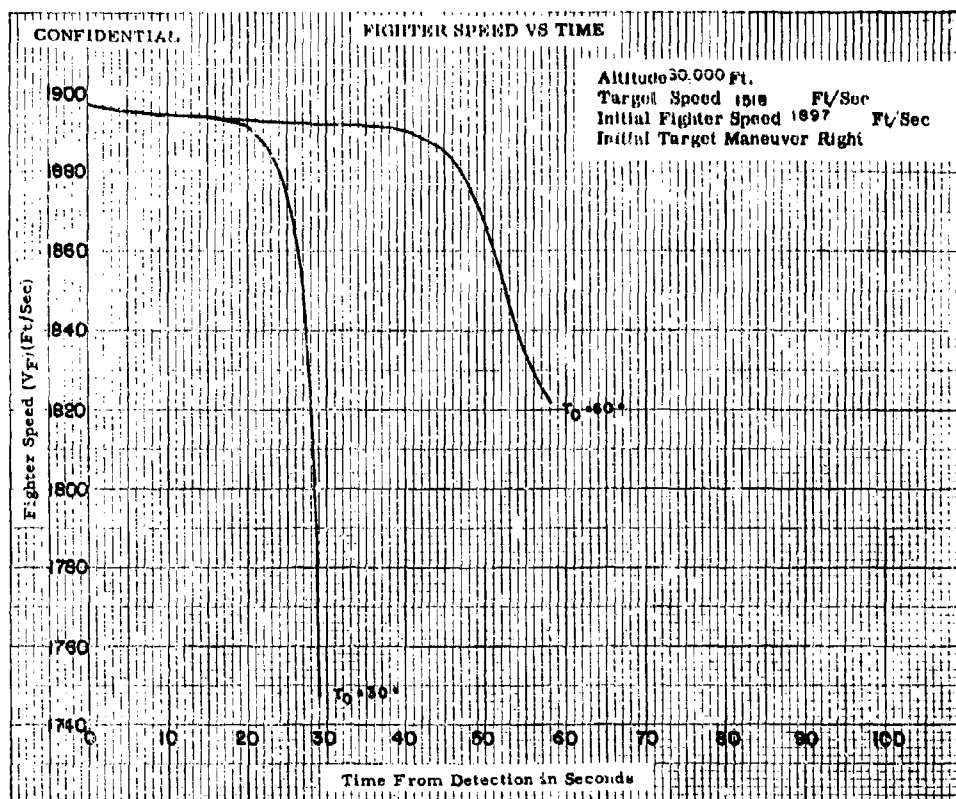


Fig. X-13a

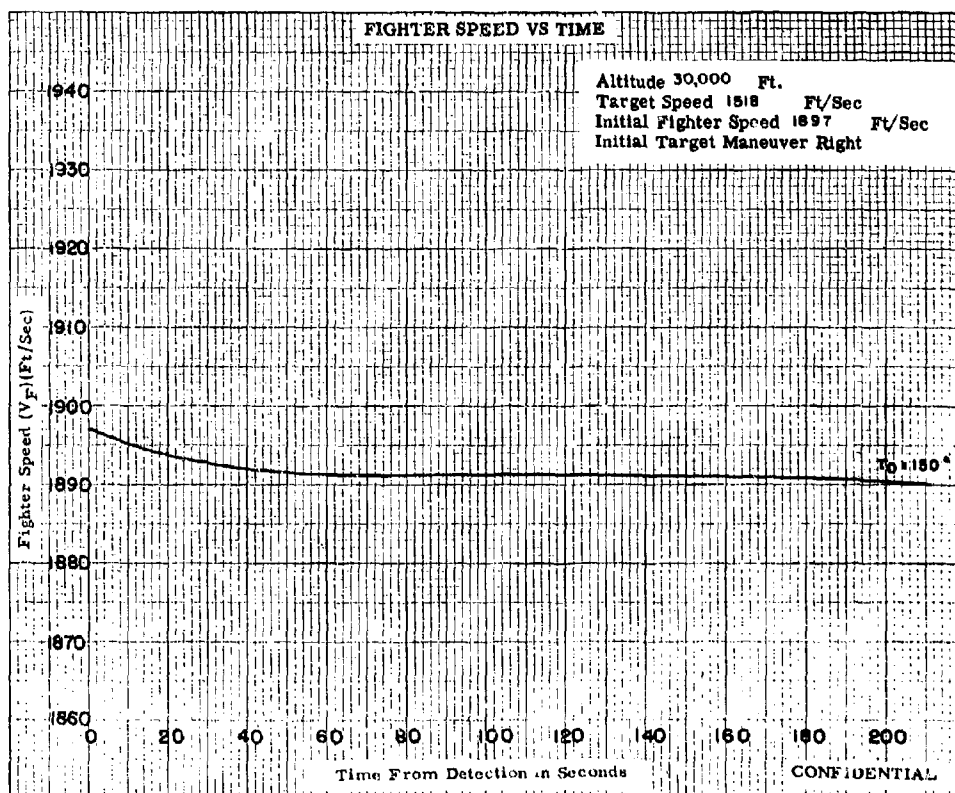
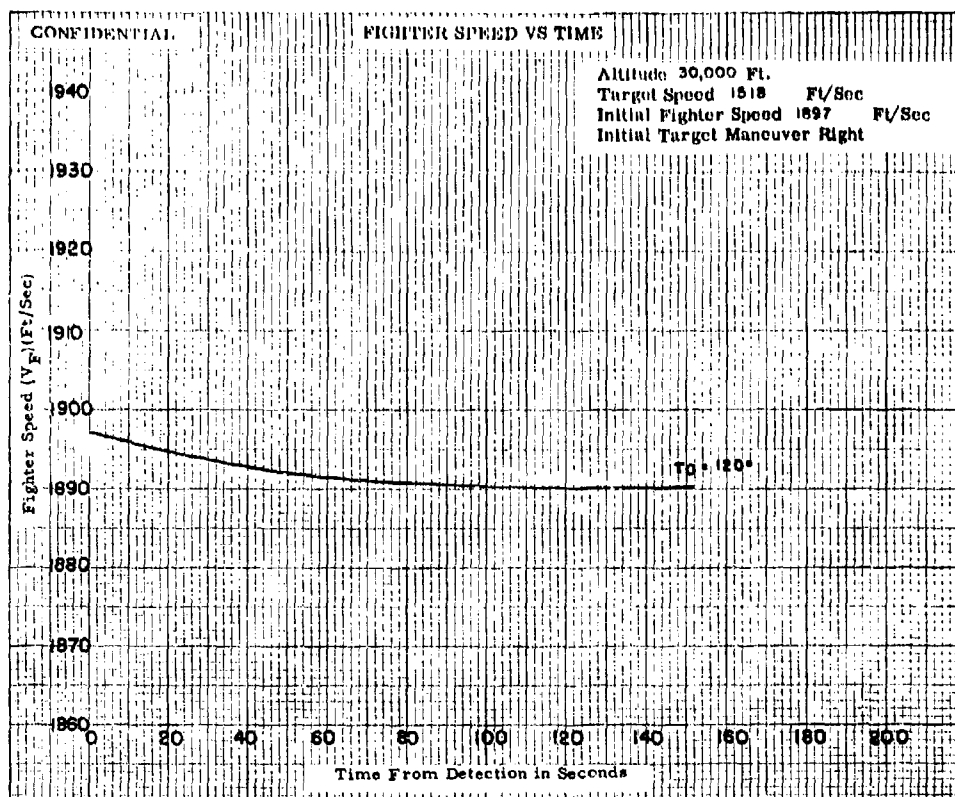


Fig. X-13b

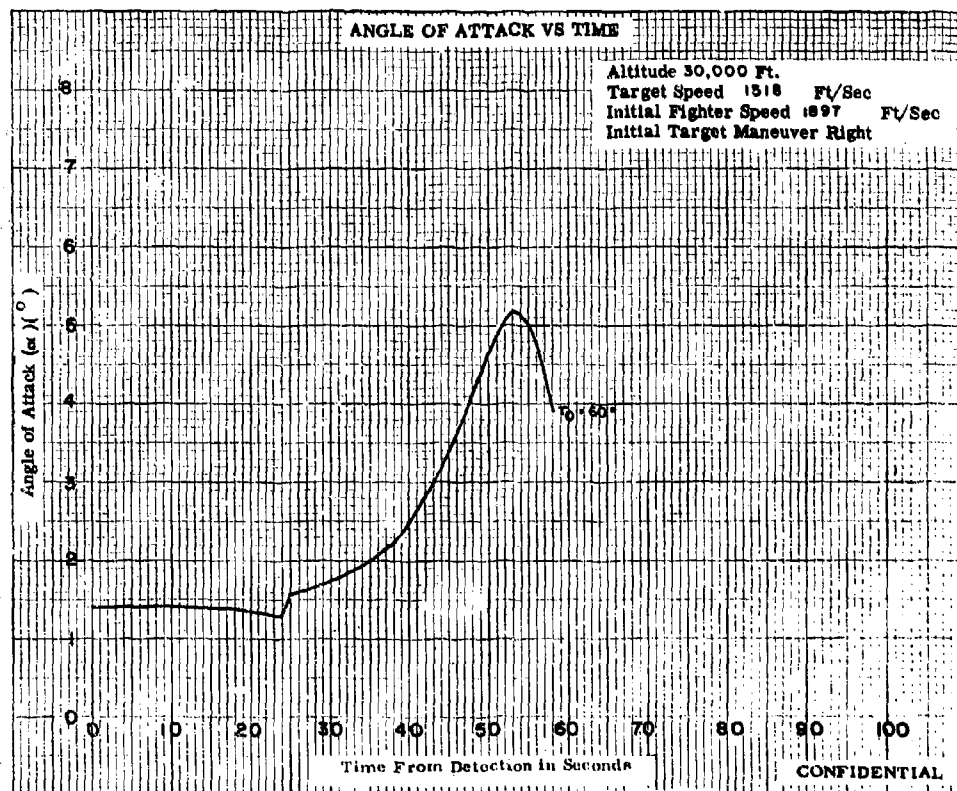
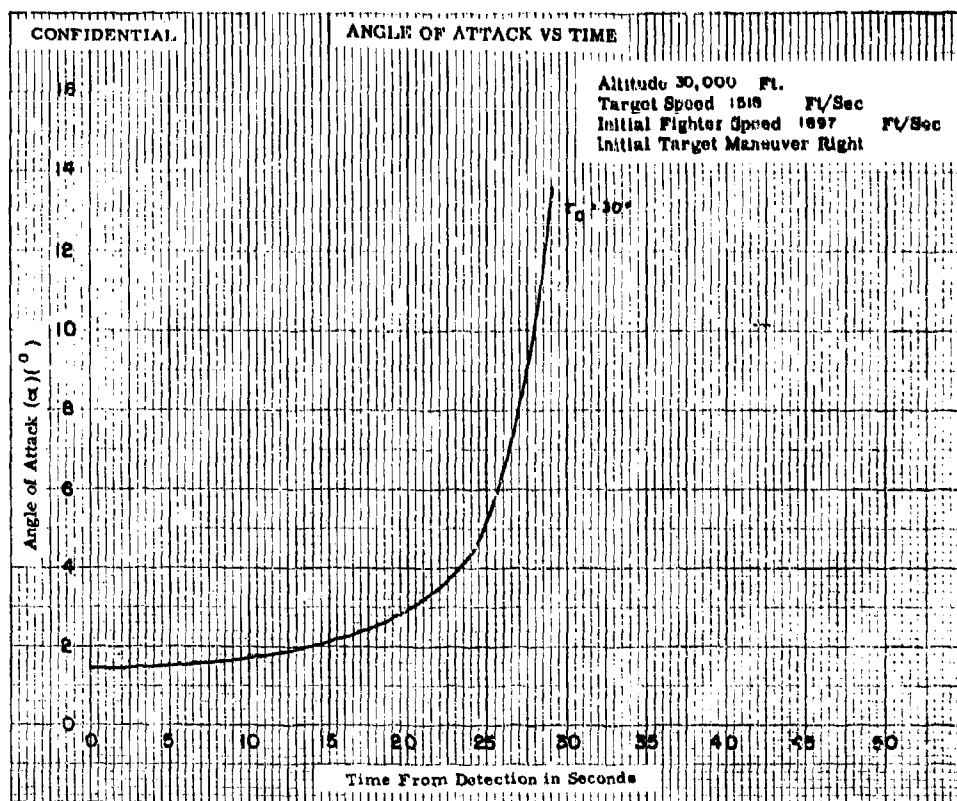


Fig. X-14a

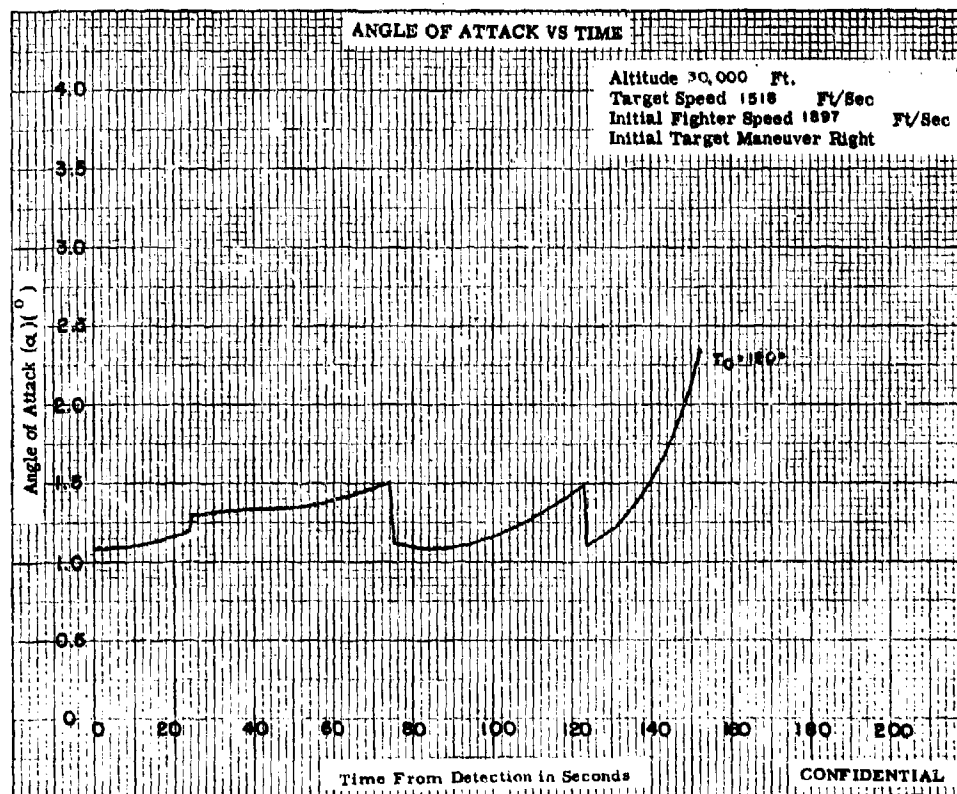
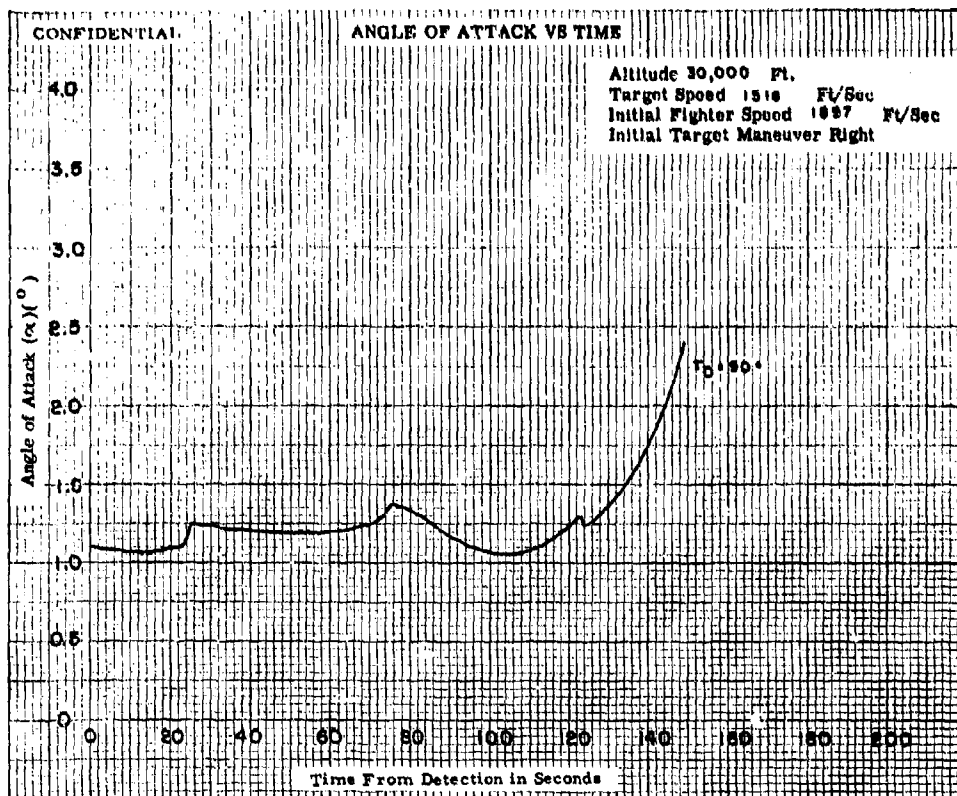


Fig. X-14b

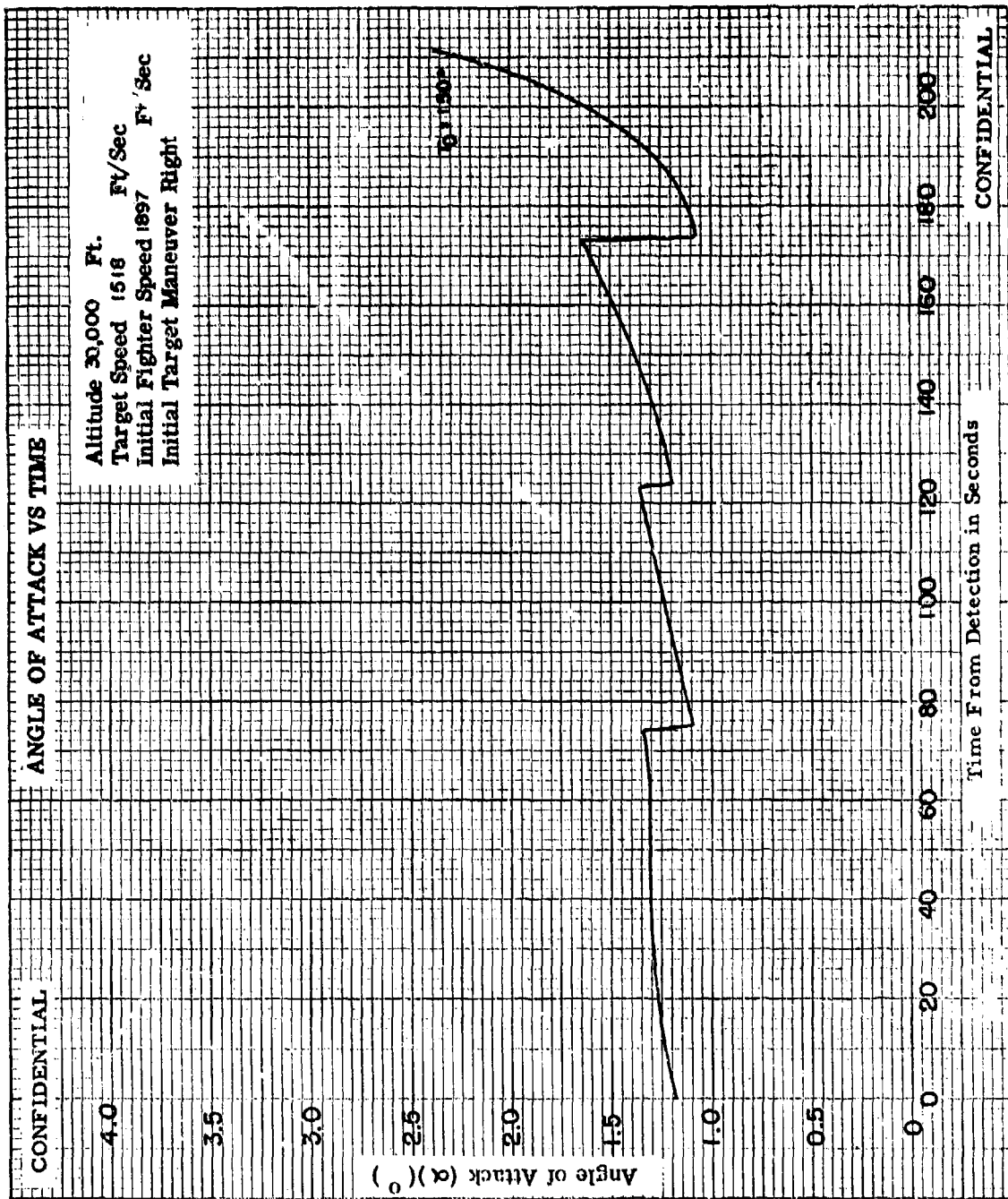
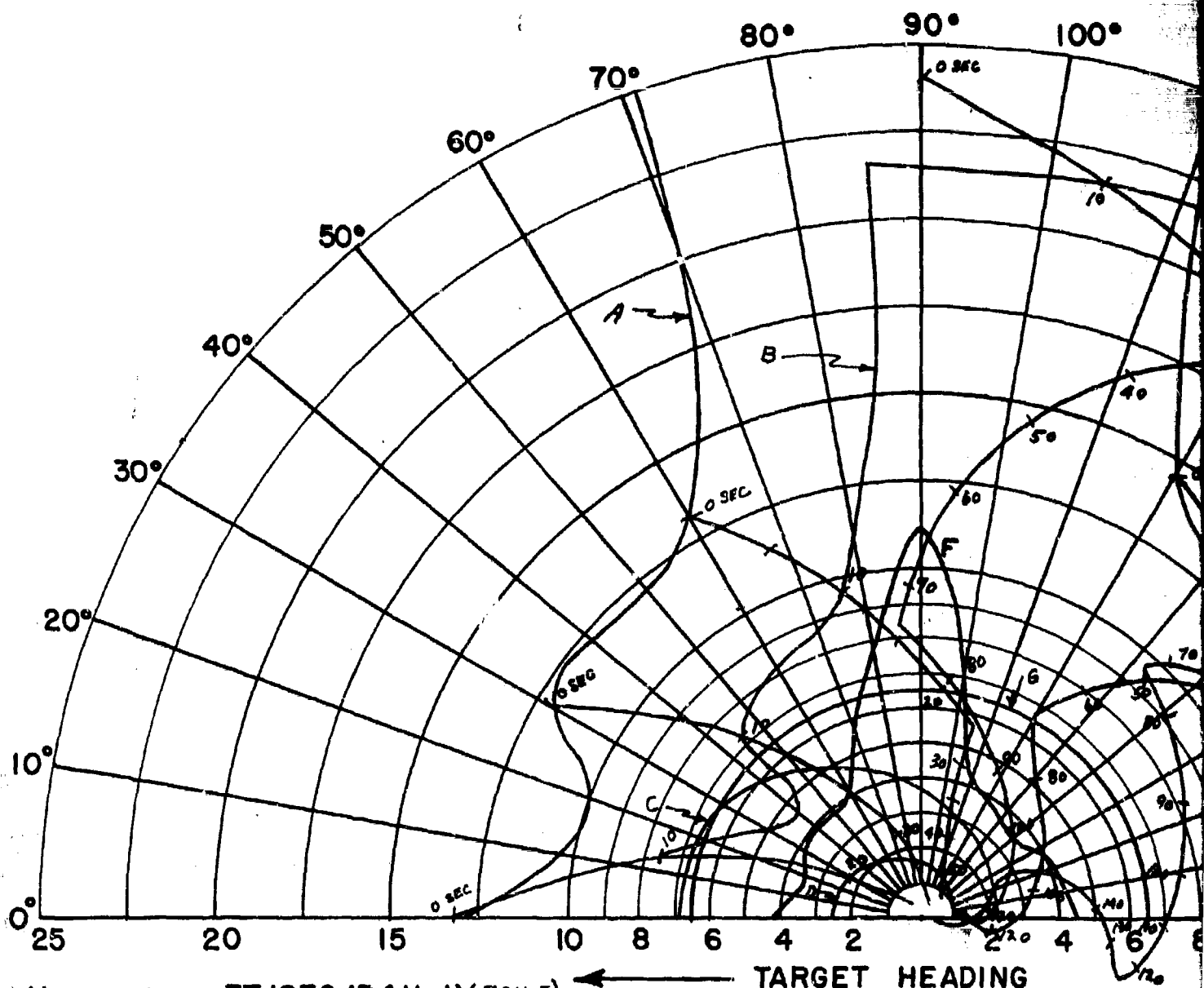


Fig. X-14c



$V_F = 1897$ FT/SEC (F4H-1)(F8U-3)

$V_T = 1518$ FT/SEC

ALTITUDE = 30,000 FT.

MANEUVERING TARGET - IN TARGET COORDINATES

INITIAL LEFT TURN

TARGET HEADING

A - 85% DETECTION RANGE

B - LOCK-ON RANGE (10 SEC. LOCK-ON T

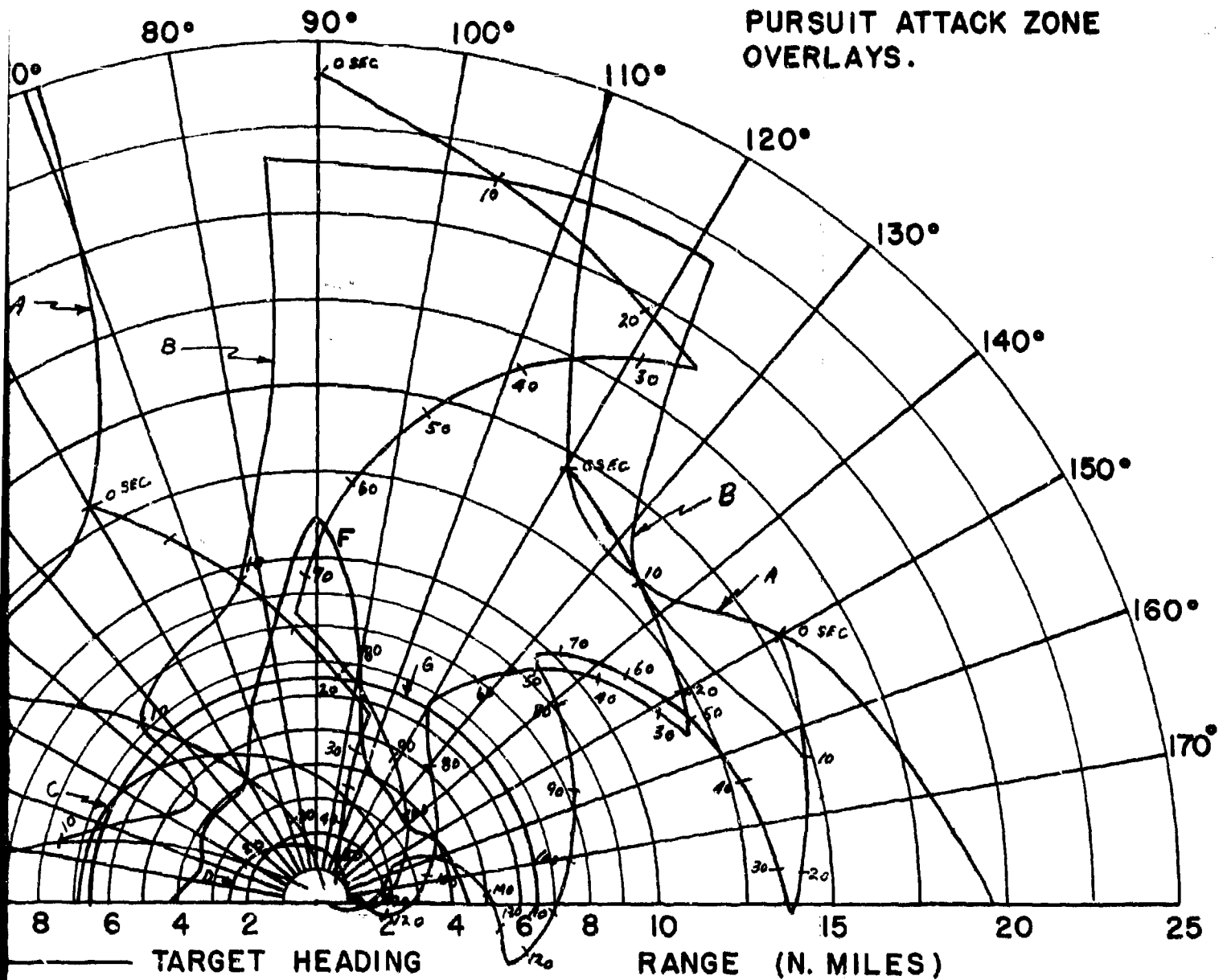
C - SPARROW III MAX. AERODYNAMIC RA

D - SPARROW III MIN. AERODYNAMIC RA

F - 90% SPARROW III SEEKER LOCK-ON

G - 6.5 N.M. INTERLOCK

FIG. XI - CO-ALTITUDE LEAD
PURSUIT ATTACK ZONE
OVERLAYS.



85% DETECTION RANGE
LOCK-ON RANGE (10 SEC. LOCK-ON TIME)
SPARROW III MAX. AERODYNAMIC RANGE
SPARROW III MIN. AERODYNAMIC RANGE

90% SPARROW III SEEKER LOCK-ON RANGE
6.5 N.M. INTERLOCK

CONFIDENTIAL

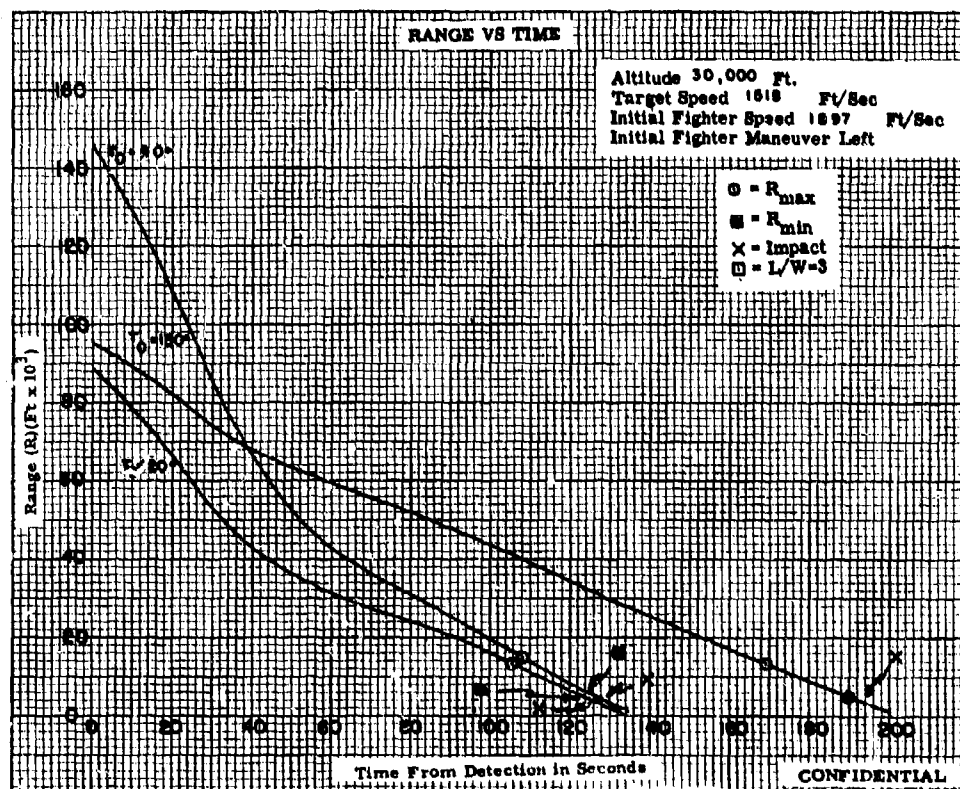
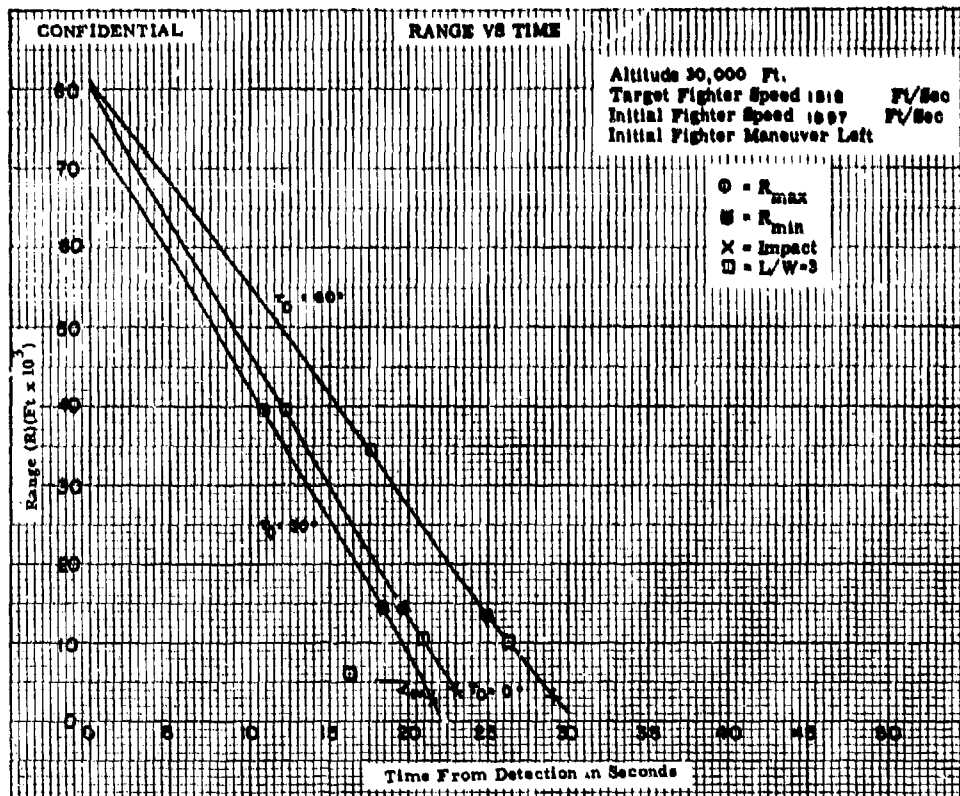


Fig. XI-1

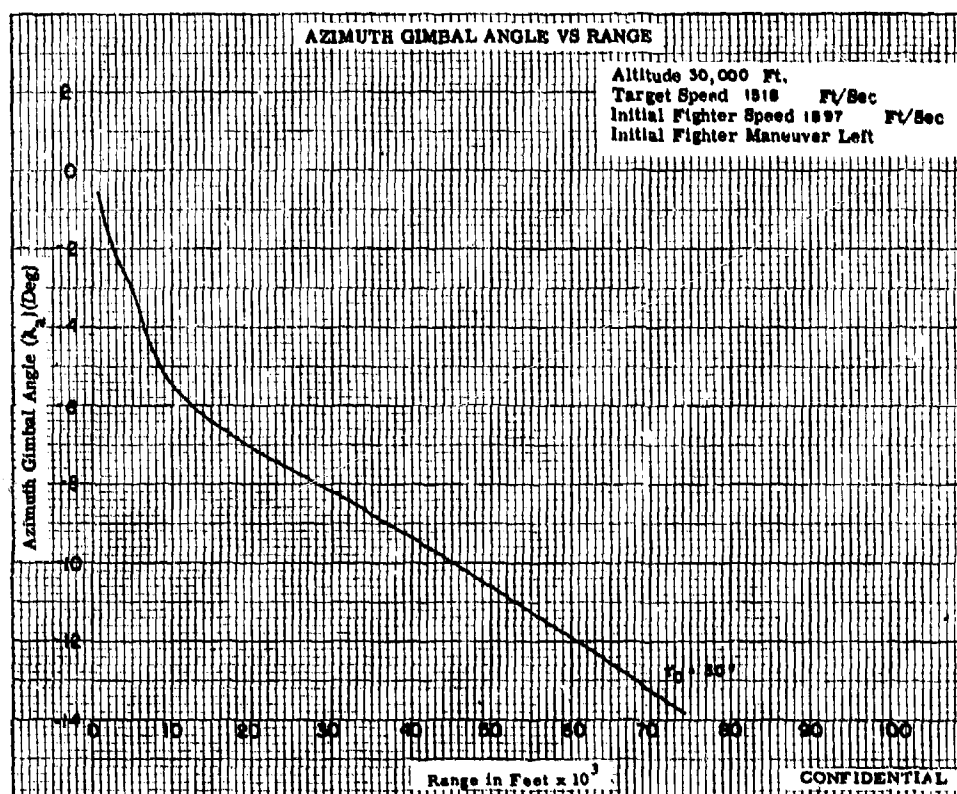
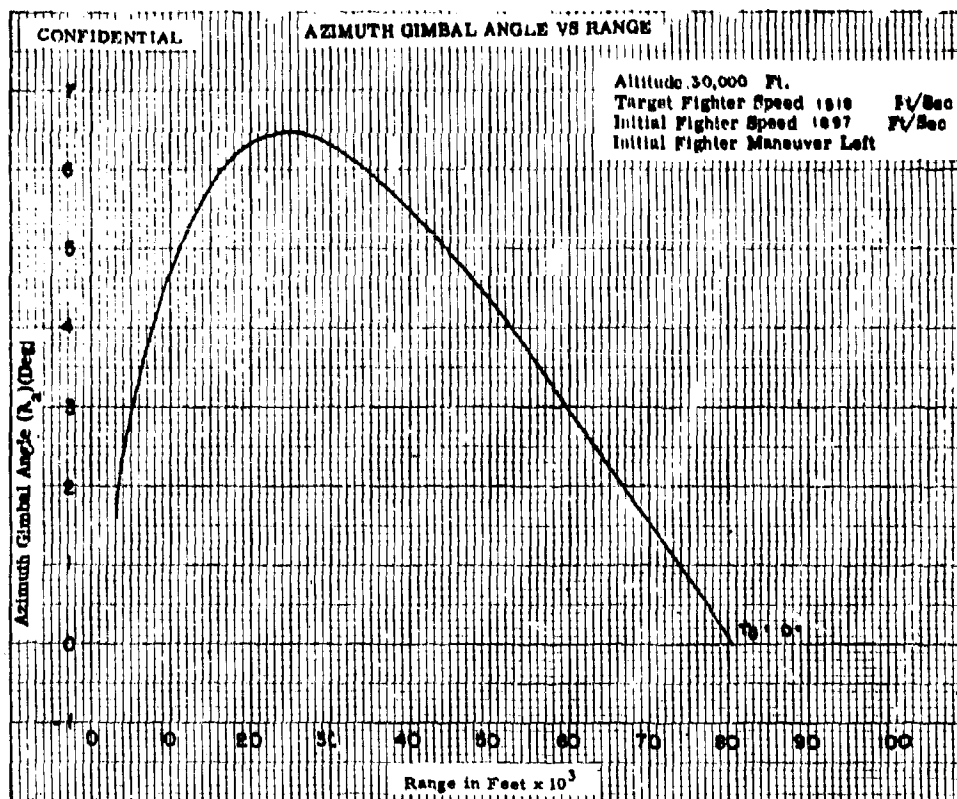


Fig. XI-2a

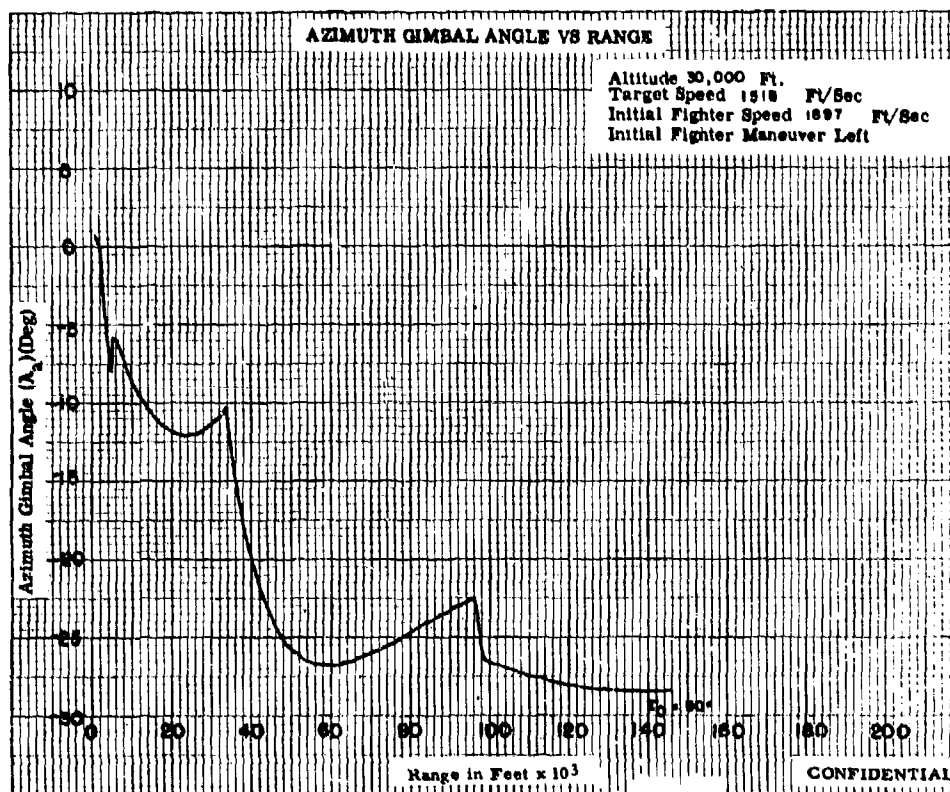
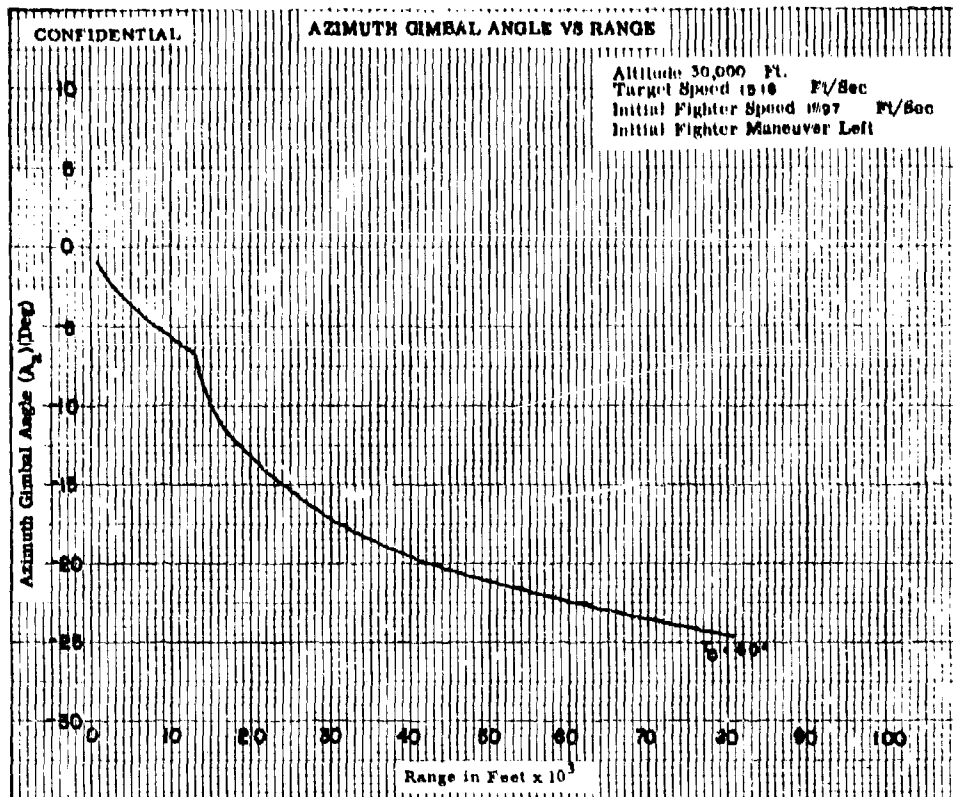


Fig. X1-2b

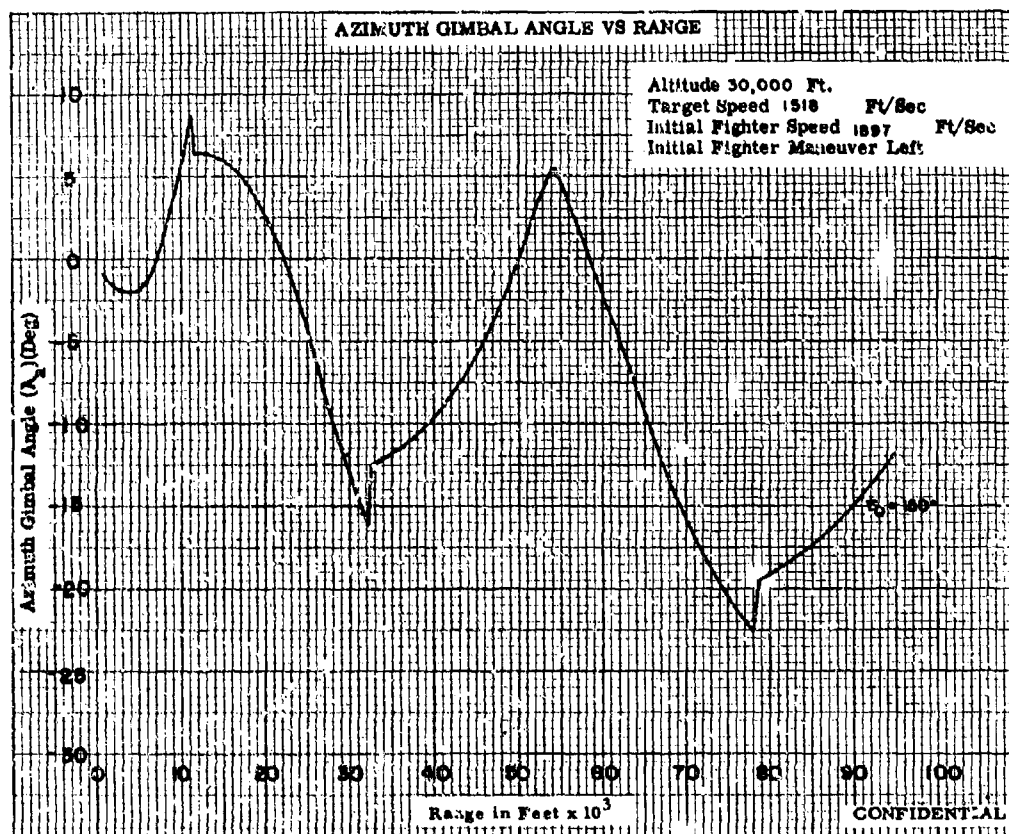
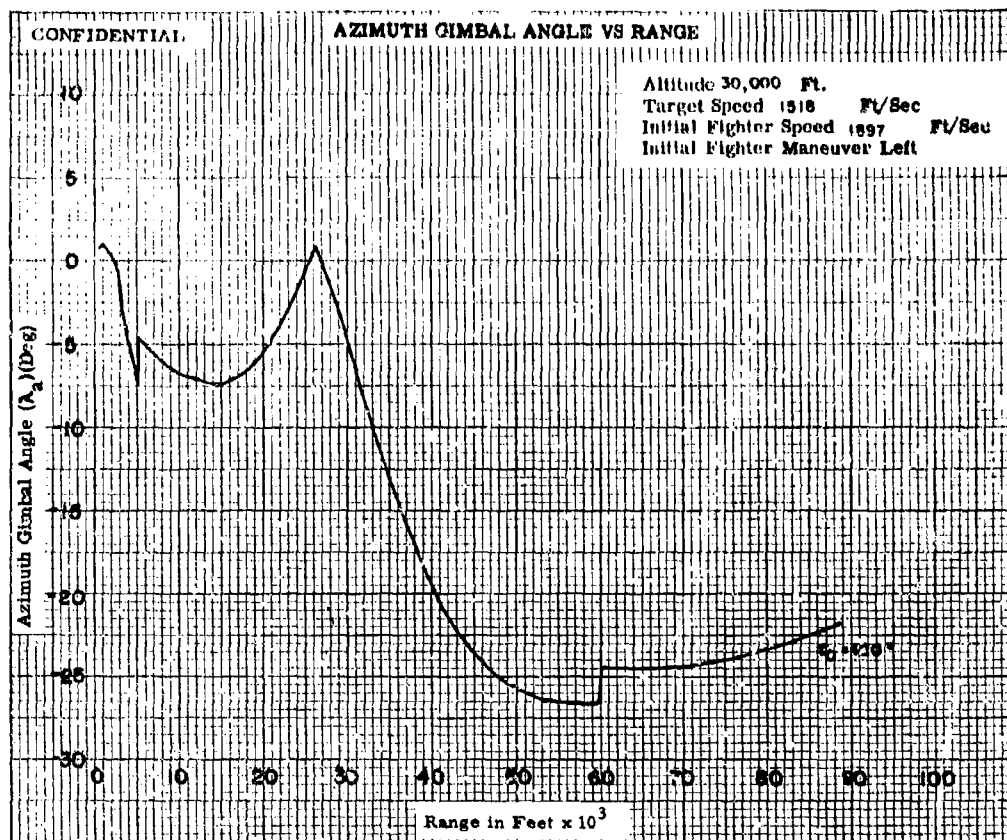


Fig. X1-2c

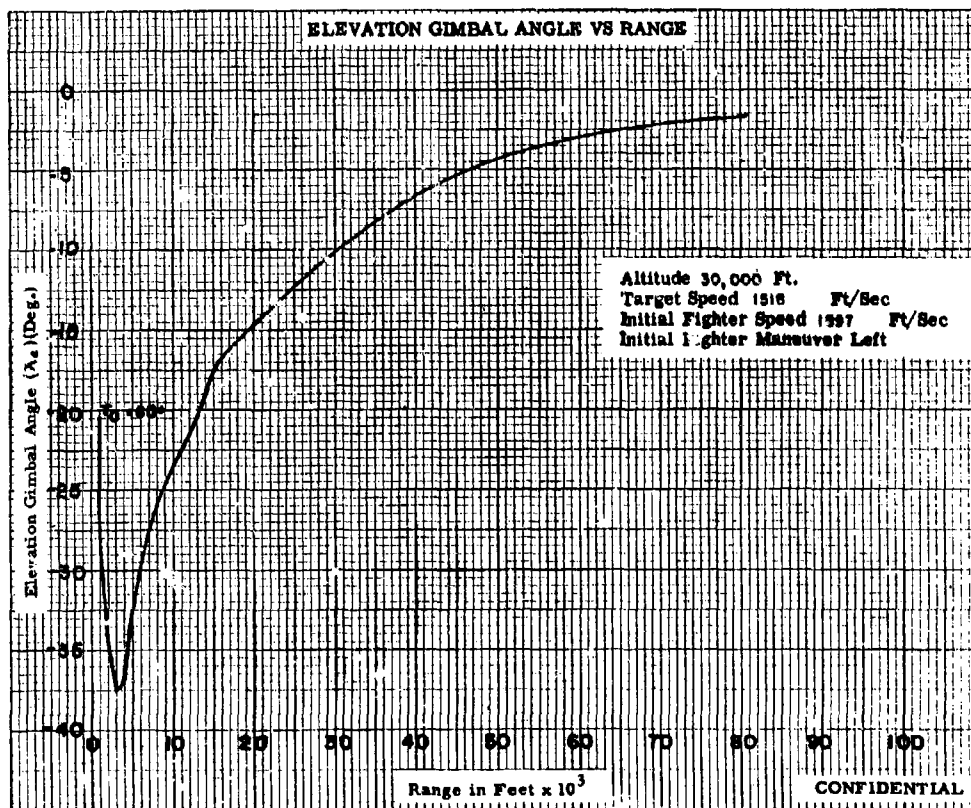
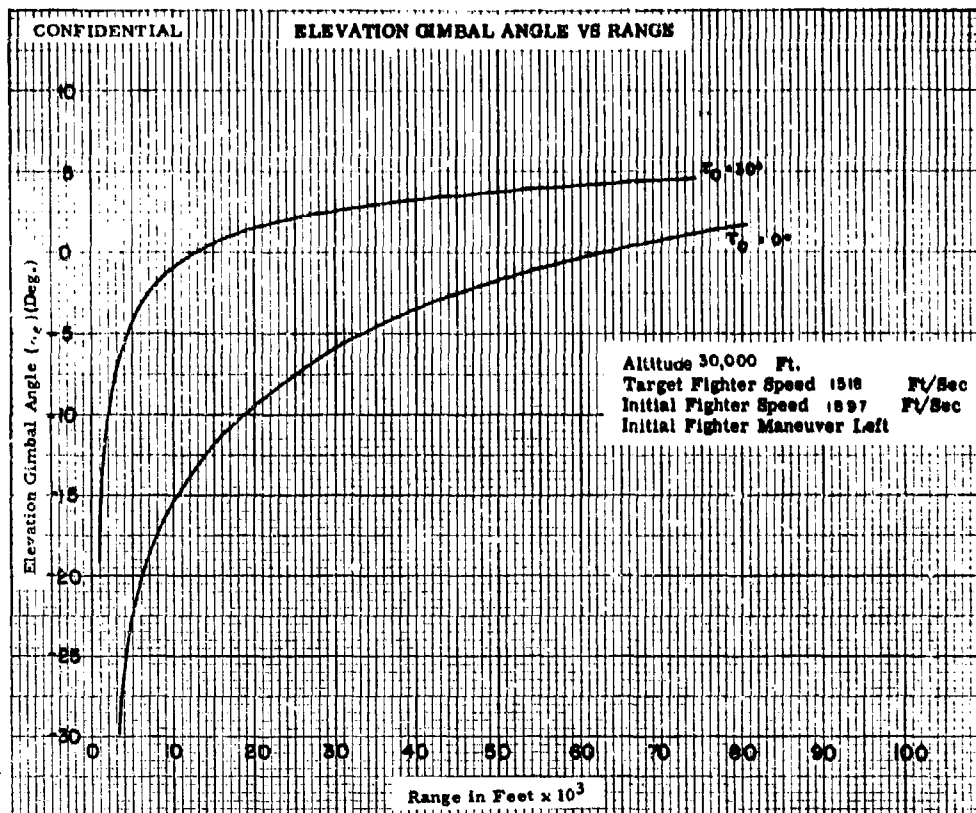


Fig. XI-3a

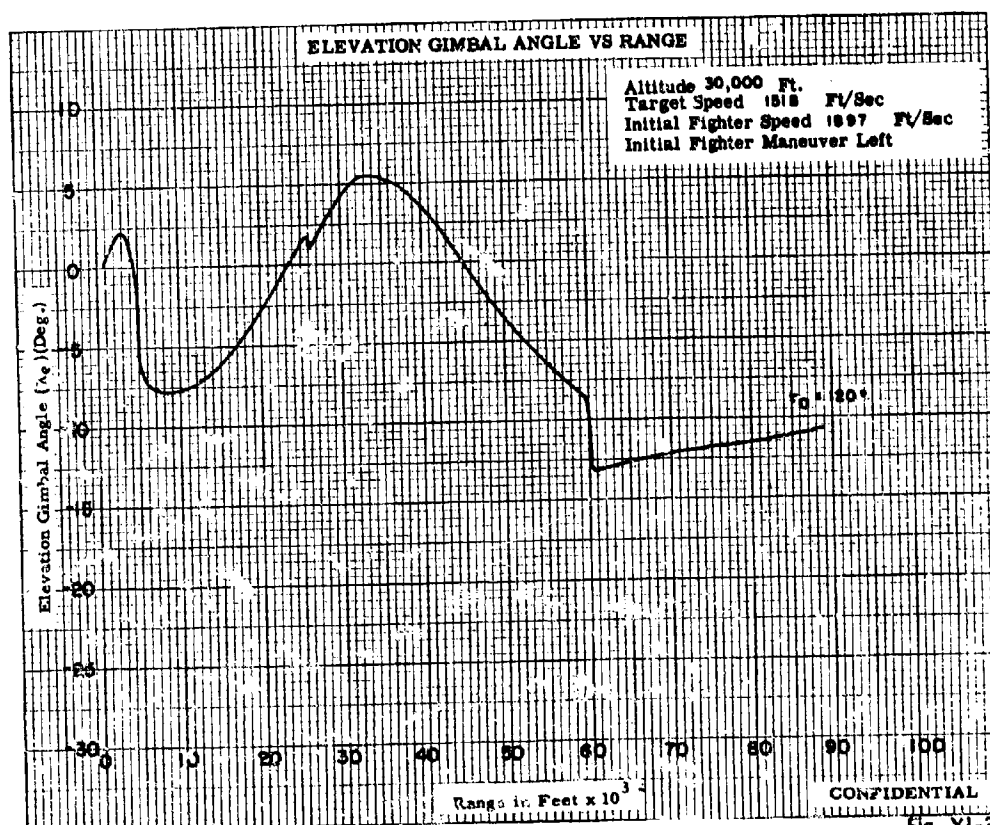
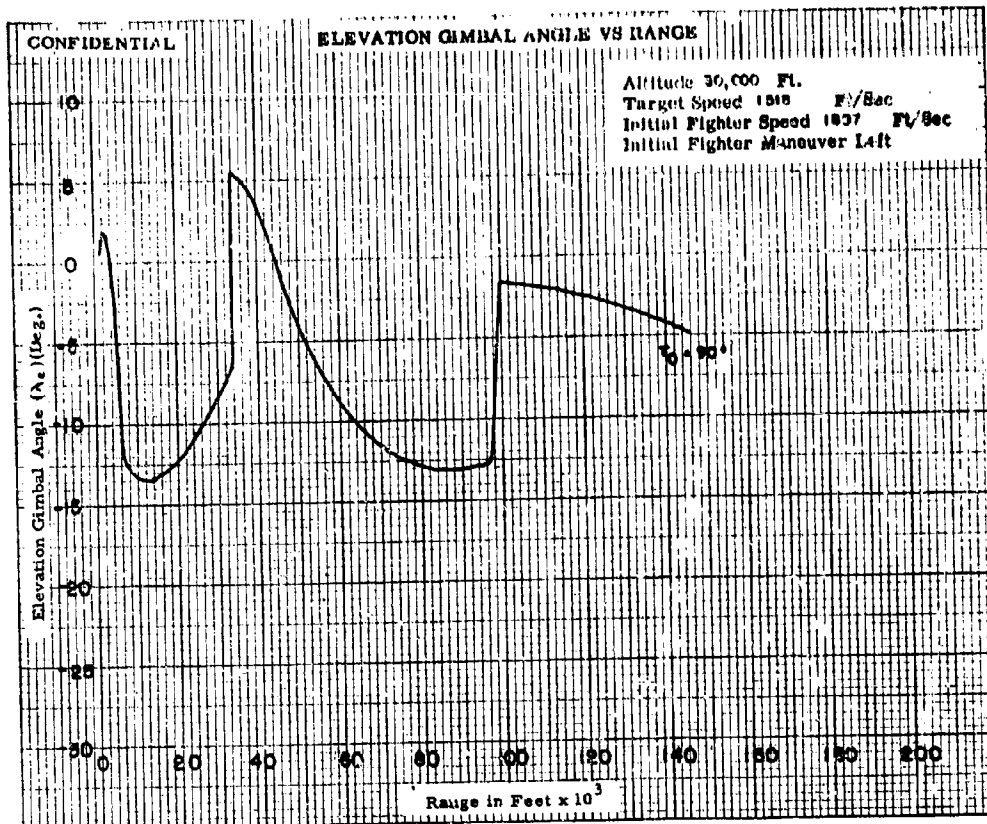


Fig. X1-3b

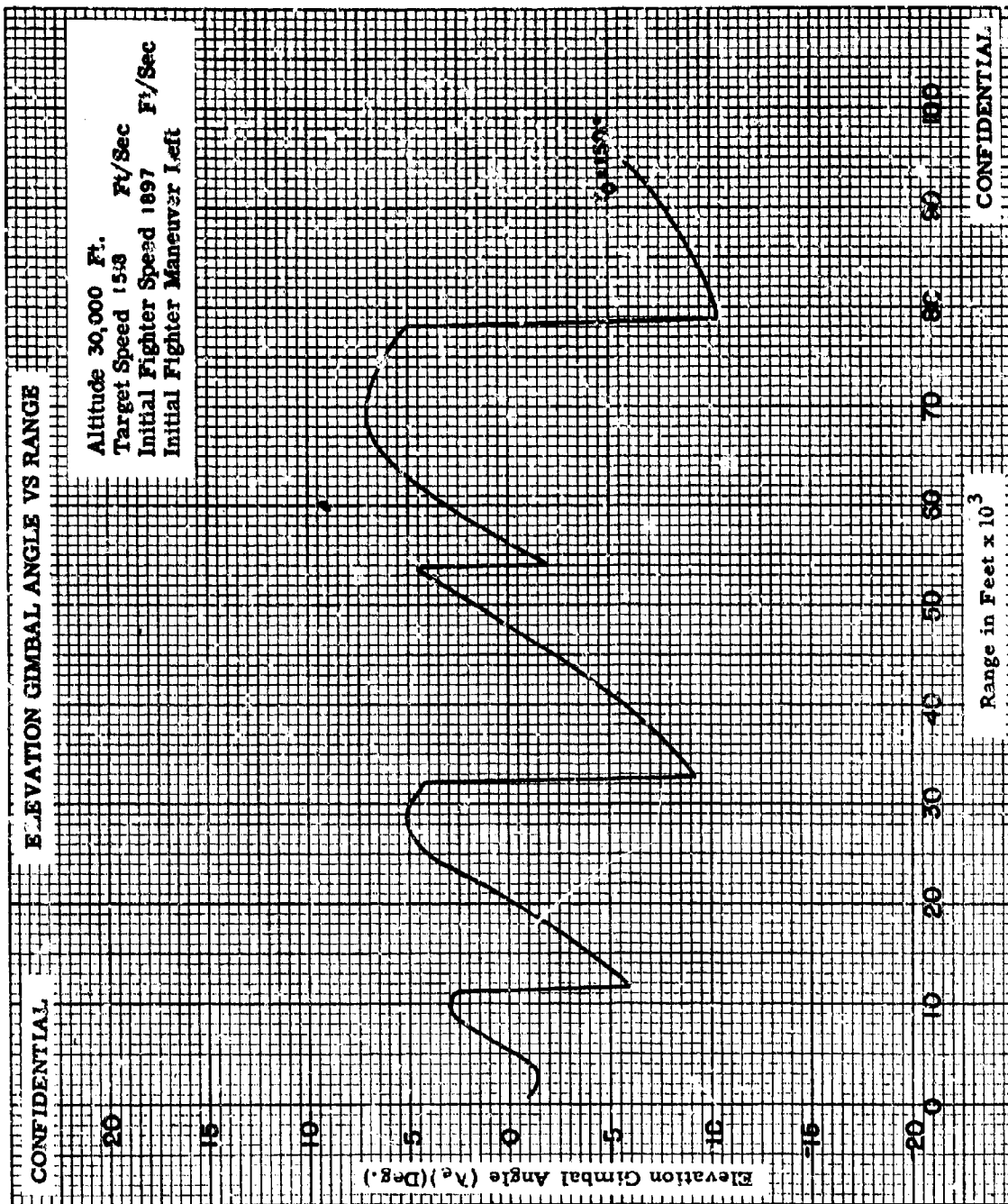


Fig. XI-3c

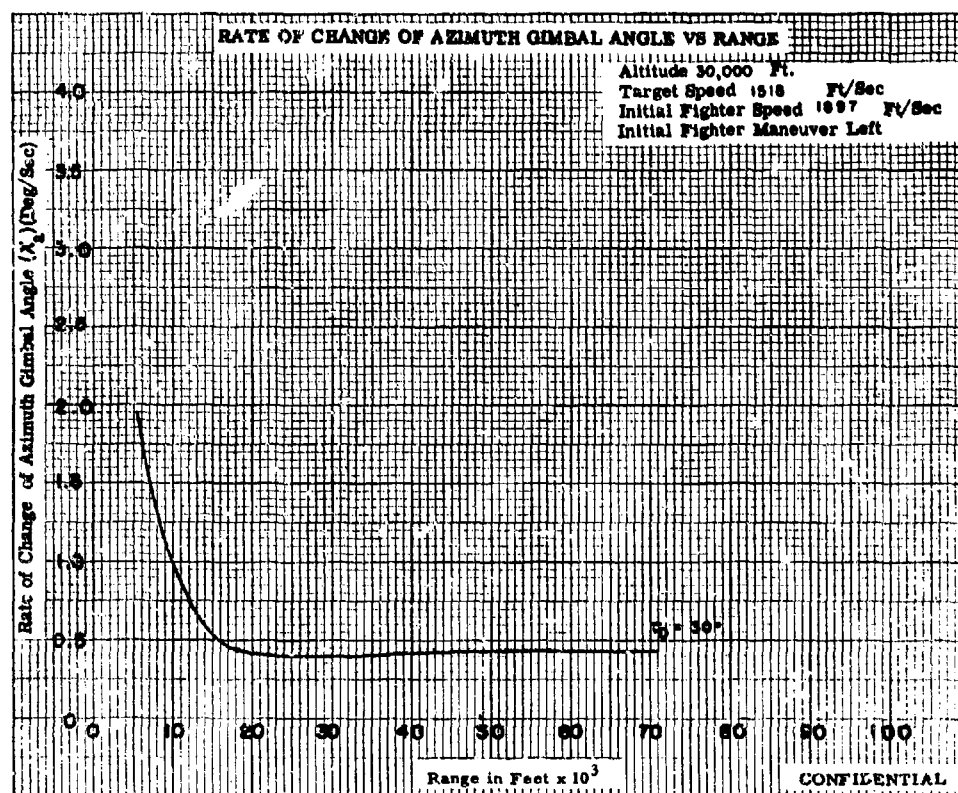
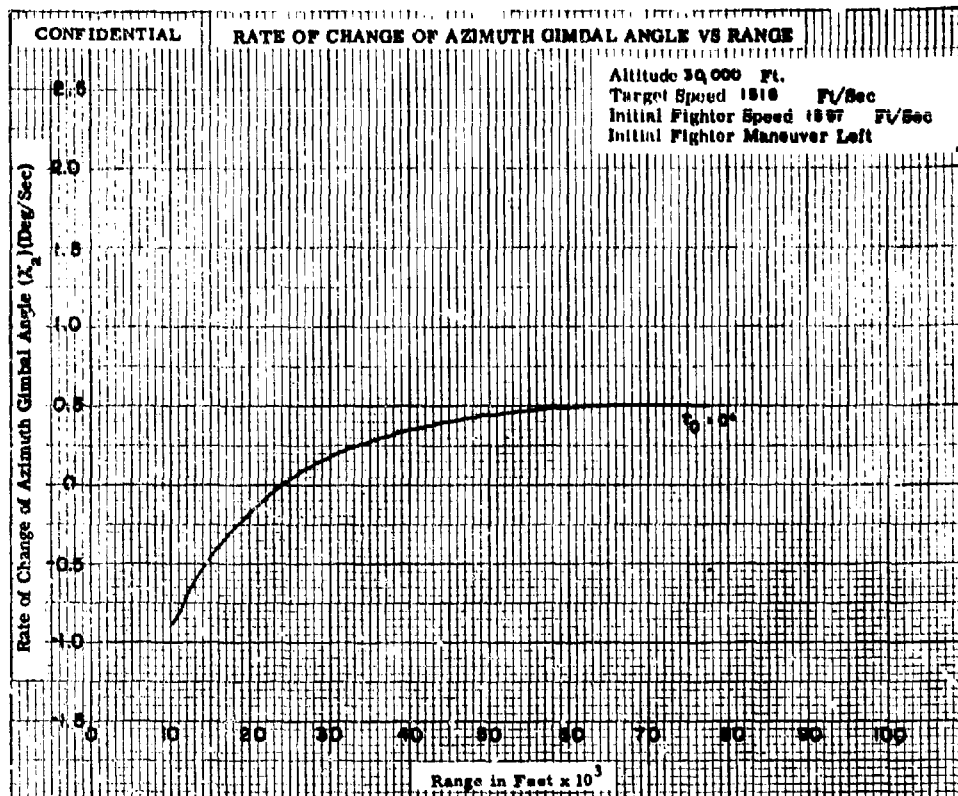


Fig. XI-4a

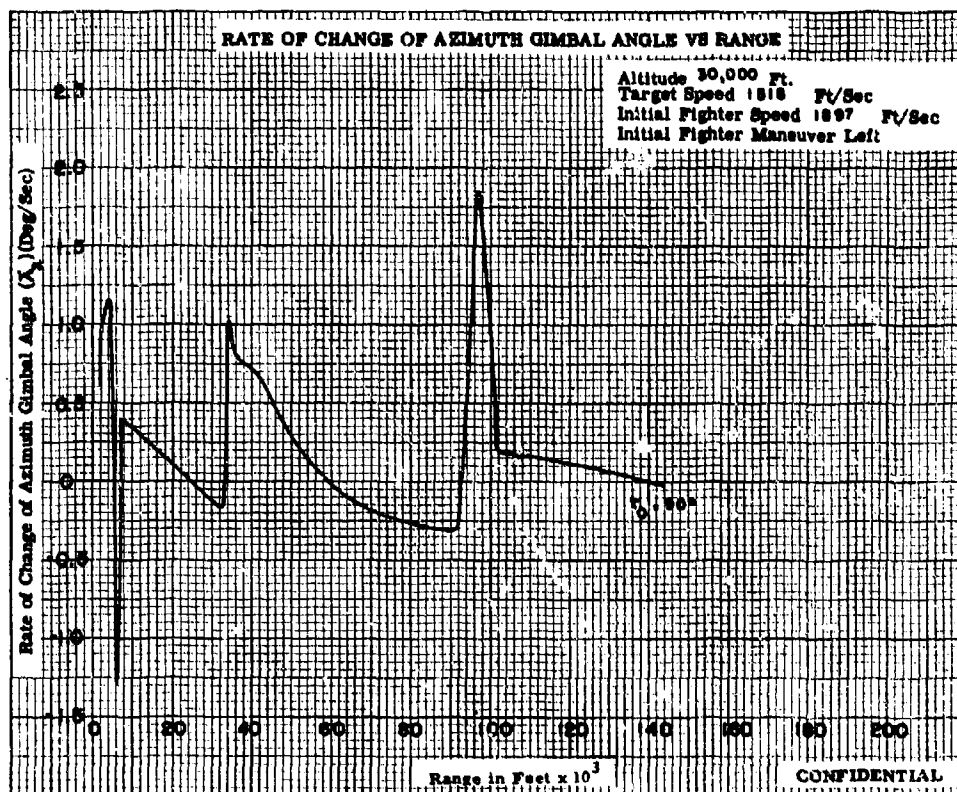
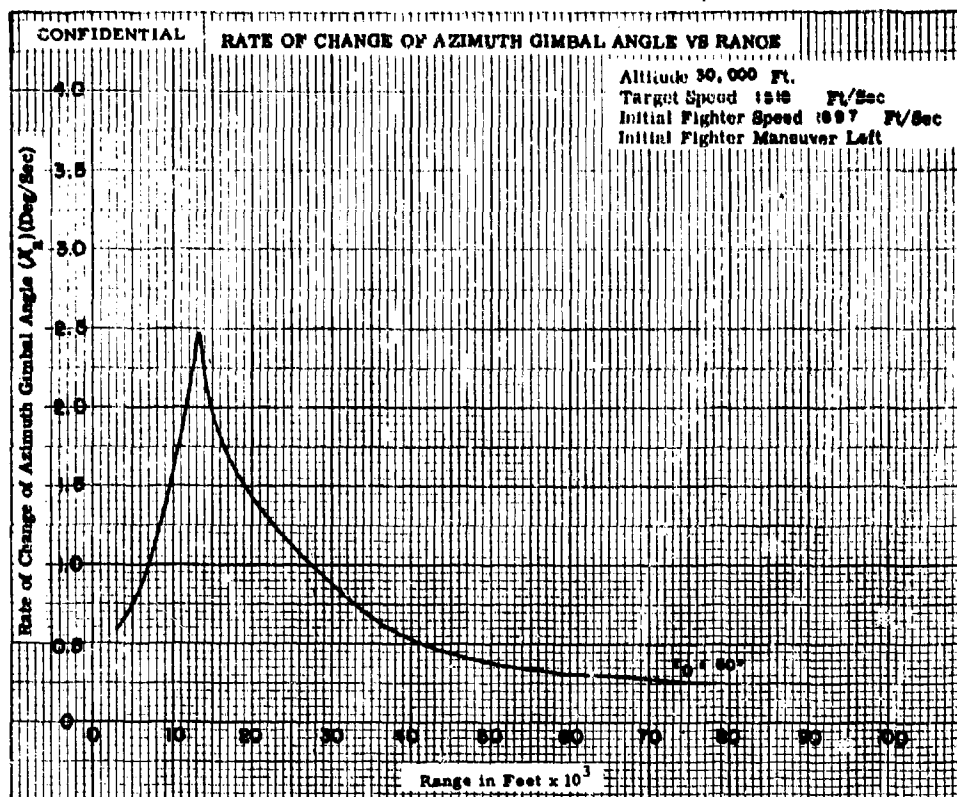


Fig. XI-4b

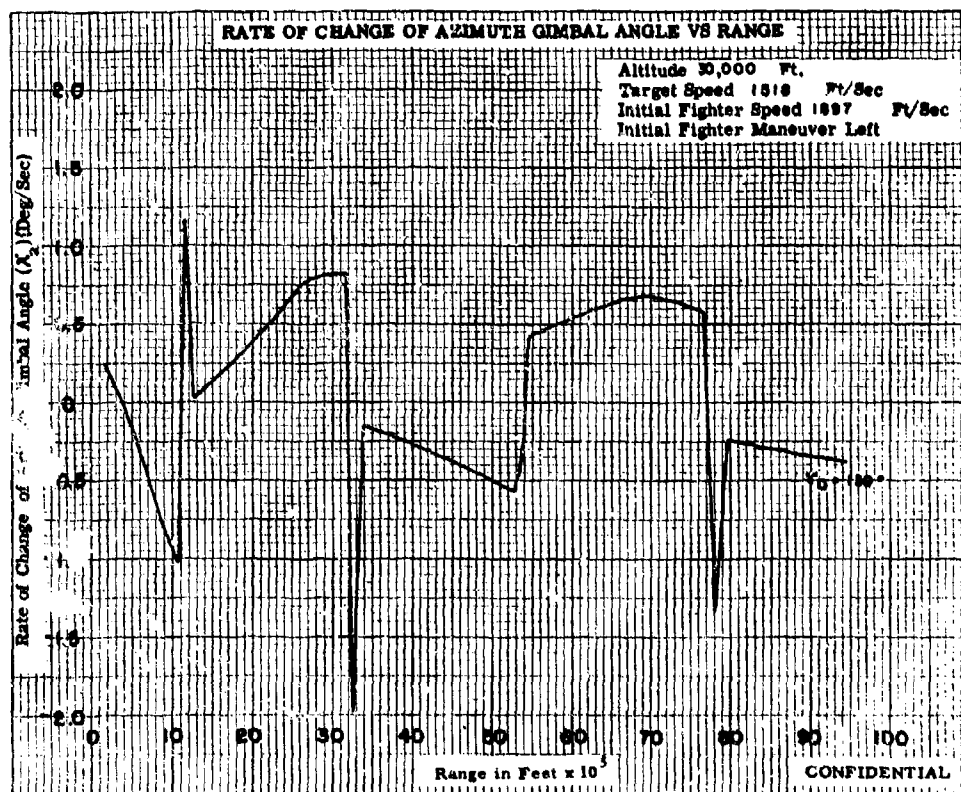
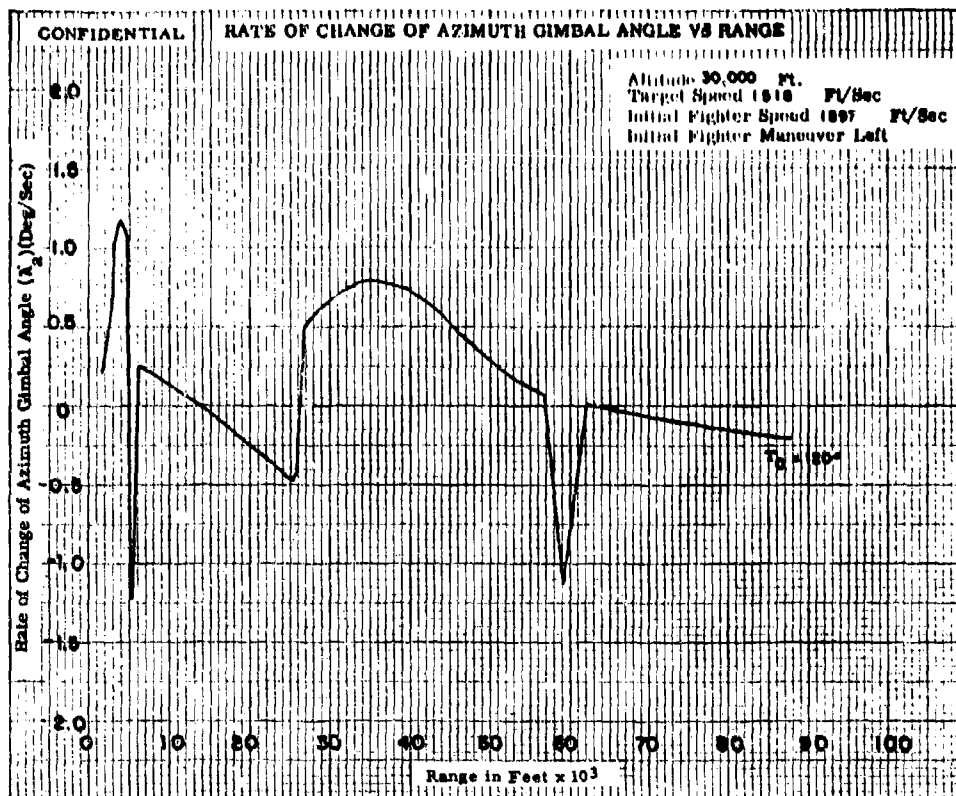


Fig. X1-4c

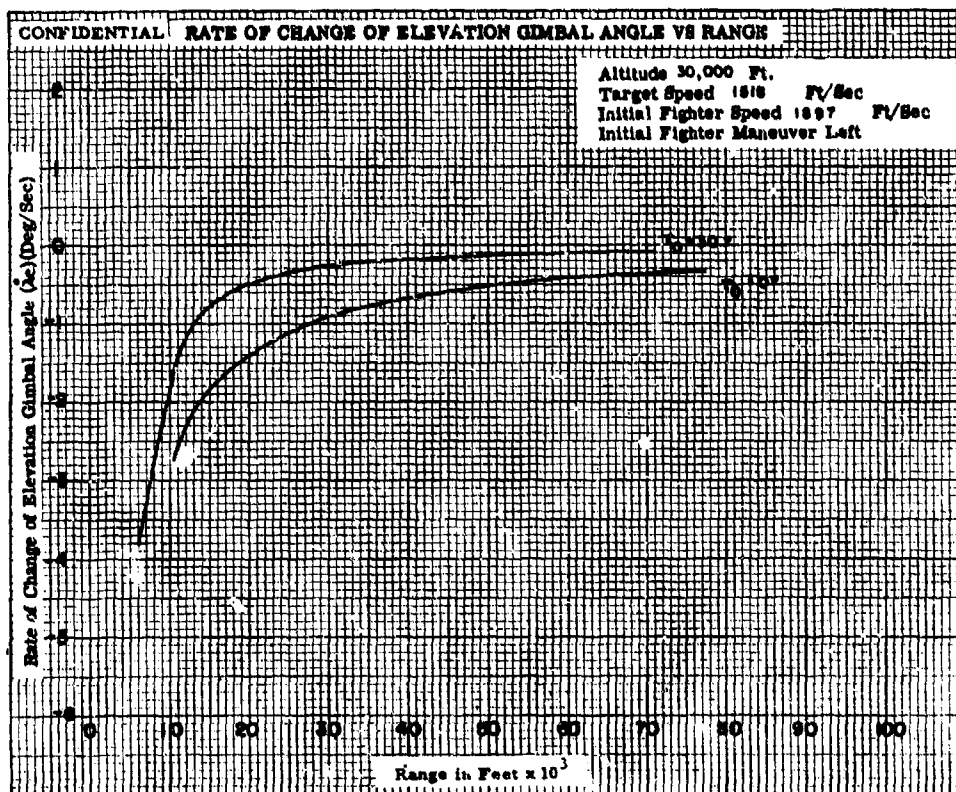
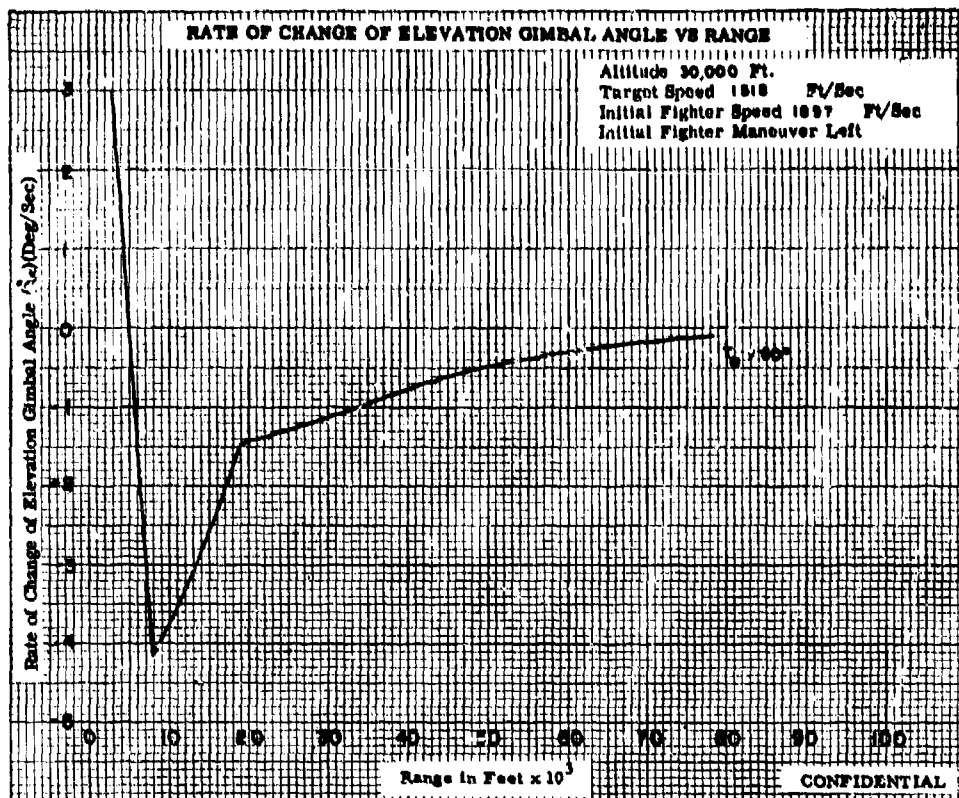


Fig. X1-5a

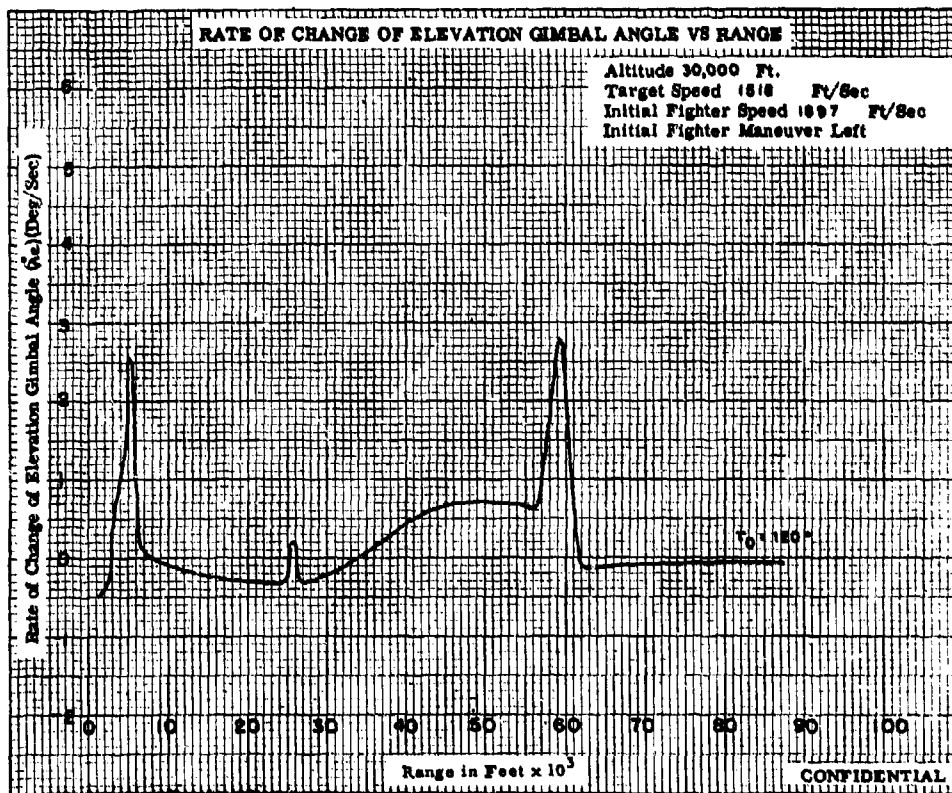
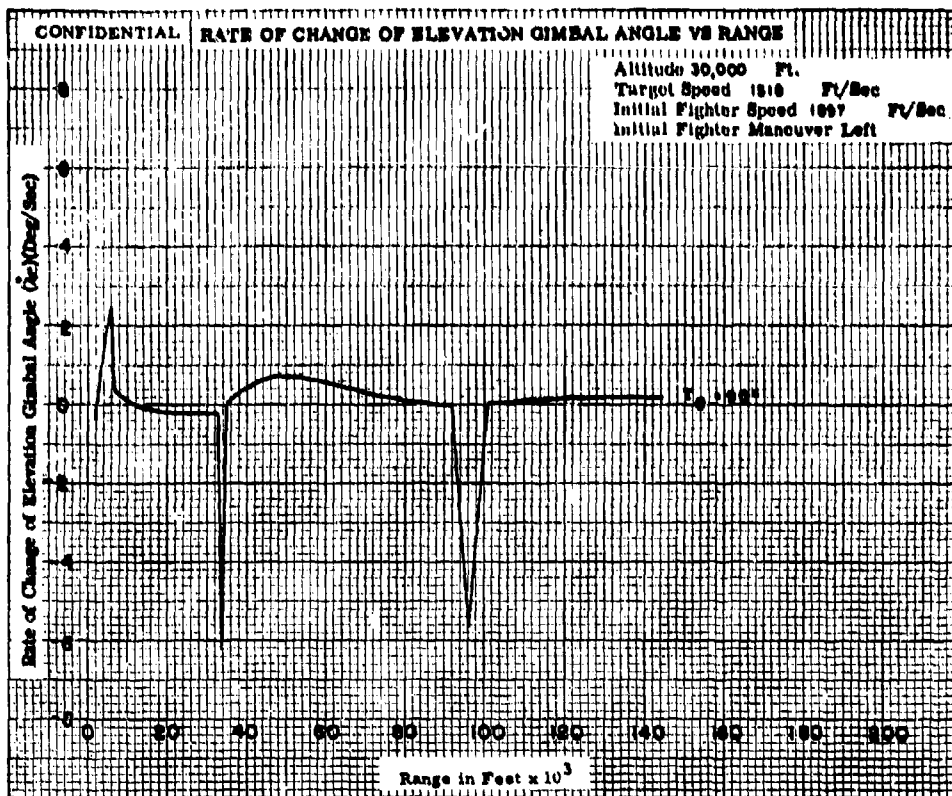


Fig. XI-5b

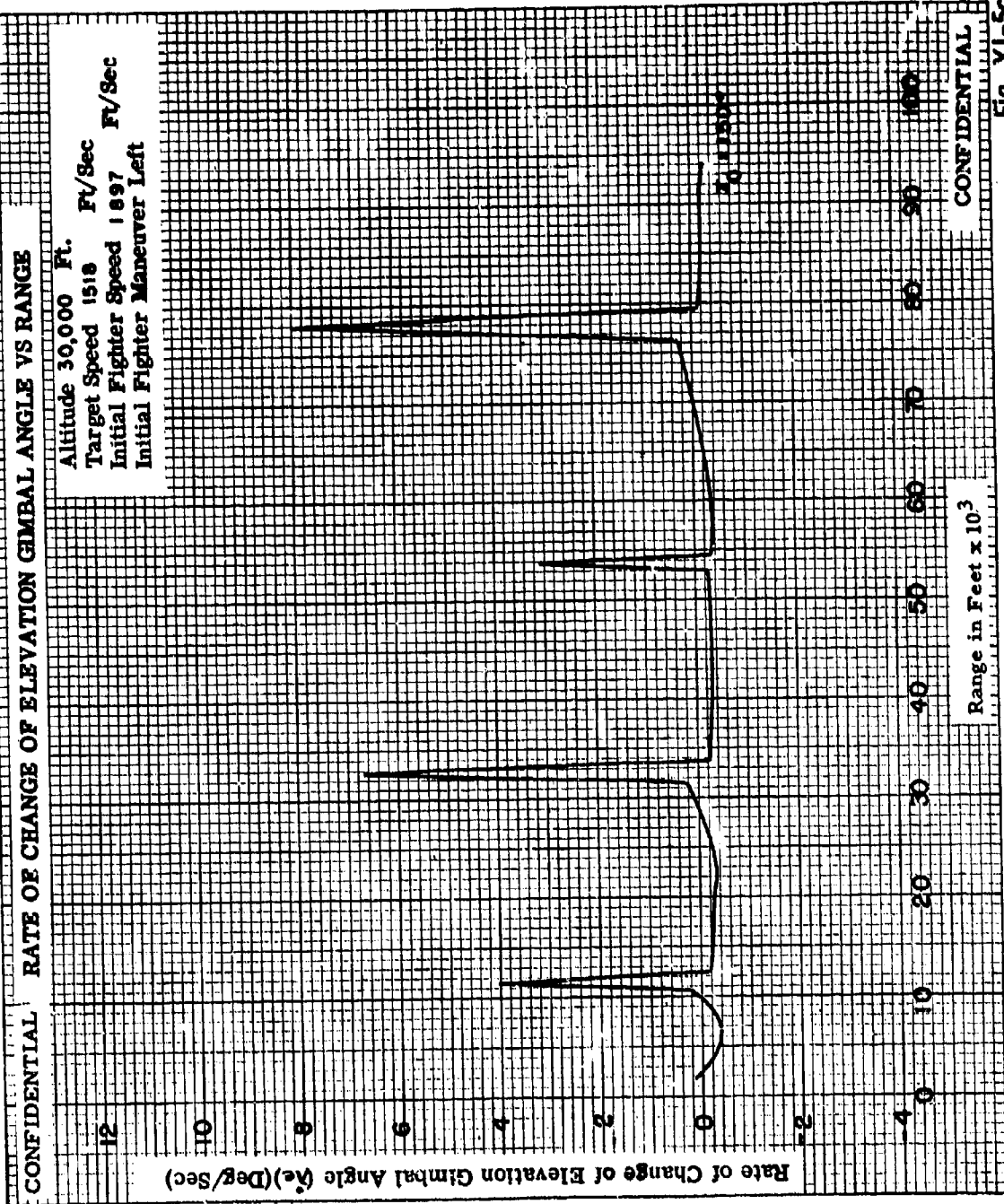


Fig XI-5c

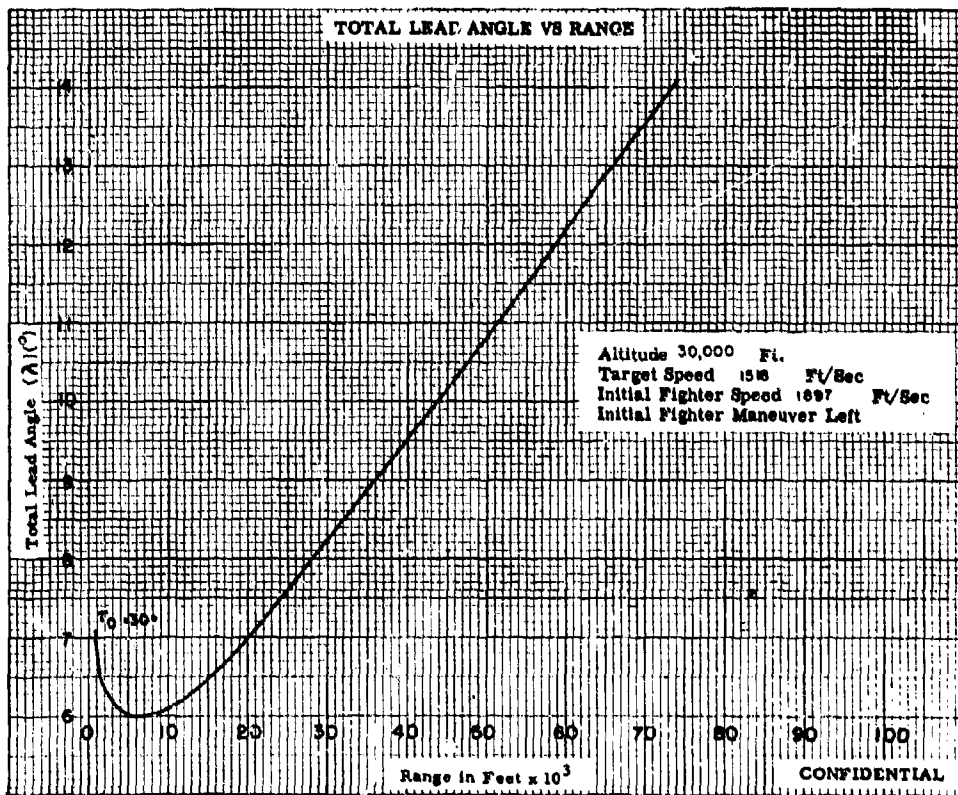
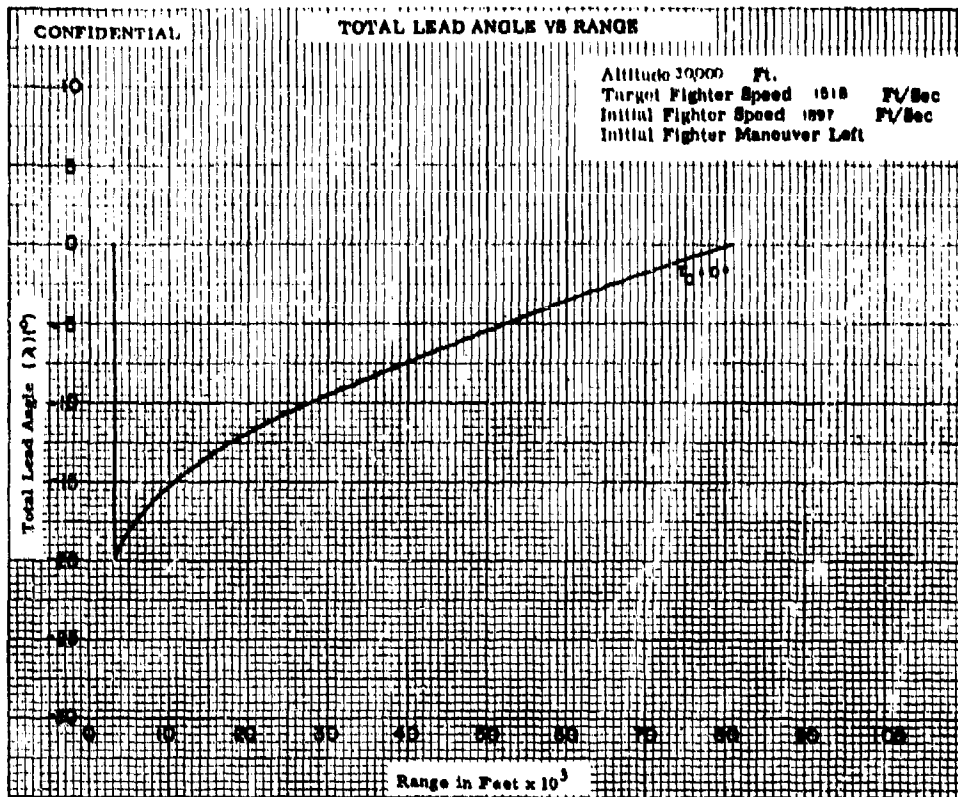


Fig. XI-6a

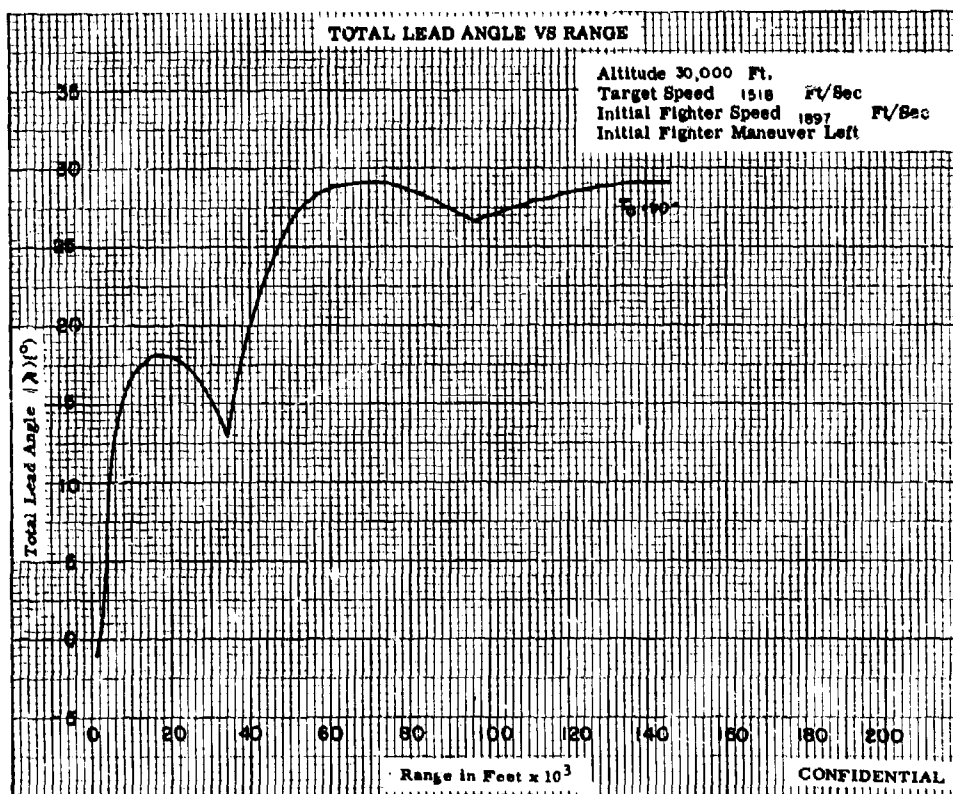
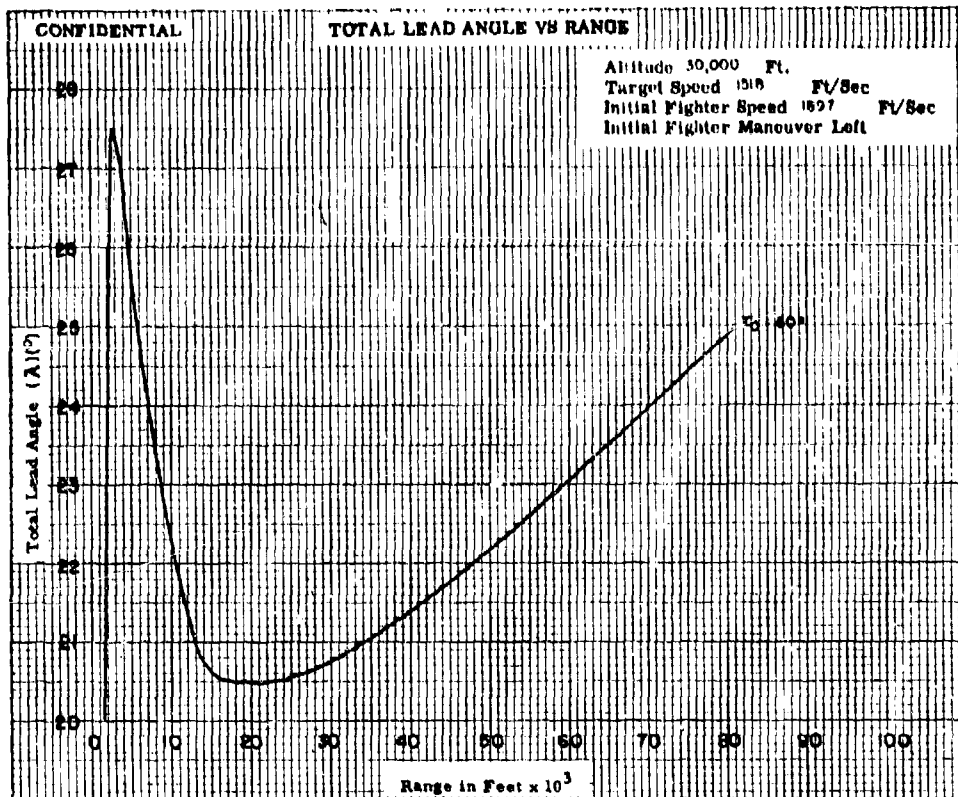


Fig. XI-6b

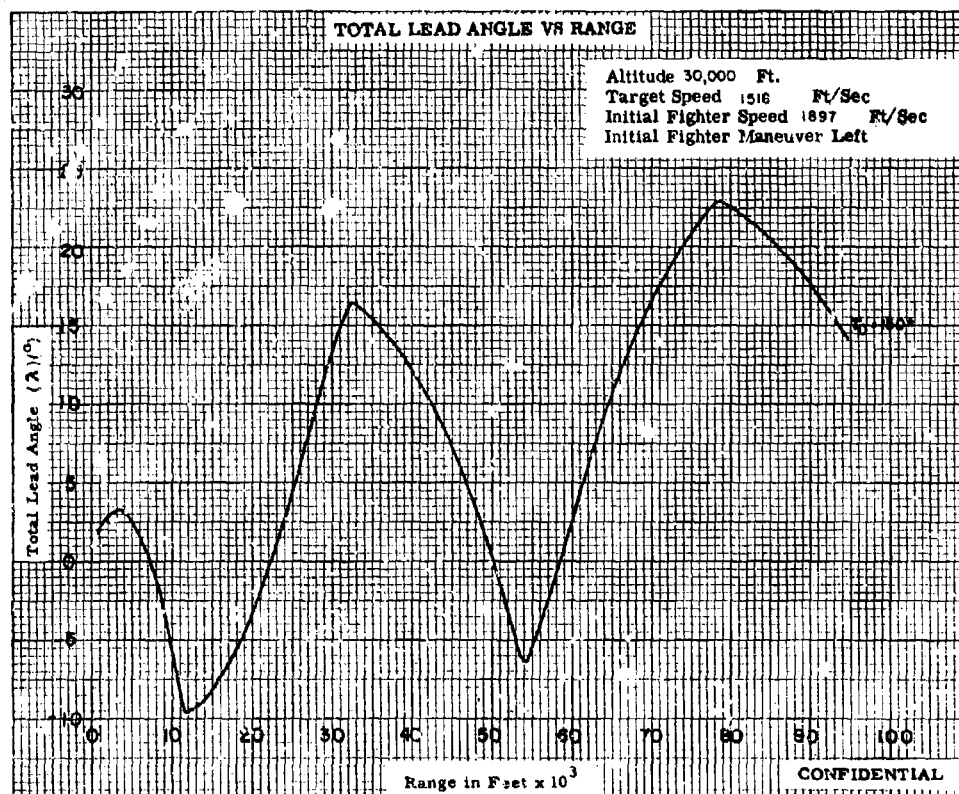
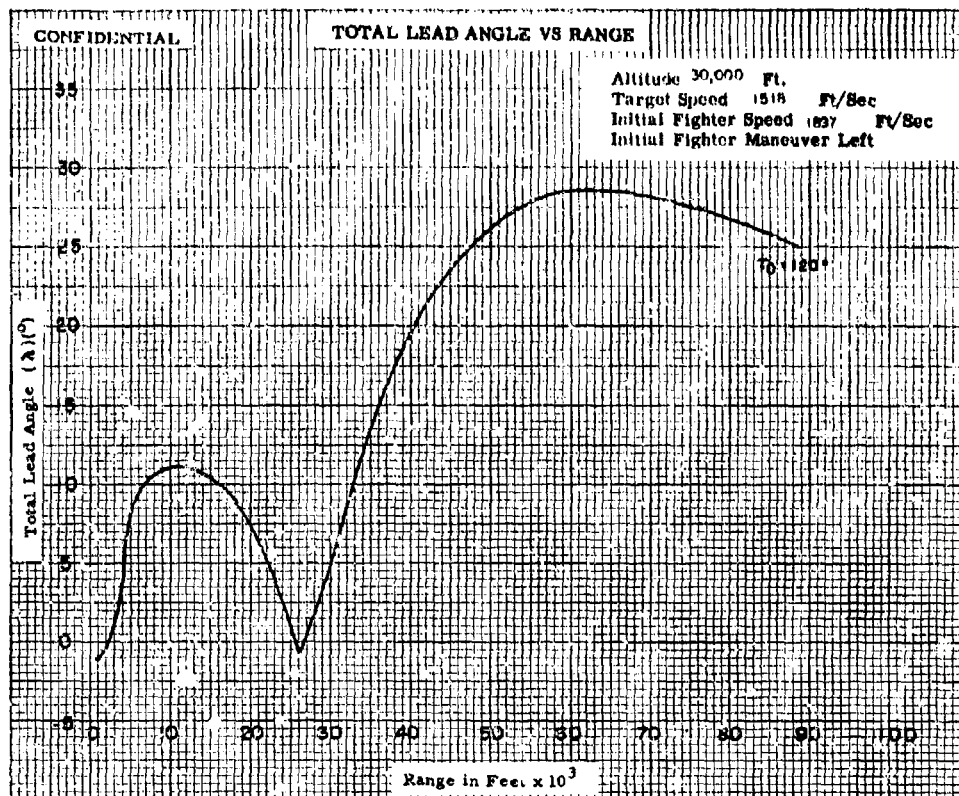


Fig. XI-6c

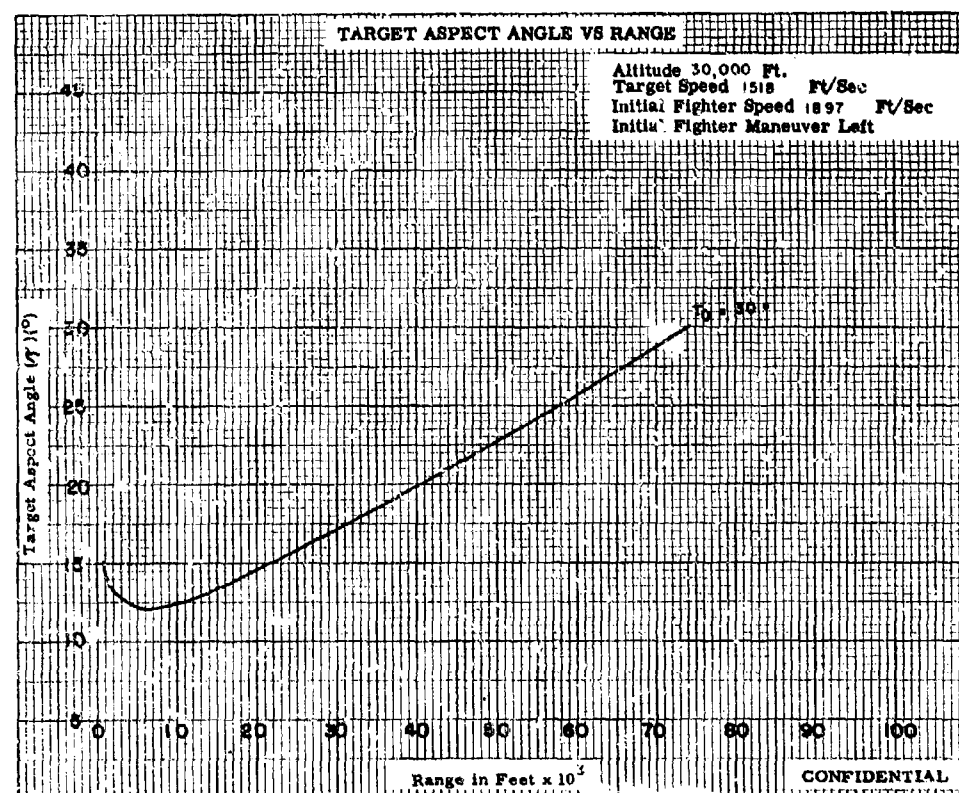
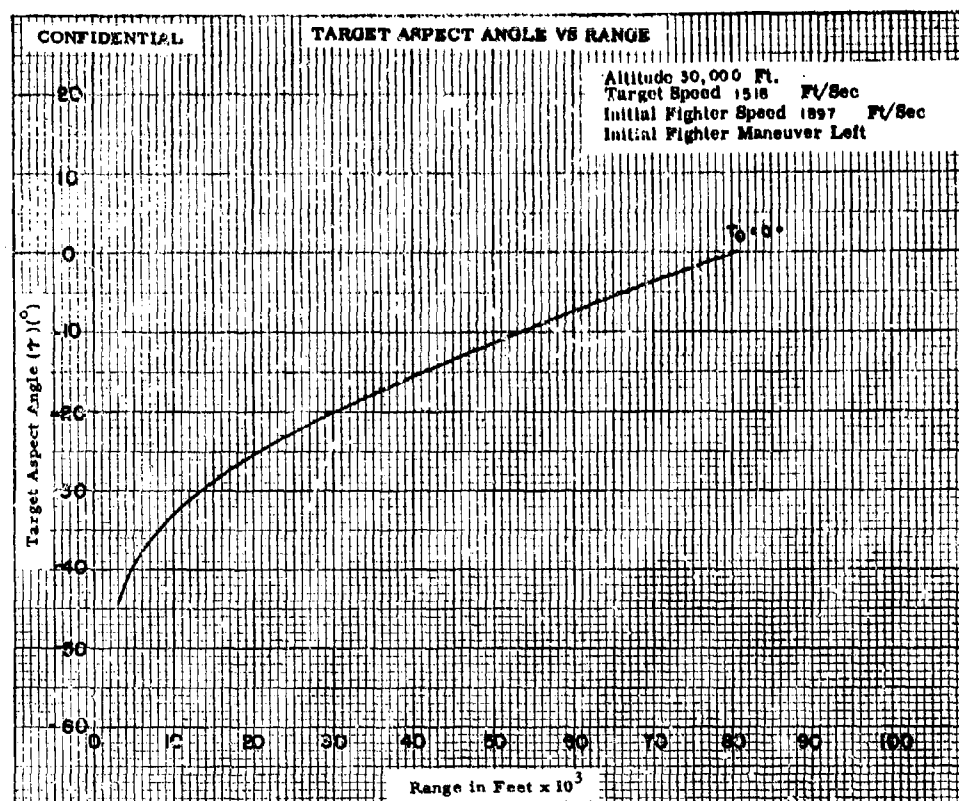


Fig. XI-7a

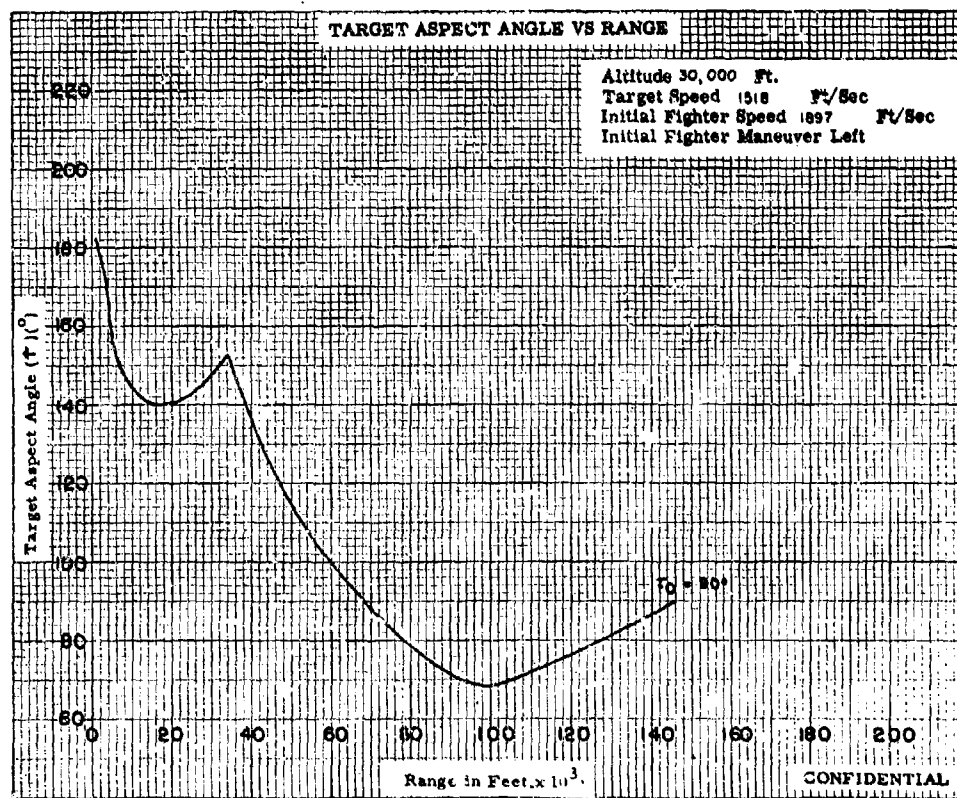
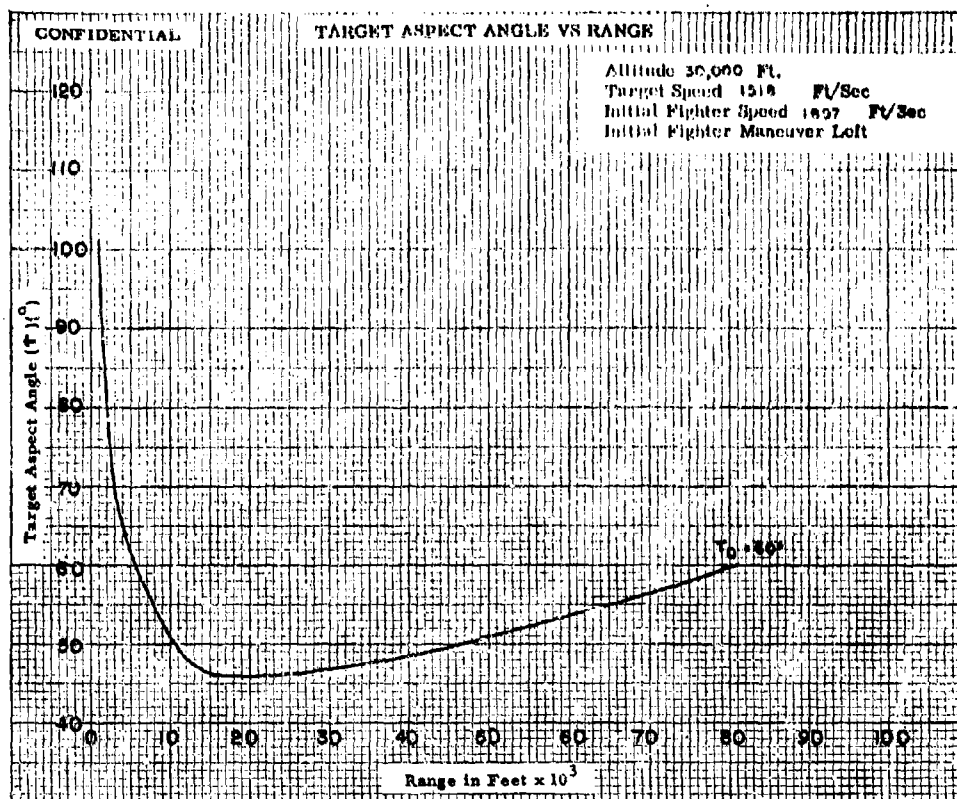


Fig. XI-7b

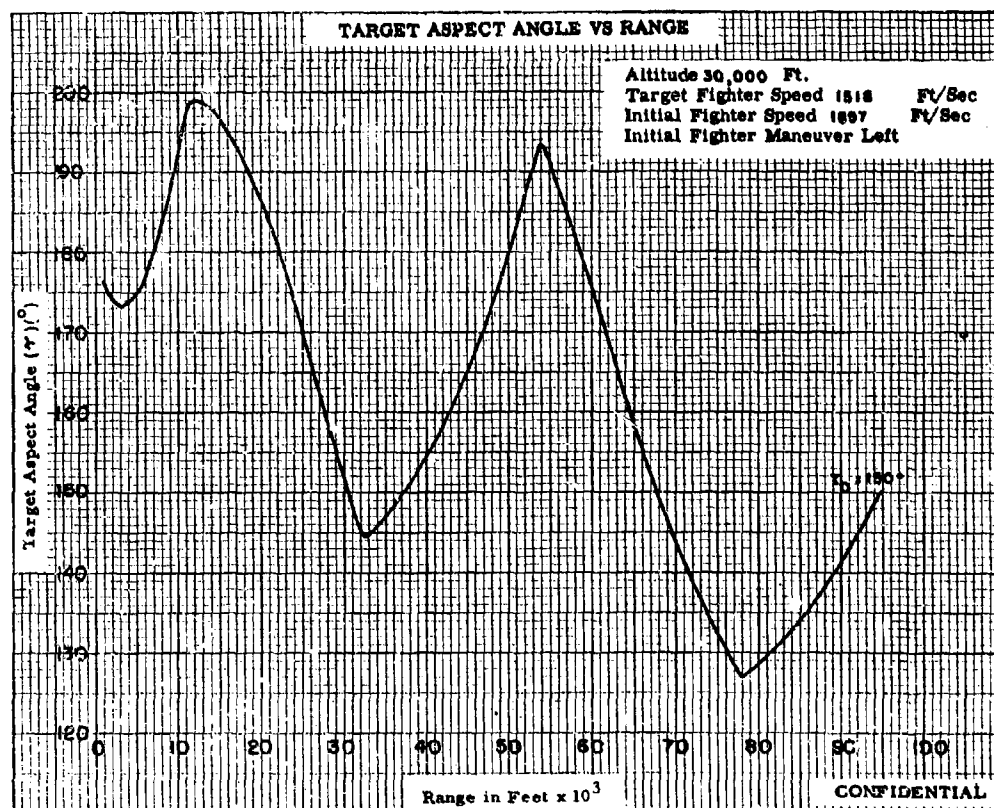
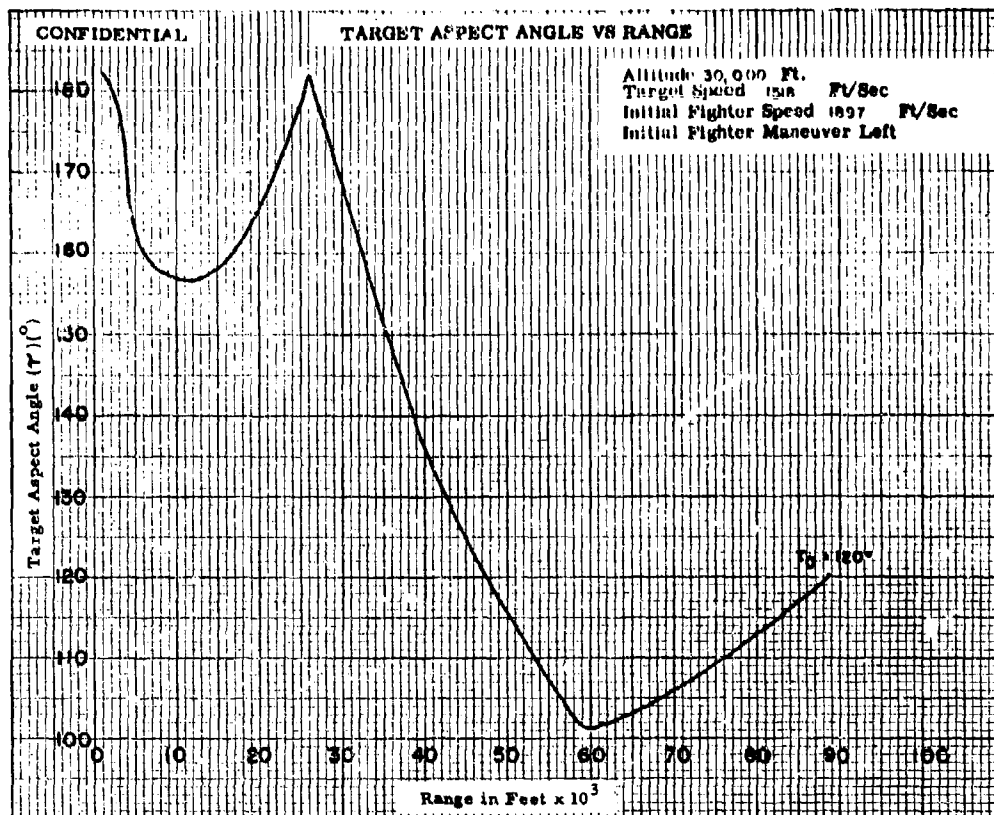


Fig. XI-7c

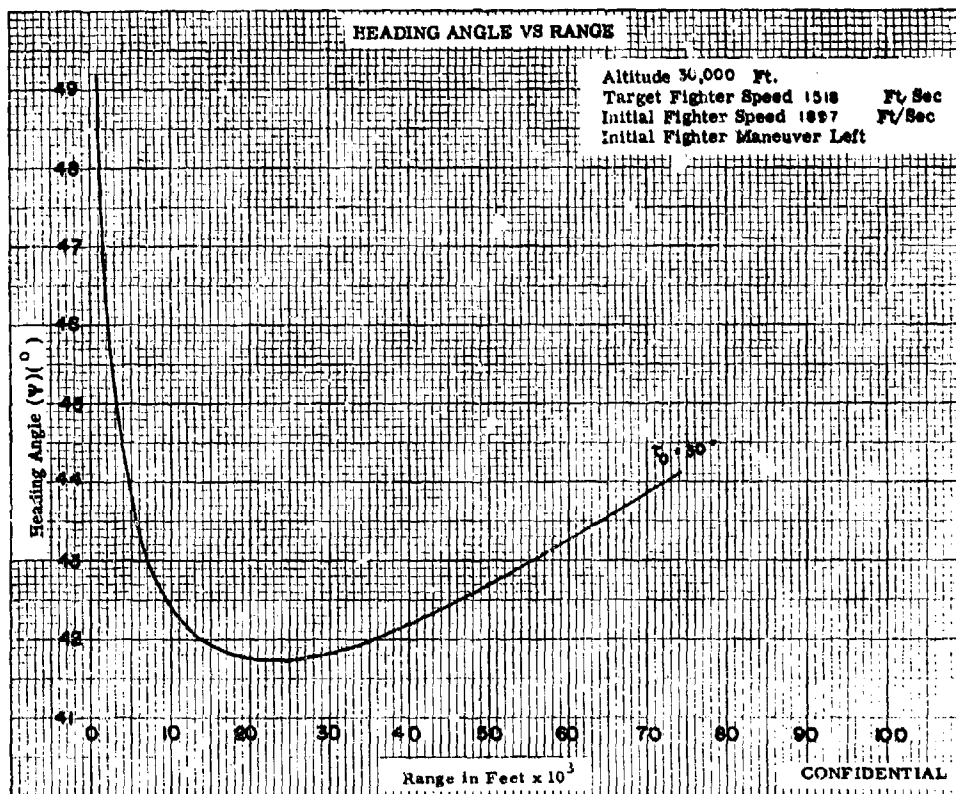
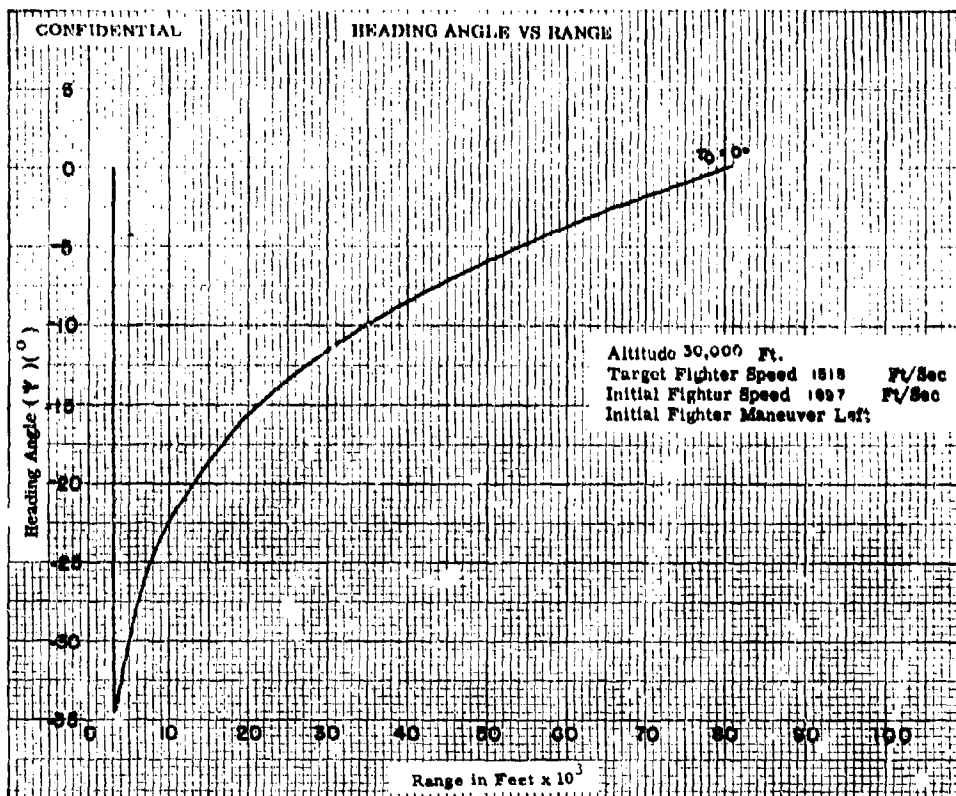


Fig. XI-8a

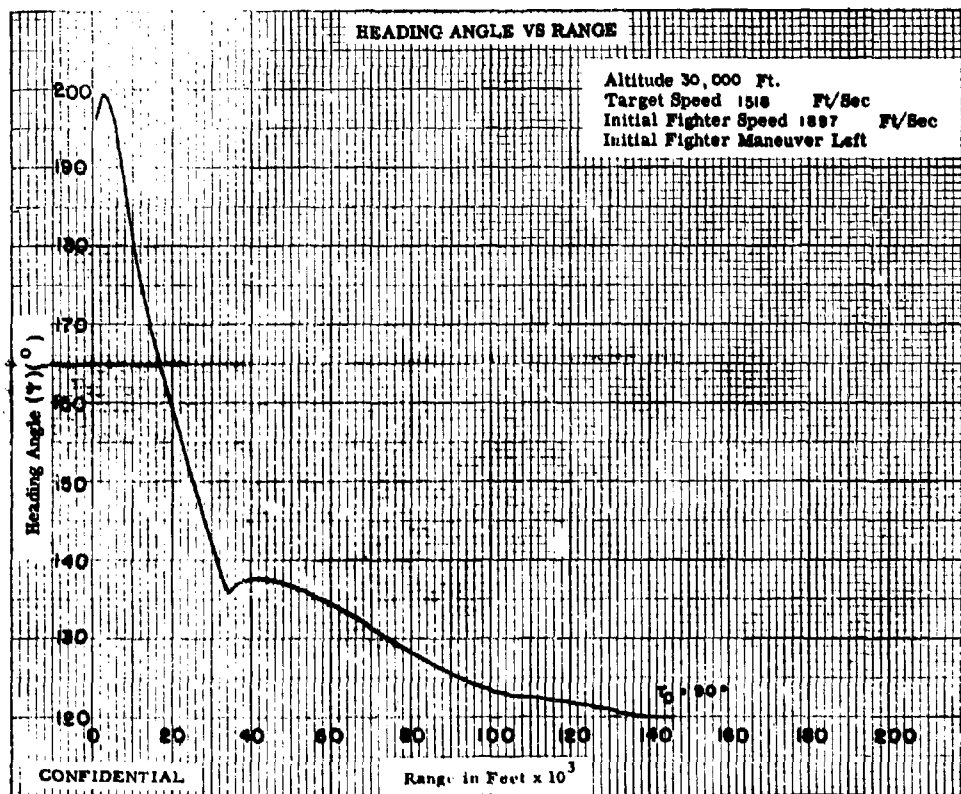
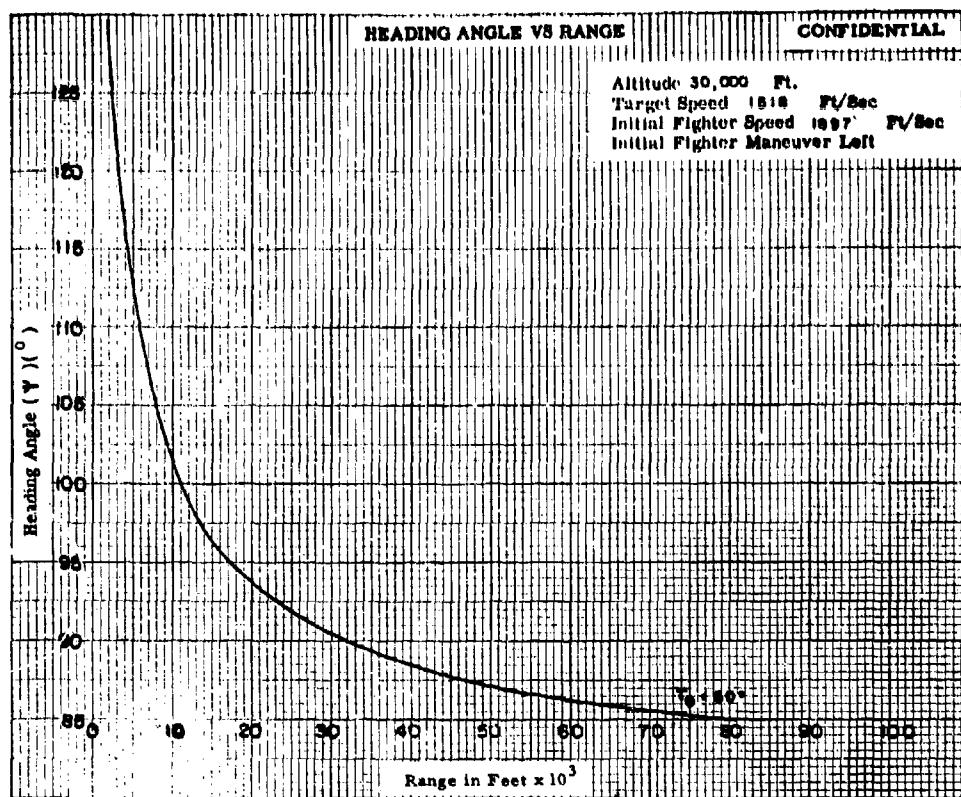


Fig. XI-80

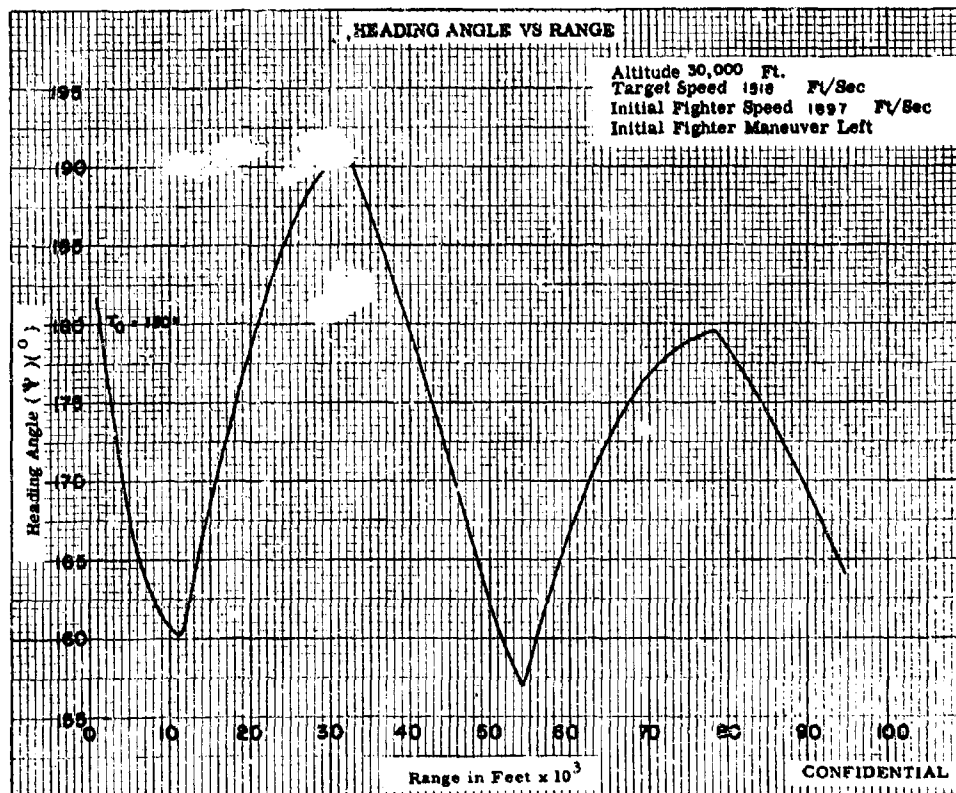
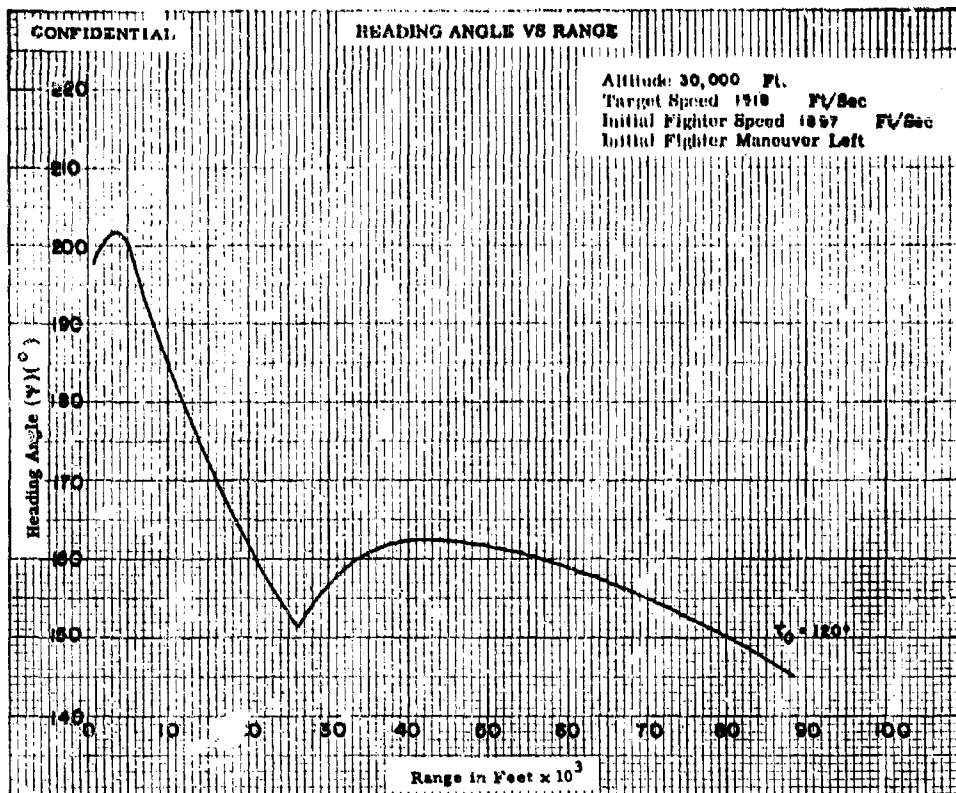


Fig. XI-8c

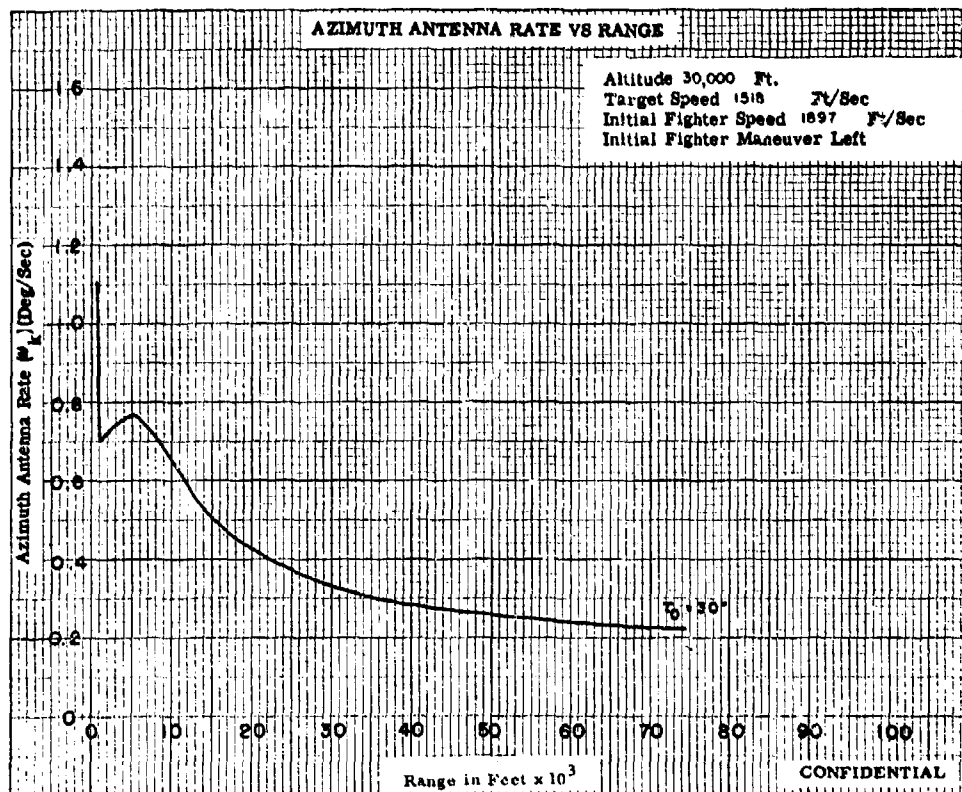
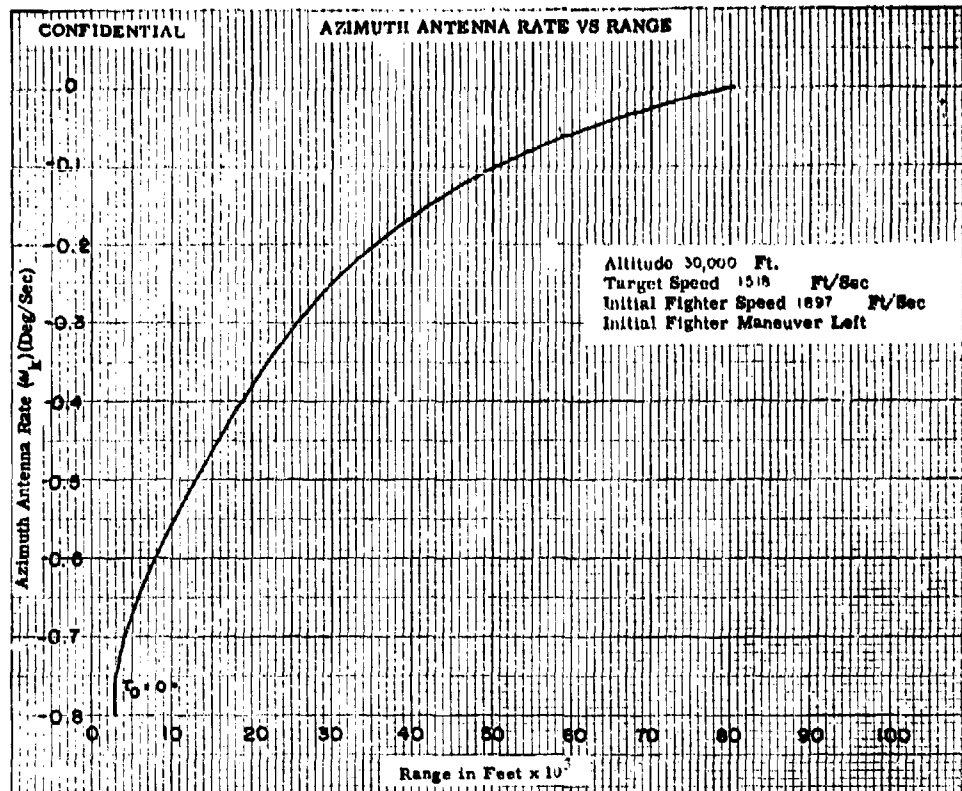


Fig. XI-9a

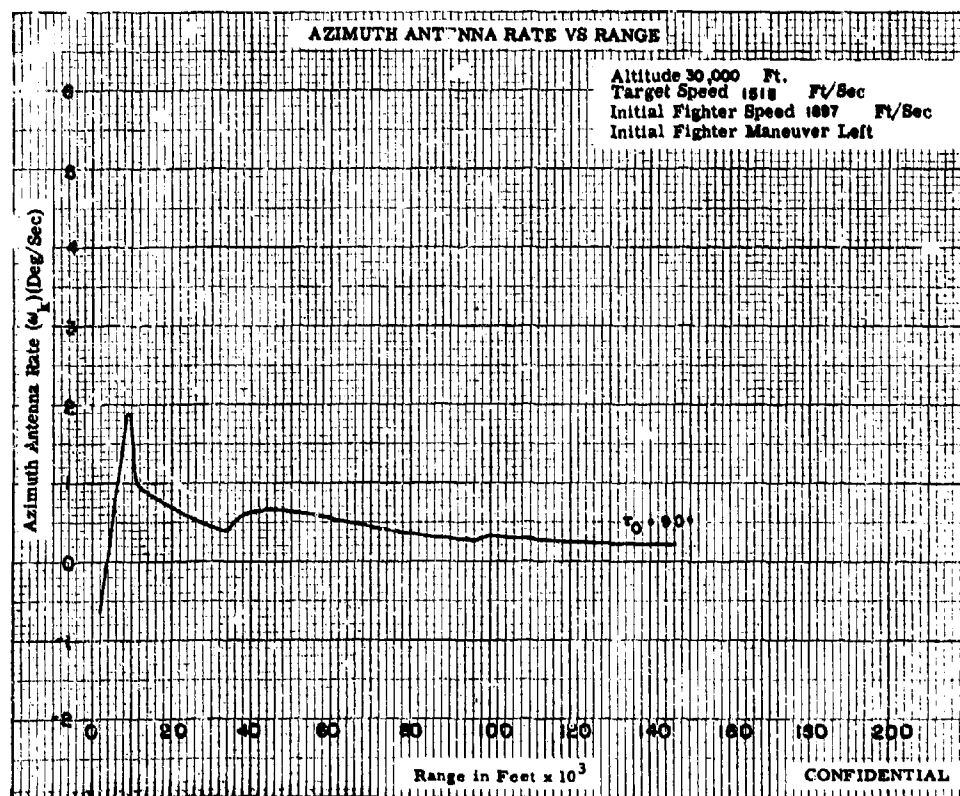
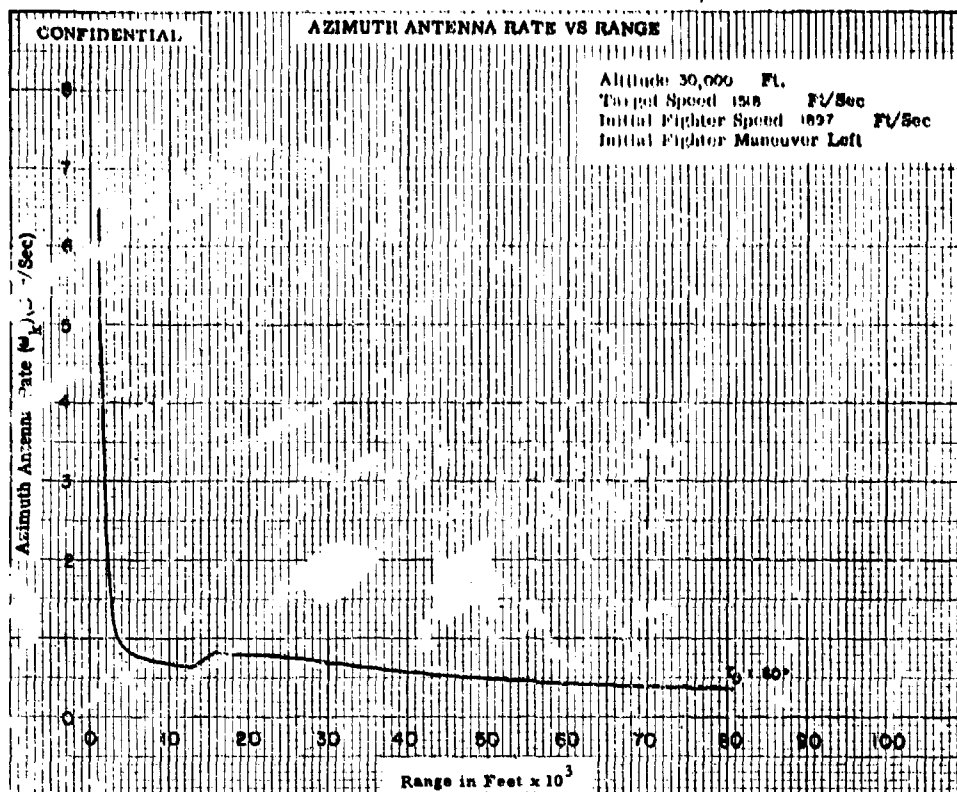


Fig. XI-9b

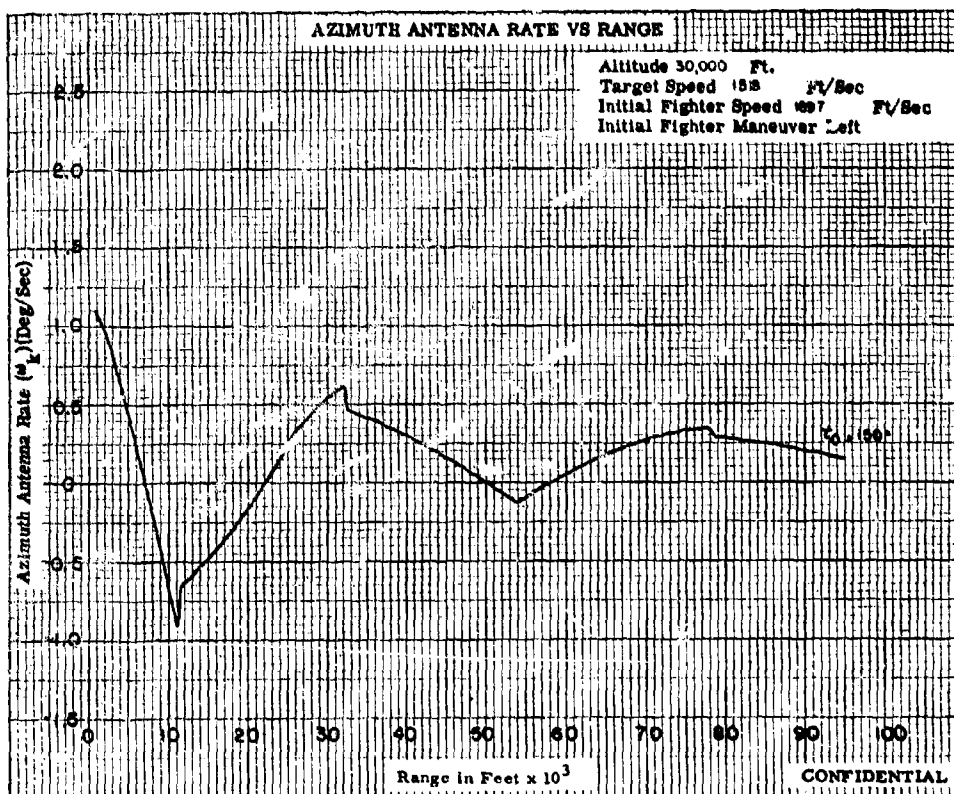
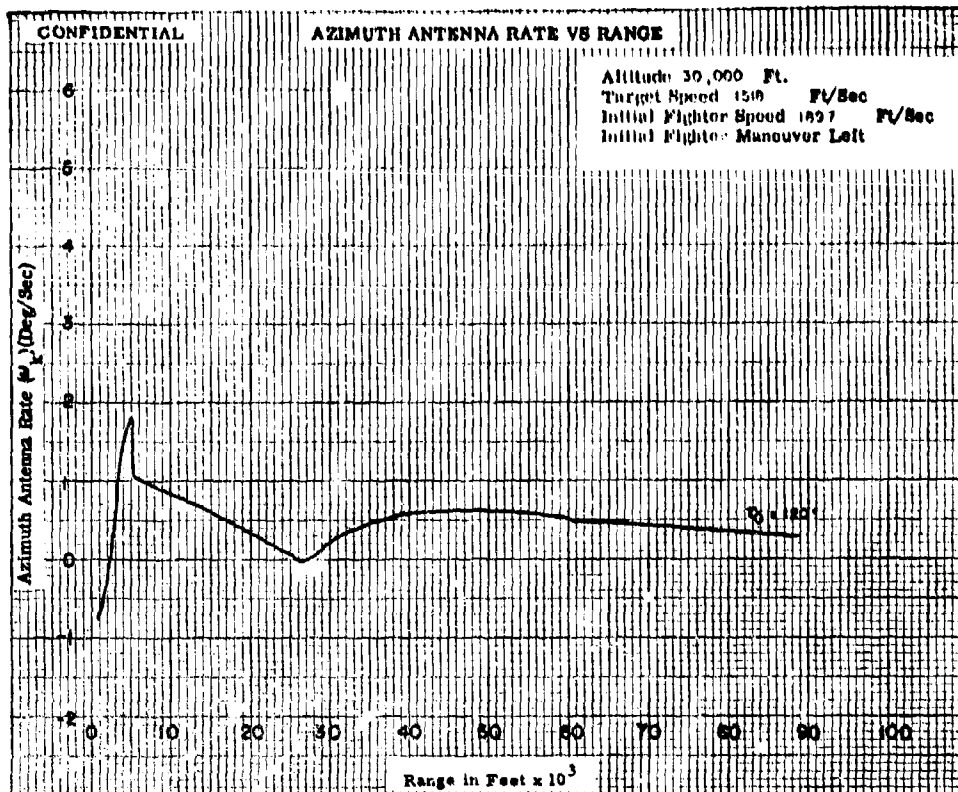


Fig. XI-9c

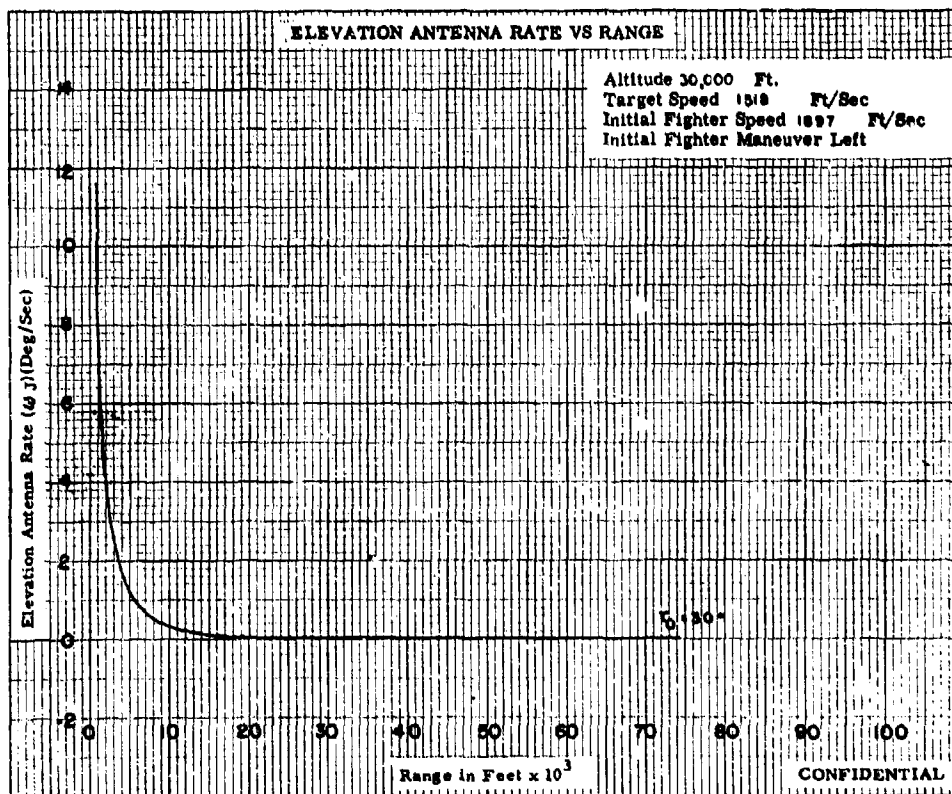
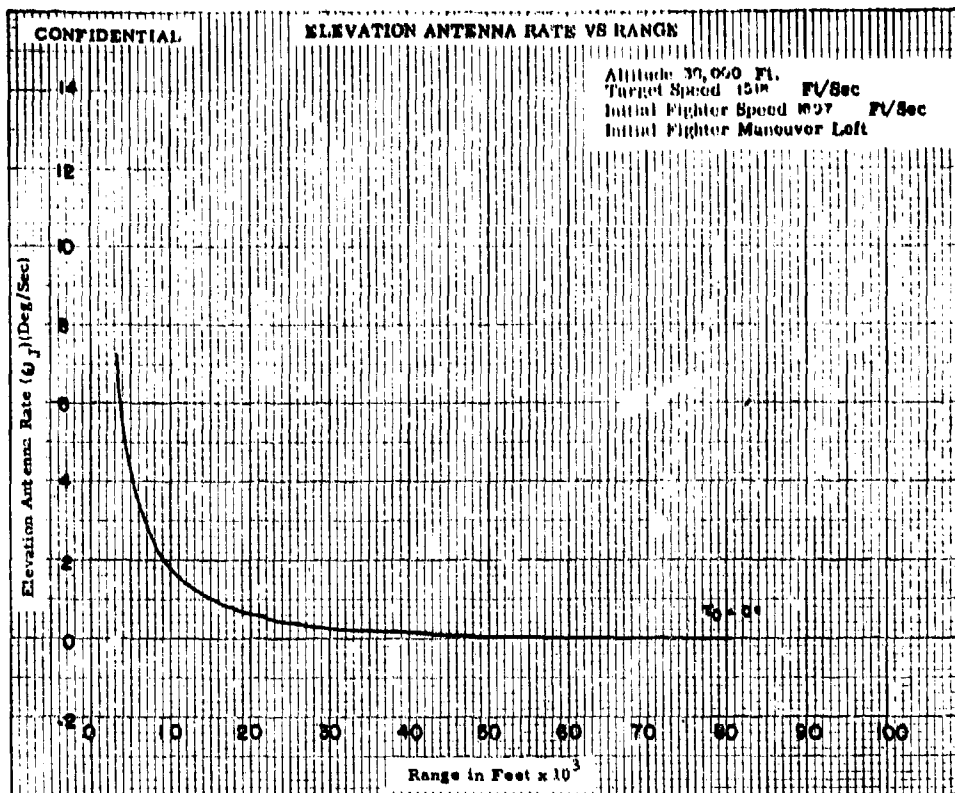


Fig. XI-10a

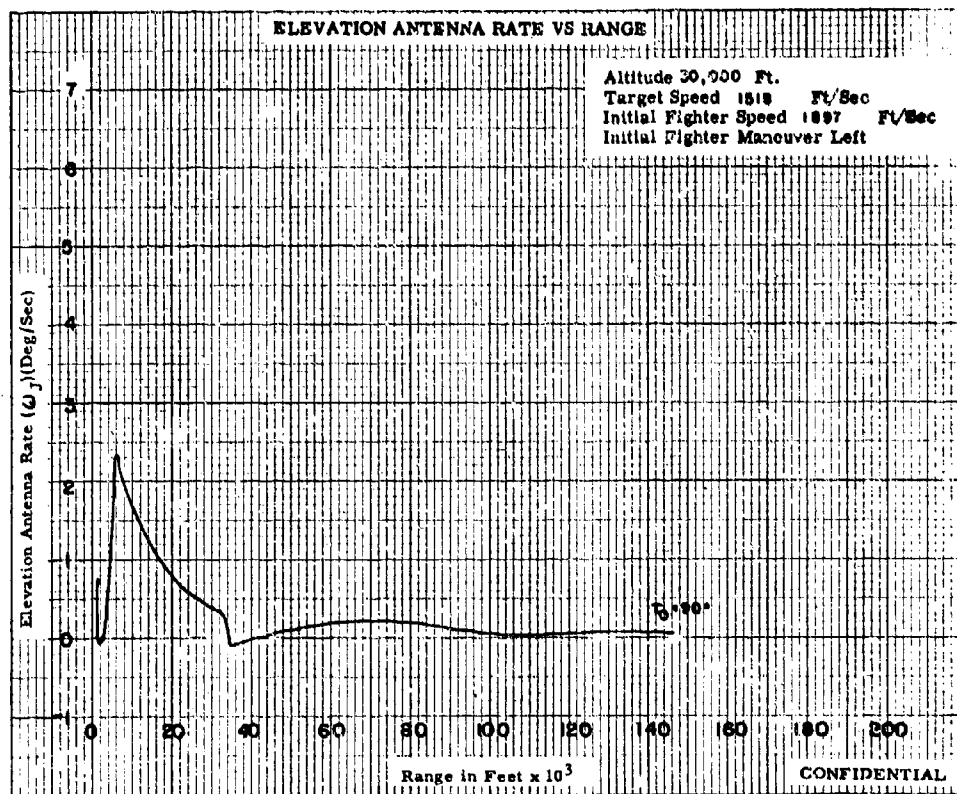
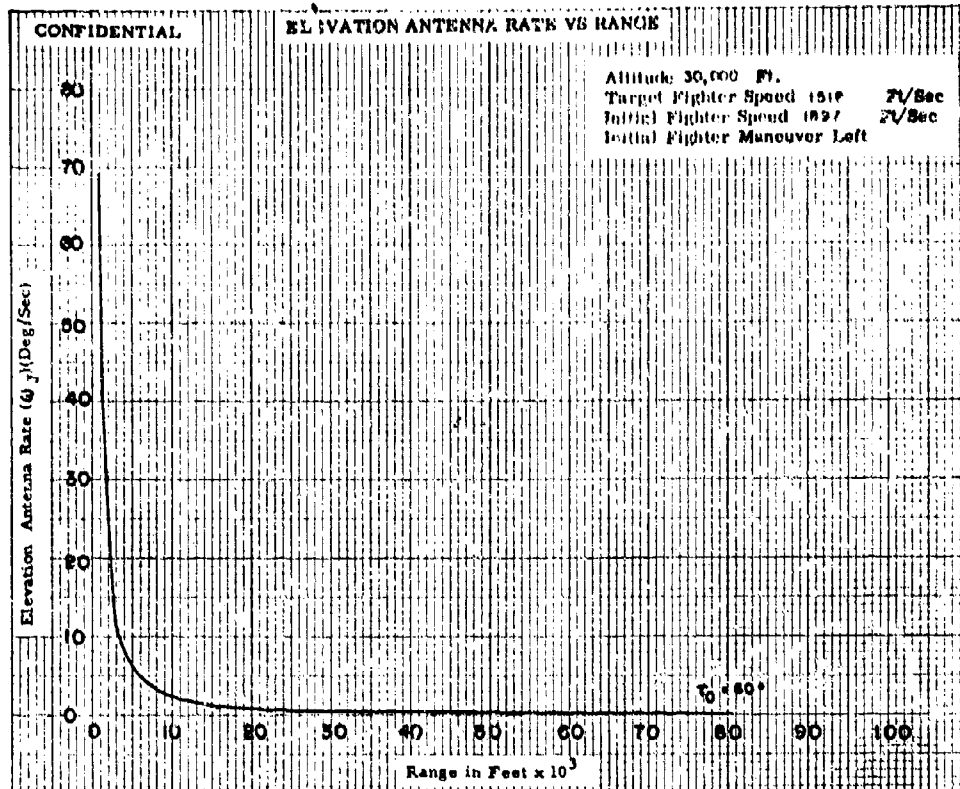


Fig. X1-10b

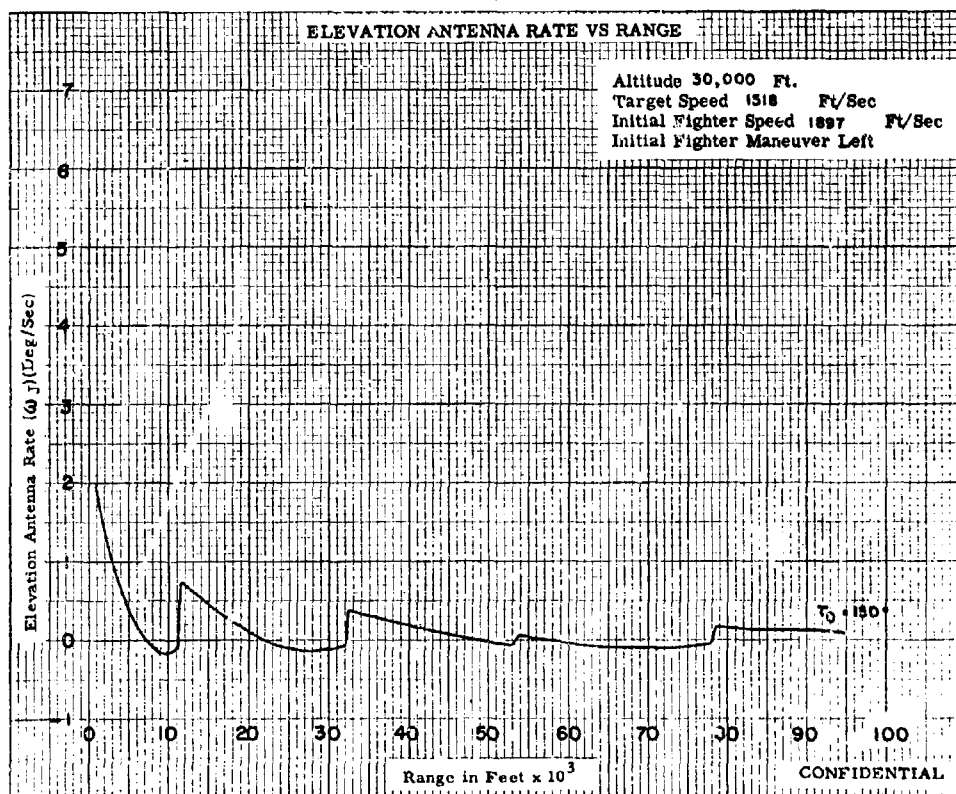
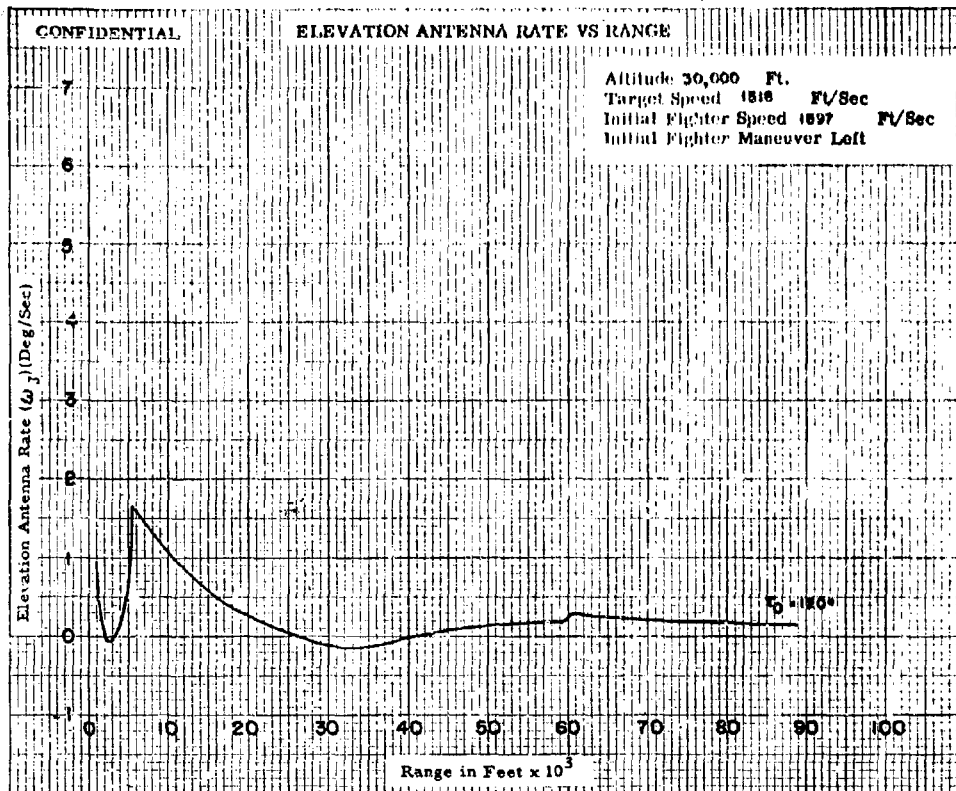


Fig. XI-10c

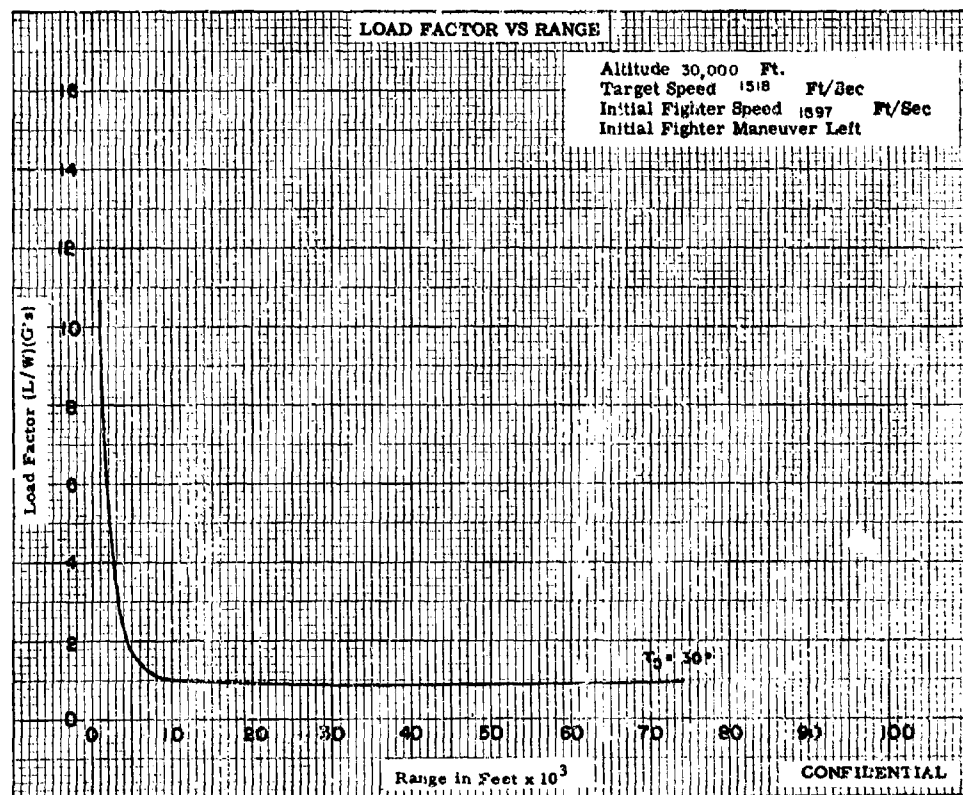
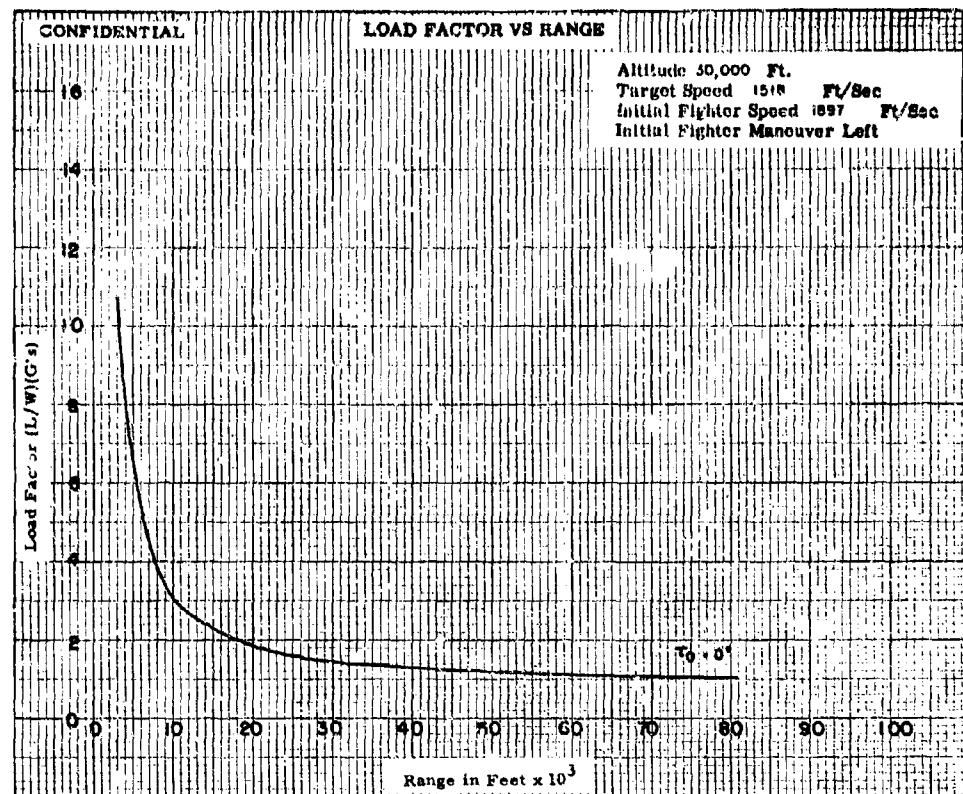


Fig. XI-11a

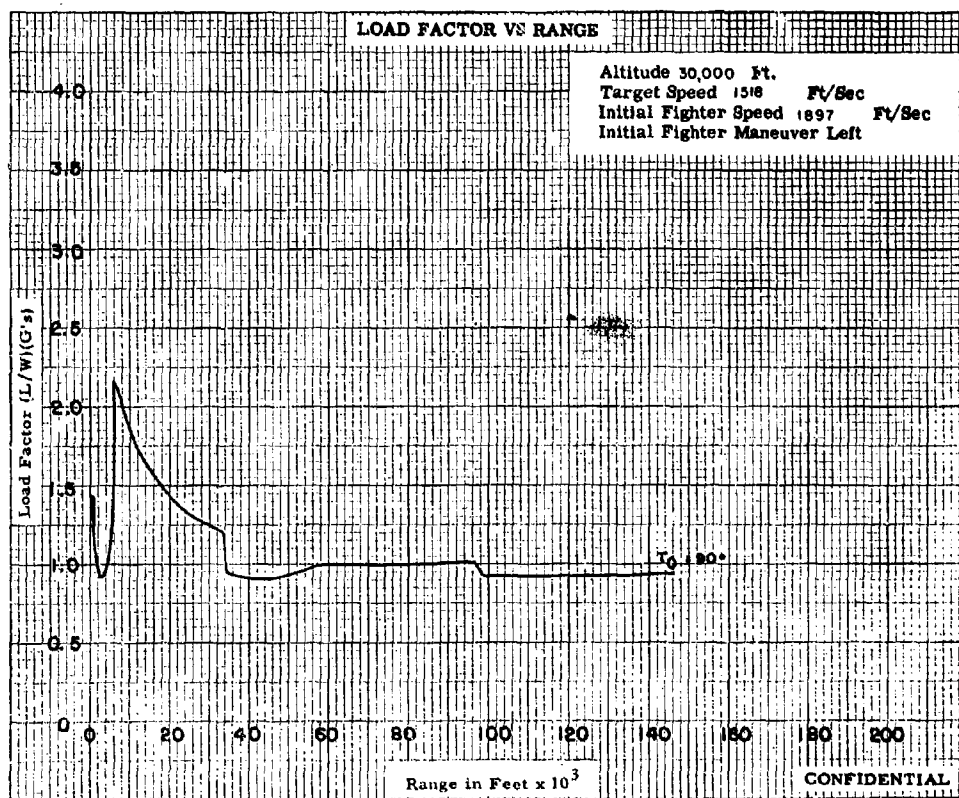
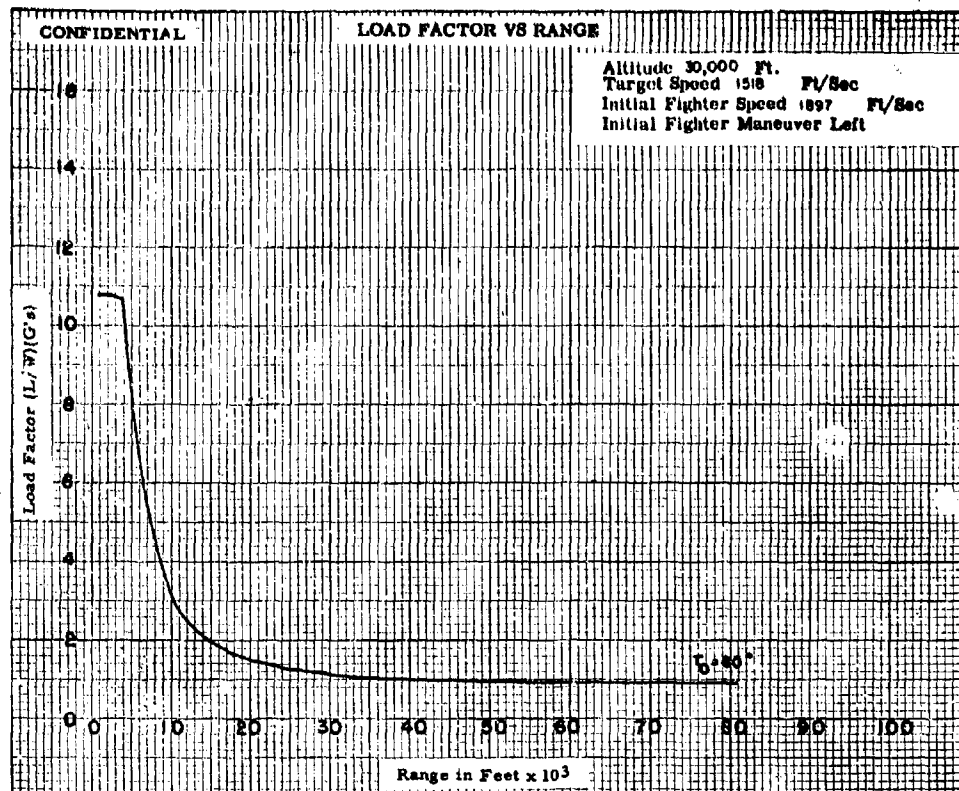


Fig. XI-11b

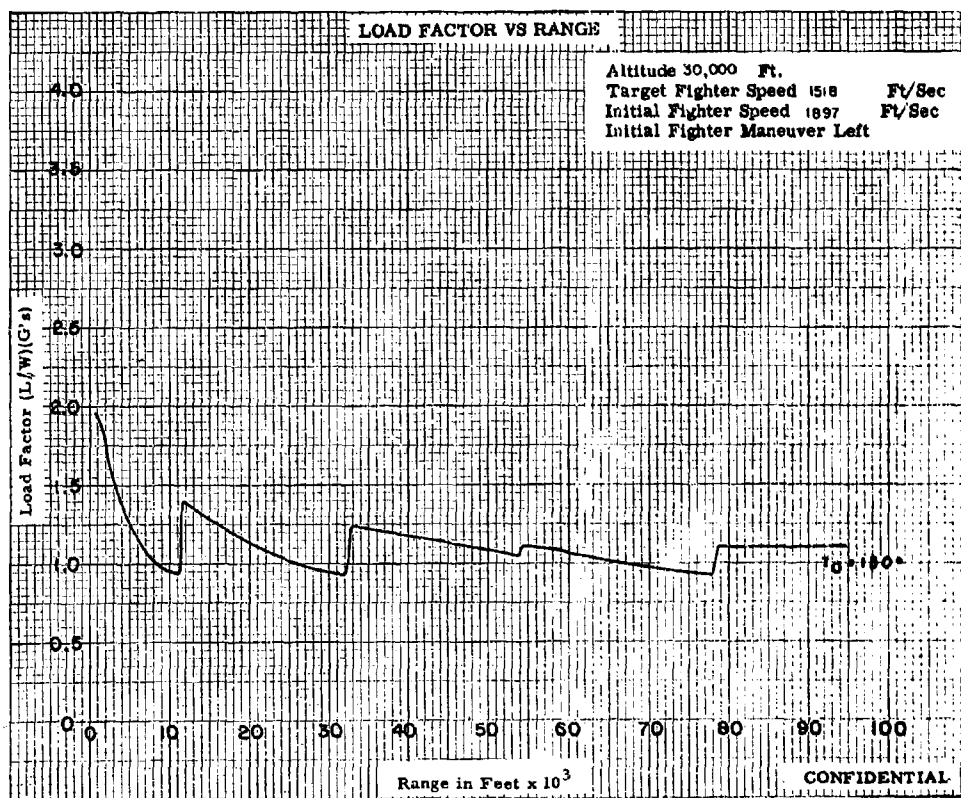
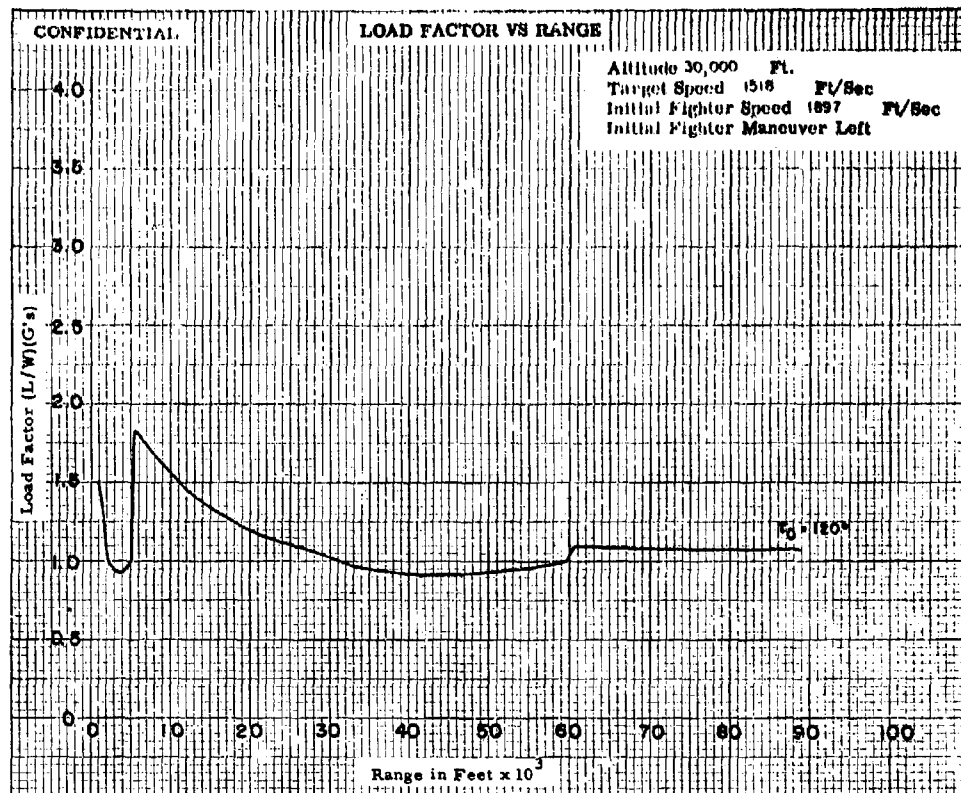


Fig. XI-11c

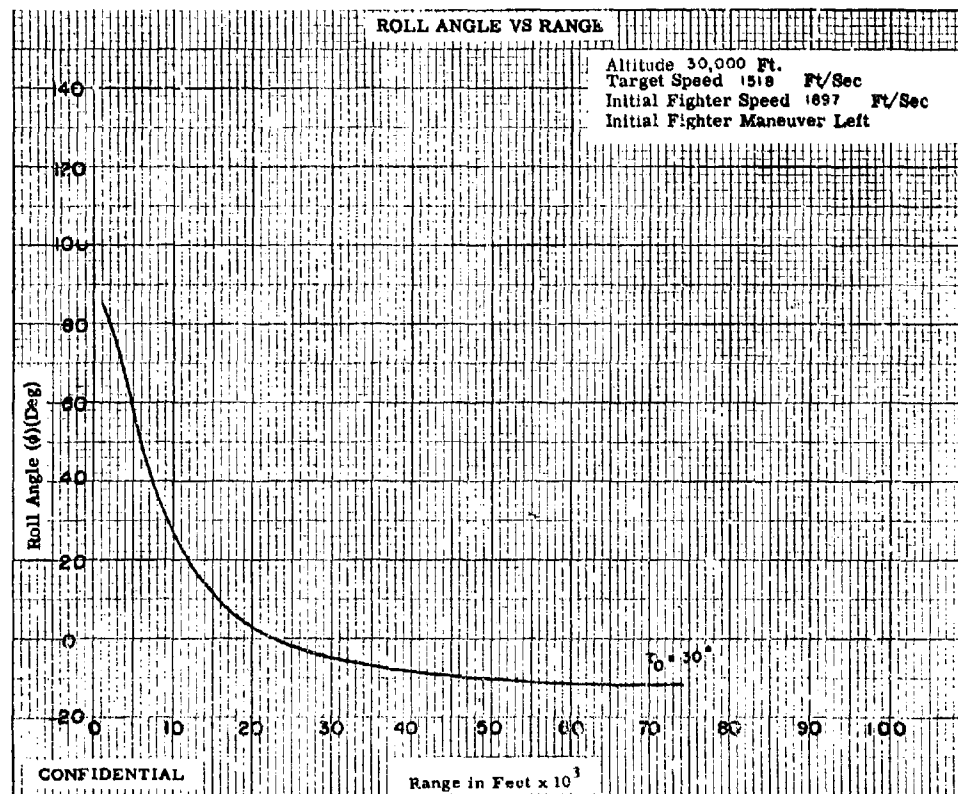
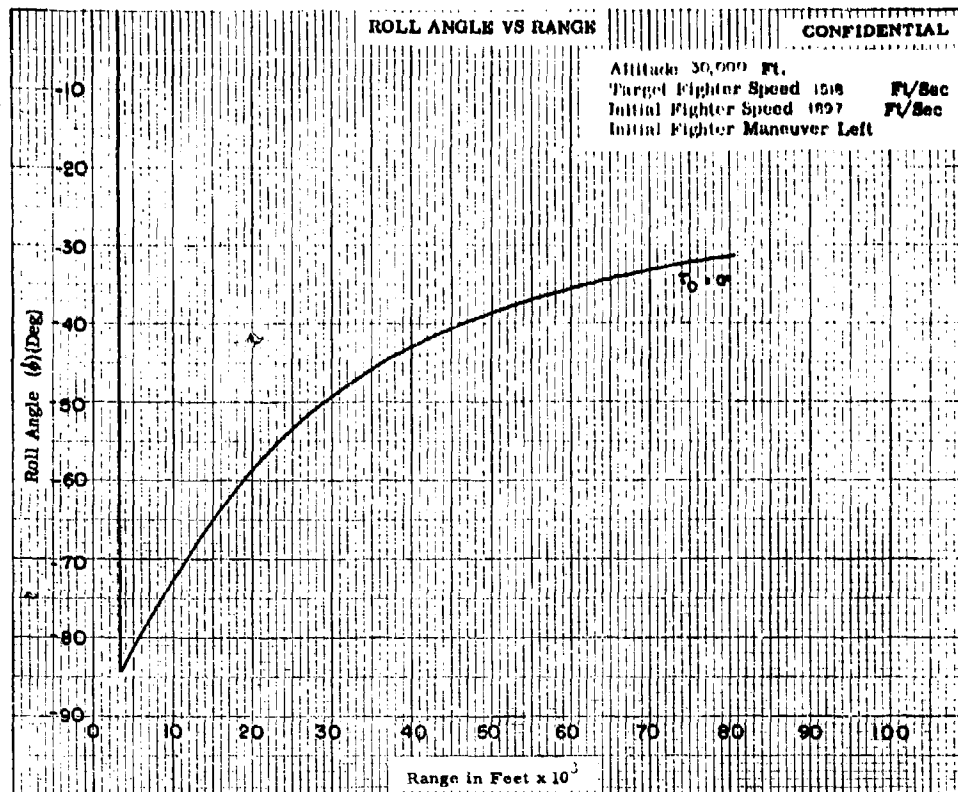


Fig. XI-12a

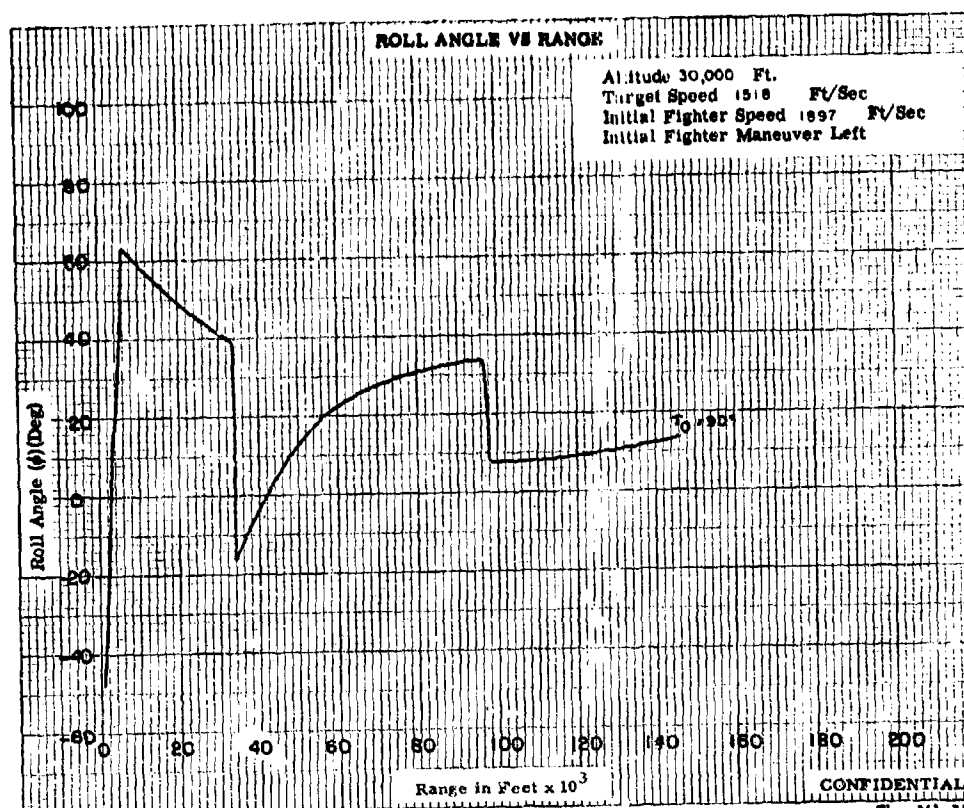
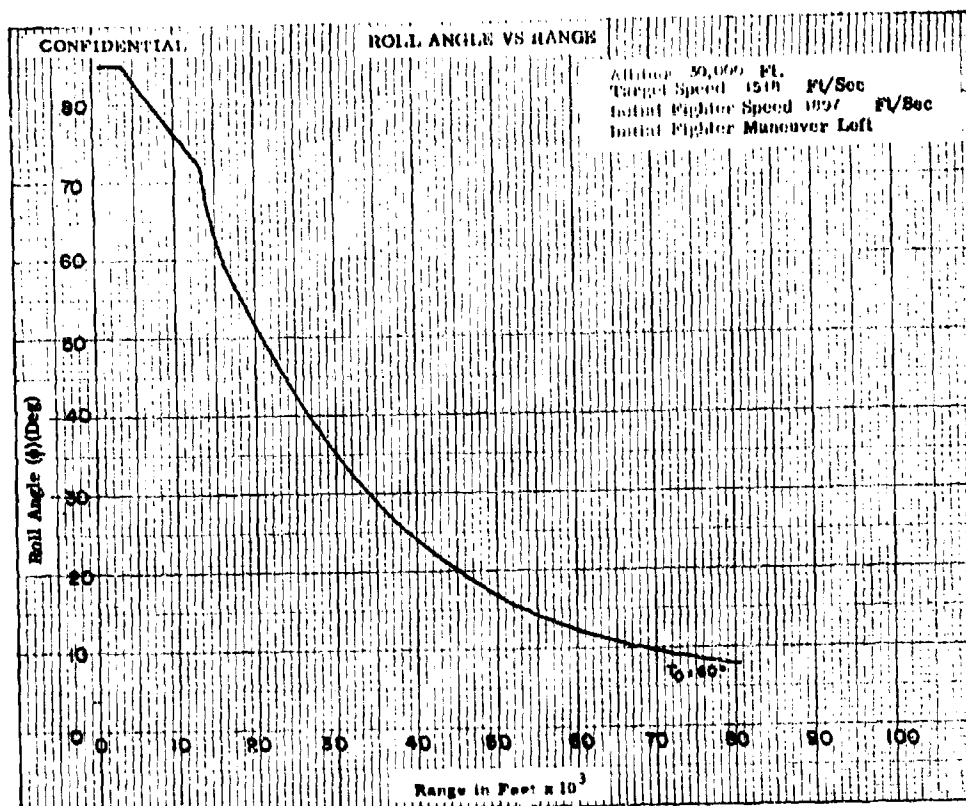


Fig. X1-12b

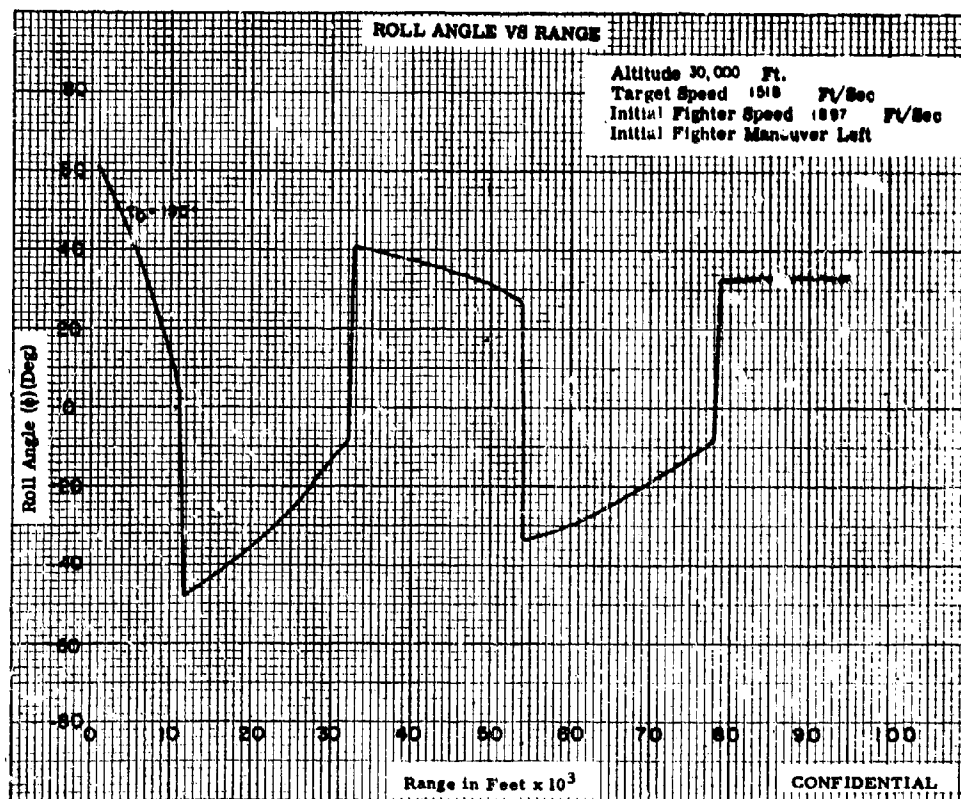
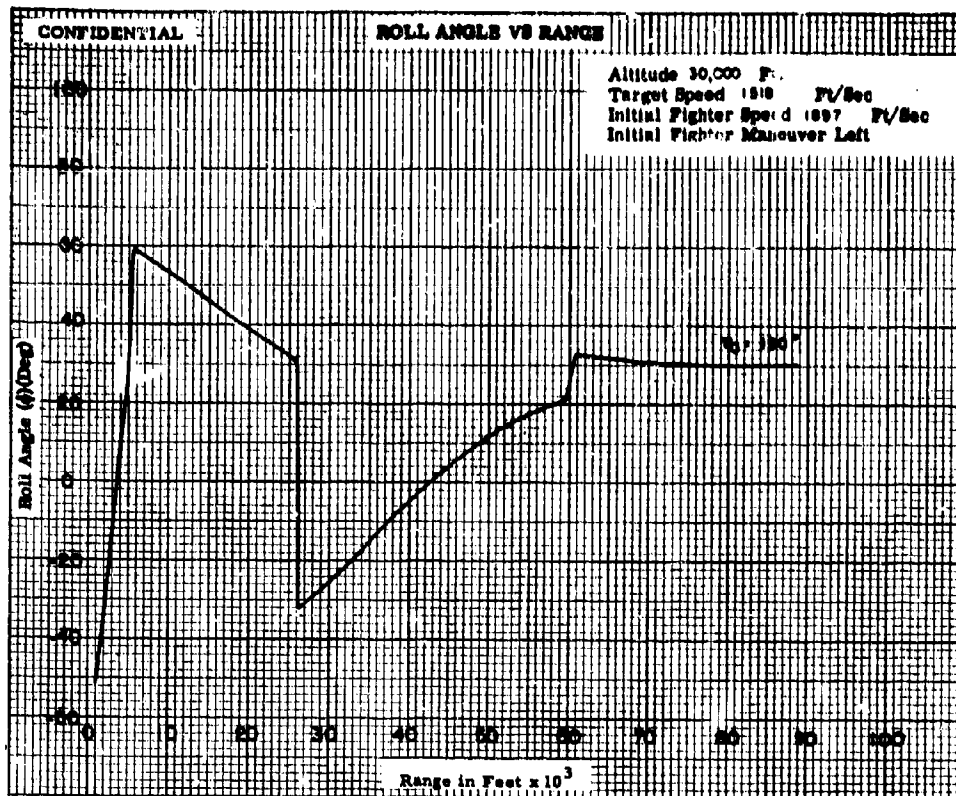


Fig. XI-12c

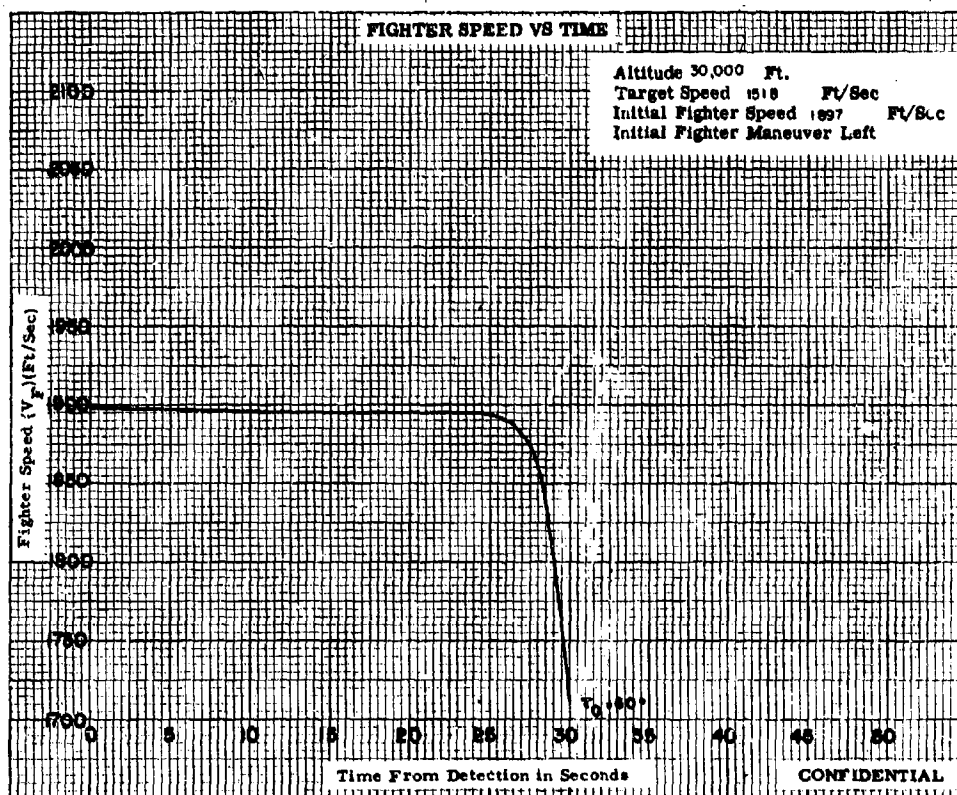
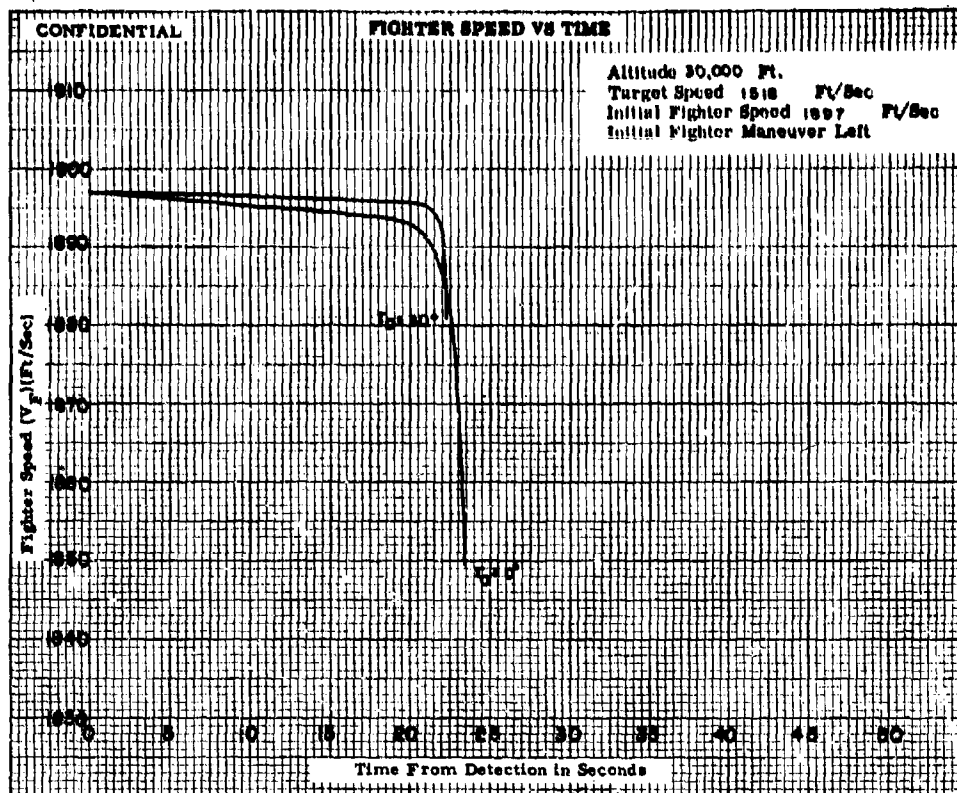


Fig. X1-13a

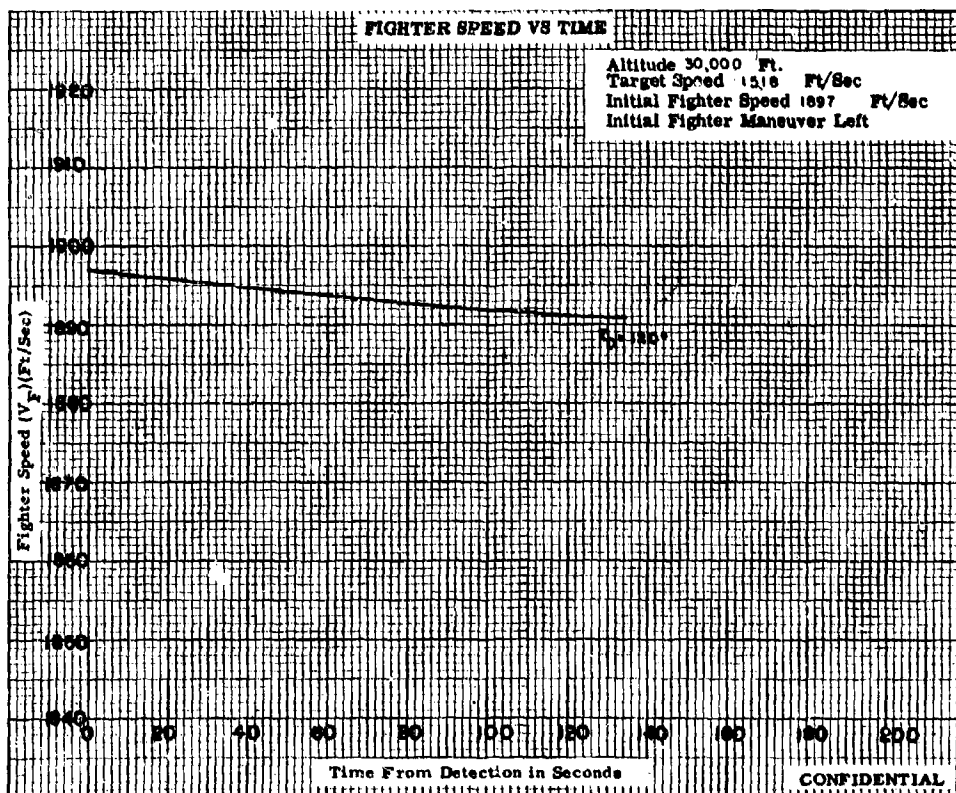
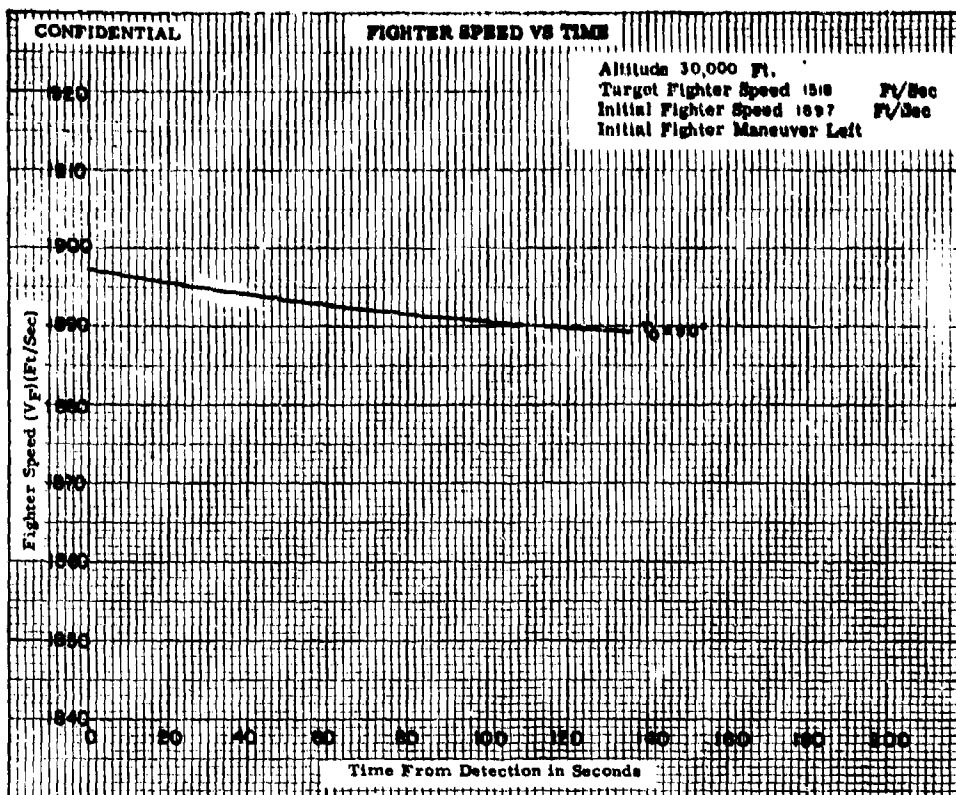


Fig. XI-13b

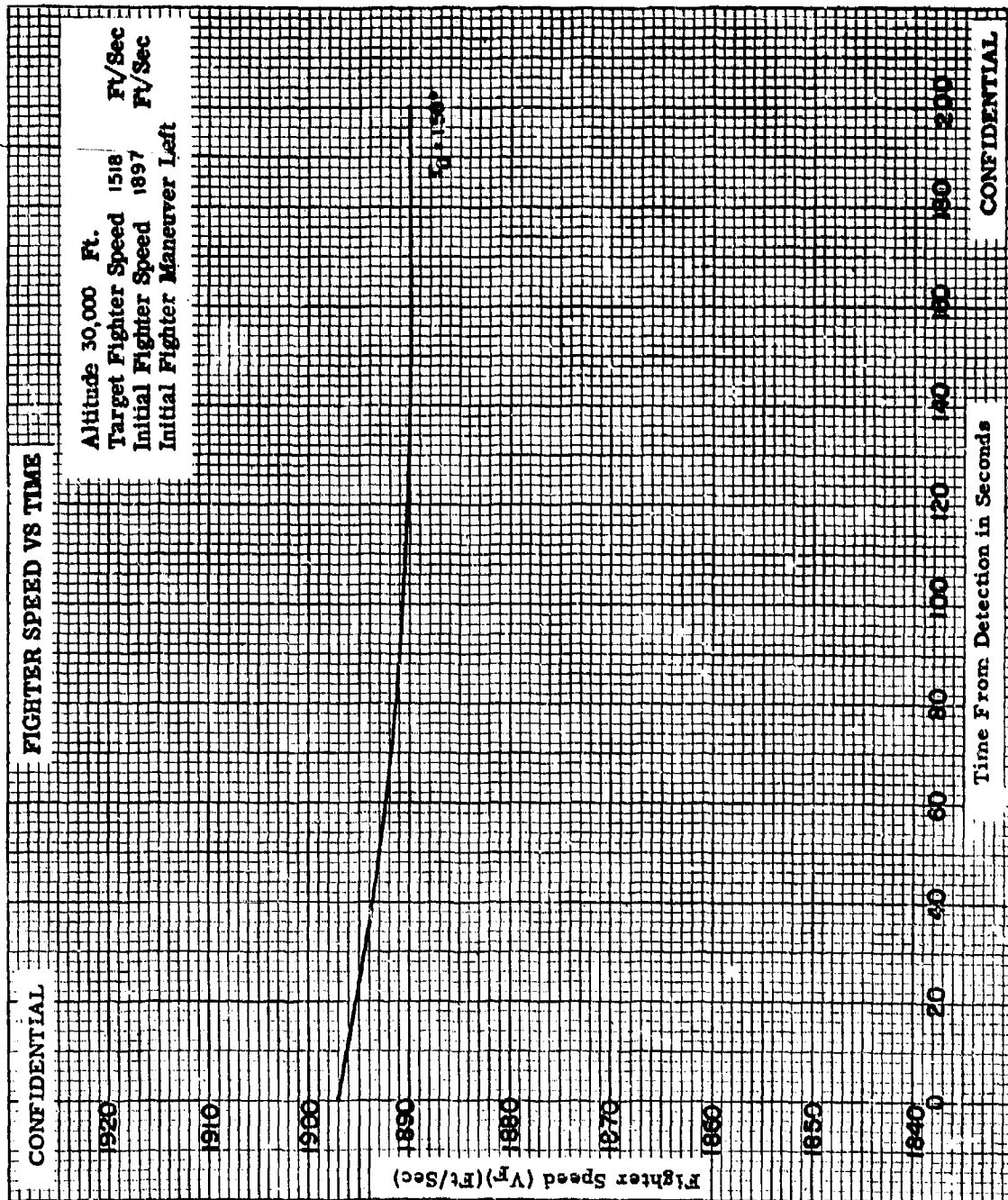


Fig. XI-13c

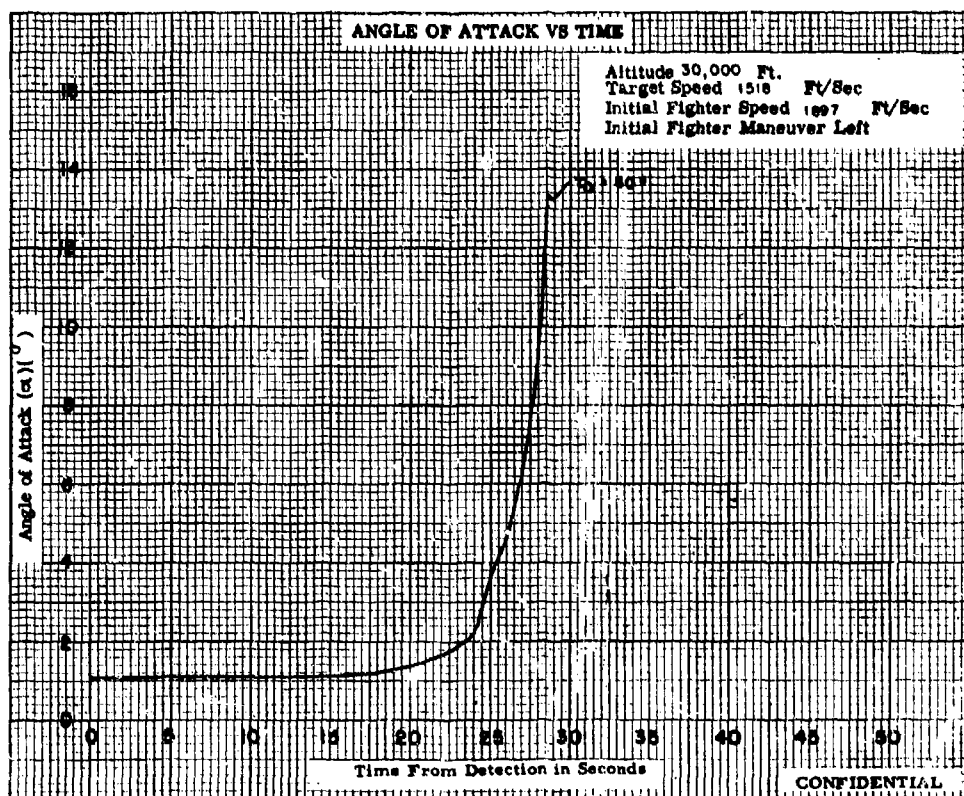
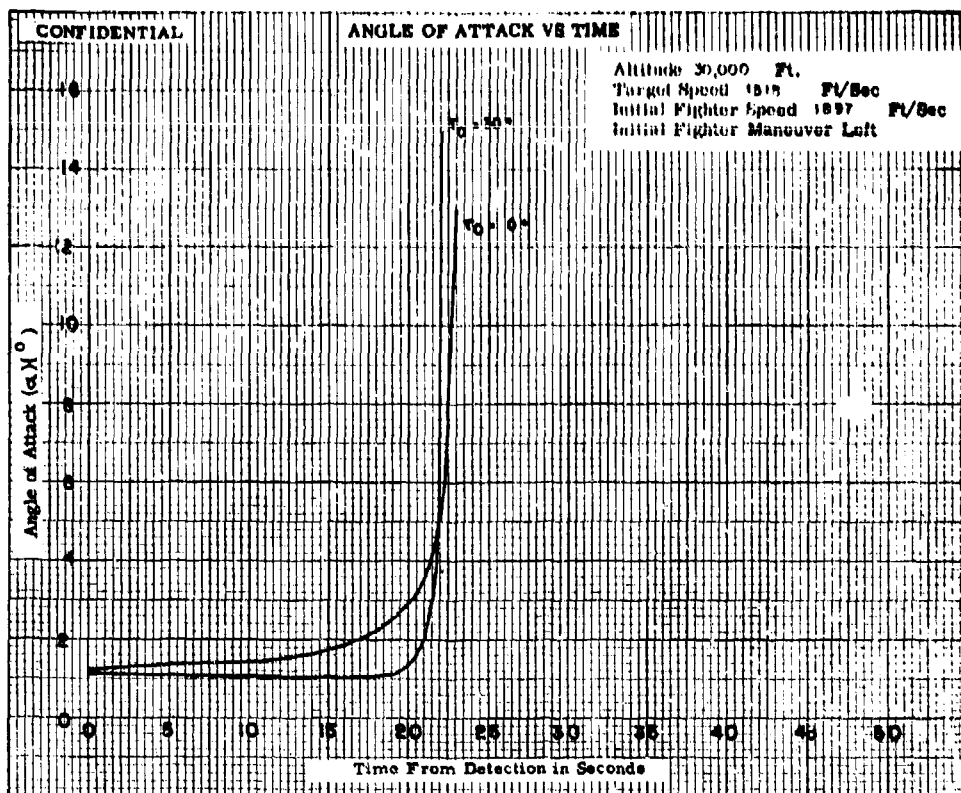


Fig. XI-14b

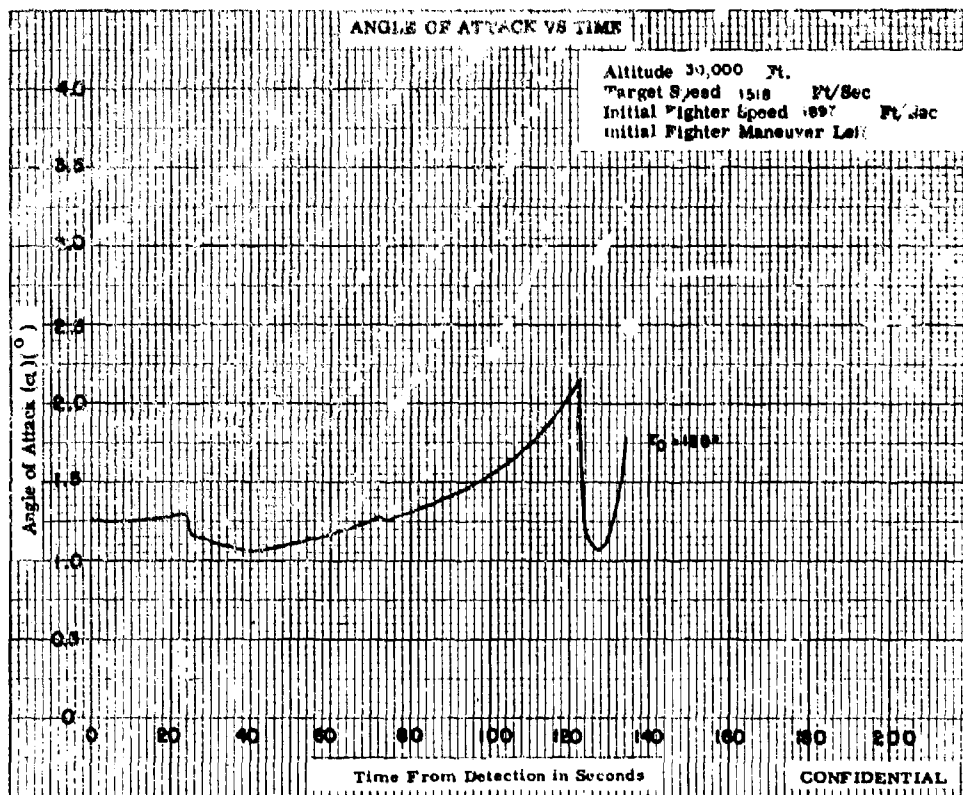
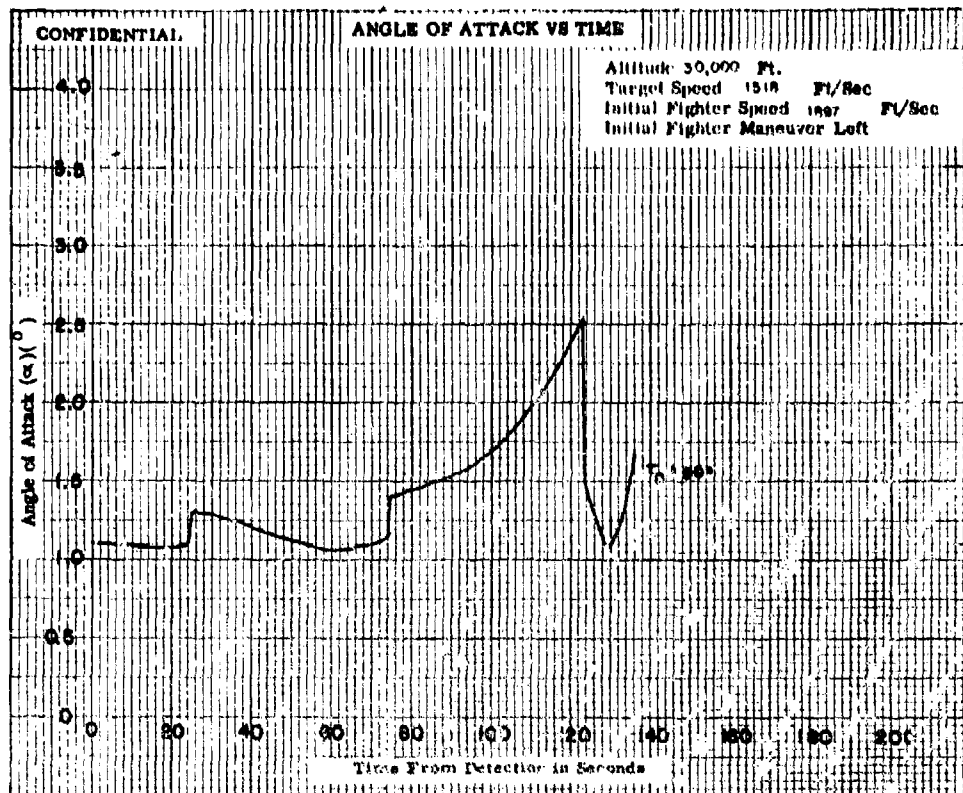


Fig. XI-14b

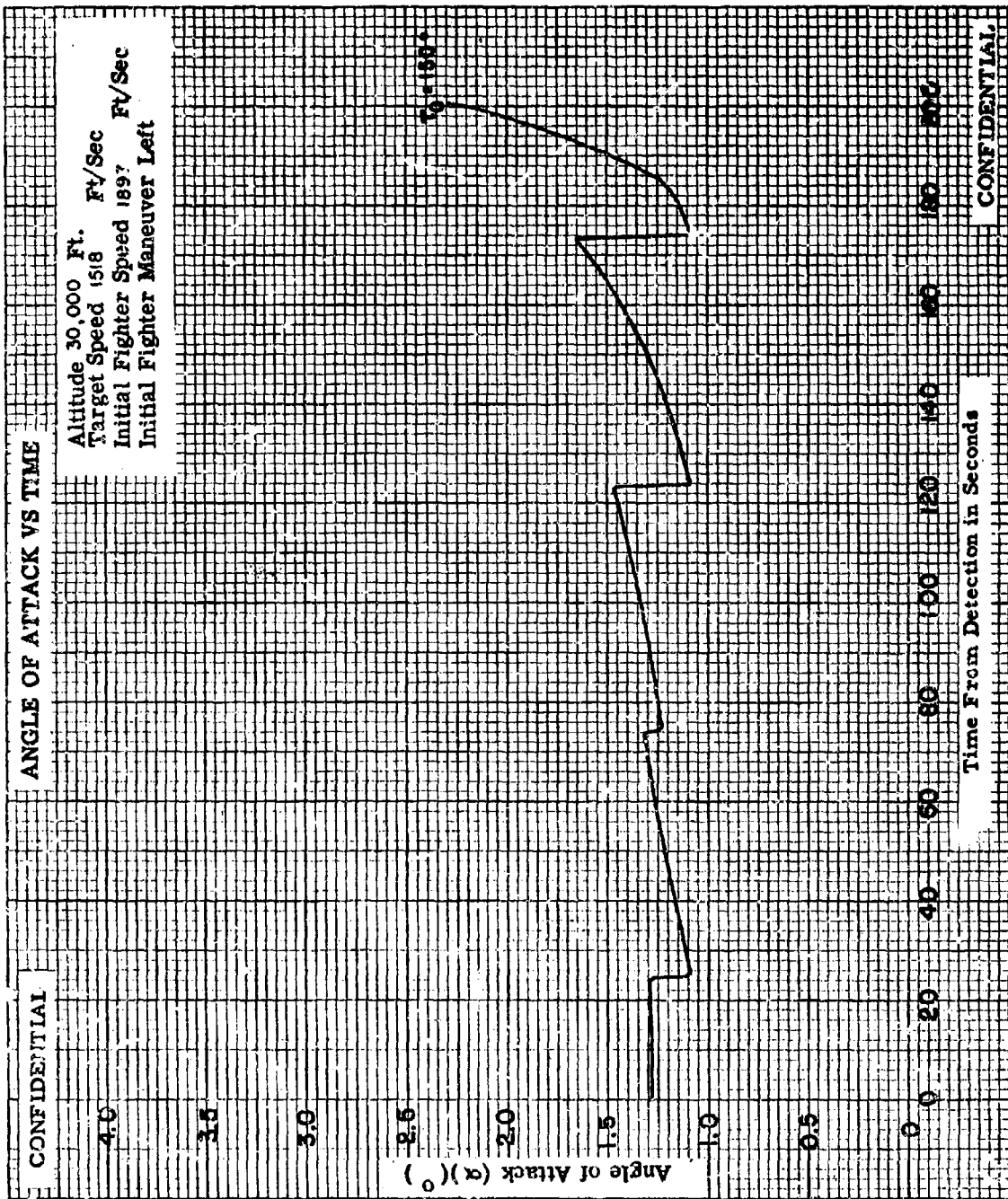


Fig. XI-14c

DATE: February 26, 2001

FROM: Mary Templeman, Code 5227

TO: **Code 5300 Paul Hughes**

CC: Tina Smallwood, Code 1221.1 *ts 3/8/01*

SUBJ: Review of NRL Reports

1. Please review NRL Report MR-754 Volumes I, II, III, IV, VII, VIII, IX, X, XI, XII, XIII, XIV, XV, MR-1372 and MR-1289 for:

- Thank you,

Mary Templeman
(202)767-3425
maryt@library.nrl.navy.mil

☒ Changed to Distribution A (Unlimited)
☐ Changed to Classification _____
☐ Other:

3-8-01
Date

** MAY CONTAIN EXPORT CONTROL DATA **

Record List

03/8/101

Page 1

AN (1) AD- 368 357/XAG
FG (2) 010100
170900
190700
CI (3) (U)
CA (5) NAVAL RESEARCH LAB WASHINGTON D C
TI (6) SUMMARY OF NAVY STUDY PROGRAM FOR F4H-1 AND F8U-3 WEAPON SYSTEMS. (PARAMETER
PLOTS FOR CO-ALTITUDE ATTACKS). VOLUME VII.
DN (9) Memo. rept.
AU (10) Bellavin ,I. N.
Lister ,R. L.
Loughmiller ,C. M.
Ryon,J. C.
RD (11) 1958
PG (12) 248 Pages
RS (14) NRL-MR-754-Vol-7
RC (20) Unclassified report
NO (21) See also Volume 4, AD-368 356L.
AL (22) Distribution: DoD only: others to Director, Naval Research Lab., Washington,
D. C. 20390.
DE (23) (*JET FIGHTERS, AERIAL WARFARE)
NAVAL AIRCRAFT, AERIAL TARGETS, TACTICAL WARFARE, FLIGHT PATHS, HIGH ALTITUDE,
PERFORMANCE(ENGINEERING), ANGLE OF ATTACK, EFFECTIVENESS (U) AIRCRAFT
INTERCEPTION, AIRCRAFT FIRE CONTROL SYSTEMS, SEARCH RADAR, TARGET ACQUISITION,
RANGE(DISTANCE), AZIMUTH, RADAR HOMING, GRAPHICS, INTERCEPT TRAJECTORIES, AIR
TO AIR MISSILES
DC (24) (U)
ID (25) AN/APQ-50, AN/APQ-72, F-4 AIRCRAFT, F-8 AIRCRAFT, SPARROW
IC (25) (U)
DL (33) 04
CC (35) 251950

APPROVED FOR PUBLIC
RELEASE - DISTRIBUTION
UNLIMITED